



viruses

Special Issue Reprint

Pseudorabies Virus, Volume II

Edited by
Yan-Dong Tang and Xiangdong Li

mdpi.com/journal/viruses



Pseudorabies Virus, Volume II

Pseudorabies Virus, Volume II

Editors

Yan-Dong Tang

Xiangdong Li



Basel • Beijing • Wuhan • Barcelona • Belgrade • Novi Sad • Cluj • Manchester

Editors

Yan-Dong Tang

Harbin Veterinary Research
Institute of Chinese Academy
of Agricultural Sciences

Harbin
China

Xiangdong Li

College of Veterinary Medicine
Yangzhou University
Yangzhou

China

Editorial Office

MDPI

St. Alban-Anlage 66

4052 Basel, Switzerland

This is a reprint of articles from the Special Issue published online in the open access journal *Viruses* (ISSN 1999-4915) (available at: www.mdpi.com/journal/viruses/special_issues/BW35V571F2).

For citation purposes, cite each article independently as indicated on the article page online and as indicated below:

Lastname, A.A.; Lastname, B.B. Article Title. <i>Journal Name</i> Year , <i>Volume Number</i> , Page Range.
--

ISBN 978-3-7258-1298-1 (Hbk)

ISBN 978-3-7258-1297-4 (PDF)

doi.org/10.3390/books978-3-7258-1297-4

© 2024 by the authors. Articles in this book are Open Access and distributed under the Creative Commons Attribution (CC BY) license. The book as a whole is distributed by MDPI under the terms and conditions of the Creative Commons Attribution-NonCommercial-NoDerivs (CC BY-NC-ND) license.

Contents

Mo Zhou, Muhammad Abid, Shinuo Cao and Shanyuan Zhu Progress of Research into Novel Drugs and Potential Drug Targets against Porcine Pseudorabies Virus Reprinted from: <i>Viruses</i> 2022 , <i>14</i> , 1753, doi:10.3390/v14081753	1
Changchao Huan, Yao Xu, Wei Zhang, Bo Ni and Song Gao Glycyrrhiza Polysaccharide Inhibits Pseudorabies Virus Infection by Interfering with Virus Attachment and Internalization Reprinted from: <i>Viruses</i> 2022 , <i>14</i> , 1772, doi:10.3390/v14081772	18
Xiangrong Li, Jingying Xie, Dianyu Li, Hongshan Li, Yuhui Niu and Bei Wu et al. HSP27 Attenuates cGAS-Mediated IFN- Signaling through Ubiquitination of cGAS and Promotes PRV Infection Reprinted from: <i>Viruses</i> 2022 , <i>14</i> , 1851, doi:10.3390/v14091851	31
Chen Li, Wen-Feng He, Long-Xi Li, Jing Chen, Guo-Qing Yang and Hong-Tao Chang et al. Interferon-Stimulated Gene 15 Knockout in Mice Impairs IFN α -Mediated Antiviral Activity Reprinted from: <i>Viruses</i> 2022 , <i>14</i> , 1862, doi:10.3390/v14091862	47
Aijing Liu, Tong Xue, Xiang Zhao, Jie Zou, Hongli Pu and Xiaoliang Hu et al. Pseudorabies Virus Associations in Wild Animals: Review of Potential Reservoirs for Cross-Host Transmission Reprinted from: <i>Viruses</i> 2022 , <i>14</i> , 2254, doi:10.3390/v14102254	59
Zhong Peng, Qingyun Liu, Yibo Zhang, Bin Wu, Huanchun Chen and Xiangru Wang Cytopathic and Genomic Characteristics of a Human-Originated Pseudorabies Virus Reprinted from: <i>Viruses</i> 2023 , <i>15</i> , 170, doi:10.3390/v15010170	71
Mo Zhou, Muhammad Abid, Shinuo Cao and Shanyuan Zhu Recombinant Pseudorabies Virus Usage in Vaccine Development against Swine Infectious Disease Reprinted from: <i>Viruses</i> 2023 , <i>15</i> , 370, doi:10.3390/v15020370	86
Li Pan, Mingzhi Li, Xinyu Zhang, Yu Xia, Assad Moon Mian and Hongxia Wu et al. Establishment of an In Vitro Model of Pseudorabies Virus Latency and Reactivation and Identification of Key Viral Latency-Associated Genes Reprinted from: <i>Viruses</i> 2023 , <i>15</i> , 808, doi:10.3390/v15030808	98
Jianle Ren, Shanshan Tan, Xinxin Chen, Jiying Yao, Zhihong Niu and Ying Wang et al. Genomic Characterization and gE/gI-Deleted Strain Construction of Novel PRV Variants Isolated in Central China Reprinted from: <i>Viruses</i> 2023 , <i>15</i> , 1237, doi:10.3390/v15061237	111
Wenwen Hou, Maodi Fan, Zhenbang Zhu and Xiangdong Li Establishment and Application of a Triplex Real-Time RT-PCR Assay for Differentiation of PEDV, PoRV, and PDCoV Reprinted from: <i>Viruses</i> 2023 , <i>15</i> , 1238, doi:10.3390/v15061238	129
Yuan Cui, Libo Huang, Jinlian Li, Gang Wang and Youfei Shi An Attempt of a New Strategy in PRV Prevention: Co-Injection with Inactivated <i>Enterococcus faecium</i> and Inactivated Pseudorabies Virus Intravenously Reprinted from: <i>Viruses</i> 2023 , <i>15</i> , 1755, doi:10.3390/v15081755	142

Zhengmin Lian, Panrao Liu, Zhenbang Zhu, Zhe Sun, Xiuling Yu and Junhua Deng et al.
Isolation and Characterization of a Novel Recombinant Classical Pseudorabies Virus in the
Context of the Variant Strains Pandemic in China
Reprinted from: *Viruses* **2023**, *15*, 1966, doi:10.3390/v15091966 **155**

Huihui Guo, Qingyun Liu, Dan Yang, Hao Zhang, Yan Kuang and Yafei Li et al.
Brincidofovir Effectively Inhibits Proliferation of Pseudorabies Virus by Disrupting Viral
Replication
Reprinted from: *Viruses* **2024**, *16*, 464, doi:10.3390/v16030464 **169**

Review

Progress of Research into Novel Drugs and Potential Drug Targets against Porcine Pseudorabies Virus

Mo Zhou ¹, Muhammad Abid ², Shinuo Cao ^{1,*} and Shanyuan Zhu ^{1,*}

¹ Jiangsu Key Laboratory for High-Tech Research and Development of Veterinary Biopharmaceuticals, Jiangsu Agri-Animal Husbandry Vocational College, Taizhou 225306, China

² Viral Oncogenesis Group, The Pirbright Institute, Ash Road Pirbright, Woking, Surrey GU24 0NF, UK

* Correspondence: shinuo_cao@163.com (S.C.); jsnm_zsy@126.com (S.Z.)

Abstract: Pseudorabies virus (PRV) is the causative agent of pseudorabies (PR), infecting most mammals and some birds. It has been prevalent around the world and caused huge economic losses to the swine industry since its discovery. At present, the prevention of PRV is mainly through vaccination; there are few specific antivirals against PRV, but it is possible to treat PRV infection effectively with drugs. In recent years, some drugs have been reported to treat PR; however, the variety of anti-pseudorabies drugs is limited, and the underlying mechanism of the antiviral effect of some drugs is unclear. Therefore, it is necessary to explore new drug targets for PRV and develop economic and efficient drug resources for prevention and control of PRV. This review will focus on the research progress in drugs and drug targets against PRV in recent years, and discuss the future research prospects of anti-PRV drugs.

Keywords: pseudorabies virus; prevention; treatment; drugs; drug targets



Citation: Zhou, M.; Abid, M.; Cao, S.; Zhu, S. Progress of Research into Novel Drugs and Potential Drug Targets against Porcine Pseudorabies Virus. *Viruses* **2022**, *14*, 1753. <https://doi.org/10.3390/v14081753>

Academic Editors: Yan-Dong Tang and Xiangdong Li

Received: 25 July 2022

Accepted: 7 August 2022

Published: 11 August 2022

Publisher's Note: MDPI stays neutral with regard to jurisdictional claims in published maps and institutional affiliations.



Copyright: © 2022 by the authors. Licensee MDPI, Basel, Switzerland. This article is an open access article distributed under the terms and conditions of the Creative Commons Attribution (CC BY) license (<https://creativecommons.org/licenses/by/4.0/>).

1. Introduction

Pseudorabies virus (PRV), also known as suid herpesvirus type 1, belongs to the Herpesviridae family along with varicella zoster virus (VZV) and equine herpesvirus [1–4]. Pigs are the natural host of PRV, though it also infects a variety of domestic and wild animals, such as cattle, sheep, dogs, cats, and other vertebrates. Pseudorabies (PR) is a major disease that affects pig production and has a mortality rate of nearly 100% in piglets [5–7]. PRV causes reproductive problems in sows and boars, such as abortion, stillbirth, mummification, and fertility issues, which result in huge economic losses for the swine industry [8,9]. It was previously thought that humans had natural resistance to PRV. However, mutated PRV has been reported to cause infections in humans. In 2018, researchers confirmed the existence of human PRV infection at the genetic level, though there has been no evidence of transmission from other animals to humans or humans to humans [10–13]. Clinical cases suggest that PRV infection is possible in humans, and a stable zoonotic strain can result from a PRV mutation.

PRV is a double-stranded DNA virus with enveloped icosahedral symmetry. It is spherical in structure and has a diameter of approximately 120–200 nm. The large PRV genome contains approximately 143,000 base pairs, consisting of unique long and unique short linear nucleotide sequences [14,15]. The viral envelope consists of at least 15 proteins, 11 of which are glycosylated (gN, gM, gL, gK, gI, gH, gB, gG, gE, gC and gD). Four glycoproteins, gB, gD, and heterodimer gH/gL are required for viral replication [16,17]. Other glycoproteins including gE, gL, membrane protein US9, and non-structural protein thymine kinase (TK) are not required for viral replication but are associated with PRV virulence [18–24].

Presently, there is no specific treatment for PRV infection in pigs. Vaccination can fundamentally prevent the infection and transmission of the PRV and is the most effective measure for preventing and controlling PR. There is still a lack of clinical consensus and

experience regarding human PRV infection because only a few confirmed cases have been reported, and patients with mild symptoms can recover without treatment. Acyclovir is recommended for treating acute retinal necrosis syndrome and encephalitis caused by VZV infection, which is also a varicella herpesvirus along with PRV. Since there are no similar treatments for PRV, it is vitally important that new drug targets should be discovered, and new antiviral drugs are being developed for the treatment, prevention, and control of PRV. This study summarizes the research results of anti-PRV drugs that have been studied in recent years and provides a theoretical basis for the development of anti-PRV drugs.

2. Natural Medicines Inhibit PRV Replication

Natural medicines have been widely accepted and used throughout history for the prevention of diseases, and interest in these medicines for use in the potential development of antiviral drugs has been increasing [25–29]. The antiviral mechanisms of natural drugs can be divided into direct inhibition and indirect inhibition. Direct inhibition refers to blocking a link during the process of viral replication, so as to remove pathogens from the body. Indirect inhibition refers to stimulating and mobilizing the immune defense system of the body to play an antiviral role [30–34]. The antiviral effect of natural drug compounds is better than with a single natural drug; however, natural drug compounds have numerous effective components and complex antiviral mechanisms. Previous research has indicated that some of these natural drugs have antiviral effects against PRV, providing a theoretical basis for the development of these compounds into anti-PRV drugs (Table 1).

Table 1. The reported anti-PRV drug.

Drug Types	Drug Names	Potential Targets	References
Natural medicines	Epigallocatechin-3-gallate	Undefined	[35]
	Resveratrol	NF- κ B signaling pathways	[36]
	Germacrone	Undefined	[37]
	Quercetin	gD-protein	[38]
	Curcumin	BDNF/TrkB signaling pathway	[39]
	Flos Lonicerae Japonicae water extract	NF- κ B signaling pathway	[40]
	Luteolin	NF- κ B signaling pathway	[41]
	Platycodon grandiflorus polysaccharides	Akt/mTOR signaling pathway	[42]
	Kaempferol	Undefined	[43]
Small molecules	2,5-dihydroxybenzoic acid-gelatin	Undefined	[44]
	Adefovir dipivoxil	Undefined	[45]
	Valproic acid derivative	Undefined	[46]
	Hydroquinone	Undefined	[47]
	Diazadispiroalkane derivatives	Heparan sulfate glycosaminoglycans	[48]
	Ivermectin	UL42	[49]
Novel materials	3D8 scFv	Undefined	[50]
	Polyvalent 2D RNAs	Undefined	[51]
		UL42	[52]
	Natural polypeptide	Undefined	[53,54]

2.1. (–)-Epigallocatechin-3-Gallate Inhibits PRV Infection through Inhibiting Virus Replication and Adsorption

Green tea, and its major constituent (–)-epigallocatechin-3-gallate (EGCG), has been reported to mitigate several chronic diseases [55,56]. In solid green tea extract, EGCG is the most abundant bioactive polyphenol, which has antibacterial, antiviral, and antioxidant properties [57–62]. EGCG prevents many viruses, including HCV, herpes simplex virus (HSV) and human immunodeficiency virus type 1 (HIV-1), from entering target cells, thus

preventing infection [35,63]. In PK15 B6 cells and Vero cells, Huan et al. reported that EGCG significantly inhibited PRV strain infectivity [35]. They also confirmed that EGCG inhibited the adhesion, entry, and replication of PRV strains *in vitro*. In addition, the survival rate of PRV-challenged mice was improved significantly by EGCG. Thus, the therapeutic effect of EGCG on PRV infection *in vivo* was demonstrated, indicating its potential as an antiviral drug.

2.2. Resveratrol Inhibits PRV Multiplication in Host Cells

When plants are stimulated, resveratrol (3,5,4-trihydroxystilbene), a nonflavonoid polyphenol organic compound, is produced. Resveratrol is produced in grape leaves and is the main bioactive ingredient in wine and grape juice [36].

Resveratrol has antioxidant, anti-inflammatory, anticancer, and cardiovascular protective properties, which have been confirmed through *in vitro* and animal experiments [64–69]. Resveratrol possesses antiviral activity against a number of different viruses, such as herpesviruses, retroviruses, respiratory syncytial viruses, and HIV-1 [70–72]. Zhao et al. evaluated the antiviral activity of resveratrol against PRV and investigated the change in relevant virus-host systems after PRV infection [36]. The mortality was reduced and the growth performance of PRV-infected piglets was increased by the treatment of resveratrol. It appears that resveratrol has antiviral properties because it inhibits viral multiplication in host cells, and it relieves PRV-induced inflammation in host cells. There is a strong correlation between I κ B kinase activity and NF- κ B activation; an important way to determine whether NF- κ B signaling is active is by measuring the levels of I κ B kinases in a cell. Zhao et al. tested the I κ B kinase activity of the host cells after PRV infection. The ability of resveratrol to inhibit I κ B kinase activity has been confirmed to suppress both NF- κ B activation and NF- κ B dependent gene expression. This suggests that resveratrol may have great potential as an antioxidant and an effective anti-PRV drug.

2.3. Germacrone Affects the Cell Antiviral Mechanism in Early Replication

Gingeraceae plants produce germacrone, a monocyclic sesquiterpene with antitumor, antiviral, antibacterial, and anti-inflammatory properties [73–75]. The action of germacrone on tumors is mediated through G2/M cell cycle arrest and apoptosis promotion [73,76,77]. In addition to its ability to inhibit influenza virus (IAV) replication, germacrone can also inhibit porcine parvovirus (PPV), feline parvovirus (FPV), and porcine enterovirus (PEV) replication [75,78–80]. An *in vitro* study conducted by He et al. showed that germacrone inhibits PRV replication dose-dependently, and a further study indicated that germacrone exerts its antiviral effect during the early stage of infection [37]. It may be useful as a therapeutic drug because germacrone inhibits PRV replication by affecting the cell antiviral mechanism during the early stages of PRV replication.

2.4. Quercetin Inhibits PRV Infections by Decreasing the Binding Activity of gD

The most widely distributed plant flavonoid is quercetin (3,3,4,5,7-pentahydroxyflavone), which can be found in fruits, vegetables, grains, Chinese herbal medicines, teas, and wines [81]. Quercetin is a flavonoid with antioxidant, anticancer, antibacterial, and antiviral activities [82–87]. Sun et al. confirmed that quercetin inhibits PRV replication dose-dependently and is effective against a wide spectrum of PRV strains [38]. Further study confirmed that quercetin inhibited PRV infections by affecting the binding ability of gD, which is important for viral infection. From *silico* molecular docking data analysis, it was discovered that quercetin interacts with PRV gD-protein, thereby blocking nectin-1 binding to gD. Quercetin also reduces PRV replication *in vivo*, reducing mortality and decreasing the viral loads in PRV-infected mice brains. Quercetin also exhibited anti-PRV activity *in vivo*; mortality was reduced and the viral loads were decreased in PRV-infected mice brains. Considering quercetin's powerful therapeutic effects against PRV infection *in vitro* and *in vivo*, it might be useful as an anti-PRV agent.

2.5. Curcumin Plays a Neuroprotective Role against PRV Infection

In turmeric, curcumin is the most active component of the curcuminoids, which have a variety of pharmacological properties, such as anti-inflammatory, antioxidant, anti-proliferative, and antiviral effects [88,89]. Several reports suggest that curcumin may be helpful against dengue [90], HSV [91], and vesicular stomatitis virus [92]. Newborn piglets with porcine PRV infection suffer from severe neurological disorders and die at an alarming rate. There are few drugs available to relieve the neurological symptoms caused by herpes virus. Curcumin may prove a promising treatment for neurodegenerative diseases because it crosses the blood–brain barrier [93,94]. Yang et al. explored novel drugs to relieve the neurological symptoms caused by PRV, and examined the role of curcumin in preventing oxidative stress, apoptosis, and mitochondrial dysfunction in rat hippocampal neurons infected by PRV [39]. By preventing neuronal cell death induced by various stimulants, the BDNF/TrkB pathway contributes to neuroprotection [95]. By upregulating the BDNF/TrkB pathway, curcumin improved the viability of PRV-infected hippocampal neurons and provided neuroprotection against infection by PRV. Therefore, curcumin has the potential for development as a novel drug for treating PRV infection in neurons.

2.6. Flos Lonicerae Japonicae Water Extract and Luteolin Suppress PRV-Induced NF- κ B Pathway Activation in RAW264.7 Cells

As an antibacterial, antiviral, anti-inflammatory, antioxidative, and hepatoprotective plant, Flos Lonicerae Japonicae (FLJ) has been used in Chinese herbal medicine for over 2000 years [40,96–100]. When phenolic acids and flavonoids are in high concentrations, cell viability increases dramatically. Hence, flavonoids and phenolic acids present in the herbs are responsible for their antioxidative activity. Lin et al. assessed the polyphenolic profile of FLJ water extract and the antiviral effects of FLJ water extract on PRV-infected RAW264.7 T cells [40]. FLJ water extract showed antiviral activity by reducing the expression of inflammatory mediators including COX-2 and iNOS, and it reduces inflammatory cytokines by inhibiting the JAK/STAT1/3-dependent NF- κ B pathway and increasing HO-1 expression. Thus, FLJ water extract can be used as a potential antiviral agent for the treatment of PRV infection.

There are high levels of luteolin (3',4',5,7-hydroxyl-flavone) present in many common medicinal herbs, including artichokes, celery, chamomile, and green pepper [41]. Liu et al. tested the anti-inflammatory effects of luteolin in PRV-infected RAW264.7 cells [101]. It was found that luteolin significantly inhibited NO and iNOS production, as well as COX-2 and inflammation-related cytokines. Moreover, luteolin inhibited PRV-induced NF- κ B through STAT1 and STAT3 phosphorylation, but not ERK1/2, p38, or JNK1/2 induction. Luteolin could be considered a potential agent for use in treating inflammation during viral infection.

2.7. Platycodon Grandiflorus Polysaccharides Inhibit PRV Replication

Ancient Chinese medicinal plants like Platycodon grandiflorus have been found to have immunomodulatory, anti-inflammatory, and antiviral properties [102,103]. The polysaccharides are believed to have antiviral properties, and the antiviral properties of polysaccharides have recently gained increased attention [42,104–107]. Xing et al. investigated the antiviral activity of total Platycodon grandiflorus polysaccharides (PGPSs) against PRV and the molecular mechanism of the anti-PRV effect [42]. PGPS decreased the viral proteins in PK-15 cells 12 h post-infection significantly. They found that PGPS affects PRV-induced autophagy, which likely explains the antiviral mechanism of PGPS. PRV-induced autophagy was downregulated by PGPS via the Akt/mTOR signaling pathway. PRV-induced, Thus, PGPS may inhibit PRV replication by targeting autophagy, and has the potential to be a novel antiviral drug.

2.8. Kaempferol can Inhibit PRV Latency

In a variety of plants, kaempferol can be found as a natural flavanol derived from ginger rhizomes [108–110]. As a treatment for diabetes and osteoporosis, kaempferol has attracted widespread attention due to its anticancer, anti-inflammatory, antioxidant, and antiviral properties [111–114]. Li et al. evaluated the ability of kaempferol to inhibit PRV replication in vitro and in vivo [43]. PRV replication was inhibited by kaempferol dose-dependently in PRV-infected cells and the survival rate of PRV-infected mice was increased.

They found that kaempferol inhibited PRV replication dose-dependently in vitro and improved the survival rate of PRV-infected mice in vivo. The expression of the IE180 gene, the major trans-activator of the PRV, required for the transcription of early genes. IE180, EPO, and TK transcriptions were inhibited simultaneously in the brain with the immediate-early IE180 gene. Kaempferol appears to inhibit latency-associated transcript expression in the brain. Latent infection is a difficult problem when treating herpesvirus infection. Inhibition of latent infection and virus activation are both especially important for the treatment of this disease. Based on the above data, kaempferol will be a novel alternative measure for control of PRV infection.

3. Small Molecules Inhibit PRV Replication

Currently, the main drug used for the treatment of HSV is acyclovir [115]. Acyclovir is a guanine nucleoside analogue, anti-DNA viral drug. Acyclovir triphosphate is phosphorylated in infected cells by HSV thymidine kinase and host cell kinase to produce acyclovir triphosphate, which competes with viral DNA polymerase inhibition or is incorporated into viral DNA, which blocks DNA synthesis [116]. However, acyclovir is associated with several drawbacks, including its short half-life and carcinogenic and embryotoxic effects. In addition, PRV strains with mutations in the viral thymidine gene have appeared, which may confer resistance to acyclovir [24]. Furthermore, acyclovir may not be able to prevent the virus from reactivating once latency was established. Therefore, research into new small molecule chemicals that can treat PRV infection is necessary (Table 1).

3.1. Polymers Inhibit the Attachment of PRV

A wide variety of naturally occurring and synthetic polymers exhibit antiviral properties by preventing the entry of herpesviruses into cells. Many negatively charged polymers also exhibit antiviral properties [117–120]. High antiviral activity of the synthetic polysaccharide dextran sulfate, sulfated chitin, and octa-decylribo-oligosaccharides have been characterized. A conjugate 2,5-dihydroxybenzoic acid-gelatin (2,5-DHBA-gelatin) was synthesized by Lisov et al., and the antiviral activity of this conjugate against PRV and bovine herpesvirus type 1 (BoHV-1) was evaluated [44]. The virucidal effect of 2,5-DHBA-gelatin conjugate was indirect, though it did inhibit the attachment of viruses to target cells during virus adsorption. Thus, this conjugate will be a promising synthetic polymer for antiviral formulations development against alpha herpesvirus infections since the adsorption of PRV to cells was strongly inhibited.

3.2. Adefovir Dipivoxil Potently Protects Mice against Lethal PRV Infection

There are 1818 kinds of drugs in the FDA-approved small-molecule library; these drugs are available for a variety of human diseases, and they are generally safe and effective. In order to develop more effective anti-PRV drugs, Wang et al. established an accurate and reliable method for screening drugs in the FDA-approved small-molecule library to determine whether they are active against PRV in vivo [45]. Several drugs inhibited PRV proliferation at nanomolar concentrations, including puromycin dihydrochloride, mitoxantrone, mitoxantrone hydrochloride, and adefovir dipivoxil. A lethal mouse model was established to confirm the effectiveness of candidate PRV drugs, in which PRV injections were administered intraperitoneal in mice. There was a noticeable reduction in clinical score in the adefovir dipivoxil treated mice compared to the untreated mice after they

were treated with adefovir dipivoxil. Therefore, adefovir dipivoxil might offer important guidance for identifying candidate drugs with the potential to control PRV epidemics.

3.3. Valproic Acid Derivative Inhibits PRV Infection

Currently there are no antiviral drugs for treating PRV infection, thus, new drugs are urgently needed. Acyclovir is a guanosine analogue, which interferes with viral DNA replication. However, as previously mentioned, acyclovir does have some advantages [121–123]. Valproic acid (VPA) is the alternative of acyclovir; it can interrupt the infectious cycle of several enveloped viruses. VPA also has hepatotoxic and teratogenic activity [124–126]; however, derivatives of VPA have been shown to be less toxic compared to VPA. To determine whether valpromide (VPD), a compound derived from VPA, has an antiviral effect against PRV infection, Andreu et al. tested the PRV-infected PK15 swine cell line and the Neuro-2a neuroblastoma cell line [46]. The inhibitory effect of VPD on PRV infection was similar with ACV in the PRV-infected cell lines. Therefore, in the future, VPD will be a viable alternative to nucleoside analogues for treating PRV-related diseases, but the pharmacokinetic study and the antiviral mechanism of VPD still need to be invested.

3.4. Hydroquinone Inhibits PRV Replication in Neurons In Vitro and In Vivo

The chemical compound hydroquinone has a variety of biological effects. High concentrations of hydroquinone are able to cause cell cycle arrest, induce apoptosis, and promote cell death in a variety of ways [47,127,128]. When macrophage-mediated inflammation occurs, hydroquinone can target AKT and promote its phosphorylation [129]. Based on a screening of 44 FDA-approved drugs, Fang and colleagues found hydroquinone to be highly anti-PRV active, inhibiting PRV adsorption on cell surfaces and internalization [47]. Further research found that the PRV inhibition induced by hydroquinone was related to AKT phosphorylation. Based on a *in vivo* experiment, they found that the viral loads in tissues and mortality in PRV-infected mice was reduced significantly in hydroquinone treated mice. Thus, hydroquinone will be an excellent therapeutic agent for the treatment of PR.

3.5. Diazadispiroalkane Derivatives Block the Attachment of PRV

Human cytomegalovirus (HCMV) is an opportunistic pathogen that can cause serious illness, including death [130–132]. Most anti-HCMV drugs, such as ganciclovir and cidofovir, inhibit the viral DNA polymerase enzyme. However, these inhibitors have some drawbacks, a low molecular weight inhibitor, N-N-(bis-5-nitropyrimidyl) dispirotriperazine derivative (DSTP-27), is a new class of non-nucleosidic antiviral agent against HSV-1 and HCMV, but DSTP-27 showed metabolic instability associated with nitric oxide release *in vivo* [133]. Two new DSTP-27 derivatives synthesized by Adfeldt et al., and the antiviral activity of these two derivatives against HCM and PRV at each stage of infection was studied [48]. Based on these results, the new derivatives of DSTP-27 may prove to be promising candidates to prevent viral attachment to cell surfaces via binding to heparan sulfate glycosaminoglycans (HS).

3.6. Ivermectin Inhibits PRV Proliferation In Vitro and In Vivo

In recent years, a small molecule macrocyclic lactone known as ivermectin, which has been approved for parasitic infections by the US Food and Drug Administration, has received renewed interest in recent years, because of its apparent potential as an antiviral drug [134]. Based on the fact that ivermectin binds to the importin α (IMP α) protein and inhibits its nuclear transport role, ivermectin appears to have broad antiviral activity. Ivermectin exhibits antiviral potential inhibits on HIV-1 and DEV proliferation by restraining nuclear transport of integrase and the non-structural protein 5 polymerase [135]. Lv et al. determined that ivermectin has antiviral effects against PRV and studied the mechanism(s) involved in this antiviral activity [49]. As a result of the treatment with ivermectin, UL42 localization at the nucleus was disrupted and subsequent progeny virus production was

significantly decreased. When PRV-infected mice were treated with ivermectin, the survival rate of mice was significantly increased, and the infection was relieved, the clinical scores were lower and the gross lesions in the brain were fewer compared with the untreated mice. Since UL42 of PRV requires importin- α/β -mediated nuclear import pathways for nuclear transport, ivermectin could serve as an anti-PRV drug candidate.

4. Application of New Technology and Materials in Anti-PRV Drug Research

The PRV has caused significant damage to the swine husbandry industry and poses a potential threat to humans. However, vaccine research has progressed relatively rapidly, resulting in the development of a vaccine against PRV. There has been much progress made in the development of vaccines against PRV, though only a few antiviral agents against PRV were available in recent years. Additionally, several novel approaches have also been used for PRV containment, including DNA replication inhibitors and viral reverse transcriptase inhibitors (Table 1).

4.1. 3D8 scFv Prevents PRV Infection in Mice

Single chain variable fragments of 3D8 are recombinant monoclonal antibodies with nuclease activity. They were originally isolated from autoimmune-prone mice and exhibit non-specific activity on DNA and RNA [136]. They are active against HSV, PRV, CSFV, murine norovirus (MNV), 2 geminiviruses, 5 tobamoviruses, and cucumaviruses [137–139]. Lee et al. purified the 3D8 scFv protein from *E. coli* and evaluated the antiviral effects in PRV-infected mice [50]. The 3D8 scFv is transmitted virtually to all organs of the mouse, localized to the cytoplasm by caveolae-mediated endocytosis, and inhibited the virus in all organs, especially in the brain. A further analysis was carried out to determine whether the 3D8 scFv damaged the viral genome directly or indirectly by inducing gene expression levels in the inflammatory pathway. The results demonstrated that 3D8 scFv induced the antiviral effects by itself directly. As the study indicates, the 3D8 scFv is a broad-spectrum, multifaceted antiviral agent that can digest viral genomes without sequence specificity, thereby inhibiting the spread of viruses, and could be used to explore novel drugs against DNA and RNA viruses in the future.

4.2. Targeting UL42 by RNAi Efficiently Inhibits PRV Replication

Gene silencing through RNA interference (RNAi) is a conserved mechanism involving small interfering RNAs that cause homologous RNAs to degrade sequence-specifically [140]. Antiviral therapies based on RNAi have shown to be novel and effective against many different viruses. As UL42 is a processivity factor for PRV, it enhances the catalytic activity of DNA polymerase and is essential for viral replication. Therefore, UL42 may be an antiviral target [52,141]. A group of researchers synthesized three siRNAs directed against UL42 in cell culture and investigated their antiviral properties [52]. The siRNAs induced potent inhibition of UL42 expression after PRV infection and decreased PRV replication. The RNAi technique may provide new clues for designing intervention strategies against herpesviruses by targeting their processivity factors.

4.3. Polyvalent 2D Entry Inhibitors Inhibit PRV Entrance

There are many biological processes in nature that involve noncovalent interactions between ligands and receptors, such as adhesion, cell-to-cell recognition, and self-organization. Among the most interesting phenomena in this context is how viruses adhere to a target cell surface, and how they enter the cell via endocytosis or cell fusion. Inhibitors targeting this process can effectively bind viral particles and block their contact with surfaces, thus preventing viral adhesion and infection. According to Haag et al., a polyglycerol sulfate-functionalized graphene sheet was synthesized and evaluated for use as an extracellular matrix-inspired entry inhibitor [51]. By binding enveloped viruses during adhesion, the developed 2D architectures demonstrated strong inhibitory activity against African swine fever virus (ASFV) and PRV. Compared to enrofloxacin and heparin, the developed 2D ar-

chitectures had equivalent or better inhibitory properties against PRV. Thus, the developed polyvalent 2D entry inhibitors could serve as efficient entry inhibitors for other enveloped viruses. The concept of the 2D molecule designs represents a novel strategy for developing novel drugs against enveloped viruses.

4.4. Natural Polypeptide Inhibits of PRV Proliferation

Antimicrobial peptide (AMP) is an effective natural polypeptide, which has gained worldwide attention as an alternative to antibiotics [53,142–145]. AMP is a new type of therapeutic agent developed for both its antibacterial and antiviral activities [122,125]. Piscidin 1 belongs to the piscidin family. It was discovered in the mast cells of fish. AMPs isolated from other hosts have been found to exert antiviral activity and can inhibit infections with enveloped viruses, such as human cytomegalovirus (HCMV), HSV-1, HSV-2, and vesicular stomatitis virus (VSV) [146]. Therefore, AMPs may be promising agents for use against herpesvirus infections. A research was performed to study the pharmacokinetics of piscidin 1 by Hu et al., [53] and the antiviral activity of piscidin was confirmed. In an evaluation of five broad-spectrum AMPs against PRV, Hu et al. found that piscidin had the strongest antiviral activity due to direct interactions with the viral particles, therefore, the cells were protected from PRV-induced apoptosis. Investigation into the protective effect of piscidin *in vivo* showed that piscidin reduced the mortality rate of PRV-infected mice. This result suggests that piscidin-1 could be a future alternative antibiotic and/or antiviral for use in clinical veterinary medicine.

Defensins are cationic peptides, a type of antimicrobial peptide. Defensins possess disulfide bonds, are widely distributed in fungi, plants, and animals and are crucial regulatory molecules in the biological immune system [147]. In many cases, defensins can kill enveloped viruses, including HIV, herpes, and vesicular stomatitis viruses [147]. These defensins work primarily by binding to the viral coat protein; this special mechanism of action also makes it difficult for microorganisms to develop resistance to them. Defensins can directly inhibit the virus, and the degree of inhibition depends on the defensin concentration and the tightness of the intramolecular disulfide bond [148]. The antiviral activity of defensin is strong under neutral and low ionic strength conditions [149]. The peptide porcine β -defensin 2 (PBD-2) has been synthesized and its antiviral activity against PRV has been evaluated both *in vivo* and *in vitro* by Huang et al. [54]. In PK15 cells, PBD-2 inhibited PRV proliferation, resulting in improved survival of PRV-infected mice. Huang et al. generated C57/BL TG mice with PBD levels 250% higher than in WT mice by overexpressing the PBD-2 gene. When C57/BLTG mice were challenged with PRV, they developed fewer lesions in their brains, spleens, and livers compared with WT littermates, while their PRV viral loads in their brains, livers, and lungs were lower. As a result, PBD-2 could provide new therapeutic and prophylactic treatment for Aujeszky's disease as well as other viral diseases.

5. Potential Targets of Anti-PRV Drugs

5.1. *NF- κ B* and *MAPK* Signaling Pathways

Infections with pathogens often cause an inflammatory response in the host. To survive in the host cell, pathogens have evolved elaborate ways to destroy the host cell's innate defenses. Pathogen-associated molecular patterns (PAMPs) are recognized by extracellular and intracellular pattern recognition receptors (PRRs), which stimulate a cascade of inflammatory signals. The mitogen-activated protein kinase (MAPK) and nuclear factor- κ B (NF- κ B) signaling pathways are activated through signal transduction when the hosts are infected by the pathogen, thus transcription of downstream anti-infection-related genes and inflammatory factors were initiated [150,151]. It has been shown that pathogen effector proteins can interfere with host inflammation by blocking MAPK and NF- κ B signaling pathways during the interaction between the pathogen and host. Animals infected with PRV often exhibit inflammation, cytokine release, and peroxide production; these are essential defense mechanisms [3,152]. Uncontrollable inflammatory responses and excessive

inflammatory cytokines may compromise the integrity and function of immune cells. As an animal's immune system weakens, PRV invades its nervous system, causing neurological symptoms [3,4]. Based on the above information, a large number of studies have concluded that the NF- κ B and MAPK signaling pathways are potential targets for drugs to treat PRV infection.

Degradation of I κ B is a crucial step in activating the NF- κ B signaling pathway, the relative levels of I κ B kinases are used as the indicator of NF- κ B signaling pathway activating. NF- κ B responsive genes are expressed more strongly following PRV-induced degradation of I κ B and translocation to the nucleus of RelA, which binds to promoter regions of these genes [153]. Resveratrol, a non-flavonoid polyphenol compound, can attenuate the degradation of I κ B α and the translocation of RelA to the nucleus in PRV-infected PK15 cells, therefore affecting virus production and infection. In addition, in vivo experiments indicated that resveratrol decreased mortality, enhanced growth performance, inhibited viral reproduction, alleviated tissue inflammation and lesions, and improved the levels of cytokines in PRV-infected piglets [152]. The inhibitory effect of resveratrol on PRV proliferation can be attributed to its immunomodulatory effects of IFN- γ .

Inflammatory genes such as iNOS and COX-2 are activated by phosphorylated NF- κ B p65 in the nucleus. According to Lin et al. and Liu et al., the FLJ water extract and luteolin suppressed the gene expression of inflammatory cytokines, COX-2 and iNOS, through the inhibition of JAK/STAT signaling [40]. Furthermore, the researchers discovered that exogenous antioxidants inhibited virus proliferative activity in vitro and reduced PRV-induced tissue damage by inhibiting oxidative stress. Additionally, using ethyl acetate fractions of polygonum hydropiper L. flavonoids, Ren et al. found a significant inhibition of phosphorylation and degradation; they also found that I κ B α and NF- κ B p65 is retained in cytoplasm and decreased in nuclei [154]. These results suggest that the NF- κ B signaling pathway could be a novel target for the anti-PRV drugs. It is well known that JNK1/2, ERK1/2, and p38 MAPK are all critical kinases in MAPK signaling pathways that regulate macrophage survival and the production of inflammatory mediators. Previous studies have shown that PRV infection increases phosphorylation of ERK1/2 and p38, treatment with ethyl acetate inhibits phosphorylation of this important kinase. Therefore, a novel anti-inflammatory role for FEA on PRV via Inhibition of the ERK/MAPK Signaling Pathway. The main drug used for the treatment of HSV is acyclovir [115]. Acyclovir is a guanine nucleoside analogue, anti-DNA viral drug. Acyclovir triphosphate is phosphorylated in infected cells by HSV thymidine kinase and host cell kinase to produce acyclovir triphosphate, which competes with viral DNA polymerase inhibition or is incorporated into viral DNA, which blocks DNA synthesis [116]. However, acyclovir is associated with several drawbacks, including its short half-life and carcinogenic and embryotoxic effects. In addition, PRV strains with mutations in the viral thymidine gene have appeared, which may confer resistance to acyclovir [24]. Furthermore, acyclovir may not be able to prevent the virus from reactivating once latency was established. Therefore, research into new small molecule chemicals that can treat PRV infection is necessary.

5.2. BDNF/TrkB Signaling Pathway

In cultured cells, PRV causes apoptosis, which is associated with neurodegenerative diseases and neuropathies. PRV infection causes oxidative stress, as well as damage to neurons, which are the targets of neuroprotective agents [155]. A major function of brain-derived neurotrophic factor (BDNF) is to modulate neuronal plasticity, mitochondrial transport, and neuronal protection, such as anti-apoptosis, anti-oxidation, and suppression of neurodegeneration. The function of BDNF is primarily regulated by the binding of transmembrane tropomyosin-related kinase B (TrkB) to the mitochondrial membrane [95]. BDNF/TrkB contributes to the neuroprotection of neurons by preventing the death of neurons induced by various stimuli [155].

A neuroprotective agent, BDNF binds to TrkB receptors to rescue neurons from various insults. BDNF plays an important role in mitochondrial dysfunction pathophysiology and

treatment. Infection with PRV may also affect levels of BDNF in hippocampal neurons [95]. Therefore, the BDNF/TrkB signaling pathway may be a drug target for the treatment of PRV infection. A study by Yang et al. found that curcumin mediated neuroprotection against PRV infection through BDNF/TrkB signaling [39]. This research suggests that the BDNF/TrkB pathway is a potential drug target for the treatment of neurological disorders caused by PRV infection.

5.3. Akt/mTOR Signaling Pathway

One of the most conserved physiologic functions of cells is autophagy, a process in which damaged organelles and pathogenic microorganisms are degraded [77,156,157]. Antiviral drugs may be able to target autophagy; the degradative process of cells is essential for adjusting to dynamic environments and coping with developmental changes. Autophagy is involved in cell regulation during the immune response. In many studies, it has been shown that low glucose concentrations inhibit the Akt/mTOR pathway involved in virus replication [42,94]. PRV infection has been found to significantly reduce the phosphorylation levels of Akt and mTOR and increase autophagosome formation in PK15 cells. PGPSs inhibited the PRV infection-induced autophagy and ameliorated PRV-suppression of the Akt/mTOR signaling pathway [42].

5.4. The Critical Factors of Attachment, Entry, and Replication

The life cycles of human and animal alpha herpesviruses are based on several major factors. When an alpha herpesvirus infects a cell, it attaches to the cell surface, fuses with plasma membrane, and enters the nucleocapsid [158–160]. The viral proteins and/or the interacting host proteins during the viral life cycle can be targets for drugs. Heparan sulfate proteoglycan on the cell surface is used by PRV for initial attachment via non-essential gC, which is critical for PRV attachment [161]. According to Adfeldt et al., two new diazadispiro-alkane derivatives are antiviral agents targeting gC's primary attachment to heparan sulfate [138]. The PRV virion envelope glycoprotein D (gD) is an essential co-factor for virus entry and is responsible for recognizing and binding the virus to specific cellular receptors. As gD binds its receptors, conformational changes occur in gD, which in turn activate a multi-glycoprotein complex for triggering viral replication [162,163]. According to the virucidal properties of quercetin and the fact that it inhibits PRV infection adsorption, quercetin may play a role in the interaction between these molecules and viral particles. Silico study indicates that quercetin might interact with the gD-protein on the surface of PRV, thereby inhibiting its replication. Furthermore, according to Lisov et al., 2,5-dihydroxybenzoic acid-gelatin conjugate significantly inhibits PRV adsorption to cells and impairs PRV attachment to target cells [44].

A number of antiviral drugs are being developed to target RNA-dependent RNA polymerase and viral DNA polymerase. PRV DNA polymerase has two subunits, UL30 and UL42. A catalytic subunit with inherent polymerase activity is UL30, while a processivity factor, UL42, enhances DNA-binding specificity and decreases dissociation between DNA polymerase and viral DNA. RNAi reduces PRV replication by reducing UL42 expression, indicating that this protein is important for virus replication in the nucleus. In mice and BHK cells, Lv et al. found that sub-cytotoxic doses of ivermectin suppressed PRV replication [140]. In mice, ivermectin prevented the translocation of UL42, an accessory subunit of DNA polymerase, resulting in a reduction in lesion severity caused by PRV infection. Thus, UL42 is a potential target for antiviral drug therapy against PRV infection.

6. Conclusions

There are limited kinds of drugs to treat herpesvirus infection. The development of anti-herpesvirus drugs has made some progress, and a large number of natural antiviral compounds have been discovered during the development of chemical synthesis technology. Natural products come from a wide range of sources, which are easy to obtain and have low toxicity. Therefore, natural products are important resources to search for antiviral

active ingredients. In addition, screening new small molecule drugs and exploring genetically engineered drugs are the main direction of anti-PRV drug development. However, the research on novel anti-PRV drugs is still in the initial stage and lacks systematic studies. Most of the antiviral activities of candidate drugs have been carried out in cell cultures, and only a few drugs have been tested in mice, and almost none in pigs. Currently, anti-PRV drug targets mainly focus on host inflammatory response related pathways, autophagy related pathways and viral replication enzymes. These studies will provide a theoretical basis for the green prevention and control of PRV and other herpesviruses.

Based on the current status of PRV drug research, the development of natural antiviral active ingredients and the screening of new small molecule drugs will be the main direction of anti-PRV drug research. The development of effective drug targets and the study of antiviral mechanisms are also the key to future anti-PRV drug research.

Author Contributions: Conceptualization, validation, M.Z., M.A., S.C. and S.Z.; investigation, M.Z. and S.C.; data curation, M.Z., M.A., S.C.; writing—original draft preparation, M.Z., M.A., S.C.; writing—review and editing, M.Z.; supervision, S.C. and S.Z.; project administration, M.Z.; funding a funding acquisition, S.Z. All authors have read and agreed to the published version of the manuscript.

Funding: This research was funded by a grant from the key project of Jiangsu Province's Key Research and Development plan (modern Agriculture) (BE2020407), Jiangsu Province high education connotation construction fund (00000221010) and the project of Jiangsu Agri-animal Husbandry Vocational College (NSF2022CB04, NSF2022CB25).

Institutional Review Board Statement: Not applicable.

Informed Consent Statement: Not applicable.

Data Availability Statement: The data presented in this study are available in the insert article.

Conflicts of Interest: The authors declare no conflict of interest.

References

- Sun, W.; Liu, S.; Lu, A.; Yang, F.; Duan, J. In vitro anti-PRV activity of dihydromyricetin from *Ampelopsis grossedentata*. *Nat. Prod. Res.* **2021**, *29*, 1–4. [CrossRef] [PubMed]
- Pannwitz, G.; Freuling, C.; Denzin, N.; Schaarschmidt, U.; Nieper, H.; Hlinak, A.; Burkhardt, S.; Klopries, M.; Dedek, J.; Hoffmann, L.; et al. A long-term serological survey on Aujeszky's disease virus infections in wild boar in East Germany. *Epidemiol. Infect.* **2012**, *140*, 348–358. [CrossRef] [PubMed]
- Klupp, B.G. Pseudorabies Virus Infections. *Pathogens* **2021**, *10*, 719. [CrossRef] [PubMed]
- Pomeranz, L.E.; Reynolds, A.E.; Hengartner, C.J. Molecular biology of pseudorabies virus: Impact on neurovirology and veterinary medicine. *Microbiol. Mol. Biol. Rev.* **2005**, *69*, 462–500. [CrossRef] [PubMed]
- Ye, C.; Guo, J.C.; Gao, J.C.; Wang, T.Y.; Zhao, K.; Chang, X.B.; Wang, Q.; Peng, J.M.; Tian, Z.J.; Cai, X.H.; et al. Genomic analyses reveal that partial sequence of an earlier pseudorabies virus in China is originated from a Bartha-vaccine-like strain. *Virology* **2016**, *491*, 56–63. [CrossRef]
- Yu, X.; Zhou, Z.; Hu, D.; Zhang, Q.; Han, T.; Li, X.; Gu, X.; Yuan, L.; Zhang, S.; Wang, B.; et al. Pathogenic pseudorabies virus, China, 2012. *Emerging Infect. Dis.* **2014**, *20*, 102–104. [CrossRef]
- Tan, L.; Yao, J.; Yang, Y.; Luo, W.; Yuan, X.; Yang, L.; Wang, A. Current Status and Challenge of Pseudorabies Virus Infection in China. *Virol Sin* **2021**, *36*, 588–607. [CrossRef]
- Zhang, R.; Chen, S.; Zhang, Y.; Wang, M.; Qin, C.; Yu, C.; Zhang, Y.; Li, Y.; Chen, L.; Zhang, X.; et al. Pseudorabies Virus DNA Polymerase Processivity Factor UL42 Inhibits Type I IFN Response by Preventing ISGF3-ISRE Interaction. *J. Immunol. (Baltim. Md. 1950)* **2021**, *207*, 613–625. [CrossRef]
- Zhang, L.; Ruan, K.; Sang, G.; Xu, Z.; Tong, W.; Yu, H.; Shan, T.; Gao, F.; Li, L.; Kong, N.; et al. Tk-deleted Pseudorabies Virus Retains High Pathogenicity in Rats. *J. Vet. Res.* **2021**, *65*, 401–405. [CrossRef]
- Zhou, Y.; Nie, C.; Wen, H.; Long, Y.; Zhou, M.; Xie, Z.; Hong, D. Human viral encephalitis associated with suid herpesvirus 1. *Neurol. Sci.* **2022**, *43*, 2681–2692. [CrossRef]
- Zheng, L.; Liu, X.; Yuan, D.; Li, R.; Lu, J.; Li, X.; Tian, K.; Dai, E. Dynamic cerebrospinal fluid analyses of severe pseudorabies encephalitis. *Transbound Emerg. Dis.* **2019**, *66*, 2562–2565. [CrossRef] [PubMed]
- Zhao, W.L.; Wu, Y.H.; Li, H.F.; Li, S.Y.; Fan, S.Y.; Wu, H.L.; Li, Y.J.; Lü, Y.L.; Han, J.; Zhang, W.C.; et al. Clinical experience and next-generation sequencing analysis of encephalitis caused by pseudorabies virus. *Zhonghua Yi Xue Za Zhi* **2018**, *98*, 1152–1157. [PubMed]

13. Yang, H.; Han, H.; Wang, H.; Cui, Y.; Liu, H.; Ding, S. A Case of Human Viral Encephalitis Caused by Pseudorabies Virus Infection in China. *Front. Neurol.* **2019**, *10*, 534. [CrossRef] [PubMed]
14. Ziemann, K.; Mettenleiter, T.C.; Fuchs, W. Gene arrangement within the unique long genome region of infectious laryngotracheitis virus is distinct from that of other alphaherpesviruses. *J. Virol.* **1998**, *72*, 847–852. [CrossRef]
15. Ye, G.; Liu, H.; Zhou, Q.; Liu, X.; Huang, L.; Weng, C. A Tug of War: Pseudorabies Virus and Host Antiviral Innate Immunity. *Viruses* **2022**, *14*, 547. [CrossRef]
16. Vallbracht, M.; Brun, D.; Tassinari, M.; Vaney, M.C.; Pehau-Arnaudet, G.; Guardado-Calvo, P.; Haouz, A.; Klupp, B.G.; Mettenleiter, T.C.; Rey, F.A.; et al. Structure-Function Dissection of Pseudorabies Virus Glycoprotein B Fusion Loops. *J. Virol.* **2018**, *92*, e01203–e01217. [CrossRef]
17. Trybala, E.; Bergström, T.; Spillmann, D.; Svennerholm, B.; Olofsson, S.; Flynn, S.J.; Ryan, P. Mode of interaction between pseudorabies virus and heparan sulfate/heparin. *Virology* **1996**, *218*, 35–42. [CrossRef]
18. Zhao, Y.; Wang, L.Q.; Zheng, H.H.; Yang, Y.R.; Liu, F.; Zheng, L.L.; Jin, Y.; Chen, H.Y. Construction and immunogenicity of a gE/gI/TK-deleted PRV based on porcine pseudorabies virus variant. *Mol. Cell. Probes* **2020**, *53*, 101605. [CrossRef]
19. Yao, L.; Hu, Q.; Chen, S.; Zhou, T.; Yu, X.; Ma, H.; Ghonaim, A.H.; Wu, H.; Sun, Q.; Fan, S.; et al. Recombinant Pseudorabies Virus with TK/gE Gene Deletion and Flt3L Co-Expression Enhances the Innate and Adaptive Immune Response via Activating Dendritic Cells. *Viruses* **2021**, *13*, 691. [CrossRef]
20. Xu, X.J.; Xu, G.Y.; Chen, H.C.; Liu, Z.F.; He, Q.G. Construction and characterization of a pseudorabies virus TK-/gG- mutant. *Sheng Wu Gong Cheng Xue Bao* **2004**, *20*, 532–535.
21. Wang, J.; Cui, X.; Wang, X.; Wang, W.; Gao, S.; Liu, X.; Kai, Y.; Chen, C. Efficacy of the Bartha-K61 vaccine and a gE(-)/gI(-)/TK(-) prototype vaccine against variant porcine pseudorabies virus (vPRV) in piglets with sublethal challenge of vPRV. *Res. Vet. Sci.* **2020**, *128*, 16–23. [CrossRef] [PubMed]
22. Wang, J.; Song, Z.; Ge, A.; Guo, R.; Qiao, Y.; Xu, M.; Wang, Z.; Liu, Y.; Zheng, Y.; Fan, H.; et al. Safety and immunogenicity of an attenuated Chinese pseudorabies variant by dual deletion of TK&gE genes. *BMC Vet. Res.* **2018**, *14*, 287.
23. Liu, Z.; Chen, H.; He, Q.; Zhou, F.; Fang, L. Construction of pseudorabies virus Ea TK-/gE-/gp63- mutant strain and the study on its biological property. *Wei Sheng Wu Xue Bao* **2002**, *42*, 370–374. [PubMed]
24. Kit, S.; Kit, M.; Pirtle, E.C. Attenuated properties of thymidine kinase-negative deletion mutant of pseudorabies virus. *Am. J. Vet. Res.* **1985**, *46*, 1359–1367. [PubMed]
25. Żyżyńska-Granica, B.; Trzaskowski, B.; Dutkiewicz, M.; Zegrocka-Stendel, O.; Machcińska, M.; Bocian, K.; Kowalewska, M.; Koziak, K. The anti-inflammatory potential of cefazolin as common gamma chain cytokine inhibitor. *Sci. Rep.* **2020**, *10*, 2886. [CrossRef]
26. Zwirner, N.W.; Fernández-Viña, M.A.; Stastny, P. MICA, a new polymorphic HLA-related antigen, is expressed mainly by keratinocytes, endothelial cells, and monocytes. *Immunogenetics* **1998**, *47*, 139–148. [CrossRef]
27. Zu, X.; Xie, X.; Zhang, Y.; Liu, K.; Bode, A.M.; Dong, Z.; Kim, D.J. Lapachol is a novel ribosomal protein S6 kinase 2 inhibitor that suppresses growth and induces intrinsic apoptosis in esophageal squamous cell carcinoma cells. *Phytother. Res.* **2019**, *33*, 2337–2346. [CrossRef]
28. Zuo, G.; Li, Z.; Chen, L.; Xu, X. Activity of compounds from Chinese herbal medicine *Rhodiola kirilowii* (Regel) Maxim against HCV NS3 serine protease. *Antiviral Res.* **2007**, *76*, 86–92. [CrossRef]
29. Zou, J.; Zhao, L.; Yi, P.; An, Q.; He, L.; Li, Y.; Lou, H.; Yuan, C.; Gu, W.; Huang, L.; et al. Quinolizidine Alkaloids with Antiviral and Insecticidal Activities from the Seeds of *Sophora tonkinensis* Gagnep. *J. Agric. Food Chem.* **2020**, *68*, 15015–15026. [CrossRef]
30. Zorrilla, J.G.; Rial, C.; Cabrera, D.; Molinillo, J.; Varela, R.M.; Macías, F.A. Pharmacological Activities of Aminophenoxazinones. *Molecules* **2021**, *26*, 3453. [CrossRef]
31. Zhou, Y.; He, Y.J.; Wang, Z.J.; Hu, B.Y.; Xie, T.Z.; Xiao, X.; Zhou, Z.S.; Sang, X.Y.; Luo, X.D. A review of plant characteristics, phytochemistry and bioactivities of the genus *Glechoma*. *J. Ethnopharmacol.* **2021**, *271*, 113830. [CrossRef] [PubMed]
32. Zhou, L.M.; Qu, R.Y.; Yang, G.F. An overview of spirooxindole as a promising scaffold for novel drug discovery. *Expert Opin. Drug Discov.* **2020**, *15*, 603–625. [CrossRef] [PubMed]
33. Zhou, X.; Xia, W.; Zhang, Y.; Ma, J.; Zhou, H.; Dong, L.; Fu, X. *Cynanchum paniculatum* (Bunge) Kitag. ex H. Hara: A review of its ethnopharmacology, phytochemistry and pharmacology. *J. Ethnopharmacol.* **2020**, *260*, 112994. [CrossRef] [PubMed]
34. Zhao, G.; Tong, Y.; Luan, F.; Zhu, W.; Zhan, C.; Qin, T.; An, W.; Zeng, N. Alpinetin: A Review of Its Pharmacology and Pharmacokinetics. *Front. Pharmacol.* **2022**, *13*, 814370. [CrossRef]
35. Huan, C.; Xu, W.; Guo, T.; Pan, H.; Zou, H.; Jiang, L.; Li, C.; Gao, S. (-)-Epigallocatechin-3-Gallate Inhibits the Life Cycle of Pseudorabies Virus In Vitro and Protects Mice Against Fatal Infection. *Front. Cell. Infect. Microbiol.* **2020**, *10*, 616895. [CrossRef]
36. Zhao, X.; Cui, Q.; Fu, Q.; Song, X.; Jia, R.; Yang, Y.; Zou, Y.; Li, L.; He, C.; Liang, X.; et al. Antiviral properties of resveratrol against pseudorabies virus are associated with the inhibition of IκB kinase activation. *Sci. Rep.* **2017**, *7*, 8782. [CrossRef]
37. He, W.; Zhai, X.; Su, J.; Ye, R.; Zheng, Y.; Su, S. Antiviral Activity of Germacrone against Pseudorabies Virus in Vitro. *Pathogens* **2019**, *8*, 258. [CrossRef] [PubMed]
38. Sun, Y.; Li, C.; Li, Z.; Shangguan, A.; Jiang, J.; Zeng, W.; Zhang, S.; He, Q. Quercetin as an antiviral agent inhibits the Pseudorabies virus in vitro and in vivo. *Virus Res.* **2021**, *305*, 198556. [CrossRef] [PubMed]
39. Yang, B.; Luo, G.; Zhang, C.; Feng, L.; Luo, X.; Gan, L. Curcumin protects rat hippocampal neurons against pseudorabies virus by regulating the BDNF/TrkB pathway. *Sci. Rep.* **2020**, *10*, 22204. [CrossRef]

40. Lin, H.W.; Lee, Y.J.; Yang, D.J.; Hsieh, M.C.; Chen, C.C.; Hsu, W.L.; Chang, Y.Y.; Liu, C.W. Anti-inflammatory effects of *Flos Loniceræ Japonicæ* Water Extract are regulated by the STAT/NF- κ B pathway and HO-1 expression in Virus-infected RAW264.7 cells. *Int. J. Med. Sci.* **2021**, *18*, 2285–2293. [CrossRef]
41. Zhou, Z.; Zhang, L.; Liu, Y.; Huang, C.; Xia, W.; Zhou, H.; Zhou, Z.; Zhou, X. Luteolin Protects Chondrocytes from H (2)O(2)-Induced Oxidative Injury and Attenuates Osteoarthritis Progression by Activating AMPK-Nrf2 Signaling. *Oxid. Med. Cell. Longev.* **2022**, *2022*, 5635797. [CrossRef]
42. Xing, Y.; Wang, L.; Xu, G.; Guo, S.; Zhang, M.; Cheng, G.; Liu, Y.; Liu, J. Platycodon grandiflorus polysaccharides inhibit Pseudorabies virus replication via downregulating virus-induced autophagy. *Res. Vet. Sci.* **2021**, *140*, 18–25. [CrossRef]
43. Li, L.; Wang, R.; Hu, H.; Chen, X.; Yin, Z.; Liang, X.; He, C.; Yin, L.; Ye, G.; Zou, Y.; et al. The antiviral activity of kaempferol against pseudorabies virus in mice. *BMC Vet. Res.* **2021**, *17*, 247. [CrossRef] [PubMed]
44. Lisov, A.; Vrublevskaia, V.; Lisova, Z.; Leontievsky, A.; Morenkov, O. A 2,5-Dihydroxybenzoic Acid-Gelatin Conjugate: The Synthesis, Antiviral Activity and Mechanism of Antiviral Action Against Two Alphaherpesviruses. *Viruses* **2015**, *7*, 5343–5360. [CrossRef]
45. Wang, G.; Chen, R.; Huang, P.; Hong, J.; Cao, J.; Wu, Q.; Zheng, W.; Lin, L.; Han, Q.; Chen, Y.; et al. Adefovir dipivoxil efficiently inhibits the proliferation of pseudorabies virus in vitro and in vivo. *Antiviral Res.* **2021**, *186*, 105014. [CrossRef]
46. Andreu, S.; Ripa, I.; Praena, B.; López-Guerrero, J.A.; Bello-Morales, R. The Valproic Acid Derivative Valpromide Inhibits Pseudorabies Virus Infection in Swine Epithelial and Mouse Neuroblastoma Cell Lines. *Viruses* **2021**, *13*, 2522. [CrossRef]
47. Fang, L.; Gao, Y.; Lan, M.; Jiang, P.; Bai, J.; Li, Y.; Wang, X. Hydroquinone inhibits PRV infection in neurons in vitro and in vivo. *Vet. Microbiol.* **2020**, *250*, 108864. [CrossRef]
48. Adfeldt, R.; Schmitz, J.; Kropff, B.; Thomas, M.; Monakhova, N.; Hölper, J.E.; Klupp, B.G.; Mettenleiter, T.C.; Makarov, V.; Bogner, E. Diazadispiroalkane Derivatives Are New Viral Entry Inhibitors. *Antimicrob. Agents Chemother.* **2021**, *65*, e02103–e02120. [CrossRef]
49. Lv, C.; Liu, W.; Wang, B.; Dang, R.; Qiu, L.; Ren, J.; Yan, C.; Yang, Z.; Wang, X. Ivermectin inhibits DNA polymerase UL42 of pseudorabies virus entrance into the nucleus and proliferation of the virus in vitro and vivo. *Antiviral Res.* **2018**, *159*, 55–62. [CrossRef]
50. Lee, G.; Cho, S.; Hoang, P.M.; Kim, D.; Lee, Y.; Kil, E.J.; Byun, S.J.; Lee, T.K.; Kim, D.H.; Kim, S.; et al. Therapeutic Strategy for the Prevention of Pseudorabies Virus Infection in C57BL/6 Mice by 3D8 scFv with Intrinsic Nuclease Activity. *Mol. Cells* **2015**, *38*, 773–780. [CrossRef] [PubMed]
51. Ziem, B.; Rahn, J.; Donskyi, I.; Silberreis, K.; Cuellar, L.; Dervede, J.; Keil, G.; Mettenleiter, T.C.; Haag, R. Polyvalent 2D Entry Inhibitors for Pseudorabies and African Swine Fever Virus. *Macromol. Biosci.* **2017**, *17*, 1600499. [CrossRef]
52. Wang, Y.P.; Du, W.J.; Huang, L.P.; Wei, Y.W.; Wu, H.L.; Feng, L.; Liu, C.M. The Pseudorabies Virus DNA Polymerase Accessory Subunit UL42 Directs Nuclear Transport of the Holoenzyme. *Front. Microbiol.* **2016**, *7*, 124. [CrossRef]
53. Hu, H.; Guo, N.; Chen, S.; Guo, X.; Liu, X.; Ye, S.; Chai, Q.; Wang, Y.; Liu, B.; He, Q. Antiviral activity of Piscidin 1 against pseudorabies virus both in vitro and in vivo. *Virol. J.* **2019**, *16*, 95. [CrossRef] [PubMed]
54. Huang, J.; Qi, Y.; Wang, A.; Huang, C.; Liu, X.; Yang, X.; Li, L.; Zhou, R. Porcine β -defensin 2 inhibits proliferation of pseudorabies virus in vitro and in transgenic mice. *Virol. J.* **2020**, *17*, 18. [CrossRef]
55. Chacko, S.M.; Thambi, P.T.; Kuttan, R.; Nishigaki, I. Beneficial effects of green tea: A literature review. *Chin. Med.* **2010**, *5*, 13. [CrossRef]
56. McKay, D.L.; Blumberg, J.B. The role of tea in human health: An update. *J. Am. Coll. Nutr.* **2002**, *21*, 1–13. [CrossRef] [PubMed]
57. Haqqi, T.M.; Anthony, D.D.; Gupta, S.; Ahmad, N.; Lee, M.S.; Kumar, G.K.; Mukhtar, H. Prevention of collagen-induced arthritis in mice by a polyphenolic fraction from green tea. *Proc. Natl. Acad. Sci. USA* **1999**, *96*, 4524–4529. [CrossRef] [PubMed]
58. Osada, K.; Takahashi, M.; Hoshina, S.; Nakamura, M.; Nakamura, S.; Sugano, M. Tea catechins inhibit cholesterol oxidation accompanying oxidation of low-density lipoprotein in vitro. *Comp. Biochem. Physiol. C Toxicol. Pharmacol.* **2001**, *128*, 153–164. [CrossRef]
59. Sudano Roccaro, A.; Blanco, A.R.; Giuliano, F.; Rusciano, D.; Enea, V. Epigallocatechin-gallate enhances the activity of tetracycline in staphylococci by inhibiting its efflux from bacterial cells. *Antimicrob. Agents Chemother.* **2004**, *48*, 1968–1973. [CrossRef]
60. Donà, M.; Dell’Aica, I.; Calabrese, F.; Benelli, R.; Morini, M.; Albini, A.; Garbisa, S. Neutrophil restraint by green tea: Inhibition of inflammation, associated angiogenesis, and pulmonary fibrosis. *J. Immunol. (Baltim. Md. 1950)* **2003**, *170*, 4335–4341. [CrossRef]
61. Weber, J.M.; Ruzindana-Umunyana, A.; Imbeault, L.; Sircar, S. Inhibition of adenovirus infection and adenain by green tea catechins. *Antivir. Res.* **2003**, *58*, 167–173. [CrossRef]
62. Sartippour, M.R.; Shao, Z.M.; Heber, D.; Beatty, P.; Zhang, L.; Liu, C.; Ellis, L.; Liu, W.; Go, V.L.; Brooks, M.N. Green tea inhibits vascular endothelial growth factor (VEGF) induction in human breast cancer cells. *J. Nutr.* **2002**, *132*, 2307–2311. [CrossRef] [PubMed]
63. Yamaguchi, K.; Honda, M.; Ikgai, H.; Hara, Y.; Shimamura, T. Inhibitory effects of (-)-epigallocatechin gallate on the life cycle of human immunodeficiency virus type 1 (HIV-1). *Antiviral Res.* **2002**, *53*, 19–34. [CrossRef]
64. Zykova, T.A.; Zhu, F.; Zhai, X.; Ma, W.Y.; Ermakova, S.P.; Lee, K.W.; Bode, A.M.; Dong, Z. Resveratrol directly targets COX-2 to inhibit carcinogenesis. *Mol. Carcinog.* **2008**, *47*, 797–805. [CrossRef]

65. Zunino, S.J.; Hwang, D.H.; Huang, S.; Storms, D.H. Resveratrol increases phagocytosis and lipopolysaccharide-induced interleukin-1 β production, but decreases surface expression of Toll-like receptor 2 in THP-1 monocytes. *Cytokine* **2018**, *102*, 141–144. [CrossRef]
66. Zulueta, A.; Caretti, A.; Signorelli, P.; Ghidoni, R. Resveratrol: A potential challenger against gastric cancer. *World. J. Gastroenterol.* **2015**, *21*, 10636–10643. [CrossRef]
67. Zou, Y.; Zuo, Q.; Huang, S.; Yu, X.; Jiang, Z.; Zou, S.; Fan, M.; Sun, L. Resveratrol inhibits trophoblast apoptosis through oxidative stress in preeclampsia-model rats. *Molecules* **2014**, *19*, 20570–20579. [CrossRef]
68. Zhu, Y.; Takayama, T.; Wang, B.; Kent, A.; Zhang, M.; Binder, B.Y.; Urabe, G.; Shi, Y.; DiRenzo, D.; Goel, S.A.; et al. Restenosis Inhibition and Re-differentiation of TGF β /Smad3-activated Smooth Muscle Cells by Resveratrol. *Sci. Rep.* **2017**, *7*, 41916. [CrossRef]
69. Zhuang, Y.; Wu, H.; Wang, X.; He, J.; He, S.; Yin, Y. Resveratrol Attenuates Oxidative Stress-Induced Intestinal Barrier Injury through PI3K/Akt-Mediated Nrf2 Signaling Pathway. *Oxid. Med. Cell. Longev.* **2019**, *2019*, 7591840. [CrossRef] [PubMed]
70. Song, P.; Yu, X.; Yang, W.; Wang, Q. Natural phytoalexin stilbene compound resveratrol and its derivatives as anti-tobacco mosaic virus and anti-phytopathogenic fungus agents. *Sci. Rep.* **2021**, *11*, 16509. [CrossRef] [PubMed]
71. Liu, T.; Zang, N.; Zhou, N.; Li, W.; Xie, X.; Deng, Y.; Ren, L.; Long, X.; Li, S.; Zhou, L.; et al. Resveratrol inhibits the TRIF-dependent pathway by upregulating sterile alpha and armadillo motif protein, contributing to anti-inflammatory effects after respiratory syncytial virus infection. *J. Virol.* **2014**, *88*, 4229–4236. [CrossRef] [PubMed]
72. Annunziata, G.; Maisto, M.; Schisano, C.; Ciampaglia, R.; Narciso, V.; Tenore, G.C.; Novellino, E. Resveratrol as a Novel Anti-Herpes Simplex Virus Nutraceutical Agent: An Overview. *Viruses* **2018**, *10*, 473. [CrossRef]
73. Liu, Y.; Wang, W.; Fang, B.; Ma, F.; Zheng, Q.; Deng, P.; Zhao, S.; Chen, M.; Yang, G.; He, G. Anti-tumor effect of germacrone on human hepatoma cell lines through inducing G2/M cell cycle arrest and promoting apoptosis. *Eur. J. Pharmacol.* **2013**, *698*, 95–102. [CrossRef]
74. Wu, J.; Feng, Y.; Han, C.; Huang, W.; Shen, Z.; Yang, M.; Chen, W.; Ye, L. Germacrone derivatives: Synthesis, biological activity, molecular docking studies and molecular dynamics simulations. *Oncotarget* **2017**, *8*, 15149–15158. [CrossRef]
75. Wu, H.; Liu, Y.; Zu, S.; Sun, X.; Liu, C.; Liu, D.; Zhang, X.; Tian, J.; Qu, L. In vitro antiviral effect of germacrone on feline calicivirus. *Arch. Virol.* **2016**, *161*, 1559–1567. [CrossRef]
76. Zhao, Y.; Cai, J.; Shi, K.; Li, H.; Du, J.; Hu, D.; Liu, Z.; Wang, W. Germacrone induces lung cancer cell apoptosis and cell cycle arrest via the Akt/MDM2/p53 signaling pathway. *Mol. Med. Rep.* **2021**, *23*, 452. [CrossRef]
77. Yu, Z.; Xu, J.; Shao, M.; Zou, J. Germacrone Induces Apoptosis as Well as Protective Autophagy in Human Prostate Cancer Cells. *Cancer Manag. Res.* **2020**, *12*, 4009–4016. [CrossRef]
78. Liao, Q.; Qian, Z.; Liu, R.; An, L.; Chen, X. Germacrone inhibits early stages of influenza virus infection. *Antiviral Res.* **2013**, *100*, 578–588. [CrossRef]
79. Feng, J.; Bai, X.; Cui, T.; Zhou, H.; Chen, Y.; Xie, J.; Shi, Q.; Wang, H.; Zhang, G. In Vitro Antiviral Activity of Germacrone Against Porcine Reproductive and Respiratory Syndrome Virus. *Curr. Microbiol.* **2016**, *73*, 317–323. [CrossRef]
80. Chen, Y.; Dong, Y.; Jiao, Y.; Hou, L.; Shi, Y.; Gu, T.; Zhou, P.; Shi, Z.; Xu, L.; Wang, C. In vitro antiviral activity of germacrone against porcine parvovirus. *Arch. Virol.* **2015**, *160*, 1415–1420. [CrossRef] [PubMed]
81. Donoso, F.; Ramirez, V.T.; Golubeva, A.V.; Moloney, G.M.; Stanton, C.; Dinan, T.G.; Cryan, J.F. Naturally Derived Polyphenols Protect Against Corticosterone-Induced Changes in Primary Cortical Neurons. *Int. J. Neuropsychopharmacol.* **2019**, *22*, 765–777. [CrossRef] [PubMed]
82. Rather, R.A.; Bhagat, M. Quercetin as an innovative therapeutic tool for cancer chemoprevention: Molecular mechanisms and implications in human health. *Cancer Med.* **2020**, *9*, 9181–9192. [CrossRef]
83. Gibellini, L.; Pinti, M.; Nasi, M.; Montagna, J.P.; De Biasi, S.; Roat, E.; Bertocelli, L.; Cooper, E.L.; Cossarizza, A. Quercetin and cancer chemoprevention. *Evid Based Complement Altern. Med.* **2011**, *2011*, 591356. [CrossRef]
84. Bagde, A.; Patel, K.; Mondal, A.; Kotlehria, S.; Chowdhury, N.; Gebeyehu, A.; Patel, N.; Kumar, N.; Singh, M. Combination of UVB Absorbing Titanium Dioxide and Quercetin Nanogel for Skin Cancer Chemoprevention. *AAPS PharmSciTech* **2019**, *20*, 240. [CrossRef]
85. Abbasi, A.; Mostafavi-Pour, Z.; Amiri, A.; Keshavarzi, F.; Nejabat, N.; Ramezani, F.; Sardarian, A.; Zal, F. Chemoprevention of Prostate Cancer Cells by Vitamin C plus Quercetin: Role of Nrf2 in Inducing Oxidative Stress. *Nutr. Cancer* **2021**, *73*, 2003–2013. [CrossRef]
86. Lee, S.; Lee, H.H.; Shin, Y.S.; Kang, H.; Cho, H. The anti-HSV-1 effect of quercetin is dependent on the suppression of TLR-3 in Raw 264.7 cells. *Arch. Pharm. Res.* **2017**, *40*, 623–630. [CrossRef]
87. Lopes, B.; da Costa, M.F.; Genova Ribeiro, A.; da Silva, T.F.; Lima, C.S.; Caruso, I.P.; de Araujo, G.C.; Kubo, L.H.; Iacovelli, F.; Falconi, M.; et al. Quercetin pentaacetate inhibits in vitro human respiratory syncytial virus adhesion. *Virus Res.* **2020**, *276*, 197805. [CrossRef]
88. Motterlini, R.; Foresti, R.; Bassi, R.; Green, C.J. Curcumin, an antioxidant and anti-inflammatory agent, induces heme oxygenase-1 and protects endothelial cells against oxidative stress. *Free Radic. Biol. Med.* **2000**, *28*, 1303–1312. [CrossRef]
89. Zhu, L.; Ding, X.; Zhang, D.; Ch, Y.; Wang, J.; Ndegwa, E.; Zhu, G. Curcumin inhibits bovine herpesvirus type 1 entry into MDBK cells. *Acta Virol.* **2015**, *59*, 221–227. [CrossRef]

90. Padilla-S, L.; Rodríguez, A.; Gonzales, M.M.; Gallego-G, J.C.; Castaño-O, J.C. Inhibitory effects of curcumin on dengue virus type 2-infected cells in vitro. *Arch. Virol.* **2014**, *159*, 573–579. [CrossRef] [PubMed]
91. Kutluay, S.B.; Doroghazi, J.; Roemer, M.E.; Triezenberg, S.J. Curcumin inhibits herpes simplex virus immediate-early gene expression by a mechanism independent of p300/CBP histone acetyltransferase activity. *Virology* **2008**, *373*, 239–247. [CrossRef] [PubMed]
92. Moghadamtousi, S.Z.; Kadir, H.A.; Hassandarvish, P.; Tajik, H.; Abubakar, S.; Zandi, K. A review on antibacterial, antiviral, and antifungal activity of curcumin. *Biomed Res. Int.* **2014**, *2014*, 186864. [PubMed]
93. Zou, X.; Himbert, S.; Dujardin, A.; Juhasz, J.; Ros, S.; Stöver, H.; Rheinstädter, M.C. Curcumin and Homotaurine Suppress Amyloid- β (25-35) Aggregation in Synthetic Brain Membranes. *ACS Chem. Neurosci.* **2021**, *12*, 1395–1405. [CrossRef]
94. Zhuang, X.X.; Wang, S.F.; Tan, Y.; Song, J.X.; Zhu, Z.; Wang, Z.Y.; Wu, M.Y.; Cai, C.Z.; Huang, Z.J.; Tan, J.Q.; et al. Pharmacological enhancement of TFEB-mediated autophagy alleviated neuronal death in oxidative stress-induced Parkinson's disease models. *Cell Death Dis.* **2020**, *11*, 128. [CrossRef]
95. Zhu, H.F.; Shao, Y.; Qin, L.; Wang, J.H.; Feng, S.; Jiang, Y.B.; Wan, D. Catalpol Enhances Neurogenesis and Inhibits Apoptosis Of New Neurons Via BDNF, But Not The BDNF/Trkb Pathway. *Drug Des. Devel. Ther.* **2019**, *13*, 4145–4157. [CrossRef]
96. Zhou, W.; Yin, A.; Shan, J.; Wang, S.; Cai, B.; Di, L. Study on the Rationality for Antiviral Activity of Flos Lonicerae Japonicae-Fructus Forsythiae Herb Chito-Oligosaccharide via Integral Pharmacokinetics. *Molecules* **2017**, *22*, 654. [CrossRef] [PubMed]
97. Zhao, H.; Zeng, S.; Chen, L.; Sun, Q.; Liu, M.; Yang, H.; Ren, S.; Ming, T.; Meng, X.; Xu, H. Updated pharmacological effects of Lonicerae japonicae flos, with a focus on its potential efficacy on coronavirus disease-2019 (COVID-19). *Curr. Opin. Pharmacol.* **2021**, *60*, 200–207. [CrossRef] [PubMed]
98. Mi, H.J.; Wang, Y.X.; Meng, J.; Wang, X.H.; Tao, Y.H.; Wang, Z.Z. Preliminary analysis on spectrum-efficient correlation model for anti-influenza virus of Lonicerae Japonicae Flos by partial least squares method. *Zhongguo Zhong Yao Za Zhi* **2015**, *40*, 4650–4654. [PubMed]
99. Kao, S.T.; Liu, C.J.; Yeh, C.C. Protective and immunomodulatory effect of flos Lonicerae japonicae by augmenting IL-10 expression in a murine model of acute lung inflammation. *J. Ethnopharmacol.* **2015**, *168*, 108–115. [CrossRef]
100. Hua, R.; Ding, Y.; Liu, X.; Niu, B.; Chen, X.; Zhang, J.; Liu, K.; Yang, P.; Zhu, X.; Xue, J.; et al. Lonicerae Japonicae Flos Extract Promotes Sleep in Sleep-Deprived and Lipopolysaccharide-Challenged Mice. *Front. Neurosci.* **2022**, *16*, 848588. [CrossRef]
101. Liu, C.W.; Lin, H.W.; Yang, D.J.; Chen, S.Y.; Tseng, J.K.; Chang, T.J.; Chang, Y.Y. Luteolin inhibits viral-induced inflammatory response in RAW264.7 cells via suppression of STAT1/3 dependent NF- κ B and activation of HO-1. *Free Radic. Biol. Med.* **2016**, *95*, 180–189. [CrossRef]
102. Kang, S.H.; Kim, T.H.; Shin, K.C.; Ko, Y.J.; Oh, D.K. Biotransformation of Food-Derived Saponins, Platycosides, into Deglycosylated Saponins Including Deglycosylated Platycodin D and Their Anti-Inflammatory Activities. *J. Agric. Food Chem.* **2019**, *67*, 1470–1477. [CrossRef]
103. Zhang, L.; Wang, Y.; Yang, D.; Zhang, C.; Zhang, N.; Li, M.; Liu, Y. Platycodon grandifloras—An ethnopharmacological, phytochemical and pharmacological review. *J. Ethnopharmacol.* **2015**, *164*, 147–161. [CrossRef]
104. Zheng, P.; Fan, W.; Wang, S.; Hao, P.; Wang, Y.; Wan, H.; Hao, Z.; Liu, J.; Zhao, X. Characterization of polysaccharides extracted from Platycodon grandiflorus (Jacq.) A.D.C. affecting activation of chicken peritoneal macrophages. *Int. J. Biol. Macromol.* **2017**, *96*, 775–785. [CrossRef] [PubMed]
105. Wang, C.; Cheng, G.; Yang, S.; Li, L.; Zhang, Y.; Zhao, X.; Liu, J. Protective effects of Platycodon grandiflorus polysaccharides against apoptosis induced by carbonyl cyanide 3-chlorophenylhydrazone in 3D4/21 cells. *Int. J. Biol. Macromol.* **2019**, *141*, 1220–1227. [CrossRef] [PubMed]
106. Zou, Y.F.; Chen, M.; Fu, Y.P.; Zhu, Z.K.; Zhang, Y.Y.; Paulsen, B.S.; Rise, F.; Chen, Y.L.; Yang, Y.Z.; Jia, R.Y.; et al. Characterization of an antioxidant pectic polysaccharide from Platycodon grandiflorus. *Int. J. Biol. Macromol.* **2021**, *175*, 473–480. [CrossRef]
107. Kim, S.R.; Park, E.J.; Dusabimana, T.; Je, J.; Jeong, K.; Yun, S.P.; Kim, H.J.; Cho, K.M.; Kim, H.; Park, S.W. Platycodon grandiflorus Fermented Extracts Attenuate Endotoxin-Induced Acute Liver Injury in Mice. *Nutrients* **2020**, *12*, 2802. [CrossRef] [PubMed]
108. Imran, M.; Rauf, A.; Shah, Z.A.; Saeed, F.; Imran, A.; Arshad, M.U.; Ahmad, B.; Bawazeer, S.; Atif, M.; Peters, D.G.; et al. Chemo-preventive and therapeutic effect of the dietary flavonoid kaempferol: A comprehensive review. *Phytother. Res.* **2019**, *33*, 263–275. [CrossRef]
109. Chen, A.Y.; Chen, Y.C. A review of the dietary flavonoid, kaempferol on human health and cancer chemoprevention. *Food Chem.* **2013**, *138*, 2099–2107. [CrossRef]
110. Calderón-Montaña, J.M.; Burgos-Morón, E.; Pérez-Guerrero, C.; López-Lázaro, M. A review on the dietary flavonoid kaempferol. *Mini Rev. Med. Chem.* **2011**, *11*, 298–344. [CrossRef]
111. Zhu, L.; Wang, P.; Yuan, W.; Zhu, G. Kaempferol inhibited bovine herpesvirus 1 replication and LPS-induced inflammatory response. *Acta Virol.* **2018**, *62*, 220–225. [CrossRef]
112. Zhu, L.; Xue, L. Kaempferol Suppresses Proliferation and Induces Cell Cycle Arrest, Apoptosis, and DNA Damage in Breast Cancer Cells. *Oncol. Res.* **2019**, *27*, 629–634. [CrossRef]
113. Zhu, J.; Tang, H.; Zhang, Z.; Zhang, Y.; Qiu, C.; Zhang, L.; Huang, P.; Li, F. Kaempferol slows intervertebral disc degeneration by modifying LPS-induced osteogenesis/adipogenesis imbalance and inflammation response in BMSCs. *Int. Immunopharmacol.* **2017**, *43*, 236–242. [CrossRef] [PubMed]

114. Zhuang, Z.; Ye, G.; Huang, B. Kaempferol Alleviates the Interleukin-1 β -Induced Inflammation in Rat Osteoarthritis Chondrocytes via Suppression of NF- κ B. *Med. Sci. Monit.* **2017**, *23*, 3925–3931. [CrossRef] [PubMed]
115. Reardon, J.E.; Spector, T. Herpes simplex virus type 1 DNA polymerase. Mechanism of inhibition by acyclovir triphosphate. *J. Biol. Chem.* **1989**, *264*, 7405–7411. [CrossRef]
116. Yedidag, E.N.; Koffron, A.J.; Mueller, K.H.; Kaplan, B.; Kaufman, D.B.; Fryer, J.P.; Stuart, F.P.; Abecassis, M. Acyclovir triphosphate inhibits the diagnostic polymerase chain reaction for cytomegalovirus. *Transplantation* **1996**, *62*, 238–242. [CrossRef]
117. Lüscher-Mattli, M. Polyanions—A lost chance in the fight against HIV and other virus diseases. *Antivir. Chem. Chemother.* **2000**, *11*, 249–259. [CrossRef]
118. Baranova, E.O.; Shastina, N.S.; Shvets, V.I. Polyanionic inhibitors of HIV adsorption. *Bioorg. Khim.* **2011**, *37*, 592–608. [CrossRef]
119. Ishihara, C.; Yoshimatsu, K.; Tsuji, M.; Arikawa, J.; Saiki, I.; Tokura, S.; Azuma, I. Anti-viral activity of sulfated chitin derivatives against Friend murine leukaemia and herpes simplex type-1 viruses. *Vaccine* **1993**, *11*, 670–674. [CrossRef]
120. Mbemba, E.; Chams, V.; Gluckman, J.C.; Klatzmann, D.; Gattegno, L. Molecular interaction between HIV-1 major envelope glycoprotein and dextran sulfate. *Biochim. Biophys. Acta* **1992**, *1138*, 62–67. [CrossRef]
121. Ghodke-Puranik, Y.; Thorn, C.F.; Lamba, J.K.; Leeder, J.S.; Song, W.; Birnbaum, A.K.; Altman, R.B.; Klein, T.E. Valproic acid pathway: Pharmacokinetics and pharmacodynamics. *Pharmacogenet. Genom.* **2013**, *23*, 236–241. [CrossRef] [PubMed]
122. Vázquez-Calvo, A.; Saiz, J.C.; Sobrino, F.; Martín-Acebes, M.A. Inhibition of enveloped virus infection of cultured cells by valproic acid. *J. Virol.* **2011**, *85*, 1267–1274. [CrossRef] [PubMed]
123. Gil, M.; González-González, R.; Vázquez-Calvo, A.; Álvarez-Gutiérrez, A.; Martín-Acebes, M.A.; Praena, B.; Bello-Morales, R.; Saiz, J.C.; López-Guerrero, J.A.; Tabarés, E.; et al. Clinical Infections by Herpesviruses in Patients Treated with Valproic Acid: A Nested Case-Control Study in the Spanish Primary Care Database, BIFAP. *J. Clin. Med.* **2019**, *8*, 1442. [CrossRef] [PubMed]
124. Shiraki, K. Antiviral Drugs Against Alphaherpesvirus. *Adv. Exp. Med. Biol.* **2018**, *1045*, 103–122.
125. Kukhanova, M.K.; Korovina, A.N.; Kochetkov, S.N. Human herpes simplex virus: Life cycle and development of inhibitors. *Biochemistry. Biokhimiia* **2014**, *79*, 1635–1652. [CrossRef]
126. Kudin, A.P.; Mawasi, H.; Eisenkraft, A.; Elger, C.E.; Bialer, M.; Kunz, W.S. Mitochondrial Liver Toxicity of Valproic Acid and Its Acid Derivatives Is Related to Inhibition of α -Lipoamide Dehydrogenase. *Int. J. Mol. Sci.* **2017**, *18*, 1912.
127. Luo, H.; Liang, H.; Chen, J.; Xu, Y.; Chen, Y.; Xu, L.; Yun, L.; Liu, J.; Yang, H.; Liu, L.; et al. Hydroquinone induces TK6 cell growth arrest and apoptosis through PARP-1/p53 regulatory pathway. *Environ. Toxicol.* **2017**, *32*, 2163–2171. [CrossRef]
128. Byeon, S.E.; Yi, Y.S.; Lee, J.; Yang, W.S.; Kim, J.H.; Kim, J.; Hong, S.; Kim, J.H.; Cho, J.Y. Hydroquinone Exhibits In Vitro and In Vivo Anti-Cancer Activity in Cancer Cells and Mice. *Int. J. Mol. Sci.* **2018**, *19*, 903. [CrossRef] [PubMed]
129. Kang, K.W.; Cho, M.K.; Lee, C.H.; Kim, S.G. Activation of phosphatidylinositol 3-kinase and Akt by tert-butylhydroquinone is responsible for antioxidant response element-mediated rGSTA2 induction in H4IIE cells. *Mol. Pharmacol.* **2001**, *59*, 1147–1156. [CrossRef] [PubMed]
130. Zvezdaryk, K.J.; Ferris, M.B.; Strong, A.L.; Morris, C.A.; Bunnell, B.A.; Dhurandhar, N.V.; Gimble, J.M.; Sullivan, D.E. Human cytomegalovirus infection of human adipose-derived stromal/stem cells restricts differentiation along the adipogenic lineage. *Adipocyte* **2016**, *5*, 53–64. [CrossRef]
131. Zu, C.; Xu, Y.; Wang, Y.; Zhang, M.; Zhao, H.; Fang, X.; Huang, H.; Hu, Y. Cytomegalovirus Retinitis and Retinal Detachment following Chimeric Antigen Receptor T Cell Therapy for Relapsed/Refractory Multiple Myeloma. *Curr. Oncol. (Tor. Ont.)* **2022**, *29*, 490–496. [CrossRef]
132. Zlatkin, R.; Bilavsky, E.; Pardo, J.; Salman, L.; Bardin, R.; Hadar, E.; Shmueli, A. The association between maternal cytomegalovirus urinary excretion and congenital infection rate. *BMC Pregnancy Childbirth* **2021**, *21*, 741. [CrossRef]
133. Biron, K.K. Antiviral drugs for cytomegalovirus diseases. *Antiviral Res.* **2006**, *71*, 154–163. [CrossRef]
134. Jans, D.A.; Wagstaff, K.M. Ivermectin as a Broad-Spectrum Host-Directed Antiviral: The Real Deal. *Cells* **2020**, *9*, 2100. [CrossRef] [PubMed]
135. Wagstaff, K.M.; Sivakumaran, H.; Heaton, S.M.; Harrich, D.; Jans, D.A. Ivermectin is a specific inhibitor of importin α / β -mediated nuclear import able to inhibit replication of HIV-1 and dengue virus. *Biochem. J.* **2012**, *443*, 851–856. [CrossRef]
136. Kim, Y.R.; Kim, J.S.; Lee, S.H.; Lee, W.R.; Sohn, J.N.; Chung, Y.C.; Shim, H.K.; Lee, S.C.; Kwon, M.H.; Kim, Y.S. Heavy and light chain variable single domains of an anti-DNA binding antibody hydrolyze both double- and single-stranded DNAs without sequence specificity. *J. Biol. Chem.* **2006**, *281*, 15287–15295. [CrossRef] [PubMed]
137. Hoang, P.M.; Cho, S.; Kim, K.E.; Byun, S.J.; Lee, T.K.; Lee, S. Development of Lactobacillus paracasei harboring nucleic acid-hydrolyzing 3D8 scFv as a preventive probiotic against murine norovirus infection. *Appl. Microbiol. Biotechnol.* **2015**, *99*, 2793–2803. [CrossRef] [PubMed]
138. Jun, H.R.; Pham, C.D.; Lim, S.I.; Lee, S.C.; Kim, Y.S.; Park, S.; Kwon, M.H. An RNA-hydrolyzing recombinant antibody exhibits an antiviral activity against classical swine fever virus. *Biochem. Biophys. Res. Commun.* **2010**, *395*, 484–489. [CrossRef] [PubMed]
139. Lee, G.; Budhathoki, S.; Lee, G.Y.; Oh, K.J.; Ham, Y.K.; Kim, Y.J.; Lim, Y.R.; Hoang, P.T.; Lee, Y.; Lim, S.W.; et al. Broad-Spectrum Antiviral Activity of 3D8, a Nucleic Acid-Hydrolyzing Single-Chain Variable Fragment (scFv), Targeting SARS-CoV-2 and Multiple Coronaviruses In Vitro. *Viruses* **2021**, *13*, 650. [CrossRef] [PubMed]
140. Zhu, K.Y.; Palli, S.R. Mechanisms, Applications, and Challenges of Insect RNA Interference. *Annu. Rev. Entomol.* **2020**, *65*, 293–311. [CrossRef]

141. Weisshart, K.; Chow, C.S.; Coen, D.M. Herpes simplex virus processivity factor UL42 imparts increased DNA-binding specificity to the viral DNA polymerase and decreased dissociation from primer-template without reducing the elongation rate. *J. Virol.* **1999**, *73*, 55–66. [CrossRef]
142. Zannella, C.; Chianese, A.; Palomba, L.; Maccocci, M.E.; Bellavita, R.; Merlino, F.; Grieco, P.; Folliero, V.; De Filippis, A.; Mangoni, M.; et al. Broad-Spectrum Antiviral Activity of the Amphibian Antimicrobial Peptide Temporin L and Its Analogs. *Int. J. Mol. Sci.* **2022**, *23*, 2060. [CrossRef]
143. Liu, R.; Liu, Z.; Peng, H.; Lv, Y.; Feng, Y.; Kang, J.; Lu, N.; Ma, R.; Hou, S.; Sun, W.; et al. Bomidin: An Optimized Antimicrobial Peptide with Broad Antiviral Activity Against Enveloped Viruses. *Front. Immunol.* **2022**, *13*, 851642. [CrossRef]
144. Liang, X.; Zhang, X.; Lian, K.; Tian, X.; Zhang, M.; Wang, S.; Chen, C.; Nie, C.; Pan, Y.; Han, F.; et al. Antiviral effects of Bovine antimicrobial peptide against TGEV in vivo and in vitro. *J. Vet. Sci.* **2020**, *21*, e80. [CrossRef] [PubMed]
145. Huang, H.N.; Pan, C.Y.; Chen, J.Y. Grouper (*Epinephelus coioides*) antimicrobial peptide epinecidin-1 exhibits antiviral activity against foot-and-mouth disease virus in vitro. *Peptides* **2018**, *106*, 91–95. [CrossRef] [PubMed]
146. Jenssen, H. Anti-herpes simplex virus activity of lactoferrin/lactoferricin—An example of antiviral activity of antimicrobial protein/peptide. *Cell. Mol. Life Sci.* **2005**, *62*, 3002–3013. [CrossRef]
147. Holly, M.K.; Diaz, K.; Smith, J.G. Defensins in Viral Infection and Pathogenesis. *Annu. Rev. Virol.* **2017**, *4*, 369–391. [CrossRef]
148. Zhao, L.; Lu, W. Defensins in innate immunity. *Curr. Opin. Hematol.* **2014**, *21*, 37–42. [CrossRef]
149. Zhao, W.Y.; Dong, B.R.; Zhou, Y. In vitro antimicrobial activity of defensins from rabbit neutrophils against *Pseudomonas aeruginosa* and its multiple-drug-resistance strains. *Sichuan Da Xue Xue Bao Yi Xue Ban* **2005**, *36*, 83–85.
150. Zheng, Y.; Chen, J.; Wu, X.; Zhang, X.; Hu, C.; Kang, Y.; Lin, J.; Li, J.; Huang, Y.; Zhang, X.; et al. Enhanced Anti-Inflammatory Effects of Silibinin and Capsaicin Combination in Lipopolysaccharide-Induced RAW264.7 Cells by Inhibiting NF- κ B and MAPK Activation. *Front. Chem.* **2022**, *10*, 934541. [CrossRef]
151. Chen, Y.; Lin, W.; Zhong, L.; Fang, Z.; Ye, B.; Wang, Z.; Chattipakorn, N.; Huang, W.; Liang, G.; Wu, G. Bicyclol Attenuates Obesity-Induced Cardiomyopathy via Inhibiting NF- κ B and MAPK Signaling Pathways. *Cardiovasc. Drugs Ther.* **2022**. [CrossRef] [PubMed]
152. Zhao, X.; Tong, W.; Song, X.; Jia, R.; Li, L.; Zou, Y.; He, C.; Liang, X.; Lv, C.; Jing, B.; et al. Antiviral Effect of Resveratrol in Piglets Infected with Virulent Pseudorabies Virus. *Viruses* **2018**, *10*, 457. [CrossRef] [PubMed]
153. Li, G.; Wu, H.; Sun, L.; Cheng, K.; Lv, Z.; Chen, K.; Qian, F.; Li, Y. (-)- α -Bisabolol Alleviates Atopic Dermatitis by Inhibiting MAPK and NF- κ B Signaling in Mast Cell. *Molecules* **2022**, *27*, 3985. [CrossRef]
154. Ren, C.Z.; Hu, W.Y.; Li, J.C.; Xie, Y.H.; Jia, N.N.; Shi, J.; Wei, Y.Y.; Hu, T.J. Ethyl acetate fraction of flavonoids from *Polygonum hydropiper* L. modulates pseudorabies virus-induced inflammation in RAW264.7 cells via the nuclear factor-kappa B and mitogen-activated protein kinase pathways. *J. Vet. Med. Sci.* **2020**, *82*, 1781–1792. [CrossRef] [PubMed]
155. Mysona, B.A.; Zhao, J.; Bollinger, K.E. Role of BDNF/TrkB pathway in the visual system: Therapeutic implications for glaucoma. *Expert. Rev. Ophthalmol.* **2017**, *12*, 69–81. [CrossRef]
156. Zou, W.; Song, Y.; Li, Y.; Du, Y.; Zhang, X.; Fu, J. The Role of Autophagy in the Correlation Between Neuron Damage and Cognitive Impairment in Rat Chronic Cerebral Hypoperfusion. *Mol. Neurobiol.* **2018**, *55*, 776–791. [CrossRef]
157. Zou, W.; Wang, X.; Vale, R.D.; Ou, G. Autophagy genes promote apoptotic cell corpse clearance. *Autophagy* **2012**, *8*, 1267–1268. [CrossRef]
158. Norberg, P. Divergence and genotyping of human alpha-herpesviruses: An overview. *Infect. Genet. Evol.* **2010**, *10*, 14–25. [CrossRef]
159. Marin, M.S.; Quintana, S.; Leunda, M.R.; Odeón, A.C.; Pérez, S.E. Distribution of bovine alpha-herpesviruses and expression of toll-like receptors in the respiratory system of experimentally infected calves. *Res. Vet. Sci.* **2016**, *105*, 53–55. [CrossRef]
160. Golais, F.; Mrázová, V. Human alpha and beta herpesviruses and cancer: Passengers or foes. *Folia Microbiol. (Praha)* **2020**, *65*, 439–449. [CrossRef]
161. Zhu, Z.; Gershon, M.D.; Gabel, C.; Sherman, D.; Ambron, R.; Gershon, A. Entry and egress of varicella-zoster virus: Role of mannose 6-phosphate, heparan sulfate proteoglycan, and signal sequences in targeting virions and viral glycoproteins. *Neurology* **1995**, *45*, S15–S17. [CrossRef] [PubMed]
162. Schmidt, J.; Gerdts, V.; Beyer, J.; Klupp, B.G.; Mettenleiter, T.C. Glycoprotein D-independent infectivity of pseudorabies virus results in an alteration of in vivo host range and correlates with mutations in glycoproteins B and H. *J. Virol.* **2001**, *75*, 10054–10064. [CrossRef] [PubMed]
163. Nixdorf, R.; Klupp, B.G.; Mettenleiter, T.C. Role of the cytoplasmic tails of pseudorabies virus glycoproteins B, E and M in intracellular localization and virion incorporation. *J. Gen. Virol.* **2001**, *82*, 215–226. [CrossRef] [PubMed]

Article

Glycyrrhiza Polysaccharide Inhibits Pseudorabies Virus Infection by Interfering with Virus Attachment and Internalization

Changchao Huan ^{1,2,3} , Yao Xu ^{1,2,3}, Wei Zhang ^{1,2,3}, Bo Ni ⁴ and Song Gao ^{1,2,3,5,*}

¹ Institutes of Agricultural Science and Technology Development, College of Veterinary Medicine, Yangzhou University, Yangzhou 225009, China

² Jiangsu Co-Innovation Center for Prevention and Control of Important Animal Infectious Diseases and Zoonoses, Yangzhou 225009, China

³ Key Laboratory of Avian Bioproduct Development, Ministry of Agriculture and Rural Affairs, Yangzhou 225009, China

⁴ Institutes of Agricultural Science and Technology Development, Yangzhou University, Yangzhou 225009, China

⁵ China Animal Health and Epidemiology Center, Qingdao 266011, China

* Correspondence: gsong@yzu.edu.cn

Abstract: Pseudorabies virus (PRV) is one of the most important pathogens causing serious diseases and leads to huge economic losses in the global swine industry. With the continuous emergence of PRV variants and the increasing number of cases of human infection, there is an urgent need to develop antiviral drugs. In this study, we discover that Glycyrrhiza polysaccharide (GCP) has anti-PRV infection activity in vitro, and 600 µg/mL GCP can completely block viral infection. The addition of GCP simultaneously with or after PRV infection had a significant inhibitory effect on PRV. Addition of GCP at different times of the virus life cycle mainly led to the inhibition of the attachment and internalization of PRV but does not affect viral replication and release. Our findings suggest that GCP has potential as a drug against PRV infection.

Keywords: Glycyrrhiza polysaccharide; pseudorabies virus; antiviral activity; attachment; internalization



Citation: Huan, C.; Xu, Y.; Zhang, W.; Ni, B.; Gao, S. Glycyrrhiza Polysaccharide Inhibits Pseudorabies Virus Infection by Interfering with Virus Attachment and Internalization. *Viruses* **2022**, *14*, 1772. <https://doi.org/10.3390/v14081772>

Academic Editors: Yan-Dong Tang and Xiangdong Li

Received: 27 July 2022

Accepted: 12 August 2022

Published: 14 August 2022

Publisher's Note: MDPI stays neutral with regard to jurisdictional claims in published maps and institutional affiliations.



Copyright: © 2022 by the authors. Licensee MDPI, Basel, Switzerland. This article is an open access article distributed under the terms and conditions of the Creative Commons Attribution (CC BY) license (<https://creativecommons.org/licenses/by/4.0/>).

1. Introduction

Pseudorabies (PR) is an acute infectious disease caused by the pseudorabies virus (PRV), which was first discovered in Hungary in 1902, and still causes serious disease and economic loss in the world [1,2]. In China, PRV was first isolated from cats in 1948, and has since been reported in domestic economic animals, such as pigs, cattle, and foxes [3]. Vaccination is the most common method to prevent PR [4,5]. The widespread introduction of the Bartha K61 vaccine from Hungary to China has brought the PR epidemic in China under control [6]. However, since 2011, highly pathogenic PRV variants have emerged in China, and the classic Bartha K61 vaccine does not provide complete protection [7,8]. Therefore, it is important to develop new vaccines and antiviral drugs to control the transmission of PRV variants.

The first step of the virus life cycle is viral entry. PRV entry into cells is mediated by viral glycoproteins, which can be divided into two stages: attachment and internalization. First, PRV virions attach to cells through glycoprotein C (gC) interaction with heparan sulfate proteoglycan in the extracellular matrix. Then, PRV glycoprotein D (gD) binds to specific cellular receptors [9]. Finally, PRV glycoprotein B (gB), glycoprotein H (gH), and glycoprotein L (gL) mediate an energy- and temperature-dependent fusion of the viral envelope and cell membrane that enables internalization of the viral capsid into the cytoplasm [10,11].

Licorice belongs to the family Leguminosae and is distributed all over the world. In China, it is mainly distributed in Xinjiang, Gansu, Shaanxi, and other northwest regions [12].

Licorice is one of the most widely used herbs in the world, and has a long history of application [13]. Polysaccharides are one of the main bioactive components of licorice. Studies have shown that Glycyrrhiza polysaccharide (GCP) has biological activities such as immune regulation [14] and antioxidant [15], antitumor [16], antiviral [17], and antibacterial properties [18]. Therefore, GCP has wide prospective applications. At present, research on GCP has mainly focused on its immunomodulatory activity; it has been reported that GCP can activate macrophages and dendritic cells [19,20]. GCP can also facilitate immune response by promoting the proliferation of lymphocytes [21]. However, the effectiveness of GCP in anti-PRV infection is still unknown.

In this study, we explored the antiviral effects of GCP on PRV infection and further explored its antiviral mechanisms. Our data showed that GCP exhibited better antiviral effects in the early stages of PRV infection, and its antiviral mechanism inhibited viral binding and internalization. Our findings suggest that GCP has potential for use as a treatment against PRV infection.

2. Materials and Methods

2.1. Cells and Virus

PK-15 cells were maintained in Dulbecco's Modified Eagle Medium (DMEM; Sigma, Canada) containing 5% fetal bovine serum (FBS; Lonsa, Uruguay, South America). Vero cells were cultured in DMEM containing 6% FBS. All cells were cultured at 37 °C with 5% CO₂. PRV XJ5, PRV NT, and PRV Ra were preserved in our laboratory.

2.2. Reagents and Antibodies

GCP \geq 98% (Ultraviolet, UV) was purchased from Ci Yuan Biotechnology Co., Ltd. (Shaanxi, China), and was diluted to 50 mg/mL with phosphate buffer saline (PBS). We purchased 4',6-diamidino-2-phenylindole (DAPI) (C1005), β -Actin mouse monoclonal antibodies (AF5001), and HRP-labeled goat anti-mouse IgG (H + L) (A0216) from Beyotime Biotechnology (Shanghai, China). Anti-gB mouse monoclonal antibodies and PRV-positive sera were prepared in our laboratory. FITC-conjugated goat anti-mouse IgG antibodies (AP124F) and FITC-conjugated rabbit anti-pig IgG antibodies (F1638) were purchased from Sigma-Aldrich (St. Louis, MO, USA).

2.3. Cell Viability Assay

The viability of PK-15 cells after GCP treatment was determined by using the Enhanced Cell Counting Kit-8 (CCK-8) (Beyotime, Shanghai, China), following the manufacturer's instructions. In brief, PK-15 cells were cultured in a 96-well plate and incubated at different concentrations (100, 200, 400, and 600 μ g/mL) of GCP at 37 °C for 24 h. Then the cells in each well were added to 10 μ L of CCK-8 solution and incubated for another 2 h at 37 °C. Absorbance was measured at 450 nm and cell viability was expressed as a percentage of control cell viability.

2.4. Infectivity Assay

PK-15 cells were seeded onto 6-well plates and cultured at 37 °C. When the cell density reached 70–80%, the original culture medium was discarded, and the cells were washed thrice with PBS. Then the cells were pre-treated with GCP (100, 200, 400, and 600 μ g/mL) in DMEM at 37 °C for 1 h, followed by infection by PRV XJ5 at a multiplicity of infection (MOI) of 0.1 at 37 °C for 1 h. After 1 h of infection, the infected cells were washed thrice with PBS and cultured in DMEM containing 2% FBS in the presence of corresponding concentrations of GCP at 37 °C for 24h. The antiviral activity of GCP was measured by cytopathic effects (CPE), a Western blot, 50% tissue culture infective dose (TCID₅₀), and an indirect immunofluorescence assay (IFA).

2.5. Time-of-Addition Assays

Time-of-addition assays were performed. PK-15 cells were either pre-treated, co-treated, or post-treated with GCP (100, 200, 400, and 600 µg/mL) during PRV infection. In brief: (i) Pre-treatment: PK-15 cells were inoculated with GCP at 37 °C for 1 h and subsequently washed thrice with PBS to remove GCP, then the cells were infected with PRV XJ5 (MOI = 0.1) for 1 h and subsequently washed thrice with PBS to remove unbound viruses. (ii) Co-treatment: PK-15 cells were simultaneously treated with PRV XJ5 (MOI = 0.1) and GCP at 37 °C for 1 h, then the cells were washed thrice with PBS to remove GCP and unbound viruses. (iii) Post-treatment: PK-15 cells were infected with PRV XJ5 (MOI = 0.1) at 37 °C for 1 h and subsequently washed thrice with PBS, then the cells were treatment with GCP at 37 °C. All the above-treated cells were then further cultured at 37°C for 24 h.

2.6. Viral Attachment, Internalization, Replication, and Release Assays

In the viral attachment assay, PK-15 cells were incubated with PRV XJ5 (MOI = 0.1) and GCP (100, 200, 400, 600 µg/mL) at 4 °C for 1 h, then the infected cells were washed thrice with ice-cold PBS and cultured in DMEM containing 2% FBS at 37 °C for 24 h.

In the viral internalization assay, PK-15 cells were infected with PRV XJ5 (MOI = 0.1) at 4 °C for 1 h and subsequently washed thrice with chilled PBS to remove unbound viruses, then the infected cells were inoculated with GCP (100, 200, 400, and 600 µg/mL) at 37 °C for 1 h to initiate internalization. After 1 h, the cells were washed thrice with citric acid (40 mM citric acid, 10 mM KCl, 135 mM NaCl, pH 3.0) followed by PBS to remove PRV bound to the cell surface. Then the cells were cultured in DMEM containing 2% FB at 37 °C for 24 h.

In the viral replication assay, PK-15 cells were infected with PRV XJ5 (MOI = 0.1) at 37 °C for 1 h, then washed thrice with PBS. Then the infected cells were incubated with GCP (100, 200, 400, and 600 µg/mL) at 37 °C. At 4 and 6 hpi, the cells were collected to quantify the viral DNA by quantitative real-time PCR (qRT-PCR).

In the viral release assay, PK-15 cells were infected with PRV XJ5 (MOI = 0.1) at 37 °C and at 24 hpi, then the infected cells were washed thrice with PBS and cultured with GCP (100, 200, 400, and 600 µg/mL) in DMEM at 37 °C for another 4 h. Then the supernatants were collected to quantify the viral DNA by qRT-PCR.

2.7. Western Blot

The collected cells were lysed by 2 × SDS-PAGE loading buffer and boiled in a metal bath (96 °C, 15 min). The samples separated by 12% SDS-PAGE were then transferred from the gel to the nitrocellulose (NC) membrane. The NC membrane was blocked in PBST with 5% nonfat milk for 2 h at room temperature. The NC membrane was washed thrice with PBST and then incubated with anti-PRV glycoprotein B (gB) monoclonal antibodies (1:200) or anti-actin monoclonal antibodies (1:5000) overnight, at 4 °C. The next day, the NC membrane was washed thrice with PBST and incubated with HRP-conjugated secondary antibodies (1:5000) for 2 h at room temperature. Finally, an enhanced chemiluminescence (ECL) reagent (Share Biotechnology, Shanghai, China) was used to analyze the banding results of the immune complexes.

2.8. Viral Titer Assay

The viral titers were evaluated by the TCID₅₀ assay. Vero cells were cultured with DMEM containing 6% fetal bovine serum (FBS) and inoculated in 96-well plates. The collected virus samples were diluted from 10⁻¹ to 10⁻⁷ in DMEM successively. Then the diluted virus samples were inoculated to cells at 37 °C for 1.5 h. Finally, the virus-DMEM mixture was removed, and the infected cells were cultured in DMEM containing 2% FBS at 37 °C. After 72 h of culturing, the CPE on Vero cells were counted by a microscope and the TCID₅₀ was calculated by the Reed-Muench method.

2.9. IFA

Cells were immobilized with 4% paraformaldehyde at 37 °C for 30 min, then incubated with 0.1% Triton X-100 at 37 °C for 10 min, followed by blocking with 5% BSA overnight at 4 °C. The next day, cells were incubated with PRV-positive serum (1:200) at 37 °C for 1 h, followed by incubation with FITC-conjugated rabbit anti-pig IgG secondary antibodies at 37 °C for 30 min. Finally, cells were stained with DAPI for 7 min and the results were observed with a fluorescence microscope.

2.10. qRT-PCR

Total DNA from cells or cell supernatants were extracted using the phenol chloride method [22]. Viral DNA was quantified by qRT-PCR. In brief, the standard curve of each experiment was constructed with PRV-gB standard plasmids. The primers were as follows: 1) gB-F: ACAAGTTCAAGGCCACATCTAC and 2) gB-R: GTCCGTGAAGCGGTTTCGTGAT. The conditions were as follows: 95 °C for 60 s, followed by 45 cycles of 95 °C for 10 s, then 62 °C for 20 s. The copy number of virus genome DNA was calculated according to the CT value of the sample and the standard curve.

2.11. Statistical Analysis

All results were obtained from three independent experiments and were presented in means \pm SD. All experimental groups were compared with the 0-concentration group. All data were analyzed using GraphPad Prism 8.0 via one-way ANOVAs. Significance levels were as follows: ns, not significant; * $p < 0.05$; ** $p < 0.01$; and *** $p < 0.001$.

3. Results

3.1. Toxicity of GCP toward PK-15 Cells

The cytotoxic effect of GCP on PK-15 cells was determined by the CCK-8 method after 24 h co-incubation; the concentrations of GCP were 100, 200, 400, and 600 $\mu\text{g}/\text{mL}$. Results revealed no cytotoxic effects of GCP from 100 to 600 $\mu\text{g}/\text{mL}$ (compared with the 0 concentration group) (Figure 1). Therefore, GCP concentrations of 100 to 600 $\mu\text{g}/\text{mL}$ were selected for the following experiments.

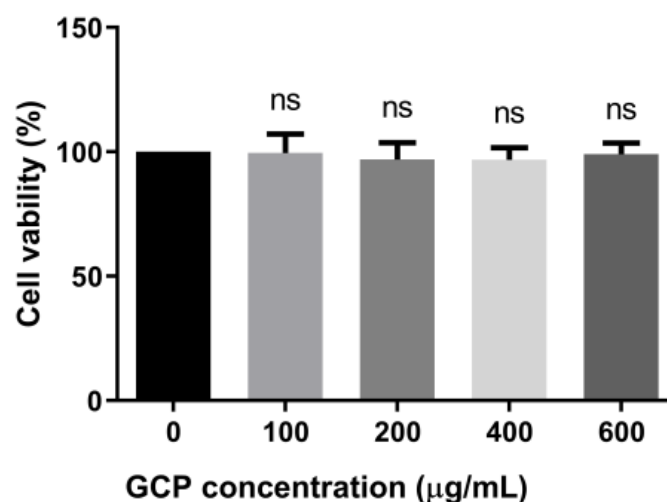


Figure 1. GCP cytotoxicity in PK-15 cells was detected with the Enhanced Cell Counting Kit-8. PK-15 cells were cultured in the presence of different concentrations of GCP for 24 h, and then added with 10 μL CCK-8 solution for another 2 h. Absorbance was measured at 450 nm (ns, not significant).

3.2. The Inhibitory Effect of GCP on PRV

To examine the antiviral effect of GCP against PRV—infected cells, PK-15 cells were pre—treated with GCP at 37 °C for 1 h and then infected with PRV XJ5 (MOI = 0.1) for 1 h. The infected cells were washed thrice with PBS and cultured with GCP in DMEM

containing 2% FBS at 37 °C (Figure 2A). At 24 hpi, the CPE caused by PRV infection was observed through a microscope. Figure 2B shows that GCP significantly reduced PRV—induced CPE. Moreover, Western blot, TCID₅₀, and IFA assays were performed to further confirm this inhibitory effect. As shown in Figure 2C, the expression levels of the PRV gB protein showed a dose-dependent decrease, and no viral protein expression was observed at concentrations of 400 and 600 µg/mL GCP. The results of the TCID₅₀ assay shows that virus titers in cell supernatants significantly decreased by GCP—treatment compared with control cells, and the decrease rate was about 45.6% at 600 µg/mL of GCP (Figure 2E). Similarly, IFA results also confirmed the inhibitory effect, and the higher the concentration of GCP, the stronger the inhibitory effect (Figure 2D).

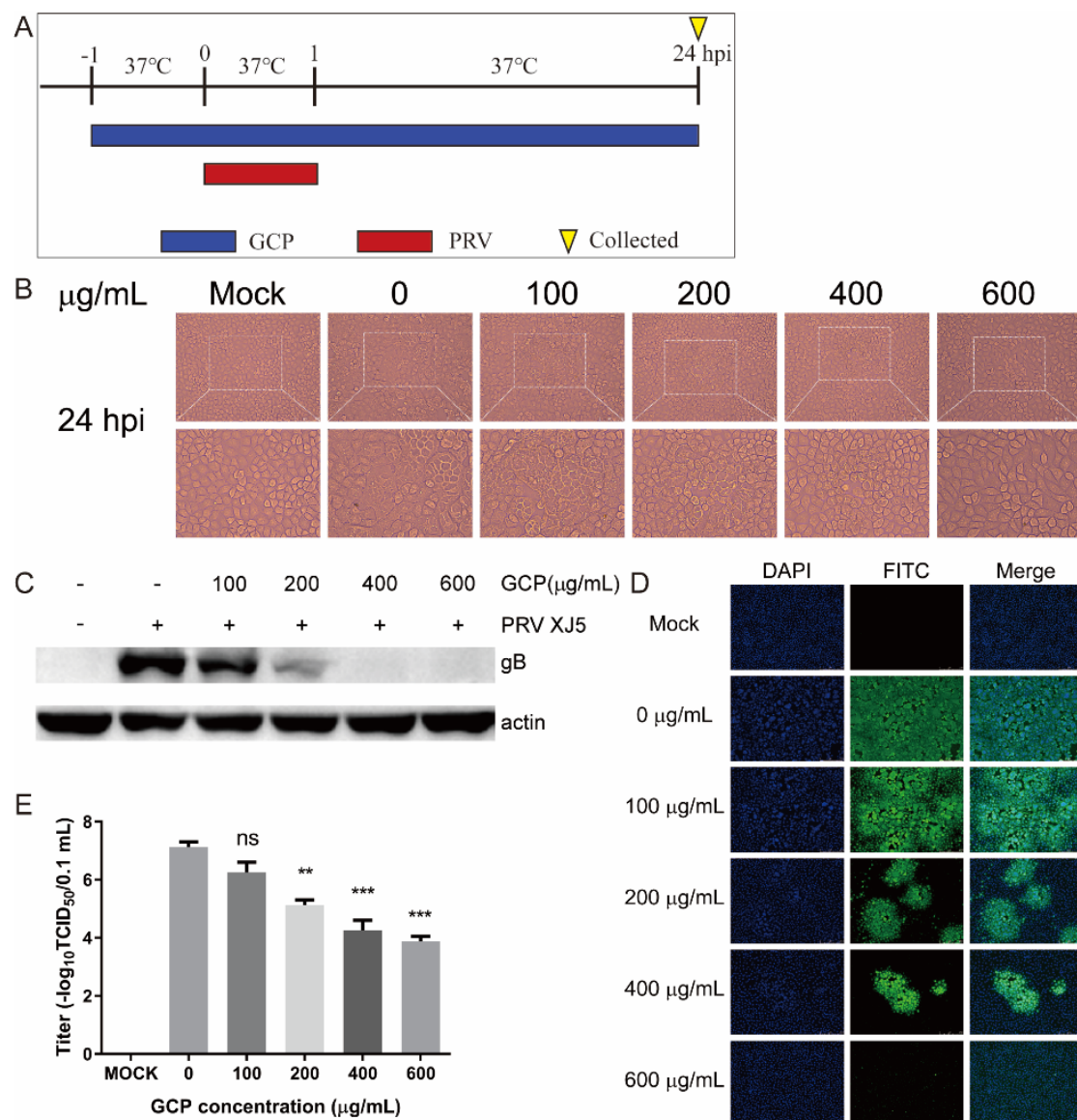


Figure 2. GCP inhibited PRV infection. (A) PK-15 cells were treated with GCP for 1 h and then infected with PRV XJ5 (MOI = 0.1) for 1 h. Cells were washed thrice with PBS and then incubated with GCP for another 24 h. (B) CPE observed by a microscope. (C) Expression levels of gB protein and actin analyzed by Western blot. (D) The internalized virus was detected by immunofluorescence assay. (E) The viral titer in supernatants was quantified by TCID₅₀. All results were obtained from three independent experiments and were presented in means ± SD (ns, not significant; ** $p < 0.01$; *** $p < 0.001$).

To rule out the possibility that the dose of virus infection had an effect, we performed assays with PRV XJ5 at an MOI of 0.1, 0.5, 1, or 2 in PK-15 cells as described above. Compared with the gB protein levels of the control cells, gB protein levels of the GCP—treated cells were significantly decreased at all tested MOI in PK-15 cells (Figure 3A–D), suggesting that the inhibitory effect of GCP on PRV infection was independent of the dose of virus infection. We further evaluated the antiviral effect of GCP on PRV NT and PRV Ra; we found that GCP had a strong inhibitory effect on different PRV strains (Figure 3E,F).

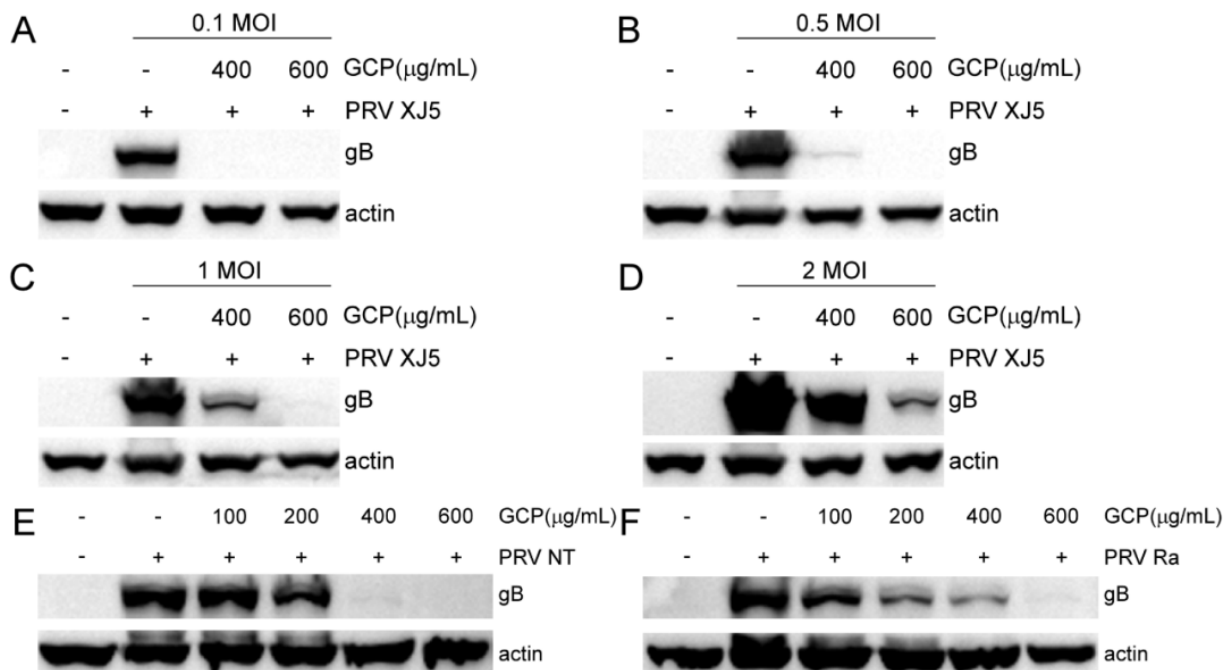


Figure 3. GCP reduced different MOI and PRV strains of infection. (A–D) GCP—preincubated PK-15 cells were incubated with PRV XJ5 at an MOI of 0.1, 0.5, 1, or 2. The expression levels of gB protein and actin were analyzed by Western blot. (E,F) GCP—preincubated PK-15 cells were incubated with PRV NT (MOI = 0.1) or PRV Ra (MOI = 0.1). The expression levels of gB protein and actin were analyzed by Western blot.

3.3. GCP Affects the Initial Stages of PRV Infection

We next investigated which stage of PRV infection was affected by GCP. Three different treatment schemes were used when adding GCP to the cells (Figure 4A). At 24 hpi, the virus titers in the supernatants of the infected cells were evaluated by TCID₅₀. The expression levels of PRV gB protein were evaluated by Western blot. According to the results of the Western blot and TCID₅₀, co—treatment demonstrated inhibition rates of about 80.6 and 42.6% at 600 μg/mL GCP, based on gB protein levels and virus titers (Figure 4D,E). Post—treatment showed inhibition rates of 17.7 and 25.9% at 600 μg/mL GCP, based on gB protein levels and virus titers (Figure 4F,G). Therefore, the inhibitory effect was most significant in GCP co—treatment with PRV. In contrast, pre—treatment of cells had no effect (Figure 4B,C). These results suggest that GCP plays an inhibitory role in the early stages of PRV infection.

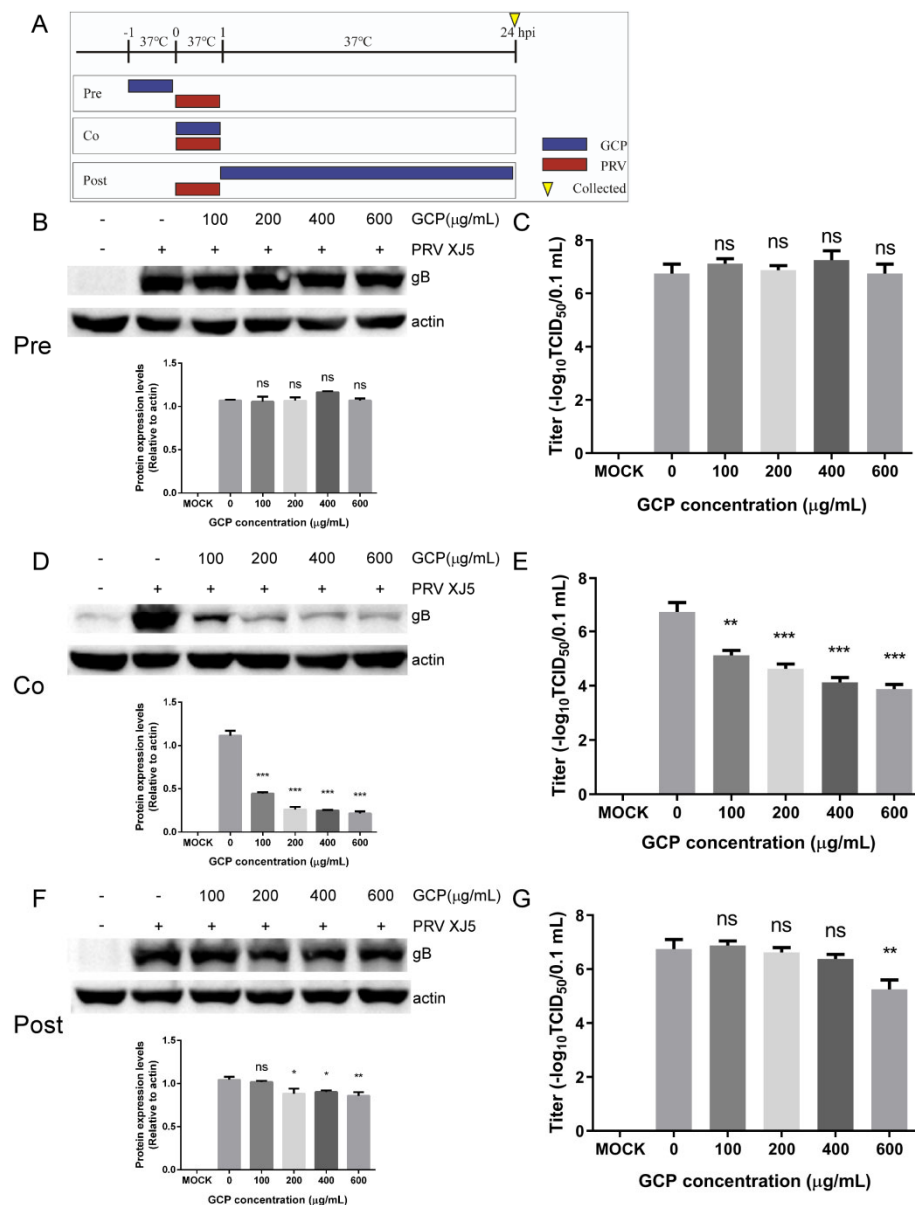


Figure 4. GCP inhibited the early stages of PRV infection. (A) Schematic diagram of GCP administration. PK-15 cells were infected with PRV XJ5 (MOI = 0.1) for 1 h and cells were treated with GCP at different hpi, designated pre—treatment (pre), co—treatment (co), or post—treatment (post). (B,C) Western blot for detection of gB expression and TCID₅₀ for detection of viral titer after pre-treatment with GCP. (D,E) Western blot for detection of gB expression and TCID₅₀ for detection of viral titer after co—treatment with GCP. (F,G) Western blot for detection of gB expression and TCID₅₀ for detection of viral titer after post—treatment with GCP. All results were obtained from three independent experiments and were presented in means ± SD (ns, not significant; * $p < 0.05$; ** $p < 0.01$; *** $p < 0.001$).

3.4. GCP Inhibits PRV Binding

Binding to the cell surface is the first step of early—stage PRV infection. So, we explored whether GCP inhibits PRV binding. PK-15 cells were incubated with PRV XJ5 (MOI = 0.1) and corresponding concentrations of GCP at 4 °C for 1 h, then the infected cells were washed thrice with chilled PBS and cultured at 37 °C (Figure 5A). At 24 hpi, PRV gB protein levels were determined by Western blot. We found that compared with control cells, the gB protein level of GCP—treated cells had decreased in a concentration—dependent manner, and 600 µg/mL of GCP almost completely blocked PRV binding (Figure B). In

the same way, according to the IFA assay, GCP decreased the numbers of infected cells (Figure 5C).

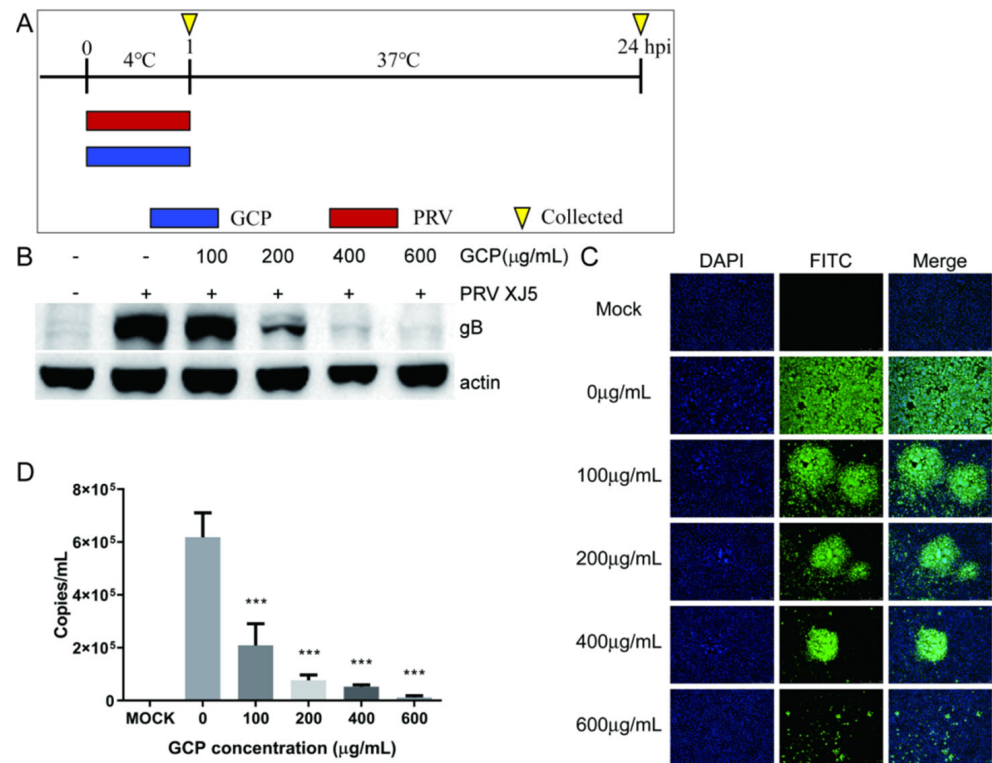


Figure 5. GCP decreased PRV binding (A) PK-15 cells were incubated with PRV XJ5 (MOI = 0.1) and GCP at 4 °C for 1 h, then cells were collected at 1 hpi or 24 hpi. (B,C) At 24 hpi, the expression levels of gB protein and actin were analyzed by Western blot and the internalized virus was detected by immunofluorescence assay. (D) At 1 hpi, the copy numbers of PRV DNA were quantified by qRT-PCR. All results were obtained from three independent experiments and were presented in means ± SD (***) $p < 0.001$).

To further verify these results, we performed a qRT-PCR assay to quantify PRV particles on the cell surface. PK-15 cells were processed as described above. At 1 hpi, the cells were washed with chilled PBS and collected to measure virus DNA copies by qRT-PCR. As expected, we found that the viral DNA copy level of GCP—treated cells had significantly decreased, which confirmed that GCP inhibits PRV binding to PK-15 cells (Figure D).

3.5. GCP Inhibits the Internalization of PRV

PRV is internalized into cells through the viral protein-mediated fusion of the viral envelope and the cellular membrane. Therefore, we tested whether GCP inhibits the internalization of PRV following viral attachment in PK-15 cells. A schematic of this timeline is shown in Figure 6A. At 24 hpi, the cells were collected to determine the expression of the PRV gB protein. We found that expression of gB was reduced compared with the control group, with an inhibition rate of 43.2% at 600 μg/mL GCP (Figure 6B). Meanwhile, similar dose—dependent inhibition of virus internalization was observed by the IFA assay (Figure 6C).

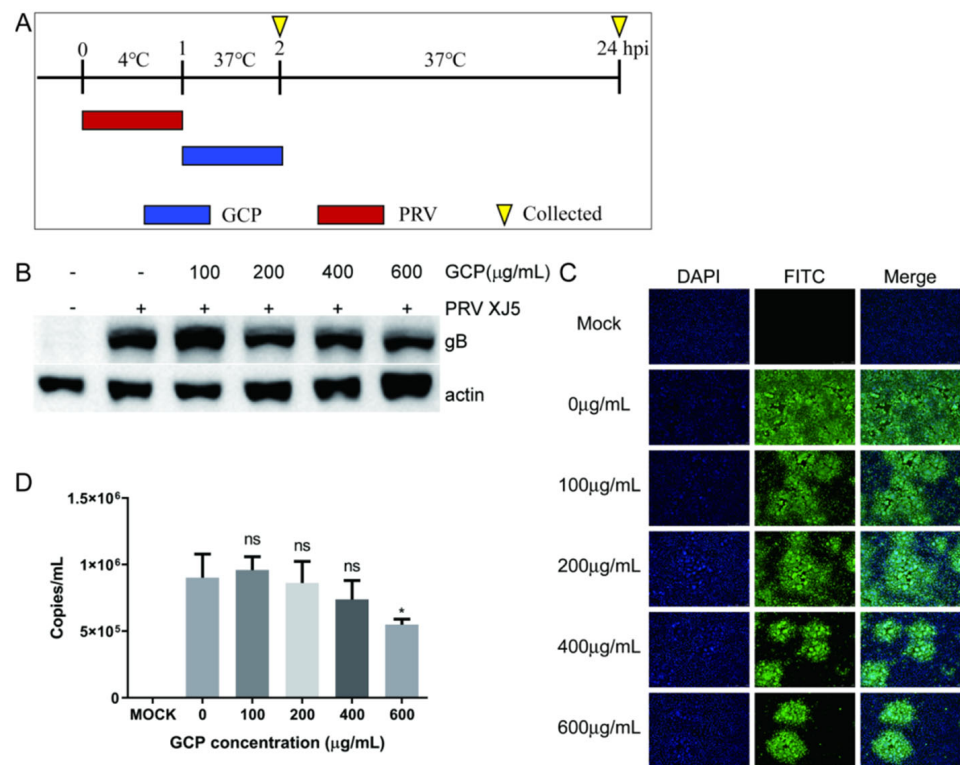


Figure 6. GCP decreased the internalization of PRV. (A) PK-15 cells were first infected with PRV XJ5 (MOI = 0.1) at 4 °C for 1 h, then incubated with GCP for another 1 h at 37 °C. (B,C) At 24 hpi, the expression levels of gB protein and actin were analyzed by Western blot and the internalized virus was detected by immunofluorescence assay. (D) At 2 hpi, the copy numbers of PRV DNA were quantified by qRT-PCR. All results were obtained from three independent experiments and were presented in means ± SD (ns, not significant; * $p < 0.05$).

We also performed a qRT-PCR assay to further verify these results. At 2 hpi, the washed cells were lysed for qRT-PCR to determine viral DNA copy levels. The results showed that GCP treatment inhibited PRV internalization into PK-15 cells; 600 μg/mL of GCP prevented 39.1% of virus internalization into cells (Figure 6D). Interestingly, the inhibition effect of GCP on PRV internalization was not as significant as that on PRV binding.

3.6. Effect of GCP on PRV Replication and Release

For the viral replication assay, PK-15 cells were infected with PRV XJ5 (MOI = 0.1) at 37 °C for 1 h, then washed thrice with PBS. The infected cells were then incubated with corresponding concentrations of GCP at 37 °C. At 4 and 6 hpi, the cells were washed and collected to determine the viral DNA levels by qRT-PCR. We found that there was no significant difference in viral DNA levels between GCP—treated PK-15 cells and control cells, suggesting that GCP had no effect on PRV replication (Figure 7A,B).

For the viral release assay, PK-15 cells were infected with PRV XJ5 (MOI = 0.1) at 37 °C and at 24 hpi, then the infected cells were washed thrice with PBS and cultured with corresponding concentrations of GCP at 37 °C for another 4 h. The cell culture supernatant was then collected to measure the viral DNA levels. The results showed that GCP did not inhibit PRV release (Figure 7C,D).

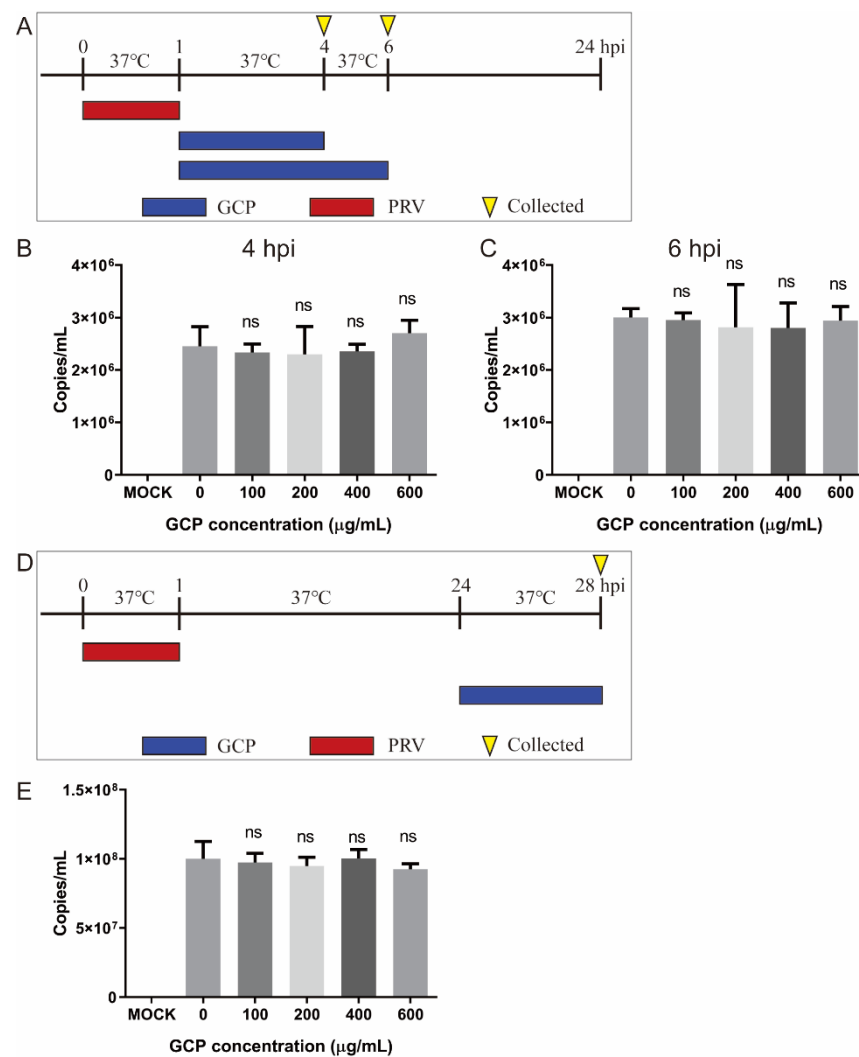


Figure 7. GCP had no effect on PRV replication and release. (A–C) PK-15 cells were infected with PRV XJ5 (MOI = 0.1) at 37 °C for 1 h, then incubated with GCP at 37 °C. At 4 and 6 hpi, the copy numbers of PRV DNA were quantified by qRT-PCR. (D,E) PK-15 cells were infected with PRV XJ5 (MOI = 0.1) for 24 h, washed, and incubated with fresh DMEM containing GCP for another 4 h. The copy numbers of PRV DNA in supernatants were quantified by qRT-PCR. All results were obtained from three independent experiments and were presented in means ± SD (ns, not significant).

4. Discussion

Vaccination is considered to be one of the most effective methods to control PR and reduce economic losses in the swine industry [5]. For nearly 40 years, the classic Bartha-K61 vaccine has been widely used to prevent and control the disease in China [23], but at the end of 2011, many vaccinated pig farms in China experienced outbreaks of PR [7,8]. Research suggests that this new outbreak was caused by a mutated strain of PRV [24,25]. More importantly, these PRV variants can infect humans and cause endophthalmitis and encephalitis [26,27]. In 2020, a PRV variant was isolated for the first time in a human case of acute encephalitis [28]. Therefore, it is necessary to develop an effective drug to control the transmission of these PRV variants. In this study, we verified the effective inhibitory effect of GCP on PRV infection *in vitro* for the first time.

PRV infection can be divided into four different stages: (1) Viral binding to the cell surface; (2) Viral internalization into the cell; (3) Viral genome replication; and (4) Viral release [10,29]. Each stage is a potential target for antiviral drugs. Studies have reported the effect of different stages of drug-resistance to PRV infection. Meclizine interfered with

PRV entry and release [30]. Germacrone, (S)-10-hydroxycamptothecin, and resveratrol inhibited viral replication in the early stages of infection [31–33]. Quercetin interacted with the PRV gD protein to block virus adsorption and entry [29]. In this study, using the time-of-addition assay, we found that cells pre-treated with GCP did not cause a decrease in PRV infectivity, suggesting that cellular factors, including cellular receptors for PRV, may not be sensitive to GCP [34]. When GCP and PRV were added simultaneously, GCP showed strong antiviral activity, suggesting that GCP mainly inhibits the early stages of PRV infection.

The first step of viral infection is to bind to a receptor on the cell surface to cause stable and irreversible adsorption, resulting in the subsequent entry process [35]. Blocking virus adsorption to the cell surface can prevent viral infection more effectively than administering drug treatments after viral infection. At 4 °C, the virus can only be adsorbed on the cell surface, and cannot enter the cell. So, GCP was added at 4 °C to verify the effect of GCP on virus adsorption [36]. We found a significant decrease in virus adsorption on the surface of GCP-treated cells. When the virus was adsorbed to the cell surface, GCP could also inhibit virus internalization. However, the inhibitory effects on virus internalization were not as significant as those on virus adsorption. Sulfated polysaccharides, such as sulfated Chuanmingshen violaceum polysaccharides [37], can block the positive charges on the cell surface using the negative charge of its sulfate group, causing interference in the viral adsorption process [35]. It has also been reported that the anti-HIV activity of sulfated polysaccharides is induced by the electrostatic interaction between the negative charge of the sulfate group and the positive charge of HIV gp120 [38]. In addition, polysaccharides can compete with viruses to bind to cell-surface receptors, or bind to the viruses themselves, preventing the viruses from attaching to cells [39–41]. However, the mechanism of GCP inhibiting PRV adsorption and internalization needs further study.

To sum up, this study first reported the significant anti-PRV activity of GCP. GCP played an inhibitory role in the early stages of PRV infection and inhibited PRV infection by blocking viral adsorption and internalization. This study provides a potential therapeutic agent to be used against PRV infection. However, the antiviral effect of GCP in vivo remains to be further studied. In addition, GCP shows antiviral effects only when added simultaneously with the virus, which may limit its application.

Author Contributions: Writing—original draft preparation, C.H.; writing—review and editing, C.H. and Y.X.; software, W.Z.; formal analysis, B.N.; project administration, S.G.; funding acquisition, C.H. and S.G. All authors have read and agreed to the published version of the manuscript.

Funding: This research was funded by the National Natural Science Foundation of China (31902253), Jiangsu Provincial Natural Science Fund for Excellent Young Scholars (BK20220114), China Postdoctoral Science Foundation (2018M632399), Priority Academic Program Development of Jiangsu Higher Education Institutions (PAPD), the earmarked fund of Jiangsu Agricultural Industry Technology System, and the Top-Level Talents Support Program of Yangzhou University.

Conflicts of Interest: The authors declare no conflict of interest.

References

1. Mettenleiter, T.C. Molecular biology of pseudorabies (Aujeszky's disease) virus. *Comp. Immunol. Microbiol. Infect. Dis.* **1991**, *14*, 151–163. [CrossRef]
2. Lee, J.Y.; Wilson, M.R. A review of pseudorabies (Aujeszky's disease) in pigs. *Can. Vet. J.* **1979**, *20*, 65–69. [PubMed]
3. Tan, L.; Yao, J.; Yang, Y.; Luo, W.; Yuan, X.; Yang, L.; Wang, A. Current Status and Challenge of Pseudorabies Virus Infection in China. *Virol. Sin.* **2021**, *36*, 588–607. [CrossRef] [PubMed]
4. Stegeman, A. Pseudorabies virus eradication by area-wide vaccination is feasible. *Vet. Q.* **1995**, *17*, 150–156. [CrossRef] [PubMed]
5. Freuling, C.M.; Muller, T.F.; Mettenleiter, T.C. Vaccines against pseudorabies virus (PrV). *Vet. Microbiol.* **2017**, *206*, 3–9. [CrossRef] [PubMed]
6. Delva, J.L.; Nauwynck, H.J.; Mettenleiter, T.C.; Favoreel, H.W. The Attenuated Pseudorabies Virus Vaccine Strain Bartha K61: A Brief Review on the Knowledge Gathered During 60 Years of Research. *Pathogens* **2020**, *9*, 897. [CrossRef] [PubMed]
7. An, T.Q.; Peng, J.M.; Tian, Z.J.; Zhao, H.Y.; Li, N.; Liu, Y.M.; Chen, J.Z.; Leng, C.L.; Sun, Y.; Chang, D.; et al. Pseudorabies virus variant in Bartha-K61-vaccinated pigs, China, 2012. *Emerg. Infect. Dis.* **2013**, *19*, 1749–1755. [CrossRef] [PubMed]

8. Tong, W.; Liu, F.; Zheng, H.; Liang, C.; Zhou, Y.J.; Jiang, Y.F.; Shan, T.L.; Gao, F.; Li, G.X.; Tong, G.Z. Emergence of a Pseudorabies virus variant with increased virulence to piglets. *Vet. Microbiol.* **2015**, *181*, 236–240. [CrossRef] [PubMed]
9. Li, A.; Lu, G.; Qi, J.; Wu, L.; Tian, K.; Luo, T.; Shi, Y.; Yan, J.; Gao, G.F. Structural basis of nectin-1 recognition by pseudorabies virus glycoprotein D. *PLoS Pathog.* **2017**, *13*, e1006314. [CrossRef] [PubMed]
10. Pomeranz, L.E.; Reynolds, A.E.; Hengartner, C.J. Molecular biology of pseudorabies virus: Impact on neurovirology and veterinary medicine. *Microbiol. Mol. Biol. Rev.* **2005**, *69*, 462–500. [CrossRef] [PubMed]
11. Spear, P.G.; Longnecker, R. Herpesvirus entry: An update. *J. Virol.* **2003**, *77*, 10179–10185. [CrossRef] [PubMed]
12. Yang, R.; Wang, L.Q.; Yuan, B.C.; Liu, Y. The Pharmacological Activities of Licorice. *Planta Med.* **2015**, *81*, 1654–1669. [CrossRef] [PubMed]
13. Yang, L.; Jiang, Y.; Zhang, Z.; Hou, J.; Tian, S.; Liu, Y. The anti-diabetic activity of licorice, a widely used Chinese herb. *J. Ethnopharmacol.* **2020**, *263*, 113216. [CrossRef] [PubMed]
14. Li, C.; Zhao, P.; Shao, Q.; Chen, W.; Huang, S.; Wang, X.; Zhang, C.; He, L. Effects of dietary Glycyrrhiza polysaccharide on growth performance, blood parameters and immunity in weaned piglets. *J. Anim. Physiol. Anim. Nutr.* **2022**, 13692. [CrossRef] [PubMed]
15. Mutaillifu, P.; Bobakulov, K.; Abuduwaili, A.; Huojiaihemaiti, H.; Nuexiati, R.; Aisa, H.A.; Yili, A. Structural characterization and antioxidant activities of a water soluble polysaccharide isolated from Glycyrrhiza glabra. *Int. J. Biol. Macromol.* **2020**, *144*, 751–759. [CrossRef]
16. Ayeka, P.A.; Bian, Y.; Githaiga, P.M.; Zhao, Y. The immunomodulatory activities of licorice polysaccharides (*Glycyrrhiza uralensis* Fisch.) in CT 26 tumor-bearing mice. *BMC Complement. Altern. Med.* **2017**, *17*, 536. [CrossRef] [PubMed]
17. Wang, Y.; Wang, X.; Zhang, K.; Zhang, X.; Li, S.; Li, Y.; Fan, W.; Leng, F.; Yang, M.; Chen, J. Extraction kinetics, thermodynamics, rheological properties and anti-BVDV activity of the hot water assisted extraction of Glycyrrhiza polysaccharide. *Food Funct.* **2020**, *11*, 4067–4080. [CrossRef]
18. Wittschier, N.; Faller, G.; Hensel, A. Aqueous extracts and polysaccharides from liquorice roots (*Glycyrrhiza glabra* L.) inhibit adhesion of *Helicobacter pylori* to human gastric mucosa. *J. Ethnopharmacol.* **2009**, *125*, 218–223. [CrossRef]
19. Cheng, A.; Wan, F.; Wang, J.; Jin, Z.; Xu, X. Macrophage immunomodulatory activity of polysaccharides isolated from *Glycyrrhiza uralensis* Fish. *Int. Immunopharmacol.* **2008**, *8*, 43–50. [CrossRef] [PubMed]
20. Aipire, A.; Yuan, P.; Aimaier, A.; Cai, S.; Mahabati, M.; Lu, J.; Ying, T.; Zhang, B.; Li, J. Preparation, Characterization, and Immuno-Enhancing Activity of Polysaccharides from *Glycyrrhiza uralensis*. *Biomolecules* **2020**, *10*, 159. [CrossRef] [PubMed]
21. Wu, Y.; Yi, L.; Li, E.; Li, Y.; Lu, Y.; Wang, P.; Zhou, H.; Liu, J.; Hu, Y.; Wang, D. Optimization of Glycyrrhiza polysaccharide liposome by response surface methodology and its immune activities. *Int. J. Biol. Macromol.* **2017**, *102*, 68–75. [CrossRef] [PubMed]
22. Zhou, J.; Li, S.; Wang, X.; Zou, M.; Gao, S. Bartha-k61 vaccine protects growing pigs against challenge with an emerging variant pseudorabies virus. *Vaccine* **2017**, *35*, 1161–1166. [CrossRef] [PubMed]
23. De Leeuw, P.W.; van Oirschot, J.T. Vaccines against Aujeszky's disease: Evaluation of their efficacy under standardized laboratory conditions. *Vet. Q.* **1985**, *7*, 191–197. [CrossRef] [PubMed]
24. Luo, Y.; Li, N.; Cong, X.; Wang, C.H.; Du, M.; Li, L.; Zhao, B.; Yuan, J.; Liu, D.D.; Li, S.; et al. Pathogenicity and genomic characterization of a pseudorabies virus variant isolated from Bartha-K61-vaccinated swine population in China. *Vet. Microbiol.* **2014**, *174*, 107–115. [CrossRef]
25. Fan, J.; Zeng, X.; Zhang, G.; Wu, Q.; Niu, J.; Sun, B.; Xie, Q.; Ma, J. Molecular characterization and phylogenetic analysis of pseudorabies virus variants isolated from Guangdong province of southern China during 2013–2014. *J. Vet. Sci.* **2016**, *17*, 369–375. [CrossRef] [PubMed]
26. Zheng, L.; Liu, X.; Yuan, D.; Li, R.; Lu, J.; Li, X.; Tian, K.; Dai, E. Dynamic cerebrospinal fluid analyses of severe pseudorabies encephalitis. *Transbound. Emerg. Dis.* **2019**, *66*, 2562–2565. [CrossRef] [PubMed]
27. Ai, J.W.; Weng, S.S.; Cheng, Q.; Cui, P.; Li, Y.J.; Wu, H.L.; Zhu, Y.M.; Xu, B.; Zhang, W.H. Human Endophthalmitis Caused by Pseudorabies Virus Infection, China, 2017. *Emerg. Infect. Dis.* **2018**, *24*, 1087–1090. [CrossRef]
28. Liu, Q.; Wang, X.; Xie, C.; Ding, S.; Yang, H.; Guo, S.; Li, J.; Qin, L.; Ban, F.; Wang, D.; et al. A Novel Human Acute Encephalitis Caused by Pseudorabies Virus Variant Strain. *Clin. Infect. Dis.* **2021**, *73*, e3690–e3700. [CrossRef]
29. Sun, Y.; Li, C.; Li, Z.; Shangguan, A.; Jiang, J.; Zeng, W.; Zhang, S.; He, Q. Quercetin as an antiviral agent inhibits the Pseudorabies virus in vitro and in vivo. *Virus Res.* **2021**, *305*, 198556. [CrossRef]
30. Liu, P.; Hu, D.; Yuan, L.; Lian, Z.; Yao, X.; Zhu, Z.; Nowotny, N.; Shi, Y.; Li, X. Meclizine Inhibits Pseudorabies Virus Replication by Interfering With Virus Entry and Release. *Front. Microbiol.* **2021**, *12*, 795593. [CrossRef]
31. He, W.; Zhai, X.; Su, J.; Ye, R.; Zheng, Y.; Su, S. Antiviral Activity of Germacrone against Pseudorabies Virus in Vitro. *Pathogens* **2019**, *8*, 258. [CrossRef] [PubMed]
32. Liu, X.; Lv, L.; Jiang, C.; Bai, J.; Gao, Y.; Ma, Z.; Jiang, P. A natural product, (S)-10-Hydroxycamptothecin inhibits pseudorabies virus proliferation through DNA damage dependent antiviral innate immunity. *Vet. Microbiol.* **2022**, *265*, 109313. [CrossRef] [PubMed]
33. Zhao, X.; Tong, W.; Song, X.; Jia, R.; Li, L.; Zou, Y.; He, C.; Liang, X.; Lv, C.; Jing, B.; et al. Antiviral Effect of Resveratrol in Piglets Infected with Virulent Pseudorabies Virus. *Viruses* **2018**, *10*, 457. [CrossRef]
34. Sui, X.; Yin, J.; Ren, X. Antiviral effect of diammonium glycyrrhizinate and lithium chloride on cell infection by pseudorabies herpesvirus. *Antiviral Res.* **2010**, *85*, 346–353. [CrossRef]

35. Chen, L.; Huang, G. The antiviral activity of polysaccharides and their derivatives. *Int. J. Biol. Macromol.* **2018**, *115*, 77–82. [CrossRef] [PubMed]
36. Wang, X.; Luo, J.; Wen, Z.; Shuai, L.; Wang, C.; Zhong, G.; He, X.; Cao, H.; Liu, R.; Ge, J.; et al. Diltiazem inhibits SARS-CoV-2 cell attachment and internalization and decreases the viral infection in mouse lung. *PLoS Pathog.* **2022**, *18*, e1010343. [CrossRef]
37. Song, X.; Yin, Z.; Zhao, X.; Cheng, A.; Jia, R.; Yuan, G.; Xu, J.; Fan, Q.; Dai, S.; Lu, H.; et al. Antiviral activity of sulfated Chuanmingshen violaceum polysaccharide against Newcastle disease virus. *J. Gen. Virol.* **2013**, *94*, 2164–2174. [CrossRef] [PubMed]
38. Battulga, T.; Tumurbaatar, O.; Ganzorig, O.; Ishimura, T.; Kanamoto, T.; Nakashima, H.; Miyazaki, K.; Yoshida, T. Analysis of interaction between sulfated polysaccharides and HIV oligopeptides by surface plasmon resonance. *Int. J. Biol. Macromol.* **2019**, *125*, 909–914. [CrossRef]
39. Hidari, K.I.; Takahashi, N.; Arihara, M.; Nagaoka, M.; Morita, K.; Suzuki, T. Structure and anti-dengue virus activity of sulfated polysaccharide from a marine alga. *Biochem. Biophys. Res. Commun.* **2008**, *376*, 91–95. [CrossRef]
40. Gao, Y.; Liu, W.; Wang, W.; Zhang, X.; Zhao, X. The inhibitory effects and mechanisms of 3,6-O-sulfated chitosan against human papillomavirus infection. *Carbohydr. Polym.* **2018**, *198*, 329–338. [CrossRef]
41. Liu, H.; Geng, M.; Xin, X.; Li, F.; Zhang, Z.; Li, J.; Ding, J. Multiple and multivalent interactions of novel anti-AIDS drug candidates, sulfated polymannuronate (SPMG)-derived oligosaccharides, with gp120 and their anti-HIV activities. *Glycobiology* **2005**, *15*, 501–510. [CrossRef] [PubMed]

Article

HSP27 Attenuates cGAS-Mediated IFN- β Signaling through Ubiquitination of cGAS and Promotes PRV Infection

Xiangrong Li ^{1,2,†} , Jingying Xie ^{1,3,†}, Dianyu Li ^{1,3}, Hongshan Li ^{1,3}, Yuhui Niu ^{1,3}, Bei Wu ^{1,3}, Yanmei Yang ^{1,3}, Zhenfang Yan ^{1,3}, Xiangbo Zhang ^{1,3}, Lei Chen ^{1,3} and Ruofei Feng ^{1,2,*} 

- ¹ Key Laboratory of Biotechnology and Bioengineering of State Ethnic Affairs Commission, Biomedical Research Center, Northwest Minzu University, Lanzhou 730030, China
² Gansu Tech Innovation Center of Animal Cell, Biomedical Research Center, Northwest Minzu University, Lanzhou 730030, China
³ College of Life Science and Engineering, Northwest Minzu University, Lanzhou 730030, China
* Correspondence: fengruofei@xbmu.edu.cn
† These authors contributed equally to this work.

Abstract: Pseudorabies (PR) is a domestic and wild animal infectious disease caused by the pseudorabies virus (PRV) and is one of the major infectious diseases that endanger the global swine industry. Studies have reported that PRV may achieve cross-species transmission from pigs to humans in recent years. Therefore, in-depth exploration of the relationship between PRV and host proteins is of great significance for elucidating the pathogenic mechanism of PRV and anti-PRV infection. Here, we report that heat shock protein 27 (HSP27) ubiquitinates and degrades cyclic GMP-AMP synthase (cGAS) and attenuates cGAS-mediated antiviral responses, thereby promoting PRV infection. Overexpression of HSP27 promoted PRV proliferation in vitro, while knockdown of HSP27 inhibited PRV infection. Importantly, we found that HSP27 inhibited PRV infection or poly(dA:dT)-activated IFN- β expression. Further studies found that HSP27 may inhibit cGAS-STING-mediated IFN- β expression through targeting cGAS. In addition, we found that HSP27 can suppress the expression of endogenous cGAS in different cells at both gene transcription and protein expression levels, and that HSP27 interacts with and ubiquitinates cGAS. In conclusion, we reveal for the first time that HSP27 is a novel negative regulator of the cGAS-STING signaling pathway induced by PRV infection or poly(dA:dT) activation and demonstrate that HSP27 plays a crucial role in PRV infection.

Keywords: pseudorabies virus; heat shock protein 27; cyclic GMP-AMP synthase; cGAS-STING signaling pathway; ubiquitination



Citation: Li, X.; Xie, J.; Li, D.; Li, H.; Niu, Y.; Wu, B.; Yang, Y.; Yan, Z.; Zhang, X.; Chen, L.; et al. HSP27 Attenuates cGAS-Mediated IFN- β Signaling through Ubiquitination of cGAS and Promotes PRV Infection. *Viruses* **2022**, *14*, 1851. <https://doi.org/10.3390/v14091851>

Academic Editors: Yan-Dong Tang and Xiangdong Li

Received: 31 July 2022

Accepted: 19 August 2022

Published: 23 August 2022

Publisher's Note: MDPI stays neutral with regard to jurisdictional claims in published maps and institutional affiliations.



Copyright: © 2022 by the authors. Licensee MDPI, Basel, Switzerland. This article is an open access article distributed under the terms and conditions of the Creative Commons Attribution (CC BY) license (<https://creativecommons.org/licenses/by/4.0/>).

1. Introduction

Innate immune response is the body's first line of defense against viral infection. Virus infection could induce host innate immune responses, and this plays an important as well as decisive role in the outcome of the infected host. The crucial point is that the host can establish an antiviral status to antagonize the invasion of the virus via identifying the components of invading virus through pattern recognition receptors (PRRs), which activate signaling pathways to produce type I interferons (IFN-I) [1]. The released IFN-I then binds to IFN receptors (IFNAR1 and/or IFNAR2) to activate the downstream JAK-STAT signaling pathway, eventually leading to the expression of a series of interferon-stimulated genes (ISGs). ISGs could realize numerous cellular consequences, including antiviral defense, antiproliferative activities, and stimulation of adaptive immunity [2–4].

For DNA virus, Toll-like receptor 9 (TLR9), cyclic GMP-AMP (cGAMP) synthase (cGAS), DAI (DLM-1/ZBP1), absent in melanoma 2 (AIM2), and IFN gamma-inducible protein 16 (IFI16) serve as the main PRRs that recognize viral DNA [5,6]. PRRs then recruit a series of signal transduction molecules, such as myeloid differentiation primary response gene 88 (MyD88), mitochondrial antiviral-signaling protein (MAVS), intracellular

stimulator of IFN genes (STING). These proteins then transfer the different signals to the downstream molecules in different signaling pathways, which eventually lead to activation and translocation of several transcription factors, including NF- κ B, interferon regulatory factor 3 (IRF3), and IRF7 into the nucleus to induce the expression of IFN-I and proinflammatory cytokines [7–9].

Pseudorabies virus (PRV) is a typical DNA virus. It belongs to the family *Herpesviridae*, subfamily *Alphaherpesvirinae*, genus *Varicellovirus*. PRV is the causative agent of Aujeszky's disease (AD, pseudorabies). Although the natural host of PRV is swine, it also threatens a wide range of other mammals [10–13]. PRV has a large linear double-stranded DNA genome that encodes more than 70 functional proteins [14]. PRV Bartha-K61 strain is a classic PRV vaccine strain commonly used worldwide. It naturally lacks the gE/gI gene, and its safety and effectiveness have been widely recognized. Recently, multiple PRV-encoded viral proteins were reported to inhibit host innate antiviral response which facilitate replication and latent viral infection [15]. For example, it has been reported that the viral glycoprotein gE/gI complex reduces the phosphorylation of ERK1/2 to suppress production of type I IFNs in plasmacytoid dendritic cells [16]. PRV UL50 suppresses type I IFN signaling by promoting lysosomal degradation of IFNAR1 [17]. In addition, PRV US3 inhibits IFN signaling by promoting degradation of the host protein Bclaf1 and IRF3 [18,19]. However, research about host proteins participating in mediating PRV immune evasion is limited.

Bcl2-associated athanogene (BAG) 3, which is a chaperone-mediated selective autophagy protein, plays a pivotal role in modulating the life cycle of a wide variety of viruses. During PRV infection, researchers found that PRV protein UL56 served as a novel BAG3 interactor by co-immunoprecipitation and co-localization analyses. The overexpression of pUL56 induced a significant degradation of BAG3 at protein level via the lysosome pathway. Overexpression of BAG3 significantly suppressed PRV proliferation, while knock-down of BAG3 resulted in increased viral replication in HEK293T cells [20]. Peroxiredoxin 1 (PRDX1) is a cellular antioxidant enzyme that is crucial for diverse fundamental biological processes, such as autophagy, inflammation, and carcinogenesis. Lin et al. reported that PRDX1 positively regulates interferon (IFN) induction and that pseudorabies virus (PRV) targets PRDX1 to evade IFN induction [21]. In addition, there are studies on the role of host restriction factors in the process of PRV infection, such as IFITM2 [22], ISG15 [23], ISG20 [24], and p53 [25]. They all play an inhibition role during PRV infection.

Heat-shock proteins (HSPs) were a conserved protein family whose major roles seemed to promote the correct folding and assembly of target proteins as well as prevent their aggregation [26]. Heat shock protein 27 (HSP27) is a member of a small heat shock protein family; it acts as both a protein chaperone and an antioxidant, involved in the inhibition of apoptosis and actin cytoskeletal remodeling [27]. Researchers have reported that HSP27 is a ubiquitin-binding protein, mediating I κ B α proteasomal degradation [28]. It also has been reported to interact with viral proteins and to be involved in viral replication [29–31]. Here, we demonstrate that HSP27 positively regulates PRV replication through attenuating the cGAS-STING signaling pathway.

2. Materials and Methods

2.1. Cells and Virus Strain

PK15, BHK-21, and HEK293 cells were cultured at 37 °C under 5% CO₂ incubator in Dulbecco's modified Eagle's medium (DMEM) containing 10% (*v/v*) new bovine serum (NBS). HEK293T cells were cultured at 37 °C under 5% CO₂ incubator in DMEM containing 10% (*v/v*) fetal bovine serum (FBS). PRV gE/gI-deleted vaccine strain Bartha-K61 was propagated and titrated in BHK-21 cells.

2.2. Plasmids and Reagents

A plasmid encoding Myc-tagged HSP27 was constructed by standard molecular cloning techniques. The expression plasmids HA-cGAS, Myc-STING, FLAG-TBK1, FLAG-

IRF3/5D (the active mutant of IRF3), and Myc-Ub were all constructed in the lab. All recombinant plasmids were identified by sequencing.

The antibodies and chemical reagents used in this study were as follows: anti-Myc tag (60003-2-Ig), anti-Flag tag (20543-1-AP), anti-HA tag (51064-2-AP), anti-IRF3 (11312-1-AP), anti-HSP27 (18284-1-AP), and anti-GAPDH (60004-1-Ig) were purchased from Proteintech (Wuhan, China); anti-TBK1 (38066) and anti-STING (D2P2F) were purchased from Cell Signaling Technology (Boston, MA, USA); anti-phospho-IRF3 (AP0623) was purchased from ABclonal Technology (Wuhan, China); anti-cGAS (D163570) and anti-Ub (D220023) were purchased from Sangon Biotech (Shanghai, China); horseradish peroxidase (HRP) affinity-purified goat anti-mouse IgG (115-035-003) and anti-rabbit IgG (111-035-003) were purchased from Jackson ImmunoResearch Laboratories (West Grove, PA, USA). Lipofectamine 2000 (11668019) and lipofectamine 3000 (L3000015) were purchased from Invitrogen (Waltham, MA, USA). Evo M-MLV Mix Kit with gDNA Clean for qPCR (AG11728) was purchased from Accurate Biology (Changsha, China). TransStart Top Green qPCR SuperMix (+Dye II) was purchased from Transgen Biotech (Beijing, China). NP-40 lysis buffer (P0013F), RIPA lysis buffer (P0013K), protease and phosphatase inhibitor (P1050), Protein G Agarose (P2009), caspase 3 inhibitor Ac-DEVD-CHO (C1206) and proteasome inhibitor MG132 (S1748) were purchased from Beyotime Biotechnology (Shanghai, China). Endosomal acidification and autophagy inhibitor chloroquine (ttrl-chq) and poly (dA:dT) (ttrl-patn) were obtained from InvivoGen (San Diego, CA, USA). Western lightning plus chemiluminescence reagent (NEL105001EA) was purchased from PerkinElmer (Waltham, MA, USA).

2.3. Transfection and RNA Interference

BHK-21, HEK293, or HEK293T cells in 6-well plates were transiently transfected with indicated plasmids or siRNA oligos using Lipofectamine 2000 (Invitrogen, Waltham, MA, USA) according to the manufacturer's instructions. PK15 cells in 6-well plates were transfected with indicated plasmids, siRNA oligos, or poly (dA:dT) (InvivoGen, San Diego, CA, USA) using Lipofectamine 3000 (Invitrogen, Waltham, MA, USA) according to the manufacturer's instructions. The siRNA targeting HSP27 (siHSP27, 5'-GCUGCAAAAUCCGAUGAGA-3') and siRNA of negative control (siNC, 5'-GUUCUCCGAACGUGTCACGU-3') were synthesized by Guangzhou Ribo Biotechnology (Guangzhou, China). At 24 h post-transfection, the effects of HSP27 overexpression or interference were identified by Western blotting.

2.4. RNA Extraction and Quantitative Real-Time PCR

Cellular RNA was extracted from RNAiso Plus (Takara, Beijing, China) and transcribed into cDNA by Evo M-MLV Mix Kit with gDNA Clean for qPCR (Accurate, Changsha, China). A TransStart Top Green qPCR SuperMix (+Dye II) (Transgen, Beijing, China) was used for relative real-time quantitative PCR (RT-qPCR). The mRNA expression levels of IFN- β and cGAS were normalized to that of β -actin using the $\Delta\Delta C_t$ method, respectively. The primer sequences used were as follows: Homo sapiens IFN- β -qF, 5'-TTGTTGAGAACCTCCTGGCT-3'; Homo sapiens IFN- β -qR, 5'-TGACTATGGTCCAGGCA CAG-3'; Homo sapiens cGAS-qF, 5'-AGGAAGCAACTACGACTAAAGCC-3'; Homo sapiens cGAS-qR, 5'-CGATGTGAGAGAAGGATAGCCG-3'; Homo sapiens β -actin-qF, 5'-TGGCACCCAGCACAATGAA-3'; Homo sapiens β -actin-qR, 5'-CTAAGTCATAGTCCGCC TAGAAGCA-3'; Sus scrofa IFN- β -qF, 5'-TCCACCACAGCTCTTCCAT-3'; Sus scrofa IFN- β -qR, 5'-CTGGAATTGTGGTGGTTGCA-3'; Sus scrofa cGAS-qF, 5'-GCACCGGAGCTAC TATGAG-3'; Sus scrofa cGAS-qR, 5'-CTCTCCACAGTGACACCTTCT-3'; Sus scrofa β -actin-qF, 5'-CAAGGACCTCTACGCCAACAC-3'; Sus scrofa β -actin-qR, 5'-TGGAGGCGCGATG ATCTT-3'.

2.5. Co-Immunoprecipitation and Western Blotting

Cells were lysed with NP-40 lysis buffer (50 mM Tris [pH 7.4], 150 mM NaCl, 1% NP-40, EDTA, leupeptin), or RIPA lysis buffer (50 mM Tris [pH 7.4], 150 mM NaCl, 1% Triton X-100, 1% sodium deoxycholate, 0.1% SDS) containing a protease and phosphatase inhibitor (52.5 mM AEBSF, 40 μ M Aprotinin, 2.5 mM Bestatin, 0.75 mM E64, 1 mM Leupeptin, 0.75 mM Pepstatin A, 250 mM sodium fluoride, 50 mM sodium pyrophosphate, 50 mM β -glycerophosphate, 50 mM sodium orthovanadate) for 30 min on ice. For immunoprecipitation assay, the supernatant after centrifugation was incubated with anti-Myc antibody or anti-HA antibody (Proteintech, Wuhan, China) for 12 h at 4 °C, and the re-suspended Protein G Agrose (Beyotime, Shanghai, China) was added and incubated for 4 h at 4 °C. The complexes were centrifuged and washed 5 times with pre-chilled lysis buffer. Precipitates or cell extracts were suspended in 1x SDS loading buffer, boiled at 95 °C for 10 min, and used for Western blotting analysis. These samples were isolated in 10% SDS-PAGE gel and transferred to PVDF membranes (Merck, Darmstadt, Germany). PVDF membranes were sequentially incubated with the indicated primary antibodies and HRP-labeled goat anti-mouse IgG or goat anti-rabbit IgG (Jackson ImmunoResearch, West Grove, PA, USA). These bound protein bands were detected using Western Lightning Plus chemiluminescence reagent (PerkinElmer, Waltham, MA, USA).

2.6. PRV Infection and Infectivity Assays

For in vitro virus infection, treated or untreated PK15 cells or HEK293 cells were washed 3 times with PBS and infected with PRV Bartha-K61 strain (MOI = 0.001) for 24 h or 48 h in a 37 °C, 5% CO₂ incubator. After freeze-thawing of the cell suspension 3 times, the supernatant was collected by centrifugation. The DNA was extracted from the viral stock using TIANamp virus DNA/RNA Kit (TIANGEN, Beijing, China), and the copy number of PRV UL37 gene was detected by absolute RT-qPCR using the Premix Ex Taq Probe qPCR (Takara, Beijing, China); the viral stock was serially diluted 10 times, and the PRV titers were detected in BHK-21 cells by the Reed-Muench method. The primers and probe sequences of absolute RT-qPCR used were as follows: PRV-UL37-qF, 5'-GGACTACATGTTCCCCACGG-3'; PRV-UL37-qR, 5'-TAGAACGGCGTCAGGAATCG-3'; PRV probe, 5'-(FAM) CCACGGCCGTCACGA (Eclipse)-3'.

2.7. Inhibitor Treatment Assay

HEK293 cells cultured in 6-well plates were transfected with Myc-HSP27 plasmid or pCMV-Myc plasmid (empty vector, EV) using Lipofectamine 2000. At 24 h post-transfection, the cells were treated with proteasome inhibitor MG132 (Beyotime, Shanghai, China), endosomal acidification and autophagy inhibitor chloroquine (InvivoGen, San Diego, CA, USA), caspase 3 inhibitor Ac-DEVD-CHO (Beyotime, Shanghai, China), or DMSO for 12 h, respectively. The supernatant after cell lysis was collected and subjected to Western blotting analysis.

2.8. cGAS Polyubiquitination Assay

The experiment was performed as described previously [32,33]. HEK293 cells were cotransfected with HA-cGAS, Myc-Ub, and EV or Myc-HSP27 plasmid using the Lipofectamine 2000. At 24 h post-transfection, cells were lysed and cGAS-ubiquitin complexes were immunoprecipitated with anti-HA antibody, and the ubiquitinated protein was detected with anti-Myc antibody.

2.9. Statistical Analysis

Data analyses were performed using GraphPad Prism 9.0 software. One-way ANOVA or two-way ANOVA were used to evaluate statistical significance. Among them, a *p* value of <0.05 was considered statistically significant, and *p* values of <0.01 or 0.001 were considered highly statistically significant.

3. Results

3.1. Overexpression of HSP27 Facilitates PRV Infection In Vitro

To explore the role of HSP27 in the process of PRV infection, PK15 cells were transfected with EV or Myc-HSP27 plasmid and then infected with PRV (MOI = 0.001) for 24 h or 48 h. We observed that endogenous and exogenous HSP27 proteins could be detected simultaneously only in the Myc-HSP27 transfection group, and the exogenous HSP27 protein expression showed an increasing trend with the prolongation of PRV infection time (Figure 1A). Overexpression of HSP27 significantly increased the viral copy number and titers of PRV in a time-dependent manner (Figure 1B,C), indicating that overexpression of HSP27 can promote PRV proliferation in PK15 cells.

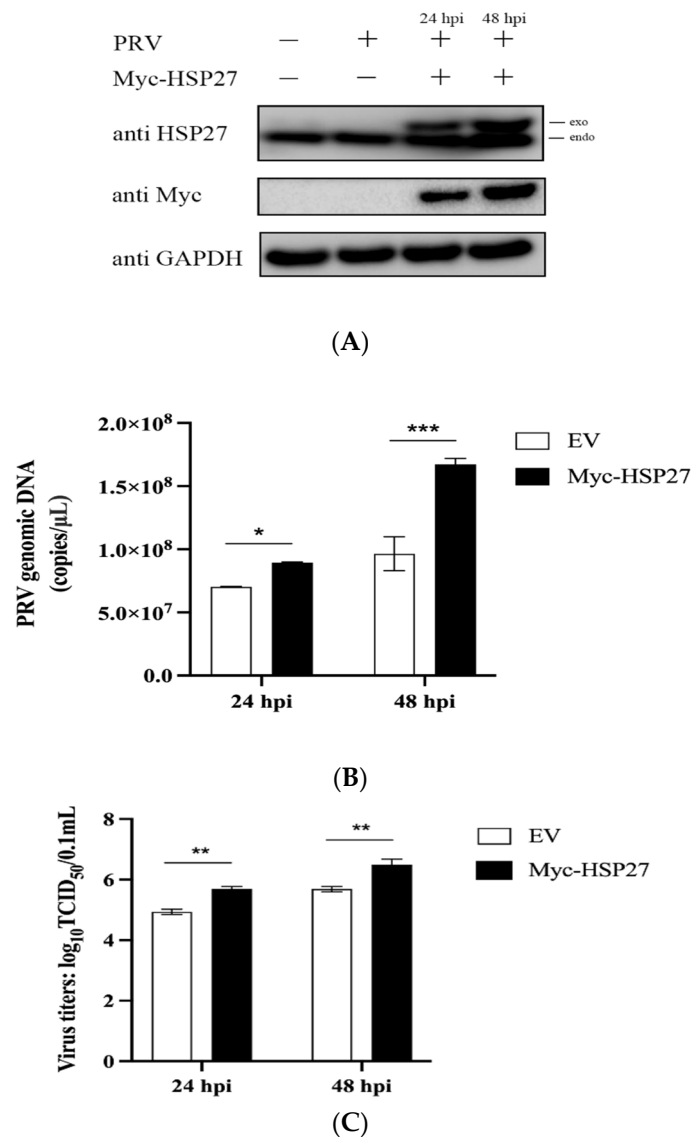


Figure 1. Overexpression of HSP27 facilitates PRV infection in PK15 cells. PK15 cells were transiently transfected with 1 μg of EV or Myc-HSP27 plasmid using Lipofectamine 3000 for 24 h followed by PRV infection (MOI = 0.001) for 24 h or 48 h. (A) Western blotting was used to detect endogenous and exogenous HSP27 proteins expression. GAPDH was used as a loading control. (B) Absolute RT-qPCR and (C) TCID₅₀ assay (Reed-Muench method) were used to detect viral copy number and titers of PRV. All the data were represented as mean ± standard deviation (SD) of three independent experiments and analyzed by two-way ANOVA in B and C, * $p < 0.05$, ** $p < 0.01$, *** $p < 0.001$.

3.2. Interfering with HSP27 Restrains PRV Infection In Vitro

We next transfected PK15 with siNC or siHSP27 for 24 h and then infected it with PRV (MOI = 0.001) for 24 h or 48 h. In contrast to the above results of overexpressing of HSP27, knockdown of endogenous HSP27 expression in PK15 cells reduced the viral copy number of PRV (Figure 2A), and similar results were also detected in HEK293 cells (Figure 2B). Taken together, these results suggested that HSP27 is a positive regulator during infection.

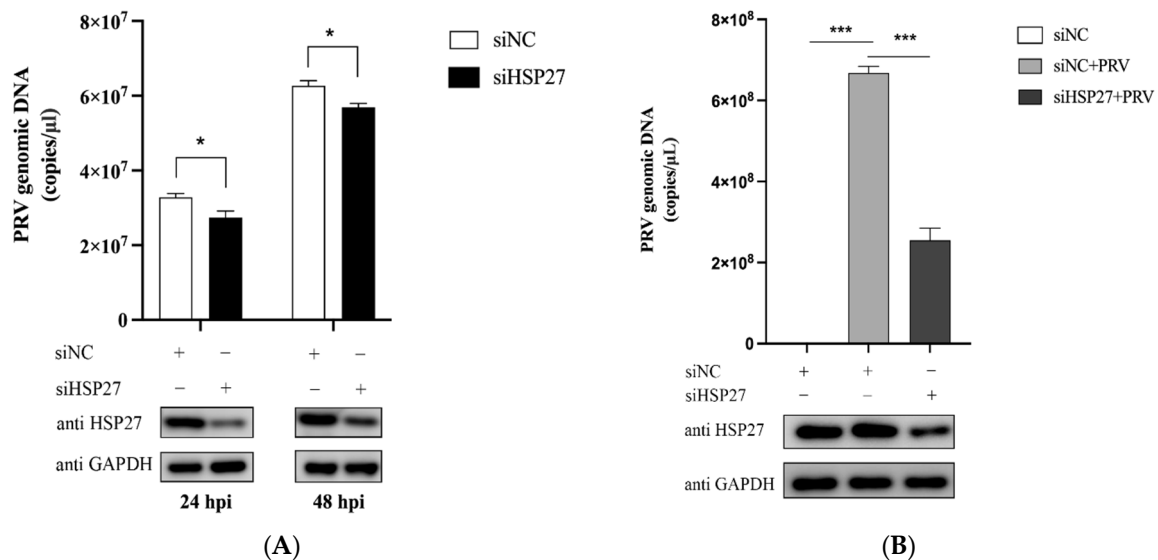


Figure 2. Interference with HSP27 inhibits PRV proliferation in PK15 and HEK293 cells. (A) PK15 cells were transiently transfected with siNC or siHSP27 using Lipofectamine 3000 for 24 h followed by PRV infection (MOI = 0.001) for 24 h or 48 h. Absolute RT-qPCR (upper panel) was used to detect the viral copy number of PRV. Western blotting (lower panel) was used to detect endogenous HSP27 protein expression. GAPDH was used as a loading control. (B) HEK293 cells were transiently transfected with siNC or siHSP27 using Lipofectamine 2000 for 24 h followed by PRV infection (MOI = 0.001) for 60 h. Absolute RT-qPCR (upper panel) was used to detect viral copy number of PRV. Western blotting (lower panel) was used to detect endogenous HSP27 protein expression. GAPDH was used as a loading control. All the data were represented as mean \pm SD of three independent experiments and analyzed by two-way ANOVA in A or one-way ANOVA in B, * $p < 0.05$, *** $p < 0.001$.

3.3. HSP27 Inhibits PRV Infection or Poly(dA:dT)-Activated IFN- β Expression

To further explore whether HSP27 assisting PRV infection is related to IFN- β production, PK15 cells were transfected with Myc-HSP27 plasmid for 24 h and then infected with PRV. Results showed that PRV infection could indeed significantly enhance IFN- β mRNA expression level in PK15 cells; however, this activation was significantly reduced when HSP27 was overexpressed (Figure 3A). Poly(dA:dT) is a repetitive synthetic double-stranded DNA sequence of poly(dA-dT):poly(dT-dA) and a synthetic analog of B-DNA, which acts as an agonist of cytosolic DNA sensors in this study, such as cGAS [34]. PK15 cells were transfected with Myc-HSP27 plasmid before poly(dA:dT) transfection to determine the effect of HSP27 on poly(dA:dT)-activated IFN- β expression. Interestingly, poly(dA:dT) stimulated a much lower level of IFN- β expression in HSP27-overexpressing PK15 cells (Figure 3B). Moreover, we also found that the IFN- β expression activated by PRV infection was even more intense when endogenous HSP27 expression was downregulated in HEK293 cells (Figure 3C). Collectively, these results demonstrated that HSP27 negatively regulates PRV-triggered or poly(dA:dT)-activated IFN- β expression.

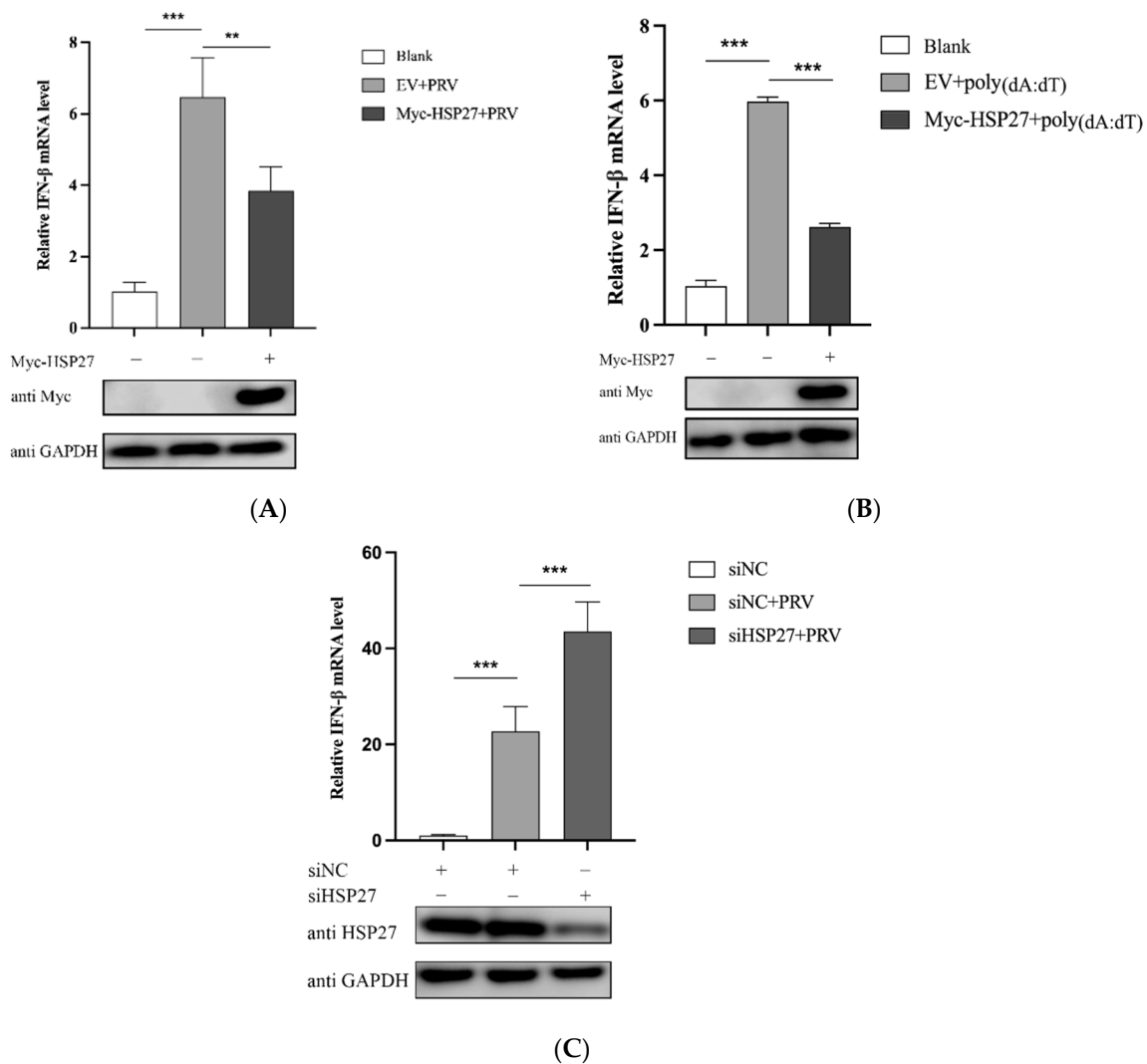


Figure 3. HSP27 negatively regulates PRV-triggered or poly(dA:dT)-activated IFN- β expression. (A) PK15 cells were transiently transfected with 1 μ g of EV or Myc-HSP27 plasmid using Lipofectamine 3000 for 24 h followed by PRV infection (MOI = 0.001) for 24 h. RT-qPCR (upper panel) was used to detect the relative expression level of IFN- β mRNA. Western blotting (lower panel) was used to detect Myc-tagged HSP27 protein expression. GAPDH was used as a loading control. (B) PK15 cells were transiently transfected with 1 μ g of EV or Myc-HSP27 plasmid using Lipofectamine 3000 for 24 h followed by poly(dA:dT) transfection for 24 h. RT-qPCR (upper panel) was used to detect the relative expression level of IFN- β mRNA. Western blotting (lower panel) was used to detect Myc-tagged HSP27 protein expression. GAPDH was used as a loading control. (C) HEK293 cells were transiently transfected with siNC or siHSP27 using Lipofectamine 2000 for 24 h followed by PRV infection (MOI = 0.001) for 24 h. RT-qPCR (upper panel) was used to detect the relative expression level of IFN- β mRNA. Western blotting (lower panel) was used to detect endogenous HSP27 protein expression. GAPDH was used as a loading control. All the data were represented as mean \pm SD of three independent experiments and analyzed by one-way ANOVA in A–C, ** $p < 0.01$, *** $p < 0.001$.

3.4. HSP27 Attenuates PRV-Triggered cGAS-Mediated Signaling Cascade

Given that PRV is a DNA virus that activates IFN- β production mainly through the cGAS-STING signaling cascade [19,35], we next examined whether HSP27 affects the expression of adaptor molecules in the PRV-triggered cGAS-STING signaling pathway. As shown in Figure 4, PRV infection did enhance the protein expression of adaptor molecules in the cGAS-STING signaling pathway, such as cGAS, STING, TBK1, and phosphorylated

IRF3. Furthermore, we also found that the protein expression of cGAS and phosphorylated IRF3 were dramatically reduced in the HSP27-overexpressing PK15 cells, while the protein expression of STING, TBK1, and IRF3 were not significantly different from those in the EV group. These data all indicated that HSP27 could impair the PRV-induced activation of the cGAS-STING signaling pathway.

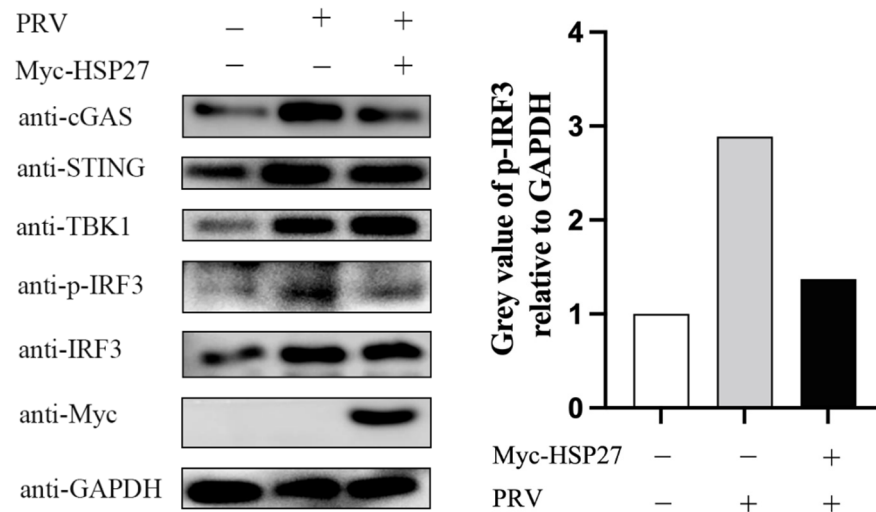


Figure 4. HSP27 inhibits the protein expression levels of adaptor molecules in the cGAS-STING signaling pathway induced by PRV. PK15 cells were transiently transfected with 1 μ g of EV or Myc-HSP27 plasmid using Lipofectamine 3000 for 24 h followed by PRV infection (MOI = 0.001) for 24 h. Western blotting was used to detect the protein expression of cGAS, STING, TBK1, IRF3, phosphorylated IRF3, and Myc-tagged HSP27. GAPDH was used as a loading control (left). Greyscale analysis was used to measure the protein expression level of phosphorylated IRF3 relative to GAPDH (right).

3.5. HSP27 Inhibits cGAS-STING-Mediated IFN- β Expression through Targeting cGAS

To further clarify which one or several of adaptor molecules in the cGAS-STING pathway were specifically inhibited by HSP27, we cotransfected PK15 cells with Myc-HSP27 and HA-cGAS, Myc-STING, FLAG-TBK1, or FLAG-IRF3/5D, respectively. The results showed that HSP27 clearly reduced the gene transcriptional expression of IFN- β activated by cGAS (Figure 5A), STING (Figure 5B), TBK1 (Figure 5C), or IRF3 (Figure 5D). Moreover, HSP27 significantly weakened the protein expression of exogenous cGAS (Figure 5A), and had no effect on the protein expression of exogenous STING, TBK1, and IRF3 (Figure 5B–D). Western blotting analysis of HEK293 cells also showed similar results (Figure 5E). Based on all the current results, we speculated that cGAS is a target molecule for HSP27 to attenuate cGAS-STING-mediated IFN- β production.

3.6. HSP27 Suppresses Endogenous cGAS Expression in Different Cells

Next, in order to explore whether HSP27 affects the protein expression of endogenous cGAS, STING, TBK1, and IRF3, we transfected EV or Myc-HSP27 plasmid into PK15, HEK293 and BHK-21 cells for 24 h, respectively. The results showed that endogenous cGAS proteins were degraded to varying degrees in different types of HSP27-overexpressing cells, while the protein expression of other adaptor molecules did not change significantly (Figure 6A). Similar results were also detected in gene transcriptional expression of cGAS in the HSP27-overexpressing PK15 or HEK293 cells (Figure 6B). These results indicated that HSP27 represses the gene transcription and protein expression of endogenous cGAS.

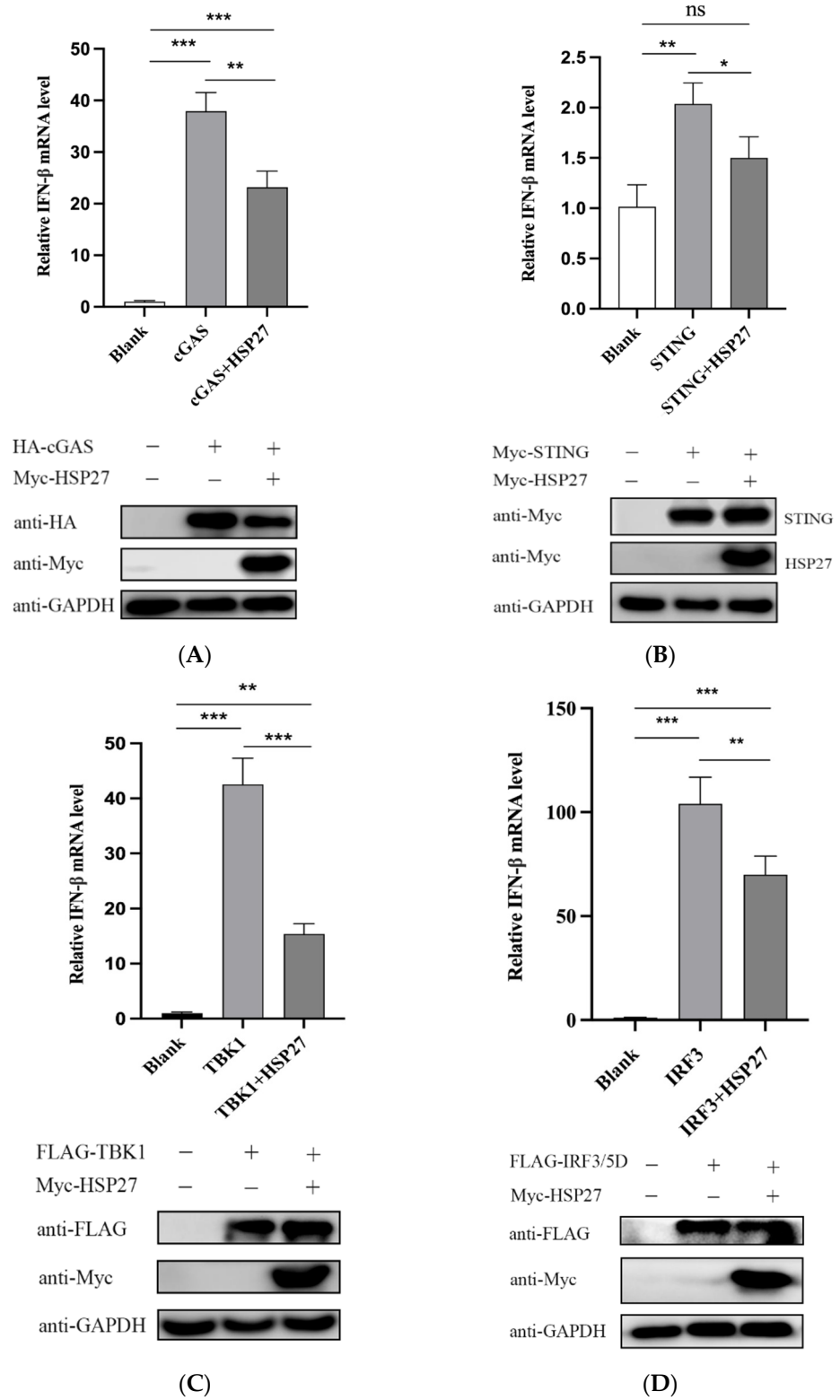


Figure 5. Cont.

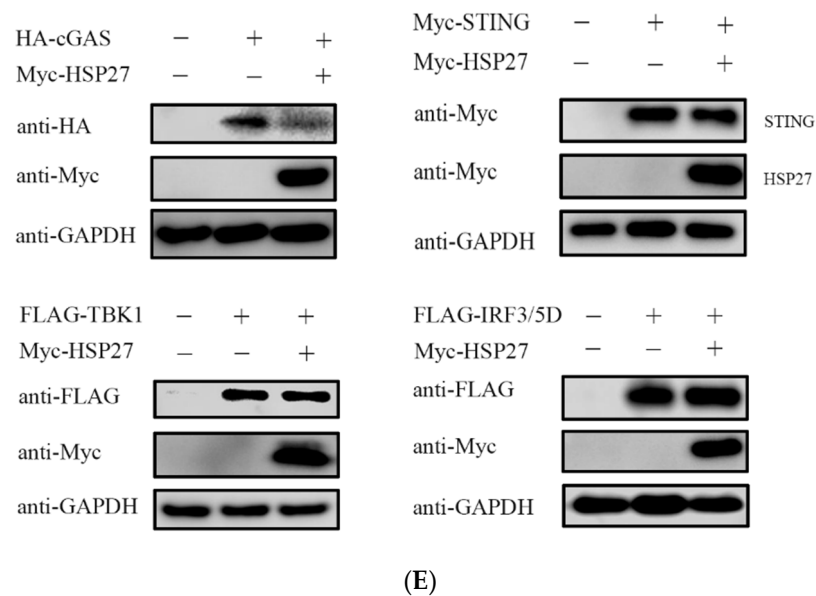


Figure 5. HSP27 inhibits cGAS-STING-mediated IFN- β expression through targeting cGAS. PK15 cells were cotransfected with EV or Myc-HSP27 plasmid and HA-cGAS, Myc-STING, FLAG-TBK1, or FLAG-IRF3/5D plasmid using Lipofectamine 3000 for 24 h, respectively. (A) RT-qPCR (upper panel) was used to detect the relative expression level of IFN- β mRNA. Western blotting (lower panel) was used to detect the protein expression of HA-tagged cGAS and Myc-tagged HSP27. GAPDH was used as a loading control. (B) RT-qPCR (upper panel) was used to detect the relative expression level of IFN- β mRNA. Western blotting (lower panel) was used to detect the protein expression of Myc-tagged STING and Myc-tagged HSP27. GAPDH was used as a loading control. (C) RT-qPCR (upper panel) was used to detect the relative expression level of IFN- β mRNA. Western blotting (lower panel) was used to detect the protein expression of FLAG-tagged TBK1 and Myc-tagged HSP27. GAPDH was used as a loading control. (D) RT-qPCR (upper panel) was used to detect the relative expression level of IFN- β mRNA. Western blotting (lower panel) was used to detect the protein expression of FLAG-tagged IRF3 and Myc-tagged HSP27. GAPDH was used as a loading control. (E) HEK293 cells were cotransfected with EV or Myc-HSP27 plasmid and HA-cGAS, Myc-STING, FLAG-TBK1, or FLAG-IRF3/5D plasmid using Lipofectamine 2000 for 24 h, respectively. Western blotting was used to detect the protein expression of HA-tagged cGAS, Myc-tagged STING, FLAG-tagged TBK1, FLAG-tagged IRF3 and Myc-tagged HSP27, respectively. GAPDH was used as a loading control. All the data were represented as mean \pm SD of three independent experiments and analyzed by one-way ANOVA in A–D, * $p < 0.05$, ** $p < 0.01$, *** $p < 0.001$.

3.7. HSP27 Interacts with cGAS and Promotes cGAS Ubiquitination

To verify whether there is a physical interaction between HSP27 and cGAS, we cotransfected HEK293T cells with Myc-HSP27 and HA-cGAS for 24 h. Cells were harvested and lysed for co-immunoprecipitation experiment. The results showed that HA-tagged cGAS protein could be immunoprecipitated after coating Protein G Agarose with Myc-tagged antibody (Figure 7A). Likewise, Myc-tagged HSP27 protein could be immunoprecipitated after coating Protein G Agarose with HA-tagged antibody (Figure 7B). These data fully supported that HSP27 binds directly to cGAS.

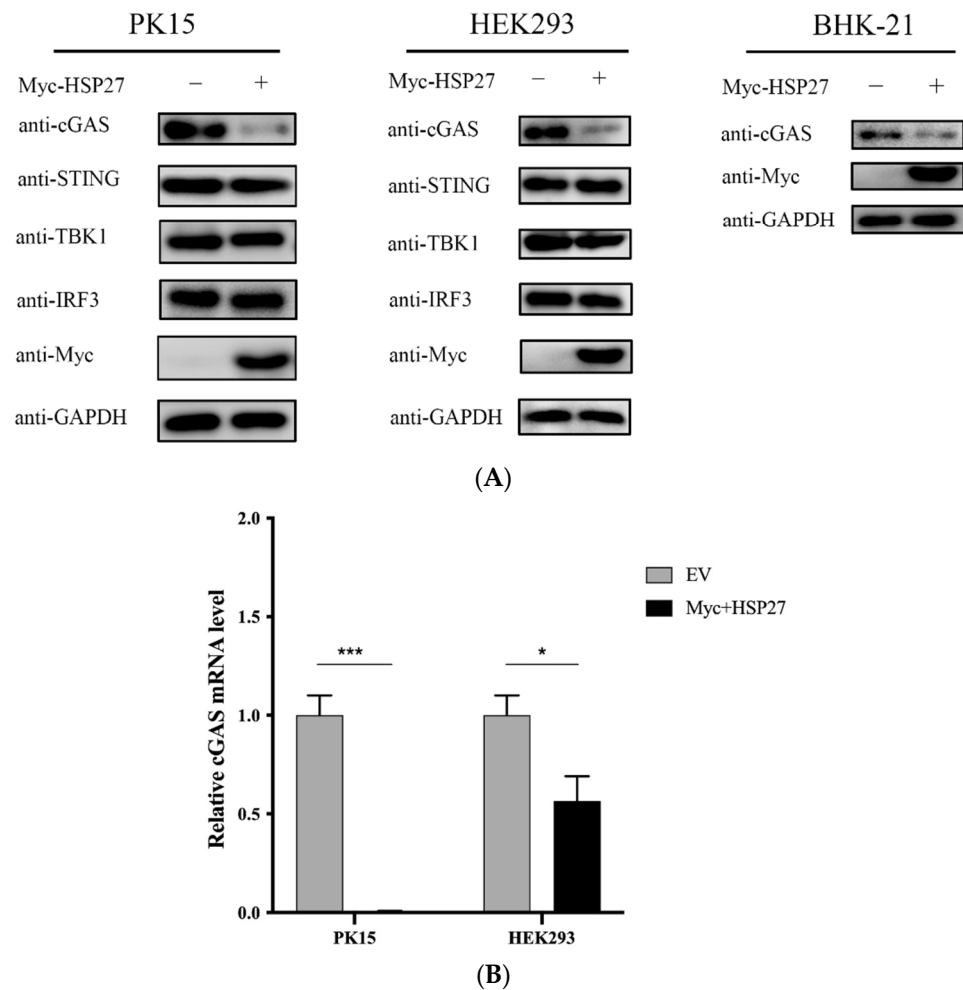


Figure 6. HSP27 suppresses the gene transcription and protein expression levels of endogenous cGAS in different cells. PK15, HEK293 or BHK-21 cells were transiently transfected with 1 μ g EV or Myc-HSP27 plasmid using Lipofectamine 3000 or Lipofectamine 2000 for 24 h, respectively. **(A)** Western blotting was used to detect the protein expression of endogenous cGAS, STING, TBK1, IRF3, and Myc-tagged HSP27 in the above-transfected PK15 and HEK293 cells. Western blotting was used to detect the protein expression of endogenous cGAS and Myc-tagged HSP27 in the above-transfected BHK-21 cells. GAPDH was used as a loading control. **(B)** RT-qPCR was used to detect the relative expression level of cGAS mRNA in the above-transfected PK15 and HEK293 cells. All the data were represented as mean \pm SD of three independent experiments and analyzed by two-way ANOVA in B, * $p < 0.05$, *** $p < 0.001$.

For the sake of exploring whether HSP27-mediated cGAS degradation is dependent on the endosomal acidification and autophagy pathway, the caspase-3-dependent apoptosis pathway, or the ubiquitin-proteasome pathway, HEK293 cells were first transfected with Myc-HSP27 plasmid for 24 h, followed by treatment with endosomal acidification and autophagy inhibitor chloroquine (CQ), caspase 3 inhibitor Ac-DEVD-CHO (DEVD), ubiquitin-proteasome inhibitor MG132, or DMSO for 12 h, respectively. It was found that HSP27-mediated cGAS degradation was blocked by MG132, but not CQ or DEVD (Figure 7C), suggesting that HSP27 degrades cGAS mainly through the ubiquitin-proteasome pathway. It has been reported that ubiquitination modification can strictly regulate the stability and activity of cGAS [36], so we hypothesized that HSP27 affects the ubiquitination of cGAS, and subsequent ubiquitination assay confirmed this hypothesis (Figure 7D).

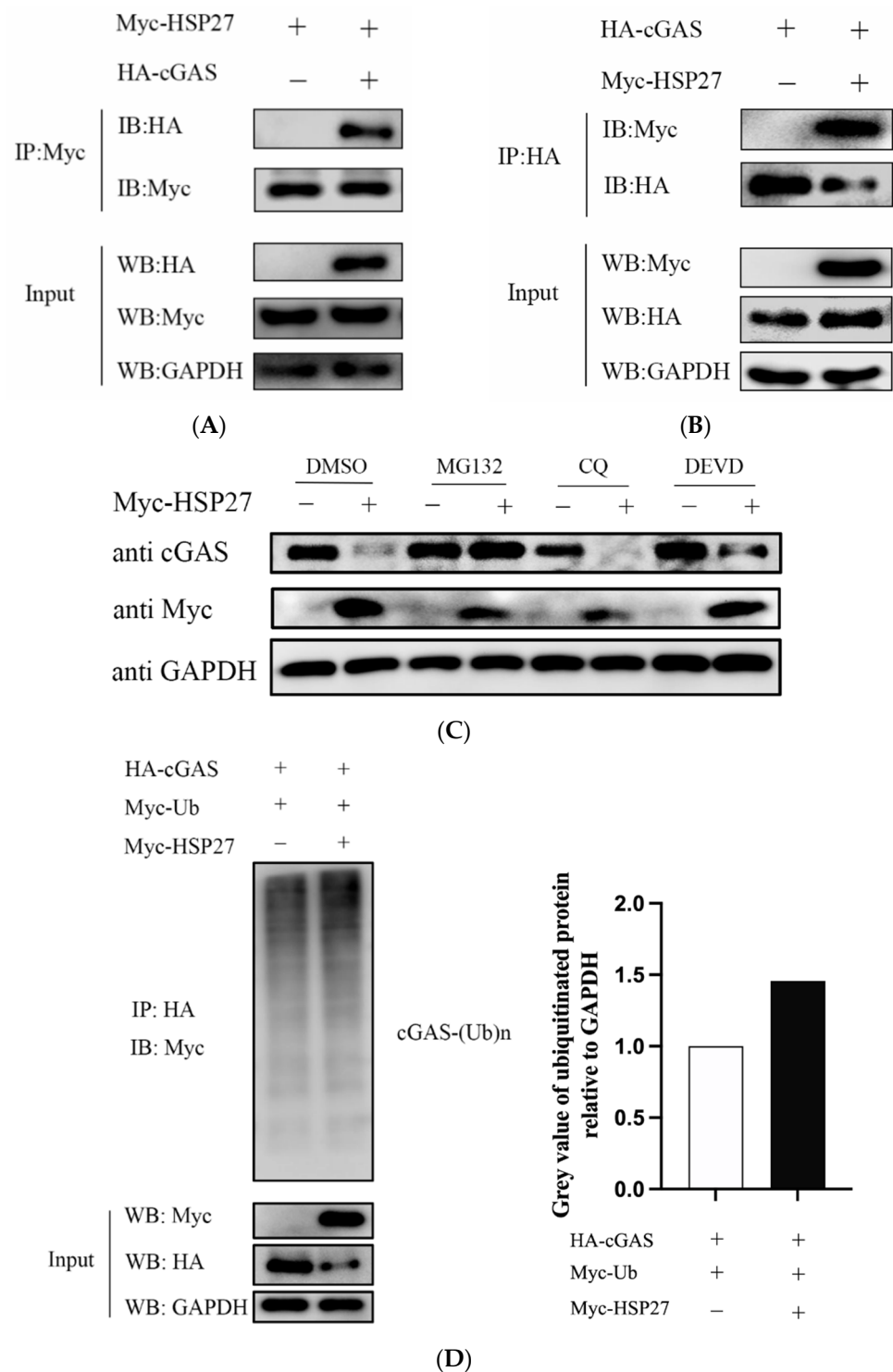


Figure 7. HSP27 interacts with cGAS and promotes cGAS ubiquitination. **(A)** HEK293T cells were cotransfected with Myc-HSP27 plasmid and pCMV-HA or HA-cGAS plasmid using Lipofectamine 2000 for 24 h, respectively. Cells were then lysed and immunoprecipitated with anti-Myc antibody. Western blotting was used to detect Myc-tagged HSP27 protein and HA-tagged cGAS protein in the whole cell lysates (Input) and immunoprecipitation (IP) complexes, respectively. **(B)** HEK293T cells were cotransfected with HA-cGAS plasmid and EV or Myc-HSP27 plasmid using Lipofectamine 2000 for 24 h, respectively. Cells were then lysed and immunoprecipitated with anti-HA antibody. Western blotting was used to detect HA-tagged cGAS protein and Myc-tagged HSP27 protein in the Input

and IP complexes, respectively. (C) HEK293 cells were transiently transfected with 1 µg of EV or Myc-HSP27 plasmid using Lipofectamine 2000 for 24 h and then treated for 12 h with MG132 (7.5 µM), CQ (50 µM), DEVD (50 µM), or DMSO, respectively. Western blotting was used to detect the protein expression of endogenous cGAS and Myc-tagged HSP27. GAPDH was used as a loading control. (D) HEK293 cells were cotransfected with HA-cGAS + Myc-Ub + EV or HA-cGAS + Myc-Ub + Myc-HSP27 plasmid at a 1:1:1 ratio using the Lipofectamine 2000 for 24 h, respectively. Cells were then lysed, and cGAS-ubiquitin complexes were immunoprecipitated with anti-HA antibody and immunoblotted with anti-Myc antibody to detect ubiquitinated protein. GAPDH was used as a loading control (left). Greyscale analysis was used to measure the protein expression level of ubiquitinated protein relative to GAPDH (right).

4. Discussion

Although the natural host of PRV is swine, it can also infect a variety of livestock and wildlife. In recent years, some cases of pseudorabies have been reported at home and abroad, but there is no conclusive evidence. In 2019, domestic researchers successfully isolated a human PRV strain hSD-1/2019 from the cerebrospinal fluid of patients for the first time [37], which provides direct evidence for the cross-species transmission of PRV from pigs to humans, suggesting that PRV may have the importance of zoonosis. Therefore, it is even more urgent to clarify the molecular mechanism of PRV pathogenesis. In-depth exploration of the relationship between PRV and host proteins is of great significance for elucidating the pathogenic mechanism of PRV and anti-PRV infection.

PRV has broad cell tropism and can proliferate in a variety of cell lines, such as PK15, Vero, MDBK and BHK-21 cells. Our research group also found that PRV can replicate effectively in human-derived cell lines, such as HEK293 cells. Therefore, PK15 cells, BHK-21 cells and HEK293 cells were used in this study. The results showed that HSP27 can not only degrade the protein expression of exogenous cGAS, but also weaken the gene transcription and protein expression of endogenous cGAS. Moreover, HSP27 could degrade the expression of porcine-derived, murine-derived and human-derived cGAS, indicating that HSP27 has specificity and universality for the recognition and degradation of cGAS. Because HEK293T cells lack endogenous cGAS [38], HEK293T cells are mainly used for co-immunoprecipitation assay of exogenous cGAS and HSP27. Subsequent results showed that HSP27 directly binds to cGAS and promotes the ubiquitination and degradation of cGAS. There are about more than 70 kinds of structural and nonstructural proteins in PRV [14]. Although the roles of some viral proteins in viral infection have been confirmed [15–19,32,35], the role of a considerable number of viral proteins remain unknown. Further studies are needed to confirm whether the viral proteins of PRV participate in the regulation of HSP27 on cGAS-STING signaling pathway to achieve active immune escape.

Many studies have shown that HSP27 regulates the proliferation of RNA viruses, mainly through the NF-κB signaling pathway, RLR signaling pathway, or autophagy pathway. HSP27 promotes the replication of foot-and-mouth disease virus (FMDV) by interacting with the structural protein VP2 of FMDV and activating the autophagy-related pathway EIF2S1-ATF4-AKT-MTOR [39]. HSP27 inhibits the proliferation of encephalomyocarditis virus (EMCV) by stabilizing the expression of MDA5 and thus positively regulating the RLR/MDA5 signaling pathway [31]. HSP27 negatively regulates the replication of classical swine fever virus (CSFV) by directly interacting with non-structural protein NS5A and promoting the activation of the NF-κB signaling pathway [40]. However, there are few studies on the mechanism of HSP27 regulating DNA virus proliferation. This study is the first to report the relationship between HSP27 and cGAS, a cytosolic DNA sensor, which provides a reference for future research of HSP27 in DNA viruses. Given that HSP27 is a multifunctional protein that can participate in multiple immunomodulatory processes of the body, whether it also regulates other signal pathway related molecules in PRV infection still needs to be further explored. HSP27 contributes to PRV infection, so HSP27 inhibitors

are expected to be candidates for PRV-targeted therapy, and HSP27 stable cell lines may also be used in large-scale culture and proliferation of PRV.

There are four main modifications of cGAS: ubiquitination, phosphorylation, acetylation, and palmitoylation [36,41–43]. Among them, ubiquitination modification is an important form of protein post-translational modification, which can regulate and change the properties and functions of proteins, such as activity and stability. It is widely involved in many physiological processes, such as protein degradation, cell cycle regulation, immune response regulation, and DNA damage repair. Here, we report that HSP27 attenuates the cGAS-mediated interferon signaling cascade by promoting cGAS ubiquitination and proteasomal-dependent degradation. K48-linked ubiquitination modification is the most common of all ubiquitin chains, accounting for about 50% of all ubiquitination modifications, and it is closely related to proteasomal degradation. Therefore, it is speculated that the way that HSP27 ubiquitinates cGAS may be K48-linked, which requires further investigation.

In this study, we found that overexpression of HSP27 contributed to PRV infection, and knockdown of HSP27 suppressed PRV infection in vitro. HSP27 inhibited PRV infection or poly(dA:dT)-activated IFN- β expression. Interestingly, we found that HSP27 attenuated cGAS-STING-mediated IFN- β expression through targeting cGAS. Further studies found that HSP27 bound directly to cGAS and promoted cGAS degradation by ubiquitination, and impaired the cGAS-mediated signaling cascade and IFN- β expression, thereby promoting PRV infection (Figure 8). In conclusion, we demonstrate for the first time that HSP27 is a novel negative regulator of the cGAS-STING signaling pathway, reveal a novel mechanism by which HSP27 facilitates PRV infection, and confirm that HSP27 plays a crucial role in PRV infection.

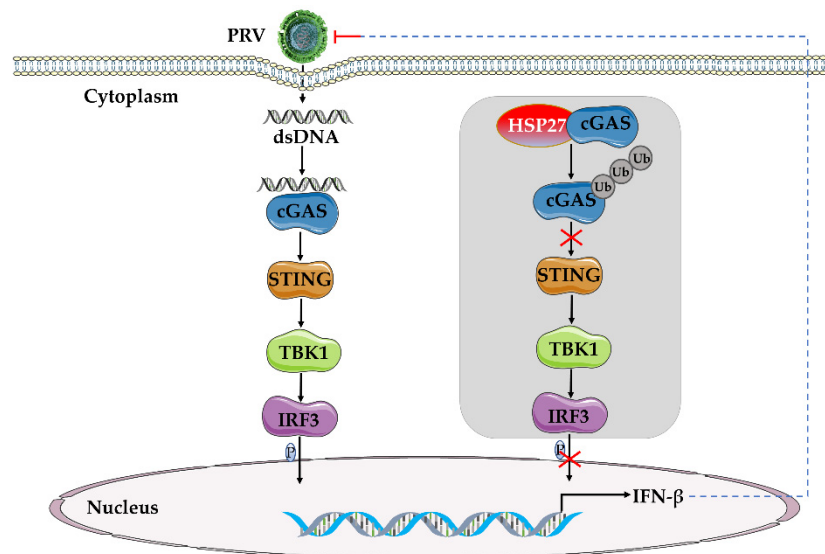


Figure 8. Schematic model of HSP27 negatively regulating cGAS-STING-mediated IFN- β expression upon PRV proliferation. cGAS recognizes the dsDNA of PRV and then activates cGAS-STING-mediated IFN- β signaling pathway. HSP27 directly binds to cGAS, promotes cGAS degradation through ubiquitination, attenuates cGAS-STING axis signaling transduction, and inhibits IRF3 phosphorylation and IFN- β expression, thereby promoting PRV infection.

Author Contributions: Methodology, X.L., J.X. and D.L.; software, X.L. and D.L.; validation, H.L., B.W., Z.Y. and X.Z.; formal analysis, Y.N.; resources, R.F.; data curation, X.L. and D.L.; writing—original draft preparation, X.L., J.X. and D.L.; writing—review and editing, X.L., J.X. and R.F.; visualization, Y.Y. and L.C.; supervision, R.F.; project administration, X.L. and R.F.; funding acquisition, X.L., J.X. and R.F. All authors have read and agreed to the published version of the manuscript.

Funding: This research was funded by the Fundamental Research Funds for the Central Universities, grant number [31920220068, 31920190003], Open Funds of the Biomedical Research Center from Northwest Minzu University, grant number [EB202101] and Gansu Youth Science and Technology Fund Project, grant number [20JR5RA501].

Institutional Review Board Statement: Not applicable.

Informed Consent Statement: Not applicable.

Data Availability Statement: All available data are presented in the article.

Conflicts of Interest: The authors declare no conflict of interest.

References

1. Akira, S.; Uematsu, S.; Takeuchi, O. Pathogen recognition and innate immunity. *Cell* **2006**, *124*, 783–801. [CrossRef] [PubMed]
2. Müller, U.; Steinhoff, U.; Reis, L.F.; Hemmi, S.; Pavlovic, J.; Zinkernagel, R.M.; Aguet, M. Functional role of type I and type II interferons in antiviral defense. *Science* **1994**, *264*, 1918–1921. [CrossRef] [PubMed]
3. Sadler, A.J.; Williams, B.R. Interferon-inducible antiviral effectors. *Nat. Rev. Immunol.* **2008**, *8*, 559–568. [CrossRef] [PubMed]
4. Schoggins, J.W. Interferon-Stimulated Genes: What Do They All Do? *Annu. Rev. Virol.* **2019**, *6*, 567–584. [CrossRef]
5. Brennan, K.; Bowie, A. Activation of host pattern recognition receptors by viruses. *Curr. Opin. Microbiol.* **2010**, *13*, 503–507. [CrossRef]
6. Xia, P.; Wang, S.; Gao, P.; Gao, G.; Fan, Z. DNA sensor cGAS-mediated immune recognition. *Protein Cell* **2016**, *7*, 777–791. [CrossRef]
7. Wan, D.; Jiang, W.; Hao, J. Research Advances in How the cGAS-STING Pathway Controls the Cellular Inflammatory Response. *Front. Immunol.* **2020**, *11*, 615. [CrossRef]
8. Koyama, S.; Ishii, K.; Coban, C.; Akira, S. Innate immune response to viral infection. *Cytokine* **2008**, *43*, 336–341. [CrossRef]
9. Hu, M.M.; Shu, H.B. Innate Immune Response to Cytoplasmic DNA: Mechanisms and Diseases. *Annu. Rev. Immunol.* **2020**, *38*, 79–98. [CrossRef]
10. Minamiguchi, K.; Kojima, S.; Sakumoto, K.; Kirisawa, R. Isolation and molecular characterization of a variant of Chinese gC-genotype II pseudorabies virus from a hunting dog infected by biting a wild boar in Japan and its pathogenicity in a mouse model. *Virus Genes* **2019**, *55*, 322–331. [CrossRef]
11. Kong, H.; Zhang, K.; Liu, Y.; Shang, Y.; Wu, B.; Liu, X. Attenuated live vaccine (Bartha-K16) caused pseudorabies (Aujeszky's disease) in sheep. *Vet. Res. Commun.* **2013**, *37*, 329–332. [CrossRef]
12. Jin, H.L.; Gao, S.M.; Liu, Y.; Zhang, S.F.; Hu, R.L. Pseudorabies in farmed foxes fed pig offal in Shandong province, China. *Arch. Virol.* **2016**, *161*, 445–448. [CrossRef] [PubMed]
13. Cheng, Z.; Kong, Z.; Liu, P.; Fu, Z.; Zhang, J.; Liu, M.; Shang, Y. Natural infection of a variant pseudorabies virus leads to bovine death in China. *Transbound. Emerg. Dis.* **2020**, *67*, 518–522. [CrossRef] [PubMed]
14. Pomeranz, L.E.; Reynolds, A.E.; Hengartner, C.J. Molecular biology of pseudorabies virus: Impact on neurovirology and veterinary medicine. *Microbiol. Mol. Biol. Rev.* **2005**, *69*, 462–500. [CrossRef] [PubMed]
15. Yang, L.; Wang, M.; Cheng, A.; Yang, Q.; Wu, Y.; Jia, R.; Liu, M.; Zhu, D.; Chen, S.; Zhang, S. Innate Immune Evasion of Alphaherpesvirus Tegument Proteins. *Front. Immunol.* **2019**, *10*, 2196. [CrossRef]
16. Lamote, J.A.S.; Kestens, M.; Van Waesberghe, C.; Delva, J.; De Pelsmaeker, S.; Devriendt, B.; Favoreel, H.W. The Pseudorabies Virus Glycoprotein gE/gI Complex Suppresses Type I Interferon Production by Plasmacytoid Dendritic Cells. *J. Virol.* **2017**, *91*, e02276-16. [CrossRef]
17. Zhang, R.; Xu, A.; Qin, C.; Zhang, Q.; Chen, S.; Lang, Y.; Wang, M.; Li, C.; Feng, W.; Zhang, R.; et al. Pseudorabies Virus dUTPase UL50 Induces Lysosomal Degradation of Type I Interferon Receptor 1 and Antagonizes the Alpha Interferon Response. *J. Virol.* **2017**, *91*, e01148-17. [CrossRef]
18. Qin, C.; Zhang, R.; Lang, Y.; Shao, A.; Xu, A.; Feng, W.; Han, J.; Wang, M.; He, W.; Yu, C.; et al. Bclaf1 critically regulates the type I interferon response and is degraded by alphaherpesvirus US3. *PLoS Pathog.* **2019**, *15*, e1007559. [CrossRef]
19. Xie, J.; Zhang, X.; Chen, L.; Bi, Y.; Idris, A.; Xu, S.; Li, X.; Zhang, Y.; Feng, R. Pseudorabies Virus US3 Protein Inhibits IFN- β Production by Interacting with IRF3 to Block Its Activation. *Front. Microbiol.* **2021**, *12*, 761282. [CrossRef]
20. Lyu, C.; Li, W.D.; Wang, S.W.; Peng, J.M.; Yang, Y.B.; Tian, Z.J.; Cai, X.H. Host BAG3 Is Degraded by Pseudorabies Virus pUL56 C-Terminal ^{181}L - ^{185}L and Plays a Negative Regulation Role during Viral Lytic Infection. *Int. J. Mol. Sci.* **2020**, *21*, 3148. [CrossRef]
21. Lv, L.; Bai, J.; Gao, Y.; Jin, L.; Wang, X.; Cao, M.; Liu, X.; Jiang, P. Peroxiredoxin 1 Interacts with TBK1/IKK ϵ and Negatively Regulates Pseudorabies Virus Propagation by Promoting Innate Immunity. *J. Virol.* **2021**, *95*, e0092321. [CrossRef] [PubMed]
22. Xie, J.; Bi, Y.; Xu, S.; Han, Y.; Idris, A.; Zhang, H.; Li, X.; Bai, J.; Zhang, Y.; Feng, R. Host antiviral protein IFITM2 restricts pseudorabies virus replication. *Virus Res.* **2020**, *287*, 198105. [CrossRef] [PubMed]
23. Liu, H.; Li, S.; Yang, X.; Wang, X.; Li, Y.; Wang, C.; Chen, L.; Chang, H. Porcine ISG15 modulates the antiviral response during pseudorabies virus replication. *Gene* **2018**, *679*, 212–218. [CrossRef] [PubMed]
24. Chen, X.; Sun, D.; Dong, S.; Zhai, H.; Kong, N.; Zheng, H.; Tong, W.; Li, G.; Shan, T.; Tong, G. Host Interferon-Stimulated Gene 20 Inhibits Pseudorabies Virus Proliferation. *Virol. Sin.* **2021**, *36*, 1027–1035. [CrossRef]

25. Li, X.; Zhang, W.; Liu, Y.; Xie, J.; Hu, C.; Wang, X. Role of p53 in pseudorabies virus replication, pathogenicity, and host immune responses. *Vet. Res.* **2019**, *50*, 9. [CrossRef]
26. Yang, K.; Shi, H.; Qi, R.; Sun, S.; Tang, Y.; Zhang, B.; Wang, C. Hsp90 regulates activation of interferon regulatory factor 3 and TBK-1 stabilization in Sendai virus-infected cells. *Mol. Biol. Cell* **2006**, *17*, 1461–1471. [CrossRef]
27. Acunzo, J.; Andrieu, C.; Baylot, V.; So, A.; Rocchi, P. Hsp27 as a therapeutic target in cancers. *Curr. Drug Targets* **2014**, *15*, 423–431. [CrossRef]
28. Parcellier, A.; Schmitt, E.; Gurbuxani, S.; Seigneurin-Berny, D.; Pance, A.; Chantôme, A.; Plenchette, S.; Khochbin, S.; Solary, E.; Garrido, C. HSP27 is a ubiquitin-binding protein involved in I-kappaBalpha proteasomal degradation. *Mol. Cell. Biol.* **2003**, *23*, 5790–5802. [CrossRef]
29. Liu, J.; Zhang, L.; Zhu, X.; Bai, J.; Wang, L.; Wang, X.; Jiang, P. Heat shock protein 27 is involved in PCV2 infection in PK-15 cells. *Virus Res.* **2014**, *189*, 235–242. [CrossRef]
30. Choi, Y.W.; Tan, Y.J.; Lim, S.G.; Hong, W.; Goh, P.Y. Proteomic approach identifies HSP27 as an interacting partner of the hepatitis C virus NS5A protein. *Biochem. Biophys. Res. Commun.* **2004**, *318*, 514–519. [CrossRef]
31. Li, X.; Ma, R.; Wu, B.; Niu, Y.; Li, H.; Li, D.; Xie, J.; Idris, A.; Feng, R. HSP27 Protein Dampens Encephalomyocarditis Virus Replication by Stabilizing Melanoma Differentiation-Associated Gene 5. *Front. Microbiol.* **2021**, *12*, 788870. [CrossRef] [PubMed]
32. Zhang, X.; Xie, J.; Gao, M.; Yan, Z.; Chen, L.; Wei, S.; Feng, R. Pseudorabies Virus ICP0 Abolishes Tumor Necrosis Factor Alpha-Induced NF- κ B Activation by Degrading P65. *Viruses* **2022**, *14*, 954. [CrossRef] [PubMed]
33. Han, Y.; Xie, J.; Xu, S.; Bi, Y.; Li, X.; Zhang, H.; Idris, A.; Bai, J.; Feng, R. Encephalomyocarditis Virus Abrogates the Interferon Beta Signaling Pathway via Its Structural Protein VP2. *J. Virol.* **2021**, *95*, e01590-20. [CrossRef] [PubMed]
34. Unterholzner, L. The interferon response to intracellular DNA: Why so many receptors? *Immunobiology* **2013**, *218*, 1312–1321. [CrossRef]
35. Kong, Z.; Yin, H.; Wang, F.; Liu, Z.; Luan, X.; Sun, L.; Liu, W.; Shang, Y. Pseudorabies virus tegument protein UL13 recruits RNF5 to inhibit STING-mediated antiviral immunity. *PLoS Pathog.* **2022**, *18*, e1010544. [CrossRef]
36. Zhang, Q.; Tang, Z.; An, R.; Ye, L.; Zhong, B. USP29 maintains the stability of cGAS and promotes cellular antiviral responses and autoimmunity. *Cell Res.* **2020**, *30*, 914–927. [CrossRef]
37. Liu, Q.; Wang, X.; Xie, C.; Ding, S.; Yang, H.; Guo, S.; Li, J.; Qin, L.; Ban, F.; Wang, D.; et al. A Novel Human Acute Encephalitis Caused by Pseudorabies Virus Variant Strain. *Clin. Infect. Dis.* **2021**, *73*, e3690–e3700. [CrossRef]
38. Ran, Y.; Li, D.; Xiong, M.G.; Liu, H.N.; Feng, T.; Shi, Z.W.; Li, Y.H.; Wu, H.N.; Wang, S.Y.; Zheng, H.X. African swine fever virus I267L acts as an important virulence factor by inhibiting RNA polymerase III-RIG-I-mediated innate immunity. *PLoS Pathog.* **2022**, *18*, e1010270. [CrossRef]
39. Sun, P.; Zhang, S.; Qin, X.; Chang, X.; Cui, X.; Li, H.; Zhang, S.; Gao, H.; Wang, P.; Zhang, Z.; et al. Foot-and-mouth disease virus capsid protein VP2 activates the cellular EIF2S1-ATF4 pathway and induces autophagy via HSPB1. *Autophagy* **2018**, *14*, 336–346. [CrossRef]
40. Ling, S.; Luo, M.; Jiang, S.; Liu, J.; Ding, C.; Zhang, Q.; Guo, H.; Gong, W.; Tu, C.; Sun, J. Cellular Hsp27 interacts with classical swine fever virus NS5A protein and negatively regulates viral replication by the NF- κ B signaling pathway. *Virology* **2018**, *518*, 202–209. [CrossRef]
41. Yang, X.; Shi, C.; Li, H.; Shen, S.; Su, C.; Yin, H. MARCH8 attenuates cGAS-mediated innate immune responses through ubiquitylation. *Sci. Signal.* **2022**, *15*, eabk3067. [CrossRef] [PubMed]
42. Dai, J.; Huang, Y.J.; He, X.; Zhao, M.; Wang, X.; Liu, Z.S.; Xue, W.; Cai, H.; Zhan, X.Y.; Huang, S.Y.; et al. Acetylation Blocks cGAS Activity and Inhibits Self-DNA-Induced Autoimmunity. *Cell* **2019**, *176*, 1447–1460.e14. [CrossRef] [PubMed]
43. Shi, C.; Yang, X.; Liu, Y.; Li, H.; Chu, H.; Li, G.; Yin, H. ZDHHC18 negatively regulates cGAS-mediated innate immunity through palmitoylation. *EMBO J.* **2022**, *41*, e109272. [CrossRef] [PubMed]

Article

Interferon-Stimulated Gene 15 Knockout in Mice Impairs IFN α -Mediated Antiviral Activity

Chen Li ^{1,†}, Wen-Feng He ^{1,†} , Long-Xi Li ¹, Jing Chen ¹ , Guo-Qing Yang ¹, Hong-Tao Chang ^{2,*} and Hui-Min Liu ^{1,*} 

¹ College of Life Science, Henan Agricultural University, Zhengzhou 450002, China

² College of Animal Veterinary Medicine, Henan Agricultural University, Zhengzhou 450002, China

* Correspondence: ndcht@163.com (H.-T.C.); liuhuimin@henau.edu.cn (H.-M.L.)

† These authors contributed equally to this work.

Abstract: Type I interferon (IFN) plays an important role in the host defense against viral infection by inducing expression of interferon-stimulated genes (ISGs). In a previous study, we found that porcine interferon-stimulated gene 15 (ISG15) exhibited antiviral activity against PRV in vitro. To further investigate the antiviral function of ISG15 in vivo, we utilized ISG15 knockout (ISG15^{-/-}) mice in this study. Here, we demonstrate that ISG15^{-/-} mice were highly susceptible to PRV infection in vivo, as evidenced by a considerably reduced survival rate, enhanced viral replication and severe pathological lesions. However, we observed no significant difference between female and male infected WT and ISG15^{-/-} mice. Moreover, ISG15^{-/-} mice displayed attenuated antiviral protection as a result of considerably reduced expression of IFN β and relevant ISGs during PRV replication. Furthermore, excessive production of proinflammatory cytokines may be closely related to encephalitis and pneumonia. In further studies, we found that the enhanced sensitivity to PRV infection in ISG15^{-/-} mice might be caused by reduced phosphorylation of STAT1 and STAT2, thereby inhibiting type I IFN-mediated antiviral activity. Based on these findings, we conclude that ISG15 is essential for host type I IFN-mediated antiviral response.

Keywords: pseudorabies virus; ISG15 knockout mice; in vivo; susceptibility; type I IFN; impair



Citation: Li, C.; He, W.-F.; Li, L.-X.; Chen, J.; Yang, G.-Q.; Chang, H.-T.; Liu, H.-M. Interferon-Stimulated Gene 15 Knockout in Mice Impairs IFN α -Mediated Antiviral Activity. *Viruses* **2022**, *14*, 1862. <https://doi.org/10.3390/v14091862>

Academic Editors: Yan-Dong Tang and Xiangdong Li

Received: 17 July 2022

Accepted: 19 August 2022

Published: 24 August 2022

Publisher's Note: MDPI stays neutral with regard to jurisdictional claims in published maps and institutional affiliations.



Copyright: © 2022 by the authors. Licensee MDPI, Basel, Switzerland. This article is an open access article distributed under the terms and conditions of the Creative Commons Attribution (CC BY) license (<https://creativecommons.org/licenses/by/4.0/>).

1. Introduction

Pseudorabies virus (PRV), also called Aujeszky's disease virus or suid herpesvirus 1 (SuHV-1), is a large, enveloped DNA virus that belongs to the subfamily Alphaherpesvirinae [1]. Although pigs are the natural reservoir for the virus, a wide variety of mammals are also susceptible to PRV [2]. Recent studies revealed that humans might also be a potential host of PRV [3–5]. PRV infection poses a major threat to the pig industry, and various types of vaccines are usually used to control the disease [6]. Although vaccines can eliminate viral infection, emerging PRV variants have caused frequent outbreaks of PRV infection since late 2011 [7]. Thus, novel antiviral agents need to be developed as a to complement vaccination.

Type I interferon (IFN) represents the first line of defense to combat viral infections. Interferon-stimulated gene 15 (ISG15), an IFN- α / β -inducible, ubiquitin-like molecule, has been reported to play an antiviral role in viral infection [8–11]. We previously reported that porcine ISG15 plays an antiviral role during PRV infection [1]. However, there are large differences among species with respect to the role of ISG15 in host–virus interactions; unlike human ISG15, which stabilizes USP18, the murine orthologue does not exert such activity [12]. In vitro studies in mouse cells have demonstrated an antiviral role of ISG15 during several viral infections [13–16], although there are some reports of viruses displaying no enhanced replication when ISG15 is deficient [16,17]. Knocking down ISG15 in human cells has also suggested an antiviral role of ISG15 during infection with numerous viruses [13,18–20], whereas other studies have suggested no role at

all [21,22]. Furthermore, mice lacking ISG15 exhibit enhanced susceptibility to some but not all viruses [23,24], whereas ISG15 deficiency in humans has been reported to enhance viral resistance [12,25–27]. According to these results, ISG15 deficiency may actually increase resistance to severe viral infections.

Type I IFN stimulation has been shown to inhibit PRV replication due to the induction of several ISGs that function as general antivirals. Among these, we found that ISG15 significantly upregulated and further demonstrated an antiviral role of ISG15 during PRV infection in vitro [28], although nothing is known about the exact role of ISG15 in type I IFN-mediated antiviral response against PRV in vivo. Here, for the first time, we examine the antiviral effect of ISG15 in vivo and show that mice lacking ISG15 were highly susceptible to PRV infection. Moreover, ISG15 deficiency in mice resulted in attenuated IFN α -mediated antiviral protection by considerably reducing the expression of IFN β and relevant ISGs. We found that excessive production of proinflammatory cytokines in ISG15^{-/-} mice may be closely related to encephalitis and pneumonia. Finally, we found that the enhanced sensitivity of ISG15^{-/-} mice to PRV infection might be associated with reduced phosphorylation of STAT1 and STAT2.

2. Materials and Methods

2.1. Virus and Reagents

Pseudorabies virus (PRV) strain QXX was propagated in porcine kidney 15 (PK15) cells (CCL-33, ATCC) and titered by plaque assay. The primary antibodies used for Western blotting included rabbit anti-STAT1, anti-STAT2 (Proteintech, Wuhan, China), rabbit anti-phospho-Tyr701 STAT1, rabbit anti-phospho-Tyr690 STAT2 (Abcam, Cambridge, UK), anti-ISG15 and anti- β -actin (Proteintech).

2.2. Mouse Experiments

C57BL/6N (WT) and ISG15^{-/-} mice were purchased from Cyagen Biosciences, Inc. (Guangzhou, China). The mice were mated, bred and genotyped in the animal facility. The genotype of bred mice was determined by PCR. Animal experiments were performed in accordance with protocols approved by the Use of National Research Center for Veterinary Medicine (Permit 20180521047).

Mice were represented in both the control and infected groups. Mice (both male and female) aged 7–9 weeks were intraperitoneally inoculated with 50–200 plaque-forming units (PFU) of PRV diluted in 40 μ L sterile DMEM. Mice were monitored daily for body weight and clinical symptoms. Brain, lung and spleen tissues were collected to determine viral loads, mRNA level of ISGs and expression of proinflammatory cytokines for histological analysis.

2.3. PCR, Quantitative Real-Time PCR and Western Blotting

Total RNA from the tissues was extracted using RNAiso Plus reagent (Takara, Dalian, China) and was reverse transcribed to cDNA using a PrimeScriptTM RT reagent kit with gDNA Eraser (Takara) according to the manufacturer's protocols. The genes used in this study were amplified by PCR using Prime STAR[®] Max DNA Polymerase (Takara) or with real-time PCR using TB Green Premix Ex Taq II (Takara). Quantitative real-time PCR (RT-qPCR) was carried out utilizing SYBR Green PCR Master Mix (Promega, Beijing, China). The mRNA level of each target gene was normalized to that of β -actin mRNA.

Protein was extracted from the homogenized tissues using a lysis buffer, and total protein concentration was determined with a BCA protein assay kit (Beyotime Biotechnology, Shanghai, China). An equal amount (30 μ g) of protein from tissues of WT and ISG15^{-/-} mice was resolved on 10% SDS-PAGE gels and transferred to a PVDF membrane (Pall Corporation, Ann Arbor, MI, USA). The membrane was probed with corresponding antibodies, followed by horseradish peroxidase-conjugated anti-rabbit IgG (Servicebio, Wuhan, China). The protein bands were visualized by chemiluminescence using ECL (Beyotime Biotechnology, Shanghai, China). The intensities of the protein bands were

quantified using Image J software and standardized against β -actin. All data are presented as three independent experiments in duplicate.

2.4. Enzyme-Linked Immunosorbent Assay (ELISA)

Protein concentration of the cytokines, including interleukin (IL)-6, IL-1 β and tumor necrosis factor (TNF)- α , from organs of infected mice were measured by ELISA using mouse IL-6, IL-1 β and TNF- α kits (Meimian, Nanjing, China). The absorbance was read with an automated ELISA plate reader at 450 nm.

2.5. Histopathological Analysis

On day 4 post infection, mice were sacrificed, and lungs and brains were collected for histological analysis. Tissues were fixed and dehydrated and embedded in paraffin, followed by sectioning (4–5 μ m) and staining with hematoxylin–eosin (HE). Pathological changes were determined through observation of the morphologic characteristics.

2.6. Statistical Analysis

Statistical analyses were performed using GraphPad Prism. The difference between groups was calculated using Student's t-tests, and the differences were considered to be significant when * $p < 0.05$, ** $p < 0.01$ or *** $p < 0.001$. The standard errors of the mean (SEM) of at least three independent experiments are shown for each data.

3. Results

3.1. Mice Lacking ISG15 Are More Susceptible to PRV Infection

PRV can infect a wide variety of mammals, including rodents; therefore a mouse model has been widely used to study PRV pathogenesis [29]. To determine whether ISG15 also exhibits antiviral activity against PRV *in vivo*, ISG15-deficient mice were generated on a C57BL/6N background by targeting ISG15 for deletion using CRISPR-Cas9 technology. Seven-week-old female and male mice were injected intraperitoneally with PRV, and their clinical symptoms, body weight and survival rate were monitored daily. The results show that the ISG15^{-/-} mice displayed typical neurological symptoms, including considerably reduced activity and pruritus at 3 days post infection (dpi), with death beginning at 4 dpi, whereas WT mice developed only mild symptoms at 5 dpi under the same conditions (Figure 1A). On the other hand, the ISG15^{-/-} mice lost weight more rapidly than WT mice by day 6, and the surviving WT mice continued to lose weight (Figure 1B).

Next, the mortality of wild-type (WT) and ISG15^{-/-} mice was monitored for 10 days after PRV infection. We found that all ISG15^{-/-} mice died within 6 days after PRV infection, whereas 53.3% of the WT mice remained alive under the same conditions. As illustrated in Figure 1C, ISG15^{-/-} mice had a survival rate of 0, whereas WT mice had a survival rate of 53.3%, suggesting that ISG15^{-/-} mice are more sensitive to PRV than WT mice. Furthermore, PRV loads in the brain, lungs and spleen were assayed at 4 dpi. The viral loads of the ISG15^{-/-} mice were markedly higher than those in the same tissues of WT mice (Figure 1D). Moreover, no significant difference between female and male mice was observed in terms of body weight, survival rate or viral load (data not shown). The above results indicate that ISG15 deficiency enhances susceptibility to PRV infection *in vivo*.

3.2. ISG15 Deficiency Promotes PRV Infection Pathogenicity in Mice

PRV infection mainly leads to neurological and respiratory symptoms, and encephalitis is a contributing factor to animal death [30]. To detect the degree of pneumonia and encephalitis in infected mice, we histopathologically analyzed the brains and lungs at 4 dpi. As shown in Figure 2A, the brains of ISG15^{-/-} mice showed a substantial number of necrotic neurons and more necrotic Purkinje cells than those in WT mice (Figure 2A). Furthermore, microgliosis and hyperemia were more obvious in the brains of ISG15^{-/-} mice. Histological analyses of infected lungs showed increased inflammatory cell infiltration, severe congestion and higher levels of lung tissue impairment in ISG15^{-/-} mice in comparison with

WT mice (Figure 2B). These results indicate that ISG15 deletion aggravated virus-induced pathogenicity during PRV infection in vivo.

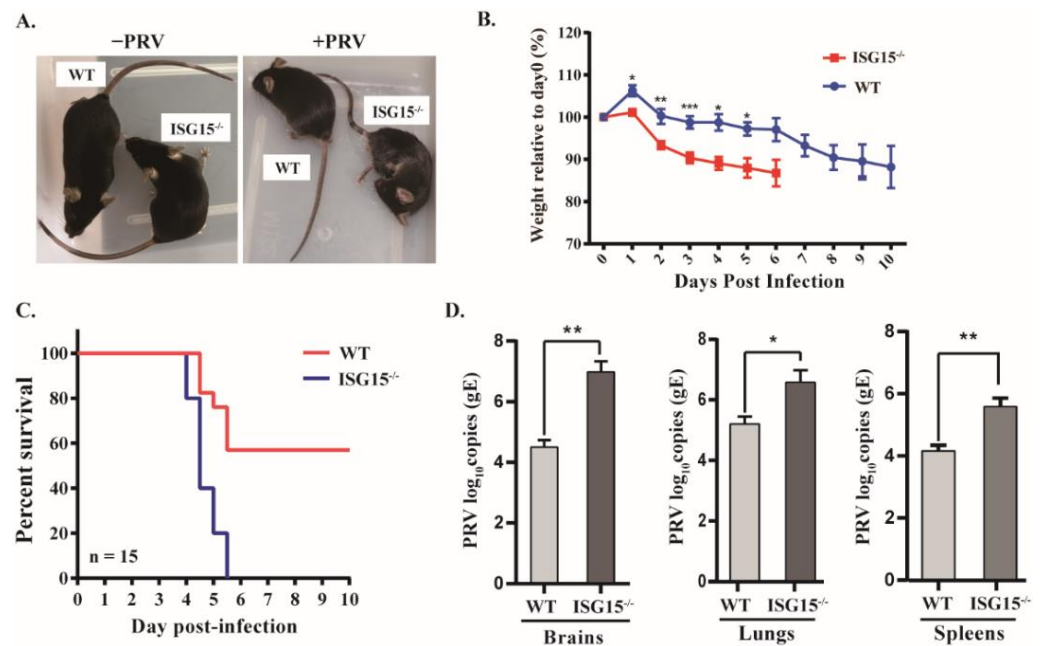


Figure 1. Mice lacking ISG15 are more susceptible to PRV than WT mice. (A) The clinical aspects of WT and ISG15-deficient (ISG15^{-/-}) mice infected intraperitoneally with PRV are shown. (B,C) Body weight (B) and survival (C) were monitored for 10 dpi (WT: $n = 15$; ISG15^{-/-}: $n = 15$). Data are shown as percent change of body weight relative to the starting weight on day 0 (mean \pm SEM). Survival curves were compared using a log-rank test. (D) At 4 dpi, the brain, lung and spleen tissues of the infected mice were harvested and homogenized, and PRV gE gene copies were assayed by quantitative real-time PCR (RT-qPCR). PRV-infected ISG15^{-/-} mice vs. PRV-infected WT mice. * $p < 0.05$; ** $p < 0.01$; *** $p < 0.001$.

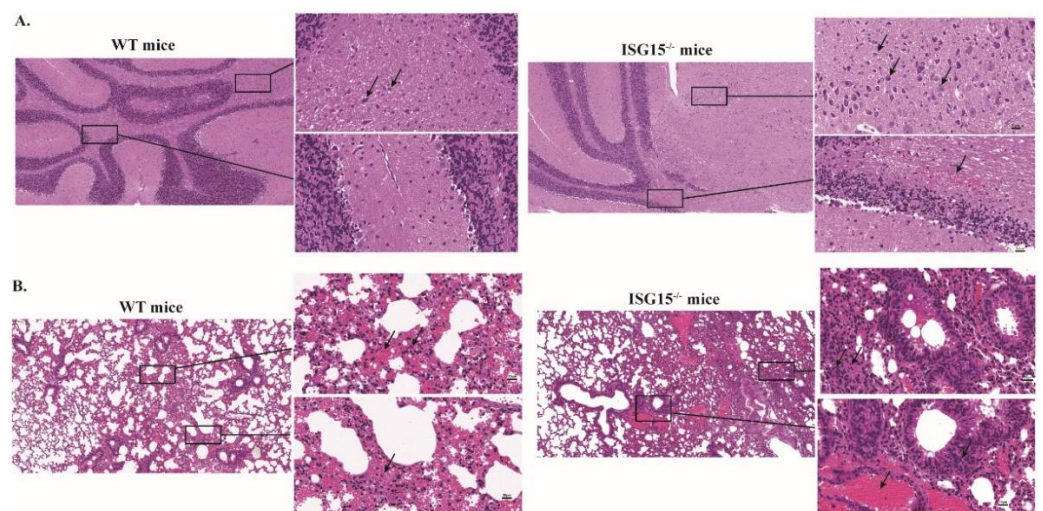


Figure 2. Histopathological examination of brains and lungs of infected ISG15^{-/-} and WT mice. WT ($n = 10$) and ISG15^{-/-} ($n = 10$) mice were intraperitoneally infected with PRV. At 4 dpi, the brains and lungs of infected mice were collected, sectioned and stained with hematoxylin-eosin. Magnified regions are indicated with rectangles in (A,B). Scale bar: 100 μ m and 20 μ m.

3.3. ISG15 Deficiency Impairs Type I IFN Production

Type I IFN (IFN- α/β) signaling is critical for host restriction of viral infection [31]. To test whether ISG15 is involved in type I IFN-mediated antiviral innate immune response *in vivo*, we first compared the body weight between WT and ISG15^{-/-} mice after infection with PRV with or without IFN α treatment. Starting on day 6, the infected mice pretreated with IFN α started to recover their body weight, albeit at a significantly lower rate compared to WT mice (Figure 3A). Moreover, ISG15^{-/-} mice pretreated with IFN α exhibited a dramatically reduced mortality rate, with no significant difference compared with WT counterparts (Figure 3B). We also compared the body weight and survival rate between female and male mice, with no significant difference observed (data not shown).

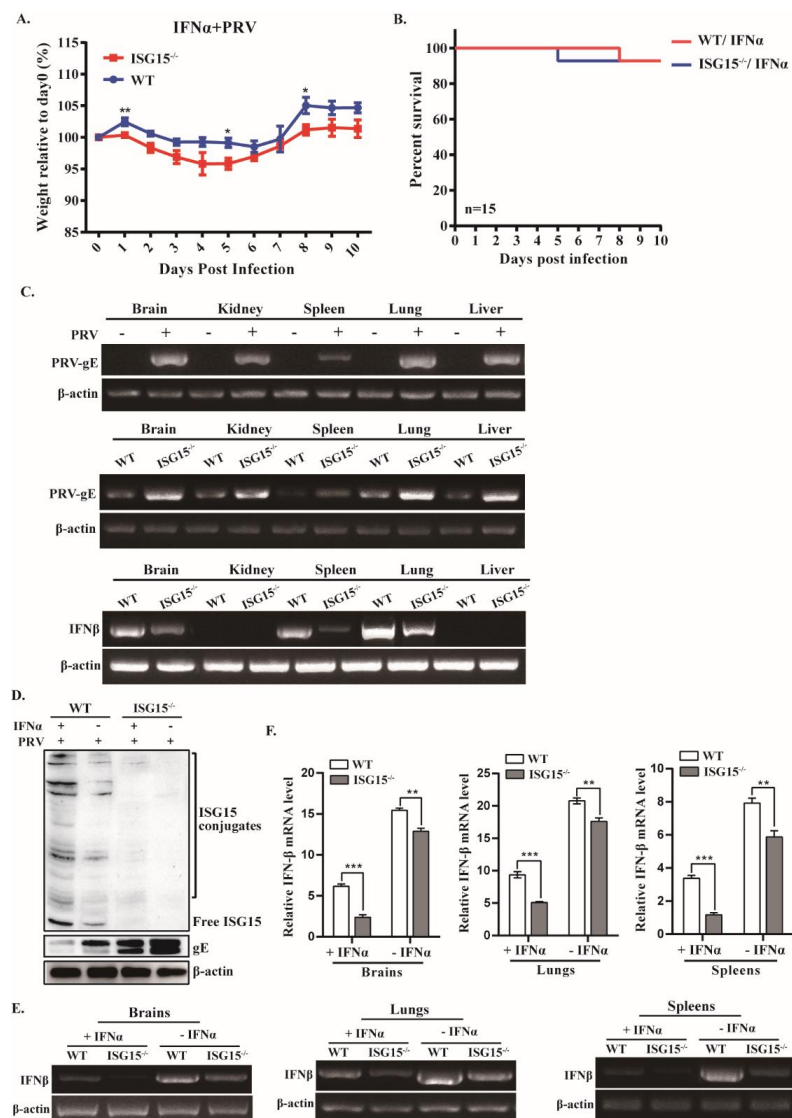


Figure 3. Expression of IFN β is reduced in ISG15^{-/-} mice after PRV infection. (A,B) Body weight and survival rate of infected WT and ISG15^{-/-} mice with IFN α treatment were monitored for 10 days. (C) WT and ISG15^{-/-} mice were infected intraperitoneally with PRV for 4 days, followed by PCR for detection of viral DNA levels in the indicated tissues from infected mice and RT-PCR for detection of IFN β levels in indicated organs of WT and ISG15^{-/-} mice (C). (D) The protein expression of ISG15 and PRV-gE in brains of WT and ISG15^{-/-} mice were analyzed by Western blotting. (E,F) IFN β levels in the indicated tissues of infected mice were examined by RT-PCR (E) and RT-qPCR (F). The average results from three independent experiments are plotted. * $p < 0.05$; ** $p < 0.01$; *** $p < 0.001$.

To analyze the tissue distribution of the PRV genome in organs of infected mice, we detected DNA of PRV-gE in different tissues after PRV infection for 4 dpi. Higher levels of PRV-gE DNA were found in infected tissues from ISG15^{-/-} mice in comparison with those from WT mice (Figure 3C). Additionally, expression of IFN β was significantly down-regulated in various tissues from ISG15^{-/-} mice in response to PRV infection (Figure 3C). To further test the effect of ISG15 on IFN β production induced by PRV infection, we first examined the association between ISG15 expression patterns and PRV replication *in vivo*. We found that the high expression of ISG15 in brains of infected WT mice inhibited PRV growth, whereas ISG15 deficiency significantly promoted PRV replication (Figure 3D). Moreover, the PRV load in IFN α -treated ISG15^{-/-} mice showed a much higher fold than that in WT mice, suggesting that ISG15 plays an important role in promoting IFN-mediated antiviral response. Thus, we next detected the levels of IFN β in brains, lungs and spleens between WT and ISG15^{-/-} mice infected with PRV untreated or treated with IFN α . We found that the expression of IFN β was considerably reduced in infected ISG15^{-/-} mice pretreated with IFN α as compared to that in WT counterparts (Figure 3E). These findings were further confirmed by RT-qPCR (Figure 3F).

Taken together, these data suggest that ISG15 deficiency impairs type I IFN production and promotes PRV replication.

3.4. ISG15 Deficiency Suppresses the Expression of Some ISGs in Response to PRV Infection

The data reported above show that ISG15 knockout considerably reduced IFN β production. Therefore, we analyzed the expression of several key ISGs, including IFIT1, OAS1 and Mx1 in various tissues of infected mice. Results indicate that the ISG15 knockout resulted in impaired expression of IFIT1, OAS1 and Mx1 in the brain during PRV infection (Figure 4A), which was further confirmed by RT-qPCR (Figure 4B). To verify this finding, the expression of these ISGs in the lungs and spleens were also detected, and similar results were obtained by RT-PCR and RT-qPCR (Figure 4C–F). These findings suggest that ISG15 may be involved in antiviral immune responses by modulating type I IFN signaling.

3.5. Mice Lacking ISG15 Produce Excessive Inflammation in Response to PRV Infection

Cytokines are crucial in combating viral infection and are involved in the regulation of immune and inflammatory responses, including interleukin 1 β (IL-1 β), interleukin-6 (IL-6) and tumor necrosis factor alpha (TNF- α) [32]. The mRNA levels of IL-1 β , IL-6 and TNF- α were markedly elevated in brains, lungs and spleens of infected ISG15^{-/-} mice relative to WT mice (Figure 5A–E). After treatment with IFN α , the mRNA levels of these cytokines were significantly reduced, whereas their expression levels were still higher in ISG15^{-/-} mice than WT mice (Figure 5A–E). Furthermore, the protein concentrations of IL-1 β , IL-6 and TNF- α were measured using ELISA assay, and a similar tendency was observed in protein levels. As shown in Figure 5G, IL-1 β , IL-6 and TNF- α protein levels were significantly higher in the serum of ISG15^{-/-} mice than those in WT mice with or without IFN α treatment (Figure 5G). These data suggest that ISG15^{-/-} mice displayed a more severe inflammatory response than WT mice, indicating that ISG15 deficiency leads to excessive production of inflammatory cytokines.

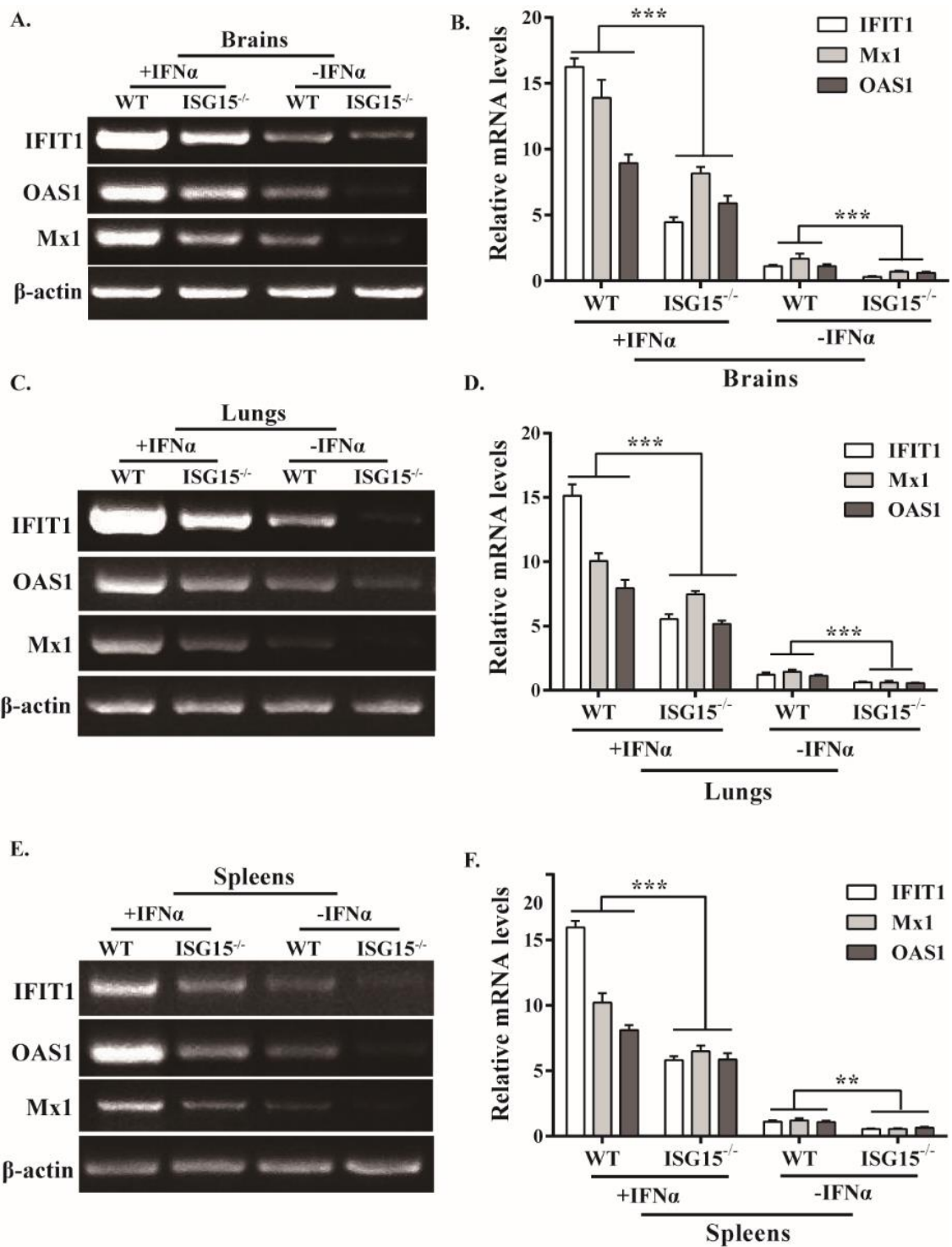


Figure 4. Several ISGs mRNA levels are downregulated in infected ISG15^{-/-} mice. WT and ISG15^{-/-} mice were intraperitoneally infected with PRV and pretreated or untreated with IFNα. At 4 dpi, the mRNA levels of IFIT1, OAS1 and Mx1 in brains (A), lungs (C) and spleens (E) of infected mice were examined by RT-PCR and RT-qPCR (B,D,F), respectively. ** *p* < 0.01; *** *p* < 0.001.

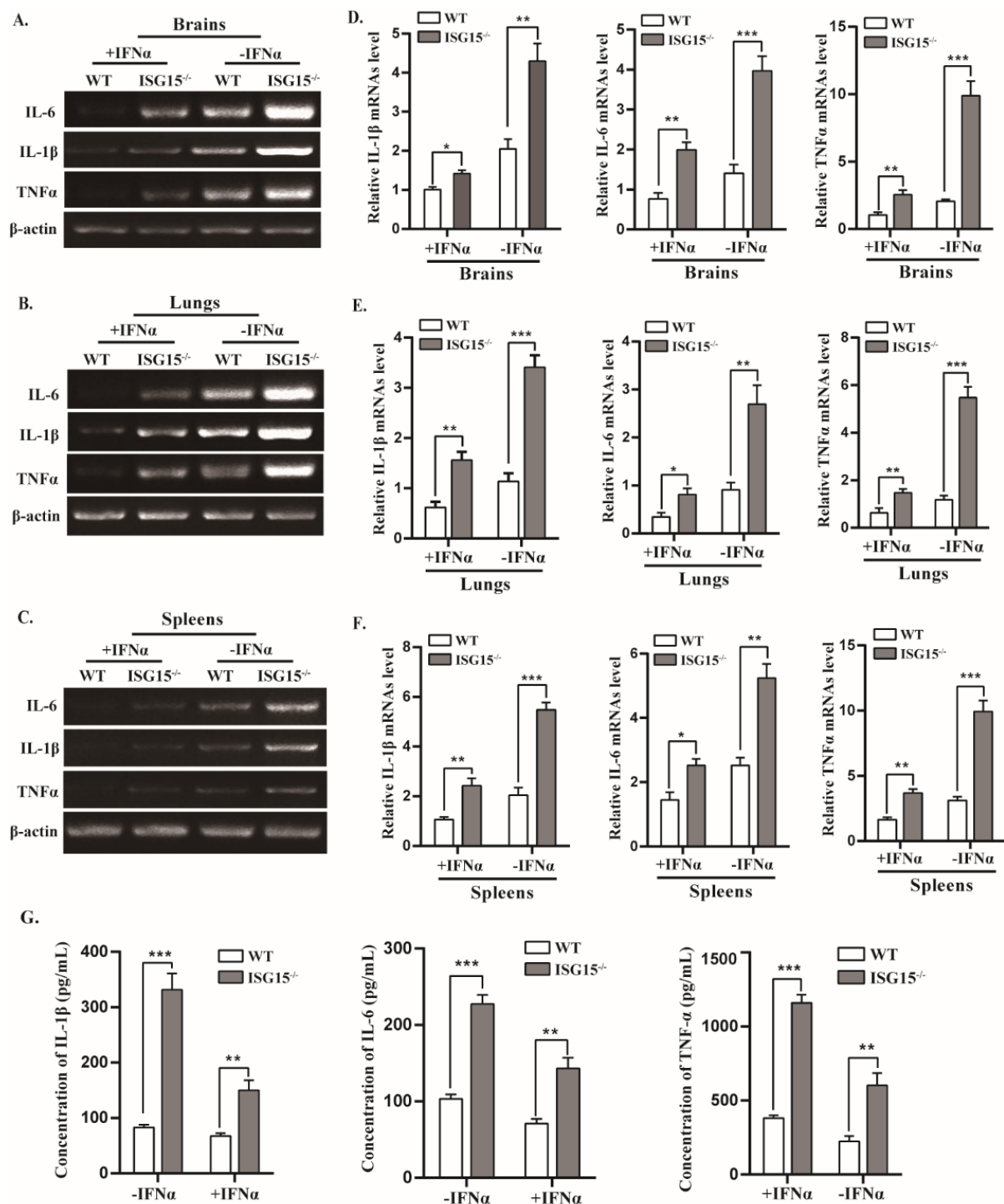


Figure 5. Expression of inflammatory cytokines was significantly increased in infected ISG15^{-/-} mice. (A–F) The RNA levels of IL-1 β , IL-6 and TNF α in the indicated tissues from PRV-infected WT and ISG15^{-/-} mice by RT-PCR and RT-qPCR, respectively. The data were normalized to β -actin. (G) The protein levels were measured by ELISA. * $p < 0.05$; ** $p < 0.01$; *** $p < 0.001$.

3.6. ISG15 Deficiency Potentiates Viral Replication by Blocking STAT1/STAT2 Phosphorylation

Because ISG15 deficiency impaired IFN β expression in response to PRV infection, as shown in Figure 3, we speculated that ISG15 may affect IFN β production by targeting phosphorylated STAT1 (pSTAT1) or/and STAT2 (pSTAT2). Therefore, we tested whether ISG15 deficiency affects the expression of pSTAT1 and pSTAT2 in tissues of infected mice by Western blot. We found that the expression of pSTAT1 and pSTAT2 was significantly

reduced in brains of ISG15^{-/-} mice in comparison with WT counterparts. Moreover, IFN α stimulation promoted the expression of pSTAT1 and pSTAT2 in the brains of infected mice (Figure 6A,B). Similar results were observed in the lungs of infected mice (Figure 6C,D). These data reveal that the ISG15 deficiency inhibits the expression of pSTAT1 and pSTAT2, which is most likely responsible for reduced IFN β production during PRV infection, suggesting that ISG15 deficiency impairs host antiviral activity against PRV by attenuating the expression of pSTAT1 and pSTAT2.

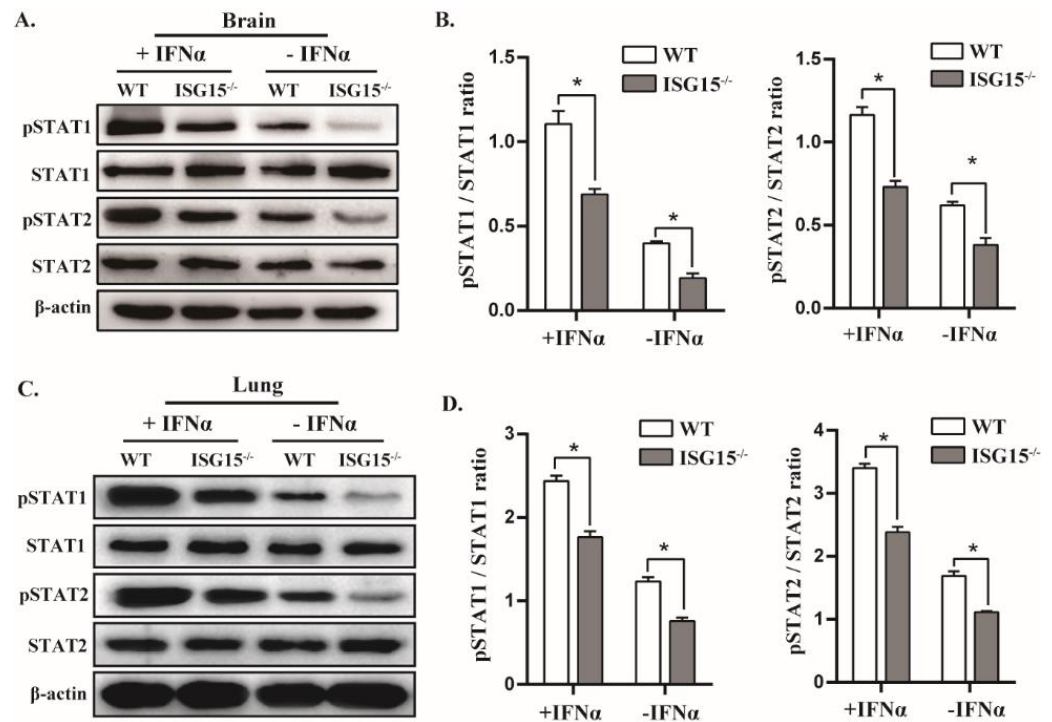


Figure 6. STAT1 and STAT2 phosphorylation are considerably reduced in infected ISG15^{-/-} mice. The tissues of infected WT and ISG15^{-/-} mice either pretreated or left untreated were harvested and analyzed by Western blotting with the indicated antibodies (A,C). Phosphorylated STAT1 or STAT2 levels relative to STAT1 or STAT2 were quantitated by densitometry and normalized to β -actin (B,D). The average of three independent replicates were plotted (means \pm SD). * $p < 0.05$.

4. Discussion

The function of ISG15 in herpesvirus remains an area of active investigation [28,33]. In vitro studies in PK15 cells revealed that ISG15 plays an antiviral role in the context of PRV infection. To examine whether ISG15 exhibit an antiviral response against PRV in vivo, we used ISG15^{-/-} mice and found that mice lacking ISG15 were more sensitive to PRV infection relative to WT mice (Figure 1). ISG15^{-/-} mice showed a decreased body weight, increased PRV growth and increased disease severity (Figures 1 and 2). Our findings are in line with the previous results showing that mice lacking ISG15 exhibit enhanced susceptibility to challenge with many viruses [17,23,24]. Furthermore, PRV infection caused more severe damage in the brain and lung tissues of ISG15^{-/-} mice than those of WT mice, indicating that ISG15 deficiency could worsen histopathological changes.

It has been reported that PRV infection could activate the immune response in the rodent brain, including type I IFN and inflammatory cytokines, to allow PRV to establish a persistent infection [34]. Although considerable progress had been made in terms of understanding the pathogenesis of PRV [35], the function of ISG15 in type I IFN-mediated antiviral response during PRV infection is not fully understood. Here, we found that mice lacking ISG15 had significantly downregulated expression of IFN β and several critical ISGs (Figures 3 and 4), which may be responsible for the increased susceptibility of ISG15^{-/-} mice to PRV infection. Although inflammatory response is the first line of defense to

prevent the spread of viral infections, uncontrolled inflammatory response usually leads to severe inflammation, which may cause damage to the host [29]. In this study, excessive production of cytokines, including IL6, IL-1 β and TNF- α , was observed in infected ISG15^{-/-} mice, indicating that ISG15 is critically involved in antiviral response. Cytokines are the key regulators of host defense against viral infection; however, excessive inflammatory response induced by viral infection is associated with viral pathogenesis. It has been reported that a cytokine storm (excessive production of IL-6, IL-1 β and TNF α) caused by highly pathogenic influenza virus infection can injure host organs, resulting in severe disease and even death [36,37]. Thus, it is very likely that the considerably elevated levels of inflammatory cytokines in infected ISG15^{-/-} mice contribute to the pathogenesis of PRV.

It has been reported that IFN α and IFN β serve as homeostatic agents during inflammatory response [37,38]. Consistent with this view, we found that ISG15 knockout not only resisted IFN β production but also increased expression of inflammatory cytokines. However, after IFN α treatment, the expression of cytokines was reduced in infected ISG15^{-/-} mice. These observations confirm that IFN α and IFN β play a critical role in the control of inflammation. In addition, downregulated phosphorylation of STAT1 and STAT2 were observed in ISG15^{-/-} mice after infection with PRV in vivo. Therefore, we speculate that reduced pSTAT1 and pSTAT2 may be associated with elevated inflammatory response. Our observation indicates that mice lacking ISG15 blocked type I IFN signaling by inhibiting phosphorylation of STAT1 and STAT2, thereby preventing an antiviral response. We observed that the expression of pSTAT1 and pSTAT2 was reduced in the brains and lungs of infected ISG15^{-/-} mice, although similar reductions were not detected in other tissues. One possible interpretation for these observations is that an excessive inflammatory response in brains and lungs may be responsible for encephalitis and pneumonia caused by PRV infection. Further studies are needed to address this possibility.

5. Conclusions

Altogether, our findings indicate that ISG15 precisely regulates the host antiviral response by controlling STAT1/2 activation and IFN β production. These results provide a new perspective on the functions of ISG15; moreover, the results of our study may provide a useful strategy for the prevention and control of this viral disease.

Author Contributions: Conceptualization, H.-M.L. and H.-T.C.; methodology, C.L.; software, W.-F.H.; validation, G.-Q.Y., J.C. and L.-X.L.; formal analysis, H.-T.C.; investigation, C.L.; resources, H.-T.C. data curation, W.-F.H.; writing—original draft preparation, C.L. and H.-M.L.; writing—review and editing, H.-T.C.; supervision, J.C.; project administration, G.-Q.Y.; funding acquisition, H.-M.L. All authors have read and agreed to the published version of the manuscript.

Funding: This research was funded by the National Natural Science Foundation of China (grant number 31902268) and the Youth Backbone Teachers' Training Program of Colleges and Universities of Henan Province, grant number 2021GGJS034.

Institutional Review Board Statement: The animal experiments were approved by the Use of National Research Center for Veterinary Medicine (Permit 20180521047).

Informed Consent Statement: Not applicable.

Data Availability Statement: All available data are presented in the article.

Conflicts of Interest: The authors declare no conflict of interest.

References


1. Ye, C.; Chen, J.; Wang, T.; Xu, J.; Zheng, H.; Wu, J.; Li, G.; Yu, Z.; Tong, W.; Cheng, X.; et al. Generation and characterization of UL41 null pseudorabies virus variant in vitro and in vivo. *Viol. J.* **2018**, *15*, 119. [CrossRef] [PubMed]
2. Tirabassi, R.S.; Enquist, L.W. Role of the Pseudorabies Virus gI Cytoplasmic Domain in Neuroinvasion, Virulence, and Posttranslational N-Linked Glycosylation. *J. Virol.* **2000**, *74*, 3505–3516. [CrossRef]
3. Liu, Q.; Wang, X.; Xie, C.; Ding, S.; Yang, H.; Guo, S.; Li, J.; Qin, L.; Ban, F.; Wang, D.; et al. A Novel Human Acute Encephalitis Caused by Pseudorabies Virus Variant Strain. *Clin. Infect. Dis.* **2021**, *73*, e3690–e3700. [CrossRef] [PubMed]

4. Hou, Y.; Wang, Y.; Zhang, Y.; Yu, H.; Zhao, Y.; Yi, A. Human Encephalitis Caused by Pseudorabies Virus in China: A Case Report and Systematic Review. *Vector Borne Zoonotic Dis.* **2022**, *22*, 391–396. [CrossRef]
5. Li, X.D.; Fu, S.H.; Chen, L.Y.; Li, F.; Deng, J.H.; Lu, X.C.; Wang, H.Y.; Tian, K.G. Detection of Pseudorabies Virus Antibodies in Human Encephalitis Cases. *Biomed. Environ. Sci.* **2020**, *33*, 444–447. [CrossRef]
6. Freuling, C.M.; Müller, T.F.; Mettenleiter, T.C. Vaccines against pseudorabies virus (PrV). *Vet. Microbiol.* **2017**, *206*, 3–9. [CrossRef]
7. Yu, X.; Zhou, Z.; Hu, D.; Zhang, Q.; Han, T.; Li, X.; Gu, X.; Yuan, L.; Zhang, S.; Wang, B.; et al. Pathogenic Pseudorabies Virus, China, 2012. *Emerg. Infect. Dis.* **2014**, *20*, 102–104. [CrossRef]
8. Zhao, C.; Collins, M.N.; Hsiang, T.-Y.; Krug, R.M. Interferon-induced ISG15 pathway: An ongoing virus–host battle. *Trends Microbiol.* **2013**, *21*, 181–186. [CrossRef]
9. Dzimianski, J.V.; Scholte, F.E.M.; Bergeron, E.; Pegan, S.D. ISG15: It’s Complicated. *J. Mol. Biol.* **2019**, *431*, 4203–4216. [CrossRef]
10. Freitas, B.T.; Scholte, F.E.M.; Bergeron, E.; Pegan, S.D. How ISG15 combats viral infection. *Virus Res.* **2020**, *286*, 198036. [CrossRef]
11. Perng, Y.-C.; Lenschow, D.J. ISG15 in antiviral immunity and beyond. *Nat. Rev. Microbiol.* **2018**, *16*, 423–439. [CrossRef] [PubMed]
12. Speer, S.D.; Li, Z.; Buta, S.; Payelle-Brogard, B.; Qian, L.; Vigant, F.; Rubino, E.; Gardner, T.J.; Wedeking, T.; Hermann, M.; et al. ISG15 deficiency and increased viral resistance in humans but not mice. *Nat. Commun.* **2016**, *7*, 11496. [CrossRef] [PubMed]
13. Okumura, A.; Pitha, P.M.; Harty, R.N. ISG15 inhibits Ebola VP40 VLP budding in an L-domain-dependent manner by blocking Nedd4 ligase activity. *Proc. Natl. Acad. Sci. USA* **2008**, *105*, 3974–3979. [CrossRef] [PubMed]
14. Dai, J.; Pan, W.; Wang, P. ISG15 facilitates cellular antiviral response to dengue and west nile virus infection in vitro. *Virol. J.* **2011**, *8*, 468. [CrossRef]
15. Holthaus, D.; Vasou, A.; Bamford, C.G.G.; Andrejeva, J.; Paulus, C.; Randall, R.E.; McLauchlan, J.; Hughes, D.J. Direct Antiviral Activity of IFN-Stimulated Genes Is Responsible for Resistance to Paramyxoviruses in ISG15-Deficient Cells. *J. Immunol.* **2020**, *205*, 261–271. [CrossRef]
16. Giannakopoulos, N.V.; Arutyunova, E.; Lai, C.; Lenschow, D.J.; Haas, A.L.; Virgin, H.W. ISG15 Arg151 and the ISG15-Conjugating Enzyme Ube1L Are Important for Innate Immune Control of Sindbis Virus. *J. Virol.* **2009**, *83*, 1602–1610. [CrossRef]
17. Lenschow, D.J.; Lai, C.; Frias-Staheli, N.; Giannakopoulos, N.V.; Lutz, A.; Wolff, T.; Osiak, A.; Levine, B.; Schmidt, R.E.; García-Sastre, A.; et al. IFN-stimulated gene 15 functions as a critical antiviral molecule against influenza, herpes, and Sindbis viruses. *Proc. Natl. Acad. Sci. USA* **2007**, *104*, 1371–1376. [CrossRef]
18. Tang, Y.; Zhong, G.; Zhu, L.; Liu, X.; Shan, Y.; Feng, H.; Bu, Z.; Chen, H.; Wang, C. Herc5 Attenuates Influenza A Virus by Catalyzing ISGylation of Viral NS1 Protein. *J. Immunol.* **2010**, *184*, 5777–5790. [CrossRef]
19. Kuang, Z.; Seo, E.J.; Leis, J. Mechanism of Inhibition of Retrovirus Release from Cells by Interferon-Induced Gene ISG15. *J. Virol.* **2011**, *85*, 7153–7161. [CrossRef]
20. Shi, H.-X.; Yang, K.; Liu, X.; Liu, X.-Y.; Wei, B.; Shan, Y.-F.; Zhu, L.-H.; Wang, C. Positive Regulation of Interferon Regulatory Factor 3 Activation by Herc5 via ISG15 Modification. *Mol. Cell. Biol.* **2010**, *30*, 2424–2436. [CrossRef]
21. Broering, R.; Zhang, X.; Kottlilil, S.; Trippler, M.; Jiang, M.; Lu, M.; Gerken, G.; Schlaak, J.F. The interferon stimulated gene 15 functions as a proviral factor for the hepatitis C virus and as a regulator of the IFN response. *Gut* **2010**, *59*, 1111–1119. [CrossRef] [PubMed]
22. Chua, P.K.; McCown, M.F.; Rajyaguru, S.; Kular, S.; Varma, R.; Symons, J.; Chiu, S.S.; Cammack, N.; Nájera, I. Modulation of alpha interferon anti-hepatitis C virus activity by ISG15. *J. Gen. Virol.* **2009**, *90*, 2929–2939. [CrossRef] [PubMed]
23. Werneke, S.W.; Schilte, C.; Rohatgi, A.; Monte, K.J.; Michault, A.; Arenzana-Seisdedos, F.; VanLandingham, D.L.; Higgs, S.; Fontanet, A.; Albert, M.L.; et al. ISG15 Is Critical in the Control of Chikungunya Virus Infection Independent of Ube1L Mediated Conjugation. *PLoS Pathog.* **2011**, *7*, e1002322. [CrossRef] [PubMed]
24. Rodriguez, M.R.; Monte, K.; Thackray, L.B.; Lenschow, D.J. ISG15 Functions as an Interferon-Mediated Antiviral Effector Early in the Murine Norovirus Life Cycle. *J. Virol.* **2014**, *88*, 9277–9286. [CrossRef]
25. Zhang, X.; Bogunovic, D.; Payelle-Brogard, B.; Francois-Newton, V.; Speer, S.D.; Yuan, C.; Volpi, S.; Li, Z.; Sanal, O.; Mansouri, D.; et al. Human intracellular ISG15 prevents interferon- α/β over-amplification and auto-inflammation. *Nature* **2015**, *517*, 89–93. [CrossRef]
26. Bogunovic, D.; Byun, M.; Durfee, L.A.; Abhyankar, A.; Sanal, O.; Mansouri, D.; Salem, S.; Radovanovic, I.; Grant, A.V.; Adimi, P.; et al. Mycobacterial Disease and Impaired IFN- γ Immunity in Humans with Inherited ISG15 Deficiency. *Science* **2012**, *337*, 1684–1688. [CrossRef]
27. Taft, J.; Bogunovic, D. The Goldilocks Zone of Type I IFNs: Lessons from Human Genetics. *J. Immunol.* **2018**, *201*, 3479–3485. [CrossRef]
28. Liu, H.; Li, S.; Yang, X.; Wang, X.; Li, Y.; Wang, C.; Chen, L.; Chang, H. Porcine ISG15 modulates the antiviral response during pseudorabies virus replication. *Gene* **2018**, *679*, 212–218. [CrossRef]
29. Wei, J.; Ma, Y.; Wang, L.; Chi, X.; Yan, R.; Wang, S.; Li, X.; Chen, X.; Shao, W.; Chen, J.-L. Alpha/beta interferon receptor deficiency in mice significantly enhances susceptibility of the animals to pseudorabies virus infection. *Vet. Microbiol.* **2017**, *203*, 234–244. [CrossRef]
30. Mettenleiter, T.C. Aujeszky’s disease (pseudorabies) virus: The virus and molecular pathogenesis—State of the art, June 1999. *Vet. Res.* **2000**, *31*, 99–115. [CrossRef]
31. Hata, N.; Sato, M.; Takaoka, A.; Asagiri, M.; Tanaka, N.; Taniguchi, T. Constitutive IFN-alpha/beta signal for efficient IFN-alpha/beta gene induction by virus. *Biochem. Biophys. Res. Commun.* **2001**, *285*, 518–525. [CrossRef] [PubMed]

32. Kim, E.Y.; Moudgil, K.D. Immunomodulation of autoimmune arthritis by pro-inflammatory cytokines. *Cytokine* **2017**, *98*, 87–96. [CrossRef] [PubMed]
33. Jacobs, S.R.; Stopford, C.M.; West, J.A.; Bennett, C.L.; Giffin, L.; Damania, B. Kaposi's Sarcoma-Associated Herpesvirus Viral Interferon Regulatory Factor 1 Interacts with a Member of the Interferon-Stimulated Gene 15 Pathway. *J. Virol.* **2015**, *89*, 11572–11583. [CrossRef]
34. Dénes, A.; Boldogkői, Z.; Hornyák, A.; Palkovits, M.; Kovács, K.J. Attenuated pseudorabies virus-evoked rapid innate immune response in the rat brain. *J. Neuroimmunol.* **2006**, *180*, 88–103. [CrossRef] [PubMed]
35. Cong, X.; Lei, J.-L.; Xia, S.-L.; Wang, Y.-M.; Li, Y.; Li, S.; Luo, Y.; Sun, Y.; Qiu, H.-J. Pathogenicity and immunogenicity of a gE/gI/TK gene-deleted pseudorabies virus variant in susceptible animals. *Vet. Microbiol.* **2016**, *182*, 170–177. [CrossRef] [PubMed]
36. La Gruta, N.L.; Kedzierska, K.; Stambas, J.; Doherty, P.C. A question of self-preservation: Immunopathology in influenza virus infection. *Immunol. Cell Biol.* **2007**, *85*, 85–92. [CrossRef]
37. Gough, D.J.; Messina, N.L.; Clarke, C.J.; Johnstone, R.W.; Levy, D.E. Constitutive Type I Interferon Modulates Homeostatic Balance through Tonic Signaling. *Immunity* **2012**, *36*, 166–174. [CrossRef]
38. Amadori, M. The role of IFN-alpha as homeostatic agent in the inflammatory response: A balance between danger and re-sponse? *J. Interferon Cytokine Res.* **2007**, *27*, 181–189. [CrossRef]

Review

Pseudorabies Virus Associations in Wild Animals: Review of Potential Reservoirs for Cross-Host Transmission

Aijing Liu ^{1,2}, Tong Xue ³, Xiang Zhao ¹, Jie Zou ¹, Hongli Pu ¹, Xiaoliang Hu ¹  and Zhige Tian ^{1,*}

¹ Yibin Key Laboratory of Zoological Diversity and Ecological Conservation, Faculty of Agriculture, Forestry, and Food Engineering, Yibin University, Yibin 644000, China

² State Key Laboratory of Veterinary Biotechnology, Harbin Veterinary Research Institute, Chinese Academy of Agricultural Sciences, Harbin 150001, China

³ School of Mathematical Science, Harbin Normal University, Harbin 150001, China

* Correspondence: beishugege@126.com

Abstract: Pseudorabies virus (PRV) has received widespread attention for its potential health effects on humans, wildlife, domestic animals, and livestock. In this review, we focus on PRV dynamics in wildlife, given the importance of wild-origin PRV transmission to domestic and farm animals. Wild boars, pigs, and raccoons can serve as reservoirs of PRV, with viral transmission to domestic livestock occurring via several routes, such as wild herd exposure, contaminated meat consumption, and insect vector transmission. Many endangered feline and canine species can be infected with PRV, with acute disease and death within 48 h. The first confirmed human case of PRV infection in mainland China was reported in 2017. Thus, PRV exhibits potentially dangerous cross-host transmission, which is likely associated with inappropriate vaccination, poor awareness, and insufficient biosecurity. Currently, no vaccine provides full protection against PRV in all animals. Here, we summarize the epidemiology and pathogenesis of PRV infection in wild, domestic, and farmed animals, which may facilitate the design of novel therapeutics and strategies for controlling PRV infection and improving wildlife protection in China.

Keywords: pseudorabies virus; wildlife; cross-host transmission; vaccination



Citation: Liu, A.; Xue, T.; Zhao, X.; Zou, J.; Pu, H.; Hu, X.; Tian, Z. Pseudorabies Virus Associations in Wild Animals: Review of Potential Reservoirs for Cross-Host Transmission. *Viruses* **2022**, *14*, 2254. <https://doi.org/10.3390/v14102254>

Academic Editors: Xiangdong Li and Yan-Dong Tang

Received: 29 September 2022

Accepted: 12 October 2022

Published: 14 October 2022

Publisher's Note: MDPI stays neutral with regard to jurisdictional claims in published maps and institutional affiliations.



Copyright: © 2022 by the authors. Licensee MDPI, Basel, Switzerland. This article is an open access article distributed under the terms and conditions of the Creative Commons Attribution (CC BY) license (<https://creativecommons.org/licenses/by/4.0/>).

1. Introduction

Belonging to the family *Herpesviridae* and subfamily *Alphaherpesvirinae* [1], the pseudorabies virus (PRV) is the causative agent of pseudorabies (PR) or Aujeszky's disease, which can lead to acute infection and significant economic losses in pigs and other animals. The alphaherpesvirus genomes are divided into six classes (A–F) [2] based on the arrangement of repeat sequences (inverted and tandem repeats) and unique regions (short and long). The PRV genome belongs to the D class [3] and is approximately 140 kb in length.

Wild boars and pigs are the primary natural hosts of PRV and the only latent carriers [4]. PRV-related morbidity and mortality depend on various factors, such as animal health, viral strain, and infectious dose [5]. To date, PRV has been detected in various wild animals, including boars [6], rats [7], bears [8,9], raccoons [10,11], panthers [12], Iberian lynx [13], wolves [14], bats [15], and cats [16], as well as in domestic and farm animals, such as dogs [17–19], cattle [20–22], cats [23], sheep [24,25], foxes [26–28], and minks [29–32]. Furthermore, PRV infection is also a potential threat to humans [33–36].

In this review, we provide a brief overview of the traceability, transmission, and vaccination of PRV infection in animals with the aim to strengthen PR control measures.

2. Possible Transmission Route of PRV Infection

At present, the epizootiology of PR disease is not completely understood. One hypothesis for herd-to-herd transmission is that wild animals (e.g., wild boars and Norway rats) act as disease reservoir hosts and spread the virus from one farm to another [37].

Alternatively, wild animals may become directly infected with PRV due to consumption of wild boar meat [38] or via insect-borne vectors such as winter ticks [39]. However, previous research on infected wild panthers found that the isolated PRV strain did not match that found in wild boars [12]. Thus, the origin of PRV in wild animals remains unresolved. In this review, we summarize current knowledge of PRV infection in natural and non-natural hosts (Figure 1).

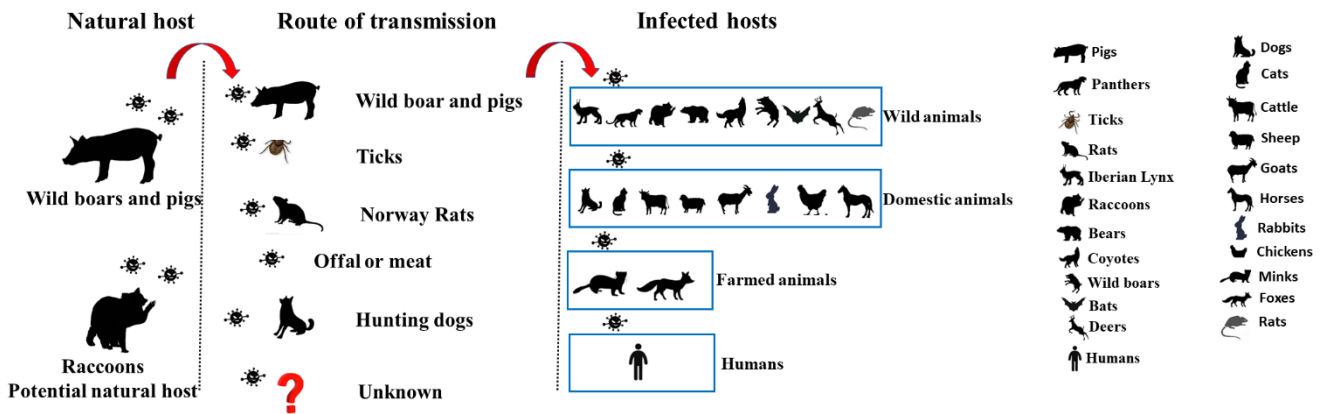


Figure 1. Schematic of PRV transmission. Wild boars and pigs are natural hosts of the PRV, while raccoons are potential natural hosts of the PRV. Five known transmission routes are described. Infected hosts include humans and wild, domestic, and farm animals.

3. PRV Infection in Wild, Domestic, and Farm Animals

3.1. PRV Infection in Wild Animals

3.1.1. Wild Boars

Wild boars are reservoirs for various infectious diseases in livestock and humans, including classical (CSFV) and African swine fever viruses (ASFV), porcine circovirus 2 (PCV2), porcine reproductive and respiratory syndrome virus (PRRSV), porcine parvovirus (PPV), hepatitis E virus (HEV), swine influenza virus (SIV), Japanese encephalitis virus (JEV), and torque teno virus (TTV) [6,40].

PRV infection is enzootic and widespread in Eurasian wild boars [41,42], with the first cases reported in Italy, former Yugoslavia, and USA [43]. Following successful prevention and eradication programs, PRV has been largely eliminated from domestic pigs in many parts of Europe, including Austria, Cyprus, Denmark, Finland, The Netherlands, and Great Britain (England, Scotland, and Wales) [41]. However, PRV infections remain widespread in many wild boar populations in the Czech Republic [44], Germany [41,45], France [46], Croatia [47], USA [48–50], Japan [51], Italy [16,52,53], Switzerland [52], Spain [53,54], Slovenia [55], Serbia [56], Brazil [57], Romania [58], Russia [59], Poland [60], and Belgium [61]. To date, however, there is little epidemiological information regarding PRV infection in Chinese wild boar populations. Considering that the number of wild boars in China is increasing year by year, epidemiological surveillance of PRV is urgently needed.

As wild boar populations expand their range, there is increased potential risk for disease transmission that may affect healthy of humans and domestic swine, and conservation of wildlife. Based on long-term serological field studies, PRV is considered endemic in wild boar populations in the USA, including in the southern and central states (California [62], Southeast [63], Hawaii, Texas [64], Arizona [65], North Carolina [66,67]), as well as in Guam [68], Nebraska, Michigan [69], and Oklahoma [49]. Seroprevalence varies from 0.5% to 64.4% at the regional level [68,70,71]. In Europe, PRV-infected wild boar populations are present in Germany, Italy, Belgium, Croatia, the Czech Republic, former Yugoslavia, France, the Netherlands, Poland, Romania, Russia, Slovenia, Spain, and Switzerland, with average seroprevalence ranging from 0.3% to 66%. Based on 7209 samples collected from 2000 to 2011, average seroprevalence in Germany is 6.8% [45]. Based on 5000 wild boar

samples collected from 2006 to 2020, average seroprevalence in Italy ranges from 3.8% to 30.9% [70–73].

Characterization of PRV from wild swine is helpful to understand population diversity and could trace back the infection route [43]. In Europe, phylogenetic analysis of partial sequences of the glycoprotein C gene suggests that wild boar isolates can be differentiated into clades A and B [61,74]. Clade A isolates originate from Austria, France, Germany, Hungary, Italy, and Slovakia, while clade B isolates originate from southwestern Europe, including Germany, France, and Spain [74]. Thus, the clade A and B isolates overlap geographically in central Europe, Germany, and France [74]. PRV isolated from USA was distinct from European isolates and was closely related to domestic pig isolates. It may represent a transmission from domestic to feral swine [6,75,76].

3.1.2. Bears

Detection of antibodies to canine distemper virus (CDV), canine herpesvirus type 1 (CHV-1), canine parvovirus type 2 (CPV-2), canine parainfluenza virus type 2 (CPIV-2), canine coronavirus (CCV), West Nile virus (WNV), and PRV is positive in European brown bears (*Ursus arctos*) [77]. Previous studies have reported PRV-positive blood samples in free-ranging Eurasian brown bears (*Ursus arctos*) in Slovakia [77] and PRV-positive tissues and antibodies in captive bears fed raw pig heads [8,9,76,77].

In most cases, PR disease is fatal in bears, with death occurring within 1–3 days of clinical symptoms. Upon consuming infected pig offal or pig heads, bears can show acute and asymptomatic infections. In Himalayan bears, however, only mild clinical signs are reported, with negative neutralizing antibody tests [8].

3.1.3. Raccoons

Raccoons (*Procyon lotor*) are considered a natural reservoir of PRV [10]. The clinical signs of PRV infection in raccoons resemble those of rabies and distemper [78]. Avirulent strain K is naturally occurring in the raccoon population [79]. Raccoons infected with virulent PRV strains (e.g., Be, S62/26, and 429) can transmit the virus to uninfected raccoons via contact. In raccoons, all virulent PRV strains are lethal, while avirulent strain K has a mortality rate of only 18% (2/11). Furthermore, when raccoons are infected with avirulent strain K, they may be re-infected with virulent strains, suggesting that virulent PRV may be circulating in raccoon populations [10,78].

3.1.4. Other Wild Animals

PRV not only infects wild boars, bears, and raccoons, but also can infect many wild animals, especially rare and endangered animals [12,53].

Panthers

The Florida panther (*Felis concolor coryi*) is an endangered feline species [12]. Similar to the infection process in domestic cats, PRV infection is fatal in panthers [80]. Necropsies of infected panthers have detected residual swine hair in the digestive tract, confirming ingestion of wild boar meat and identifying the potential route of PRV exposure. Based on sequence analysis, the isolated panther strain has been identified as a wild-type gI⁺ and TK⁺ genotype [81].

Iberian Lynx

The Iberian lynx (*Lynx pardinus*), one of the most endangered feline species in the world [53], preys on small ungulates, birds, reptiles, and occasionally wild boar [82] and is positive for feline leukemia provirus (FeLV), feline parvovirus (FPV), and *Cytauxzoon* sp. by using PCR assay [13]. A previously captured lynx was found to be PRV-positive based on blood, oropharyngeal swab, and rectal swab samples, with PRV antigens also detected in the tonsils, brain, and gastric glandular epithelial cells [53]. Histopathological analysis of the central nervous system (CNS) further showed meningoencephalitis similar to that

reported in domestic cats [83,84], dogs [85–87], foxes [88], and coyotes [89]. These results suggest that the Iberian lynx is susceptible to PRV and may be exposed to the virus via the consumption of wild boar meat [82]. Molecular and seroepidemiological analysis further confirmed the emergence of PRV in the Iberian lynx population (11.8%, 2/17) [13].

Coyotes

PRV infection has been reported in coyotes (*Canis latrans*) based on the testing of brain tissue. Clinical symptoms include anorexia, abnormal vocalizations, and nervousness [14,87,88]. PRV isolated from Belgian coyotes is similar to the Kaplan reference strain, the most common type present in European wild boars, suggesting potential infection via consumption of PRV-infected boar meat [14]. In China, a PRV strain was isolated from a coyote showing various clinical symptoms, including vomiting, dyspnea, circular movements, processed moaning, uneasy behavior, intense pruritus, paroxysmal convulsions, and quadriplegia. Sequence analysis of the Chinese PRV strain, which contained the glycoprotein E gene, indicated that it may be a field strain rather than a vaccine strain [90].

3.2. PRV Infections in Domestic Animals

3.2.1. Dogs

Because of the recent incidents of PRV infecting people, the dog in PRV infection has aroused great concern. PRV is prevalent in dogs, including working and hunting dogs, in the USA [17,89,90], Belgium [91], Italy [19,75,92], France [93], Spain [85,94], Japan [95,96], Austria [97–99], China [18], Serbia [100], Argentina [101], and Germany [74], with infection via direct or indirect contact with wild boars and pigs [6,74]. Dogs with PRV infection display neurological signs, anorexia, intense muzzle itch, and respiratory distress [1,96], and usually die within 48 h of clinical symptom onset [19].

3.2.2. Cattle

PRV infection can occur in cattle [6,20,21], especially when housed with pigs. PRV-infected cattle present with neurological symptoms and usually die within 24 h, with necropsy showing leptomenigeal hyperemia and lung consolidation [21]. Furthermore, under experimental infection, PRV has been isolated from the retropharyngeal lymph nodes [102] and pituitary, pharynx, and submaxillary lymph nodes of cattle [103].

3.2.3. Cats

Cats can be infected with PRV under natural and experimental conditions [81,82,103]. The disease is sporadic and mainly transmits through the consumption of pig offal. Clinical symptoms include anorexia and pruritus, with death occurring within 12–48 h of clinical onset [83]. The virus is transmitted via the oral route, typically replicating in the tonsils and pharynx, then spreading through the CNS and excreted through oral and nasal secretions [83,104].

3.2.4. Sheep

Sheep in contact with pigs are also susceptible to field strains of PRV. Previous studies have reported clinical signs of lethargy, fever, pruritus, and death in sheep following PRV infection, despite vaccination with the Bartha vaccine strain [24]. Even without direct contact with pigs, sheep exhibiting CNS symptoms have been found to be PRV positive in postmortem tissue samples, with sequence analysis of the viral genome showing close identity to the Buk T-900 reference strain [105]. China has also reported outbreaks of PR in sheep following vaccination with attenuated live vaccines (i.e., Bartha-K16), resulting in clinical symptoms such as intense rubbing and licking. These results suggest that certain vaccines may be unsuitable for use in sheep [25].

3.2.5. Horses

Previous reported that horses with experimentally induced PRV infection had severe clinical signs, but no pruritus [106]. PRV antigens and DNA have also been detected in the neurons of horses presenting with neurological signs and severe meningoencephalitis, with PRV infection potentially occurring via aerosolized pig slurry [106]. While other non-porcine species typically succumb to PRV infection within 48 h, PRV-infected horses exhibit a longer course of infection (more than 7 days) without pruritus, and eventually survive [106,107].

3.2.6. Chickens

In addition to infecting mammals, PRV can also infect birds such as chickens, which are susceptible to PRV infection under both experimental and natural conditions [108–110]. For example, Kouwenhoven (1982) isolated a PRV strain from farm chickens, which was pathogenic to 7-day-old chicks but could be neutralized by known PRV antisera and showed cross-reactivity with infectious bovine rhinotracheitis. The strain was originally derived from a PRV vaccine adapted to chicken cells and did not cause classical inclusion bodies in the neural tissue [110].

3.3. PRV Infections in Farm Animals

3.3.1. Foxes

Foxes fed pig offal can become infected with PRV, as reported in Italy [26,28] and China [27]. Foxes with PRV infection display neurological signs, ataxia, fever, vomiting, dyspnea, intense pruritus, and frequent snarling, with death usually occurring within a few hours to three days. Studies have reported a high morbidity rate (80%; 1200/1500) in PRV-infected foxes, especially symptomatic foxes [27]. Previous epidemiological analysis of strains isolated from dead foxes found a close relationship to domestic field strains in China, rather than vaccine strains [27]. However, the epidemiological link between the isolated strain and wild animal populations or domestic pigs is unclear.

3.3.2. Minks

Outbreaks of PRV in minks have been reported in many countries [111–115]. Brain samples collected from dead minks have been identified as PRV-positive, with necropsy also showing organ hemorrhage and endotheliotropic vessels, although no neurological signs were evident before death [29,30]. In 2014, a serious outbreak of PRV was reported in a mink farm in Shandong Province, China. The minks exhibited severe clinical signs, including diarrhea, anorexia, and abdominal and facial skin scratching, and a high morbidity rate of 87% (3522/4028). Out of 566 minks, 33 tested PRV-positive by polymerase chain reaction (PCR), and the isolated strain clustered with vaccine-resistant Chinese porcine PRV isolates [31,32].

3.4. PRV Infections in Humans

Although humans were previously considered a non-susceptible host for PRV infection, a PRV variant causing infectious endophthalmitis has been reported in China in recent years [36], thought to have originated from sewage containing pig excrement. In 2020, four patients with acute encephalitis were diagnosed with PRV infection and presented with respiratory dysfunction and acute neurological symptoms. The PRV strain (hSD-1/2019) isolated from the cerebrospinal fluid of one of the patients was closely related to a PRV variant known to cause high pathogenicity and acute neurological symptoms in pigs [35].

4. Transmission Models and Cross-Host Transmission Routes for PRV

There are two competing models of PRV transmission in wild boars, i.e., age-dependent and sexual transmission models. The age-dependent model suggests that PRV seroprevalence differs between older and younger animals, with older boars showing significantly

higher prevalence than younger individuals [16,116–119]. In contrast, preferential sexual transmission may occur under random or polygynous boar mating systems [48], whereby polygamy and mate guarding behavior may impact the seroprevalence of PRV in males and females differently. For example, under a 1:1 sex ratio, predicted seroprevalence is the same for both at-risk males and at-risk females; however, as wild boars are highly polygynous [120,121], the predicted seroprevalence is different for at-risk males and at-risk females [48].

Although data on the origin and transmission of PRV field strains are limited, we suggest several possible transmission routes: (1) non-natural hosts may become infected via contact with immunized pigs [122]; (2) before succumbing to illness, PRV-infected non-natural hosts may travel within their territories, leading to transmission to other individuals; (3) due to inappropriate biosecurity measures, non-natural hosts may come into indirect contact with carcasses contaminated with PRV [9]; (4) as anthropogenic-impacted landscapes change wild animal habitat availability, frequent contact between wild animals may result in an increase in PRV infection. Thus, appropriate measures should be taken to disrupt these transmission routes and control animal infection.

5. Vaccination

PRV has a wide host range and can be transmitted across wild, domestic, and farm animals. The DIVA strategy (i.e., differentiating infected from vaccinated animals) has been used in various European countries and the USA based on gE- or gI-deleted vaccines [67,72]. Attenuated live vaccines (e.g., gE-gene, gE/gI/TK-gene, TK/gG-gene, gE/gI-gene, TK/gE-gene and gE/US2-gene deleted) have been used in China since the early 1990s for the control of PR in pig farms [123–127]. However, while these vaccines provide effective protection for pigs, they do not appear to provide full protection for all animals or species. Previous reports suggest that virulent strain DCD1 and attenuated strain HB98 can cause clinical signs and pathological lesions and induce death within 24 h of the onset of symptoms [128]. Interestingly, in transmission experiments using the Bartha-K61 vaccine, viruses with longer incubation periods and lower replication rates take longer to cause lesions in dogs than the HB98 and DCD-1 strains [128]. In addition, US7/US8/UL23-deleted recombinant PRV vaccines provide effective protection in pigs but show obvious neural symptoms and virulence in dogs [129], while the Bartha-K16 vaccine can also induce PR in sheep and goat populations [25]. Thus, commercial vaccines may not be safe for dogs or certain farm animals [129]. These findings suggest that genes deleted in commercial vaccines may be associated with replication rates and tissue tropism *in vivo*, resulting in changes in PRV pathogenicity [128]. In contrast, modified live PRV vaccines with gG-gE/TK deletion have been shown to induce an immune response against the virulent Shope strain and may play a role in preventing PRV transmission in raccoons [11]. In general, however, present-day vaccines used in pig farms do not provide complete protection for all farm and domestic animals. As such, novel and safe vaccines must be developed for different animals, particularly those that are endangered.

6. Interspecies Transmission

PRV was previously considered to be limited to host species only. However, there are three possible pathways that have allowed cross-host transmission from wild boars and pigs to non-natural hosts, namely, positive selection, adaptive evolution, and recombination. The *gB*, *gC*, *gD*, and *gE* genes play central roles in receptor binding, pathogenicity, and induction of antibodies, with various residues shown to be under positive selection, including residues 43, 75, 848, and 922 in the *gB* protein, residues 59 and 194 in the *gC* protein, and residue 348 in *gE* protein [130], thus suggesting that PRV may undergo host adaptation. Further research has revealed that two sites on *gB* in clade 2 of PRV (929 and 934), four sites on *gC* in clade 1 of PRV (59, 75, 76, and 191), and two sites on *gE* in clade 2 of PRV (495 and 540) may be related to adaptive evolution after cross-host transmission [130]. Thus, these two pathways suggest that mutations on the PRV glycoprotein may play a

role in facilitating cross-host transmission from natural to non-natural hosts (including humans). Recombination also plays a vital role in the evolution of viruses, allowing the emergence of new strains with altered virulence and immunogenicity [131]. Intraclade and interclade recombinations have occurred in the PRV genome. For example, the SC strain is thought to have recombined with PRV strains in clade 2 and the PRV ZJ01 strain is thought to have originated by recombination between clade 1 or clade 2.1 isolates [132]. These recombinations can cause enhanced virulence, failed immunity, or new genotypes [130], and may increase the probability of cross-host transmission of PRV.

In addition, the receptors of PRV have been identified, including 3-O-sulfonated-heparan sulfate (3-O-S-HS) [133], the herpes virus entry mediator A (HveA, also known as HVEM), a TNF receptor-related protein [134], and three immunoglobulin superfamily members: HveB (PRR2, nectin-2) [135], HveC (PRR1, nectin-1) and HveD (PRV, CD155) [136]. Among these molecules, nectin-1 is highly conserved in mammalian animals and serves as a broadly used receptor mediating the entry of PRV [136]. Previous reports suggested that PRV infects host cells via both human and swine nectin-1, and that its gD exhibits similar binding affinities for nectin-1 of the two species [137]. These structural observations provide a systematic view on the receptor binding mechanism for cross-host transmission of PRV.

7. Conclusions

In this review, we summarize the epidemiology and pathogenesis of PRV infection in wild, domestic, and farm animals. Recently, various field strains have shown virulence against non-natural hosts, such as bears, coyotes, and panthers, with some found to be epidemiologically associated with swine isolates, wild boar isolates, and vaccine strains. Thus, novel and safe vaccines should be developed for different animals, particularly endangered species, to control cross-host transmission of PRV.

Author Contributions: Conceptualization, supervision, and project administration: Z.T. and X.H.; investigation, visualization, and writing of original draft preparation: A.L., T.X., J.Z., X.Z. and H.P.; funding acquisition: X.H. and Z.T. All authors have read and agreed to the published version of the manuscript.

Funding: This work was supported by the Doctor Launch Project of Yibin University (2019QD09 and 2019QD10) and Provincial First-Class Undergraduate Major-Biological Engineering (155-SYLZY201901).

Institutional Review Board Statement: Not applicable.

Informed Consent Statement: Not applicable.

Data Availability Statement: All data generated or analyzed during this study are included in the published article.

Conflicts of Interest: The authors declare no conflict of interest.

References

1. Nauwynck, H.; Glorieux, S.; Favoreel, H.; Pensaert, M. Cell biological and molecular characteristics of pseudorabies virus infections in cell cultures and in pigs with emphasis on the respiratory tract. *Vet. Res.* **2007**, *38*, 229–241. [CrossRef] [PubMed]
2. Roizman, B. The family Herpesviridae: A brief introduction. *Fields Virol.* **2001**, *2*, 2387–2397.
3. Ben-Porat, T.; Kaplan, A.S. Molecular biology of pseudorabies virus. In *The Herpesviruses*; Springer: Berlin/Heidelberg, Germany, 1985; pp. 105–173.
4. Sun, Y.; Luo, Y.; Wang, C.-H.; Yuan, J.; Li, N.; Song, K.; Qiu, H.-J. Control of swine pseudorabies in China: Opportunities and limitations. *Vet. Microbiol.* **2016**, *183*, 119–124. [CrossRef] [PubMed]
5. Pomeranz, L.E.; Reynolds, A.E.; Hengartner, C.J. Molecular biology of pseudorabies virus: Impact on neurovirology and veterinary medicine. *Microbiol. Mol. Biol. Rev.* **2005**, *69*, 462–500. [CrossRef]
6. Müller, T.; Hahn, E.C.; Tottewitz, F.; Kramer, M.; Klupp, B.G.; Mettenleiter, T.C.; Freuling, C. Pseudorabies virus in wild swine: A global perspective. *Arch. Virol.* **2011**, *156*, 1691–1705. [CrossRef]
7. Shope, R.E. Experiments on the Epidemiology of Pseudorabies: II. Prevalence of the Disease among Middle Western Swine and the Possible Role of Rats in Herd-to-Herd Infections. *J. Exp. Med.* **1935**, *62*, 101–117. [CrossRef]

8. Banks, M.; Torracca, L.S.; Greenwood, A.G.; Taylor, D.C. Aujeszky's disease in captive bears. *Vet. Rec.* **1999**, *145*, 362–365. [CrossRef]
9. Zanin, E.; Capua, I.; Casaccia, C.; Zuin, A.; Moresco, A. Isolation and characterization of Aujeszky's disease virus in captive brown bears from Italy. *J. Wildl. Dis.* **1997**, *33*, 632–634. [CrossRef]
10. Platt, K.B.; Graham, D.L.; Faaborg, R.A. Pseudorabies: Experimental studies in raccoons with different virus strains. *J. Wildl. Dis.* **1983**, *19*, 297–301. [CrossRef]
11. Weigel, R.M.; Hahn, E.C.; Scherba, G. Survival and immunization of raccoons after exposure to pseudorabies (Aujeszky's disease) virus gene-deleted vaccines. *Vet. Microbiol.* **2003**, *92*, 19–24. [CrossRef]
12. Glass, C.M.; McLean, R.G.; Katz, J.B.; Maehr, D.S.; Cropp, C.B.; Kirk, L.J.; McKeiman, A.J.; Evermann, J.F. Isolation of pseudorabies (Aujeszky's disease) virus from a Florida panther. *J. Wildl. Dis.* **1994**, *30*, 180–184. [CrossRef]
13. Nájera, F.; Grande-Gómez, R.; Peña, J.; Vázquez, A.; Palacios, M.J.; Rueda, C.; Corona-Bravo, A.; Zorrilla, I.; Revuelta, L.; Gil-Molino, M.; et al. Disease Surveillance during the Reintroduction of the Iberian Lynx (*Lynx pardinus*) in Southwestern Spain. *Animals* **2021**, *11*, 547. [CrossRef]
14. Verpeest, S.; Cay, A.B.; Bertrand, O.; Saulmont, M.; De Regge, N. Isolation and characterization of pseudorabies virus from a wolf (*Canis lupus*) from Belgium. *Eur. J. Wildl. Res.* **2014**, *60*, 149–153. [CrossRef]
15. Reagan, R.L.; Day, W.C.; Marley, R.T.; Brueckner, A.L. Effect of pseudorabies virus (Aujeszky strain) in the large brown bat (*Eptesicus fuscus*). *Am. J. Vet. Res.* **1953**, *14*, 331–332.
16. Lari, A.; Lorenzi, D.; Nigrelli, D.; Brocchi, E.; Faccini, S.; Poli, A. Pseudorabies virus in European wild boar from central Italy. *J. Wildl. Dis.* **2006**, *42*, 319–324. [CrossRef]
17. Cramer, S.D.; Campbell, G.A.; Njaa, B.L.; Morgan, S.E.; Smith, S.K., II; McLin, W.R., IV; Brodersen, B.W.; Wise, A.G.; Scherba, G.; Langohr, I.M.; et al. Pseudorabies virus infection in Oklahoma hunting dogs. *J. Vet. Diagn. Investig. Off. Publ. Am. Assoc. Vet. Lab. Diagn.* **2011**, *23*, 915–923. [CrossRef]
18. Zhang, L.; Zhong, C.; Wang, J.; Lu, Z.; Liu, L.; Yang, W.; Lyu, Y. Pathogenesis of natural and experimental Pseudorabies virus infections in dogs. *Virology* **2015**, *12*, 44. [CrossRef]
19. Abbate, J.M.; Giannetto, A. First Isolation and Molecular Characterization of Pseudorabies Virus in a Hunting Dog in Sicily (Southern Italy). *Vet. Sci.* **2021**, *8*, 296. [CrossRef]
20. Bitsch, V. A study of outbreaks of Aujeszky's disease in cattle. I. Virological and epidemiological findings. *Acta Vet. Scand.* **1975**, *16*, 420–433. [CrossRef]
21. Cheng, Z.; Kong, Z.; Liu, P.; Fu, Z.; Zhang, J.; Liu, M. Natural infection of a variant pseudorabies virus leads to bovine death in China. *Transbound. Emerg. Dis.* **2020**, *67*, 518–522. [CrossRef]
22. Ciarello, F.P.; Capucchio, M.T.; Ippolito, D.; Colombino, E.; Gibelli, L.R.M.; Fiasconaro, M.; Moreno Martin, A.M.; Di Marco Lo Presti, V. First Report of a Severe Outbreak of Aujeszky's Disease in Cattle in Sicily (Italy). *Pathogens* **2020**, *9*, 954. [CrossRef]
23. Pensaert, M.; Kluge, J. Pseudorabies virus (Aujeszky's disease). *Virus Infect. Porc.* **1989**, *2*, 39–65.
24. Jacobs, L.; Mulder, W.; Dercksen, D.; Vos, J.; Raymakers, R.; Kimman, T. Detection of wild-type Aujeszky's disease virus by polymerase chain reaction in sheep vaccinated with a modified live vaccine strain. *Res. Vet. Sci.* **1997**, *62*, 271–274. [CrossRef]
25. Kong, H.; Zhang, K.; Liu, Y.; Shang, Y.; Wu, B.; Liu, X. Attenuated live vaccine (Bartha-K16) caused pseudorabies (Aujeszky's disease) in sheep. *Vet. Res. Commun.* **2013**, *37*, 329–332. [CrossRef]
26. Moreno, A.; Chiapponi, C.; Sozzi, E.; Morelli, A.; Silenzi, V.; Gobbi, M.; Lavazza, A.; Paniccia, M. Detection of a gE-deleted Pseudorabies virus strain in an Italian red fox. *Vet. Microbiol.* **2020**, *244*, 108666. [CrossRef]
27. Jin, H.-L.; Gao, S.-M.; Liu, Y.; Zhang, S.-F.; Hu, R.-L. Pseudorabies in farmed foxes fed pig offal in Shandong province, China. *Arch. Virol.* **2016**, *161*, 445–448. [CrossRef]
28. Caruso, C.; Dondo, A.; Cerutti, F.; Masoero, L.; Rosamilia, A.; Zoppi, S.; D'Errico, V.; Grattarola, C.; Acutis, P.L.; Peletto, S. Aujeszky's disease in red fox (*Vulpes vulpes*): Phylogenetic analysis unravels an unexpected epidemiologic link. *J. Wildl. Dis.* **2014**, *50*, 707–710. [CrossRef]
29. Kimman, T.G.; van Oirschot, J.T. Pathology of Aujeszky's disease in mink. *Vet. Pathol.* **1986**, *23*, 303–309. [CrossRef]
30. Marcaccini, A.; Peña, M.L.; Quiroga, M.I.; Bermúdez, R.; Nieto, J.M.; Alemañ, N. Pseudorabies virus infection in mink: A host-specific pathogenesis. *Vet. Immunol. Immunopathol.* **2008**, *124*, 264–273. [CrossRef]
31. Wang, G.-S.; Du, Y.; Wu, J.-Q.; Tian, F.-L.; Yu, X.-J.; Wang, J.-B. Vaccine resistant pseudorabies virus causes mink infection in China. *BMC Vet. Res.* **2018**, *14*, 20. [CrossRef]
32. Liu, H.; Li, X.-T.; Hu, B.; Deng, X.-Y.; Zhang, L.; Lian, S.-Z.; Zhang, H.-L.; Lv, S.; Xue, X.-H.; Lu, R.-G.; et al. Outbreak of severe pseudorabies virus infection in pig-offal-fed farmed mink in Liaoning Province, China. *Arch. Virol.* **2017**, *162*, 863–866. [CrossRef] [PubMed]
33. Ou, J.; Cai, S.; Zheng, F.; Lu, G.; Zhang, G. Human pseudorabies virus infection: A new threat in China. *J. Infect.* **2020**, *80*, 578–606. [CrossRef] [PubMed]
34. Sehl, J.; Teifke, J.P. Comparative Pathology of Pseudorabies in Different Naturally and Experimentally Infected Species—A Review. *Pathogens* **2020**, *9*, 633. [CrossRef] [PubMed]
35. Liu, Q.; Wang, X.; Xie, C.; Ding, S.; Yang, H.; Guo, S.; Li, J.; Qin, L.; Ban, F.; Wang, D.; et al. A Novel Human Acute Encephalitis Caused by Pseudorabies Virus Variant Strain. *Clin. Infect. Dis. Off. Publ. Infect. Dis. Soc. Am.* **2021**, *73*, e3690–e3700. [CrossRef]

36. Ai, J.-W.; Weng, S.-S.; Cheng, Q.; Cui, P.; Li, Y.-J.; Wu, H.-L.; Zhu, Y.-M.; Xu, B.; Zhang, W.-H. Human Endophthalmitis Caused by Pseudorabies Virus Infection, China, 2017. *Emerg. Infect. Dis.* **2018**, *24*, 1087–1090. [CrossRef] [PubMed]
37. Shope, R.E. Experiments on the Epidemiology of Pseudorabies: I. Mode of Transmission of the Disease in Swine and Their Possible Role in Its Spread to Cattle. *J. Exp. Med.* **1935**, *62*, 85–99. [CrossRef]
38. Haddane, B.; Essalhi, A. (Eds.) An outbreak of Aujeszky's disease in the hunting dog (*Lycaon Pictus*). In *European Association of Zoo-and Wildlife Veterinarians (EAZVV); Second Scientific Meeting*; 1998.
39. Musante, A.R.; Pedersen, K.; Hall, P. First reports of pseudorabies and winter ticks (*Dermacentor albipictus*) associated with an emerging feral swine (*Sus scrofa*) population in New Hampshire. *J. Wildl. Dis.* **2014**, *50*, 121–124. [CrossRef]
40. Meng, X.-J.; Lindsay, D.S.; Sriranganathan, N. Wild boars as sources for infectious diseases in livestock and humans. *Philos. Trans. R. Soc. Lond. Ser. B Biol. Sci.* **2009**, *364*, 2697–2707. [CrossRef]
41. Pannwitz, G.; Freuling, C.; Denzin, N.; Schaarschmidt, U.; Nieper, H.; Hlinak, A.; Burkhardt, S.; Klopries, M.; Dedek, J.; Hoffmann, L.; et al. A long-term serological survey on Aujeszky's disease virus infections in wild boar in East Germany. *Epidemiol. Infect.* **2012**, *140*, 348–358. [CrossRef]
42. Ruiz-Fons, F. A Review of the Current Status of Relevant Zoonotic Pathogens in Wild Swine (*Sus scrofa*) Populations: Changes Modulating the Risk of Transmission to Humans. *Transbound. Emerg. Dis.* **2017**, *64*, 68–88. [CrossRef]
43. Muller, T.; Conraths, F.J.; Hahn, E.C. Pseudorabies virus infection (Aujeszky's disease) in wild swine. *Infect. Dis. Rev.* **2000**, *2*, 27–34.
44. Sedlak, K.; Bartova, E.; Machova, J. Antibodies to selected viral disease agents in wild boars from the Czech Republic. *J. Wildl. Dis.* **2008**, *44*, 777–780. [CrossRef]
45. Denzin, N.; Borgwardt, J.; Freuling, C.; Müller, T. Spatio-temporal analysis of the progression of Aujeszky's disease virus infection in wild boar of Saxony-Anhalt, Germany. *Geospat. Health* **2013**, *8*, 203–213. [CrossRef]
46. Albina, E.; Mesplède, A.; Chenut, G.; Le Potier, M.F.; Bourbao, G.; Le Gal, S.; Leforban, Y. A serological survey on classical swine fever (CSF), Aujeszky's disease (AD) and porcine reproductive and respiratory syndrome (PRRS) virus infections in French wild boars from 1991 to 1998. *Vet. Microbiol.* **2000**, *77*, 43–57. [CrossRef]
47. Zupancić, Z.; Jukić, B.; Lojkić, M.; Cac, Z.; Jemersić, L.; Staresina, V. Prevalence of antibodies to classical swine fever, Aujeszky's disease, porcine reproductive and respiratory syndrome, and bovine viral diarrhoea viruses in wild boars in Croatia. *J. Vet. Med. B Infect. Dis. Vet. Public Health* **2002**, *49*, 253–256. [CrossRef]
48. Smith, G. Preferential sexual transmission of pseudorabies virus in feral swine populations may not account for observed seroprevalence in the USA. *Prev. Vet. Med.* **2012**, *103*, 145–156. [CrossRef]
49. Gaskamp, J.A.; Gee, K.L.; Campbell, T.A.; Silvy, N.J.; Webb, S.L. Pseudorabies Virus and *Brucella abortus* from an Expanding Wild Pig (*Sus scrofa*) Population in Southern Oklahoma, USA. *J. Wildl. Dis.* **2016**, *52*, 383–386. [CrossRef]
50. Corn, J.L.; Stallknecht, D.E.; Mechlin, N.M.; Luttrell, M.P.; Fischer, J.R. Persistence of pseudorabies virus in feral swine populations. *J. Wildl. Dis.* **2004**, *40*, 307–310. [CrossRef]
51. Mahmoud, H.Y.; Suzuki, K.; Tsuji, T.; Yokoyama, M.; Shimojima, M.; Maeda, K. Pseudorabies virus infection in wild boars in Japan. *J. Vet. Med. Sci.* **2011**, *73*, 1535–1537. [CrossRef]
52. Meier, R.; Ryser-Degiorgis, M. Wild boar and infectious diseases: Evaluation of the current risk to human and domestic animal health in Switzerland: A review. *Schweiz. Arch. Tierheilkd.* **2018**, *160*, 443–460. [CrossRef]
53. Masot, A.J.; Gil, M.; Risco, D.; Jiménez, O.M.; Núñez, J.I.; Redondo, E. Pseudorabies virus infection (Aujeszky's disease) in an Iberian lynx (*Lynx pardinus*) in Spain: A case report. *BMC Vet. Res.* **2017**, *13*, 6. [CrossRef]
54. Vicente, J.; Ruiz-Fons, F.; Vidal, D.; Höfle, U.; Acevedo, P.; Villanúa, D.; Fernández-De-Mera, I.G.; Martín, M.P.; Gortázar, C. Serosurvey of Aujeszky's disease virus infection in European wild boar in Spain. *Vet. Rec.* **2005**, *156*, 408–412. [CrossRef]
55. Vengust, G.; Valencak, Z.; Bidovec, A. Presence of antibodies against Aujeszky's disease virus in wild boar (*Sus scrofa*) in Slovenia. *J. Wildl. Dis.* **2005**, *41*, 800–802. [CrossRef]
56. Milicevic, V.; Radojicic, S.; Valcic, M.; Ivovic, V.; Radosavljevic, V. Evidence of Aujeszky's disease in wild boar in Serbia. *BMC Vet. Res.* **2016**, *12*, 134. [CrossRef]
57. Kmetiuk, L.B.; Cassaro Villalobos, E.M.; do Carmo Custódio de Souza Hunold Lara, M.; Machado, F.P.; Lipinski, L.C.; Dos Santos, A.P.; Biondo, A.W.; de Barros Filho, I.R. Serosurvey for Pseudorabies (Aujeszky's Disease) in Free-Range Wild Boars (*Sus scrofa*) of Brazil. *J. Wildl. Dis.* **2020**, *56*, 959–961. [CrossRef]
58. Vuta, V.; Barboi, G.; Olvedi, I.; Nicolae, S.; Leau, S.; Zamfir, L. The presence of antibodies to Aujeszky's Disease, Bovine Viral Diarrhoea and Porcine Reproductive and Respiratory Syndrome in wild boars. *Prelim. Data Rev. Română Med. Vet.* **2009**, *19*, 75–81.
59. Shcherbakov, A.; Kukushkin, S.; Timina, A.; Baibikov, T.; Kovalishin, V.; Kan'shina, A.; B''adovskaia, O.P.; Prokhvatilova, L.; Ruchnova, O.I.; Bakunov, I.N.; et al. Monitoring of infectious diseases among wild boars. *Vopr. Virusol.* **2007**, *52*, 29–33.
60. Szweda, W.; Lipowski, A.; Ciecierski, H.; Zalewski, K.; Pirus, T. European wild boar (*Sus scrofa* L.) as a reservoir of Herpesvirus suis 1. *Med. Weter.* **1998**, *54*, 541–544.
61. Verpoest, S.; Cay, A.B.; De Regge, N. Molecular characterization of Belgian pseudorabies virus isolates from domestic swine and wild boar. *Vet. Microbiol.* **2014**, *172*, 72–77. [CrossRef]
62. Clark, R.K.; Jessup, D.A.; Hird, D.W.; Ruppanner, R.; Meyer, M.E. Serologic survey of California wild hogs for antibodies against selected zoonotic disease agents. *J. Am. Vet. Med. Assoc.* **1983**, *183*, 1248–1251.


63. Nettles, V.; Erickson, G. (Eds.) Pseudorabies in wild swine. In Proceedings of the Annual Meeting-United States Animal Health Association, Louisville, KY, USA, 2–7 November 1984; Volume 88, pp. 505–506.
64. Corn, J.; Swiderek, P.; Blackburn, B.; Erickson, G.; Thiermann, A.; Nettles, V. Survey of selected diseases in wild swine in Texas. *J. Am. Vet. Med. Assoc.* **1986**, *189*, 1029–1032. [PubMed]
65. Corn, J.L.; Lee, R.M.; Erickson, G.A.; Murphy, C. Serologic survey for evidence of exposure to vesicular stomatitis virus, pseudorabies virus, brucellosis and leptospirosis in collared peccaries from Arizona. *J. Wildl. Dis.* **1987**, *23*, 551–557. [CrossRef] [PubMed]
66. Cunha, E.; Nassar, A.; Lara, M.; Bersano, J.; Villalobos, E.; Oliveira, J. Antibodies against pseudorabies virus in feral swine in southeast Brazil. *Arq. Bras. Med. Vet. Zootec.* **2006**, *58*, 462–466. [CrossRef]
67. Sandfoss, M.R.; DePerno, C.S.; Betsill, C.W.; Palamar, M.B.; Erickson, G.; Kennedy-Stoskopf, S. A serosurvey for *Brucella suis*, classical swine fever virus, porcine circovirus type 2, and pseudorabies virus in feral swine (*Sus scrofa*) of eastern North Carolina. *J. Wildl. Dis.* **2012**, *48*, 462–466. [CrossRef]
68. Cleveland, C.A.; DeNicola, A.; Dubey, J.; Hill, D.E.; Berghaus, R.D.; Yabsley, M.J. Survey for selected pathogens in wild pigs (*Sus scrofa*) from Guam, Mariana Islands, USA. *Vet. Microbiol.* **2017**, *205*, 22–25. [CrossRef]
69. Wilson, S.; Doster, A.R.; Hoffman, J.D.; Hygnstrom, S.E. First record of pseudorabies in feral swine in Nebraska. *J. Wildl. Dis.* **2009**, *45*, 874–876. [CrossRef]
70. Caruso, C.; Vitale, N.; Prato, R.; Radaelli, M.C.; Zoppi, S.; Possidente, R.; Dondo, A.; Chiavacci, L.; Martin, A.M.M.; Masoero, L. Pseudorabies virus in North-West Italian wild boar (*Sus scrofa*) populations: Prevalence and risk factors to support a territorial risk-based surveillance. *Vet. Ital.* **2018**, *54*, 337–341.
71. Verin, R.; Varuzza, P.; Mazzei, M.; Poli, A. Serologic, molecular, and pathologic survey of pseudorabies virus infection in hunted wild boars (*Sus scrofa*) in Italy. *J. Wildl. Dis.* **2014**, *50*, 559–565. [CrossRef]
72. Chiari, M.; Ferrari, N.; Bertolotti, M.; Avisani, D.; Cerioli, M.; Zanoni, M.; Alborali, L.G.; Lanfranchi, P.; Lelli, D.; Martin, A.M.; et al. Long-Term Surveillance of Aujeszky’s Disease in the Alpine Wild Boar (*Sus scrofa*). *EcoHealth* **2015**, *12*, 563–570. [CrossRef]
73. Pacini, M.I.; Forzan, M. Detection and Characterization of Viral Pathogens Associated with Reproductive Failure in Wild Boars in Central Italy. *Animals* **2021**, *11*, 304. [CrossRef]
74. Müller, T.; Klupp, B.; Freuling, C.; Hoffmann, B.; Mojczic, M.; Capua, I.; Palfi, V.; Toma, B.; Lutz, W.; Ruiz-Fon, F.; et al. Characterization of pseudorabies virus of wild boar origin from Europe. *Epidemiol. Infect.* **2010**, *138*, 1590–1600. [CrossRef]
75. Capua, I.; Fico, R.; Banks, M.; Tamba, M.; Calzetta, G. Isolation and characterisation of an Aujeszky’s disease virus naturally infecting a wild boar (*Sus scrofa*). *Vet. Microbiol.* **1997**, *55*, 141–146. [CrossRef]
76. Capua, I.; Casaccia, C.; Calzetta, G.; Caporale, V. Characterisation of Aujeszky’s disease viruses isolated from domestic animals and from a wild boar (*Sus scrofa*) in Italy between 1972 and 1995. *Vet. Microbiol.* **1997**, *57*, 143–149. [CrossRef]
77. Vitásková, E.; Molnár, L.; Holko, I.; Supuka, P.; Černíková, L.; Bártová, E.; Sedlak, K. Serologic Survey of Selected Viral Pathogens in Free-Ranging Eurasian Brown Bears (*Ursus arctos arctos*) from Slovakia. *J. Wildl. Dis.* **2019**, *55*, 499–503.
78. Thawley, D.G.; Wright, J.C. Pseudorabies virus infection in raccoons: A review. *J. Wildl. Dis.* **1982**, *18*, 113–116. [CrossRef]
79. Bartha, A. Kísérletek az Aujeszky-Féle Vírus Virulenciájának Szelídítésére. 1961. Available online: <http://hdl.handle.net/10832/46> (accessed on 20 August 2022).
80. Roelke, M.E.; Forrester, D.J.; Jacobson, E.R.; Kollias, G.V.; Scott, F.W.; Barr, M.C.; Evermann, J.F.; Pirtle, E.C. Seroprevalence of infectious disease agents in free-ranging Florida panthers (*Felis concolor coryi*). *J. Wildl. Dis.* **1993**, *29*, 36–49. [CrossRef]
81. Maehr, D.S.; Belden, R.C.; Land, E.D.; Wilkins, L. Food habits of panthers in southwest Florida. *J. Wildl. Manag.* **1990**, *54*, 420–423. [CrossRef]
82. Boadella, M.; Gortázar, C.; Vicente, J.; Ruiz-Fons, F. Wild boar: An increasing concern for Aujeszky’s disease control in pigs? *BMC Vet. Res.* **2012**, *8*, 7. [CrossRef]
83. Thiry, E.; Addie, D.; Belák, S.; Boucraut-Baralon, C.; Egberink, H.; Frymus, T.; Gruffydd-Jones, T.; Hartmann, K.; Hosie, M.J.; Lloret, A.; et al. Aujeszky’s disease/pseudorabies in cats: ABCD guidelines on prevention and management. *J. Feline Med. Surg.* **2013**, *15*, 555–556. [CrossRef]
84. Hagemoser, W.A.; Kluge, J.P.; Hill, H.T. Studies on the pathogenesis of pseudorabies in domestic cats following oral inoculation. *Can. J. Comp. Med. Rev. Can. Med. Comp.* **1980**, *44*, 192–202.
85. Quiroga, M.I.; Nieto, J.M.; Sur, J.; Osorio, F. Diagnosis of Aujeszky’s disease virus infection in dogs by use of immunohistochemistry and in-situ hybridization. *Zent. Vet. Reihe A* **1998**, *45*, 75–81. [CrossRef]
86. Shell, L.G.; Ely, R.W.; Crandell, R.A. Pseudorabies in a dog. *J. Am. Vet. Med. Assoc.* **1981**, *178*, 1159–1161.
87. Schöniger, S.; Klose, K.; Werner, H.; Schwarz, B.-A.; Müller, T.; Schoon, H.-A. Nonsuppurative encephalitis in a dog. *Vet. Pathol.* **2012**, *49*, 731–734. [CrossRef]
88. Quiroga, M.; Vázquez, S.; López-Peña, M.; Guerrero, F.; Nieto, J. Experimental Aujeszky’s Disease in Blue Foxes (*Alopex lagopus*). *J. Vet. Med. Ser. A* **1995**, *42*, 649–657. [CrossRef]
89. Raymond, J.T.; Gillespie, R.G.; Woodruff, M.; Janovitz, E.B. Pseudorabies in captive coyotes. *J. Wildl. Dis.* **1997**, *33*, 916–918. [CrossRef]
90. Lian, K.; Zhang, M.; Zhou, L.; Song, Y.; Wang, G.; Wang, S. First report of a pseudorabies-virus-infected wolf (*Canis lupus*) in China. *Arch. Virol.* **2020**, *165*, 459–462. [CrossRef]

91. Cay, A.; Letellier, C. Isolation of Aujeszky's disease virus from two hunting dogs in Belgium after hunting wild boars. *Vlaams Diergeneesk. Tijdschr.* **2009**, *78*, 194–195.
92. Moreno, A.; Sozzi, E.; Grilli, G.; Gibelli, L.R.; Gelmetti, D.; Lelli, D.; Chiari, M.; Prati, P.; Alborali, G.L.; Boniotti, M.B.; et al. Detection and molecular analysis of Pseudorabies virus strains isolated from dogs and a wild boar in Italy. *Vet. Microbiol.* **2015**, *177*, 359–365. [CrossRef]
93. Toma, B.; Dufour, B. Transmission de la maladie d'Aujeszky des sangliers sauvages aux suidés domestiques. *Epidémiol. Santé Anim.* **2004**, *45*, 115–119.
94. Cano-Terriza, D.; Martínez, R.; Moreno, A.; Pérez-Marín, J.E.; Jiménez-Ruiz, S.; Paniagua, J.; Borge, C.; García-Bocanegra, I. Survey of Aujeszky's Disease Virus in Hunting Dogs from Spain. *EcoHealth* **2019**, *16*, 351–355. [CrossRef]
95. Irie, T.; Yamaguchi, Y.; Doanh, P.N.; Guo, Z.H.; Habe, S.; Horii, Y.; Nonaka, N. Infection with *Paragonimus westermani* of boar-hunting dogs in Western Japan maintained via artificial feeding with wild boar meat by hunters. *J. Vet. Med. Sci.* **2017**, *79*, 1419–1425. [CrossRef] [PubMed]
96. Kaneko, C.; Kaneko, Y.; Sudaryatma, P.E.; Mekata, H.; Kirino, Y.; Yamaguchi, R.; Okabayashi, T. Pseudorabies virus infection in hunting dogs in Oita, Japan: Report from a prefecture free from Aujeszky's disease in domestic pigs. *J. Vet. Med. Sci.* **2021**, *83*, 680–684. [CrossRef] [PubMed]
97. Thaller, D.; Bilek, A.; Revilla-Fernandez, S.; Bago, Z.; Schildorfer, H.; Url, A.; Weikel, J.; Weissenböck, H. Diagnosis of Aujeszky's disease in a dog in Austria. *Wien. Tierarztl. Mon.* **2006**, *93*, 62–67.
98. Steinrigl, A.; Revilla-Fernández, S.; Kolodziejek, J.; Wodak, E.; Bagó, Z.; Nowotny, N.; Schmoll, F.; Köfer, J. Detection and molecular characterization of Suid herpesvirus type 1 in Austrian wild boar and hunting dogs. *Vet. Microbiol.* **2012**, *157*, 276–284. [CrossRef]
99. Leschnik, M.; Gruber, A.; Kübber-Heiss, A.; Bagó, Z.; Revilla-Fernández, S.; Wodak, E.; Müller, E.; Rath, H.; Deutz, A. Epidemiologische Aspekte der Aujeszky'schen Krankheit in Österreich anhand von sechs aktuellen Fällen beim Hund. *Wien. Tierarztl. Mon.* **2012**, *99*, 82.
100. Lazić, G.; Petrović, T.; Lupulović, D.; Topalski, B.; Božić, B.; Lazić, S. Aujeszky's disease in a dog-case report. *Arch. Vet. Med.* **2018**, *11*, 61–69. [CrossRef]
101. Serena, M.S.; Metz, G.E.; Lozada, M.I.; Aspitia, C.G.; Nicolino, E.H.; Pidone, C.L.; Fossaroli, M.; Balsalobre, A.; Quiroga, M.A.; Echeverria, M.G. First isolation and molecular characterization of Suid herpesvirus type 1 from a domestic dog in Argentina. *Open Vet. J.* **2018**, *8*, 131–139. [CrossRef]
102. Wittmann, G.; Rziha, H.-J. Aujeszky's disease (pseudorabies) in pigs. In *Herpesvirus Diseases of Cattle, Horses, and Pigs*; Springer: Berlin/Heidelberg, Germany, 1989; pp. 230–325.
103. McFerran, J.B.; Dow, C. Virus Studies on Experimental Aujeszky's Disease in Calves. *J. Comp. Pathol.* **1964**, *74*, 173–179. [CrossRef]
104. Hara, M.; Shimizu, T.; Nemoto, S.; Fukuyama, M.; Ikeda, T.; Kiuchi, A.; Tabuchi, K.; Nomura, Y.; Shirota, K.; Une, Y.; et al. A natural case of Aujeszky's disease in the cat in Japan. *J. Vet. Med. Sci.* **1991**, *53*, 947–949. [CrossRef]
105. Salwa, A. A natural outbreak of Aujeszky's disease in farm animals. *Pol. J. Vet. Sci.* **2004**, *7*, 261–266.
106. Van den Ingh, T.; Binkhorst, G.; Kimman, T.; Vreeswijk, J.; Pol, J.; Van Oirschot, J. Aujeszky's disease in a horse. *J. Vet. Med. Ser. B* **1990**, *37*, 532–538. [CrossRef]
107. Crandell, R. Selected animal herpesviruses: New concepts and technologies. *Adv. Vet. Sci. Comp. Med.* **1985**, *29*, 281–327.
108. Ramachandran, S.P.; Fraser, G. Studies on the virus of Aujeszky's disease. II. Pathogenicity for chicks. *J. Comp. Pathol.* **1971**, *81*, 55–62. [CrossRef]
109. Bang, F.B. Experimental Infection of the Chick Embryo with the Virus of Pseudorabies. *J. Exp. Med.* **1942**, *76*, 263–270. [CrossRef]
110. Kouwenhoven, B.; Davelaar, F.G.; Burger, A.G.; van Walsum, J. A case of Aujeszky's disease virus infection in young chicks. *Vet. Q.* **1982**, *4*, 145–154. [CrossRef]
111. Christodoulou, T.; Tsiroyiannis, E.; Papado-poulos, O.; Tsangaris, T. An outbreak of Aujeszky's disease in minks. *Cornell Vet.* **1970**, *60*, 65–73.
112. Geurden, L.; Devos, A.; Viaene, N.; Stoelens, M. Ziekte van Aujeszky bij nertsen. *Vlaams Dierg Tijdschr.* **1963**, *32*, 36.
113. Hartung, J.; Fritsch, W. Aujeszky'sche Krankheit bei Nerz und Fuchs. (*Aujeszky's Dis. Mink Foxes*) *Mh Vet.-Med.* **1964**, *19*, 422–427.
114. Lapcevic, E. Ein Beitrag zur Kenntnis der Aujeszky'schen Krankheit bei Nerzen. *Dtsch Tierärztl Wschr.* **1964**, *71*, 273.
115. Lyubashenko, S.; Tyul'Panova, A.; Grishin, V. Aujeszky's disease in mink, arctic fox, and silver fox. *Veterinariya* **1958**, *35*, 37–41.
116. Lutz, W.; Junghans, D.; Schmitz, D.; Müller, T. A long-term survey of pseudorabies virus infections in European wild boar of western Germany. *Z. Jagdwiss.* **2003**, *49*, 130–140. [CrossRef]
117. Müller, T.; Teuffert, J.; Ziedler, K.; Possardt, C.; Kramer, M.; Staubach, C.; Conraths, F.J. Pseudorabies in the European wild boar from eastern Germany. *J. Wildl. Dis.* **1998**, *34*, 251–258. [CrossRef]
118. van der Leek, M.L.; Becker, H.N.; Pirtle, E.C.; Humphrey, P.; Adams, C.L.; All, B.P.; Erickson, G.A.; Belden, R.C.; Frankenberger, W.B.; Gibbs, E.P.J. Prevalence of pseudorabies (Aujeszky's disease) virus antibodies in feral swine in Florida. *J. Wildl. Dis.* **1993**, *29*, 403–409. [CrossRef]
119. Pirtle, E.C.; Sacks, J.M.; Nettles, V.F.; Rollor, E.A., III. Prevalence and transmission of pseudorabies virus in an isolated population of feral swine. *J. Wildl. Dis.* **1989**, *25*, 605–607. [CrossRef]
120. Boitani, L.; Mattei, L.; Nonis, D.; Corsi, F. Spatial and activity patterns of wild boars in Tuscany, Italy. *J. Mammal.* **1994**, *75*, 600–612. [CrossRef]

121. Poteaux, C.; Baubet, E.; Kaminski, G.; Brandt, S.; Dobson, F.; Baudoin, C. Socio-genetic structure and mating system of a wild boar population. *J. Zool.* **2009**, *278*, 116–125. [CrossRef]
122. Soulsbury, C.D.; Iossa, G.; Baker, P.J.; White, P.C.; Harris, S. Behavioral and spatial analysis of extraterritorial movements in red foxes (*Vulpes vulpes*). *J. Mammal.* **2011**, *92*, 190–199.
123. Zhiwen, X.; Wanzhu, G.; Ling, Z.; Shanhu, T. Study on the hereditary stability of pseudorabies virus three-gene-deleted strain (SA215). *Xu Mu Shou Yi Xue Bao = Acta Vet. Zootech. Sin.* **2004**, *35*, 694–697.
124. He, Q.; Fang, L.; Wu, B. The preparation of gene-deleted vaccine against swine pseudorabies, measurement of its safety, immunogenicity, shelf life and the evaluation of vaccine by field trials. *Acta Vet. Zootech. Sin.* **2005**, *36*, 1055.
125. Tong, W.; Li, G.; Liang, C.; Liu, F.; Tian, Q.; Cao, Y.; Li, L.; Zheng, X.; Zheng, H.; Tong, G. A live, attenuated pseudorabies virus strain JS-2012 deleted for gE/gI protects against both classical and emerging strains. *Antivir. Res.* **2016**, *130*, 110–117.
126. Yin, Y.; Xu, Z.; Liu, X.; Li, P.; Yang, F.; Zhao, J.; Fan, Y.; Sun, X.; Zhu, L. A live gI/gE-deleted pseudorabies virus (PRV) protects weaned piglets against lethal variant PRV challenge. *Virus Genes* **2017**, *53*, 565–572. [CrossRef] [PubMed]
127. Wang, J.; Song, Z.; Ge, A.; Guo, R.; Qiao, Y.; Xu, M.; Wang, Z.; Liu, Y.; Zheng, Y.; Fan, H.; et al. Safety and immunogenicity of an attenuated Chinese pseudorabies variant by dual deletion of TK&gE genes. *BMC Vet. Res.* **2018**, *14*, 287.
128. Lin, W.; Shao, Y.; Tan, C.; Shen, Y.; Zhang, X.; Xiao, J.; Wu, Y.; He, L.; Shao, G.; Han, M.; et al. Commercial vaccine against pseudorabies virus: A hidden health risk for dogs. *Vet. Microbiol.* **2019**, *233*, 102–112. [CrossRef] [PubMed]
129. Yin, H.; Li, Z.; Zhang, J.; Huang, J.; Kang, H.; Tian, J.; Qu, L. Construction of a US7/US8/UL23/US3-deleted recombinant pseudorabies virus and evaluation of its pathogenicity in dogs. *Vet. Microbiol.* **2020**, *240*, 108543. [CrossRef] [PubMed]
130. He, W.; Auclert, L.Z.; Zhai, X.; Wong, G.; Zhang, C.; Zhu, H.; Xing, G.; Wang, S.; He, W.; Li, K.; et al. Interspecies Transmission, Genetic Diversity, and Evolutionary Dynamics of Pseudorabies Virus. *J. Infect. Dis.* **2019**, *219*, 1705–1715. [CrossRef] [PubMed]
131. Chen, S.; Liu, D.; Tian, J.; Kang, H.; Guo, D.; Jiang, Q.; Liu, J.; Li, Z.; Hu, X.; Qu, L. Molecular characterization of HLJ-073, a recombinant canine coronavirus strain from China with an ORF3abc deletion. *Arch. Virol.* **2019**, *164*, 2159–2164. [CrossRef] [PubMed]
132. Ye, C.; Guo, J.-C.; Gao, J.-C.; Wang, T.-Y.; Zhao, K.; Chang, X.-B.; Wang, Q.; Peng, J.-M.; Tian, Z.-J.; Cai, X.-H.; et al. Genomic analyses reveal that partial sequence of an earlier pseudorabies virus in China is originated from a Bartha-vaccine-like strain. *Virology* **2016**, *491*, 56–63. [CrossRef]
133. Shukla, D.; Liu, J.; Blaiklock, P.; Shworak, N.W.; Bai, X.; Esko, J.D.; Cohen, G.H.; Eisenberg, R.J.; Rosenberg, R.D.; Spear, P.G. A novel role for 3-O-sulfated heparan sulfate in herpes simplex virus 1 entry. *Cell* **1999**, *99*, 13–22. [CrossRef]
134. Montgomery, R.I.; Warner, M.S.; Lum, B.J.; Spear, P.G. Herpes simplex virus-1 entry into cells mediated by a novel member of the TNF/NGF receptor family. *Cell* **1996**, *87*, 427–436. [CrossRef]
135. Warner, M.S.; Geraghty, R.J.; Martinez, W.M.; Montgomery, R.I.; Whitbeck, J.C.; Xu, R.; Eisenberg, R.J.; Cohen, G.H.; Spear, P.G. A cell surface protein with herpesvirus entry activity (HveB) confers susceptibility to infection by mutants of herpes simplex virus type 1, herpes simplex virus type 2, and pseudorabies virus. *Virology* **1998**, *246*, 179–189. [CrossRef]
136. Geraghty, R.J.; Krummenacher, C.; Cohen, G.H.; Eisenberg, R.J.; Spear, P.G. Entry of alphaherpesviruses mediated by poliovirus receptor-related protein 1 and poliovirus receptor. *Science* **1998**, *280*, 1618–1620. [CrossRef]
137. Li, A.; Lu, G.; Qi, J.; Wu, L.; Tian, K.; Luo, T.; Shi, Y.; Yan, J.; Gao, G.F. Structural basis of nectin-1 recognition by pseudorabies virus glycoprotein D. *PLoS Pathog.* **2017**, *13*, e1006314. [CrossRef]

Article

Cytopathic and Genomic Characteristics of a Human-Originated Pseudorabies Virus

Zhong Peng^{1,2,3,4,†}, Qingyun Liu^{1,2,3,4,†}, Yibo Zhang^{1,2}, Bin Wu^{1,2,3,4}, Huanchun Chen^{1,2,3,4} and Xiangru Wang^{1,2,3,4,*}

- ¹ State Key Laboratory of Agricultural Microbiology, College of Veterinary Medicine, Huazhong Agricultural University, Wuhan 430070, China
- ² Key Laboratory of Preventive Veterinary Medicine in Hubei Province, The Cooperative Innovation Center for Sustainable Pig Production, Huazhong Agricultural University, Wuhan 430070, China
- ³ Key Laboratory of Development of Veterinary Diagnostic Products, Ministry of Agriculture of China, Huazhong Agricultural University, Wuhan 430070, China
- ⁴ International Research Center for Animal Disease, Ministry of Science and Technology of China, Wuhan 430070, China
- * Correspondence: wangxr228@mail.hzau.edu.cn
- † These authors contributed equally to this work.

Abstract: Pseudorabies virus (PRV) generally infects pigs and threatens the pig industry. However, recently we have isolated a PRV strain designated hSD-1/2019 from infected humans. In this study, we compared the complete genome sequence of hSD-1/2019 with those of pig-originated PRV strains. Sequence alignments revealed that the genome sequence of hSD-1/2019 was highly homologous to those of the porcine PRV strains. Phylogenetic analyses found that hSD-1/2019 was the closest related to porcine PRV endemic strains in China, particularly the variant strains circulating recently. We also showed that the glycoproteins important for the multiplication and pathogenesis of hSD-1/2019 were highly similar to those of the pig endemic strains. Diversifying selection analyses revealed that hSD-1/2019 and pig variant strains are under diversifying selection. Recombination analysis indicated that hSD-1/2019 was a recombinant of several PRV variant strains and an earlier PRV classic strain. Finally, we found that both human and pig-originated PRV strains could induce cytopathic effects in cells from humans, pigs, and mice, but only the human PRV and pig-variant PRV formed large syncytia in human cell lines. The data presented in this study contribute to our understanding of the molecular basis for the pathogenesis of human PRV from a genomic aspect.

Keywords: pseudorabies virus; human; pig; complete genome sequence; comparative genomics



Citation: Peng, Z.; Liu, Q.; Zhang, Y.; Wu, B.; Chen, H.; Wang, X. Cytopathic and Genomic Characteristics of a Human-Originated Pseudorabies Virus. *Viruses* **2023**, *15*, 170. <https://doi.org/10.3390/v15010170>

Academic Editor: Yan-Dong Tang

Received: 14 December 2022

Revised: 3 January 2023

Accepted: 3 January 2023

Published: 5 January 2023



Copyright: © 2023 by the authors. Licensee MDPI, Basel, Switzerland. This article is an open access article distributed under the terms and conditions of the Creative Commons Attribution (CC BY) license (<https://creativecommons.org/licenses/by/4.0/>).

1. Introduction

The world is now under the One Health Initiative, in which there is no dividing line between human and animal medicine [1]. Indeed, approximately 61% of the infectious organisms affecting humans are zoonotic [2]. The epidemic or pandemic of wildlife-origin pathogens, including Ebola and Marburg virus, human immunodeficiency virus (HIV)-1 and HIV-2, Sin Nombre virus, Nipah, Hendra and Menangle virus, West Nile virus, *Borrelia burgdorferi*, SARS coronavirus, MERS coronavirus, and more recently, SARS-CoV-2, have caused huge morbidity, mortality, and economic loss for humans. However, much of the knowledge about the pathogenesis and interspecies transmission of these pathogens is poorly understood.

Pseudorabies virus (PRV) is a double-stranded DNA virus belonging to the genus *Varicellovirus* of the subfamily *Alphaherpesvirinae*, family *Herpesviridae* [3]. PRV generally possesses a linear DNA genome with high G+C content (approximately 74%); this 143-kb genome encodes 70~100 proteins involved in the formation of viral capsid, tegument, and envelope. Among these proteins, glycoproteins gB, gD, gH, gL, and gK are necessary

for virus multiplication, while gE, gL, gG, gC, gM, and gN are the main virulence determinants [4]. It is worth noting that gC protein has also been used as a marker for PRV genotyping, and based on this gene, PRV strains are divided into two genotypes: genotype I and genotype II [5]. In general, PRV strains cause lethal infections in many animal species, with the exception of pigs, and reproductive failure in sows, as well as respiratory and neurological symptoms in piglets, are the common manifestations in pigs [6,7]. In China, the first report of a PRV outbreak in pigs occurred in the 1950s, and an inactivated vaccine consisting of PRV strain Bartha was imported into China in the 1970s [6]. Between 1990 and 2011, the wide vaccination of this inactivated vaccine in pig herds contributed to the control of PRV outbreaks well in China [8]. However, in late 2011, PRV variant strains emerged and circulated in many Bartha-K61-vaccinated pig farms in China [9,10]. These viruses display higher pathogenicity than PRV strains circulating in China before, and they show a different genotype from the Bartha strain [6].

For a very long time, whether humans are susceptible to PRV infection has been the subject of controversy, although several pieces of serological evidence have been found [7]. However, 25 cases of suspected PRV infection in humans were reported in China between 2017 and 2021, and all of the infected individuals in these cases had a history of working near pigs or in pork production [11–18]. These reported cases suggested that PRV infection might represent a new threat to humans in China. While in most of these cases, PRV-specific sequences have been determined in patients' tissues, none of them have reported the successful isolation of PRV. Recently, our group reported the isolation of the first PRV strain from the cerebrospinal fluid (CSF) of an infected patient with acute encephalitis in China [18]. To further explore the genetic characteristics of this human-originated PRV strain and its association with the pig PRV strains, we performed a comparative genomic analysis of the pseudorabies virus originating from humans and pigs in this study. Our aim is to provide more knowledge about the pathogenesis and interspecies transmission of PRV from a genomic perspective.

2. Materials and Methods

2.1. PRV Strains, Cells, Culture Conditions, and Whole-Genome Sequences

The PRV strains used in this study included hSD-1/2019 (GenBank accession no. MT468550), HuBXY/2018 (GenBank accession no. MT468549), and Ea (GenBank accession no. KX423960). These three PRV strains are all clinical isolates preserved in our laboratory: hSD-1/2019 was isolated from the CSF of an infected veterinarian with acute encephalitis in a pig farm of Shandong Province in China 2019 [18]; HuBXY/2018 is a variant isolated from the brain tissue of a piglet with neurological symptoms in Hubei Province in 2018; and Ea is a classic PRV epidemic strain isolated from pigs in China in the 1990s. The detailed steps for the isolation of hSD-1/2019 using PK-15 cells (ATCC, CCL-33) have been documented in our recent publication [18].

Cell lines, including PK-15 (Porcine Kidney-15; ATCC, CCL-33), ST (Swine Testis Cells; ATCC, CRL-1746), HT-22 (Mouse Hippocampal neuronal cell line; Sigma-Aldrich, SCC129), ARPE-19 (Adult Retinal Pigment Epithelial cell line-19; ATCC, CRL-2302), hBMEC (Human Brain Microvascular Endothelial Cells; gifted by Prof. Kwang Sik Kim at Johns Hopkins University School of Medicine), SK-N-SH (human neuroblastoma cell; ATCC, HTB-11), and hUVEC (Human Umbilical Vein Endothelial Cells; ATCC, CRL-1730) were used in this study. Among these cells, the PK-15, ST, HT-22, and ARPE-19 cells were maintained in Dulbecco's Modified Eagle Medium (DMEM; Gibco, Thermo Fisher Scientific, Waltham, MA, USA) supplemented with 10% fetal bovine serum (Genimi Bio, Calabasas, CA, USA); the hBMEC cells were cultured using RPMI 1640 medium (Gibco, Thermo Fisher Scientific, Waltham, MA, USA) supplemented with 10% fetal bovine serum; the SK-N-SH cells were maintained in Minimum Essential Medium (MEM; Gibco, Thermo Fisher Scientific, Waltham, MA, USA) supplemented with 10% fetal bovine serum.

The whole-genome sequences used for the analyses in this study included those of 55 pig epidemic strains that we isolated in China between 2011 and 2018 [6], as well as

those of several other pig-originated epidemic strains in China. The genome sequences of all of these PRV strains were retrieved from NCBI, and their GenBank accession numbers are listed in Table S1 in the Supplementary Materials.

2.2. Genomic DNA Extraction and Pacific Biosciences (PacBio) Sequencing

To obtain high-quality genomic DNA for PacBio sequencing, the isolated human PRV strain, hSD-1/2019, was passaged using PK-15 cells for 5 generations and was then inoculated in PK-15 cells at 0.1 MOI. A total of 100 mL of the viral culture was prepared. The viral culture was centrifuged together with a sucrose solution (30% *m/v*) at 26,000 rpm for 3 h; then the viral pellets were washed and resuspended in PBS. The genomic DNA was extracted using the phenol–chloroform protocol, as described previously [19]. The DNA concentration, quality, and integrity were evaluated using a Qubit Fluorometer (Invitrogen, Thermo Fisher Scientific, Waltham, MA, USA) and a NanoDrop Spectrophotometer (Thermo Scientific, Waltham, MA, USA). Afterward, a TruSeq DNA Sample Preparation Kit (Illumina, San Diego, CA, USA) and a Template Prep Kit (Pacific Biosciences, CA, USA) were used for the preparation of the 20-kb sequencing libraries, which were then sequenced on the Pacific Bio sciences platform and the Illumina Miseq platform at Personal Biotechnology Company (Shanghai, China). This sequencing strategy yielded 324,157,231-bp raw reads (N_{50} , 13277 bp). In the next step, the adapter contaminations were removed and the data were filtered by using AdapterRemoval [20] and SOAPdenovo2 [21]. Through this approach, a total of 7,708,624-bp clean reads (Q20% > 96.63%; Q30% > 88.84%) were obtained for de novo assembly using SPAdes [22] and A5-miseq [23] to construct the scaffolds and contigs. The Canu v1.5 [24] package was used to assemble the data obtained through the PacBio sequencing. All of the assembled data were integrated to generate a complete sequence. The final genome sequence was acquired after the rectification by using pilon software [25].

2.3. Bioinformatic Analysis

The sequence alignments were performed by using the EasyFig package (version 2.2.3_win) [26] and/or the MAFFT package (version 7.471) [27]. The nucleotide similarities at the genome level were calculated and visualized by using the SimPlot software (version 3.5.1), and the data were regenerated by using GraphPad Prism 8. GeneDoc (version 2.7) was used to visualize the sequence alignments of the genes or proteins. The average nucleotide identity (ANI) between the two genome sequences was calculated by using the ANI calculator [28]. Phylogenetic analysis was performed using the Beast 2 program (version 2.6.3) [29]. By using this program, maximum likelihood trees were generated through the Gamma correction for site heterogeneity and the GTR model [30]. A bootstrap value of 1000 was also applied, and the tree was visualized by using the iTOL tool [31]. The single-nucleotide polymorphisms (SNPs) between the different PRV strains were determined by using the MUMmer software (version 3.23) [32]. The coding effects of the SNPs were determined by using a local Perl command described previously [33]. The recombinant sequences were determined by using the Recombination Detection Program (RDP) package Beta 4.100 [34]. A recombination event with a significance of $p < 0.01$ in at least three out of seven of the selected algorithms: RDP, GENECONV, BootScan, Maxchi, Chimaera, SiScan, and 3Seq, was considered to be reliable, as previously described [35].

2.4. Cells Infection Tests

The cell monolayers were infected with PRV hSD-1/2019 (human-originated strain), HuBXY/2018 (pig-originated clinical variant strain), or Ea (pig-originated clinical classic strain) at 5 MOI and were incubated at 37 °C. At 12 h post-infection, the cytopathic effects were observed and recorded using the EVOS[®] FL Auto Imaging System (Thermo Fisher Scientific, Waltham, MA, USA).

3. Results

3.1. Overview of the Human-Originated PRV Genome

The sequencing using PacBio technology generated a complete genome sequence 143,905 bp in length with a G+C content of 73.66% for the human-originated PRV strain hSD-1/2019. A total of 68 genes were annotated. Comparative analysis revealed that the genome sequence of the human-originated PRV genome was highly homologous to those of the pig-originated PRV strains from China (Figure 1A, Table 1). In particular, the glycoproteins-encoding genes *UL27* (encoding gB), *UL44* (encoding gC), *US6* (encoding gD), *US8* (encoding gE), *US4* (encoding gG), *UL22* (encoding gH), *US7* (encoding gI), *US3* (encoding gK), *UL1* (encoding gL), *UL10* (encoding gM), and *UL49.5* (encoding gN) harbored by the human-originated PRV strain hSD-1/2019 were also highly homologous to those of the pig-originated PRV strains from China (Figure 1B, Table 1).

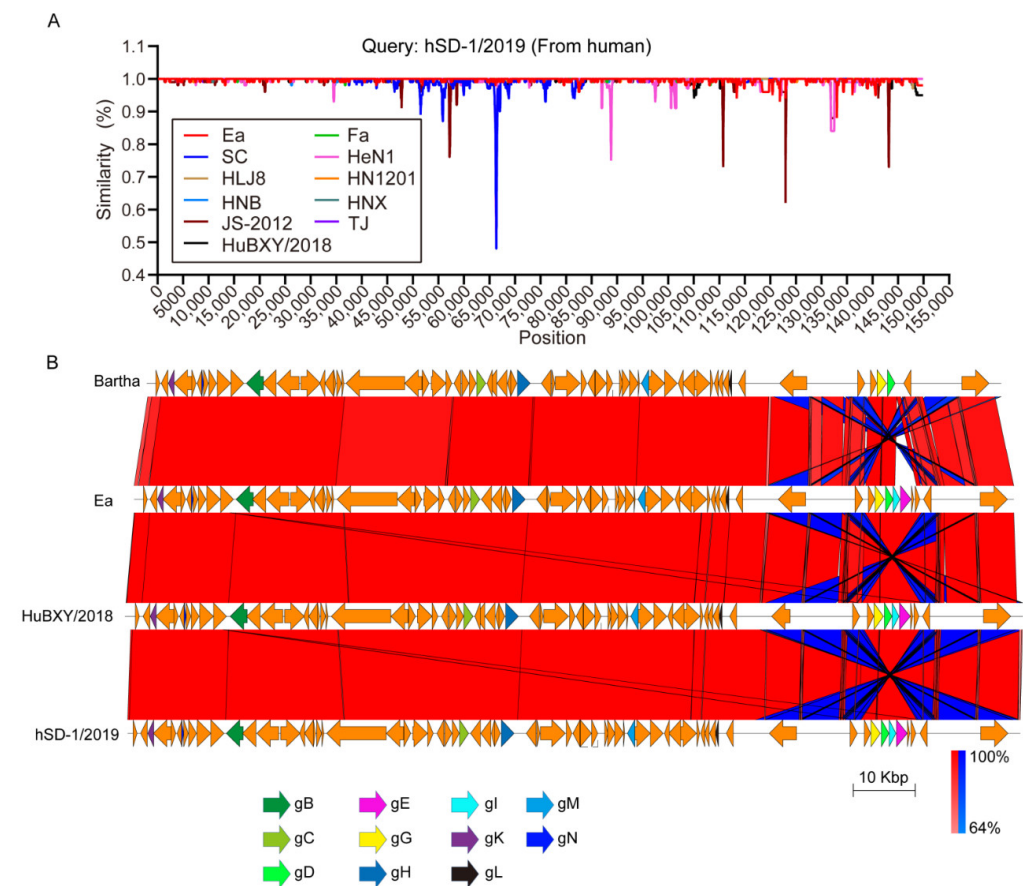


Figure 1. Sequence comparisons of human-originated and pig-originated PRV strains (A) Nucleotide similarities of the human-originated PRV strain hSD-1/2019 and the pig-originated PRV variant strains (HeN1, HLJ8, HN1201, HNB, HNX, JS-2012, TJ, and HuBXY/2018), as well as the pig-originated PRV classic strains (Ea, Fa, SC). (B) Comparative genomic analyses of the human-originated PRV strain hSD-1/2019, the pig-originated PRV variant strain HuBXY/2018, the pig-originated PRV strain Ea, and the vaccine strain Bartha. Color code stands for BLASTn identity of those regions between genomes. Arrows in the same colors represent putative CDSs with similar roles in different genomes.

Table 1. Nucleotide sequence identities between hSD-1/2019 and pig PRV representative strains.

Average Nucleotide Identity (%)												
hSD-1/2019 (Human PRV; GenBank Accession No. MT468550)												
Type	Pig PRV Classic Strain			Pig PRV Variant Strain								Vaccine Strain
Strain	Ea	Fa	SC	HeN1	HLJ8	HN1201	HNB	HNX	JS-2012	TJ	HuBXY/2018	Bartha
GenBank accession	KX423960	KM189913	KT809429	KP098534	KT824771	KP722022	KM189914	KM189912	KP257591	KJ789182	MT468549	JF797217
Year of isolation	1990	1990	1990	2012	2014	2012	2012	2012	2012	2012	2018	1950s
Place of isolation	China	China	China	China	China	China	China	China	China	China	China	Hungry
Complete genome	99.36%	99.44%	99.03%	99.45%	99.83%	99.82%	99.83%	99.90%	99.65%	99.80%	99.62%	96.73%
UL27	99.82%	99.82%	99.82%	100%	100%	100%	100%	100%	100%	100%	99.96%	98.14%
UL44	99.66%	99.73%	95.83%	100%	100%	100%	100%	100%	99.93%	100%	100%	95.11%
US6	99.18%	99.18%	99.18%	100%	100%	100%	100%	100%	100%	100%	100%	98.43%
US8	99.41%	99.48%	99.48%	99.89%	99.94%	100.00%	100.00%	100.00%	100.00%	99.83%	100.00%	Deletion
US4	99.93%	99.93%	99.93%	100.00%	100.00%	99.87%	100.00%	100.00%	99.93%	100.00%	100.00%	99.13%
UL22	99.95%	99.95%	99.95%	99.61%	100.00%	100.00%	100.00%	100.00%	99.90%	99.95%	99.95%	99.85%
US7	99.82%	99.82%	99.82%	99.91%	99.91%	100.00%	99.91%	100.00%	100.00%	99.91%	100.00%	Deletion
US3	99.90%	99.90%	99.90%	100.00%	100.00%	100.00%	100.00%	100.00%	99.90%	100.00%	100.00%	98.71%
UL1	100.00%	96.91%	100.00%	96.82%	100.00%	100.00%	100.00%	100.00%	100.00%	100.00%	100.00%	95.97%
UL10	99.92%	99.92%	99.07%	100%	100%	100%	100%	100%	99.92%	100%	99.92%	98.73%
UL49.5	99.33%	99.33%	99.33%	100%	100%	100%	100%	100%	99.67%	99.67%	100%	93.81%

3.2. Phylogenetic Relationship of the Human and Pig-Originated PRV Strains

It has been reported that PRV strains are phylogenetically divided into two genotypes according to the gC gene [5]. Therefore, we first performed a phylogenetic analysis of the human- and pig-originated PRV strains. Most of the pig-originated PRV strains included in the current analysis are our previously collected variant strains from the pseudorabies (PR) outbreaks in China between 2012 and 2017 [6]. Several other variant strains from the outbreaks in China after 2011, as well as PRV strains isolated in China before 2011 and/or from other countries, are also included (Table S1 in Supplementary Materials). The phylogenetic analysis based on the gC gene showed that the human-originated strain, hSD-1/2019, and the swine PRV strains from China were included in one clade, while the PRV strains from the other countries, including the vaccine strain Bartha, formed another clade (Figure 2A). We also performed a phylogenetic analysis on these strains according to their genome sequences. The maximum likelihood tree also revealed that the human-originated strain hSD-1/2019 and the Chinese swine PRV strains formed a phylogenetic clade, which showed a distinct relatedness to another phylogenetic clade, which was mainly composed of the pig-originated PRV strains from the other countries, including the vaccine strain Bartha (Figure 2B).

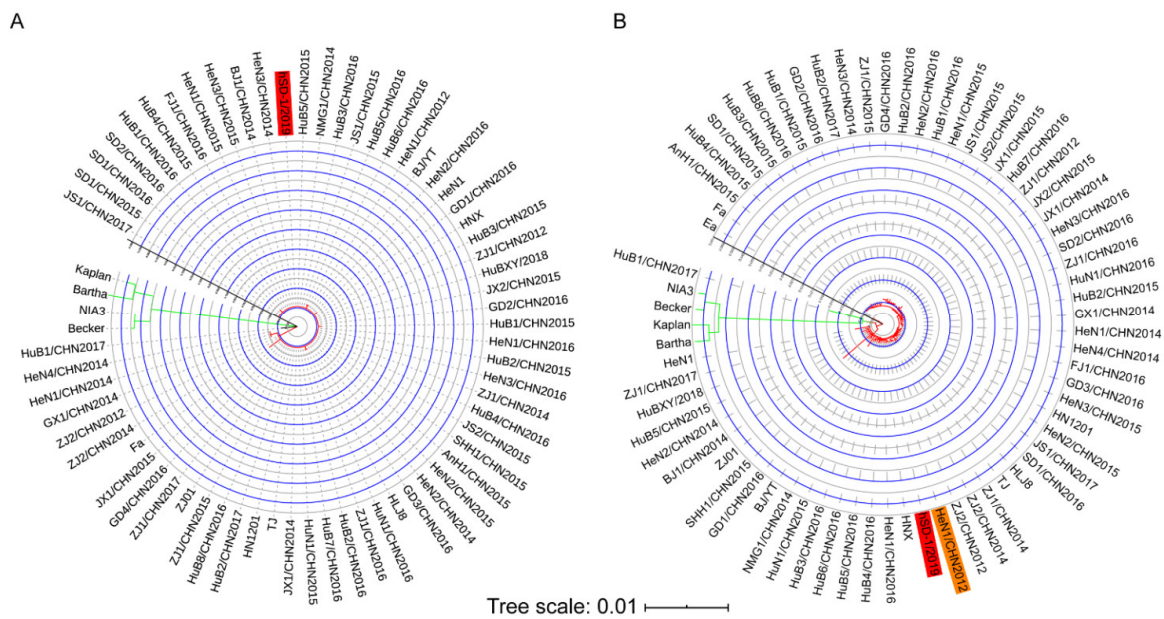


Figure 2. Phylogenetic analyses of human-originated and pig-originated PRV strains (A) A maximum likelihood tree was generated based on the full length of the gC coding gene. (B) A maximum likelihood tree was generated based on the complete genome sequences. Maximum likelihood trees were generated by using the Beast 2 program (version 2.6.3) through the Gamma correction for site heterogeneity and the GTR model. A bootstrap value of 1000 was also applied, and the tree was visualized by using the iTOL tool.

3.3. Glycoproteins of the Human and Pig-Originated PRV Strains

Glycoproteins play key roles in virus multiplication and pathogenesis [4], we, therefore, analyzed the 11 glycoproteins of the human- and pig-originated PRV strains. Overall, there were no significant differences in the amino acid components between these 11 glycoproteins of human PRV and the pig PRV variant strains (Figure 3). However, several characteristic amino acid changes were observed in glycoproteins gB, gD, gE, gG, and/or gN of the human PRV and the pig PRV variant strains compared to those of the pig PRV classic strains (Figure 3). In gB, the pig PRV classic strains possessed amino acids “T”, “H”, “T”, and “V” at sites 82, 560, 737, and 895, while the human PRV and the pig PRV variant strains all had “A”, “Q”, “A”, and “A” at these sites, respectively (Figure 3); in the gD of the human PRV and the pig PRV variant strains, the deletions of two amino acids and one amino acid change (“V→A”) occurred at sites 267, 268, and 338, compared to that of the pig PRV classic strains, respectively (Figure 3); in gE of the human PRV and the pig PRV variant strains, amino acid changes at sites 54 (“G→D”), 403 (“P→A”), 518 (“S→P”), and an insertion of one amino acid (“D”) at site 492 were observed compared to that of the pig PRV classic strains, respectively (Figure 3); in gG of the human PRV and the pig PRV variant strains, an amino acid change at site 82 (“S→P”) was observed compared to that of the classic PRV pig strains, while in the gN of the human PRV and the pig PRV variant strains, an amino acid change at site 49 (“A→T”) was observed compared to that of the classic PRV pig strains (Figure 3).

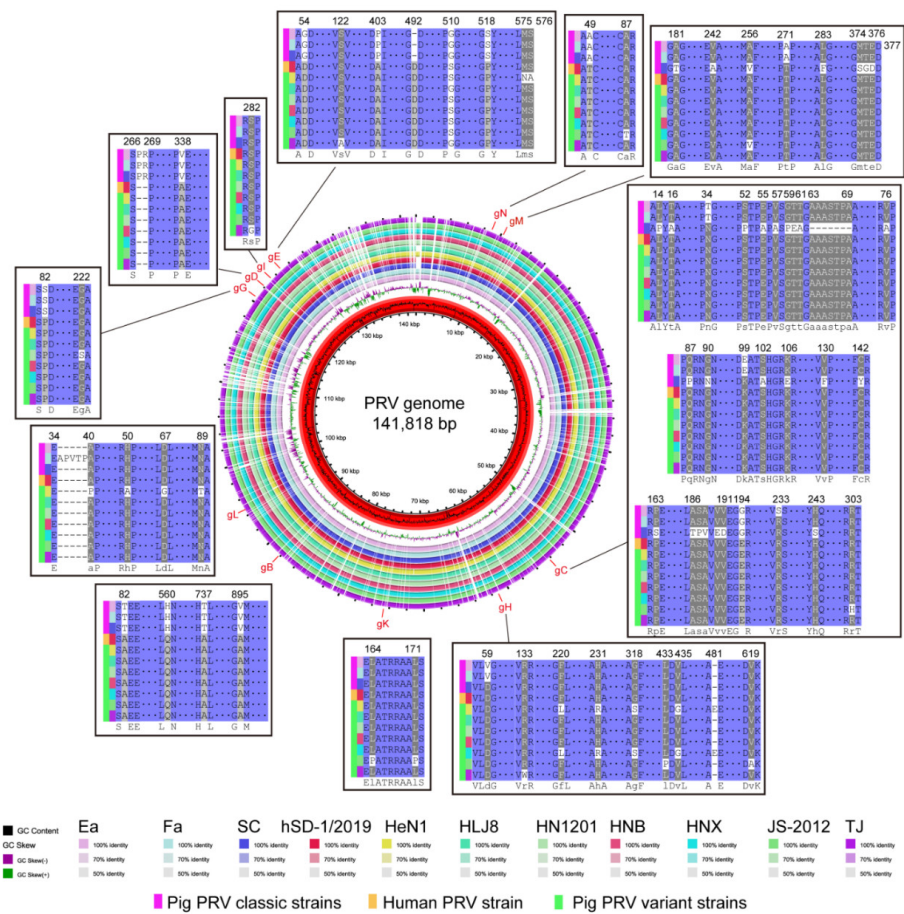


Figure 3. Circle map showing complete genome sequence alignments of human-originated and pig-originated PRV strains. Alignments of amino acid sequences of glycoproteins between different PRV strains were also displayed. Only sites with different amino acid residues are shown.

3.4. Diversifying Selection Analyses of the Human and Pig-Originated PRV Strains

To explore the diversifying selection of different PRV types, the SNPs of the human-originated PRV strain hSD-1/2019, a pig PRV variant strain HeN1 (GenBank accession no. KP098534), and a classic PRV pig strain Ea (GenBank accession no. KX423960) were determined by using MUMmer software (version 3.23) [32]. A total of 508, 363, and 258 SNPs were identified in the genomes of HeN1, hSD-1/2019, and hSD-1/2019 compared to the genomes of Ea, Ea, and HeN1, respectively (Table 2). By using a local Perl command described previously [33], the coding effects of these SNPs were determined. Compared to the genome sequence of Ea, 292 SNPs determined in the genome sequence of hSD-1/2019 had coding effects, of which 153 SNPs were identified as non-synonymous SNPs and 139 SNPs were identified as synonymous SNPs (Table 2). The overall ratio between the non-synonymous to synonymous substitutions (dN/dS) of all of the coding regions of strain hSD-1/2019 compared to strain Ea was 1.10 (Table 2). In total, there were 257 SNPs with coding effects in the genome sequence of HeN1 compared to that of Ea, with 145 SNPs being identified as non-synonymous SNPs and 112 SNPs being identified as synonymous SNPs (Table 2). The dN/dS ratio between the two genome sequences was 1.29 (Table 2). Only 101 SNPs in the genome sequence of hSD-1/2019 compared to that of HeN1 were determined to have coding effects, among which 56 SNPs and 45 SNPs were identified as non-synonymous SNPs and synonymous SNPs, respectively (Table 2). The dN/dS ratio between the two genome sequences was 1.24 (Table 2). Among different comparisons (hSD-1/2019 vs. Ea; HeN1 vs. Ea; hSD-1/2019 vs. HeN1), the highest numbers of SNPs were observed in several genes such as UL47, UL36, UL8, UL1, and US1 (Figure 4). In

addition, high dN/dS ratios were observed in several glycoprotein-encoding genes, such as US8, which encodes gE (Figure 4B–D).

Table 2. Single nucleotide polymorphisms (SNPs) analyses of different PRV strains.

Comparisons	Non-Synonymous	Synonymous	dN/dS Ratio
hSD-1/2019 vs. Ea	153	139	1.10
HeN1 vs. Ea	145	112	1.29
hSD-1/2019 vs. HeN1	56	45	1.24

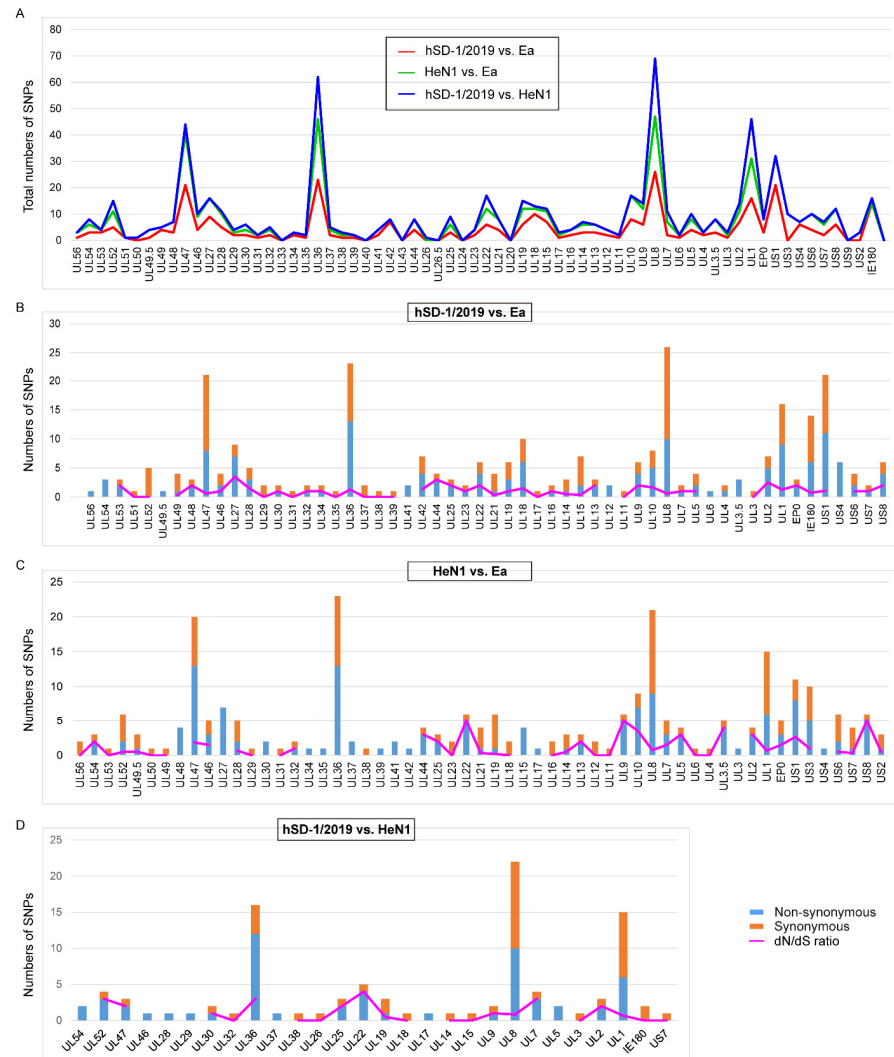


Figure 4. Single-nucleotide polymorphisms (SNPs) of the human- and pig-originated PRV strains (A) Graph showing the numbers of total SNPs identified in the complete genome sequences of human-originated PRV strain hSD-1/2019 and pig-originated PRV variant strain HeN1 compared to those of strains Ea and/or HeN1, respectively. (B) Graph showing the numbers of non-synonymous SNPs and synonymous SNPs, as well as the ratio of non-synonymous to synonymous substitutions (dN/dS) in the complete genome sequences of hSD-1/2019 compared to that of Ea. (C) Graph showing the numbers of non-synonymous SNPs and synonymous SNPs, as well as the dN/dS ratio in the complete genome sequences of HeN1 compared to that of Ea. (D) Graph showing the numbers of non-synonymous SNPs and synonymous SNPs, as well as the dN/dS ratio in the complete genome sequences of hSD-1/2019 compared to that of HeN1.

3.5. Genomic Recombinant Analyses of the Human and Pig-Originated PRV Strains

We used the Recombination Detection Program (RDP) package Beta 4.100 [34] to determine the recombinant sequences in the default mode and a recombination event with a significance of $p < 0.01$ in at least three out of seven selected algorithms: RDP, GENECONV, BootScan, Maxchi, Chimaera, SiScan, and 3Seq, was considered to be reliable [35]. The results revealed that the human-originated PRV strain hSD-1/2019 was highly probable homologous recombinant resulting from HuBXY/2018 (GenBank accession no. MT468549), HeN1 (GenBank accession no. KP098534), Ea (GenBank accession no. KX423960), TJ (GenBank accession no. KJ789182), and HLJ8 (GenBank accession no. KT824771) (Table 3). One recombinant event appeared with a beginning breakpoint at around 1 (without gaps) and an ending breakpoint at around 2,279 (without gaps), with the major parent strain of HuBXY/2018 and a minor parent strain of HeN1, encompassing the genes *UL56* and *UL54* partially; another recombinant event appeared with a beginning breakpoint at around 65,809 (without gaps) and an ending breakpoint at around 66,710 (without gaps), with the major parent strain of HuBXY/2018 and a minor parent strain of Ea, including partial *UL21*, *UL20*, and partial *UL19*; a third recombinant event appeared with a beginning breakpoint at around 117,180 (without gaps) and an ending breakpoint at around 128,177 (without gaps), with the major parent strain of TJ and a minor parent strain of HLJ8, encompassing the genes *US3*, *US4*, *US6*, *US7*, *US8*, *US9*, and *US2* as well as partial *US1*; the last recombinant event appeared with a beginning breakpoint at around 143,787 (without gaps) and an ending breakpoint at around 143,906 (without gaps), with the major parent strain of HNX and a minor parent strain of JS-2012, encompassing parts of a repeat region (Figure 5A). BootScan analysis was performed to confirm the recombination events within the genome of hSD-1/2019 by using SimPlot software (Figure 5B).

Table 3. Algorithms of the RDP4 package used to predict the recombination event.

Recombinant Strain	Parent Major/Minor	Recombinant Region in Alignment	Model (Average p -Value)						
			RDP	GENECONV	BootScan	MaxChi	Chimaera	SiScan	Phylpro
hSD-1/2019	HuBXY/HeN1	1–2279	1.73×10^{-2}	-	-	4.35×10^{-2}	2.4×10^{-2}	-	3.54×10^{-2}
	HuBXY/Ea	65,809–66,710	1.98×10^{-8}	2.99×10^{-8}	1.96×10^{-9}	1.22×10^{-2}	1.20×10^{-2}	9.60×10^{-9}	9.47×10^{-6}
	TJ/HLJ8	117,180–128,177	6.74×10^{-12}	3.21×10^{-14}	7.85×10^{-8}	1.62×10^{-8}	1.18×10^{-4}	4.28×10^{-30}	4.02×10^{-10}
	HNX/JS	143,787–143,906	1.69×10^{-19}	4.29×10^{-22}	1.23×10^{-20}	5.84×10^{-7}	-	3.35×10^{-10}	-

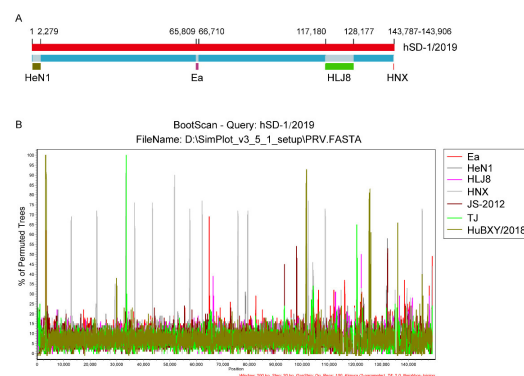


Figure 5. Genomic recombinant analyses of the complete genome of human-originated PRV strain hSD-1/2019 (A) Recombination events determined in the genome of hSD-1/2019. hSD-1/2019 genome are shown in red. The likely backbone is shown in blue. Recombination events predicted by RDP4 were shown as dark gold, purple, green, and red, respectively. Likely breakpoint positions were shown above the genome. (B) BootScan analysis of the complete genome sequence of hSD-1/2019. The complete genome sequence of hSD-1/2019 was used as the query sequence and compared with those of Ea, HeN1, HLJ8, HNX, JS-2012, TJ, and HuBXY/2018. The default setting of SimPlot software was used as follows: window size 200 bp, step size 20 bp.

3.6. Cytopathic Effects Induced by Human and Pig-Originated PRV Strains in Different Cell Lines

The above comparative analyses revealed that the genomic characteristics of the human-originated PRV strain were more similar to those of the pig PRV variant strains rather than those of the classic PRV pig strains. Therefore, we investigated the cytopathic effects induced by the human-originated PRV strain (hSD-1/2019), pig-originated PRV variant strain (HuBXY/2018), and the classic pig-originated PRV strain (Ea) in different cell lines. Strikingly, both the human-originated PRV strain and the pig-originated variant strain formed large syncytia in the human-sourced cells (ARPE-19, hBMEC, and SK-N-SH), while the human cells treated with the classic pig-originated strain showed cytopathic effects characterized with single, rounded, and swollen cells (Figure 6). However, in the porcine cells (PK-15, ST) and murine cells (HT22), the three tested PRV strains induced similar cytopathic effects, which were characterized by single, rounded, and swollen cells (Figure 7).

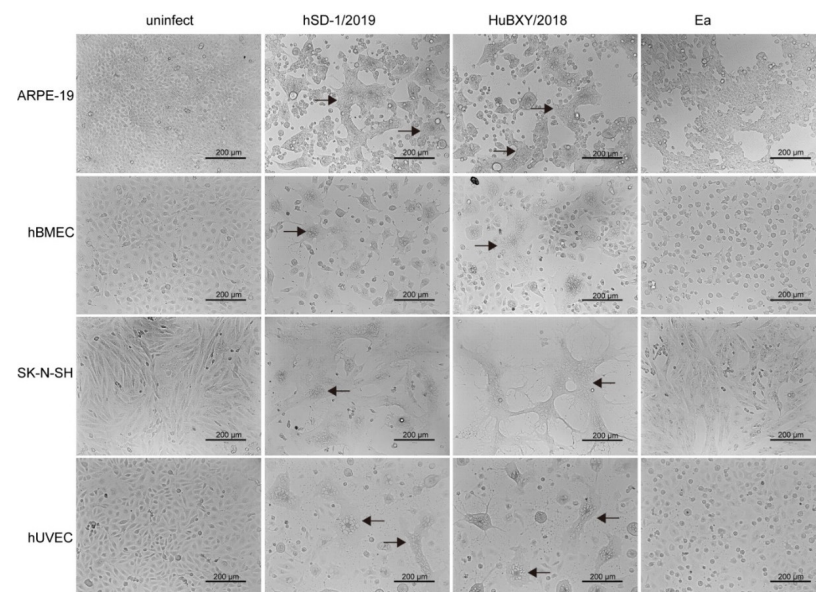


Figure 6. Cytopathic effects of PRV strains in different human cells. In ARPE, hBMEC, SK-N-SH, and hUVEC cells, hSD-1/2019, and HuBXY/2018 induced large syncytia, while the Ea-infected cells showed cytopathic effects characterized by single, rounded, and swollen cells. Syncytia are indicated using black arrows.

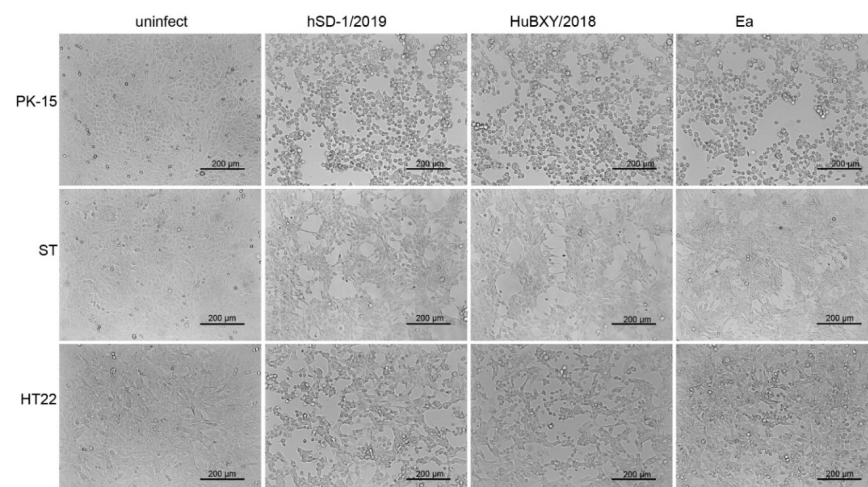


Figure 7. The cytopathic effects of PRV strain in swine and mouse cells. PRV strain hSD-1/2019, HuBXY/2018, and Ea induced similar cytopathic effects in PK-15, ST, and HT22 cells, respectively, which were characterized by single, rounded, and swollen cells.

4. Discussion

Although there has been a long documented history of suspected PRV infection in humans since 1914 [36], the virus had not been isolated from infected humans until recently [18]. As the first PRV isolates from humans, knowledge about the genomic characteristics of hSD-1/2019 and its association with pig-originated PRV strains is poorly understood. In this study, sequence comparisons revealed that the genome sequence of the human-originated PRV strain hSD-1/2019 was highly homologous to (average nucleotide identity $\geq 99\%$) those of the PRV strains originated from pigs, including the classical strains that spread in China before 2011 (e.g., strain Ea, Fa, SC) and the variant strains isolated after 2011 (e.g., strain HuBXY/2018, HeN1, HLJ8, HN1201, HNB, HNX, JS-2012, TJ). In particular, the glycoproteins gB, gC, gD, gE, gG, gH, gI, gK, gL, gM, and gN harbored by the human-originated PRV strain hSD-1/2019 were also highly homologous to those of the pig-originated PRV strains. It is known that these glycoproteins are necessary for virus multiplication and have important roles in the pathogenesis of the virus [4]. The above findings suggested that, from the genomic level, the human-originated PRV strain exhibited similar characteristics to the pig-originated PRV strains, and the human-originated PRV might display a similar mechanism for pathogenesis.

Previously, both the gC gene and the whole-genome sequence were used to analyze the phylogeny of PRV strains in epidemiology studies [5,6,37], and according to the gC gene, the PRV strains from pigs are divided into two genotypes (genotype I and II); of which genotype II strains are mainly the PRV strains circulating in China while genotype I strains are swine PRV strains isolated from the other regions [5]. Our phylogenetic analysis based on gC revealed that the human-originated strain hSD-1/2019 belonged to genotype II and was closest to the epidemic swine variant strains isolated in China after 2011. A similar result was illustrated by the phylogenetic analysis using the whole-genome sequence. Additionally, from the result of the phylogenetic analysis based on the whole-genome sequence, we found that the human-originated strain hSD-1/2019 was closest related to one of our previously collected pig-originated strain HeN1/CHN2012 (GenBank accession no. MK642583) at the whole-genome level. HeN1/CHN2012, also named SMX, was isolated from neonatal piglets with severe neurological disorders, including tremble, convulsion, and opisthotonus, in May 2012 in a PR-outbreak pig farm that used commercial Bartha-K61 vaccine as a routine vaccination procedure in Henan province in China [38]. Our previous study revealed that the virus variants with defects in TK, gE, and gI from this strain protected growing pigs against the lethal challenge of PRV variant strains, while the known vaccine strain Bartha could not [38]. These findings suggest that the human-originated strain hSD-1/2019 has a very close phylogenetic relationship with the pig epidemic variant strain in China, highlighting the possibility that hSD-1/2019 is a pig-originated strain and it may transmit to humans in a certain condition.

PRV strains encode 11 glycoproteins, which are beneficial for their multiplication and pathogenesis [4]. Of particular note is gD, which mediates the binding to the host cell by using the nectin-1 receptor and, therefore, contributes to the viral entry into the host cells [39,40]. It has been shown that the gD protein from pig-originated PRV strains engages both human and swine-origin nectin-1 with similar binding affinities, and the nectin-1 proteins and those key amino acid residues required for virus binding in this protein are conserved across many different species (including pig, human, mouse, bovine species, sheep, goat, cat, dog, bat) [7,39]. The sequence alignments revealed that the gD protein of the human PRV was highly homologous (100% amino acid similarity) to that of the pig-originated PRV variant strains. The above findings might provide evidence to explain why PRV strains can infect both pigs and humans. We also determined several characteristic amino acid changes in the gD protein of the human PRV and pig-originated PRV variant strains compared to that of the pig-originated PRV classic strains. However, these changes might have no effect on the function of gD binding to nectin-1 because the binding of gD protein from a classic PRV pig strain Becker to both human and pig-origin nectin-1 proteins has been shown [39]. In addition to gD, the other glycoproteins, such as the gB of the

human-originated PRV strain, were also highly homologous to those of the pig PRV variant strains. These findings may explain why hSD-1/2019 exhibits similar immunogenicity as PRV variant strains, as determined by our previous cross-neutralizing assays [18].

The analyses of the SNPs revealed high dN/dS ratios of the human-originated PRV strain and the pig-originated PRV variant strain compared to the pig-originated PRV classic strain, which suggests that the human-originated PRV strain and the pig-originated PRV variant strain are under diversifying selection, as dN/dS ratio is commonly used as a measure of purifying versus diversifying selection [41]. From the import of an inactivated vaccine derived from PRV strain Bartha in the 1970s to the circulation of pig PRV variant strains in late 2011 [9], pig herds in China had been vaccinated with Bartha-K61 or the other vaccines derived from PRV classic strains such as Ea for over 40 years. The long-time continuous and wide application of these vaccines might be an important contributor to the diversifying selection that led to the emergence of PRV variant strains. High dN/dS ratios were also found in several glycoprotein encoding genes, suggesting these genes are also under diversifying selection, which might be due to their frequent interactions with the host immune systems. Recombinant detection found several recombinant events in the genome of the human-originated PRV strain hSD-1/2019. These recombinant events resulted from several pig-originated PRV variant strains, which were isolated recently (between 2012 and 2018), and a classic PRV pig strain Ea, which was isolated in 1990. In addition, hSD-1/2019 also has a close relationship to these strains. While reports of recombination of PRV between endemic variant strains and classic strains are limited, recombination between PRV endemic strains and vaccine strains has been reported, and this recombination is speculated to be responsible for the emergence of novel strains [42]. Therefore, it may also be speculated that PRV endemic strains and earlier strains in China are probably the parental strains of human-originated PRV. These above findings may also remind us to take into consideration the recombination of different types of PRV strains during taking actions to control PRV infections in China, although the evolutionary rate of herpesvirus is very low [42].

Our cell infection experiments revealed that both human- and pig-originated PRV strains displayed a good adaptation and could induce cytopathic effects in different cells from both humans, pigs, and mice. It is not a surprise to obtain these results since previous studies have found that the key receptor (nectin-1) contributing to PRV entry into the host cells is conserved across many different species, including pigs, humans, and mice [7,39], and our comparative analysis performed in this study revealed that the viral protein (gD) engaging this receptor was conserved between the human and pig-originated PRV strains. More strikingly, we found that both human PRV and pig variant PRV formed large syncytia in human cell lines (ARPE, hBMEC, and SK-N-SH); while the classic pig PRV did not. These findings indicate that both human PRV and pig variant PRV strains demonstrate a better cell-associated spread, as syncytia formation contributes to the spread of the virus between cells [43]. Although detailed mechanisms for this difference should be further explored, a recent study has found SARS-CoV-2 B.1.617 variants could also form prominent syncytia, and this capacity facilitates the furin-mediated spike cleavage and enhances and accelerates cell–cell fusion [44]. Correspondingly, the capacity of both human PRV and pig variant PRV forming syncytia may also contribute to the virus spread and immune escape. In the next step, we intend to investigate this hypothesis.

Among the different proteins of PRV, gB, gH/gL, and gK that have been demonstrated to be necessary for virus-mediated syncytia formation, while gE/gI and gM are not necessary, but they could regulate cell fusions [43]. Several previous studies showed that amino acid mutations in gB, including lacking the C-terminal 29 amino acids [45] or the mutation of the dileucine motif in the gB tail [46], were beneficial for syncytia formation and cell spread, while syncytia formation was significantly decreased in mutants deficient in gE [47]. In this study, we also found several amino acid mutations in the main glycoproteins of the human- and pig-originated variant strains compared to those of the pig-originated classic strains (Figure 3). However, it remains to be addressed whether these mutations

are associated with the observation that the variant strains demonstrate better syncytia formation than the classic strains in human cell lines. Currently, the host factors associated with PRV-mediated syncytia formation has not been well revealed. It was reported that Isobavachalcone, an Akt signaling pathway inhibitor, could inhibit PRV by impairing virus-mediated cell-to-cell fusion [48]. In addition, it was stated that syncytia were formed by the fusion of adjacent cells through the binding of viral glycoproteins expressed on the infected cell membrane with the corresponding receptors expressed on adjacent uninfected cell membranes [43]. Clearly, the identification of viral glycoproteins and corresponding receptors is necessary for clarifying the mechanism of syncytial formation.

5. Conclusions

We reported the complete genome sequence and the genomic characteristics of the first human-originated PRV strain hSD-1/2019. Genomic comparative analyses of human-originated and pig-originated PRV strains revealed that the complete genome sequence of hSD-1/2019 was highly homologous to those of the pig PRV strains. Phylogenetic analyses revealed a very close relationship between hSD-1/2019 and PRV endemic strains in China, particularly the variant strains circulating recently. In addition, our sequence alignments found the glycoproteins important for viral multiplication and pathogenesis in hSD-1/2019 were highly similar to those of the pig endemic strains, and recombination detection suggested that hSD-1/2019 was probably the recombinant of several PRV variant strains and the earlier classic strain. The initial cell infection assays showed that both human- and pig-originated PRV strains displayed a good adaptation and could induce cytopathic effects in cells from humans, pigs, and mice. Moreover, both human PRV and pig variant PRV formed large syncytia in human cell lines. These findings further expand the current understanding of the molecular basis for the pathogenesis and interspecies transmission of PRV.

Supplementary Materials: The following supporting information can be downloaded at: <https://www.mdpi.com/article/10.3390/v15010170/s1>, Table S1: PRV strains used for bioinformatical analyses in the present study.

Author Contributions: Bioinformatic analysis, Z.P. and Q.L.; Infection tests, Q.L. and Y.Z.; Funding acquisition, X.W.; Material providing, B.W., H.C. and X.W.; Writing—original draft, Z.P. and Q.L.; Writing—review and editing, X.W. All authors have read and agreed to the published version of the manuscript.

Funding: This work was supported by grants from the National Natural Science Foundation of China (32122086), the National Key Research and Development Program of China (2021YFD1800800), and the Walmart Foundation as well as Walmart Food Safety Collaboration Center (Project #61626817). The funder had no role in the study design, data collection, data analysis, data interpretation, or manuscript writing.

Institutional Review Board Statement: Not applicable.

Informed Consent Statement: Not applicable.

Data Availability Statement: All data generated or analyzed during this study are included in this published article. The complete genome sequence of PRV strain hSD-1/2019 is deposited in NCBI. GenBank accession number is MT468550.

Conflicts of Interest: The authors declare no conflict of interest.

References

1. Ryu, S.; Kim, B.I.; Lim, J.S.; Tan, C.S.; Chun, B.C. One Health Perspectives on Emerging Public Health Threats. *J. Prev. Med. Public Health* **2017**, *50*, 411–414. [CrossRef] [PubMed]
2. Taylor, L.H.; Latham, S.M.; Woolhouse, M.E. Risk factors for human disease emergence. *Philos. Trans. R. Soc. B Biol. Sci.* **2001**, *356*, 983–989. [CrossRef] [PubMed]
3. Mettenleiter, T.C. Aujeszky's disease (pseudorabies) virus: The virus and molecular pathogenesis—state of the art, June 1999. *Vet. Res.* **2000**, *31*, 99–115. [CrossRef] [PubMed]

4. Pomeranz, L.E.; Reynolds, A.E.; Hengartner, C.J. Molecular biology of pseudorabies virus: Impact on neurovirology and veterinary medicine. *Microbiol. Mol. Biol. Rev.* **2005**, *69*, 462–500. [CrossRef] [PubMed]
5. Ye, C.; Zhang, Q.Z.; Tian, Z.J.; Zheng, H.; Zhao, K.; Liu, F.; Guo, J.C.; Tong, W.; Jiang, C.G.; Wang, S.J.; et al. Genomic characterization of emergent pseudorabies virus in China reveals marked sequence divergence: Evidence for the existence of two major genotypes. *Virology* **2015**, *483*, 32–43. [CrossRef]
6. Sun, Y.; Liang, W.; Liu, Q.; Zhao, T.; Zhu, H.; Hua, L.; Peng, Z.; Tang, X.; Stratton, C.W.; Zhou, D.; et al. Epidemiological and genetic characteristics of swine pseudorabies virus in mainland China between 2012 and 2017. *PeerJ* **2018**, *6*, e5785. [CrossRef]
7. Wong, G.; Lu, J.; Zhang, W.; Gao, G.F. Pseudorabies virus: A neglected zoonotic pathogen in humans? *Emerg. Microbes Infect.* **2019**, *8*, 150–154. [CrossRef]
8. Ou, J.; Cai, S.; Zheng, F.; Lu, G.; Zhang, G. Human pseudorabies virus infection: A new threat in China. *J. Infect.* **2020**, *80*, 578–606. [CrossRef]
9. An, T.Q.; Peng, J.M.; Tian, Z.J.; Zhao, H.Y.; Li, N.; Liu, Y.M.; Chen, J.Z.; Leng, C.L.; Sun, Y.; Chang, D.; et al. Pseudorabies virus variant in Bartha-K61-vaccinated pigs, China, 2012. *Emerg. Infect. Dis.* **2013**, *19*, 1749–1755. [CrossRef]
10. Luo, Y.; Li, N.; Cong, X.; Wang, C.H.; Du, M.; Li, L.; Zhao, B.; Yuan, J.; Liu, D.D.; Li, S.; et al. Pathogenicity and genomic characterization of a pseudorabies virus variant isolated from Bartha-K61-vaccinated swine population in China. *Vet. Microbiol.* **2014**, *174*, 107–115. [CrossRef]
11. Ai, J.W.; Weng, S.S.; Cheng, Q.; Cui, P.; Li, Y.J.; Wu, H.L.; Zhu, Y.M.; Xu, B.; Zhang, W.H. Human Endophthalmitis Caused By Pseudorabies Virus Infection, China, 2017. *Emerg. Infect. Dis.* **2018**, *24*, 1087–1090. [CrossRef]
12. Wang, D.; Tao, X.; Fei, M.; Chen, J.; Guo, W.; Li, P.; Wang, J. Human encephalitis caused by pseudorabies virus infection: A case report. *J. Neurovirol* **2020**, *26*, 442–448. [CrossRef]
13. Wang, Y.; Nian, H.; Li, Z.; Wang, W.; Wang, X.; Cui, Y. Human encephalitis complicated with bilateral acute retinal necrosis associated with pseudorabies virus infection: A case report. *Int. J. Infect. Dis.* **2019**, *89*, 51–54. [CrossRef]
14. Yang, H.; Han, H.; Wang, H.; Cui, Y.; Liu, H.; Ding, S. A Case of Human Viral Encephalitis Caused by Pseudorabies Virus Infection in China. *Front. Neurol.* **2019**, *10*, 534. [CrossRef]
15. Yang, X.; Guan, H.; Li, C.; Li, Y.; Wang, S.; Zhao, X.; Zhao, Y.; Liu, Y. Characteristics of human encephalitis caused by pseudorabies virus: A case series study. *Int. J. Infect. Dis.* **2019**, *87*, 92–99. [CrossRef]
16. Zhao, W.L.; Wu, Y.H.; Li, H.F.; Li, S.Y.; Fan, S.Y.; Wu, H.L.; Li, Y.J.; Lü, Y.L.; Han, J.; Zhang, W.C.; et al. Clinical experience and next-generation sequencing analysis of encephalitis caused by pseudorabies virus. *Zhonghua Yi Xue Za Zhi* **2018**, *98*, 1152–1157. [CrossRef]
17. Zheng, L.; Liu, X.; Yuan, D.; Li, R.; Lu, J.; Li, X.; Tian, K.; Dai, E. Dynamic cerebrospinal fluid analyses of severe pseudorabies encephalitis. *Transbound. Emerg. Dis.* **2019**, *66*, 2562–2565. [CrossRef]
18. Liu, Q.; Wang, X.; Xie, C.; Ding, S.; Yang, H.; Guo, S.; Li, J.; Qin, L.; Ban, F.; Wang, D.; et al. A novel human acute encephalitis caused by pseudorabies virus variant strain. *Clin. Infect. Dis.* **2021**, *73*, 3690–3700. [CrossRef]
19. Szpara, M.L.; Tafuri, Y.R.; Enquist, L.W. Preparation of viral DNA from nucleocapsids. *J. Vis. Exp.* **2011**, *10*, 3151. [CrossRef]
20. Lindgreen, S. AdapterRemoval: Easy cleaning of next-generation sequencing reads. *BMC Res. Notes* **2012**, *5*, 337. [CrossRef]
21. Luo, R.; Liu, B.; Xie, Y.; Li, Z.; Huang, W.; Yuan, J.; He, G.; Chen, Y.; Pan, Q.; Liu, Y.; et al. SOAPdenovo2: An empirically improved memory-efficient short-read de novo assembler. *GigaScience* **2012**, *1*, 18. [CrossRef] [PubMed]
22. Bankevich, A.; Nurk, S.; Antipov, D.; Gurevich, A.A.; Dvorkin, M.; Kulikov, A.S.; Lesin, V.M.; Nikolenko, S.I.; Pham, S.; Pribelski, A.D.; et al. SPAdes: A new genome assembly algorithm and its applications to single-cell sequencing. *J. Comput. Biol.* **2012**, *19*, 455–477. [CrossRef] [PubMed]
23. Coil, D.; Jospin, G.; Darling, A.E. A5-miseq: An updated pipeline to assemble microbial genomes from Illumina MiSeq data. *Bioinformatics* **2015**, *31*, 587–589. [CrossRef] [PubMed]
24. Koren, S.; Walenz, B.P.; Berlin, K.; Miller, J.R.; Bergman, N.H.; Phillippy, A.M. Canu: Scalable and accurate long-read assembly via adaptive k-mer weighting and repeat separation. *Genome Res.* **2017**, *27*, 722–736. [CrossRef] [PubMed]
25. Walker, B.J.; Abeel, T.; Shea, T.; Priest, M.; Abouelliel, A.; Sakthikumar, S.; Cuomo, C.A.; Zeng, Q.; Wortman, J.; Young, S.K.; et al. Pilon: An integrated tool for comprehensive microbial variant detection and genome assembly improvement. *PLoS ONE* **2014**, *9*, e112963. [CrossRef] [PubMed]
26. Sullivan, M.J.; Petty, N.K.; Beatson, S.A. Easyfig: A genome comparison visualizer. *Bioinformatics* **2011**, *27*, 1009–1010. [CrossRef]
27. Rozewicki, J.; Li, S.; Amada, K.M.; Standley, D.M.; Katoh, K. MAFFT-DASH: Integrated protein sequence and structural alignment. *Nucleic Acids Res.* **2019**, *47*, 5–10. [CrossRef]
28. Goris, J.; Konstantinidis, K.T.; Klappenbach, J.A.; Coenye, T.; Vandamme, P.; Tiedje, J.M. DNA-DNA hybridization values and their relationship to whole-genome sequence similarities. *Int. J. Syst. Evol. Microbiol.* **2007**, *57*, 81–91. [CrossRef]
29. Bouckaert, R.; Vaughan, T.G.; Barido-Sottani, J.; Duchêne, S.; Fourment, M.; Gavryushkina, A.; Heled, J.; Jones, G.; Kühnert, D.; De Maio, N.; et al. BEAST 2.5: An advanced software platform for Bayesian evolutionary analysis. *PLoS Comput. Biol.* **2019**, *15*, e1006650. [CrossRef]
30. Gatto, L.; Catanzaro, D.; Milinkovitch, M.C. Assessing the applicability of the GTR nucleotide substitution model through simulations. *Evol. Bioinform.* **2007**, *2*, 145–155. [CrossRef]
31. Letunic, I.; Bork, P. Interactive Tree Of Life (iTOL) v4: Recent updates and new developments. *Nucleic Acids Res.* **2019**, *47*, W256–W259. [CrossRef]

32. Kurtz, S.; Phillippy, A.; Delcher, A.L.; Smoot, M.; Shumway, M.; Antonescu, C.; Salzberg, S.L. Versatile and open software for comparing large genomes. *Genome Biol.* **2004**, *5*, 12. [CrossRef]
33. Peng, Z.; Liang, W.; Liu, W.; Wu, B.; Tang, B.; Tan, C.; Zhou, R.; Chen, H. Genomic characterization of *Pasteurella multocida* HB01, a serotype A bovine isolate from China. *Gene* **2016**, *581*, 85–93. [CrossRef]
34. Martin, D.P.; Murrell, B.; Golden, M.; Khoosal, A.; Muhire, B. RDP4: Detection and analysis of recombination patterns in virus genomes. *Virus Evol.* **2015**, *1*, 003. [CrossRef]
35. Yu, J.; Zhao, S.; Rao, H. Whole genomic analysis of a potential recombinant human adenovirus type 1 in Qinghai plateau, China. *Virol. J.* **2020**, *17*, 111. [CrossRef]
36. Mravak, S.; Bienzle, U.; Feldmeier, H.; Hampl, H.; Habermehl, K.O. Pseudorabies in man. *Lancet* **1987**, *1*, 501–502. [CrossRef]
37. Zhai, X.; Zhao, W.; Li, K.; Zhang, C.; Wang, C.; Su, S.; Zhou, J.; Lei, J.; Xing, G.; Sun, H.; et al. Genome Characteristics and Evolution of Pseudorabies Virus Strains in Eastern China from 2017 to 2019. *Virol. Sin.* **2019**, *34*, 601–609. [CrossRef]
38. Hu, R.M.; Zhou, Q.; Song, W.B.; Sun, E.C.; Zhang, M.M.; He, Q.G.; Chen, H.C.; Wu, B.; Liu, Z.F. Novel pseudorabies virus variant with defects in TK, gE and gI protects growing pigs against lethal challenge. *Vaccine* **2015**, *33*, 5733–5740. [CrossRef]
39. Li, A.; Lu, G.; Qi, J.; Wu, L.; Tian, K.; Luo, T.; Shi, Y.; Yan, J.; Gao, G.F. Structural basis of nectin-1 recognition by pseudorabies virus glycoprotein D. *PLoS Pathog.* **2017**, *13*, e1006314. [CrossRef]
40. Zhang, N.; Yan, J.; Lu, G.; Guo, Z.; Fan, Z.; Wang, J.; Shi, Y.; Qi, J.; Gao, G.F. Binding of herpes simplex virus glycoprotein D to nectin-1 exploits host cell adhesion. *Nat. Commun.* **2011**, *2*, 577. [CrossRef]
41. Rocha, E.P.; Smith, J.M.; Hurst, L.D.; Holden, M.T.; Cooper, J.E.; Smith, N.H.; Feil, E.J. Comparisons of dN/dS are time dependent for closely related bacterial genomes. *J. Theor. Biol.* **2006**, *239*, 226–235. [CrossRef] [PubMed]
42. Ye, C.; Guo, J.C.; Gao, J.C.; Wang, T.Y.; Zhao, K.; Chang, X.B.; Wang, Q.; Peng, J.M.; Tian, Z.J.; Cai, X.H.; et al. Genomic analyses reveal that partial sequence of an earlier pseudorabies virus in China is originated from a Bartha-vaccine-like strain. *J. Virol.* **2016**, *491*, 56–63. [CrossRef] [PubMed]
43. Nauwynck, H.; Glorieux, S.; Favoreel, H.; Pensaert, M. Cell biological and molecular characteristics of pseudorabies virus infections in cell cultures and in pigs with emphasis on the respiratory tract. *Vet. Res.* **2007**, *38*, 229–241. [CrossRef] [PubMed]
44. Saito, A.; Nasser, H.; Uriu, K.; Kosugi, Y.; Irie, T.; Shirakawa, K.; Sadamasu, K.; Kimura, I.; Ito, J.; Wu, J. SARS-CoV-2 spike P681R mutation enhances and accelerates viral fusion. *bioRxiv* **2021**. [CrossRef]
45. Klupp, B.G.; Nixdorf, R.; Mettenleiter, T.C. Pseudorabies virus glycoprotein M inhibits membrane fusion. *J. Virol.* **2000**, *74*, 6760–6768. [CrossRef]
46. Favoreel, H.W.; Van Minnebruggen, G.; Nauwynck, H.J.; Enquist, L.W.; Pensaert, M.B. A tyrosine-based motif in the cytoplasmic tail of pseudorabies virus glycoprotein B is important for both antibody-induced internalization of viral glycoproteins and efficient cell-to-cell spread. *J. Virol.* **2002**, *76*, 6845–6851. [CrossRef]
47. Zsak, L.; Zuckermann, F.; Sugg, N.; Ben-Porat, T. Glycoprotein gI of pseudorabies virus promotes cell fusion and virus spread via direct cell-to-cell transmission. *J. Virol.* **1992**, *66*, 2316–2325. [CrossRef]
48. Wang, Y.; Liu, T.X.; Wang, T.Y.; Tang, Y.D.; Wei, P. Isobavachalcone inhibits Pseudorabies virus by impairing virus-induced cell-to-cell fusion. *Virol. J.* **2020**, *17*, 39. [CrossRef]

Disclaimer/Publisher’s Note: The statements, opinions and data contained in all publications are solely those of the individual author(s) and contributor(s) and not of MDPI and/or the editor(s). MDPI and/or the editor(s) disclaim responsibility for any injury to people or property resulting from any ideas, methods, instructions or products referred to in the content.

Review

Recombinant Pseudorabies Virus Usage in Vaccine Development against Swine Infectious Disease

Mo Zhou ¹, Muhammad Abid ², Shinuo Cao ^{1,*} and Shanyuan Zhu ^{1,*}

¹ Jiangsu Key Laboratory for High-Tech Research and Development of Veterinary Biopharmaceuticals, Engineering Technology Research Center for Modern Animal Science and Novel Veterinary Pharmaceutic Development, Jiangsu Agri-Animal Husbandry Vocational College, Taizhou 225306, China

² Viral Oncogenesis Group, The Pirbright Institute, Ash Road Pirbright, Woking, Surrey GU24 0NF, UK

* Correspondence: shinuo_cao@163.com (S.C.); jsnm_zsy@126.com (S.Z.); Tel.: +86-150-0469-3053 (S.C.)

Abstract: Pseudorabies virus (PRV) is the pathogen of pseudorabies (PR), which belongs to the alpha herpesvirus subfamily with a double stranded DNA genome encoding approximately 70 proteins. PRV has many non-essential regions for replication, has a strong capacity to accommodate foreign genes, and more areas for genetic modification. PRV is an ideal vaccine vector, and multivalent live virus-vectored vaccines can be developed using the gene-deleted PRV. The immune system continues to be stimulated by the gene-deleted PRVs and maintain a long immunity lasting more than 4 months. Here, we provide a brief overview of the biology of PRV, recombinant PRV construction methodology, the technology platform for efficiently constructing recombinant PRV, and the applications of recombinant PRV in vaccine development. This review summarizes the latest information on PRV usage in vaccine development against swine infectious diseases, and it offers novel perspectives for advancing preventive medicine through vaccinology.

Keywords: pseudorabies virus; virus modification; virus-vectored vaccines; recombinant PRV; swine infectious disease



Citation: Zhou, M.; Abid, M.; Cao, S.; Zhu, S. Recombinant Pseudorabies Virus Usage in Vaccine Development against Swine Infectious Disease. *Viruses* **2023**, *15*, 370. <https://doi.org/10.3390/v15020370>

Academic Editors: Yan-Dong Tang and Xiangdong Li

Received: 30 December 2022

Revised: 19 January 2023

Accepted: 20 January 2023

Published: 28 January 2023



Copyright: © 2023 by the authors. Licensee MDPI, Basel, Switzerland. This article is an open access article distributed under the terms and conditions of the Creative Commons Attribution (CC BY) license (<https://creativecommons.org/licenses/by/4.0/>).

1. Introduction

Pseudorabies virus (PRV) is the etiological agent of pseudorabies (PR), belonging to the *Herpesviridae* family, primarily affects pigs and can occasionally be transmitted to cattle, goats, sheep, cats, and dogs [1–5]. The PRV virus is a double-stranded DNA virus approximately 143 kb in size, consisting of unique long (UL), internal repeat short (IRS), unique short (US), and a terminal repeat short (TRS) [6–8]. There is a minimum of 70 open reading frames (ORFs) in the genome encoding 70–100 viral proteins, including virulence-related proteins and replicase, as well as many proteins that are not essential for PRV replication [9,10]. The large PRV genome allows the insertion of several kilobases (kb) foreign DNA sequences. The expression of foreign genes does not influence the virus replication [11]. Therefore, multivalent vaccines were developed using PRV as a vector, in which the major antigen of different swine pathogens was expressed [12].

Live vector vaccine can stimulate humoral immunity and solid cellular immunity, which is the main goal for developing a swine infectious disease vaccine. Scientists have generated PRV vaccine strains with few side effects and good immunity by inserting foreign genes or knocking out self-virulence genes. This review summarizes the biological characteristics of PRV, the methodological principle and technology platform for constructing characteristics of PRV, the methodological principle and technology platform for constructing PRV recombinants efficiently, and the applications of PRV recombinants in vaccine development. This review is intended to serve as a reference for PRV live vector vaccine research and development.

2. The Biological Characteristics of PRV

There are 10 glycoproteins encoded by PRV, which are divided into two groups (essential or non-essential glycoproteins) according to the degree to which viral replication depends on them [13,14]. The glycoprotein B (gB) plays a crucial role in membrane fusion during infection and in spreading viruses from cell to cell [15–17]. A major glycoprotein encoded by the glycoprotein C gene mediates the attachment of PRV to target cells through heparin-binding domains [11,18–20]. In susceptible animals, the protective immune responses were induced by gB, gC, and glycoprotein D (gD) [21–23]. In the viral envelope of infected cells, a heterodimer complex formed by glycoprotein I (gI) and glycoprotein E (gE) plays a crucial role in PR infection and transmission [24–27].

Bartha-K61, the original PRV vaccine strain, contains the deletion of US2, gE, gI, and US9 genes. This vaccine strain has been widely used to control PR worldwide. Since the 1990s, few swine PR cases have been reported due to PRV Bartha-K61 [4,28–31]. However, the PR outbreak occurred at the farm where pigs were vaccinated with Bartha-K61, which was caused by PRV variants and resulted in severe economic losses from 2011 [32–38]. Vaccines remain the most effective method to control PRV infection. Consequently, the PRV variant has been used to generate several gene mutant vaccines with gE, gI, and TK deletions. When challenged with PRV variants, these mutants provided adequate protection [39–48]. By introducing foreign genes derived from other porcine pathogens into the PRV variants and subsequent vaccination, it is possible to establish immune protection against these swine infectious diseases.

3. PRV Recombinants Construction

There are some non-essential regions in the large genome of PRV. As a result of this character, several kb of foreign DNA can be accommodated by PRV without compromising its stability. Reverse genetics plays a crucial role in PRV gene modification, and with the development of molecular biology techniques, many reverse genetic techniques have been used to construct the recombinant PRV.

3.1. Homologous Recombination

In the past, PRV recombinants were generated by homologous recombination (HR) in permissive cells. The construction of recombinant viruses based on the principle of HR can be divided into two steps: construction of a transfer plasmid and screening of the recombinant virus. Usually, the virus genome is used as a template to amplify the two gene fragments used as recombinant homologous arms by PCR technology, and then the foreign gene expression cassette is inserted between the homologous arms to construct the transfer vector containing the foreign gene expression cassette and the left and right homologous arms. Gene deletion or replacement is achieved by homologous recombination of the transfer vector and parent strain in eukaryotic susceptible cells. At present, there are two methods used for transfection. One method is co-transfection of the transfer vector and the parent virus genome, and another method is transfection of the transfer vector first and then inoculation of the virus. The reporter gene carried on the transfer vector is used to screen the plaque of the recombinant virus. Generally, the recombinant virus with infective activity can be obtained after 5–10 generations of screening. By using this method, Tong et al. and Wang et al., constructed a recombinant PRV strain expressing the E2 protein of CSFV in a gE-deleted PRV variant strain [49,50]; Yan et al. constructed the recombinant virus with additional expression of the gC gene [51]; Zheng et al. produced recombinant PRV that expressed VP2 protein of porcine parvovirus and porcine IL-6 [52]. Because of the low efficiency of HR, it is not commonly used in the construction of PRV recombinants.

3.2. Bacterial Artificial Chromosome

In comparison with homologous recombination, bacterial artificial chromosomes (BAC) are more efficient. Red/ET recombination technology can be used to modify BAC in *Escherichia coli*, which can be divided into two steps [53]. The first step is to construct an ex-

pression cassette with marker genes and both ends containing homologous arm sequences and transform them into competent cells containing viral BAC by electroporation. After resistance screening, correct recombinants were obtained. The second step was constructing an expression cassette with foreign genes and both ends containing homologous arm sequences. The recombinants with deleted marker genes were obtained by counter-resistance screening. Zhang et al. construct a TK/gE-deleted AH02LA BAC using the virulent PRV AH02LA strain and inserted the pig epidemic diarrhea virus (PEDV) variant spike (S) expression cassette in four different noncoding regions using the En Passant mutagenesis method [54]. Furthermore, to develop the recombinant vaccine against the PRV variants, Zhang et al. constructed a BAC clone of Bartha-K61. Using Bartha-K61 BAC as the backbone, the gD and gC of Bartha were replaced with that of PRV variants (AH02LA) via the En Passant method. When compared to the parental Bartha-K61, there was no difference in growth properties in the gD/gC-substituted Bartha-K61 ST cells [22].

3.3. Fosmid Library

The traditional HR method is not efficient in obtaining recombinant viruses. Creating recombinant BAC constructs is a labor-intensive and time-consuming process. When the whole genome PRV is cloned to the BAC plasmid, fragment deletion often occurs during the electroporation process, affecting recombination efficiency. In contrast, fosmid library generation is more efficient. The huge genome of PRV is randomly sheared into various fragments, then each segment is ligated with a fosmid vector to screen out the various combinations covering the whole genome of PRV, and the fosmid combination was co-transfected into virus-susceptible eukaryotic cells to rescue the virus [55,56]. Construction of recombinant virus only needs to modify the corresponding fosmid in *E. coli*. Since the fosmid only contains part of the PRV genome, the efficiency of obtaining virus mutants is greatly improved. Modification of fosmid in *E. coli* can also utilize Red/ET recombination technology. A fosmid library based on the PRV-TJ strain was constructed by Zhou et al., and recombinant PRV was rescued by transfecting a group of fosmid directly into Vero cells. Furthermore, the green fluorescent protein-expressing reporter virus was rescued successfully by the Red/ET system [55]. Abid et al. constructed a PRV co-expressing E2 of classical swine fever virus (CSFV) and Cap of porcine circovirus type 2 (PCV2) by using this fosmid library platform [57]. In addition, Qi et al. constructed a fosmid library for the PRV-SC strain. The EGFP gene was inserted into the N-terminal of the UL 36 gene of PRV-SC via the Red/ET recombination [56].

3.4. CRISPR/Cas9

Molecular biotechnology has dramatically contributed to studying viruses' replication and vaccines. The CRISPR /Cas9-mediated genome editing system has been widely applied as a powerful tool to construct PRV mutants. The researchers used CRISPR/Cas9 technology to construct PRV gE, gI, or TK gene-deleted recombinants [42,43,46]. Furthermore, CRISPR/Cas9 can be used in combination with HR and BAC technology to improve the efficiency of recombination [53,58]. Fu et al., used CRISPR/Cas9 gene-editing technology to construct a double reporter virus with stable expression of EGFP and firefly luciferase [59]. Feng et al. used this technology to insert the African swine fever virus (ASFV) CD2v gene into the TK, gE, and gI-deleted PRV Fa strain. The ASFV CD2v was stability expressed in the recombinant virus [12]. Wu et al. inserted the tandem repeats of the ORF2 gene into PRV gE and gG sites through CRISPR/Cas9 mediated HR and constructed a bivalent vaccine based on the PRV-HNX strain [60]. To optimize the method used for generating infectious recombinant PRV expressing predicted or known ASFV immunogenic proteins, Fuchs et al. developed an efficient strategy for the insertion of foreign genes in PRV vector based on marker-enforced recombination and CRISPR/Cas9. They co-transfected the defective PRV Bartha-K61 BAC DNA (possesses a deletion of glycoprotein G and an additional deletion encompassing the initiation codon and promoter of glycoprotein D, which plays an essential role in binding to receptors), the rescue transfer plasmid (A PRV-encoded

transgene flanked by homologous recombination sequences and an intact gD promoter are included in this construct), and the CRISPR/Cas9 plasmid to the cell. Transgene substitutions were observed in 99% of the obtained progeny viruses [61]. Additionally, CRISPR/Cas9 and Cre/Lox greatly improved multi-gene editing efficiency and reduced vaccine development time. Yao et al. combined the Cre/Lox and CRISPR/Cas9-mediated gene insertion system, deleted the TK and gE gene, and inserted the immunoregulatory factor gene simultaneously [62].

Homologous recombination is the traditional method to generate the recombinant PRV. BAC was used later and allowed manipulation of the whole genome in *Escherichia coli*. The homologous recombination method is labor-intensive due to several rounds of plaque purification. The BAC system was more efficient than homologous recombination, but the generation of recombinant BAC construct is time-consuming, and the huge PRV genome is easily broken. The fosmid library and CRISPR/Cas9-based genetic manipulation platform for PRV offer several advantages over the conventional technology, but some disadvantages still appeared during the construction of the recombinants (Table 1). Therefore, we need to consider the advantages of various approaches and develop a more efficient way to construct the recombinant PRV.

Table 1. Advantages and disadvantages of recombinant PRV construction approaches.

Approaches	Advantages	Disadvantages
Homologous recombination (HR)	The procedure is relatively easy; Site-specific insertion of foreign genes.	Construction of transfer vector is time-consuming and labor-intensive; The efficiency of homologous recombination is low; The purification of viruses is time-consuming.
Bacterial Artificial Chromosome (BAC)	More efficient than homologous recombination; Cloning the entire genome into a plasmid facilitates genome modification.	Generation of recombinant BAC construct is time-consuming; The PRV genome is easily broken, and once the genome is broken, infectivity is lost and a recombinant virus cannot be obtained.
Fosmid library	Generation of the fosmid library is more efficient; High structural stability.	The fractured genome was inserted into 5-6 fosmids; 5-6 fosmids need to be co-transfected.
CRISPR/Cas9 system	Highly efficient; Simultaneous targeting of multiple sites.	It is necessary to construct homologous arms; Off-target effects usually occurred; This method also requires the purification of the virus.

4. Principle behind Recombinant PRV

The expression of foreign genes is an important index to evaluate the efficacy of the live recombinant vaccine, which is affected by the promoter and the insertion site of the foreign gene.

4.1. Promoter Affects Foreign Gene Expression

The initial transcription of foreign genes is the critical step of gene expression, and the rate of transcription initiation is the rate-limiting step of gene expression. The promoters and related regulatory sequences are the premises of constructing a good expression system. The regulation elements of exogenous gene expression include a promoter, enhancer, Kozak sequence, and stop codon. The expression level of the foreign gene in PRV mainly depends on the strength of the upstream promoter, and a generally strong promoter is selected. The gG and gE promoters were always chosen to construct recombinant PRV, which have unique structures and vigorous activity [57,60]. A more potent heterologous enhancer or promoter, such as the HCMV or MCMV promoter, was also evaluated instead of the gG promoter [50,54]. Different promoters were tested to express the ASFV gene in PRV, such as HCMV, MCMV, and a chimeric promoter (CAG) consisting of the HCMV enhancer and the chicken beta-actin promoter [61]. Compared with cytomegalovirus immediate-early promoters, the CAG promoter enhanced the expression of foreign genes in PRV.

4.2. Insertion Site Is the Main Factor, Affects the Expression of Foreign Genes

For a live vector vaccine strain, genetic stability is crucial. The PRV genome contains numerous sites for inserting and expressing heterologous genes, but almost all are located near the gI/gE, TK, or gG genes. In a study by Tong et al., the gD and gG genes were inserted with E2 expression cassettes, and insertion of the cassettes did not significantly affect in vitro replication of the recombinant virus. And the piglets challenged with virulent PRV are protected by recombinant viruses [50]. Wu et al. also inserted the tandem repeats of the PCV2 Cap protein gene into PRV gG and gE sites. A high level of PCV2 Cap protein expression was detected in this recombinant PRV [60]. Intergenic regions between gG and gD proved to be excellent sites for expressing foreign genes, according to these results. To identify suitable areas to insert foreign genes into PRV genomes, Zhang et al. inserted an S protein expression cassette of a PEDV variant in different noncoding regions of the PRV genome with deletion of TK, gE, and gI, such as US2-1, UL11-10, UL46-27, and UL35-36. The US2-1 area is critical for PRV replication, as the insertion of a foreign gene failed to rescue the virus, another three noncoding regions are suitable sites for the insertion of the S gene; S gene mRNA expression was higher when it was inserted in the location of UL11-10 [50,54]. Therefore, the UL11-10 is a new suitable insertion site for S gene expression.

So far, when selecting the insertion sites of foreign genes, researchers have considered the non-essential regions of virus replication first. Although the genome sequence of PRV contains a large number of non-essential regions for replication, the basic theories of the relationship between these regions and virus virulence, immune escape mechanism, or host range need to be further studied. At the same time, the expression of exogenous genes in the vector is affected by the size of the exogenous fragment, the promoter of the expression vector, and the insertion site effect caused by the insertion of exogenous genes. Therefore, a certain size of a foreign gene, stable insertion sites of a foreign gene, and safe and efficient expression elements are the basis for the application of recombinant live vector vaccines.

5. Applications of Recombinant PRV

The large genome of PRV contains numerous insertion sites that allow heterologous genes to be integrated and expressed. Consequently, PRV has developed into a powerful vector system for expressing foreign proteins.

5.1. PRV Bartha K61 Strain as a Vector for Expressing Exogenous Antigens

In pigs, PRV Bartha K61 replicates reliably and elicits a wide range of humoral and cellular immune responses. Additionally, in order to establish clinical protection against different pathogens, foreign antigens can be introduced into the Bartha K61 backbone and vaccinated. By introducing the GP5 gene from the porcine reproductive and respiratory syndrome virus (PRRSV) into Bartha K61, and subsequently vaccinating, significant clinical protection was achieved, and pathological lesions were reduced after the PRRSV challenge in piglets [63]. Further, mice were protected against virulent challenges with swine influenza H3N2 by vaccination with a Bartha vector that expressed the hemagglutinin of swine influenza H3N2 [64]. Furthermore, pigs vaccinated with Bartha vectors expressing the pandemic H1N1 swine-origin influenza virus hemagglutinin or neuraminidase also demonstrated significant inhibition of virus replication after a challenge with the H1N1 virus [65]. Due to the limitations of Bartha K61 in protecting against PRV variants, Zhang et al. constructed the gD/gC-substituted Bartha K61, in which the gD/gC of Bartha K61 was substituted with the gD/gC of PRV variants (AH02LA). The gD/gC-substituted Bartha K61 was safe, and it effectively protected against virulent PRV variants [22]. Therefore, Bartha K61 was a safe and effective backbone for multivalent vaccine development.

5.2. Attenuated PRV Variant as a Vector for Expressing Exogenous Antigens

Since 2011, farms immunized with Bartha-K61 have experienced PR outbreaks caused by PRV variants. Therefore, the researchers try to generate several gene mutant vaccines involving gE/TK, gI/gE, and gI/gE/TK deletion based on different PRV variants. These

vaccines provided adequate protection against the PRV variant challenge. These gene mutant vaccines also are used as a vector system for foreign proteins to develop multivalent live virus-vectored vaccines against several swine infectious diseases. Tong et al. and Wang et al. constructed a recombinant expressing the CSFV E2 protein and evaluated its efficacy against both CSFV and PRV variant strains [49,50]. The recombinant PRV appears to be a promising recombinant vaccine candidate for the control and eradication of PRV variants and CSFV. Through the fosmid library platform, Abid et al. constructed a recombinant co-expressing E2 of CSFV and Cap of PCV2 with gE/gI/TK gene deletions [57]. The recombinant strain was safe for pigs and rabbits, and anti-PRV antibodies could be detected in the serum of immunized rabbits and pigs. But anti-E2 and PCV2 antibodies could not be detected, which was presumed to be because the expression level of E2 and Cap proteins are too low to induce antibody production. In addition, a tandem repeat of PCV2 Cap protein gene ORF2 that links with a protein quantitation rationing linker was constructed by Wu et al., and endogenous PRV promoters were used to drive PCV2 Cap2 expression in PRV [60]. High levels of neutralizing antibodies were detected 14 days after immunization of the recombinant bivalent vaccine candidate, which was maintained at days 21, 42, and 60. In wild boars and domestic pigs, the African swine fever virus (ASFV) causes a fatal disease, and there is no effective vaccine against the ASFV. In order to develop the live vector vaccine against ASFV, Feng et al. insert the CD2v into the PRV variant Fa stain (TK, gE, and gI deleted) and obtained a recombinant strain expressing CD2v gene [12]. The recombinant virus stimulated the production of anti-CD2v antibodies and specific cellular immune responses. Furthermore, the recombinant virus could protect mice against the virulent strain (PRV-Fa) infection.

5.3. Attenuated PRV Variant as a Vector for Expressing Immunoregulatory Factors

Lymphokine-activated killer cells recognize infected cells associated with PRV gC during cell-mediated immunity, and PRV gC plays a role in cytotoxic T-lymphocytes recognition of infected cells [22,66,67]. To enhance gC expression, Yan et al. inserted an additional expression cassette of the gC gene into the gI and gE deletion regions [51]. Additional gC gene expression enhanced the efficacy of the PRV gI/gE-deleted vaccine in pigs. A hematopoietic growth factor, Fms-related tyrosine kinase 3 ligand (Flt3L), plays an important role in hematopoietic cell differentiation. In the periphery, FLT3L and its receptor regulate homeostatic DC division [68,69]. An FLT3L-dependent pathway mediates vaccine-induced protective immunity and enhances the activation of T cells [70]. Based on the immunomodulatory functions of Flt3L, a TK/gE gene deleted and Flt3L co-expressed recombinant PRV was constructed by Yao et al. [62]. The recombinant gene showed potential function in DC activation and protective immune response enhancement. These results indicated that t Flt3L is an ideal adjuvant, and the PRV can load the immunoregulatory factors and achieve simultaneous immunization with the adjuvant and vaccine.

5.4. Attenuated PRV Variant as Vector for Expressing Reporter Genes

Up to now, the mechanism of PRV variant virulence enhancement is unknown. A reporter virus is a valuable tool for basic virology studies. Therefore, Fu et al. constructed a double reporter virus with stable expression of EGFP and firefly luciferase based on the PRV variant [59]. The recombinant virus showed similar biological characteristics to the parental strain, including a stable viral titer and luciferase activity throughout 20 passages. Furthermore, Zhou and Qi constructed the reporter virus based on the PRV variant and classical stain, respectively [55,56]. The EGFP was fused into the amino-terminal of UL36 in these recombinants. The single viral particles with green fluorescence were used to monitor retrograde and anterograde moving virions in the axon, these reported viruses will accelerate the understanding of the biology of the PRV variant.

6. Conclusions and Prospects

The genetically engineered live vector vaccine can effectively avoid the traditional vaccines' defects, simplify the breeding industry's immunization procedures, and improve the efficiency of epidemic prevention and control. Attenuated PRV-based vector vaccines do not induce any clinical signs of PR, but provide complete protection against PRV and other swine pathogens, and it has been widely used in the study of a recombinant multivalent vaccine against swine infectious disease. The BAC technology, CRISPR/Cas9 technology, and fosmid library were used to construct PRV recombinant, significantly improving the efficiency of exogenous gene expression (Table 2). But we still need to consider how to ensure the genetic stability of the immune genes, and how to ensure the safety of recombinant viruses during live vector vaccine development. The significant virulence genes were deleted during the development of the recombinant PRV live vector vaccine, significantly reducing its virulence to animals, However, the safety of the recombinants still needs to be analyzed in detail. There are extensive replication non-essential regions in the PRV genome, which provide a basis for optimizing recombinant sites. The selection of better insertion sites and safer and more efficient expression elements, especially an efficient promoter, is the basis of recombinant live vector vaccine application. Further research and utilization of the advantages of recombinant PRV live vector vaccine will play an essential role in the prevention and control of animal diseases. The recombinant herpes virus live vector vaccine will play an important role in animal disease prevention and control in the future.

Table 2. The characteristic features of recombinant PRV.

Vector	Exogenous Genes	Insertion Sites	Promoters	Modification of PRV	Immunization Dose/Route	Animal Model	Efficacy	Reference
Bartha-K61	respiratory syndrome virus (PRRSV) GP5	UL23 (TK) site	CMV promoter	homologous recombination (HR)	$10^{7.0}$ plaque-forming unit (PFU)/ intranasally (i.n.) and intramuscularly (i.m.)	4-week-old piglet	confer significant protection against clinical disease and reduce pathogenic lesions induced by PRRSV challenge in vaccinated pigs	[63]
Bartha-K61	hemagglutinin (HA) gene of swine influenza virus (SIV)	not mentioned	SV40 promoter	HR	$10^{5.0}$ PFU/i.n.	8-week-old mice	protect mice from heterologous virulent challenge	[64]
Bartha-K61	HA of swine-origin H1N1 virus.	gG gene locus	MCMV promoter	bacterial artificial chromosome (BAC) technology-mediated HR	$2 \times 10^{7.0}$ PFU/i.n.	7-week-old pigs	protected pig from clinical signs after challenge with a related swine-origin H1N1 influenza A virus	[65]
Bartha-K61	gD and gC genes of the AH02LA strain	gD and gC gene locus		BAC technology and HR	$10^{6.0}$ TCID ₅₀ / i.m	4-week-old piglet	PRV B-gD&gC S is safe for piglets, and provides complete clinical protection against a pseudorabies variant (AH02-LA) challenge	[22]

Table 2. Cont.

Vector	Exogenous Genes	Insertion Sites	Promoters	Modification of PRV	Immunization Dose/Route	Animal Model	Efficacy	Reference
Bartha-K61	open reading frames E199L, CP204L (p30) and KP177R (p22) of African swine fever virus.	gG gene locus	CAG promoters	BAC technology and CRISPR/Cas9				[61]
PRV variant (HN1201strain)	enhanced green fluorescent protein (EGFP) and firefly luciferase	between gE partial and gI partial	EGFP expression was under the control of the CAG promoter (a synthetic promoter composed of a CMV enhancer and chicken β -actin promoter); the firefly luciferase expression cassette was under the control of the SV40 promoter	CRISPR/Cas9				[59]
PRV variant (AH strain)	glycoprotein C	between gD and US9	CMV promoter	HR	$10^{7.0}$ TCID ₅₀ / i.m (piglet); $10^{5.0}$ TCID ₅₀ / i.m (mice)	4-week-old piglet; 4-week-old SPF Kunming mice	additional insertion of gC gene could enhance the protective efficacy in PRV gI/gE-deleted vaccine in pigs	[51]
PRV variant (HNX strain)	cytokine Fms-related tyrosine kinase 3 ligand (Flt3L)	after gD	gD promoter	CRISPR/Cas9 and Cre/Lox systems	$10^{5.0}$ TCID ₅₀ / i.m	Six-week-old female BALB/c mice	Flt3L can activate DCs and enhance protective immune responses of recombinant pseudorabies virus with TK/gE gene deletion	[62]
PRV variant (TJ strain)	classical swine fever virus (CSFV) E2 glycoprotein and capsid (Cap) protein of porcine circovirus type 2 (PCV2)	E2 expression cassette was inserted after US9; Cap was fused with gG and co-expressed with gG	E2 expression was under the control of CMV promoter; Cap was under the control of the gG promoter	fosmid library platform and Red/ET systems	10^7 , 10^6 , and 10^5 TCID ₅₀ / i.m (rabbit); $10^{6.0}$ TCID ₅₀ / i.m (pig)	6-week-old rabbits; 6-week-old pigs	rPRV[TJ]-delgE/gI/TK-E2-Cap elicited detectable anti-PRV antibodies, but not anti-PCV2 or anti-CSFV antibodies	[57]
PRV variant (AH02LA strain)	S gene of a Porcine epidemic diarrhea virus (PEDV) variant	UL11-10, UL35-36, UL46-27	MCMV promoter	BAC technology and En Passant method				[54]
PRV variant (JS-2012)	CSFV E2 glycoprotein	between the gG and gD genes	not mentioned	HR	$10^{5.0}$ TCID ₅₀ / i.m	3-week-old piglets	induce the production of Abs to the gE protein of PRV or to the CSFV proteins other than E2	[50]

Table 2. Cont.

Vector	Exogenous Genes	Insertion Sites	Promoters	Modification of PRV	Immunization Dose/Route	Animal Model	Efficacy	Reference
PRV variant (TJ strain)	CSFV E2 glycoprotein	between gE partial and gI partial	CMV promoter	HR	10^4 , 10^5 , and 10^6 TCID ₅₀ / i.m	6-week-old piglets	provided complete protection against the lethal challenge with either the PRV TJ strain or the CSFV Shimen strain	[49]
PRV variant (HNX strain)	tandem repeats of porcine circovirus type 2 (PCV2) Capprotein gene ORF2	gE and gG sites		CRISPR/Cas9 and HR	$10^{5.8}$ TCID ₅₀ / i.m	4-week-old female BALB/c mice	high titer of specific antibodies for PRV and neutralized antibodies for PCV2 were detected	[60]
PRV (Fa strain)	CD2v of African swine fever virus	PRV UL23 (TK) site	CMV promoter	CRISPR/Cas9 and HR	$10^{5.0}$ TCID ₅₀ / i.m	5-week-old SPF mice (ICR)	PRV-ΔgE/ΔgI/ΔTK-(CD2v) recombinant strain has strong immunogenicity	[12]
PRV	P12A and 3C of Foot-and-mouth disease virus (FMDV)	between gE partial and gI partial	CMV promoter	HR	$10^{6.0}$ TCID ₅₀ / i.m	6-week-old large white piglets	PRV-P12A3C induced a high level of neutralizing antibody and FMDV-specific lymphocytes.	[71]
PRV variant (TJ strain)	EGFP	fused with UL35	UL35 promoter	fosmid library platform and Red/ET				[55]
PRV (SC strain)	EGFP	fused with UL36	UL36 promoter	fosmid library platform and Red/ET				[56]

Author Contributions: M.Z. and S.C. are the major contributors to the review, M.Z., S.C. and S.Z. designed the concept and prepare the original draft of the review; S.Z. and M.A. conceived and revised the paper. All authors have read and agreed to the published version of the manuscript.

Funding: This work was funded by a grant from the key project of Jiangsu Province's Key Research and Development Plan (modern Agriculture) (BE2020407), the project of Jiangsu Agri-animal Husbandry Vocational College (NSF2022CB04, NSF2022CB25), the Natural Science Research Project of Higher Education of Jiangsu Province (2020220375), and the Qing Lan Project of Jiangsu Province.

Institutional Review Board Statement: Not applicable.

Informed Consent Statement: Not applicable.

Data Availability Statement: The data presented in this study are available in the insert article.

Acknowledgments: The authors would like to thank members of the Division of Swine Infectious disease prevention and control of Jiangsu Agri-animal Husbandry Vocational College for valuable discussion.

Conflicts of Interest: The authors declare that this work was conducted in the absence of any commercial or financial relationships that could be as a potential conflict of interest.

References

- Hu, R.M.; Zhou, Q.; Song, W.B.; Sun, E.C.; Zhang, M.M.; He, Q.G.; Chen, H.C.; Wu, B.; Liu, Z.F. Novel pseudorabies virus variant with defects in TK, gE and gI protects growing pigs against lethal challenge. *Vaccine* **2015**, *33*, 5733–5740. [CrossRef] [PubMed]
- Zhao, X.; Tong, W.; Song, X.; Jia, R.; Li, L.; Zou, Y.; He, C.; Liang, X.; Lv, C.; Jing, B.; et al. Antiviral Effect of Resveratrol in Piglets Infected with Virulent Pseudorabies Virus. *Viruses* **2018**, *10*, 457. [CrossRef] [PubMed]
- Yao, J.; Li, J.; Gao, L.; He, Y.; Xie, J.; Zhu, P.; Zhang, Y.; Zhang, X.; Duan, L.; Yang, S.; et al. Epidemiological Investigation and Genetic Analysis of Pseudorabies Virus in Yunnan Province of China from 2017 to 2021. *Viruses* **2022**, *14*, 895. [CrossRef] [PubMed]

4. Zheng, H.H.; Fu, P.F.; Chen, H.Y.; Wang, Z.Y. Pseudorabies Virus: From Pathogenesis to Prevention Strategies. *Viruses* **2022**, *14*, 1638. [CrossRef] [PubMed]
5. Ye, C.; Wu, J.; Tong, W.; Shan, T.; Cheng, X.; Xu, J.; Liang, C.; Zheng, H.; Li, G.; Tong, G. Comparative genomic analyses of a virulent pseudorabies virus and a series of its in vitro passaged strains. *Virol. J.* **2018**, *15*, 195. [CrossRef] [PubMed]
6. Pomeranz, L.E.; Ekstrand, M.I.; Latcha, K.N.; Smith, G.A.; Enquist, L.W.; Friedman, J.M. Gene Expression Profiling with Cre-Conditional Pseudorabies Virus Reveals a Subset of Midbrain Neurons That Participate in Reward Circuitry. *J. Neurosci.* **2017**, *37*, 4128–4144. [CrossRef]
7. Yin, Y.; Romero, N.; Favoreel, H.W. Pseudorabies Virus Inhibits Type I and Type III Interferon-Induced Signaling via Proteasomal Degradation of Janus Kinases. *J. Virol.* **2021**, *95*, e0079321. [CrossRef]
8. Yin, Y.; Ma, J.; Van Waesberghe, C.; Devriendt, B.; Favoreel, H.W. Pseudorabies virus-induced expression and antiviral activity of type I or type III interferon depend on the type of infected epithelial cell. *Front. Immunol.* **2022**, *13*, 1016982. [CrossRef]
9. Wang, Y.P.; Huang, L.P.; Du, W.J.; Wei, Y.W.; Xia, D.L.; Wu, H.L.; Feng, L.; Liu, C.M. The pseudorabies virus DNA polymerase processivity factor UL42 exists as a monomer in vitro and in vivo. *Arch. Virol.* **2016**, *161*, 1027–1031. [CrossRef]
10. Xu, C.; Wang, M.; Song, Z.; Wang, Z.; Liu, Q.; Jiang, P.; Bai, J.; Li, Y.; Wang, X. Pseudorabies virus induces autophagy to enhance viral replication in mouse neuro-2a cells in vitro. *Virus. Res.* **2018**, *248*, 44–52. [CrossRef]
11. Thomsen, D.R.; Marotti, K.R.; Palermo, D.P.; Post, L.E. Pseudorabies virus as a live virus vector for expression of foreign genes. *Gene* **1987**, *57*, 261–265. [CrossRef] [PubMed]
12. Feng, Z.; Chen, J.; Liang, W.; Chen, W.; Li, Z.; Chen, Q.; Cai, S. The recombinant pseudorabies virus expressing African swine fever virus CD2v protein is safe and effective in mice. *Virol. J.* **2020**, *17*, 180. [CrossRef] [PubMed]
13. Zhao, W.L.; Wu, Y.H.; Li, H.F.; Li, S.Y.; Fan, S.Y.; Wu, H.L.; Li, Y.J.; Lü, Y.L.; Han, J.; Zhang, W.C.; et al. Clinical experience and next-generation sequencing analysis of encephalitis caused by pseudorabies virus. *Zhonghua Yi Xue Za Zhi* **2018**, *98*, 1152–1157.
14. Zhao, N.; Wang, F.; Kong, Z.; Shang, Y. Pseudorabies Virus Tegument Protein UL13 Suppresses RLR-Mediated Antiviral Innate Immunity through Regulating Receptor Transcription. *Viruses* **2022**, *14*, 1465. [CrossRef] [PubMed]
15. Dory, D.; Rémond, M.; Béven, V.; Cariolet, R.; Backovic, M.; Zientara, S.; Jestin, A. Pseudorabies virus glycoprotein B can be used to carry foot and mouth disease antigens in DNA vaccination of pigs. *Antivir. Res.* **2009**, *81*, 217–225. [CrossRef] [PubMed]
16. Li, X.; Yang, F.; Hu, X.; Tan, F.; Qi, J.; Peng, R.; Wang, M.; Chai, Y.; Hao, L.; Deng, J.; et al. Two classes of protective antibodies against Pseudorabies virus variant glycoprotein B: Implications for vaccine design. *PLoS Pathog.* **2017**, *13*, e1006777. [CrossRef] [PubMed]
17. Chen, M.; Wang, M.H.; Shen, X.G.; Liu, H.; Zhang, Y.Y.; Peng, J.M.; Meng, F.; Wang, T.Y.; Bai, Y.Z.; Sun, M.X.; et al. Neuropilin-1 Facilitates Pseudorabies Virus Replication and Viral Glycoprotein B Promotes Its Degradation in a Furin-Dependent Manner. *J. Virol.* **2022**, *96*, e0131822. [CrossRef]
18. Trybala, E.; Bergström, T.; Spillmann, D.; Svennerholm, B.; Flynn, S.J.; Ryan, P. Interaction between pseudorabies virus and heparin/heparan sulfate. Pseudorabies virus mutants differ in their interaction with heparin/heparan sulfate when altered for specific glycoprotein C heparin-binding domain. *J. Biol. Chem.* **1998**, *273*, 5047–5052. [CrossRef]
19. Tong, T.; Fan, H.; Tan, Y.; Xiao, S.; Ling, J.; Chen, H.; Guo, A. C3d enhanced DNA vaccination induced humoral immune response to glycoprotein C of pseudorabies virus. *Biochem. Biophys. Res. Commun.* **2006**, *347*, 845–851. [CrossRef]
20. Fan, H.; Liu, Z.; Tong, T.; Liu, X.; Guo, A. C3d-M28 enhanced DNA vaccination induced humoral immune response to glycoprotein C of pseudorabies virus. *Sheng Wu Gong Cheng Xue Bao* **2009**, *25*, 987–992.
21. Li, A.; Lu, G.; Qi, J.; Wu, L.; Tian, K.; Luo, T.; Shi, Y.; Yan, J.; Gao, G.F. Structural basis of nectin-1 recognition by pseudorabies virus glycoprotein D. *PLoS Pathog.* **2017**, *13*, e1006314. [CrossRef] [PubMed]
22. Zhang, C.; Liu, Y.; Chen, S.; Qiao, Y.; Guo, M.; Zheng, Y.; Xu, M.; Wang, Z.; Hou, J.; Wang, J. A gD&gC-substituted pseudorabies virus vaccine strain provides complete clinical protection and is helpful to prevent virus shedding against challenge by a Chinese pseudorabies variant. *BMC Vet. Res.* **2019**, *15*, 2.
23. Zhang, T.; Liu, Y.; Chen, Y.; Wang, A.; Feng, H.; Wei, Q.; Zhou, E.; Zhang, G. A single dose glycoprotein D-based subunit vaccine against pseudorabies virus infection. *Vaccine* **2020**, *38*, 6153–6161. [CrossRef]
24. Tyborowska, J.; Reszka, N.; Kochan, G.; Szweczyk, B. Formation of Pseudorabies virus glycoprotein E/I complex in baculovirus recombinant system. *Acta Virol.* **2006**, *50*, 169–174. [PubMed]
25. Lu, S.; Xiang, M.; Dan, H.; Wu, B.; Gao, Q.; Huang, H.; He, Q.; Chen, H. Immune-tolerizing procedure for preparation of monoclonal antibodies against glycoprotein E of Pseudorabies virus. *Monoclon. Antib. Immunodiagn. Immunother.* **2013**, *32*, 21–25. [CrossRef]
26. Wu, C.Y.; Liao, C.M.; Chi, J.N.; Chien, M.S.; Huang, C. Growth properties and vaccine efficacy of recombinant pseudorabies virus defective in glycoprotein E and thymidine kinase genes. *J. Biotechnol.* **2016**, *229*, 58–64. [CrossRef] [PubMed]
27. Xu, J.J.; Wu, J.Q.; Cheng, X.F.; Tong, W.; Zheng, H.; Zhu, H.J.; Liu, Y.T.; Jiang, Y.F.; Gao, F.; Yu, H.; et al. Identification of two novel epitopes targeting glycoprotein E of pseudorabies virus using monoclonal antibodies. *Biochem. Biophys. Res. Commun.* **2019**, *519*, 330–336. [CrossRef] [PubMed]
28. Freuling, C.M.; Müller, T.F.; Mettenleiter, T.C. Vaccines against pseudorabies virus (PrV). *Vet. Microbiol.* **2017**, *206*, 3–9. [CrossRef]
29. Delva, J.L.; Nauwynck, H.J.; Mettenleiter, T.C.; Favoreel, H.W. The Attenuated Pseudorabies Virus Vaccine Strain Bartha K61: A Brief Review on the Knowledge Gathered During 60 Years of Research. *Pathogens* **2020**, *9*, 897. [CrossRef]


30. Mettenleiter, T.C. Aujeszky Disease and the Development of the Marker/DIVA Vaccination Concept. *Pathogens* **2020**, *9*, 563. [CrossRef]
31. Zhou, H.; Pan, Y.; Liu, M.; Han, Z. Prevalence of Porcine Pseudorabies Virus and Its Coinfection Rate in Heilongjiang Province in China from 2013 to 2018. *Viral Immunol.* **2020**, *33*, 550–554. [CrossRef] [PubMed]
32. Zheng, H.H.; Bai, Y.L.; Xu, T.; Zheng, L.L.; Li, X.S.; Chen, H.Y.; Wang, Z.Y. Isolation and Phylogenetic Analysis of Reemerging Pseudorabies Virus Within Pig Populations in Central China During 2012 to 2019. *Front. Vet. Sci.* **2021**, *8*, 764982. [CrossRef] [PubMed]
33. Zheng, H.H.; Jin, Y.; Hou, C.Y.; Li, X.S.; Zhao, L.; Wang, Z.Y.; Chen, H.Y. Seroprevalence investigation and genetic analysis of pseudorabies virus within pig populations in Henan province of China during 2018–2019. *Infect. Genet. Evol.* **2021**, *92*, 104835. [CrossRef] [PubMed]
34. Fan, J.; Zeng, X.; Zhang, G.; Wu, Q.; Niu, J.; Sun, B.; Xie, Q.; Ma, J. Molecular characterization and phylogenetic analysis of pseudorabies virus variants isolated from Guangdong province of southern China during 2013–2014. *J. Vet. Sci.* **2016**, *17*, 369–375. [CrossRef]
35. Wang, X.; Wu, C.X.; Song, X.R.; Chen, H.C.; Liu, Z.F. Comparison of pseudorabies virus China reference strain with emerging variants reveals independent virus evolution within specific geographic regions. *Virology* **2017**, *506*, 92–98. [CrossRef]
36. Zhai, X.; Zhao, W.; Li, K.; Zhang, C.; Wang, C.; Su, S.; Zhou, J.; Lei, J.; Xing, G.; Sun, H.; et al. Genome Characteristics and Evolution of Pseudorabies Virus Strains in Eastern China from 2017 to 2019. *Virol. Sin.* **2019**, *34*, 601–609. [CrossRef]
37. Liu, J.; Chen, C.; Li, X. Novel Chinese pseudorabies virus variants undergo extensive recombination and rapid interspecies transmission. *Transbound. Emerg. Dis.* **2020**, *67*, 2274–2276. [CrossRef]
38. Bo, Z.; Li, X. A Review of Pseudorabies Virus Variants: Genomics, Vaccination, Transmission, and Zoonotic Potential. *Viruses* **2022**, *14*, 1003. [CrossRef] [PubMed]
39. Wang, T.; Xiao, Y.; Yang, Q.; Wang, Y.; Sun, Z.; Zhang, C.; Yan, S.; Wang, J.; Guo, L.; Yan, H.; et al. Construction of a gE-Deleted Pseudorabies Virus and Its Efficacy to the New-Emerging Variant PRV Challenge in the Form of Killed Vaccine. *Biomed. Res. Int.* **2015**, *2015*, 684945.
40. Wang, J.; Guo, R.; Qiao, Y.; Xu, M.; Wang, Z.; Liu, Y.; Gu, Y.; Liu, C.; Hou, J. An inactivated gE-deleted pseudorabies vaccine provides complete clinical protection and reduces virus shedding against challenge by a Chinese pseudorabies variant. *BMC Vet. Res.* **2016**, *12*, 277. [CrossRef]
41. Yin, Y.; Xu, Z.; Liu, X.; Li, P.; Yang, F.; Zhao, J.; Fan, Y.; Sun, X.; Zhu, L. A live gI/gE-deleted pseudorabies virus (PRV) protects weaned piglets against lethal variant PRV challenge. *Virus. Genes.* **2017**, *53*, 565–572. [CrossRef] [PubMed]
42. Li, J.; Fang, K.; Rong, Z.; Li, X.; Ren, X.; Ma, H.; Chen, H.; Li, X.; Qian, P. Comparison of gE/gI- and TK/gE/gI-Gene-Deleted Pseudorabies Virus Vaccines Mediated by CRISPR/Cas9 and Cre/Lox Systems. *Viruses* **2020**, *12*, 369. [CrossRef] [PubMed]
43. Lin, J.; Li, Z.; Feng, Z.; Fang, Z.; Chen, J.; Chen, W.; Liang, W.; Chen, Q. Pseudorabies virus (PRV) strain with defects in gE, gC, and TK genes protects piglets against an emerging PRV variant. *J. Vet. Med. Sci.* **2020**, *82*, 846–855. [CrossRef] [PubMed]
44. Yin, H.; Li, Z.; Zhang, J.; Huang, J.; Kang, H.; Tian, J.; Qu, L. Construction of a US7/US8/UL23/US3-deleted recombinant pseudorabies virus and evaluation of its pathogenicity in dogs. *Vet. Microbiol.* **2020**, *240*, 108543. [CrossRef]
45. Zhao, Y.; Wang, L.Q.; Zheng, H.H.; Yang, Y.R.; Liu, F.; Zheng, L.L.; Jin, Y.; Chen, H.Y. Construction and immunogenicity of a gE/gI/TK-deleted PRV based on porcine pseudorabies virus variant. *Mol. Cell Probes.* **2020**, *53*, 101605. [CrossRef]
46. Lv, L.; Liu, X.; Jiang, C.; Wang, X.; Cao, M.; Bai, J.; Jiang, P. Pathogenicity and immunogenicity of a gI/gE/TK/UL13-gene-deleted variant pseudorabies virus strain in swine. *Vet. Microbiol.* **2021**, *258*, 109104. [CrossRef]
47. Xu, L.; Wei, J.F.; Zhao, J.; Xu, S.Y.; Lee, F.Q.; Nie, M.C.; Xu, Z.W.; Zhou, Y.C.; Zhu, L. The Immunity Protection of Central Nervous System Induced by Pseudorabies Virus DelgI/gE/TK in Mice. *Front. Microbiol.* **2022**, *13*, 862907. [CrossRef]
48. Zhao, J.; Zhu, L.; Xu, L.; Li, F.; Deng, H.; Huang, Y.; Gu, S.; Sun, X.; Zhou, Y.; Xu, Z. The Construction and Immunogenicity Analyses of Recombinant Pseudorabies Virus with NADC30-Like Porcine Reproductive and Respiratory Syndrome Virus-Like Particles Co-expression. *Front. Microbiol.* **2022**, *13*, 846079. [CrossRef]
49. Wang, Y.; Yuan, J.; Cong, X.; Qin, H.Y.; Wang, C.H.; Li, Y.; Li, S.; Luo, Y.; Sun, Y.; Qiu, H.J. Generation and Efficacy Evaluation of a Recombinant Pseudorabies Virus Variant Expressing the E2 Protein of Classical Swine Fever Virus in Pigs. *Clin. Vaccine Immunol.* **2015**, *22*, 1121–1129. [CrossRef]
50. Tong, W.; Zheng, H.; Li, G.X.; Gao, F.; Shan, T.L.; Zhou, Y.J.; Yu, H.; Jiang, Y.F.; Yu, L.X.; Li, L.W.; et al. Recombinant pseudorabies virus expressing E2 of classical swine fever virus (CSFV) protects against both virulent pseudorabies virus and CSFV. *Antiviral Res.* **2020**, *173*, 104652. [CrossRef]
51. Yan, Z.; Chen, M.; Tang, D.; Wu, X.; Ren, X.; Pan, H.; Li, Y.; Ji, Q.; Luo, Y.; Fan, H.; et al. Better immune efficacy triggered by the inactivated gI/gE-deleted pseudorabies virus with the additional insertion of gC gene in mice and weaned pigs. *Virus. Res.* **2021**, *296*, 198353. [CrossRef] [PubMed]
52. Zheng, H.H.; Wang, L.Q.; Fu, P.F.; Zheng, L.L.; Chen, H.Y.; Liu, F. Characterization of a recombinant pseudorabies virus expressing porcine parvovirus VP2 protein and porcine IL-6. *Virol. J.* **2020**, *17*, 19. [CrossRef] [PubMed]
53. Zheng, K.; Jiang, F.F.; Su, L.; Wang, X.; Chen, Y.X.; Chen, H.C.; Liu, Z.F. Highly Efficient Base Editing in Viral Genome Based on Bacterial Artificial Chromosome Using a Cas9-Cytidine Deaminase Fused Protein. *Virol. Sin.* **2020**, *35*, 191–199. [CrossRef] [PubMed]

54. Zhang, C.; Guo, S.; Guo, R.; Chen, S.; Zheng, Y.; Xu, M.; Wang, Z.; Liu, Y.; Wang, J. Identification of four insertion sites for foreign genes in a pseudorabies virus vector. *BMC Vet. Res.* **2021**, *17*, 190. [CrossRef]
55. Zhou, M.; Abid, M.; Yin, H.; Wu, H.; Teklue, T.; Qiu, H.J.; Sun, Y. Establishment of an Efficient and Flexible Genetic Manipulation Platform Based on a Fosmid Library for Rapid Generation of Recombinant Pseudorabies Virus. *Front. Microbiol.* **2018**, *9*, 2132. [CrossRef]
56. Qi, H.; Wu, H.; Abid, M.; Qiu, H.J.; Sun, Y. Establishment of a Fosmid Library for Pseudorabies Virus SC Strain and Application in Viral Neuronal Tracing. *Front. Microbiol.* **2020**, *11*, 1168. [CrossRef]
57. Abid, M.; Teklue, T.; Li, Y.; Wu, H.; Wang, T.; Qiu, H.J.; Sun, Y. Generation and Immunogenicity of a Recombinant Pseudorabies Virus Co-Expressing Classical Swine Fever Virus E2 Protein and Porcine Circovirus Type 2 Capsid Protein Based on Fosmid Library Platform. *Pathogens* **2019**, *8*, 279. [CrossRef]
58. Guo, J.C.; Tang, Y.D.; Zhao, K.; Wang, T.Y.; Liu, J.T.; Gao, J.C.; Chang, X.B.; Cui, H.Y.; Tian, Z.J.; Cai, X.H.; et al. Highly Efficient CRISPR/Cas9-Mediated Homologous Recombination Promotes the Rapid Generation of Bacterial Artificial Chromosomes of Pseudorabies Virus. *Front. Microbiol.* **2016**, *7*, 2110. [CrossRef]
59. Fu, P.F.; Cheng, X.; Su, B.Q.; Duan, L.F.; Wang, C.R.; Niu, X.R.; Wang, J.; Yang, G.Y.; Chu, B.B. CRISPR/Cas9-based generation of a recombinant double-reporter pseudorabies virus and its characterization in vitro and in vivo. *Vet. Res.* **2021**, *52*, 95. [CrossRef]
60. Wu, X.; Wu, H.; Wang, H.; Luo, L.; Wang, J.; Wu, B.; He, Q.; Cao, G.; Lei, Y.; Chen, X.; et al. A new strategy to develop pseudorabies virus-based bivalent vaccine with high immunogenicity of porcine circovirus type 2. *Vet. Microbiol.* **2021**, *255*, 109022. [CrossRef]
61. Hübner, A.; Keil, G.M.; Kabuuka, T.; Mettenleiter, T.C.; Fuchs, W. Efficient transgene insertion in a pseudorabies virus vector by CRISPR/Cas9 and marker rescue-enforced recombination. *J. Virol. Methods* **2018**, *262*, 38–47. [CrossRef] [PubMed]
62. Yao, L.; Hu, Q.; Chen, S.; Zhou, T.; Yu, X.; Ma, H.; H Ghonaim, A.; Wu, H.; Sun, Q.; Fan, S.; et al. Recombinant Pseudorabies Virus with TK/gE Gene Deletion and Flt3L Co-Expression Enhances the Innate and Adaptive Immune Response via Activating Dendritic Cells. *Viruses* **2021**, *13*, 691. [CrossRef] [PubMed]
63. Qiu, H.J.; Tian, Z.J.; Tong, G.Z.; Zhou, Y.J.; Ni, J.Q.; Luo, Y.Z.; Cai, X.H. Protective immunity induced by a recombinant pseudorabies virus expressing the GP5 of porcine reproductive and respiratory syndrome virus in piglets. *Vet. Immunol. Immunopathol.* **2005**, *106*, 309–319. [CrossRef] [PubMed]
64. Tian, Z.J.; Zhou, G.H.; Zheng, B.L.; Qiu, H.J.; Ni, J.Q.; Yang, H.L.; Yin, X.N.; Hu, S.P.; Tong, G.Z. A recombinant pseudorabies virus encoding the HA gene from H3N2 subtype swine influenza virus protects mice from virulent challenge. *Vet. Immunol. Immunopathol.* **2006**, *111*, 211–218. [CrossRef] [PubMed]
65. Klingbeil, K.; Lange, E.; Teifke, J.P.; Mettenleiter, T.C.; Fuchs, W. Immunization of pigs with an attenuated pseudorabies virus recombinant expressing the haemagglutinin of pandemic swine origin H1N1 influenza A virus. *J. Gen. Virol.* **2014**, *95*, 948–959. [CrossRef] [PubMed]
66. Flynn, S.J.; Ryan, P. The receptor-binding domain of pseudorabies virus glycoprotein gC is composed of multiple discrete units that are functionally redundant. *J. Virol.* **1996**, *70*, 1355–1364. [CrossRef] [PubMed]
67. Zhang, P.; Lv, L.; Sun, H.; Li, S.; Fan, H.; Wang, X.; Bai, J.; Jiang, P. Identification of linear B cell epitope on gB, gC, and gE proteins of porcine pseudorabies virus using monoclonal antibodies. *Vet. Microbiol.* **2019**, *234*, 83–91. [CrossRef]
68. Waskow, C.; Liu, K.; Darrasse-Jèze, G.; Guermonprez, P.; Ginhoux, F.; Merad, M.; Shengelia, T.; Yao, K.; Nussenzweig, M. The receptor tyrosine kinase Flt3 is required for dendritic cell development in peripheral lymphoid tissues. *Nat. Immunol.* **2008**, *9*, 676–683. [CrossRef]
69. Yuan, X.; Qin, X.; Wang, D.; Zhang, Z.; Tang, X.; Gao, X.; Chen, W.; Sun, L. Mesenchymal stem cell therapy induces FLT3L and CD1c (+) dendritic cells in systemic lupus erythematosus patients. *Nat. Commun.* **2019**, *10*, 2498. [CrossRef]
70. Wen, Y.; Wang, H.; Wu, H.; Yang, F.; Tripp, R.A.; Hogan, R.J.; Fu, Z.F. Rabies virus expressing dendritic cell-activating molecules enhances the innate and adaptive immune response to vaccination. *J. Virol.* **2011**, *85*, 1634–1644. [CrossRef]
71. Zhang, K.; Huang, J.; Wang, Q.; He, Y.; Xu, Z.; Xiang, M.; Wu, B.; Chen, H. Recombinant pseudorabies virus expressing P12A and 3C of FMDV can partially protect piglets against FMDV challenge. *Res. Vet. Sci.* **2011**, *91*, 90–94. [CrossRef] [PubMed]

Disclaimer/Publisher's Note: The statements, opinions and data contained in all publications are solely those of the individual author(s) and contributor(s) and not of MDPI and/or the editor(s). MDPI and/or the editor(s) disclaim responsibility for any injury to people or property resulting from any ideas, methods, instructions or products referred to in the content.

Article

Establishment of an In Vitro Model of Pseudorabies Virus Latency and Reactivation and Identification of Key Viral Latency-Associated Genes

Li Pan ^{1,†}, Mingzhi Li ^{1,2,†}, Xinyu Zhang ^{1,3}, Yu Xia ^{1,2}, Assad Moon Mian ¹, Hongxia Wu ^{1,*}, Yuan Sun ^{1,2} and Hua-Ji Qiu ^{1,3,*} 

¹ State Key Laboratory of Veterinary Biotechnology, Harbin Veterinary Research Institute, Chinese Academy of Agricultural Sciences, 678 Haping Road, Harbin 150069, China; sunyuan@caas.cn (Y.S.)
² School of Animal Science and Technology, Henan Institute of Science and Technology, Xinxiang 453003, China
³ School of Life Science and Engineering, Foshan University, Foshan 528225, China
* Correspondence: whx450650@163.com (H.W.); qiuhuaji@caas.cn (H.-J.Q.); Tel.: +86-130-1901-1305 (H.-J.Q.)
† These authors contributed equally at this work as first author.

Abstract: Alphaherpesviruses infect humans and most animals. They can cause severe morbidity and mortality. The pseudorabies virus (PRV) is a neurotropic alphaherpesvirus that can infect most mammals. The PRV persists in the host by establishing a latent infection, and stressful stimuli can induce the latent viruses to reactivate and cause recurrent diseases. The current strategies of antiviral drug therapy and vaccine immunization are ineffective in eliminating these viruses from the infected host. Moreover, overspecialized and complex models are also a major obstacle to the elucidation of the mechanisms involved in the latency and reactivation of the PRV. Here, we present a streamlined model of the latent infection and reactivation of the PRV. A latent infection established in N2a cells infected with the PRV at a low multiplicity of infection (MOI) and maintained at 42 °C. The latent PRV was reactivated when the infected cells were transferred to 37 °C for 12 to 72 h. When the above process was repeated with a *UL54*-deleted PRV mutant, it was observed that the *UL54* deletion did not affect viral latency. However, viral reactivation was limited and delayed. This study establishes a powerful and streamlined model to simulate PRV latency and reveals the potential role of temperature in PRV reactivation and disease. Meanwhile, the key role of the early gene *UL54* in the latency and reactivation of PRV was initially elucidated.

Keywords: pseudorabies virus; latent infection; reactivation; thermoregulation; in vitro model; *UL54*



Citation: Pan, L.; Li, M.; Zhang, X.; Xia, Y.; Mian, A.M.; Wu, H.; Sun, Y.; Qiu, H.-J. Establishment of an In Vitro Model of Pseudorabies Virus Latency and Reactivation and Identification of Key Viral Latency-Associated Genes. *Viruses* **2023**, *15*, 808. <https://doi.org/10.3390/v15030808>

Academic Editors: Yan-Dong Tang and Xiangdong Li

Received: 25 February 2023

Revised: 16 March 2023

Accepted: 17 March 2023

Published: 22 March 2023



Copyright: © 2023 by the authors. Licensee MDPI, Basel, Switzerland. This article is an open access article distributed under the terms and conditions of the Creative Commons Attribution (CC BY) license (<https://creativecommons.org/licenses/by/4.0/>).

1. Introduction

The pseudorabies virus (PRV) belongs to the subfamily *Alphaherpesvirinae* of the family *Herpesviridae* and causes a lethal viral disease in pigs, which causes severe economic losses to the swine industry around the world [1,2]. PRV is a neuroinvasive herpesvirus that causes various infections from acute to lifelong latent infections of the peripheral nervous system (PNS) [3]. However, the molecular mechanisms underlying the establishment of alphaherpesvirus latency and reactivation remain poorly understood [4–6]. For herpesviruses, primary infection begins with the productive infection of mucosal epithelial cells. In less than a day, each infected cell will produce thousands of progeny [7]. It is generally accepted that the latency of alphaherpesviruses is characterized by the episomal maintenance of the viral genome and by a state of chronic infection that does not lead to the production of infectious viral particles [8]. When known stress signaling and neuronal survival pathways are activated, the viral genome is transcribed and replicated, producing new viral particles that travel back to the original infection site to ensure the spread of infection to other hosts [9]. Chronic viruses, such as herpesviruses, influence host physiology and have evolved to use inflammation to regulate viral latency and reactivation and to modulate

Table 1. *Cont.*

Primers	Sequences (5' to 3')
UL54-rpsl-R	AACAGCAGCGGCAGCGAGGCGTCCCGGTCCGGGAGCGAG-GAGCGGCGCCCTCAGAAGAAGCTCGTCAAGAAGGC
UL54-del-F	GGTCTTGTGGGCGTGAGCCGCGCCCGGACGGGCGGC
UL54-del-R	TCCGGGCGCGGCTCACGCCACAAGACCGGCTGCGA
UL54-JC-F	CTCGCGCACGCCAGAGAGGTAC
UL54-JC-R	CGCTCGCACCGGTCATGGAG

2.2. One-Step and Multistep Growth Curves and Plaque Assay

For one-step growth curves, PK-15 cells in 24-well cell culture plates were infected with WT-PRV or rPRV-EGFP (MOI = 5) and were incubated for 2 h, and they were then washed with PBS to clear the uninfected viral particles and were cultured in fresh medium. The cell supernatants were harvested at different time points. For multistep growth curves, PK-15 cells were infected with WT-PRV or rPRV- Δ UL54-EGFP (MOI = 0.01). Growth curves were plotted based on median tissue culture infective doses (TCID₅₀) or the viral DNA copies of all the samples [19]. Plaque assay was performed as described previously [20].

2.3. PCR, qPCR, and RT-qPCR

The genomic DNA of WT-PRV, rPRV-EGFP, and rPRV- Δ UL54-EGFP was extracted and used as the template for PCR kit (catalog no. AG11510; Agbio, Changsha, China) or qPCR kit (catalog no. Q311; Vazyme, Beijing, China). Total RNA was isolated from the infected or uninfected cells, and RT-qPCR kit (catalog no. A336; Genstar, Beijing, China) was used to quantify viral mRNA. The tests were performed according to the kit instructions. The primers for PCR, qPCR, and RT-qPCR are listed in Table 2.

Table 2. Primers for PCR, qPCR, and RT-qPCR.

Primers	Sequences (5' to 3')
EGFP-JC-F(PCR)	ATGGTGAGCAAGGGCGAGGAG
EGFP-JC-R(PCR)	TTACTTGTACAGCTCGTCCAT
gB-JC-F(PCR)	ATGGACATGTACCGGATCATGT
gB-JC-R(PCR)	AGAGCGTGACGCGCAACTTTCTGC
IE180-F(qPCR/RT-qPCR)	CTGGCAGAAGTGGTTGAAGC
IE180-R(qPCR/RT-qPCR)	TCGTGCGCCTCATCTACAG
EP0-F(qPCR/RT-qPCR)	TGCGCCGATATGTCAAACAG
EP0-R(qPCR/RT-qPCR)	TCGTGGACAACATCGTCGAG
gB-F(qPCR/RT-qPCR)	TCCTCGACGATGCAGTTGAC
gB-R(qPCR/RT-qPCR)	ACCAACGACACCTACACCAAG
LAT-F(qPCR/RT-qPCR)	ACGTGACGTTTTTGCCGATG
LAT-R(qPCR/RT-qPCR)	GCGCGATATGCAGATGAGATC

2.4. Transmission Electronic Microscopy

The samples were prepared as reported previously [18]. Cell culture medium was centrifuged at 3000 × g for 10 min, the supernatant was collected and centrifuged at 10,000 × g for 10 min, and then the pellet was resuspended in PBS. The samples were negatively stained with 2% phosphotungstic acid, and the morphology of viral particles was observed under transmission electronic microscopy (TEM).

2.5. Western Blotting

The N2a cells infected with the recombinant viruses of different MOIs were cultured at 37 and 42 °C for 120 h. At 120 h postinfection (hpi), the cells were harvested, and samples were prepared for Western blotting. The mouse anti-gB and -gD monoclonal antibodies (MAbs) were from our laboratory. Anti- β -actin MAb was commercially purchased from Sigma (catalog no. A1978; Sigma, Shanghai, China). Goat antimouse FITC antibodies

(catalog no. sc-516140; Sigma, Shanghai, China) were used as secondary antibodies. Total protein extraction and Western blotting analysis were carried out following the previously described protocols [20].

2.6. Thermoregulation Model of Latent Infection and Reactivation of PRV

To establish a model of latent PRV infection, N2a, BHK-21, and PK-15 cells were seeded separately into 35 mm dishes at 5×10^5 per dish and were cultured with a complete medium. For infection, in brief, rPRV-EGFP was added to the three cell types mentioned above at MOIs of 1.0, 0.1, 0.01, and 0.001, respectively. The infected cells were incubated continuously at 37 or 42 °C for 72 or 120 h. Fluorescence was monitored at 72 hpi to investigate the optimal cell type and MOI for establishing PRV latent infection. N2a cells were infected with rPRV-EGFP (MOI = 0.01) and were incubated at 37 °C for different amounts of time to determine the optimal incubation time. To determine the incubation time for noninfectious PRV replication, the cells were then transferred to 42 °C for 120 h, and EGFP fluorescence was monitored. Subsequently, latent infection of PRV was established with optimized parameters and was maintained at 42 °C for 120 h (i.e., N2a cells were infected with rPRV-EGFP at an MOI of 0.01, were incubated at 37 °C for 2 h, and were then transferred to 42 °C). In addition, qPCR, RT-qPCR, and Western blotting were used to analyze viral DNA, mRNA, and proteins in the samples. For the reactivation of latent PRV, N2a cells were transferred from 42 to 37 °C for mild hypothermic incubation (cold stress), activating the latent PRV. At 12, 24, 48, and 72 h postreactivation (hpr), the infectious PRV was measured through EGFP fluorescence and RT-qPCR. It should be noted that the medium was changed on alternate days throughout the model experiment to maintain normal cell growth.

For the experiments of latent infection and reactivation of rPRV- Δ UL54-EGFP, the experimental details were similar to the above procedures.

2.7. Statistical Analysis

Analysis of the data was performed using GraphPad Prism 8 statistical software. Student's two-tailed *t*-test and two-way analysis of variance were used, and significant differences were defined when the *p*-value was <0.05.

3. Results

3.1. Generation and Identification of rPRV-EGFP

The recombinant PRV with the EGFP cassette was constructed using the PRV reverse genetic operating system established in our laboratory [18] (Figure 1A). The clone was identified as rPRV-EGFP after plaque purification and sequencing verification (Figure 1B). The size of the plaques produced by rPRV-EGFP was similar to that of WT-PRV (Figure 1C). Electron microscopy revealed that the rPRV-EGFP particles had an intact envelope similar to that of the parental virus (Figure 1D). Fluorescence imaging demonstrated the capability of rPRV-EGFP to express the EGFP protein (Figure 1E). The replication kinetics of rPRV-EGFP was very similar to that of the parental virus based on the one-step growth curve (Figure 1F). Overall, the recombinant PRV retained the parental phenotype, except for EGFP fluorescence.

3.2. Hyperthermic Stress Maintained PRV Latency in Neuron-like Cells

Inspired by the speculation of Markus et al. [11] and a real-world problem situation, we screened the optimal conditions for the thermoregulation model of the latent infection and reactivation of the PRV. In this study, we attempted to establish models of the latent infection and reactivation of PRV in PK-15 cells, BHK-21 cells, and N2a cells. The results showed that only the N2a cells allowed the PRV to establish a latent infection. The PRV with an MOI no more than 0.01 was able to maintain a stably latent infection at 42 °C (Figure 2).

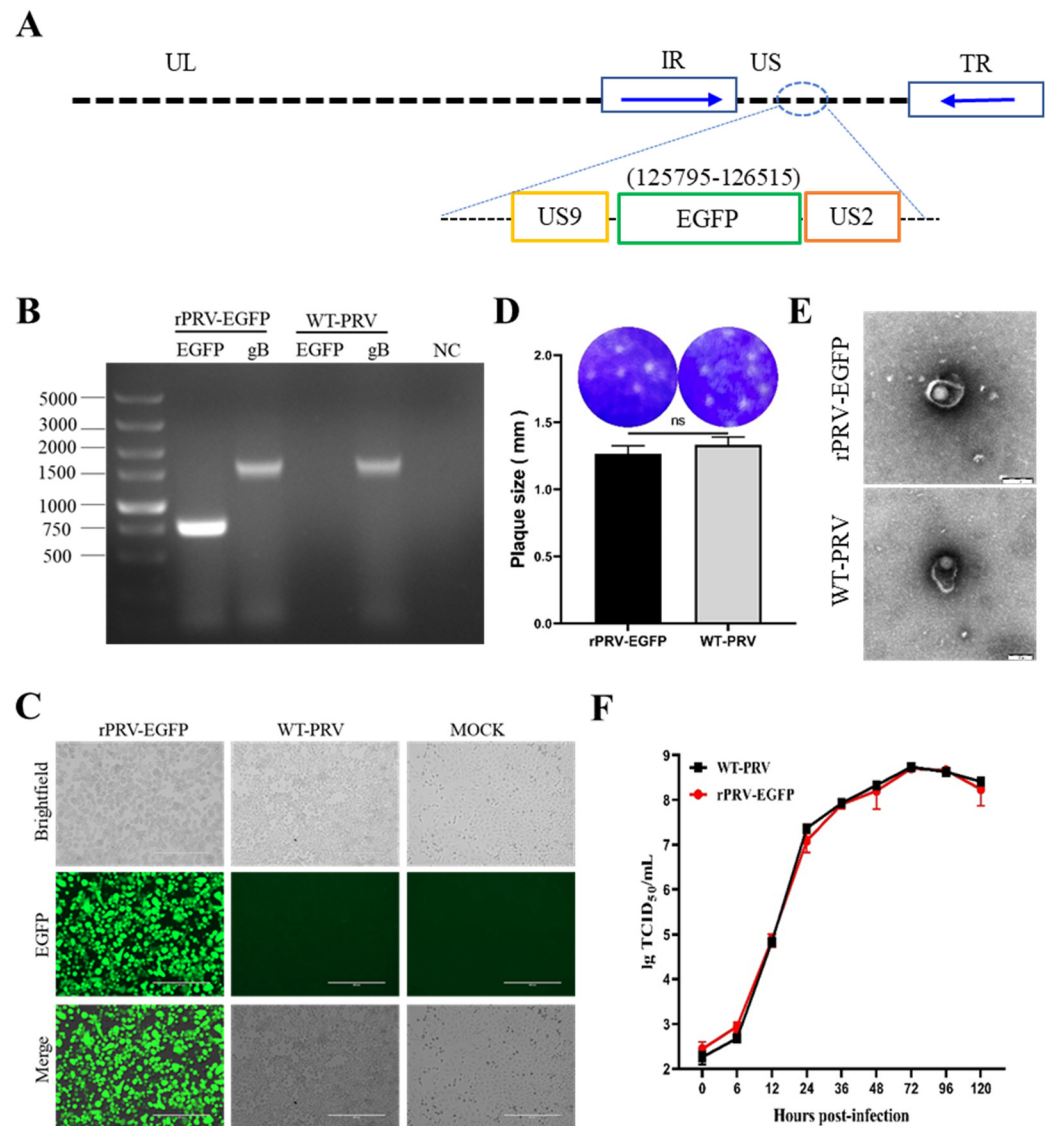


Figure 1. Generation and characterization of rPRV-EGFP. (A) Schematic diagram of the construction of the recombinant virus. Using the PRV genomic fosmid library, the EGFP sequence was inserted nondestructively downstream of the *US9* gene in the PRV genome. The relative position of the EGFP sequence in the WT-PRV genome is shown on top of the green box. (B) PCR amplification of the *EGFP* and *gB* genes from the genomes of rPRV-EGFP and WT-PRV. (C) The green fluorescence and cytopathic effects (CPEs) in the PK-15 cells infected with rPRV-EGFP and WT-PRV at 48 h postinfection (hpi). (D) Plaques of rPRV-EGFP and WT-PRV in the PK-15 cells. ns: not significant ($p \geq 0.05$). The diameters of plaques were averaged for three independent experiments. ns: not significant. (E) Transmission electron microscopy photographs of rPRV-EGFP and WT-PRV. Scale bar = 200 nm. (F) One-step growth curves of rPRV-EGFP and WT-PRV in PK-15 cells.

Moreover, the study showed that one of the key factors determining the success or failure of the model was the incubation time at 37 °C. When the PRV was incubated at 37 °C for over 3 h, the lytic infection was not prevented, even when the cells were transferred to 42 °C (Figure 3A). Surprisingly, the virus (MOI = 0.01) was incubated at 37 °C for 2 h and was then moved to 37 or 42 °C for 120 h. No lytic viral replication was observed at 42 °C (Figure 3B). During the latency phase, the viral DNA was not replicated, but the latency-associated transcript (LAT) of PRV could be detected (Figure 3C); additionally, low levels of mRNA for IE180 (the immediate early gene of the PRV) were detected (Figure 3D). The cells infected with rPRV-EGFP at different MOIs and incubated at 37 or 42 °C for 120 h

were harvested. These samples were used to detect the viral proteins gB and gD. The results showed that the virus did not produce lytic proteins at an MOI of 0.01 or at 42 °C (Figure 3E). The above results showed that, under hyperthermia stress, the viral DNA did not replicate and no viral proteins or viral particles was produced. However, the latent PRV only produced the LAT and low levels of IE180 transcripts.

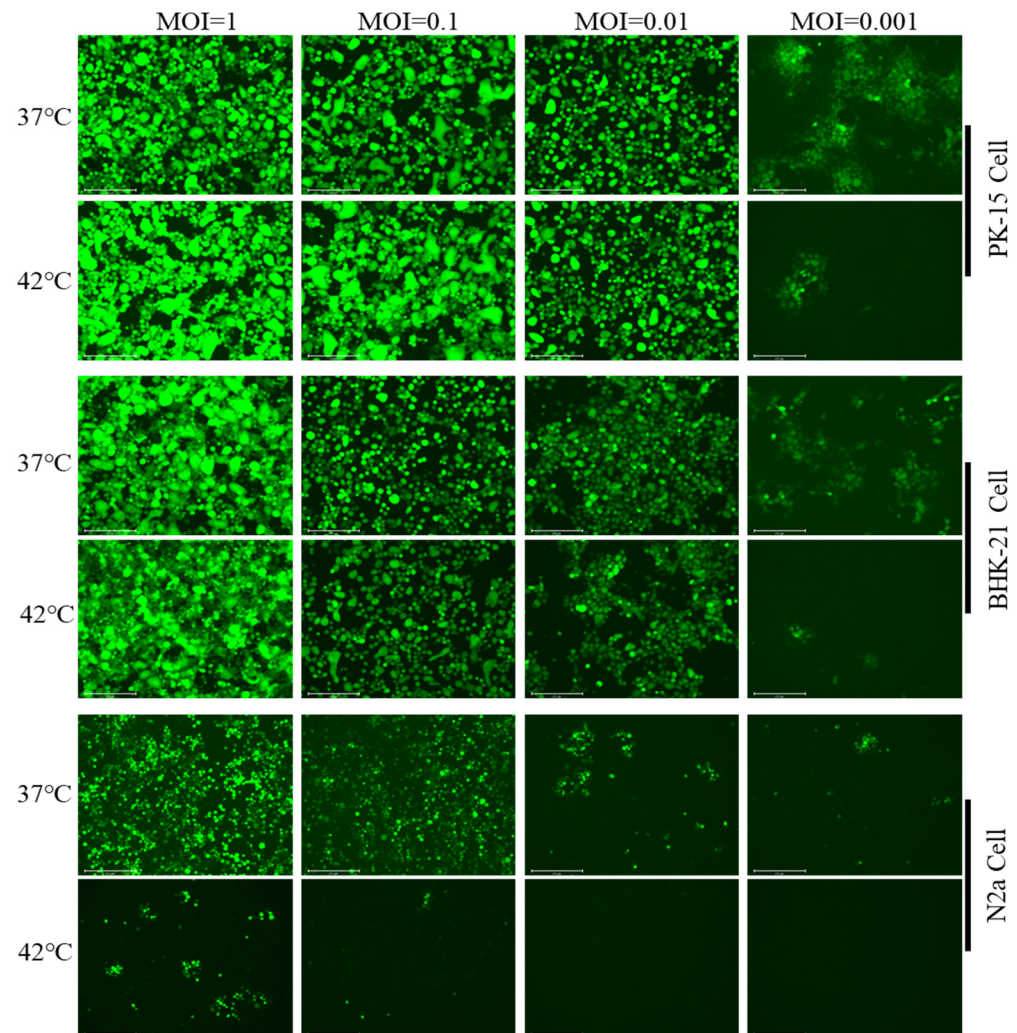


Figure 2. Screening for appropriate cell types and optimal infectious dose for in vitro PRV latent infection models. N2a, BHK-21, and PK-15 cells were seeded into 35 mm dishes at 5×10^5 per dish and were cultured with complete medium. rPRV-EGFP was added to the three cell types at an MOI of 1, 0.1, 0.01, or 0.001. The infected cells were incubated continuously at 37 or 42 °C for 72 h. Fluorescence was monitored at 72 h postinfection.

3.3. Reduced Temperature Enhanced the Reactivation of the Latent PRV

It has been shown that mild hypothermia reactivates the VZV in latently infected neurons and enhances viral replication [11,21]. Therefore, we combined the treatment of persistent latent infection with hyperthermic stress (42 °C) and incubation with mild hypothermia (37 °C). According to the results, the virus was incubated at 42 °C for 120 h and was then transferred to 37 °C for additional incubation. Infectious virus particles were produced within 12 h (Figure 4A). The number of viral DNA copies increased with the viral reactivation time (Figure 4B). Upon reactivation, the expression levels of the late viral envelope proteins gB and gD were increased over time (Figure 4C). It was easy to see that hyperthermia stress drove the viruses into a quiescent state. At the same time,

mild hypothermia could reactivate them to produce infectious viral particles and to infect other cells.

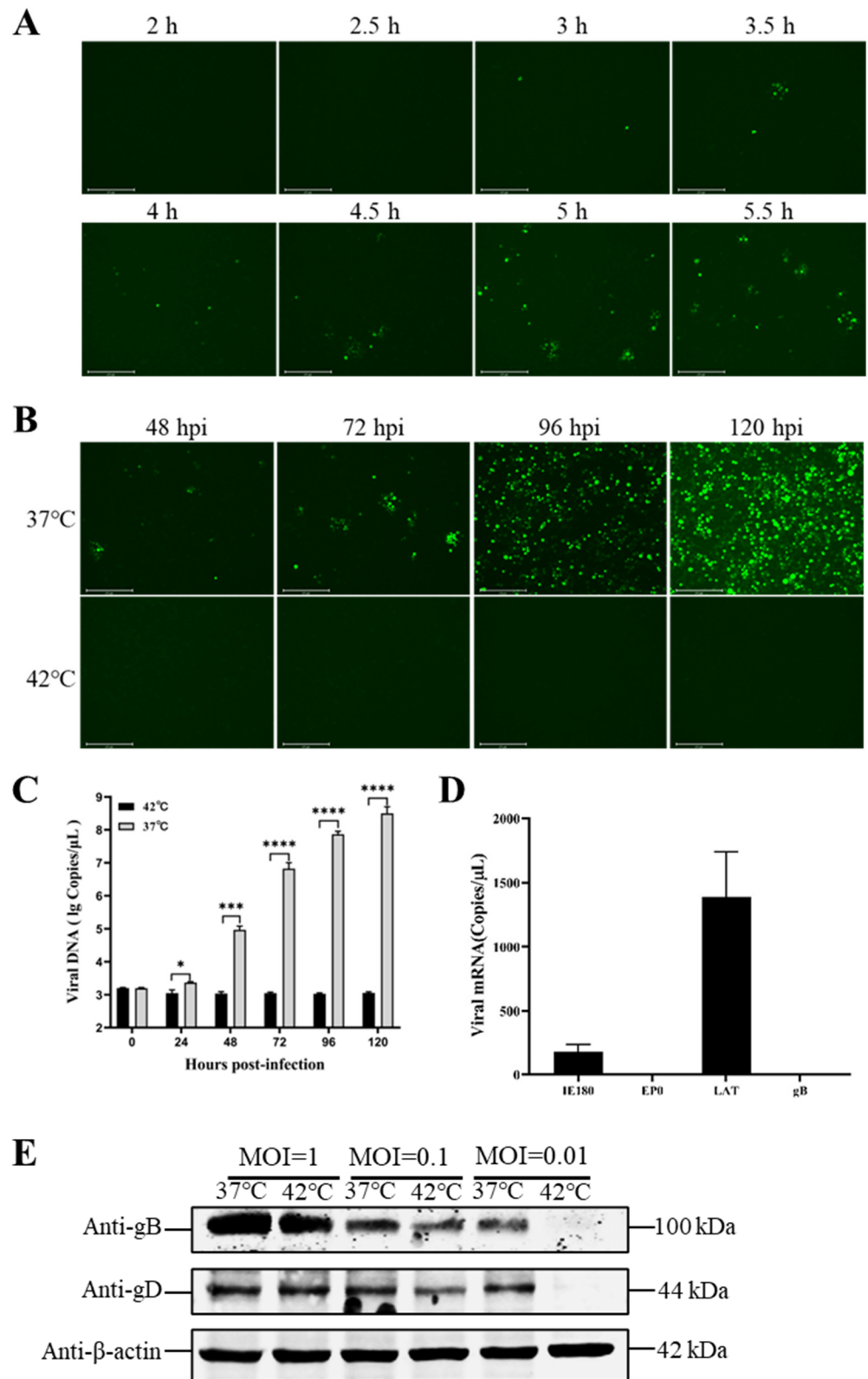


Figure 3. Optimal incubation time for screening and detection of latency indicators. (A) Optimal incubation time screening. N2a cells were infected with rPRV-EGFP (MOI = 0.01) and were incubated

at 37 °C for 2, 2.5, 3, 3.5, 4, 4.5, 5, and 5.5 h. The cells were then transferred to 42 °C for 120 h, and EGFP fluorescence was monitored. **(B)** Identification of the optimal conditions for latent PRV infection. N2a cells were infected at an MOI of 0.01, were incubated at 37 °C for 2 h, then transferred to 42 °C for 120 h. **(C)** Latent and lytic viral DNA detection. N2a cells were infected with rPRV-EGFP at an MOI of 0.01 and were incubated at 37 °C for 2 h. After rPRV-EGFP was cultured at 42 °C for 120 h, the samples were then collected, and viral DNA was extracted; additionally, the *gB* gene was detected through real-time PCR to quantify genomic DNA. **(D)** Quantification of transcripts of latent viral genes. After rPRV-EGFP was cultured at 42 °C for 120 h, the samples were then collected, and the mRNAs of *IE180*, *EP0*, *LAT*, and *gB* were detected through RT-qPCR. **(E)** Detection of late viral protein expression levels at two culture temperatures. N2a cells were infected with different doses of rPRV-EGFP (MOI = 1, 0.1, or 0.01) and were incubated at 37 or 42 °C for 120 h, respectively. At 120 h postinfection (hpi), the cells were harvested, and samples were prepared for Western blotting. The homemade mouse anti-*gB* and -*gD* monoclonal antibodies were used as primary antibodies, and goat antimouse FITC antibodies were used as secondary antibodies. Bars represent the means \pm SDs of three independent experiments. ns: not significant ($p \geq 0.05$). * $p < 0.05$, *** $p < 0.001$, and **** $p < 0.0001$.

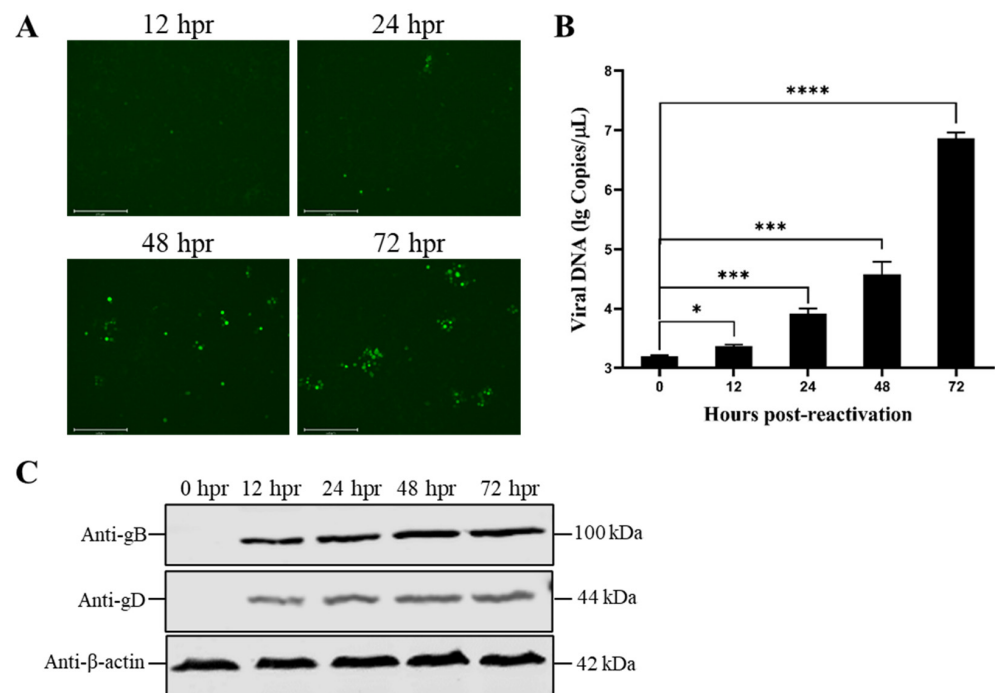


Figure 4. Reactivation of latent rPRV-EGFP. **(A)** Fluorescence spots of rPRV-EGFP during reactivation. N2a cells were infected with rPRV-EGFP (MOI = 0.01), were incubated at 42 °C for 120 h, and were then transferred to 37 °C for additional incubation. EGFP fluorescence was monitored at 12, 24, 48, and 72 h postreactivation (hpr). **(B)** Detection of viral genomic DNA during reactivation. The viral DNA was extracted, and the *gB* gene was detected at 0, 12, 24, 48, and 72 hpr. **(C)** Identification of expression levels of viral late proteins following rPRV-EGFP reactivation. N2a cells were infected with rPRV-EGFP (MOI = 0.01), were incubated at 42 °C for 120 h, and were then transferred to 37 °C. At 0, 12, 24, 48, and 72 hpr, the cells were harvested, and samples were prepared for Western blotting. The homemade mouse anti-*gB* and -*gD* monoclonal antibodies were used as primary antibodies, and goat antimouse FITC antibodies were used as secondary antibodies. Bars represent the means \pm SDs of three independent experiments. ns: not significant ($p \geq 0.05$). * $p < 0.05$, *** $p < 0.001$, and **** $p < 0.0001$.

3.4. Deleting the *UL54* Gene Affects Viral Particle Morphology and Replication Efficiency

As described in the Materials and Methods, the *UL54*-deleted mutant was constructed using rPRV-EGFP as the parental strain (Figure 5A). The same procedure as that described

above was used to describe the phenotype of rPRV- Δ UL54-EGFP, which was produced through the fosmid system. Based on these results, the deletion of the *UL54* gene was confirmed through the PCR and sequencing of rPRV- Δ UL54-EGFP (Figure 5B). This further confirmed that the EGFP expression cassette was successfully inserted into the intended location in the PRV genome, and the green fluorescent protein was expressed (Figure 5C). Due to the *UL54* gene deletion, the plaques of rPRV- Δ UL54-EGFP were significantly smaller than those of WT-PRV (Figure 5D), and they lacked an outer membrane (Figure 5E) and replicated less efficiently compared to WT-PRV (Figure 5F). The results presented in this section demonstrate that the deletion of the *UL54* gene limited the expression of the viral envelope proteins, resulting in the production of fewer infectious viral particles.

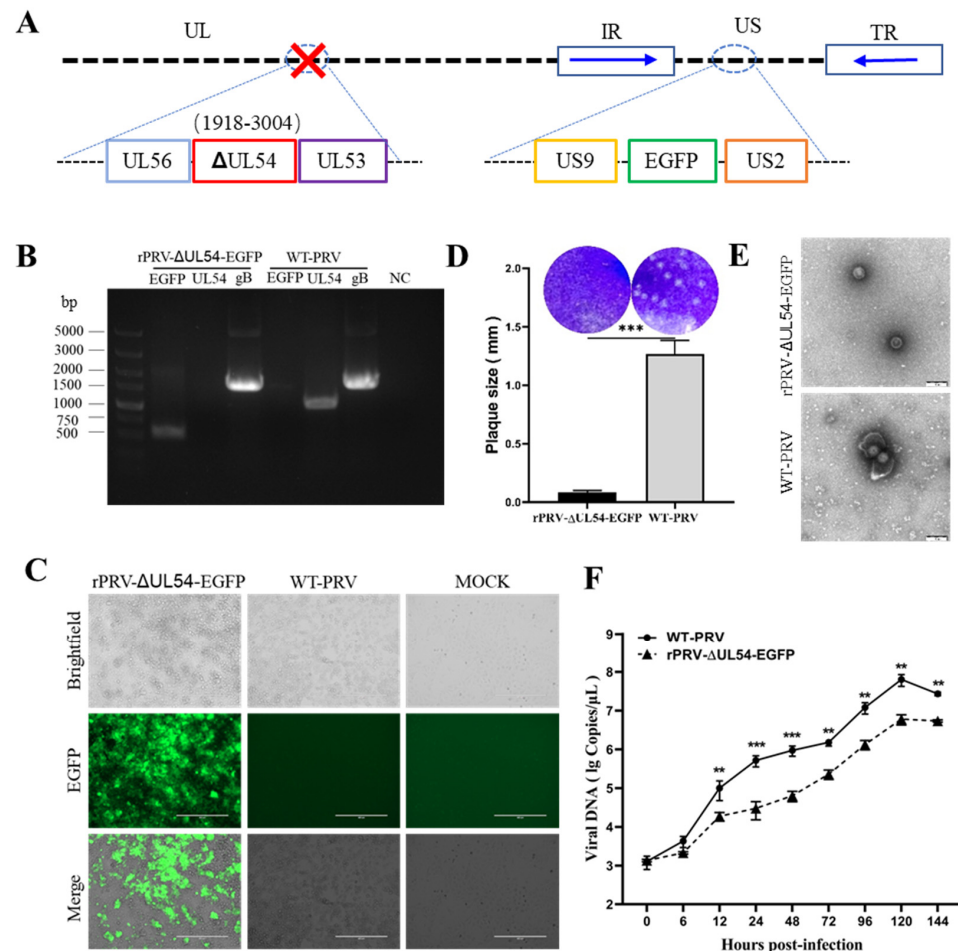


Figure 5. Generation and characterization of rPRV- Δ UL54-EGFP. (A) Schematic diagram of the construction of rPRV- Δ UL54-EGFP. Using the PRV genomic fosmid library, the *UL54* deletion mutant was constructed using rPRV-EGFP as the parental strain. The relative position of the *UL54* gene in the WT-PRV genome is shown on top of the red box. (B) PCR amplification of the *UL54*, *EGFP*, and *gB* genes from the genomes of rPRV- Δ UL54-EGFP and WT-PRV. (C) The green fluorescence and cytopathic effects (CPEs) in the PK-15 cells infected with rPRV- Δ UL54-EGFP and WT-PRV at 60 h postinfection (hpi). (D) Plaques of rPRV- Δ UL54-EGFP and WT-PRV in the PK-15 cells. The diameters of plaques were averaged for three independent experiments. (E) Transmission electron microscopy imaging of rPRV- Δ UL54-EGFP and WT-PRV. Scale bar = 200 nm. (F) Multistep growth curves of rPRV- Δ UL54-EGFP and WT-PRV in PK-15 cells. PK-15 cells were infected with rPRV- Δ UL54-EGFP and WT-PRV (MOI = 0.01). Bars represent the means \pm SDs of three independent experiments. ns: not significant ($p \geq 0.05$). ** $p < 0.01$, and *** $p < 0.001$.

3.5. Deleting the *UL54* Gene Affects PRV Reactivation without Affecting Latency

To understand the effect of the *UL54* gene on the latency and reactivation of the PRV, rPRV- Δ UL54-EGFP was tested in the model developed above. The results showed that

rPRV- Δ UL54-EGFP established a stably latent infection at 42 °C (Figure 6A). The characteristics of the latent rPRV- Δ UL54-EGFP were similar to those of rPRV-EGFP. The results showed that the rPRV- Δ UL54-EGFP infected group did not increase the DNA copies (Figure 6B), but it maintained higher levels of LAT and lower levels of IE180 transcripts (Figure 6C) and, last but not least, did not produce lytic viral proteins (Figure 6D). Subsequently, we transferred the cells from 42 to 37 °C. As expected, a few fluorescent spots appeared on the cells latently infected with rPRV-EGFP when incubated at 37 °C for 12 h. After 48 h incubation at 37 °C, the cells latently infected with rPRV- Δ UL54-EGFP showed insufficient fluorescent spots (Figure 6E). During reactivation, the DNA copies of rPRV-EGFP were significantly higher than rPRV- Δ UL54-EGFP during the same period, indicating that the deletion of the *UL54* gene significantly delayed viral reactivation (Figure 6F). As expected, the levels of viral lytic proteins were gradually increased with prolonged reactivation. The above data suggest that the early gene *UL54* plays an essential role in the reactivation of the PRV.

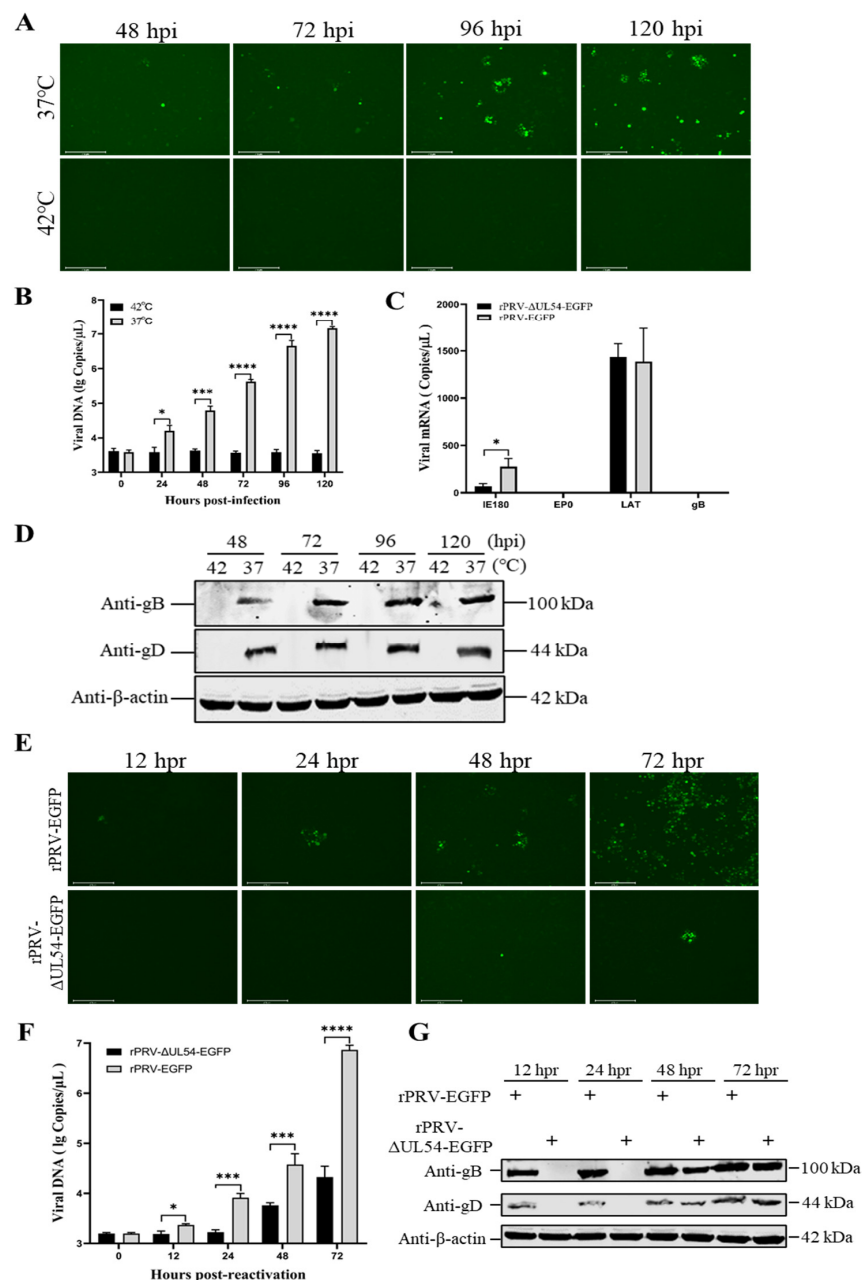


Figure 6. Latent infection and reactivation of rPRV- Δ UL54-EGFP. Based on the established model,

rPRV- Δ UL54-EGFP was tested. (A) Identification of the effect of UL54 deletion on latent infection. (B) Latent and lytic viral DNA copy detection. N2a cells were infected with rPRV- Δ UL54-EGFP at an MOI of 0.01 and were incubated at 37 °C for 2 h. After rPRV- Δ UL54-EGFP was cultured at 42 °C for 120 h, the samples were then collected, and viral DNA was extracted; additionally, the *gB* gene was detected through real-time PCR to quantify genomic DNA. (C) Quantification of the transcripts of the latency-associated viral genes. After rPRV- Δ UL54-EGFP was cultured at 42 °C for 120 h, the samples were then collected, and total RNA was extracted; additionally, the mRNA of the *IE180*, *EP0*, *LAT*, and *gB* genes was detected through RT-qPCR. (D) Inability of latent rPRV-UL54-EGFP to express lytic viral proteins. (E) Fluorescence spots of rPRV-EGFP and rPRV- Δ UL54-EGFP during reactivation. N2a cells were infected with rPRV-EGFP and rPRV- Δ UL54-EGFP (MOI = 0.01), were incubated at 42 °C for 120 h, and were then transferred to 37 °C for culture. EGFP fluorescence was monitored at 12, 24, 48, and 72 h postreactivation (hpr). (F) Detection of viral genomic DNA during reactivation. N2a cells were infected with rPRV- Δ UL54-EGFP and rPRV- Δ UL54-EGFP (MOI = 0.01). The viral DNA was extracted, and the *gB* gene was quantified at 0, 12, 24, 48, and 72 hpr. (G) Identification of expression levels of viral envelope proteins following rPRV- Δ UL54-EGFP reactivation. Bars represent the means \pm SDs of three independent experiments. ns: not significant ($p \geq 0.05$). * $p < 0.05$, *** $p < 0.001$, and **** $p < 0.0001$.

4. Discussion

In this study, we described an in vitro model of the latent infection and reactivation of the PRV through thermoregulation. Furthermore, based on this model, we described for the first time the essential role of the *UL54* gene in viral reactivation. To the best of our knowledge, this model is the most plausible and controllable model of the latent infection and reactivation of the PRV.

Alphaherpesviruses, the most common viruses in the world, can establish a lytic or latent infection in the peripheral nervous system of the host [22]. During the establishment of a latent infection, herpesviruses are maintained as epistomes in the nucleus of the host cell [23]. To elucidate the mechanisms of the latent infection and reactivation of alphaherpesviruses, several in vivo and in vitro models have been developed. The in vivo models include rhesus monkeys, domestic pigs, guinea pigs, and mice, and the in vitro models include primary neuronal cells, immortalized neuroma cells, and nonneuronal cells [11–13,22,24–29]. While most laboratories focus on their highly complex model systems and tools, the field would benefit from consolidating expertise and streamlining operational processes in a collaborative effort to address the global burden of alphaherpesviral diseases. Therefore, it is inevitable that the procedures of the model need to be simplified while ensuring its validity. Initial attempts were made to use the antiviral drug acyclovir to inhibit productive viral DNA replication in dissociated neurons to simulate culture latency. Since 1977, acyclovir has been a very effective antiherpetic drug [30]. The viral thymidine kinase in the infected cells activates the drug. Only after this activation does the drug interfere with viral DNA replication [31]. Pretreating neurons with acyclovir before viral infection prevents viral replication and forces productive infection into a dormant state, similar to latency in vivo [28]. This opened the way to a better understanding of the molecules stimulated by alphaherpesvirus reactivation. However, long-term administration cannot mimic the complex host response associated with in vivo infection. It is well known that, during infection, the ability of the host to mount an appropriate immune and inflammatory response against the pathogen is critical. Higher temperatures are expected to increase antiviral activity because fever enhances the inflammatory response to fight infection [32].

Our operational definition of experimental latency is the maintenance of viral genomes without virus production for prolonged periods that can be reactivated into productive viral infection, spreading to other cells. This definition distinguishes between latency and aborted, incomplete, or partial infection, which may apply to latency models in nonpermiss-

sive hosts or cell types that cannot support a full productive infection [11]. Understanding these factors that maintain latency and the driver of reactivation is important because understanding these processes may eventually allow us to target them to prevent reactivation. Latency involves a program of primarily suppressed regular lytic viral gene expression, leading to virion production. In addition to the previously mentioned details, we also made an initial attempt. According to the published studies, we also tried to use nonneuronal cells as models, including African green monkey kidney (Vero) cells, African green monkey embryonic kidney epithelial (MARC-145) cells, and Madin–Darby canine kidney (MDCK) cells. Unfortunately, a latent model could not be established in these cells. In addition, we tried different temperatures to establish latency. In 0.5 °C increments, the culture temperature of the cells was increased from 40 to 45 °C. Considering factors such as the physiological state of the cells and the reactivation of the virus, we selected 42 °C as the optimal incubation temperature. It has been reported that the PRV replicates rapidly in the mucosal or epithelial cells of pigs upon infection. Soon after, the intense inflammatory response induced through viral infection leads to a rapid rise in body temperature of up to 42 °C [33]. In the presence of a high temperature and the host immune defense, the residual virus enters the host’s peripheral nervous system to establish latency. Other studies have also shown that human herpes simplex virus 1 is able to maintain a latent state in human diploid fibroblasts and fetal lung cells cultured at 42 °C [34,35].

In conclusion, in the present study, in addition to the in vitro model of the PRV, we found that the *UL54* gene plays an essential role in the reactivation of the PRV. We believe that the *UL54* gene represents a potential target for latent virus clearance, and, given its importance, its exact function will be clarified in the future.

Author Contributions: Conceptualization, H.W., Y.S. and H.-J.Q.; methodology, L.P. and M.L.; writing—original draft preparation, L.P., M.L. and X.Z.; writing—review and editing, M.L., X.Z., Y.X., A.M.M., H.W., Y.S. and H.-J.Q.; funding acquisition, Y.S. and H.-J.Q. All authors have read and agreed to the published version of the manuscript.

Funding: This work was supported by the Natural Science Foundation of the Heilongjiang Province of China (grant no. JQ2022C007) and the National Natural Science Foundation of China (grant no. 31870152).

Informed Consent Statement: Not applicable.

Conflicts of Interest: The authors declare no conflict of interest.

References

1. Laval, K.; Vernejoul, J.B.; Van Cleemput, J.; Koyuncu, O.O.; Enquist, L.W. Virulent Pseudorabies Virus Infection Induces a Specific and Lethal Systemic Inflammatory Response in Mice. *J. Virol.* **2018**, *92*, 24. [CrossRef]
2. Wang, B.; Wu, H.; Qi, H.; Li, H.; Pan, L.; Li, L.F.; Zhang, K.; Yuan, M.; Wang, Y.; Qiu, H.J.; et al. Histamine is Responsible for the Neuropathic Itch Induced by the Pseudorabies Virus Variant in a Mouse Model. *Viruses* **2022**, *14*, 1067. [CrossRef]
3. Bailer, S.M. Venture from the Interior—Herpesvirus pUL31 Escorts Capsids from Nucleoplasmic Replication Compartments to Sites of Primary Envelopment at the Inner Nuclear Membrane. *Cells* **2017**, *6*, 46. [CrossRef] [PubMed]
4. Wilson, A.C.; Mohr, I. A Cultured Affair: HSV Latency and Reactivation in Neurons. *Trends Microbiol.* **2012**, *20*, 604–611. [CrossRef]
5. Bloom, D.C. Alphaherpesvirus Latency: A Dynamic State of Transcription and Reactivation. *Adv. Virus Res.* **2016**, *94*, 53–80. [PubMed]
6. Lu, J.; Yuan, W.; Zhu, Y.; Hou, S.; Wang, X. Latent Pseudorabies Virus Infection in Medulla Oblongata from Quarantined Pigs. *Transbound. Emerg. Dis.* **2021**, *68*, 543–551. [CrossRef] [PubMed]
7. Gershon, A.A.; Breuer, J.; Cohen, J.I.; Cohrs, R.J.; Gershon, M.D.; Gilden, D.; Grose, C.; Hambleton, S.; Kennedy, P.G.; Oxman, M.N.; et al. Varicella Zoster Virus Infection. *Nat. Rev. Dis. Prim.* **2015**, *1*, 15016. [CrossRef]
8. Clarke, P.; Beer, T.; Cohrs, R.; Gilden, D.H. Configuration of Latent Varicella-Zoster Virus-DNA. *J. Virol.* **1995**, *69*, 8151–8154. [CrossRef] [PubMed]
9. Smith, G. Herpesvirus Transport to the Nervous System and Back Again. *Ann. Rev. Microbiol.* **2012**, *66*, 153–176. [CrossRef]
10. Reese, T.A. Coinfections: Another Variable in the Herpesvirus Latency-Reactivation Dynamic. *J. Virol.* **2016**, *90*, 5534–5537. [CrossRef]

11. Markus, A.; Leberthal-Loinger, I.; Yang, I.H.; Kinchington, P.R.; Goldstein, R.S. An In Vitro Model of Latency and Reactivation of Varicella Zoster Virus in Human Stem Cell-Derived Neurons. *PLoS Pathog.* **2015**, *11*, 6. [CrossRef]
12. Baird, N.; Zhu, S.; Pearce, C.M.; Viejo-Borbolla, A. Current In Vitro Models to Study Varicella Zoster Virus Latency and Reactivation. *Viruses* **2019**, *11*, 103. [CrossRef] [PubMed]
13. Hu, H.; Srinivas, K.; Mohr, I.; Huang, T.; Wilson, A. Using Primary SCG Neuron Cultures to Study Molecular Determinants of HSV-1 Latency and Reactivation. *Methods Mol. Biol.* **2020**, *2060*, 263–277.
14. Huang, Y.; Chien, M.; Wu, C.; Huang, C. Mapping of Functional Regions Conferring Nuclear Localization and RNA-Binding Activity of Pseudorabies Virus Early Protein UL54. *J. Virol. Methods* **2005**, *130*, 102–107. [CrossRef]
15. Li, M.; Wang, S.; Cai, M.; Zheng, C. Identification of Nuclear and Nucleolar Localization Signals of Pseudorabies Virus (PRV) Early Protein UL54 Reveals that Its Nuclear Targeting Is Required for Efficient Production of PRV. *J. Virol.* **2011**, *85*, 10239–10251. [CrossRef] [PubMed]
16. Ostler, J.B.; Jones, C. Stress Induced Transcription Factors Transactivate the Herpes Simplex Virus 1 Infected Cell Protein 27 (ICP27) Transcriptional Enhancer. *Viruses* **2021**, *13*, 2296. [CrossRef]
17. Luo, Y.; Li, N.; Cong, X.; Wang, C.H.; Du, M.; Li, L.; Zhao, B.; Yuan, J.; Liu, D.D.; Li, S.; et al. Pathogenicity and Genomic Characterization of a Pseudorabies Virus Variant Isolated from Bartha-K61-Vaccinated Swine Population in China. *Vet. Microbiol.* **2014**, *174*, 107–115. [CrossRef]
18. Zhou, M.; Abid, M.; Yin, H.; Wu, H.; Teklue, T.; Qiu, H.J.; Sun, Y. Establishment of An Efficient and Flexible Genetic Manipulation Platform Based on a Fosmid Library for Rapid Generation of Recombinant Pseudorabies Virus. *Front. Microbiol.* **2018**, *9*, 2132. [CrossRef] [PubMed]
19. Abid, M.; Teklue, T.; Li, Y.F.; Wu, H.; Wang, T.; Qiu, H.J.; Sun, Y. Generation and Immunogenicity of a Recombinant Pseudorabies Virus Co-Expressing Classical Swine Fever Virus E2 Protein and Porcine Circovirus Type 2 Capsid Protein Based on Fosmid Library Platform. *Pathogens* **2019**, *8*, 279. [CrossRef]
20. Qi, H.; Wu, H.; Abid, M.; Qiu, H.J.; Sun, Y. Establishment of a Fosmid Library for Pseudorabies Virus SC Strain and Application in Viral Neuronal Tracing. *Front. Microbiol.* **2020**, *11*, 1168. [CrossRef]
21. Kinchington, P.R.; Bookey, D.; Turse, S.E. The Transcriptional Regulatory Proteins Encoded by Varicella-Zoster Virus Open Reading Frames (Orfs) 4 and 63, But not Orf-61, Are Associated with Purified Virus-Particles. *J. Virol.* **1995**, *69*, 4274–4282. [CrossRef]
22. McCarthy, K.M.; Tank, D.W.; Enquist, L.W. Pseudorabies Virus Infection Alters Neuronal Activity and Connectivity In Vitro. *PLoS Pathog.* **2009**, *5*, 10. [CrossRef]
23. Xiao, K.; Xiong, D.; Chen, G.; Yu, J.; Li, Y.; Chen, K.; Zhang, L.; Xu, Y.; Xu, Q.; Huang, X.; et al. RUNX1-Mediated Alphaherpesvirus-Host Trans-Species Chromatin Interaction Promotes Viral Transcription. *Sci. Adv.* **2021**, *7*, 26. [CrossRef]
24. Krishnan, R.; Stuart, P.M. Developments in Vaccination for Herpes Simplex Virus. *Front. Microbiol.* **2021**, *12*, 798927. [CrossRef]
25. Yan, C.; Luo, Z.; Li, W.; Li, X.; Dallmann, R.; Kurihara, H.; Li, Y.F.; He, R.R. Disturbed Yin-Yang Balance: Stress Increases the Susceptibility to Primary and Recurrent Infections of Herpes Simplex Virus Type 1. *Acta Pharm. Sin. B* **2020**, *10*, 383–398. [CrossRef]
26. Cohen, J.I. Herpesvirus Latency. *J. Clin. Investig.* **2020**, *130*, 3361–3369. [CrossRef]
27. St Leger, A.J.; Koelle, D.M.; Kinchington, P.R.; Verjans, G. Local Immune Control of Latent Herpes Simplex Virus Type 1 in Ganglia of Mice and Man. *Front. Immunol.* **2021**, *12*, 723809. [CrossRef]
28. Koyuncu, O.O.; MacGibeny, M.A.; Enquist, L.W. Latent Versus Productive Infection: The Alpha Herpesvirus Switch. *Future Virol.* **2018**, *13*, 431–443. [CrossRef] [PubMed]
29. Van Diemen, F.R.; Kruse, E.M.; Hooykaas, M.J.; Bruggeling, C.E.; Schurch, A.C.; van Ham, P.M.; Imhof, S.M.; Nijhuis, M.; Wiertz, E.J.; Lebbink, R.J. CRISPR/Cas9-Mediated Genome Editing of Herpesviruses Limits Productive and Latent Infections. *PLoS Pathog.* **2016**, *12*, e1005701. [CrossRef] [PubMed]
30. Elion, G.B.; Furman, P.A.; Fyfe, J.A.; de Miranda, P.; Beauchamp, L.; Schaeffer, H.J. Selectivity of Action of an Antiherpetic Agent, 9-(2-Hydroxyethoxymethyl) Guanine. *Proc. Natl. Acad. Sci. USA* **1977**, *74*, 5716–5720. [CrossRef] [PubMed]
31. Reardon, J.E.; Spector, T. Herpes Simplex Virus Type 1 DNA Polymerase. Mechanism of Inhibition by Acyclovir Triphosphate. *J. Biol. Chem.* **1989**, *264*, 7405–7411. [CrossRef]
32. Mackowiak, P.A. Concepts of Fever. *Arch. Intern. Med.* **1998**, *158*, 1870–1881. [CrossRef] [PubMed]
33. Chen, Q.Y.; Wu, X.M.; Che, Y.L.; Chen, R.J.; Hou, B.; Wang, C.Y.; Wang, L.B.; Zhou, L.J. The Immune Efficacy of Inactivated Pseudorabies Vaccine Prepared from FJ-2012ΔgE/gI Strain. *Microorganisms* **2022**, *10*, 1880. [CrossRef] [PubMed]
34. Rafael, D.; Tomer, E.; Kobiler, O. A Single Herpes Simplex Virus 1 Genome Reactivates from Individual Cells. *Microbiol. Spectr.* **2022**, *31*, e0114422. [CrossRef] [PubMed]
35. Harris, R.A.; Preston, C.M. Establishment of Latency In Vitro by the Herpes Simplex Virus Type 1 Mutant in1814. *J. Gen. Virol.* **1991**, *72*, 907–913. [CrossRef] [PubMed]

Disclaimer/Publisher’s Note: The statements, opinions and data contained in all publications are solely those of the individual author(s) and contributor(s) and not of MDPI and/or the editor(s). MDPI and/or the editor(s) disclaim responsibility for any injury to people or property resulting from any ideas, methods, instructions or products referred to in the content.

Article

Genomic Characterization and gE/gI-Deleted Strain Construction of Novel PRV Variants Isolated in Central China

Jianle Ren ¹, Shanshan Tan ¹, Xinxin Chen ², Jiying Yao ¹, Zhihong Niu ¹, Ying Wang ¹, Lei Ma ³, Xiaolong Gao ⁴, Sheng Niu ¹, Libin Liang ¹, Junping Li ¹, Yujun Zhao ¹ and Wen-xia Tian ^{1,*}

¹ College of Veterinary Medicine, Shanxi Agricultural University, Jinzhong 030801, China; renjianle0615@163.com (J.R.); tanshanshan2021@163.com (S.T.); yjy2323126320@163.com (J.Y.); nzh1217899264@163.com (Z.N.); wangying@sxau.edu.cn (Y.W.); niusheng@sxau.edu.cn (S.N.); lianglibin521@126.com (L.L.); lijunping916@163.com (J.L.); tgzhaoyujun@163.com (Y.Z.)

² Beijing Solarbio Science & Technology Co., Ltd., Beijing 101102, China; jjdswsx@126.com

³ School of Biotechnology and Food Engineering, Anyang Institute of Technology, Anyang 455000, China; nihaowsm12008@163.com

⁴ Beijing Animal Disease Prevention and Control Center, Beijing 102629, China; veterinary89@126.com

* Correspondence: wenxiatian@126.com

Abstract: Pseudorabies virus (PRV) variants have caused substantial economic losses in the swine industry in China since 2011. To surveil the genetic variation in PRV field strains, here, two novel variant strains of PRV were isolated from Shanxi Province in central China and were designated SX1910 and SX1911. To identify the genetic characteristics of the two isolates, their complete genomes were sequenced, and phylogenetic analysis and sequence alignment revealed that field PRV variants have undergone genetic variations; notably, the protein-coding sequences UL5, UL36, US1 and IE180 exhibited extensive variation and contained one or more hypervariable regions. Furthermore, we also found that the glycoproteins gB and gD of the two isolates had some novel amino acid (aa) mutations. Importantly, most of these mutations were located on the surface of the protein molecule, according to protein structure model analysis. We constructed a mutant virus of SX1911 with deletion of the gE and gI genes via CRISPR/Cas9. When tested in mice, SX1911-ΔgE/gI-vaccinated mice were protected within a comparable range to Bartha-K61-vaccinated mice. Additionally, a higher dose of inactivated Bartha-K61 protected the mice from lethal SX1911 challenge, while a lower neutralization titer, higher viral load and more severe microscopic lesions were displayed in Bartha-K61-vaccinated mice. These findings highlight the need for continuous monitoring of PRV and novel vaccine development or vaccination program design for PRV control in China.

Keywords: PRV variant; variation; vaccine; Bartha-K61; immunity protection



Citation: Ren, J.; Tan, S.; Chen, X.; Yao, J.; Niu, Z.; Wang, Y.; Ma, L.; Gao, X.; Niu, S.; Liang, L.; et al. Genomic Characterization and gE/gI-Deleted Strain Construction of Novel PRV Variants Isolated in Central China. *Viruses* **2023**, *15*, 1237. <https://doi.org/10.3390/v15061237>

Academic Editors: Yan-Dong Tang and Xiangdong Li

Received: 19 April 2023

Revised: 21 May 2023

Accepted: 22 May 2023

Published: 25 May 2023



Copyright: © 2023 by the authors. Licensee MDPI, Basel, Switzerland. This article is an open access article distributed under the terms and conditions of the Creative Commons Attribution (CC BY) license (<https://creativecommons.org/licenses/by/4.0/>).

1. Introduction

Pseudorabies virus (PRV) is a double-stranded DNA virus that belongs to the family Herpesviridae, subfamily Alphaherpesvirinae, and genus Varicellovirus [1–3]. This virus is the etiological agent of pseudorabies (PR) or Aujeszky's disease [4]. PRV exhibits a broad host range and is capable of infecting most mammals and some avian species, but pigs are the natural host of the virus [5–7]. PRV infections cause neurological and respiratory system disorders, causing high mortality in newborn piglets and reproductive disease in pregnant sows [5]. In particular, PRV can establish life-long latent infection in the neurological tissues and lymphoid tissues of recovered pigs, leading to recurrent infection [1,8,9].

Inactivated or attenuated gene-deletion vaccines, along with differential diagnosis, has proven to be the best strategy to control and eradicate PRV [6,7,10]. Due to the control efforts and strict implementation of this strategy, PRV has disappeared from domestic pig populations in several parts of the world, such as New Zealand, most European countries and the USA [6,11]. In China, the attenuated vaccine strain Bartha-K61 was imported the

1980s and has been broadly applied since, resulting in relatively favorable control of PR [5,12]. However, PR reemerged in large-scale swine herds in most regions of China in 2011 [13,14]. Subsequently, the causative agent was confirmed to be PRV variant strains. Compared with classical strains, variant strains exhibit increased virulence, causing high mortality in newborn piglets and finishing pigs and an increased abortion rate in sows [15–17]. Of note, the Bartha-K61 vaccine could not provide effective protection against PRV variants [18–21]. Genetically, PRV can be divided into two genotypes. PRV strains in China belong to genotype II, while genotype I comprises mainly strains isolated in America and Europe [22]. Within genotype II, PRV variant genomes also exhibit marked sequence divergence in comparison to classical strains [22–24]. In the last decade, PRV variants have undergone extensive intragenotype and intergenotype recombination among strains and amino acid (aa) mutation, such as that of viral glycoproteins or other viral proteins [25–27]. More PRV variants have also been isolated from cows, dogs, sheep, wolves, minks and even humans [28–31]. In this regard, recombination events and aa mutations might alter viral virulence or the immune response of novel hosts and lead to rapid interspecies transmission [26]. Thus, it is necessary to continuously monitor and analyze epidemic or genetic variation in PRV in the future, which will help facilitate PRV prevention and control.

In this study, we successfully isolated two novel PRV strains, SX1910 and SX1911, from the lung tissue samples of sick piglets on pig farms in Shanxi Province, China. By analyzing the genetic variation in and evolution of the isolates, we found that SX1910 and SX1911 were classified into genotype II and were variant strains. Furthermore, we revealed that the PRV variants isolated from the field were undergoing genetic variations, and the aa sequences of the viral proteins UL5, UL36, US1 and IE180 exhibited extensive variations, including one or more hypervariable regions. Of note, novel aa mutations in gB and gD were found in SX1910 and SX1911. Most of these mutations were located on the surface of the molecule, according to protein structure model analysis. Based on the PRV strain SX1911, we generated a mutant virus lacking the gE and gI genes (SX1911- Δ gE/gI) via CRISPR/Cas9 and the LoxP system platform. Immunization and challenge tests in mice indicated that inactivated SX1911- Δ gE/gI could provide comparable protection in comparison with inactivated Bartha-K61. However, the viral loads and microscopic lesions of Bartha-K61-vaccinated mice were much higher and more severe, respectively, than those of mice inoculated with SX1911- Δ gE/gI. These findings will help us understand the epidemic status of PRV variants and will have important implications for PRV control in China.

2. Materials and Methods

2.1. Cells, Viruses and Antibodies

Vero-CCL81 cells (ATCC, CCL81) were cultured in Dulbecco's modified Eagle's medium (DMEM) (Gibco, Grand Island, NY, USA) supplemented with 10% fetal bovine serum (FBS) (Gibco, USA) at 37 °C in a 5% CO₂ incubator. The two PRV variant strains SX1910 (GenBank no. OL606749.1) and SX1911 (GenBank no. OP376823.1) were isolated from PRV-infected piglets from pig farms in Shanxi Province in 2019. The PRV Bartha-K61 vaccine strain (Genbank no. JF797217.1) was a gift from Shanxi LUCKIER Biopharmaceutical Co., Ltd. and was preserved in our laboratory. The PRV strains were propagated in Vero-CCL81 cells maintained in DMEM supplemented with 2% FBS (Gibco, USA) at 37 °C with 5% CO₂. The anti-PRV gB monoclonal antibody was a gift from Dr. Jiangwei Song (Institute of Animal Husbandry and Veterinary Medicine, Beijing Academy of Agriculture and Forestry Sciences).

2.2. Virus Isolation and Identification

Lung tissues that were positive for PRV were homogenized in Dulbecco's modified Eagle's medium. The homogenates were centrifuged and filtered through a 0.22 μ m filter to remove bacteria, and inoculated onto Vero cells. Then, the cells were incubated at 37 °C and examined daily for a cytopathic effect (CPE). After the CPE appeared, the infected cells

were characterized via immunofluorescence assays (IFAs) using an anti-PRV gB protein monoclonal antibody and PCR targeting of the gE gene (Table S1). Finally, the viruses were purified via plaque purification, with homogeneity monitored based on the plaque sizes.

2.3. Multistep Growth Analysis

The multistep growth kinetics of PRV were measured as previously described [21]. Briefly, Vero cells were infected with PRV at a multiplicity of infection (MOI) of 0.01. After absorption for 1 h at 37 °C, the unbound viruses were removed via brief acid and PBS washing. The cells were washed twice with PBS. Then, the cells were supplemented with fresh DMEM containing 2% FBS. The cell cultures were collected at the indicated times post-infection, and the virus titers are expressed as the 50% tissue culture infectious dose (TCID₅₀), as determined according to the Reed–Muench method [32].

2.4. Plaque Size Analysis

To analyze the size of the plaques induced by PRV, the virus supernatants were diluted with DMEM at a 10-fold dilution, transferred to 6-well plates containing Vero cell monolayers at a volume of 1 mL/well and incubated to allow absorption at 37 °C for 1 h. Then, the supernatants were removed by washing the cells twice with PBS, and the cells were overlaid with 2 mL of DMEM containing 0.5% methylcellulose. After incubation at 37 °C for 60 h, the plaque sizes were analyzed using ImageJ2X software (National Institutes of Health, Bethesda, MD, USA) after staining with 4% paraformaldehyde containing 0.1% crystal violet.

2.5. Genomic Sequencing

PRV genomic DNA was extracted from infected Vero cells as previously described [33]. Five micrograms of genomic DNA were submitted to Sangon Biotech (Shanghai, China) Co., Ltd. for next-generation sequencing (NGS) using an Illumina HiSeq™. After the host sequences were removed, the raw assembled genomes were aligned using Blast software (NCBI) to analyze the spanned sequences. Then, the sequences corresponding to the remaining gaps were amplified via PCR, and the products were cloned into the pEASY-Blunt vector (TransGen, Beijing, China) for Sanger sequencing. Following assembly and annotation, the genome sequences of PRV strains SX1910 and SX1911 were submitted to the GenBank database under accession numbers OL606749.1 and OP376823.1, respectively.

2.6. Phylogenetic Analysis and Sequence Alignment

For PRV, the gC gene and whole genome have been most widely used for phylogenetic analysis. Thus, the gC gene sequences (Table S2) were collected from the GenBank database and input into MEGA 5.1 software (Mega Limited, Auckland, New Zealand) for analysis using the neighbor-joining algorithm, 1000 bootstrap replicates and the Kimura 2-parameter substitution model. Additionally, whole-genome phylogenetic analysis was performed using Geneious Prime software (version 2022.2, Biomatters, Auckland, New Zealand) with the neighbor-joining method, 100 bootstrap replicates and the Tamura–Nei genetic distance model.

The whole genomes of the SX1910 and SX1911 strains were aligned with those of eight reference PRV genomes, including the European–American strain Bartha-K61, the classical strain Fa, and variant strains (TJ, GD0304, HN1201, JS-2012 and HeN1), using the mVista genomic analysis tool (<http://genome.lbl.gov/vista/mvista/submit.shtml>, accessed on 29 October 2022) with global LAGAN alignment. Moreover, the selected gene-encoding sequences (gB, gC, gD, UL5, UL36, US1 and IE180) of the PRV strains were aligned via Geneious Prime software (version 2022.2, Biomatters, Auckland, New Zealand) with the Clustal Omega program. The reference strains used for alignment are listed in Table S2.

2.7. Construction of a gE/gI-Deleted Virus

sgRNAs targeting the gE and gI genes were designed using an online CRISPR tool (<https://www.genscript.com/gRNA-design-tool.html>, accessed on 15 May 2021). The sgRNA CRISPR/Cas9 plasmid was constructed as previously described [21]. In brief, the oligo pairs were synthesized (Table S3) and annealed under the following conditions: 5 min at 95 °C and 30 min at 25 °C. The purified product was then cloned into the plasmid pX335 (sgRNA/Cas9 expression vector) at the BbsI restriction site, followed by verification via DNA sequencing.

To delete gE and gI, the homologous arms were amplified from the variant strain SX1911. Two pairs of primers containing the Loxp site were designed (Table S3) and used to amplify GFP from the plasmid pEGFP-N2 (Clontech, Mountain View, CA, USA) via PCR using Phanta[®] Max Super-Fidelity DNA Polymerase (Vazyme, Nanjing, China). A donor GFP construct flanked by homologous arms was then constructed via overlapping PCR. To generate the recombinant virus, PRV genomic DNA was extracted from infected Vero cells as previously described [34], and cotransfected with linear donor DNA (5.0 µg) and two sgRNA plasmids (1.5 µg each) into Vero cells using Lipofectamine 2000 Reagent (Invitrogen, Carlsbad, CA, USA). The CPE was monitored daily, and the recombinant virus carrying GFP was harvested 72 h later. To delete the GFP gene, the genomic DNA of the recombinant virus and plasmid expressing Cre were cotransfected into Vero cells. Then, gE/gI-deleted viruses were screened by determining the loss of GFP fluorescence. All viruses were purified via plaque purification, with homogeneity monitored using the plaque sizes, and were verified via DNA sequencing.

2.8. Experiments in Mice

2.8.1. Pathogenicity Test

One hundred and thirty 6-week-old female SPF Kunming mice were randomly divided into 13 groups with ten mice in each group. Mice in groups 1–4, 5–8 and 9–12 were subcutaneously inoculated with 100 µL of different doses (10^3 , 10^4 , 10^5 or 10^6 TCID₅₀) of SX1910, SX1911 and SX1911ΔgE/gI, respectively. Mice in group 13 were injected with DMEM as a mock control. Clinical signs were observed daily, and the number of deaths and time of death of mice in each group were recorded. At 14 days post-challenge (dpc), all surviving mice were euthanized. The 50% lethal dose (LD₅₀) was calculated using the Reed–Muench method [32]. Additionally, a detailed description of the calculation of clinical scores is shown in Table 1.

Table 1. Clinical scores in the mice after PRV infection.

Symptoms	Clinical Scores ^a
Normal	0
Ruffled hair	1
Depression	1
Anorexia	1
Moderately labored breathing	1
Urgent breathing	2
Itching	2
Skin biting	3
Paralysis	3
Death	3
Total scores	17

^a Clinical signs are represented by +++: serious ($11 \leq$ total average score ≤ 17), ++: moderate ($5 \leq$ total average score ≤ 10), +: mild ($0 \leq$ total average score ≤ 4) and /: none.

2.8.2. Immunization and Challenge Test

Fifty-four 6-week-old female SPF Kunming mice were randomly divided into 6 groups with nine mice in each group. The mice in groups 1–2 were inoculated with 200 µL of inactivated SX1911-ΔgE/gI at a dose of 10^6 TCID₅₀/mL or 10^7 TCID₅₀/mL via both the

subcutaneous and intramuscular routes. Similarly, the mice in groups 3–4 were injected with Bartha-K61. Mice in the unvaccinated group (positive control) and negative control group received 200 μ L of DMEM, respectively. Following immunization, the clinical symptoms were recorded daily. At 14 days post-immunization (dpi), mice in groups 1–4 received a second immunization. At 28 dpi, serum samples were collected to monitor PRV-neutralizing antibody production. Then, all mice were challenged subcutaneously (i.p.) with PRV SX1911 at a dose of 200 μ L of 10^6 TCID₅₀, except for those in the negative control group. After the challenge, the clinical signs of disease were recorded and scored daily. At 14 dpc, all surviving mice were euthanized and necropsied, and the lungs were collected for viral load and histopathology analyses.

2.9. Quantitative PCR (qPCR)

The viral tissue load was measured via absolute quantitative PCR (qPCR) targeting the gB gene on a QuantStudio™ 5 Real-Time PCR Instrument (Applied Biosystem, Carlsbad, CA, USA) using previously described primers and following the manufacturer's recommendations [21]. According to the standard curve, the viral loads and virus shedding were calculated and expressed as log₁₀ copies per mouse.

2.10. Histopathological Examinations

Histopathological examination was performed as previously described [21]. Briefly, the collected lungs were fixed with a 4% paraformaldehyde solution at room temperature for 48 h. The fixed tissues were dehydrated in graded alcohol and embedded in paraffin wax. Microsections were cut, stained with hematoxylin and eosin (HE) and examined via light microscopy to identify microscopic pathological changes.

2.11. Statistical Analyses

Statistical analyses were performed using a one-way or two-way analysis of variance (ANOVA) in GraphPad Prism 5 (San Diego, CA, USA). *p* values < 0.05 were considered to indicate statistical significance; *p* values < 0.001 were considered to indicate extreme significance.

3. Results

3.1. Isolation and Identification of Virus

PRV-positive lung tissue homogenates were centrifuged, filtered through a 0.22 μ m filter to remove bacteria, and inoculated onto Vero cells. A distinct CPE was characterized by rounded cells at 36 h post-inoculation. When the Vero cells were infected with supernatant from cultures exhibiting a CPE, a positive signal for the PRV gB protein was observed in the infected region using IFA (Figure 1A). Simultaneously, viral genome DNA was extracted from the supernatant from cultures exhibiting a CPE, and the PRV gE gene was amplified via PCR using the primers gE-F/gE-R (Table S1). As shown in Figure 1B, the supernatant from cultures exhibiting a CPE was positive for the gE gene. Then, the viruses were purified via plaque purification, with homogeneity monitored using the plaque sizes, and the isolates were named SX1910 and SX1911. We also tested the multistep growth and plaque size of the two isolates, and found that the growth kinetics of SX1910 was generally similar to SX1911, and the plaque sizes of SX1910 were significantly larger than those of SX1911.

To test the pathogenicity of the two isolates, mice were infected with SX1910 or SX1911 to determine the LD₅₀. As shown in Table 2, at the same dose, mice inoculated with SX1910 died much earlier than mice inoculated with SX1911. The LD₅₀ of each strain was calculated as $10^{3.84}$ TCID₅₀ (SX1910) and $10^{4.42}$ TCID₅₀ (SX1911), respectively, indicating that the pathogenicity of SX1910 was higher than that of SX1911.

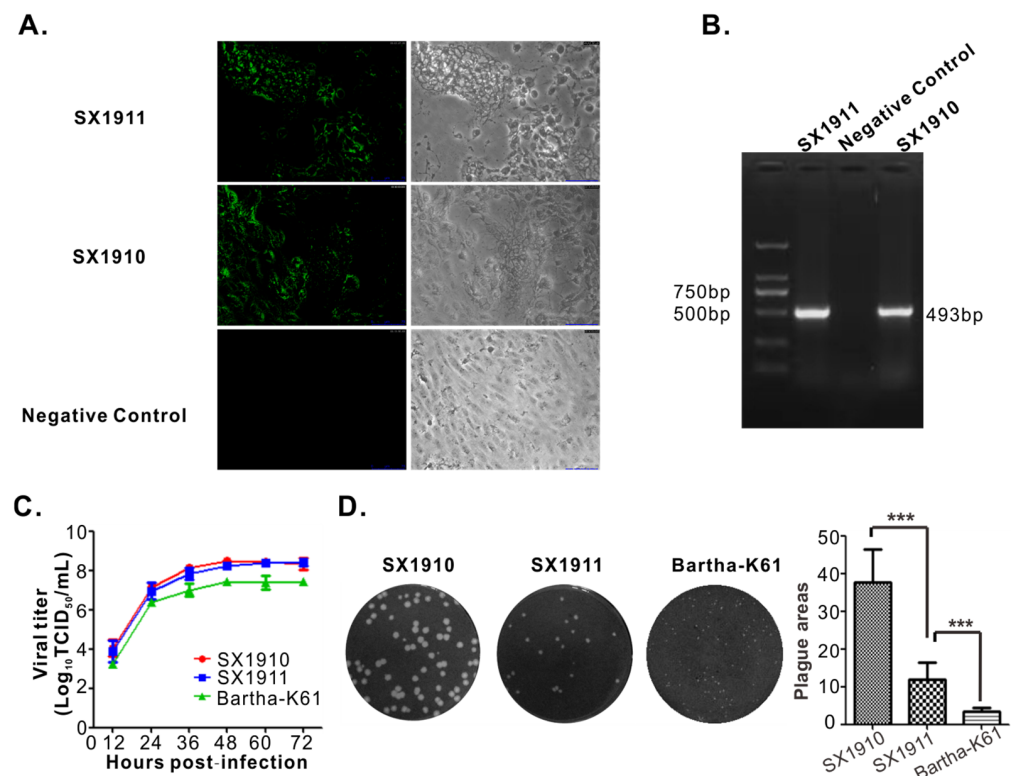


Figure 1. Identification of the isolated PRV strains. (A) Indirect immunofluorescence assay (IFA) for the detection of the PRV strains SX1910 and SX1911 (magnification 200X). Vero cells infected with the supernatant from cultures exhibiting a CPE were fixed at 48 h post-inoculation and examined via IFA using monoclonal antibodies against the gB protein. (B) PCR verification of the PRV strains SX1910 and SX1911. Vero cells were inoculated with the supernatant from cultures exhibiting a CPE and subjected to PCR amplification using the primer pair gE-F/gE-R specific for the PRV gE gene. (C) Multistep growth curve of SX1910 and SX1911 compared with Bartha-K61 in Vero cells. (D) Plaque sizes of SX1910 and SX1911 compared with Bartha-K61 in Vero cells. Data are presented as the mean \pm SD, and an asterisk indicates a significant difference ***: $p < 0.001$.

Table 2. Statistical analysis of mice infected with PRV.

Groups	Amounts	Doses (TCID ₅₀ /mL)	Clinical Signs ^a	Mortality (Mean Days to Death)	LD ₅₀
SX1910	10	10 ⁶	+++	10/10 (2.98)	10 ^{3.84}
	10	10 ⁵	+++	8/10 (3.51)	
	10	10 ⁴	++	6/10 (4.08)	
	10	10 ³	+	2/10 (4.25)	
SX1911	10	10 ⁶	+++	10/10 (3.25)	10 ^{4.42}
	10	10 ⁴	++	3/10 (4.16)	
	10	10 ³	+	1/10 (4.25)	
SX1911- Δ gE/gI	10	10 ⁶	++	5/10 (4.07)	10 ^{6.00}
	10	10 ⁵	+	2/10 (6.68)	
	10	10 ⁴	/	0/10	
DMEM	10	0.1 mL	/	0/10	

^a Clinical signs are represented by +++: serious, ++: moderate, +: mild and /: none.

3.2. Genomic Sequencing and Phylogenetic Analysis

The complete genome sequences of SX1910 and SX1911 were determined using the high-throughput Illumina platform. Following assembly and annotation, there were 69 open reading frames (ORFs) in both isolates. The complete genomes of the SX1910 and

SX1911 strains encompass 143,186 bp and 143,263 bp with GC contents of 73.71% and 73.75%, respectively. To search for the aa variations between SX1910 and SX1911, all protein-coding regions of the SX1911 strain were compared with SX1910. Sequence comparison revealed that the 19 viral proteins displayed variations in the SX1911 strain (Table 3), and most of these proteins are associated with viral DNA replication or virulence.

Table 3. Protein-coding variations of PRV SX1911, in comparison to PRV SX1910.

Protein Name ^a	Amino Acid Residues Found in PRV SX1911, which Differ from PRV SX1910 ^b
gK (UL53)	F124L
gN (UL49.5)	W42R
gB (UL27)	45 (+L), S131T, T358M
ICP18.5 (UL28)	G255A, 256 (+G)
ICP8 (UL29)	M178T
VP1/2 (UL36)	E404G, L536R, S1464P
UL37	D844G
RR1 (UL39)	G589V
UL43	G206D
Scaffold (UL26.5)	V269P
VP24 (UL26)	V515M
OBP (UL9)	L565, W723R
UL8	V5A, V293A, A532E
UL5	74–79 (PGGPAG > Δ)
ICP0 (EP0)	V345A
ICP4 (IE180)	Q98Δ, 869–880 (STKSSSSTKSSS > Δ), 448 (+S)
ICP22 (US1)	352–371(EEEEDEEEDEEEDEEEED > Δ)
gD (US6)	280–281 (RP > Δ)
gE (US8)	V386A, G510S

^a Proteins are listed in order of occurrence along the genome. ^b single AA residue changes are written in standard format, including the SX1910 strain AA, its position and the AA residue found in the PRV SX1911 protein, e.g., S100P. Insertions are indicated by the AA position in SX1910, followed by “+” and the new AAs, e.g., 100 (+RR). Deletions are indicated by the symbol Δ. Sequential changes are combined and shown with the SX1910 strain AA positions are shown first, followed by the relevant SX1910 AA residues, and then “>”, and finally, the new alternative AA residues, e.g., 100–102 (RAR > EDA).

To elucidate the genetic relationship of the two isolates, phylogenetic trees based on the gC sequences and the whole genomic sequences were constructed using a neighbor-joining method via MEGA 5.1 and Geneious Prime (version 2022.2) software. As shown in Figure 2A, the phylogenetic tree of gC showed that the PRV strains were divided into two genotypes. Genotype I is mainly composed of European–American strains, while Chinese strains belong to genotype II, which is consistent with previous studies [22]. Within genotype II, the PRV variants displayed the highest homology and were divided into the clade 2.2 group. Correspondingly, a similar result was found using whole-genome analysis (Figure 2B), but the variant strains were contained in four clades: clades 2.2, 2.3, 2.4 and 2.5. SX1910 and SX1911 were clustered into clade 2.5, together with strains HeNZM/2017, PRV GD, TJ and HLJ8. These results suggest that PRV variants are undergoing genetic variations but the genotype is unchanged.

3.3. The Extensive Variations That the Two Isolates Exhibit in the Protein-Coding Sequences UL5, UL36, US1 and IE180

To explore the genetic variations in the two isolates, using the mVista genomic analysis tool with global LAGAN alignment, the SX1910 and SX1911 whole genomes were aligned with those of the reference strains from genotype I (Bartha-K61) and different clades of genotype II, including Fa (clade 2.1), HeN1 (clade 2.2), JS-2012 (clade 2.3), HN1201 (clade 2.4), GD0304 (clade 2.4) and TJ (clade 2.5). As shown in Figures 3 and S1, compared with Bartha-K61, the variants carried gene deletions, insertions and substitutions scattered along the genome, which was consistent with previous studies [22]. Of note, among the variant strains, most genes were conserved, while the SX1910 and SX1911 strains showed extensive divergence in noncoding regions (internal/terminal repeat regions and intergenic sequences) and the protein-coding sequences UL5, UL36, US1 and IE180, which are associated with viral egress, DNA replication and transcriptional regulation.

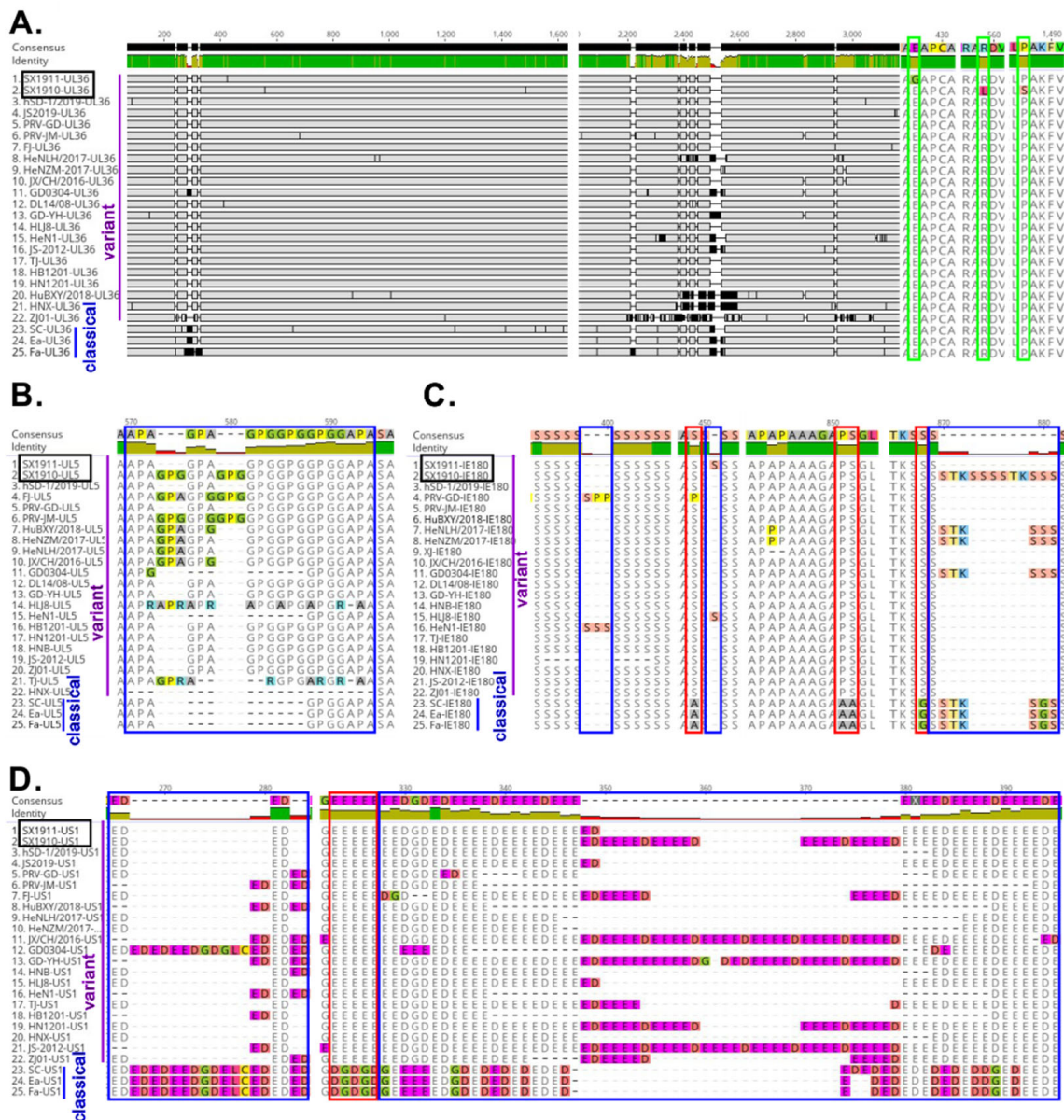


Figure 4. Multiple sequence alignment of divergent protein sequences among the genotype II strains. (A) UL36, (B) UL5, (C) IE180 and (D) US1. The novel aa mutations of the two isolates are indicated by a green box. The hypervariable aa regions are marked with blue boxes. The changes in conserved aa regions are marked with red boxes.

To further understand the characteristics of hypervariable genes, respectively, the viral UL36, UL5, US1 and IE180 protein sequences from 3 classical strains and 22 variant strains were aligned using Geneious Prime software with the Clustal Omega program. As shown in Figure 4A–D, compared with those of the reference strains, some novel aa mutations of the two isolates were observed. Specifically, two aa mutations (R559L and aa P1487S) in UL36 were identified in SX1910, and one aa mutation (E427G) was identified in SX1911. For IE180, a continuous 6 aa (SSSSTK) insertion at position 873–878 was observed in SX1910. SX1911 had an insertion of one serine (S) at position 451, identical to HLJ8. Notably, the indicated proteins had one or more hypervariable aa regions, such as UL36 (240–340 aa and 2200–2600 aa), UL5 (570–594 aa), IE180 (870–881 aa) and US1 (265–284 aa and 322–395 aa). Moreover, compared with those of classical strains, some conservative aa changes were also observed in variant strains. On the other hand, we also found that UL36 had many strain-specific aa mutations, and variation regions of the US1 protein (ICP22)

mainly exhibited a continuous repeated aa deletion/insertion (ED or E) or substitution (E-G, D-E, G-E, or G-D). Overall, these results indicate that noncoding regions and the protein-coding sequences UL36, UL5, US1 and IE180 exhibited extensive variations, and these protein-coding sequences had one or more hypervariable aa regions and strain-specific aa mutations.

3.4. The Glycoproteins gB and gD of the Two Isolates Have New Amino Acid Mutations

PRV glycoproteins play an important role in promoting virus entry, modulating virulence and inducing the immune response. To this end, we further explored the variations in gB, gC and gD of the isolated strains. In contrast with those of other variant strains, the major novel mutations occurred in gB and gD (Figure 5A,E), while gC was highly conserved. In gB alignment, two aa substitutions (S131T and T358M) in SX1911 and one aa (L) deletion at position aa 47 in SX1910 were identified. Moreover, a 2 aa (RP) insertion at position 276–277 was observed in gD of SX1910, identical to the classical strains and variant strain HLJ8. To determine whether the variation in gB and gD affects immunogenicity, we also examined the structure of the gB and gD proteins using PyMOL software (Schrodinger, Inc., New York, NY, USA). After removing the signal peptide (1–58 aa) and intracellular region (820–915 aa) of gB, we found that the mutant aa of SX1911 at position 131, which is located in coil structures, was on the surface of the molecule. Additionally, compared with those of classical strains, the two conserved mutant residues (aa 451 and 737) of the variant strains exhibited a similar result (Figure 5B,C). Furthermore, the RP at position 276–277 of gD in SX1910 was also located on the surface of the molecule (Figure 5E). These results suggest that the variation in the glycoproteins gB and gD might be involved in immunogenicity or antigenicity changes.

3.5. Construction and Biological Characterization of gE/gI-Deleted Virus of SX1911

In our study, a mutant SX1911 virus lacking the gE and gI genes was generated using the CRISPR/Cas9 and Cre-loxp systems and named SX1911-ΔgE/gI (Figure 6A,B). Then, the biological characteristics of SX1911-ΔgE/gI were tested in Vero cells. Analysis of the multistep growth kinetics of SX1911-ΔgE/gI showed a replication efficiency similar to that of SX1911 (Figure 6C). The sizes of plaques formed by SX1911-ΔgE/gI were considerably reduced compared to those of its parental virus SX1911 (Figure 6D). When the pathogenicity of the mutant virus was tested in mice, SX1911-ΔgE/gI exhibited lower virulence than SX1911. According to our analysis using the Reed–Muench method, the LD₅₀ values of SX1911-ΔgE/gI were 38-fold those of SX1911 (Table 1).

3.6. Bartha-K61 Provides a Comparable Protection Range to SX1911-ΔgE/gI

It has been reported that the Bartha-K61 vaccine cannot provide effective protection against PRV variants [18–21]. To investigate the protection efficiency of SX1911-ΔgE/gI, 6-week-old Kunming mice were vaccinated with 200 μL of either inactivated SX1911-ΔgE/gI or inactivated Bartha-K61 at doses of 10⁶ TCID₅₀ or 10⁷ TCID₅₀ via both the subcutaneous and intramuscular routes. After immunization, all mice displayed a good mental state, with normal appetite and no clinical symptoms, suggesting that these vaccines had no side effects on the mice. Serum samples were collected at 28 dpi, and neutralizing antibody levels were measured via a neutralization test. As shown in Figure 7A, the vaccines at a dose of 10⁷ TCID₅₀ could effectively induce the mice to produce neutralizing antibodies, while the neutralizing antibody titers of the SX1911-ΔgE/gI group were significantly higher than those of Bartha-K61.

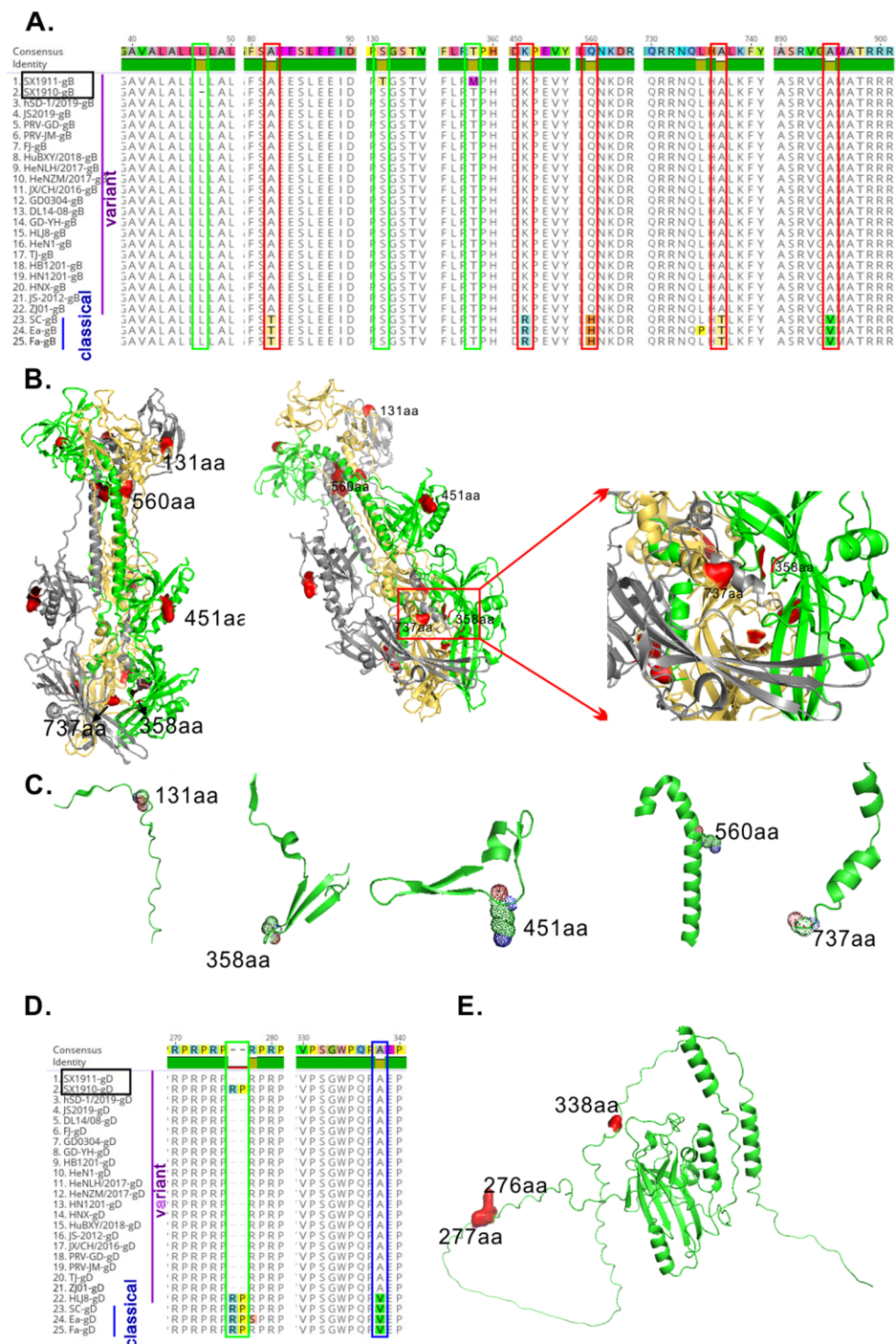


Figure 5. Analysis of the effect of aa mutations on gB and gD antigenicity, determined via bioinformatics. (A) Multiple sequence alignment of gB sequences among the genotype II strains. The novel aa mutations of the two isolates are indicated by a green box. The hypervariable aa regions are marked with blue boxes. The changes in conserved aa regions are marked with red boxes. (B) The position of aa mutations of surface residues in the structure of the PRV gB trimer (PRV strain HN1201, PDB ID: 5ys6) is shown with a cartoon representation. (C) Review of aa mutations in the gB the secondary structure. (D) Multiple sequence alignment of gD sequences among the genotype II strains. The novel aa mutations of the two isolates are indicated by a green box. The hypervariable aa regions are marked with blue boxes. The changes in conserved aa region changes are marked with red boxes. (E) The position of aa mutations of surface residues in the structure of the PRV gD is shown with a cartoon representation. Additionally, the gD structure was predicted via AlphaFold 2 combined with PRV HN1201 the gD structure (7–250 aa, PDB ID: 5X5V).

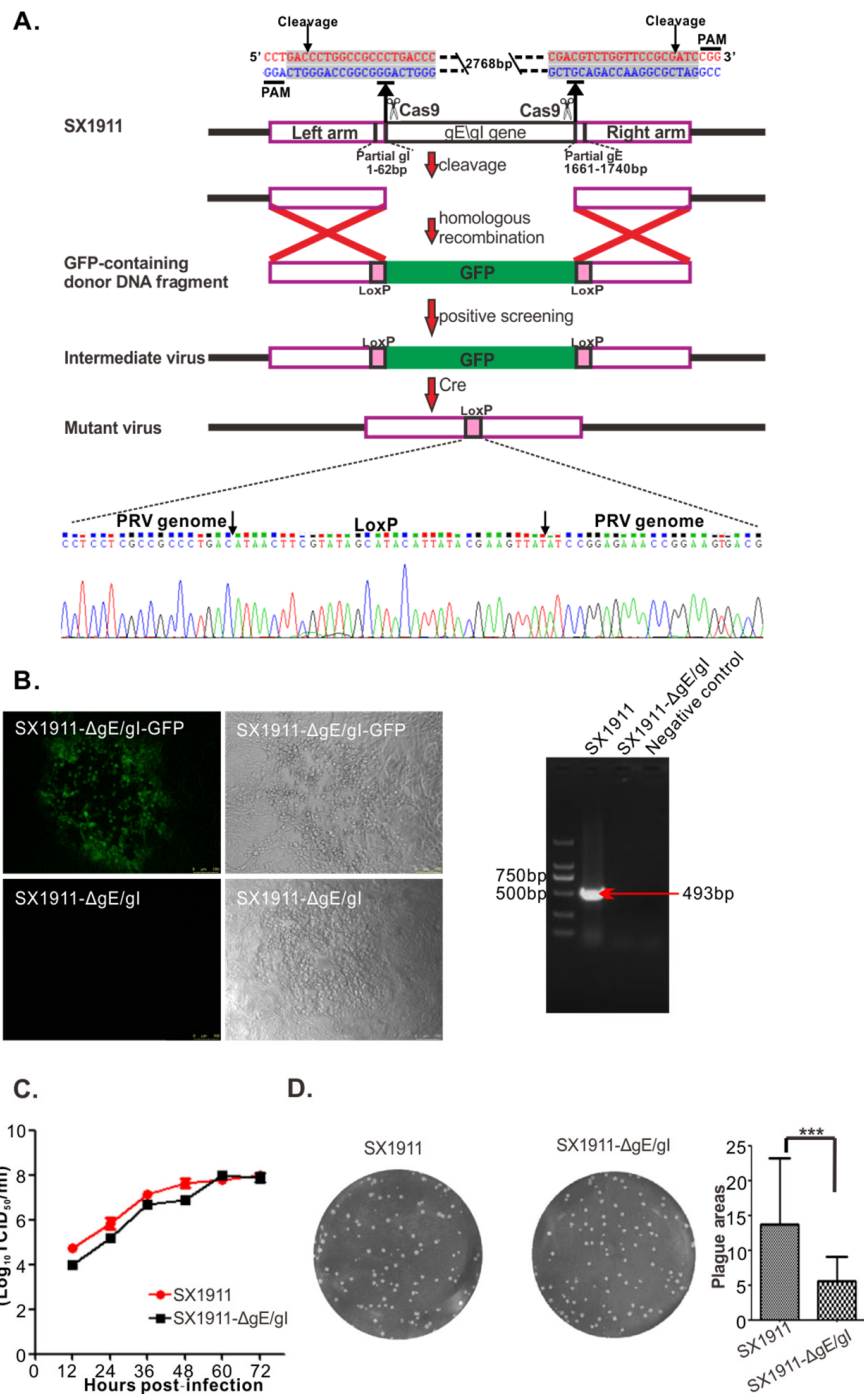


Figure 6. Construction and identification of the mutant virus SX1911-ΔgE/gI. (A) Strategy for constructing SX1911-ΔgE/gI using the CRISPR/Cas9 and LoxP systems. Two sgRNAs were designed to guide Cas9 to delete the gE and gI genes, and GFP was used for both positive and negative screening of mutant virus production. (B) Identification of SX1911-ΔgE/gI via IFA and PCR targeting the gE gene. (C) Multistep growth curve of SX1911 and SX1911-ΔgE/gI in Vero cells. (D) Plaque sizes of SX1911 and SX1911-ΔgE/gI in Vero cells. Data are presented as the mean ± SD, and an asterisk indicates a significant difference between SX1911 and SX1911-ΔgE/gI. ***: $p < 0.001$.

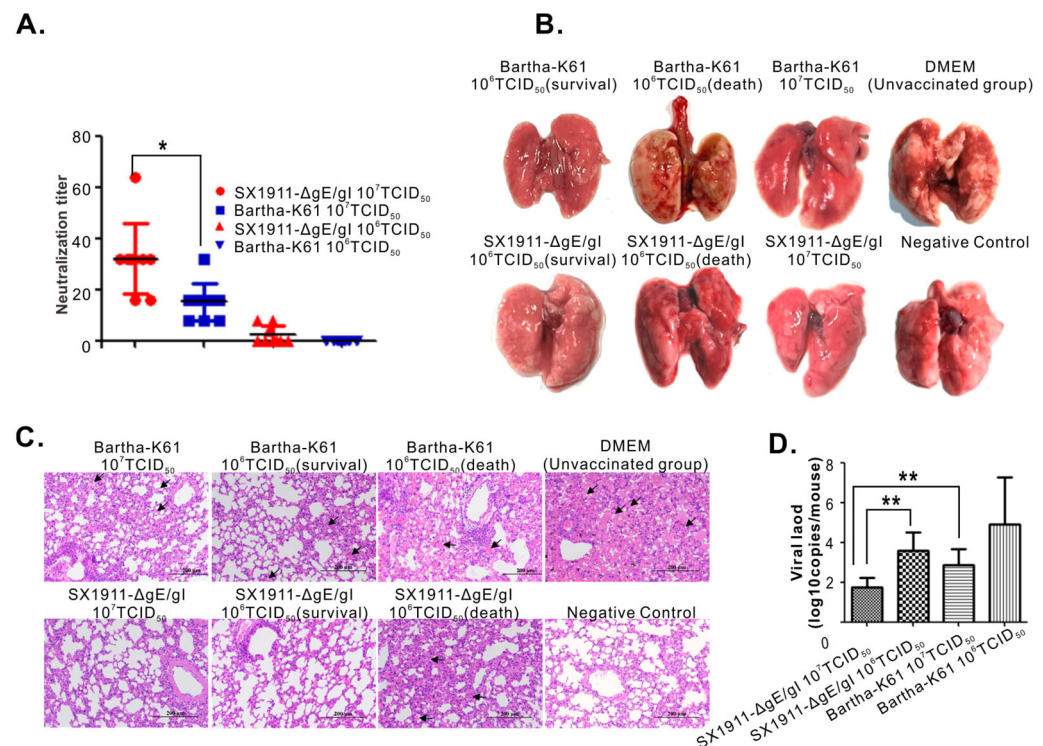


Figure 7. Protection efficiency analysis of SX1911-ΔgE/gI and Bartha-K61. (A) Neutralizing antibody titers against SX1911. Mouse sera were collected at 28 days post-immunization (dpi), and neutralizing antibodies were quantified in 96-well plates. (B) Gross lesion changes in immunized mice following challenge with SX1911. Lungs were collected and subjected to pathological examination at 14 days post-challenge (dpc). (C) Histopathological lesions of immunized mice following challenge with SX1911. The lungs were fixed, sectioned and stained with hematoxylin and eosin (HE) (200× magnification). (D) The tissue viral load of PRV in the lungs determined via qPCR. Data are presented as the mean ± SD, and an asterisk indicates a significant difference. *: $p < 0.05$; **: $p < 0.01$.

At 28 dpi, except for the negative controls, all mice were inoculated with SX1911 via the subcutaneous route at a highly lethal dose of 10⁶ TCID₅₀. Following the challenge, the DMEM group (unvaccinated group) began to exhibit obvious symptoms 72 h later, such as apathetic mood, rough hair disorder, loss of appetite, weight loss, and constant biting of the injection sites. For the immunized groups, mice immunized with a dose of 10⁷ TCID₅₀ did not show obvious clinical symptoms, except moderate or slight depression in the Bartha-K61 group. Three mice died and displayed severe symptoms in the groups receiving a challenge dose of 10⁶ TCID₅₀, including those immunized with SX1911-ΔgE/gI and Bartha-K61 (Table 4). At 14 dpc, all surviving mice were euthanized and necropsied, and the lungs were collected for pathological examination and viral load analyses. As shown in Figure 7B, postmortem necropsy showed that the dead mice receiving an immunization dose of 10⁶ TCID₅₀ had obvious consolidation and severe hemorrhage in the lung. Mice in the SX1911-ΔgE/gI group did not show a significant difference from those in the Bartha-K61 group. For the mice immunized with a dose of 10⁷ TCID₅₀, moderate or mild hemorrhagic lesions were observed in the Bartha-K61 group. However, we did not observe visible pathological lesions in the SX1911-ΔgE/gI group. Next, we also examined the histopathological changes via HE staining (Figure 7C), and found that the mice in the Bartha-K61 group developed more severe microscopic lesions than the mice in the SX1911-ΔgE/gI group, such as alveolar septal capillary dilatation, hemorrhage, congestion and alveolar destruction. Thus, the pathological examination revealed that SX1911-ΔgE/gI could more effectively reduce organ lesions compared with Bartha-K61. On the other hand, we assessed the viral load in the lungs using quantitative real-time PCR with primers targeting the gene encoding gB (Figure 7D). The results showed that a high immunization dose (10⁷ TCID₅₀) significantly

reduced the viral tissue load in the lungs compared with that after low-dose (10^6 TCID₅₀) immunization. Interestingly, at an immunization dose of 10^7 TCID₅₀, the viral load in the lungs (PRV genome copies) of mice in the SX1911-ΔgE/gI group was much lower than that the lungs of mice in the Bartha-K61 group. Overall, these data indicated that SX1911-ΔgE/gI-vaccinated mice were protected within a comparable range to Bartha-K61-vaccinated mice. Additionally, a higher dose of inactivated Bartha-K61 protected the mice from lethal SX1911 challenge, while a lower neutralization titer, higher viral load and more severe microscopic lesions were displayed in Bartha-K61-vaccinated mice.

Table 4. Statistical analysis of the protection efficiency of SX1911-ΔgE/gI in mice.

Groups	Amounts	Immunization Doses (TCID ₅₀ /mL)	Clinical Signs ^a	Mortality (Mean Days to Death)
SX1911-ΔgE/gI	9	10^6	+	3/9 (4.00)
SX1911-ΔgE/gI	9	10^7	/	0/9
Bartha-K61	9	10^6	+	3/9 (3.66)
Bartha-K61	9	10^7	+	0/9
DMEM	9	0.2 mL DMEM	+++	9/9 (4.44)
Negative control	9	0.2 mL DMEM	/	0/9

^a Clinical signs are represented by +++: serious, +: mild and /: none.

4. Discussion

Since 2011, highly virulent PRV variants have caused substantial economic losses to the swine industry in China [35]. In recent years, an increasing number of reports have indicated that PRV variants are undergoing extensive aa mutations and intragenotype and intergenotype gene recombination. In this report, to surveil the genetic variation in PRV field strains, we analyzed the genetic variation in two novel PRV variant strains (SX1910 and SX1911) isolated in Shanxi Province, China. We revealed the following findings. (i) The two isolates exhibited the greatest foci of divergence in noncoding regions and the protein-coding regions UL5, UL36, US1 and IE180, which are associated with viral egress, DNA replication and transcriptional regulation. (ii) The glycoproteins gB and gD of the isolated strains had novel aa mutations, and these mutations were mainly located on the surface of the molecule, corresponding to a higher antigenic index. (iii) High doses of Bartha-K61 alone could provide relatively better immunity in mice, and its protection efficiency exhibited a comparable range to SX1911-ΔgE/gI. The relevant significance and insights of this study are discussed below.

Phylogenetic characterization revealed that PRV variants were classified into genotype II, exhibiting remarkable divergence from genotype I strains, including Bartha-K61 and Becker [22,23,36–38]. Similarly, our study also revealed that PRV SX1910 and SX1911 were variant strains. However, SX1910 and SX1911 were also undergoing genetic variation and were clustered into clade 2.5. In addition, Hu et al. found that a unique genetic clade of PRV variants was detected via phylogenetic analysis, implying that PRV variants continuously evolved between 2012 and 2017 in China [27]. Of note, the HLJ-2013 strain is a recombinant virus that emerged from a recombination event between genotype I and genotype II strains, so HLJ-2013 is located in an independent branch [39]. Similar results were found in another study based on phylogenetic analysis of the whole genome [37].

Extensive genetic variations in the variant strains are scattered along the genome, in comparison to Bartha-K61 or Becker from genotype I [22]. However, according to the genotype II strain genome alignment, the hypervariable regions of the SX1910 and SX1911 genomes predominantly occurred in internal and terminal repeat regions, intergenic sequences and some protein-coding sequences, such as UL36, UL5, US1 and IE180. Notably, the viral proteins UL36, UL5, US1 and IE180 are responsible for viral egress, DNA replication and gene transcriptional regulation [2,40–43]. Each protein contains one or more hypervariable aa regions displaying aa deletions, insertions and substitutions. Previously, a study indicated that aa 2087–2796 in UL36 (VP1/2) is required for PRV Becker strain

virulence and retrograde axon transport in vivo [42]. Interestingly, our study showed that the hypervariable aa 2200–2600 region of UL36 (VP1/2) was located within the functional aa 2087–2796 region. This finding suggests that the variations in aa 2200–2600 might be associated with virulence attenuation or enhancement in PRV variants. US1 (ICP22) is involved in transactivation and regulatory functions in related alphaherpesviruses [40]. Ye et al. found that PRV variants exhibited the highest variation rate among all viral proteins [22]. Moreover, our study also showed that US1 protein (ICP22) variations mainly exhibited a continuous repeated aa deletion/insertion (ED or E) or substitution (E-G, D-E, G-E, or G-D). In addition, in herpes simplex virus type I (HSV-1) and duck plague virus (DPV), ICP22 is required for efficient viral replication and pathogenicity [44–47]. Therefore, it would also be interesting to explore the role and significance of US1-coding sequence variability in the future. Of note, the “hypervariable regions” also might be due to different types of repeated sequence which are not only instable but also problematic when using NGS techniques. Therefore, some of the variations in the genomes are probably due to sequencing (assembly) errors. The glycoproteins gB, gC and gD are the key proteins involved in virus entry and the induction of neutralizing antibody production or protective immunity [2]. Variations in gB, gC and gD contribute to PRV variant escape from the immunity provided by Bartha-K61 [21,48,49]. To this end, we also detected variations in gB, gC and gD in the two isolates. The results showed that most novel aa mutations of gB and gD are mainly scattered on the surface of the protein molecule. Thus, we speculated that the aa mutations of gB or gD in the two isolates might cause antigenic drift.

It has been reported that PRV variants are highly virulent [15–17]. In a mouse model, the LD₅₀ values of variant strains JS-2012 and TJ were 10^{3.0} TCID₅₀ and 10^{2.3} TCID₅₀ [15,48], respectively. However, in our study, we found that the LD₅₀ values of SX1910 (10^{3.84} TCID₅₀) and SX1911 (10^{4.42} TCID₅₀) in mice were lower than those of the JS-2012 and TJ strains, indicating that the two isolates might be less pathogenic PRV variants. Additionally, Zhou et al. isolated a moderately pathogenic PRV variant strain, SD1401, in Shandong Province, China [50]. These data suggested that some PRV variants might be undergoing low-pathogenicity evolution, which might lead to genetic diversity in variant strains in pig farms.

Previous studies indicated that the Bartha-K61 vaccine could not provide effective protection against PRV variants [18–21]. In contrast, we provided evidence that Bartha-K61 could provide better protection via a high immunization dose. In addition, Wang et al. found that Bartha-K61, at a dose of 1 × 10⁵ TCID₅₀ per animal, protected pigs from sublethal challenge with the variant strain XJ5, whereas lower doses of Bartha-K61 alone did not protect pigs against this challenge [51]. The clinical protective efficiency usually depends on the immune responses induced by the vaccine and the virulence of the virus. Thus, in addition to the immune response induced by the high dose of vaccine, we also speculated that the variant strain SX1911 is a moderately pathogenic strain, so SX1911 might not overwhelm the host immunity provided by Bartha-K61. To date, based on the genetic backbone of variant strains, more novel PRV vaccines have been constructed or licensed and put on the market [52–54]. These vaccines showed better protection than Bartha-K61 against variant strains from the field. Surprisingly, our studies showed that immunization with SX1911-ΔgE/gI and Bartha-K61 resulted in equal mortality when the mice were challenged with SX1911. However, it should be noted that a lower neutralization titer, higher viral load and more severe microscopic lesions were displayed in Bartha-K61-vaccinated mice. Collectively, our results provide useful information for vaccination interventions when choosing the Bartha-K61 vaccine to eradicate PRV variants. Moreover, SX1911-ΔgE/gI is a promising vaccine candidate for the effective control of the current epidemic of PR in China.

Supplementary Materials: The following supporting information can be downloaded at: <https://www.mdpi.com/article/10.3390/v15061237/s1>, Figure S1: Comparison of the whole-genome sequence conservation between strain SX1910 and other PRV strains; Table S1: Primers for amplification of genes in this study; Table S2: The PRV reference strains used in this study; Table S3: oligos to construct the sgRNA plasmid used in this study.

Author Contributions: J.R. and W.-x.T. conceptualized the experiments; J.R. developed the methods and performed the investigation and data validation; S.T., X.C., J.Y. and Z.N. performed the investigation; Y.W., L.M., X.G., S.N., L.L., J.L. and Y.Z. contributed reagents and analyzed the data; J.R. drafted the original manuscript and revised the paper. All authors have read and agreed to the published version of the manuscript.

Funding: This work was supported by grants from the National Natural Science Foundation of China (Grant No. 32202786), the Science and Technology Innovation Program of Shanxi Agricultural University (Grant No. 2020BQ59), the special Fund for Science and Technology Innovation Teams of Shanxi Province (Grant No. 202204051001022), the Fund for Shanxi “1331 Project” (Grant No. 20211331-13), the University Science and Technology Innovation Project of Shanxi Province (Grant No. 2021L145), the Scientific Research Project of Shanxi Province Doctoral Graduates and Postdoctoral Researchers to Work in Shanxi Province (Grant No. SXBYKY2021036), the Innovation Projects of the College of Veterinary Medicine, Shanxi Agricultural University (Grant No. DY-Q008), Shanxi Key Laboratory of Protein Structure Determination (Grant No. 202104010910006) and the Scientific Research Project of Colleges and Universities in Henan Province (Grant No. 22B230001). The funders had no role in the study design, data collection and analysis, decision to publish the paper, or preparation of the manuscript.

Institutional Review Board Statement: All the animal experiments were approved by the Laboratory Animal Ethical and Welfare Committee of Shanxi Agricultural University (license number: SXAU-EAW-2021M.JF.009012001). All animal experiments were performed according to the Chinese Regulations for Laboratory Animals—The Guidelines for the Care of Laboratory Animals (Ministry of Science and Technology of People’s Republic of China) and the Laboratory Animal Requirements for Environment and Housing Facilities (National Laboratory Animal Standardization Technical Committee).

Informed Consent Statement: Not applicable.

Data Availability Statement: All data generated or analyzed during this study are included in the published article.

Conflicts of Interest: The authors declare no conflict of interest.

References

1. Mettenleiter, T.C. Aujeszky’s disease (pseudorabies) virus: The virus and molecular pathogenesis—state of the art, June 1999. *Vet. Res.* **2000**, *31*, 99–115. [CrossRef] [PubMed]
2. Pomeranz, L.E.; Reynolds, A.E.; Hengartner, C.J. Molecular biology of pseudorabies virus: Impact on neurovirology and veterinary medicine. *Microbiol. Mol. Biol. Rev. MMBR* **2005**, *69*, 462–500. [CrossRef] [PubMed]
3. Muller, T.; Hahn, E.C.; Tottewitz, F.; Kramer, M.; Klupp, B.G.; Mettenleiter, T.C.; Freuling, C. Pseudorabies virus in wild swine: A global perspective. *Arch. Virol.* **2011**, *156*, 1691–1705. [CrossRef] [PubMed]
4. Lee, J.Y.; Wilson, M.R. A review of pseudorabies (Aujeszky’s disease) in pigs. *Can. Vet. J.* **1979**, *20*, 65–69.
5. Sun, Y.; Luo, Y.; Wang, C.H.; Yuan, J.; Li, N.; Song, K.; Qiu, H.J. Control of swine pseudorabies in China: Opportunities and limitations. *Vet. Microbiol.* **2016**, *183*, 119–124. [CrossRef]
6. Freuling, C.M.; Muller, T.F.; Mettenleiter, T.C. Vaccines against pseudorabies virus (PrV). *Vet. Microbiol.* **2017**, *206*, 3–9. [CrossRef]
7. Mettenleiter, T.C. Aujeszky’s Disease and the Development of the Marker/DIVA Vaccination Concept. *Pathogens* **2020**, *9*, 563. [CrossRef]
8. Laval, K.; Enquist, L.W. The Neuropathic Itch Caused by Pseudorabies Virus. *Pathogens* **2020**, *9*, 254. [CrossRef]
9. Zheng, H.H.; Fu, P.F.; Chen, H.Y.; Wang, Z.Y. Pseudorabies Virus: From Pathogenesis to Prevention Strategies. *Viruses* **2022**, *14*, 1638. [CrossRef]
10. Delva, J.L.; Nauwynck, H.J.; Mettenleiter, T.C.; Favoreel, H.W. The Attenuated Pseudorabies Virus Vaccine Strain Bartha K61: A Brief Review on the Knowledge Gathered during 60 Years of Research. *Pathogens* **2020**, *9*, 897. [CrossRef]
11. Pannett, G.R.; Motha, M.X.; MacDiarmid, S.C. Eradication of Aujeszky’s disease from New Zealand pig herds 1976–1997. *Vet. Rec.* **1999**, *144*, 365–369. [CrossRef] [PubMed]
12. Yang, H. Epidemic status and characteristics of swine pseudorabies [in Chinese]. *Swine Indus. Sci.* **2016**, *33*, 38.


13. An, T.Q.; Peng, J.M.; Tian, Z.J.; Zhao, H.Y.; Li, N.; Liu, Y.M.; Chen, J.Z.; Leng, C.L.; Sun, Y.; Chang, D.; et al. Pseudorabies virus variant in Bartha-K61-vaccinated pigs, China, 2012. *Emerg. Infect. Dis.* **2013**, *19*, 1749–1755. [CrossRef] [PubMed]
14. Yu, X.; Zhou, Z.; Hu, D.; Zhang, Q.; Han, T.; Li, X.; Gu, X.; Yuan, L.; Zhang, S.; Wang, B.; et al. Pathogenic pseudorabies virus, China, 2012. *Emerg. Infect. Dis.* **2014**, *20*, 102–104. [CrossRef] [PubMed]
15. Luo, Y.; Li, N.; Cong, X.; Wang, C.H.; Du, M.; Li, L.; Zhao, B.; Yuan, J.; Liu, D.D.; Li, S.; et al. Pathogenicity and genomic characterization of a pseudorabies virus variant isolated from Bartha-K61-vaccinated swine population in China. *Vet. Microbiol.* **2014**, *174*, 107–115. [CrossRef]
16. Tong, W.; Liu, F.; Zheng, H.; Liang, C.; Zhou, Y.J.; Jiang, Y.F.; Shan, T.L.; Gao, F.; Li, G.X.; Tong, G.Z. Emergence of a Pseudorabies virus variant with increased virulence to piglets. *Vet. Microbiol.* **2015**, *181*, 236–240. [CrossRef]
17. Yang, Q.Y.; Sun, Z.; Tan, F.F.; Guo, L.H.; Wang, Y.Z.; Wang, J.; Wang, Z.Y.; Wang, L.L.; Li, X.D.; Xiao, Y.; et al. Pathogenicity of a currently circulating Chinese variant pseudorabies virus in pigs. *World J. Virol.* **2016**, *5*, 23–30. [CrossRef]
18. Wang, C.H.; Yuan, J.; Qin, H.Y.; Luo, Y.; Cong, X.; Li, Y.; Chen, J.; Li, S.; Sun, Y.; Qiu, H.J. A novel gE-deleted pseudorabies virus (PRV) provides rapid and complete protection from lethal challenge with the PRV variant emerging in Bartha-K61-vaccinated swine population in China. *Vaccine* **2014**, *32*, 3379–3385. [CrossRef]
19. Gu, Z.; Dong, J.; Wang, J.; Hou, C.; Sun, H.; Yang, W.; Bai, J.; Jiang, P. A novel inactivated gE/gI deleted pseudorabies virus (PRV) vaccine completely protects pigs from an emerged variant PRV challenge. *Virus Res.* **2015**, *195*, 57–63. [CrossRef]
20. Hu, R.M.; Zhou, Q.; Song, W.B.; Sun, E.C.; Zhang, M.M.; He, Q.G.; Chen, H.C.; Wu, B.; Liu, Z.F. Novel pseudorabies virus variant with defects in TK, gE and gI protects growing pigs against lethal challenge. *Vaccine* **2015**, *33*, 5733–5740. [CrossRef]
21. Ren, J.; Wang, H.; Zhou, L.; Ge, X.; Guo, X.; Han, J.; Yang, H. Glycoproteins C and D of PRV Strain HB1201 Contribute Individually to the Escape From Bartha-K61 Vaccine-Induced Immunity. *Front. Microbiol.* **2020**, *11*, 323. [CrossRef]
22. Ye, C.; Zhang, Q.Z.; Tian, Z.J.; Zheng, H.; Zhao, K.; Liu, F.; Guo, J.C.; Tong, W.; Jiang, C.G.; Wang, S.J.; et al. Genomic characterization of emergent pseudorabies virus in China reveals marked sequence divergence: Evidence for the existence of two major genotypes. *Virology* **2015**, *483*, 32–43. [CrossRef] [PubMed]
23. Ye, C.; Guo, J.C.; Gao, J.C.; Wang, T.Y.; Zhao, K.; Chang, X.B.; Wang, Q.; Peng, J.M.; Tian, Z.J.; Cai, X.H.; et al. Genomic analyses reveal that partial sequence of an earlier pseudorabies virus in China is originated from a Bartha-vaccine-like strain. *Virology* **2016**, *491*, 56–63. [CrossRef] [PubMed]
24. Dong, J.; Gu, Z.; Jin, L.; Lv, L.; Wang, J.; Sun, T.; Bai, J.; Sun, H.; Wang, X.; Jiang, P. Polymorphisms affecting the gE and gI proteins partly contribute to the virulence of a newly-emergent highly virulent Chinese pseudorabies virus. *Virology* **2018**, *519*, 42–52. [CrossRef]
25. Zhai, X.; Zhao, W.; Li, K.; Zhang, C.; Wang, C.; Su, S.; Zhou, J.; Lei, J.; Xing, G.; Sun, H.; et al. Genome Characteristics and Evolution of Pseudorabies Virus Strains in Eastern China from 2017 to 2019. *Virol. Sin.* **2019**, *34*, 601–609. [CrossRef]
26. Liu, J.; Chen, C.; Li, X. Novel Chinese pseudorabies virus variants undergo extensive recombination and rapid interspecies transmission. *Transbound. Emerg. Dis.* **2020**, *67*, 2274–2276. [CrossRef] [PubMed]
27. Hu, R.; Wang, L.; Liu, Q.; Hua, L.; Huang, X.; Zhang, Y.; Fan, J.; Chen, H.; Song, W.; Liang, W.; et al. Whole-Genome Sequence Analysis of Pseudorabies Virus Clinical Isolates from Pigs in China between 2012 and 2017 in China. *Viruses* **2021**, *13*, 1322. [CrossRef] [PubMed]
28. Lin, W.; Shao, Y.; Tan, C.; Shen, Y.; Zhang, X.; Xiao, J.; Wu, Y.; He, L.; Shao, G.; Han, M.; et al. Commercial vaccine against pseudorabies virus: A hidden health risk for dogs. *Vet. Microbiol.* **2019**, *233*, 102–112. [CrossRef]
29. Fan, S.; Yuan, H.; Liu, L.; Li, H.; Wang, S.; Zhao, W.; Wu, Y.; Wang, P.; Hu, Y.; Han, J.; et al. Pseudorabies virus encephalitis in humans: A case series study. *J. Neurovirol.* **2020**, *26*, 556–564. [CrossRef]
30. Ou, J.; Cai, S.; Zheng, F.; Lu, G.; Zhang, G. Human pseudorabies virus infection: A new threat in China. *J. Infect.* **2020**, *80*, 578–606. [CrossRef]
31. Tu, L.; Lian, J.; Pang, Y.; Liu, C.; Cui, S.; Lin, W. Retrospective detection and phylogenetic analysis of pseudorabies virus in dogs in China. *Arch. Virol.* **2021**, *166*, 91–100. [CrossRef] [PubMed]
32. Reed, L.J.; Muench, H. A simple method of estimating fifty per cent endpoints. *Am. J. Epidemiol.* **1938**, *27*, 493–497. [CrossRef]
33. Szpara, M.L.; Tafuri, Y.R.; Enquist, L.W. Preparation of viral DNA from nucleocapsids. *J. Vis. Exp. JoVE* **2011**, *54*, e3151.
34. Hirt, B. Selective extraction of polyoma DNA from infected mouse cell cultures. *J. Mol. Biol.* **1967**, *26*, 365–369. [CrossRef] [PubMed]
35. Tan, L.; Yao, J.; Yang, Y.; Luo, W.; Yuan, X.; Yang, L.; Wang, A. Current Status and Challenge of Pseudorabies Virus Infection in China. *Virol. Sin.* **2021**, *36*, 588–607. [CrossRef] [PubMed]
36. Zheng, H.H.; Bai, Y.L.; Xu, T.; Zheng, L.L.; Li, X.S.; Chen, H.Y.; Wang, Z.Y. Isolation and Phylogenetic Analysis of Reemerging Pseudorabies Virus Within Pig Populations in Central China During 2012 to 2019. *Front. Vet. Sci.* **2021**, *8*, 764982. [CrossRef]
37. Bo, Z.; Li, X. A Review of Pseudorabies Virus Variants: Genomics, Vaccination, Transmission, and Zoonotic Potential. *Viruses* **2022**, *14*, 1003. [CrossRef]
38. Liu, Q.; Kuang, Y.; Li, Y.; Guo, H.; Zhou, C.; Guo, S.; Tan, C.; Wu, B.; Chen, H.; Wang, X. The Epidemiology and Variation in Pseudorabies Virus: A Continuing Challenge to Pigs and Humans. *Viruses* **2022**, *14*, 1463. [CrossRef]
39. Liu, H.; Shi, Z.; Liu, C.; Wang, P.; Wang, M.; Wang, S.; Liu, Z.; Wei, L.; Sun, Z.; He, X.; et al. Implication of the Identification of an Earlier Pseudorabies Virus (PRV) Strain HLJ-2013 to the Evolution of Chinese PRVs. *Front. Microbiol.* **2020**, *11*, 612474. [CrossRef]

40. Rice, S.A.; Davido, D.J. HSV-1 ICP22: Hijacking host nuclear functions to enhance viral infection. *Future Microbiol.* **2013**, *8*, 311–321. [CrossRef]
41. Takacs, I.F.; Tombacz, D.; Berta, B.; Prazsak, I.; Poka, N.; Boldogkoi, Z. The ICP22 protein selectively modifies the transcription of different kinetic classes of pseudorabies virus genes. *BMC Mol. Biol.* **2013**, *14*, 2. [CrossRef] [PubMed]
42. Zaichick, S.V.; Bohannon, K.P.; Hughes, A.; Sollars, P.J.; Pickard, G.E.; Smith, G.A. The herpesvirus VP1/2 protein is an effector of dynein-mediated capsid transport and neuroinvasion. *Cell Host Microbe* **2013**, *13*, 193–203. [CrossRef] [PubMed]
43. Zhang, Y.; Liu, S.; Jiang, H.; Deng, H.; Dong, C.; Shen, W.; Chen, H.; Gao, C.; Xiao, S.; Liu, Z.F.; et al. G(2)-quadruplex in the 3'UTR of IE180 regulates Pseudorabies virus replication by enhancing gene expression. *RNA Biol.* **2020**, *17*, 816–827. [CrossRef] [PubMed]
44. Brandt, C.R.; Kolb, A.W.; Shah, D.D.; Pumfery, A.M.; Kintner, R.L.; Jaehnig, E.; Van Gompel, J.J. Multiple determinants contribute to the virulence of HSV ocular and CNS infection and identification of serine 34 of the US1 gene as an ocular disease determinant. *Investig. Ophthalmol. Vis. Sci.* **2003**, *44*, 2657–2668. [CrossRef]
45. O'Toole, J.M.; Aubert, M.; Kotsakis, A.; Blaho, J.A. Mutation of the protein tyrosine kinase consensus site in the herpes simplex virus 1 alpha22 gene alters ICP22 posttranslational modification. *Virology* **2003**, *305*, 153–167. [CrossRef]
46. Mostafa, H.H.; Davido, D.J. Herpes simplex virus 1 ICP22 but not US 1.5 is required for efficient acute replication in mice and VICE domain formation. *J. Virol.* **2013**, *87*, 13510–13519. [CrossRef]
47. Wu, Y.; Tan, S.; He, Q.; Wang, M.; Chen, S.; Jia, R.; Yang, Q.; Zhu, D.; Liu, M.; Zhao, X.; et al. Deletion of Double Copies of the US1 Gene Reduces the Infectivity of Recombinant Duck Plague Virus In Vitro and In Vivo. *Microbiol. Spectr.* **2022**, *10*, e0114022. [CrossRef]
48. Yu, Z.Q.; Tong, W.; Zheng, H.; Li, L.W.; Li, G.X.; Gao, F.; Wang, T.; Liang, C.; Ye, C.; Wu, J.Q.; et al. Variations in glycoprotein B contribute to immunogenic difference between PRV variant JS-2012 and Bartha-K61. *Vet. Microbiol.* **2017**, *208*, 97–105. [CrossRef]
49. Zhang, C.; Liu, Y.; Chen, S.; Qiao, Y.; Guo, M.; Zheng, Y.; Xu, M.; Wang, Z.; Hou, J.; Wang, J. A gD&gC-substituted pseudorabies virus vaccine strain provides complete clinical protection and is helpful to prevent virus shedding against challenge by a Chinese pseudorabies variant. *BMC Vet. Res.* **2019**, *15*, 2.
50. Zhou, M.; Wu, X.; Jiang, D.; Sui, C.; Chen, L.; Cong, X.; Xin, X.; Wang, G.; Li, Y.; Tian, F.; et al. Characterization of a moderately pathogenic pseudorabies virus variant isolated in China, 2014. *Infect. Genet. Evol.* **2019**, *68*, 161–171. [CrossRef]
51. Wang, J.; Cui, X.; Wang, X.; Wang, W.; Gao, S.; Liu, X.; Kai, Y.; Chen, C. Efficacy of the Bartha-K61 vaccine and a gE⁻/gI⁻/TK⁻ prototype vaccine against variant porcine pseudorabies virus (vPRV) in piglets with sublethal challenge of vPRV. *Res. Vet. Sci.* **2020**, *128*, 16–23. [CrossRef] [PubMed]
52. Cong, X.; Lei, J.L.; Xia, S.L.; Wang, Y.M.; Li, Y.; Li, S.; Luo, Y.; Sun, Y.; Qiu, H.J. Pathogenicity and immunogenicity of a gE/gI/TK gene-deleted pseudorabies virus variant in susceptible animals. *Vet. Microbiol.* **2016**, *182*, 170–177. [CrossRef] [PubMed]
53. Tong, W.; Li, G.; Liang, C.; Liu, F.; Tian, Q.; Cao, Y.; Li, L.; Zheng, X.; Zheng, H.; Tong, G. A live, attenuated pseudorabies virus strain JS-2012 deleted for gE/gI protects against both classical and emerging strains. *Antivir. Res.* **2016**, *130*, 110–117. [CrossRef] [PubMed]
54. Dong, J.; Bai, J.; Sun, T.; Gu, Z.; Wang, J.; Sun, H.; Jiang, P. Comparative pathogenicity and immunogenicity of triple and double gene-deletion pseudorabies virus vaccine candidates. *Res. Vet. Sci.* **2017**, *115*, 17–23. [CrossRef] [PubMed]

Disclaimer/Publisher's Note: The statements, opinions and data contained in all publications are solely those of the individual author(s) and contributor(s) and not of MDPI and/or the editor(s). MDPI and/or the editor(s) disclaim responsibility for any injury to people or property resulting from any ideas, methods, instructions or products referred to in the content.

Article

Establishment and Application of a Triplex Real-Time RT-PCR Assay for Differentiation of PEDV, PoRV, and PDCoV

Wenwen Hou ¹, Maodi Fan ¹, Zhenbang Zhu ¹ and Xiangdong Li ^{1,2,*} 

¹ Jiangsu Co-Innovation Center for Prevention and Control of Important Animal Infectious Diseases and Zoonoses, College of Veterinary Medicine, Yangzhou University, Yangzhou 225009, China

² Key Laboratory of Protection & Utilization of Biological Resources in Tarim Basin, College of Life Sciences, Tarim University, Alar 843399, China

* Correspondence: 007352@yzu.edu.cn

Abstract: Porcine viral diarrhea is very common in clinical practice and has caused huge losses to the pig industry. Porcine epidemic diarrhea virus (PEDV), porcine rotavirus (PoRV), and porcine deltacoronavirus (PDCoV) are important pathogens of porcine viral diarrhea. Co-infection situations among these three viruses in clinics are common, which increases the difficulty of differential diagnosis. Currently, polymerase chain reaction (PCR) is commonly used to detect pathogens. TaqMan real-time PCR is more sensitive than conventional PCR and has better specificity and accuracy. In this study, a triplex real-time RT-PCR assay based on TaqMan probes was developed for differential detection of PEDV, PoRV, and PDCoV. The triplex real-time RT-PCR assay developed in this study could not detect unrelated pathogens and showed satisfactory specificity, sensitivity, repeatability, and reproducibility with a limit of detection (LOD) of 6.0×10^1 copies/ μ L. Sixteen clinical samples were used to compare the results of the commercial RT-PCR kit and the triplex RT-PCR for PEDV, PoRV, and PDCoV detection, and the results were completely consistent. A total of 112 piglet diarrhea samples collected from Jiangsu province were next used to study the local prevalence of PEDV, PoRV, and PDCoV. The positive rates of PEDV, PoRV, and PDCoV detected by the triplex real-time RT-PCR were 51.79% (58/112), 59.82% (67/112), and 2.68% (3/112), respectively. The co-infections of PEDV and PoRV were frequent (26/112, 23.21%), followed by the co-infections of PDCoV and PoRV (2/112, 1.79%). This study established a useful tool for simultaneous differentiation of PEDV, PoRV, and PDCoV in practice and provided valuable information on the prevalence of these diarrhea viral pathogens in Jiangsu province.



Citation: Hou, W.; Fan, M.; Zhu, Z.; Li, X. Establishment and Application of a Triplex Real-Time RT-PCR Assay for Differentiation of PEDV, PoRV, and PDCoV. *Viruses* **2023**, *15*, 1238. <https://doi.org/10.3390/v15061238>

Academic Editor: Douglas Gladue

Received: 4 May 2023

Revised: 22 May 2023

Accepted: 24 May 2023

Published: 25 May 2023



Copyright: © 2023 by the authors. Licensee MDPI, Basel, Switzerland. This article is an open access article distributed under the terms and conditions of the Creative Commons Attribution (CC BY) license (<https://creativecommons.org/licenses/by/4.0/>).

Keywords: triplex real-time RT-PCR; porcine epidemic diarrhea virus; porcine rotavirus; porcine deltacoronavirus

1. Introduction

Porcine viral diarrhea leads to a high mortality rate in piglets and causes serious economic losses to the pig industry all over the world [1]. Porcine epidemic diarrhea virus (PEDV), porcine rotavirus (PoRV), and porcine deltacoronavirus (PDCoV) are important clinical pathogens causing viral diarrhea in pigs [2,3]. PEDV is a member of the genus *Alphacoronavirus* in the family *Coronaviridae*, which is an enveloped, single-stranded positive-sense RNA virus. PEDV particles are spherical with different sizes; the average diameter is about 130 nm, and the total length of the PEDV genome is about 28 kb [4]. Porcine epidemic diarrhea (PED) was first reported in England in 1971 [5], then broke out again in Belgium in 1977 [6]. The first report of PED in China was in 1973, and it was not confirmed as PED until 1984 [7]. Since October 2010, PEDV has suddenly erupted on a large scale in China, and the mortality of newborn piglets has increased significantly, which indicates the emergence of a new variant virulent strain. In April 2013, the United States of America experienced the first outbreak of highly pathogenic PEDV infection [8], and the epidemic has gradually spread to a wide range. Currently, PEDV has spread

widely to many parts of the world [7]. PoRV belongs to the genus *Rotavirus* in the family *Reoviridae* [9]. PoRV is a non-enveloped, double-stranded RNA virus [10]. The full length of the PoRV genome is about 18,500 bp, which is composed of 11 segments of dsRNA. They encode six structural proteins (VP1~VP4, VP6, and VP7) and five non-structural proteins (NSP1~NSP5/6). PoRV is divided into seven serogroups (A–J) based on VP6 [11]. Subgroup A rotavirus is the main rotavirus causing gastrointestinal disease in swine, with high pathogenicity and prevalence. Subgroup B was first reported and described as a rotavirus-like agent in 1985 [12]. Subgroup C was first isolated from swine in 1980. Currently, subgroups A, B, C, E, and H have been described in swine. Due to its complex co-infection situation, high variability, and worldwide distribution, PoRV has gradually become an important porcine diarrhea pathogen [11]. PDCoV is a member of the genus *Deltacoronavirus* in the family *Coronaviridae*. PDCoV is an enveloped, single-stranded positive-stranded RNA virus, and its genome size is approximately 25.4 kb (excluding the poly A-tail) [13]. In 2012, PDCoV was first reported in Hong Kong, China [14], then it was reported in the United States of America in 2014 and quickly spread to many states in a very short time [15–17]. The virus was also detected in Canada, South Korea, and Thailand in succession [18].

PEDV, PoRV, and PDCoV can cause similar clinical symptoms, including vomiting, diarrhea, and dehydration in piglets. Meanwhile, the pathological changes among them are also very similar and difficult to distinguish. In addition, co-infections and secondary infections among PEDV, PoRV, and PDCoV are very common, which makes clinical diagnosis quite difficult [19]. Therefore, there is an urgent need in the clinic to establish a rapid and efficient molecular method to differentiate them.

2. Materials and Methods

2.1. Viruses, Primers, and Probes

The DNA samples of pseudorabies virus (PRV), porcine circovirus 2 (PCV2), porcine circovirus 3 (PCV3), and cDNA samples of PEDV, PoRV, PDCoV, classical swine fever virus (CSFV), and porcine reproductive and respiratory syndrome virus (PRRSV) were stored in our laboratory at $-20\text{ }^{\circ}\text{C}$ until use. To acquire specific primers and probes, the primers and probes of PDCoV were adapted from the reference [20]. For PEDV and PoRV, we downloaded at least 20 genome sequences of PEDV and PoRV from NCBI for comparison and analysis. Primer Express 3.0 software (Applied Biosystems, Foster City, CA, USA) was used to design the primers and probes based on their most conserved regions. The TaqMan probes for PEDV, PoRV, and PDCoV were labeled with FAM, ROX, and TAMRA at the 5' end, respectively, and all quenchers at the 3' end were MGB (Table 1). Primers and probes were synthesized in Sangon (Shanghai, China).

Table 1. Primers and probes used in this study. F, R, and P indicate forward primer, reverse primer, and probe, respectively.

Viruses	Primers/Probes	Sequences (5'–3')	Reference
PEDV	PEDV-M-F	CACTCCTTAGTGGTACATTGCTTGTAGA	This study
	PEDV-M-R	CCTTGGCGACTGTGACGAA	This study
	PEDV-M-P	FAM-ACAGGTAAGTCAATTACC-MGB	This study
PoRV	PoRV-NSP5-F	GAAGTCTCCAGAGGATATTGGACC	This study
	PoRV-NSP5-R	TCTTAAGTGCATTTCGATCTAATCGA	This study
	PoRV-NSP5-P	ROX-CTGATTCTGCTTCAAACG-MGB	This study
PDCoV	PDCoV-N-F	CCTACTACTGACGCGTCTTGGTT	Adapted from [20]
	PDCoV-N-R	TGCCACGAAACTGAGGATGA	Adapted from [20]
	PDCoV-N-P	TAMRA-TGCTCAAAGCTCAAAC-MGB	Adapted from [20]

2.2. Clinical Samples and Nucleic Acid Extraction

A total of 128 small intestine tissue samples from piglets with diarrhea symptoms were collected from 16 pig farms in 10 cities in Jiangsu province from 2021 to 2022. Among them, 16 samples were used for comparison between commercial single-plex real-time RT-PCR detection kits (Beijing Anheal Laboratories Co., Ltd.) and the established triplex real-time RT-PCR assay in this study. The rest of the 112 samples were only used to investigate the prevalence of PEDV, PoRV, and PDCoV using the triplex real-time RT-PCR assay. The mixture of intestinal contents and PBS was in a 1:5 ratio and subjected to centrifugation at 4 °C, 5000 rpm, for 10 min. The supernatant was then used to extract RNA using TRNzol Universal Reagent (DP424) (TIANGEN BIOTECH, Beijing, China) and reverse transcribe into first-strand cDNA using HiScript III 1st Strand cDNA Synthesis Kit (+gDNA wiper) (Vazyme, Nanjing, China). The steps of reverse transcription included denaturation of the RNA template, removal of genomic DNA, and synthesis of the 1st strand cDNAs. A total volume of 20 µL of reaction solution was instantly centrifuged and placed in an applied biosystems PCR cycler (Thermo Fisher Scientific, Waltham, MA USA). After 25 °C for 5 min, 37 °C for 45 min, and 85 °C for 5 s, the synthesized cDNA was used as a template for triplex real-time RT-PCR or commercial single-plex real-time RT-PCR.

2.3. Development and Optimization of the Triplex Real-Time RT-PCR

The concentrations of primers and probes were optimized as previously described [21]. After optimization, the triplex real-time RT-PCR reaction in a total volume of 20 µL was as follows: Premix Ex Taq 10 µL (Takara, China), cDNA templates 2 µL, primers (PEDV-M-F/R, PoRV-NSP5-F/R, or PDCoV-N-F/R) (10 µM) 0.5 µL for each of them, probes (PEDV-M-P, PoRV-NSP5-P, or PDCoV-N-P) (10 µM) 0.5 µL for each of them, and ddH₂O 3.5 µL. The triplex real-time RT-PCR amplification was performed on the applied biosystems QuantStudio3 (Thermo Fisher Scientific, USA); the amplification condition was set at 95 °C for 30 s, followed by 40 cycles of 95 °C for 5 s and 60 °C for 30 s, and the fluorescent signal was detected at the end of the extension step in each cycle.

2.4. Standard Curve Generation of the Triplex Real-Time RT-PCR

Amplified fragments with PEDV-M-F/R, PoRV-NSP5-F/R, or PDCoV-N-F/R were synthesized and cloned into the pUC57 vector by Genewiz (Suzhou, China). The plasmid was then used as the standard positive control. The concentration of the plasmid was converted to copy number using the following formula: y (copies/µL) = $(6.02 \times 10^{23}) \times (x(\text{ng}/\mu\text{L}) \times 10^{-9} \text{ DNA}) / (\text{DNA length} \times 660)$ [22]. The 10-fold serially diluted standard plasmids (6.0×10^1 – 6.0×10^6 copies/µL) were used as templates to generate the standard curve of the triplex real-time RT-PCR assay.

2.5. Specificity and Sensitivity of the Triplex Real-Time RT-PCR

To evaluate the specificity of the established triplex real-time RT-PCR assay, DNA samples of PRV, PCV2, PCV3, and cDNA samples of CSFV and PRRSV were applied. The sensitivity and limit of detection (LOD) of the triplex real-time RT-PCR assay developed in this study were verified by using 10-fold serially diluted standard plasmids (6.0×10^0 – 6.0×10^6 copies/µL).

2.6. Repeatability and Reproducibility of the Triplex Real-Time RT-PCR

To assess the repeatability and reproducibility of the triplex real-time RT-PCR assay, three different concentrations of 10-fold serially diluted plasmid (6.0×10^6 , 6.0×10^4 , and 6.0×10^2 copies/µL) were used to test the intra-assay variability and the inter-assay variability. For intra-assay variability, the assay was repeated three times for each dilution on the same day. As for inter-assay variability, each dilution was tested in six independent experiments by two operators on different days according to MIQE guidelines [23]. The coefficients of variation (CVs) of Ct values were calculated from the intra-assay and inter-assay results.

2.7. Comparison of the Triplex Real-Time RT-PCR with the Commercial Single-Plex RT-PCR Kit

Sixteen piglet diarrhea samples collected from Jiangsu Province that have been tested positive for PEDV, PoRV, or PDCoV by a commercial single-plex real-time RT-PCR detection kit were used to verify the established triplex real-time RT-PCR assay. The sixteen samples were tested for single infections or co-infections with PEDV, PoRV, or PDCoV.

2.8. Clinical Application of the Triplex Real-Time RT-PCR

A total of 112 small intestine tissue samples of piglets with diarrhea symptoms collected from 16 pig farms in 10 cities of Jiangsu province from 2021 to 2022 were used to study the prevalence of PEDV, PoRV, and PDCoV using the established triplex RT-PCR.

2.9. Sequencing and Phylogenetic Analysis

Representative virus strains from the positive pig farms were selected for Sanger sequencing and phylogenetic analysis (seven PEDV strains, eight PoRV strains, and one PDCoV strain). The S genes of PEDV and PDCoV and the VP4 and VP7 genes of PoRV were amplified by conventional RT-PCR. The amplicons of PEDV and PDCoV were used for sequencing, and the VP4 and VP7 genes of PoRV amplicons were linked with the pMD-19T vector before sequencing. Sequence alignments and phylogenetic trees were performed by MEGA 11 (Mega Limited, Auckland, New Zealand).

3. Results

3.1. Primers and Probes Design and Concentration Optimization

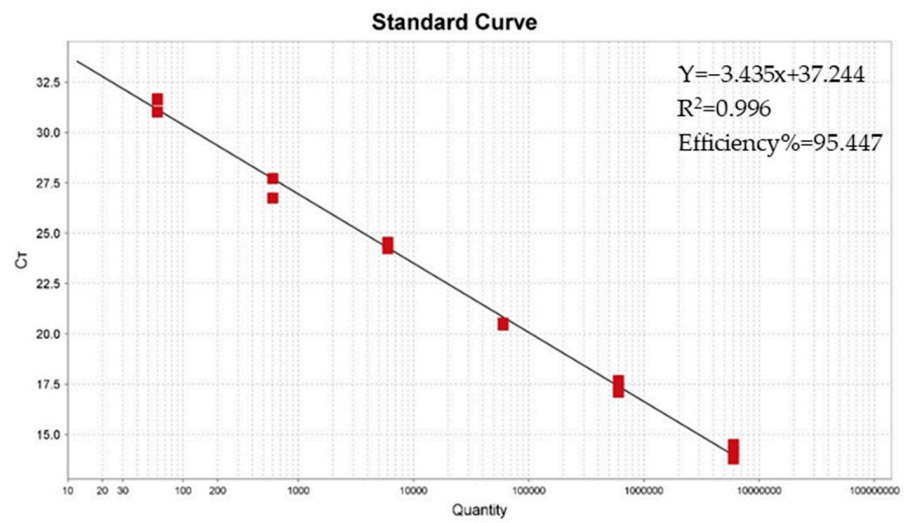
The forward primer, reverse primer, and probe of PDCoV targeted the N gene and were adapted from the reference [19]. For PEDV and PoRV, genome sequences of at least 20 reference strains were downloaded from the NCBI GenBank database for comparison and analysis. The most conserved gene sequences in the M gene of PEDV and the NSP5 gene of PoRV were selected for the design of primers and probes. The 5' ends of the probes used in this study were labeled with different fluorophores to ensure that there was no interference among the fluorescent signals of different viruses. The sequences of primers and probes were listed in Table 1. The concentrations of primers and probes were optimized as described in the Materials and Methods section. The same reaction parameters were used throughout the study.

3.2. Standard Curve of the Triplex Real-Time RT-PCR

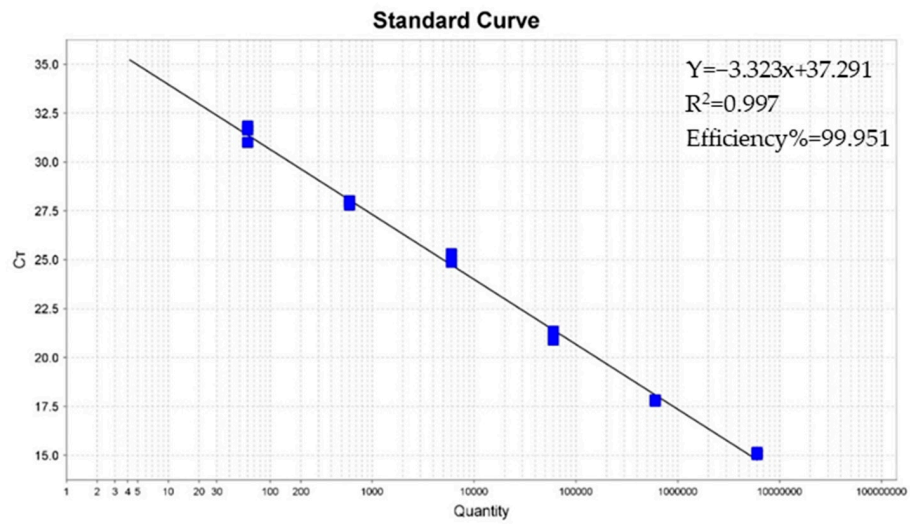
As shown in Figure 1, the standard curves of the triplex real-time RT-PCR assay were generated by using 10-fold serially diluted standard plasmids, ranging from 6.0×10^1 to 6.0×10^6 copies/ μL . The slopes of the standard curve for PEDV, PoRV, and PDCoV were -3.435 , -3.323 , and -3.753 , respectively. The correlation coefficients R^2 for PEDV, PoRV, and PDCoV were 0.996, 0.997, and 0.994, respectively.

3.3. Standard Curve of the Triplex Real-Time RT-PCR

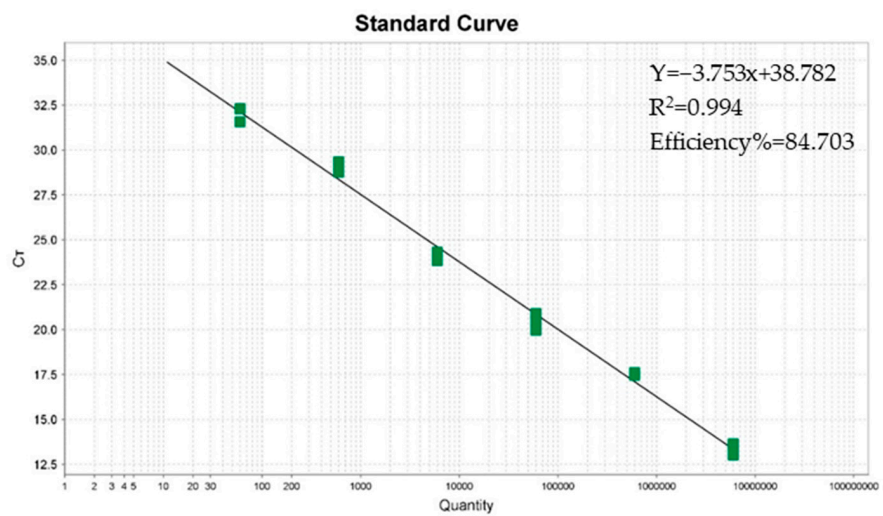
The 6.0×10^4 copies/ μL of 10-fold serially diluted standard plasmid was used as a positive control, and ddH₂O was used as a negative control. DNA samples of other common porcine viruses, including PRV, PCV2, PCV3, and cDNA samples of CSFV and PRRSV, were used to evaluate the specificity. The amplification curves showed that only corresponding FAM, ROX, and TAMRA signals for PEDV, PoRV, and PDCoV could be specifically detected, while no fluorescence signal was detected for other viruses (Figure 2). Furthermore, the fluorescent signals of these three viruses did not interfere with each other. The above results indicated that the established assay had high specificity.



(a)



(b)



(c)

Figure 1. Standard curves of the triplex real-time RT-PCR assay. (a) The standard curve for porcine epidemic diarrhea virus (PEDV); (b) the standard curve for porcine rotavirus (PoRV); (c) the standard curve for porcine deltacoronavirus (PDCoV).

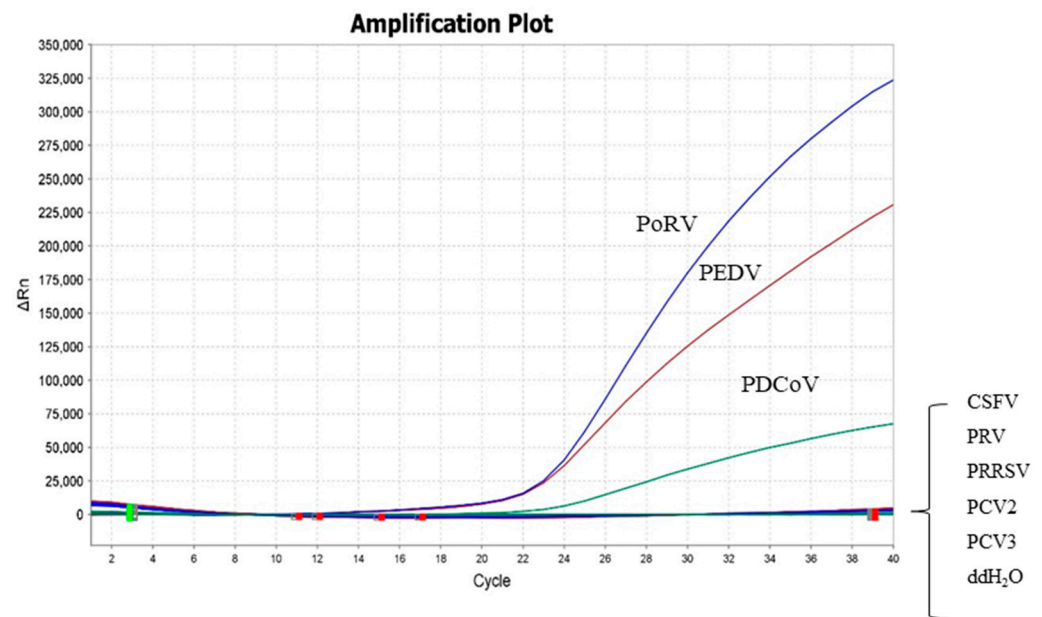


Figure 2. Specificity test of the triplex real-time RT-PCR assay. FAM, ROX, and TAMRA fluorescent signals were monitored by the triplex real-time RT-PCR assay, and the 6.0×10^4 copies/ μL of 10-fold serially diluted standard plasmid was used as a positive control. No fluorescent signal was observed for cDNA or DNA samples of other viruses.

The sensitivity of the triplex real-time RT-PCR assay was determined by using the 10-fold serially diluted standard plasmids (6.0×10^0 – 6.0×10^6 copies/ μL). ddH₂O was used as a negative control. Our results showed that the LOD of the triplex real-time RT-PCR assay for detecting PEDV, PoRV, and PDCoV was 6.0×10^1 copies/ μL (Figure 3).

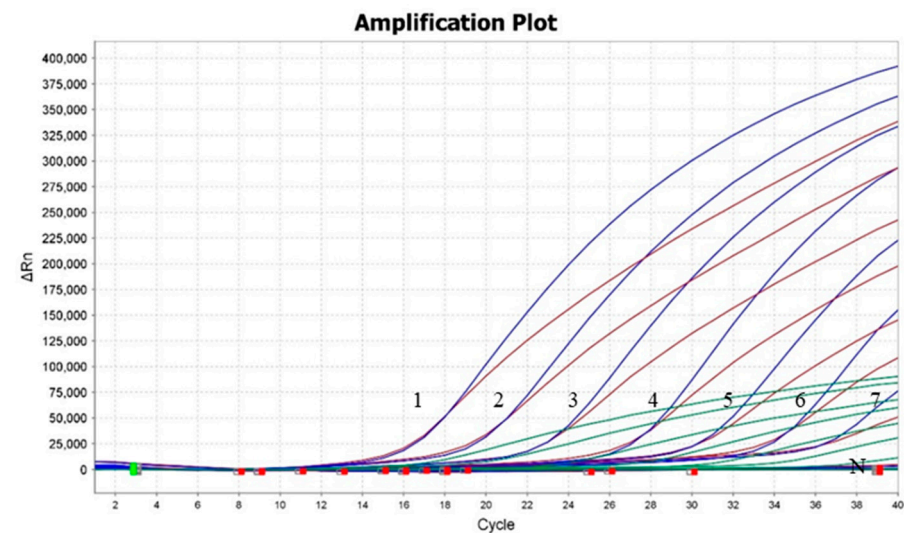


Figure 3. Sensitivity test of the triplex real-time RT-PCR assay. Labels 1–7 indicated the different concentrations of plasmids (6.0×10^6 , 6.0×10^5 , 6.0×10^4 , 6.0×10^3 , 6.0×10^2 , 6.0×10^1 , and 6.0×10^0 copies/ μL , respectively). The detection of PEDV, PoRV, and PDCoV was shown by red lines, blue lines, and green lines, respectively.

3.4. Repeatability and Reproducibility of the Triplex Real-Time RT-PCR

The intra-assay variability (repeatability) and inter-assay variability (reproducibility) were tested using three different concentrations of 10-fold serially diluted plasmid (6.0×10^2 , 6.0×10^4 , and 6.0×10^6 copies/ μL), and the results showed that the intra-assay and inter-assay CVs of Ct values ranged from 0.35% to 4.76% and 0.74% to 4.34%, respec-

tively (Table 2). The results indicated that the triplex real-time RT-PCR assay established in this study had satisfactory repeatability and reproducibility.

Table 2. Intra-repeatability and inter-reproducibility of the triplex real-time RT-PCR assay.

Standard Sample	Target	Intra-Reproductivity (Ct Value)	SD	Coefficients of Variation (%)	Inter-Reproductivity (Ct Value)	SD	Coefficients of Variation (%)
6.0×10^6 copies/ μ L	PEDV	14.15	0.36	2.56	14.35	0.49	3.41
	PoRV	15.08	0.05	0.35	15.13	0.11	0.74
	PDCoV	13.40	0.34	2.52	13.46	0.30	2.24
6.0×10^4 copies/ μ L	PEDV	20.18	0.52	2.60	20.24	0.44	2.19
	PoRV	20.99	0.10	0.48	21.08	0.20	0.93
	PDCoV	20.99	0.59	2.66	20.73	0.68	3.32
6.0×10^2 copies/ μ L	PEDV	26.00	1.12	4.32	25.23	1.02	4.04
	PoRV	27.83	1.22	4.39	27.71	1.04	3.75
	PDCoV	25.40	1.21	4.76	23.94	1.03	4.34

3.5. Comparison of the Triplex Real-Time RT-PCR with the Commercial Single-Plex Commercial RT-PCR Kit

Sixteen clinical samples were used to compare the results of the commercial RT-PCR kit and the triplex RT-PCR for PEDV, PoRV, and PDCoV detection. These 16 samples had been confirmed as PEDV, PoRV, or PDCoV positive using a commercial single-plex real-time RT-PCR detection kit. As shown in Table 3, the results shown in the commercial real-time PCR detection kit and triplex real-time RT-PCR assay were completely consistent.

Table 3. The detection results of 16 piglet diarrhea samples using the commercial single-plex real-time RT-PCR detection kit and the triplex real-time RT-PCR assay in this study.

Sample	Commercial Real-Time RT-PCR Detection Kit			Triplex Real-Time RT-PCR Assay		
	PEDV	PoRV	PDCoV	PEDV	PoRV	PDCoV
1	+	-	-	+	-	-
2	+	-	-	+	-	-
3	+	+	-	+	+	-
4	+	+	-	+	+	-
5	+	-	-	+	-	-
6	+	+	-	+	+	-
7	+	+	-	+	+	-
8	+	+	-	+	+	-
9	-	+	-	-	+	-
10	+	+	-	+	+	-
11	+	-	-	+	-	-
12	-	+	-	-	+	-
13	-	+	-	-	+	-
14	-	+	-	-	+	-
15	-	+	-	-	+	-
16	-	-	+	-	-	+

3.6. Clinical Application of the Triplex Real-Time RT-PCR

Furthermore, a total of 112 piglet diarrhea samples collected from Jiangsu province were used to investigate the local prevalence of PEDV, PoRV, and PDCoV. The positive rates of PEDV, PoRV, and PDCoV detected by the triplex real-time RT-PCR assay were 51.79% (58/112), 59.82% (67/112), and 2.68% (3/112), respectively. Furthermore, 26 out of 112 samples (23.21%) were found to be co-infected with PEDV and PoRV, and 2 out of 112 samples (1.79%) were found to be co-infected with PDCoV and PoRV (Table 4). More

specific information about the detection results of 112 clinical diarrhea samples is shown in Table S1.

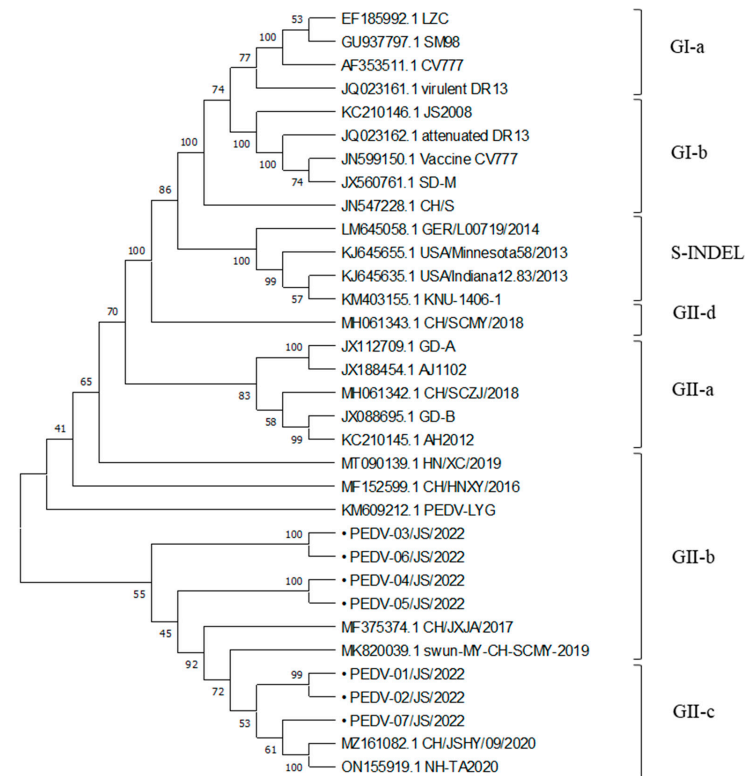
Table 4. The detection results of 112 clinical diarrhea samples.

PEDV+	PoRV+	PDCoV+	PEDV+PoRV+	PDCoV+PoRV+
58/112	67/112	3/112	26/112	2/112

3.7. Gene Sequencing and Phylogenetic Analysis

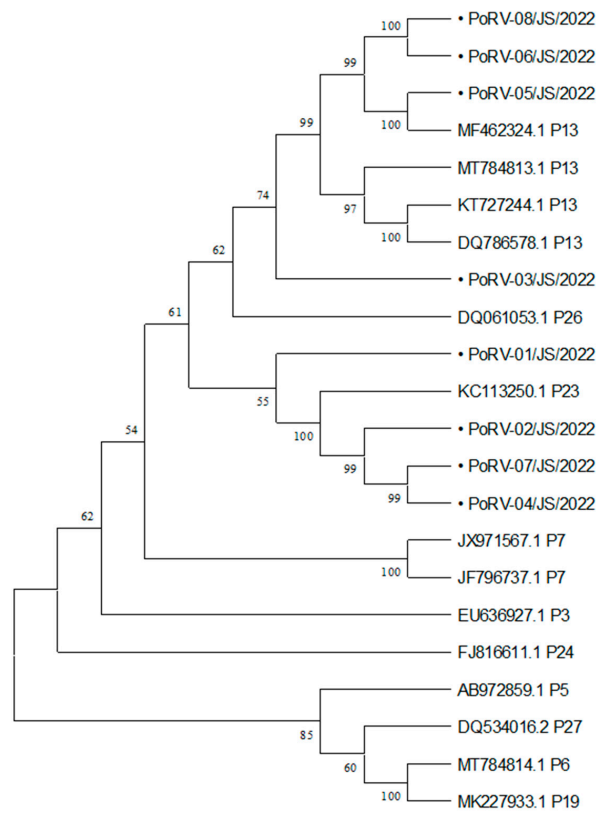
The virus strains from each positive pig farm were subjected to sequencing and phylogenetic tree analysis. The sequences have been uploaded to NCBI GenBank (PEDV S gene with GenBank accession numbers: OQ504178~OQ504184; PoRV VP4 gene with GenBank accession numbers: OQ504188~OQ504195; PoRV VP7 with GenBank accession numbers: OQ504197~OQ504204; PDCoV S gene with GenBank accession number: OQ504187).

The results of phylogenetic analysis based on the PEDV S gene showed that four PEDV-positive samples detected in this study belonged to the GII-b subtype and three samples belonged to the GII-c subtype (Figure 4a). According to the phylogenetic tree based on the PoRV VP4 gene, four strains (PoRV-01, PoRV-02, PoRV-04, and PoRV-07) belonged to the P [23] type, and another four PoRV strains (PoRV-03, PoRV-05, PoRV-06, and PoRV-08) in this study belonged to the P [13] type (Figure 4b). The results of the VP7 gene phylogenetic analysis indicated that PoRV-03, PoRV-04, and PoRV-08 strains belonged to the G4 type, PoRV-02 belonged to the G3 type, PoRV-01, PoRV-06, and PoRV-07 belonged to the G9 type, and PoRV-05 belonged to the G11 type (Figure 4c). The detailed GP types of the eight PoRV-positive samples in this study are listed in Table 5. The results of phylogenetic analysis based on the PDCoV S gene showed that one PDCoV strain in this study belonged to the China/Vietnam/Laos/Thailand branch (Figure 4d).

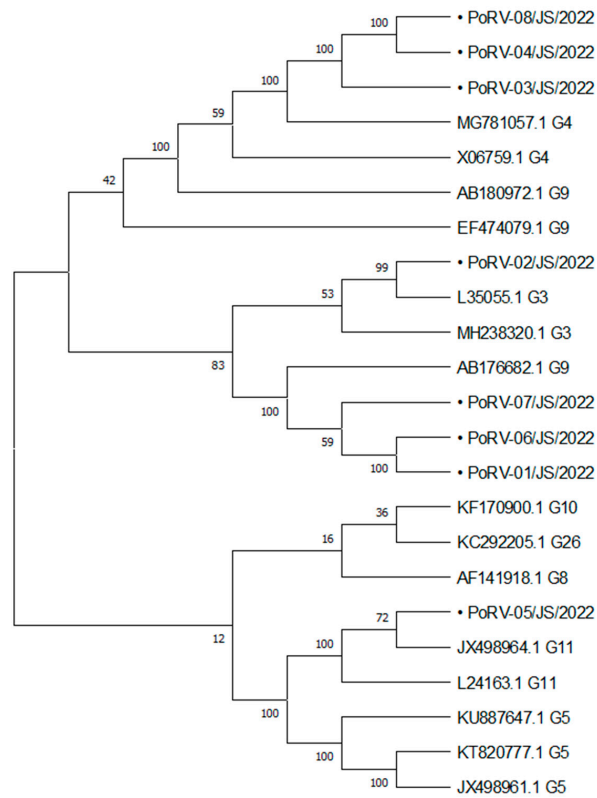


(a)

Figure 4. Cont.

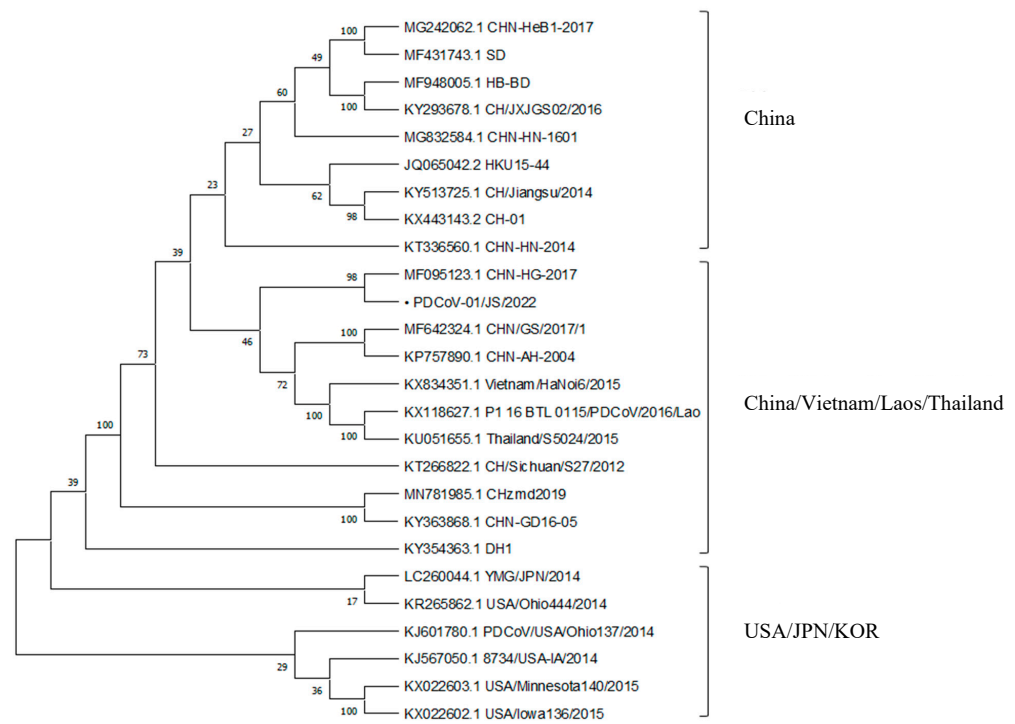


(b)



(c)

Figure 4. Cont.



(d)

Figure 4. Phylogenetic tree based on the nucleotide sequence of the PEDV S gene (a), PoRV VP4 (b), PoRV VP7 gene (c), and PDCoV S gene (d), respectively. “●” indicates the positive samples tested in this study.

Table 5. GP type of eight PoRV-positive samples in this study.

No.	Strain Name	G[P] Type
1	PoRV-01	G9 [P23]
2	PoRV-02	G3 [P23]
3	PoRV-03	G4 [P13]
4	PoRV-04	G4 [P23]
5	PoRV-05	G11 [P13]
6	PoRV-06	G9 [P13]
7	PoRV-07	G9 [P23]
8	PoRV-08	G4 [P13]

4. Discussion

Porcine viral diarrhea is a common clinical disease that can lead to a high mortality rate in piglets. PEDV, PoRV, and PDCoV are important diarrhea viruses in piglets. On account of similar clinical symptoms and co-infections among them, it presents challenges to differentiate these three important porcine diarrhea viruses in clinical practice. Since 2010, highly pathogenic strains of PEDV have appeared and spread in many countries, causing severe economic losses in the global swine industry [24]. At the same time, millions of piglets died in more than 10 provinces in southern China due to PEDV variant strains [25]. In 2014, PDCoV spread to most states in the US, which also had a huge economic impact on the local pig industry [13]. In recent years, the infection rate of PoRV has constantly increased, and the co-infection between PoRV and PEDV or PDCoV has become common. From the perspective of controlling epidemic diseases, the first step is the rapid and accurate detection of etiological pathogens. Accurate identification of pathogens and fast differential diagnosis are crucial for controlling epidemics. Therefore, it is necessary to establish a detection method to distinguish PEDV, PoRV, and PDCoV simultaneously.

Several conventional RT-PCR assays or single-plex real-time RT-PCR have been developed for the detection of PEDV, PoRV, and PDCoV [26,27]. These methods are inefficient, time-consuming, and expensive compared to multiplex RT-PCR. Therefore, we developed a triplex real-time RT-PCR detection method for PEDV, PoRV, and PDCoV differentiation in this study. The triplex real-time RT-PCR assay established in this study had satisfactory specificity, sensitivity, repeatability, and reproducibility. To evaluate the performance of the established triplex real-time RT-PCR assay, 16 clinical samples of diarrheal piglets were used to compare the results between the triplex real-time RT-PCR assay and commercial single-plex real-time RT-PCR. The results of two detection methods were confirmed to be completely consistent, which suggested the triplex real-time RT-PCR assay in this study could replace the commercial single-plex real-time RT-PCR with high efficiency to differentiate PEDV, PoRV, and PDCoV simultaneously.

Next, 112 clinical samples were detected by triplex real-time RT-PCR to investigate the prevalence of PEDV, PoRV, and PDCoV in Jiangsu province, China. The results showed that 51.79% (58/112) were PEDV positive, 59.82% (67/112) were PoRV positive, and 2.68% (3/112) were PDCoV positive, respectively. From the above results, we could conclude that PEDV and PoRV are the major porcine diarrhea pathogens in Jiangsu province. Guangming Ding et al. developed a multiplex RT-PCR for PEDV, TGEV, PoRV, porcine kobuvirus (PKV), porcine sapovirus (PsAV), and PDCoV, and the positive rates of PEDV, PoRV, and PDCoV were 19.69% (78/398), 17.59% (70/398), and 36.18% (144/398) in 398 samples collected from North, Middle, and South China between 2015 and 2017 [28]. Shuo Jia et al. established a dual priming oligonucleotide (DPO)-based real-time RT-PCR assay for PEDV, TGEV, PoRV, and PDCoV and detected 672 diarrhea samples collected in Northeast China from 2017 to 2018, and the results showed 19.05% (128/672), 4.32% (29/672), and 3.87% (26/672) positive rates for PEDV, PoRV, and PDCoV, respectively [1]. The disparity in PEDV, PRoV, and PDCoV positive rates in these studies could be attributed to differences in sample collection time and geographical distribution of sampling.

In addition, the co-infections of porcine diarrhea viruses cannot be ignored, since some co-infection status could even cause more severe symptoms. Honglei Zhang et al. conducted a prevalence analysis of PDCoV in Henan pigs. They found that co-infection between PEDV and PDCoV was approximately 60%, and the co-infection enhanced the severity of diarrhea and worsened the disease in piglets [19,29]. The co-infection of PEDV and PoRV was also supposed to be the most severe form of piglet diarrhea, and the detection rate could reach 16–25% in Northeast China. In some provinces of China, the co-infection of PEDV and PoRV even became the main reason for piglet diarrhea [30]. In our study, PoRV and PEDV co-infections accounted for 38.81% of all PoRV positive cases (26/67), PoRV and PDCoV co-infections accounted for 2.99% of all PoRV positive cases (2/67), and no PEDV and PDCoV co-infection cases were found.

To further characterize the epidemic strains of porcine diarrhea viruses in Jiangsu province, seven PEDV strains, eight PoRV strains, and one PDCoV strain were selected to construct a phylogenetic analysis. The phylogenetic tree based on the PEDV S gene could be divided into three genotypes: GI, GII, and S-INDEL. The GI type included classical strains such as CV777 and SD-M; the GII type was mainly prevalent in PEDV strains in recent years. The phylogenetic tree based on the PEDV S gene showed that four PEDV strains in this study belonged to the GII-b subtype and three strains belonged to the GII-c subtype, which were closely related to the prevalent PEDV strains in China in recent years but far from the classic PEDV strains and PEDV strains abroad. This indicated that there was a possibility of inter-provincial transmission of PEDV epidemic strains in Jiangsu province, and these strains underwent significant genomic variation compared to classic strains, which may lead to the unsatisfactory protective effect of commonly used vaccines in pig farms.

The phylogenetic tree based on the PoRV VP4 gene and the PoRV VP7 gene indicated that eight PoRV strains in this study had six different combinations: G3 [P23] type, G4 [P13] type, G4 [P23] type, G9 [P13] type, G9 [P23] type, and G11 [P13] type, respectively. Accord-

ing to previous studies, the G5P [7] type was the most widely prevalent combination type globally [31]. However, with the continuous variation and recombination in PoRV genomes, different types of virus strains have emerged in China in recent years. In this study, new combination strains of G3 [P23] type, G4 [P23] type, and G9 [P13] type have emerged, indicating that the combination types of PoRV strains in Jiangsu province are plentiful, the virus is undergoing recombination, and it has unique genetic evolution characteristics.

The phylogenetic tree based on the PDCoV S gene in this study indicated that the reference strains can be divided into three groups. The USA/JPN/KOR group was mainly composed of strains from countries such as the United States of America, Japan, and South Korea. The China group was mainly composed of Chinese strains, and the China/Vietnam/Laos/Thailand group was mainly composed of strains from Southeast Asian countries such as China, Vietnam, Laos, and Thailand. The PDCoV-01 strain in this study belonged to the China/Vietnam/Laos/Thailand groups. This may be related to the frequent animal and animal product transactions and close personnel communication between China and Southeast Asian countries in recent years.

In conclusion, we developed a triplex real-time RT-PCR assay in this study to differentiate PEDV, PoRV, and PDCoV, which showed satisfactory specificity, sensitivity, repeatability, and reproducibility. The established triplex real-time RT-PCR can be well applied to the detection of clinical samples, indicating that the assay we have established in this study is a useful detection tool for rapid differential detection of PEDV, PoRV, and PDCoV.

Supplementary Materials: The following supporting information can be downloaded at: <https://www.mdpi.com/article/10.3390/v15061238/s1>, Table S1: Specific information about the detection results of 112 clinical diarrhea samples.

Author Contributions: X.L. conceived and designed the experiments. W.H. and M.F. performed the experiments and analyzed the data. W.H. wrote the paper. X.L. and Z.Z. were involved in the interpretation of the results and critically read the manuscript. All authors have read and agreed to the published version of the manuscript.

Funding: This work was supported by the Jiangsu Agricultural Industry Technology System (JATS [2022] 361), the 111 Project D18007, and the Project of the Priority Academic Program Development of Jiangsu Higher Education Institutions (PAPD).

Data Availability Statement: All the data generated during the current study are included in the manuscript. Additional data related to this article may be requested from the corresponding authors.

Conflicts of Interest: The authors declare no conflict of interest.

References

- Jia, S.; Feng, B.; Wang, Z.; Ma, Y.; Gao, X.; Jiang, Y.; Cui, W.; Qiao, X.; Tang, L.; Li, Y.; et al. Dual priming oligonucleotide (DPO)-based real-time RT-PCR assay for accurate differentiation of four major viruses causing porcine viral diarrhea. *Mol. Cell. Probes* **2019**, *47*, 101435. [CrossRef] [PubMed]
- Theuns, S.; Desmarests, L.M.; Heylen, E.; Zeller, M.; Dedeurwaerder, A.; Roukaerts, I.D.; Van Ranst, M.; Matthijssens, J.; Nauwynck, H.J. Porcine group A rotaviruses with heterogeneous VP7 and VP4 genotype combinations can be found together with enteric bacteria on Belgian swine farms. *Vet. Microbiol.* **2014**, *172*, 23–34. [CrossRef] [PubMed]
- Jung, K.; Hu, H.; Saif, L.J. Porcine deltacoronavirus infection: Etiology, cell culture for virus isolation and propagation, molecular epidemiology and pathogenesis. *Virus Res.* **2016**, *226*, 50–59. [CrossRef] [PubMed]
- Niu, X.Y.; Wang, Q.H. Prevention and Control of Porcine Epidemic Diarrhea: The Development of Recombination-Resistant Live Attenuated Vaccines. *Viruses* **2022**, *14*, 1317. [CrossRef]
- Wood, E.N. An apparently new syndrome of porcine epidemic diarrhoea. *Vet. Rec.* **1977**, *100*, 243–244. [CrossRef]
- Pensaert, M.B.; de Bouck, P. A new coronavirus-like particle associated with diarrhea in swine. *Arch. Virol.* **1978**, *58*, 243–247. [CrossRef]
- Wang, D.; Fang, L.R.; Xiao, S.B. Porcine epidemic diarrhea in China. *Virus Res.* **2016**, *226*, 7–13. [CrossRef]
- Stevenson, G.W.; Hoang, H.; Schwartz, K.J.; Burrough, E.R.; Sun, D.; Madson, D.; Cooper, V.L.; Pillatzki, A.; Gauger, P.; Schmitt, B.J.; et al. Emergence of Porcine epidemic diarrhea virus in the United States: Clinical signs, lesions, and viral genomic sequences. *J. Vet. Diagn. Investig.* **2013**, *25*, 649–654. [CrossRef]
- Kumar, D.; Shepherd, F.K.; Springer, N.L.; Mwangi, W.; Marthaler, D.G. Rotavirus Infection in Swine: Genotypic Diversity, Immune Responses, and Role of Gut Microbiome in Rotavirus Immunity. *Pathogens* **2022**, *11*, 1078. [CrossRef]

10. Park, G.N.; Kim, D.I.; Choe, S.; Shin, J.; An, B.H.; Kim, K.S.; Hyun, B.H.; Lee, J.S.; An, D.J. Genetic Diversity of Porcine Group A Rotavirus Strains from Pigs in South Korea. *Viruses* **2022**, *14*, 2522. [CrossRef]
11. Vlasova, A.N.; Amimo, J.O.; Saif, L.J. Porcine Rotaviruses: Epidemiology, Immune Responses and Control Strategies. *Viruses* **2017**, *9*, 48. [CrossRef]
12. Theil, K.W.; Saif, L.J.; Moorhead, P.D.; Whitmoyer, R.E. Porcine rotavirus-like virus (group B rotavirus): Characterization and pathogenicity for gnotobiotic pigs. *J. Clin. Microbiol.* **1985**, *21*, 340–345. [CrossRef] [PubMed]
13. Turlewicz-Podbielska, H.; Pomorska-Mol, M. Porcine Coronaviruses: Overview of the State of the Art. *Viol. Sin.* **2021**, *36*, 833–851. [CrossRef] [PubMed]
14. Woo, P.C.Y.; Lau, S.K.P.; Lam, C.S.F.; Lau, C.C.Y.; Tsang, A.K.L.; Lau, J.H.N.; Bai, R.; Teng, J.L.L.; Tsang, C.C.C.; Wang, M.; et al. Discovery of Seven Novel Mammalian and Avian Coronaviruses in the Genus Deltacoronavirus Supports Bat Coronaviruses as the Gene Source of Alphacoronavirus and Betacoronavirus and Avian Coronaviruses as the Gene Source of Gammacoronavirus and Deltacoronavirus. *J. Virol.* **2012**, *86*, 3995–4008. [PubMed]
15. Marthaler, D.; Jiang, Y.; Collins, J.; Rossow, K. Complete Genome Sequence of Strain SDCV/USA/Illinois121/2014, a Porcine Deltacoronavirus from the United States. *Genome Announc.* **2014**, *2*, e00218-14. [CrossRef]
16. Li, G.; Chen, Q.; Harmon, K.M.; Yoon, K.-J.; Schwartz, K.J.; Hoogland, M.J.; Gauger, P.C.; Main, R.G.; Zhang, J. Full-Length Genome Sequence of Porcine Deltacoronavirus Strain USA/IA/2014/8734. *Genome Announc.* **2014**, *2*, e00278-14. [CrossRef]
17. Wang, L.Y.; Byrum, B.; Zhang, Y. Porcine Coronavirus HKU15 Detected in 9 US States, 2014. *Emerg. Infect. Dis.* **2014**, *20*, 1594–1595. [CrossRef]
18. Zhang, J.Q. Porcine deltacoronavirus: Overview of infection dynamics, diagnostic methods, prevalence and genetic evolution. *Virus Res.* **2016**, *226*, 71–84. [CrossRef]
19. Shu, X.; Han, F.; Hu, Y.; Hao, C.; Li, Z.; Wei, Z.; Zhang, H. Co-infection of porcine deltacoronavirus and porcine epidemic diarrhoea virus alters gut microbiota diversity and composition in the colon of piglets. *Virus Res.* **2022**, *322*, 198954. [CrossRef]
20. Chen, Q.; Wang, L.; Yang, C.; Zheng, Y.; Gauger, P.C.; Anderson, T.; Harmon, K.M.; Zhang, J.; Yoon, K.J.; Main, R.G.; et al. The emergence of novel sparrow deltacoronaviruses in the United States more closely related to porcine deltacoronaviruses than sparrow deltacoronavirus HKU17. *Emerg. Microbes Infect.* **2018**, *7*, 105. [CrossRef]
21. Chen, N.; Xiao, Y.; Li, X.; Li, S.; Xie, N.; Yan, X.; Li, X.; Zhu, J. Development and application of a quadruplex real-time PCR assay for differential detection of porcine circoviruses (PCV1 to PCV4) in Jiangsu province of China from 2016 to 2020. *Transbound. Emerg. Dis.* **2021**, *68*, 1615–1624. [CrossRef] [PubMed]
22. Li, X.D.; Hu, Y.X.; Liu, P.G.; Zhu, Z.B.; Liu, P.R.; Chen, C.H.; Wu, X.D. Development and application of a duplex real-time PCR assay for differentiation of genotypes I and II African swine fever viruses. *Transbound. Emerg. Dis.* **2022**, *69*, 2971–2979. [CrossRef] [PubMed]
23. Wittwer, C.T.; Vandesompele, J.; Shipley, G.L.; Pfaffl, M.W.; Nolan, T.; Mueller, R.; Kubista, M.; Huggett, J.; Hellems, J.; Garson, J.A.; et al. The MIQE Guidelines: Minimum Information for Publication of Quantitative Real-Time PCR Experiments. *Clin. Chem.* **2009**, *55*, 611–622.
24. Zhang, Y.; Chen, Y.; Zhou, J.; Wang, X.; Ma, L.; Li, J.; Yang, L.; Yuan, H.; Pang, D.; Ouyang, H. Porcine Epidemic Diarrhea Virus: An Updated Overview of Virus Epidemiology, Virulence Variation Patterns and Virus-Host Interactions. *Viruses* **2022**, *14*, 2434. [CrossRef] [PubMed]
25. Chen, J.; Liu, X.; Shi, D.; Shi, H.; Zhang, X.; Feng, L. Complete genome sequence of a porcine epidemic diarrhea virus variant. *J. Virol.* **2012**, *86*, 3408. [CrossRef]
26. Ben Salem, A.N.; Sergei, A.C.; Olga, P.B.; Olga, G.A.; Mahjoub, A.; Larissa, B.P. Multiplex nested RT-PCR for the detection of porcine enteric viruses. *J. Virol. Methods* **2010**, *165*, 283–293. [CrossRef]
27. Liu, G.P.; Jiang, Y.H.; Opriessnig, T.; Gu, K.D.; Zhang, H.L.; Yang, Z.Q. Detection and differentiation of five diarrhea related pig viruses utilizing a multiplex PCR assay. *J. Virol. Methods* **2019**, *263*, 32–37. [CrossRef]
28. Ding, G.; Fu, Y.; Li, B.; Chen, J.; Wang, J.; Yin, B.; Sha, W.; Liu, G. Development of a multiplex RT-PCR for the detection of major diarrhoeal viruses in pig herds in China. *Transbound. Emerg. Dis.* **2020**, *67*, 678–685. [CrossRef]
29. Zhang, H.; Liang, Q.; Li, B.; Cui, X.; Wei, X.; Ding, Q.; Wang, Y.; Hu, H. Prevalence, phylogenetic and evolutionary analysis of porcine deltacoronavirus in Henan province, China. *Prev. Vet. Med.* **2019**, *166*, 8–15. [CrossRef]
30. Li, W.; Lei, M.K.; Li, Z.F.; Li, H.M.; Liu, Z.; He, Q.G.; Luo, R. Development of a Genetically Engineered Bivalent Vaccine against Porcine Epidemic Diarrhea Virus and Porcine Rotavirus. *Viruses* **2022**, *14*, 1746. [CrossRef]
31. Papp, H.; Laszlo, B.; Jakab, F.; Ganesh, B.; De Grazia, S.; Matthijssens, J.; Ciarlet, M.; Martella, V.; Banyai, K. Review of group A rotavirus strains reported in swine and cattle. *Vet. Microbiol.* **2013**, *165*, 190–199. [CrossRef] [PubMed]

Disclaimer/Publisher’s Note: The statements, opinions and data contained in all publications are solely those of the individual author(s) and contributor(s) and not of MDPI and/or the editor(s). MDPI and/or the editor(s) disclaim responsibility for any injury to people or property resulting from any ideas, methods, instructions or products referred to in the content.

Article

An Attempt of a New Strategy in PRV Prevention: Co-Injection with Inactivated *Enterococcus faecium* and Inactivated Pseudorabies Virus Intravenously

Yuan Cui ¹, Libo Huang ¹, Jinlian Li ², Gang Wang ^{1,*} and Youfei Shi ^{1,*}

¹ College of Animal Science and Veterinary Medicine, Shandong Agricultural University, Tai'an 271018, China; cuiyuan1995123@163.com (Y.C.); huanglibo123@126.com (L.H.)

² College of Biology and Brewing Engineering, Taishan University, Tai'an 271021, China; lijianli1979@163.com

* Correspondence: wanggang@sdau.edu.cn (G.W.); shiyoufei@163.com (Y.S.)

Abstract: Pseudorabies virus (PRV) is one of the causative agents of common infectious diseases in swine herds. *Enterococcus faecium* is a probiotic belonging to the group of lactic acid bacteria and has excellent immunomodulatory effects. Vaccine immunization is an important approach to prevent animal diseases in the modern farming industry, and good immunization outcomes can substantially reduce the damage caused by pathogens to animals, improve the quality of animals' lives, and reduce economic losses. In the present study, we showed that inactivated *E. faecium* and inactivated PRV when co-injected intravenously significantly reduced the mortality of mice after inoculation with PRV. The inactivated *E. faecium* + inactivated PRV intravenous injection group induced more production of Th cells and Tc cells. Additionally, the inactivated *E. faecium* + inactivated PRV intravenous injection group showed higher concentrations of cytokines (IFN- γ and IL-10) and induced higher antibody production. Thus, the co-injection of inactivated *E. faecium* and inactivated PRV could remarkably prevent and control the lethality of PRV infection in mice, which is a critical finding for vaccination and clinical development.

Keywords: pseudorabies virus; *Enterococcus faecium*; immunization; intravenous



Citation: Cui, Y.; Huang, L.; Li, J.; Wang, G.; Shi, Y. An Attempt of a New Strategy in PRV Prevention: Co-Injection with Inactivated *Enterococcus faecium* and Inactivated Pseudorabies Virus Intravenously. *Viruses* **2023**, *15*, 1755. <https://doi.org/10.3390/v15081755>

Academic Editor: Xiangdong Li

Received: 30 May 2023

Revised: 9 August 2023

Accepted: 11 August 2023

Published: 17 August 2023



Copyright: © 2023 by the authors. Licensee MDPI, Basel, Switzerland. This article is an open access article distributed under the terms and conditions of the Creative Commons Attribution (CC BY) license (<https://creativecommons.org/licenses/by/4.0/>).

1. Introduction

Pseudorabies virus (PRV), the causative agent of pseudorabies, is a swine herpesvirus that belongs to the genus *Varicellovirus* in the subfamily *Alphaherpesvirinae* of the family *Herpesviridae* [1]. PRV is lethal to many domestic and wild animals, for example, cattle, sheep, and dogs, while pigs are the natural host of this virus. PRV was first reported in swine herds of China in 1956, and since 2012, several PRV variants have been detected, which has led to massive economic losses of swine farms in China. A serious concern is that PRV can be transmitted from pigs to humans, with neurological dysfunction as a typical symptom, and the disease can eventually cause vegetation or death in humans [2–5].

PRV is globally distributed and poses a high risk to livestock and human health; furthermore, vaccination is the most effective and economical approach to prevent infectious diseases [6–8]. However, because of immune evasion by the virus and the immunologically silent nature of its latency, the development of effective and safe PRV vaccines remains challenging.

Vaccine adjuvants are substances that can modulate antibody and cell-mediated adaptive immune responses, reduce the antigen dose used, and reduce the number of immunizations based on the highest immunity achieved for animals [9,10]. Probiotics play a key role in shaping the maturation and activity of the immune system in animals. Several field studies have shown the positive effects of probiotics on animal growth performance and their immune system [11,12]. Probiotics mainly activate the innate immune response. This feature of probiotics is the key for the subsequent stimulation of an adaptive immune

response [13]. Probiotics are used as vaccine adjuvants to further enhance the immunogenicity and effectiveness of live vaccines [14]. As a protective antigen delivery carrier, probiotics have the advantages of high safety, and oral or nasal mucosal administration can induce mucosal immunity, humoral immunity, and cellular immunity [15]. Following the administration through the oral route, the probiotics enter the gut and induce a systemic immune response by causing the release of cytokines via mucosal lymphoid cells [16]. In previous studies, mice were orally immunized with the *Lactobacilli plantarum* NC8-pSIP409-HA strain, and this strain induced the production of sIgA, IgG, and HI antibodies, which further induced CD8⁺ T-cell immune response. Most importantly, the oral administration approach provided complete protection against the challenge with mouse-adapted H9N2 virus. These results indicate that *L. plantarum* NC8-pSIP409-HA was more effective in inducing mucosal, humoral, and cellular immune responses [17]. *Lactobacillus acidophilus* has been used to enhance the immunogenicity of Newcastle disease virus (NDV) vaccines. In another study, oral administration of *L. acidophilus* significantly increased the IgG and HI NDV antibody levels in chicks [18]. Probiotics can stimulate the release of cytokines by macrophages and T cells, thereby modulating the mucosal immune response pathways [19,20]. Based on mouse studies, spore adjuvants can induce lung-specific immune responses when delivered as intranasal vaccines [21]. *Bacillus subtilis* spores not only enhance innate immunity for protection against respiratory infections but also induce an increase in antigen-specific antibody and T-cell responses when co-administered with a soluble antigen [22,23]. Probiotics can also be injected intramuscularly together with antigens. This approach involving vaccination with inactivated H9N2 virus together with a *B. subtilis* spore adjuvant in chickens produced a remarkable effect on antigen-specific antibody and T-cell responses against avian influenza virus. It enhanced not only H9N2 virus-specific IgG levels but also CD4⁺ and CD8⁺ T-cell responses, with an increase in proinflammatory cytokine production [24].

In a previous study, the intravenous administration of *Enterococcus faecium* after hyperbaric inactivation induced a substantial increase in nonspecific immune function in mice and restored the normal immune function of immunosuppressed mice [25]. However, presently, there are no reports of intravenous co-administration of bacteria and viruses in a specific ratio. In our preliminary experiment, we found that the intravenous administration of inactivated *E. faecium* alone could not enable mice to resist PRV infection. Therefore, we combined inactivated *E. faecium* with inactivated PRV for intravenous administration to test the experimental results. We expected that this approach could (1) serve as a reference for treating some diseases that cannot be prevented and cured by conventional treatment approaches and (2) function as a model for vaccine development and clinical application.

In the present study, we attempted intravenous co-administration of inactivated *E. faecium* and inactivated PRV to overcome PRV infection in mice. The changes in the levels of immune cells and cytokines in mice were studied to reveal the mechanism underlying the induction of immunity against PRV infection.

2. Materials and Methods

2.1. Bacterial and Viral Strains and Mice

E. faecium CICC 6049 strain was purchased from China Center of Industrial Culture Collection. The PRV Bartha-K61 vaccine strain was obtained from Boehringer Ingelheim Animal Health USA Inc. Specific pathogen free (SPF)-grade Kunming breed mice weighing 18–22 g were purchased from Shandong Taibang Biological Products Co., Ltd. (Tai'an, China).

2.2. Preparation of Inactivated *E. faecium* and Inactivated PRV

The laboratory-preserved *E. faecium* strain was inoculated in a *Lactobacillus* culture medium and incubated at 37 °C for 24 h. The suspension in the culture flask was then centrifuged at 2500 rpm for 6 min; the supernatant was discarded, and the bottom precipitate was retained. The residue was washed three times with 0.9% saline and resuspended with

a suitable volume of 0.9% saline to prepare a high concentration of *E. faecium* solution. This solution was placed in an autoclave and sterilized at 121 °C for 15 min and then stored at 4 °C. A suitable volume of the bacterial solution was diluted, and the number of bacterial cells was counted under a microscope by using a THOMA bacterial counting plate. The number of bacterial cells was adjusted to 1.0×10^9 CFU/mL, and the optical density (OD) value was measured at 690 nm. An OD value of 0.38 was assumed as $1 \times$ dose, which is the dose required for the experiment.

The solution of PRV Bartha-K61 strain inoculated and amplified on PK-15 cells was harvested, and after centrifugation to remove the sediment, sucrose density gradient centrifugation was performed to obtain ultra-pure PRV Bartha-K61 strain particles. The infectious titers of the viral solution were $10^{-7.33}$ TCID₅₀/0.1 mL. The purified viral solution was inactivated by adding a 40% formaldehyde solution and mixing it thoroughly so that the concentration of the formaldehyde solution used was 0.3% of the viral liquid volume. The inactivated PRV was inoculated into the monolayer of PK-15 cells in three cell culture bottles, cultured at 37 °C, and observed for 7 d before blind transmission of the second generation. No cytopathic effect (CPE) was observed. The inactivated viral solution was inoculated into a bouillon culture medium and a standard nutrient agar and cultured at 37 °C for 24–48 h; no bacterial growth was observed. For safety testing, 10 mice were subcutaneously inoculated with 0.2 mL of the inactivated viral solution and observed for 14 d. A control group without vaccination was also established, and no local or systemic adverse reactions caused by vaccination were observed.

2.3. Experimental Design

Animal ethics statements. The present study was conducted in accordance with recommendations from the Guide for the Care and Use of Laboratory Animals of the Ministry of Science and Technology of China. During the experiment, mice showing extreme lethargy were considered moribund and were humanely euthanized.

Sixty 4-week-old mice were divided into 6 groups (10 mice/group) as follows: negative control group (group 1), PRV model group (group 2), inactivated *E. faecium* + inactivated PRV intramuscular injection group (group 3), inactivated *E. faecium* intravenous injection group (group 4), saline + inactivated PRV intravenous injection group (group 5), and inactivated *E. faecium* + inactivated PRV intravenous injection group (group 6). After acclimatization and rearing for 3 days, the mice were treated according to the details provided in Table 1. Three days after antigen inoculation, all the experimental groups, except the negative control group, were administered 20 µL of live PRV containing $10^{6.2}$ TCID₅₀ through a nasal drip, and the negative control group was administered an equal amount of saline nasal drops. Clinical signs, including depression, rough appearance of hair coat, swollen eyes, and neurological symptoms, were monitored daily. All the mice were humanely euthanized at 5 days post challenge (except for the 21 days survival curve experiments).

Table 1. Immunization methods of mice in each group.

Group	Method of Immunization
Negative control group (group 1)	Intramuscular injection of saline
PRV model group (group 2)	Intramuscular injection of saline
Inactivated <i>E. faecium</i> + inactivated PRV intramuscular injection group (group 3)	Intramuscular injection of 1:1 mixture of inactivated <i>E. faecium</i> and inactivated PRV 0.2 mL
Inactivated <i>E. faecium</i> intravenous injection group (group 4)	Intravenous injection of 0.2 mL of inactivated <i>E. faecium</i> injection
Saline + inactivated PRV intravenous injection group (group 5)	Intravenous injection of a 1:1 mixture of saline and inactivated PRV 0.2 mL
Inactivated <i>E. faecium</i> + inactivated PRV intravenous injection group (group 6)	Intravenous injection of a 1:1 mixture of inactivated <i>E. faecium</i> and inactivated PRV 0.2 mL

2.4. Survival Curve

After subjecting the mice to immune challenge, they were fed and provided free access to water, and the number of mouse deaths within 21 days was recorded.

2.5. Histopathological Examination

During necropsy, the lungs of each group were collected and fixed in 4% phosphate-buffered formalin, embedded in paraffin, cut into 2- to 4- μ m-thick slices, and stained with hematoxylin and eosin (H&E). Lesions were observed by an experienced professional pathologist who was blinded to the study groups.

2.6. Antibody Analysis

Serum antibodies against the PRV gB protein at 5 days post-infection (DPI) were detected using the porcine pseudorabies virus ELISA antibody detection kit (Wuhan Keqian Biology Co., Ltd., Wuhan, China) in accordance with the manufacturer's instructions.

2.7. Flow Cytometry Analysis

After subjecting them to immune challenge, the mice were fed and provided free access to water for 5 d. After 5 DPI, their spleens were removed and placed in a 24-well plate; 1 mL of RPMI 1640 culture medium was added, mixed, and the culture medium was then discarded. Next, 1 mL of trypsin was injected, and the spleens were cut with sterilized scissors and incubated at 37 °C for approximately 30 min. Subsequently, 1 mL of PBS was added to terminate the digestion. The spleen was grinded, filtered through a cell sieve, and made up to the volume of 10 mL. This suspension was centrifuged at 2500 rpm for 6 min at 4 °C. The supernatant was discarded, and 10 mL of PBS was added to terminate the reaction. Next, the suspension was centrifuged at 4 °C at 2500 rpm for 6 min, the supernatant was discarded, and 1 mL PBS was added. The precipitate was mixed well, filtered through a cell sieve, and divided into two portions. Anti-mouse CD3e FITC-conjugated antibodies, anti-mouse CD4 Alexa Fluor 4700-conjugated antibodies, PE anti-mouse CD8a antibodies, anti-mouse NK1.1 antibodies, and anti-human/mouse CD45R (B220) PerCP-Cyanine 5.5 antibodies were added to approximately 30 μ L of the cell suspension. After 15 min of incubation, the samples were subjected to flow cytometry for measurement.

2.8. Cytokine Analysis

Sera collected at 5 DPI were used to detect IL-10 levels by using commercial ELISA kits (Mlbio, Inc., Shanghai, China) in accordance with the manufacturer's instructions. The concentration of cytokines (ng/L) was calculated with a standard curve generated using recombinant mouse cytokines supplied in the kits.

2.9. Data Analysis

Kaluza flow cytometric analysis software was used to analyze the results of flow cytometry. GraphPad Prism 9 software was used to prepare graphs. SPSS 23.0 software was used for statistical analysis. One-way analysis of variance (ANOVA) was performed to analyze the significance of the data. Numerical data are expressed as mean \pm standard deviation (SD). Different lowercase letters indicate significant differences ($p < 0.05$), while different uppercase letters indicate highly significant differences ($p < 0.01$).

3. Results

3.1. Clinical Signs and Survival Curve

Table 2 and Figures 1 and 2 show the results of the number of deaths in the different groups of mice within 21 days after immunization. The mice in each group showed a normal response after immunization, and their appetite for drinking water was normal. Three days after immunization, except for group 1, the remaining groups were challenged with PRV. The mice were normal in the first two days after the virus challenge. From the

third day onward, the mice in group 2 and group 4 showed shortness of breath, confusion, loss of appetite, and other clinical symptoms. In the late stage of the disease, the mice were depressed and lost their appetite. Some mice exhibited strong itching symptoms, incomplete body surface hair, and blurred flesh and blood. The mice in group 2 began to die on the 6th day after the virus challenge, and all mice died within 6–8 days. The mice in group 4 began to die on the 6th day after the virus challenge, and all mice died within 6–14 days; this finding confirmed that the inactivated *E. faecium* alone could not resist PRV infection in mice. The mice in group 3 died on the 7th day, and 6 mice died between the 7th and 13th day after the virus challenge. Two mice in group 5 died on the 9th day. Mice in group 6 did not die and showed good growth status, which indicated the advantages of intravenous vaccination. Group 6 showed an excellent immune adjuvant effect of inactivated *E. faecium* as compared to group 5.

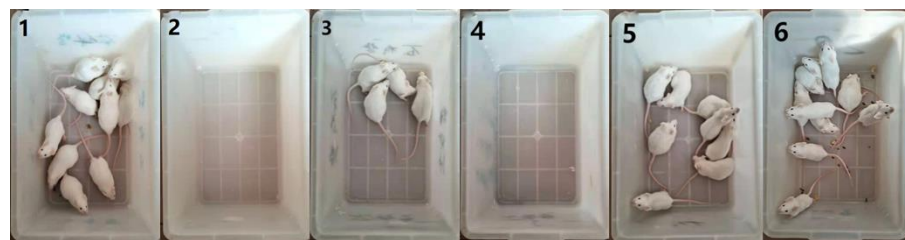


Figure 1. Survival status of mice in each group within 21 days of virus challenge. Group 1 is the negative control group; 2 is the pseudorabies virus model group; 3 is the inactivated *E. faecium* + inactivated pseudorabies virus intramuscular injection group; 4 is the inactivated *E. faecium* intravenous injection group; 5 is the saline + inactivated pseudorabies virus intravenous injection group; 6 is the inactivated *E. faecium* + inactivated pseudorabies virus intravenous injection group.

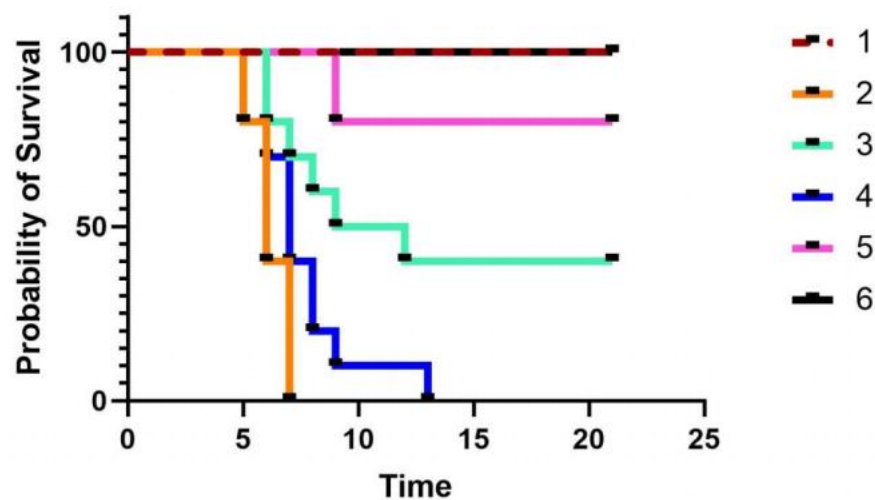


Figure 2. Survival curve of mice from the different groups. Group 1 is the negative control group; 2 is the pseudorabies virus model group; 3 is the inactivated *E. faecium* + inactivated pseudorabies virus intramuscular injection group; 4 is the inactivated *E. faecium* intravenous injection group; 5 is the saline + inactivated pseudorabies virus intravenous injection group; 6 is the inactivated *E. faecium* + inactivated pseudorabies virus intravenous injection group.

Table 2. Number of surviving mice in different groups on 21 days.

Groups	Number of Mice
1	10 ^A
2	0 ^{Ba}
3	4 ^{BCb}
4	0 ^{Ba}
5	8 ^{AC}
6	10 ^A

Group 1 is the negative control group; 2 is the pseudorabies virus model group; 3 is the inactivated *E. faecium* + inactivated pseudorabies virus intramuscular injection group; 4 is the inactivated *E. faecium* intravenous injection group; 5 is the saline + inactivated pseudorabies virus intravenous injection group; 6 is the inactivated *E. faecium* + inactivated pseudorabies virus intravenous injection group. Different lowercase letters indicate significant differences ($p < 0.05$), while different uppercase letters indicate highly significant differences ($p < 0.01$).

3.2. Histopathological Examination

Histopathological lesions in the lungs of different mice groups are shown in Figure 3. Group 1 and group 6 showed no apparent lesions, while the other four treated groups showed varying degrees of pathological changes. Mice in group 2 exhibited pulmonary hemorrhage, interstitial widening, and interstitial inflammatory cell infiltration (Figure 3B). Mice in the remaining three groups showed a widened interstitium with infiltration of interstitial inflammatory cells (Figure 3C–E).

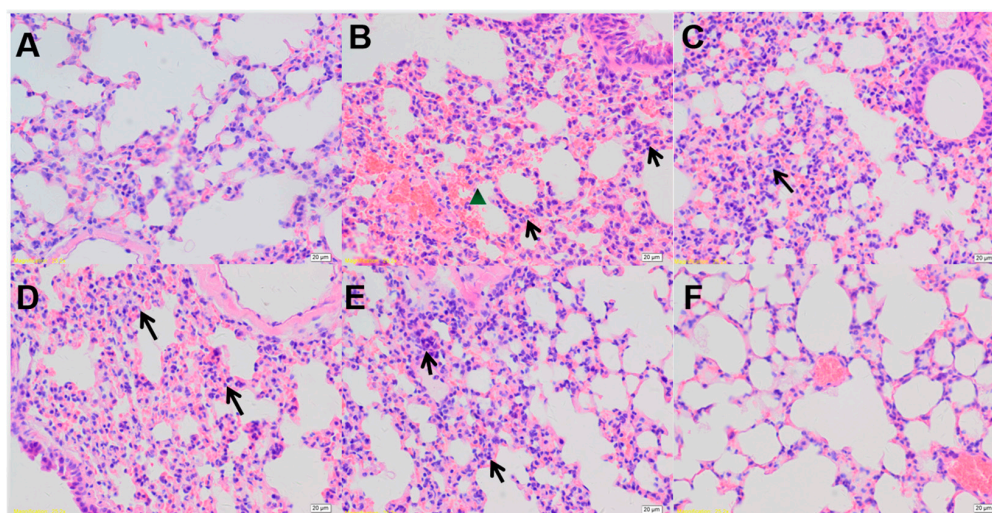


Figure 3. Histopathological changes in the lungs of mice from the different groups. Lung samples from the negative control group (A), the pseudorabies virus model group (B), the inactivated *E. faecium* + inactivated pseudorabies virus intramuscular injection group (C), the inactivated *E. faecium* intravenous injection group (D), the saline + inactivated pseudorabies virus intravenous injection group (E), and the inactivated *E. faecium* + inactivated pseudorabies virus intravenous injection group (F). Tissues were stained with hematoxylin and eosin (magnification 200 \times). The triangle in the pathological section image represents pulmonary hemorrhage; the arrow shows a widened interstitium with infiltration of interstitial inflammatory cells.

3.3. Antibody Analysis

Mice anti-PRV gB antibodies were detected using the porcine PRV ELISA antibody test kit. The secondary antibody in this kit was replaced with the horseradish peroxidase (HRP)-conjugated sheep anti-mouse IgG to determine the amount of PRV antibodies in mouse serum. The dilution of the secondary antibody was 1:5000. As shown in Table 3 and Figure 4, the original antibody solution color was replaced with the color of tetramethylbenzidine (TMB), and the absorbance value was measured at 450 nm. Group 5 and group 6 developed anti-PRV antibodies at 5 DPI. A significant difference was observed between the levels

of anti-PRV antibodies of group 5 and group 6 and the remaining groups ($p < 0.01$). No significant difference in the levels of antibodies was observed between group 5 and group 6 ($p > 0.05$). These results show that the intravenous route of vaccination can maximize the production of neutralizing antibodies and play a better role in animal immunity. This finding indicates the feasibility of intravenous vaccine administration for treating PRV infection.

Table 3. Levels of PRV antibodies in the sera of each group of mice.

Groups	PRV Antibody Concentration (OD450 Value)
1	0.124 ± 0.0172^A
2	0.176 ± 0.0256^B
3	0.237 ± 0.010^C
4	0.178 ± 0.023^B
5	0.324 ± 0.054^D
6	0.297 ± 0.046^D

Group 1 is the negative control group; 2 is the PRV model group; 3 is the inactivated *E. faecium* + inactivated PRV intramuscular injection group; 4 is the inactivated *E. faecium* intravenous injection group; 5 is the saline + inactivated PRV intravenous injection group; 6 is the inactivated *E. faecium* + inactivated PRV intravenous injection group. Different uppercase letters indicate highly significant differences ($p < 0.01$).

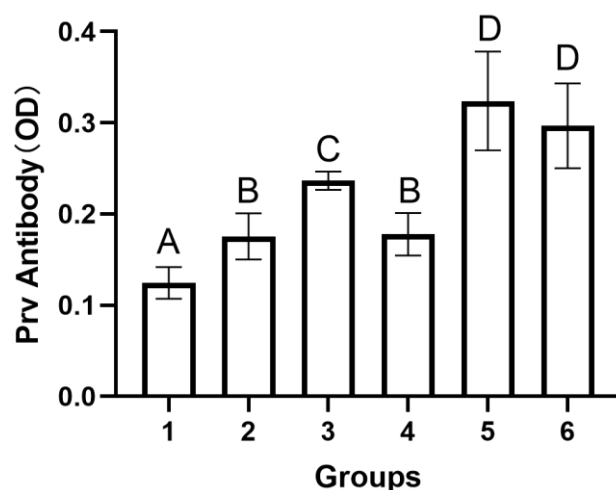


Figure 4. Levels of PRV antibodies in the sera of each group of mice. Serum samples were assayed using the porcine pseudorabies virus ELISA antibody test kit. The secondary antibody in the ELISA kit was replaced with HRP-conjugated sheep anti-mouse IgG to detect PRV antibodies in mouse serum. The dilution of the secondary antibody was 1:5000. The original antibody solution color was replaced with the color of TMB, and the absorbance value was measured at 450 nm. Sera samples were obtained from the negative control group (1), the PRV model group (2), the inactivated *E. faecium* + inactivated PRV intramuscular injection group (3), the inactivated *E. faecium* intravenous injection group (4), the saline + inactivated PRV intravenous injection group (5), and the inactivated *E. faecium* + inactivated PRV intravenous injection group (6). Each point represents mean (\pm SD) generated from all mice on 5 DPI. Different uppercase letters indicate highly significant differences ($p < 0.01$).

3.4. Flow Cytometry Analysis

As shown in Table 4 and Figure 5, the highest expression and percentage of Th and Tc cells were noted in the spleen of mice from group 3 (5468.9 ± 2443.5 vs. 3577.4 ± 1631.6 ; 23.43% vs. 10.49%), followed by group 6 (5386.8 ± 1443.9 vs. 2704.5 ± 1182.3 ; 21.58% vs. 7.92%) (Table 1 and Figure 5c,d). The expression of natural killer (NK) cells in mice spleen was the highest (1462.9 ± 869.4) in group 3 among all the groups (Table 1). These data indicate that the dosage of inactivated *E. faecium* as a vaccine adjuvant is $\times 10^9$ CFU/mL, 0.1 mL per serving, mixed with antigen 1:1. When the injection route is intramuscular, it

has a good activation effect on B cells, Th cells, Tc cells, and NK cells; when the injection route is intravenous, it has a good activation effect on Th cells.

Table 4. The number of each immune cell type in the spleen of mice from the different groups.

Groups	B Cell Count (pcs)	Th Cell Count (pcs)	Tc Cell Count (pcs)	NK Cell Count (pcs)
1	17,376.9 ± 7048.6 ^a	4055.11 ± 1130.6	2005.2 ± 593.1 ^A	1125.8 ± 367.6
2	14,265.8 ± 4364.1	2800.10 ± 529.7 ^A	2004.7 ± 622.1 ^A	885.7 ± 412.6 ^a
3	17,496.5 ± 7015.1 ^a	5468.9 ± 2443.5 ^{Bb}	3577.4 ± 1631.6 ^B	1462.9 ± 869.4 ^{Bb}
4	11,947 ± 3757.2 ^b	3140 ± 1105.5 ^A	1807.8 ± 1051.6 ^A	812.7 ± 189.1 ^{Aa}
5	15,034.7 ± 5906	3867.1 ± 1665.4 ^a	2099 ± 969.1 ^A	1283.4 ± 511.7 ^{ABb}
6	15,645.5 ± 6016	5386.8 ± 1443.9 ^{Bb}	2704.5 ± 1182.3	1070.1 ± 404.5

Group 1 is the negative control group; 2 is the PRV model group; 3 is the inactivated *E. faecium* + inactivated PRV intramuscular injection group; 4 is the inactivated *E. faecium* intravenous injection group; 5 is the saline + inactivated PRV intravenous injection group; 6 is the inactivated *E. faecium* + inactivated PRV intravenous injection group. Different lowercase letters indicate significant differences ($p < 0.05$), while different uppercase letters indicate highly significant differences ($p < 0.01$).

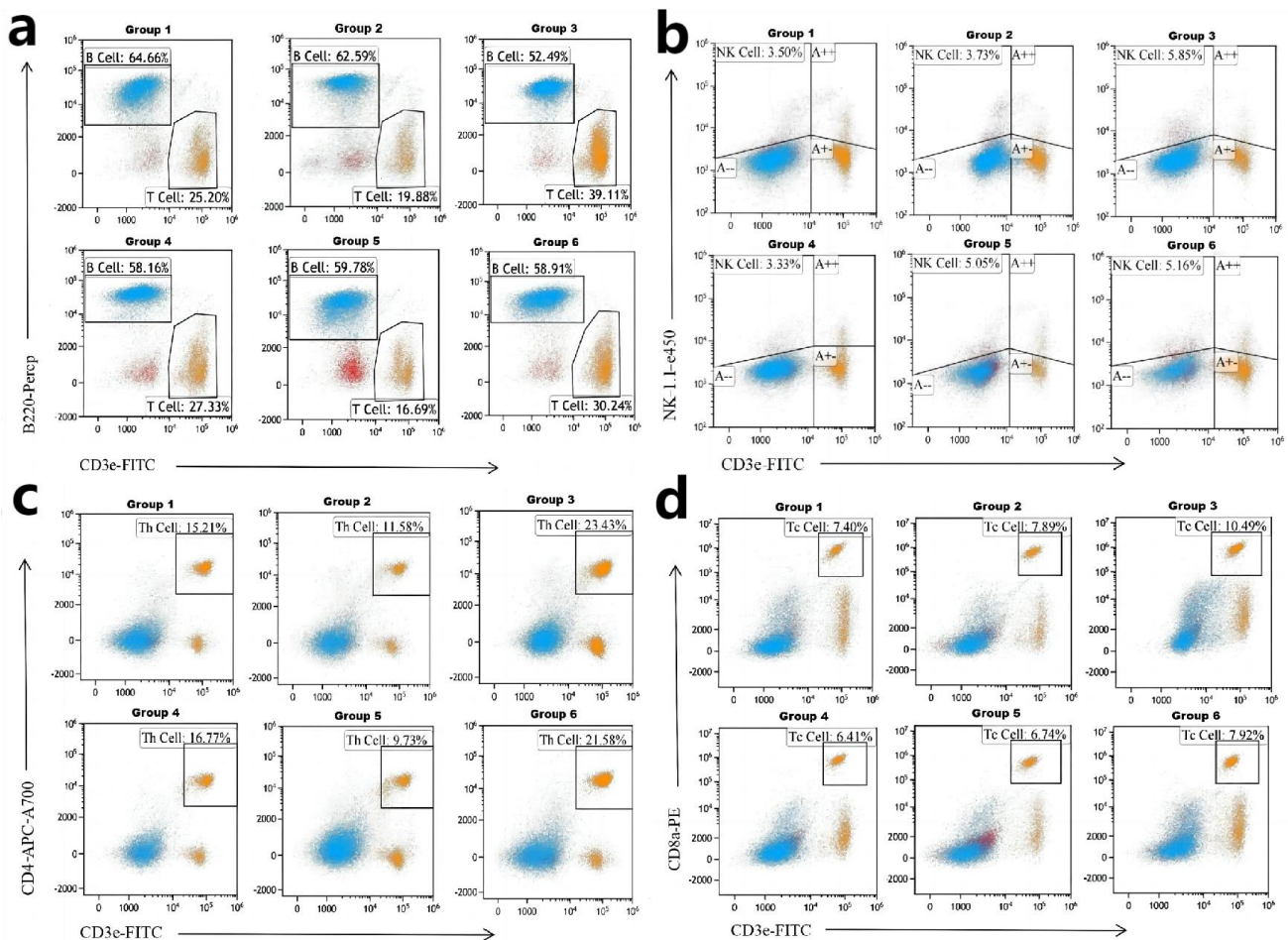


Figure 5. The proportion of each immune cell type in the spleen of mice from the different groups. (a–d) The proportion of B cells, NK cells, Th cells, and Tc cells, respectively.

3.5. Cytokine Analysis

As shown in Figure 6, IFN- γ expression was lower in group 5 than in the other groups (592.22, $p < 0.0001$); however, cytokine IL-1 β expression was higher in this group than in the other groups (278.85, $p < 0.0001$). IL-1 β expression in group 6 was almost similar to that in group 1 ($p = 0.498$). Group 6 showed the highest expression of cytokine IL-10 (320.08) among

all the experimental groups, and a significant difference ($p = 0.02$) in IL-10 expression was noted between this group and group 5. These results show that inactivated *E. faecium* could play an excellent immunomodulatory role of a probiotic when administered as a vaccine adjuvant through the intravenous route. A significant difference ($p = 0.018$) was observed in cytokine IFN- γ expression between group 3 and group 6. Furthermore, cytokine IL-10 expression showed a highly significant difference ($p = 0.003$) between group 3 and group 6. These results indicate that the intravenous route of vaccination was more effective than the intramuscular route in promoting the expression of cytokines in serum when inactivated *E. faecium* was used as a vaccine adjuvant.

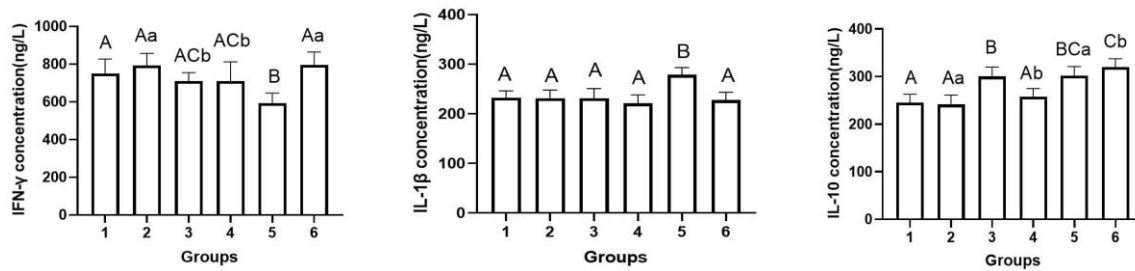


Figure 6. Changes in the expression of cytokines in the serum of mice from the different groups. Group 1 is the negative control group; 2 is the PRV model group; 3 is the inactivated *E. faecium* + inactivated PRV intramuscular injection group; 4 is the inactivated *E. faecium* intravenous injection group; 5 is the saline + inactivated PRV intravenous injection group; 6 is the inactivated *E. faecium* + inactivated PRV intravenous injection group. Different lowercase letters indicate significant differences ($p < 0.05$), while different uppercase letters indicate highly significant differences ($p < 0.01$).

4. Discussion

The present study showed that inactivated PRV when administered intravenously could reduce the mortality of PRV-infected mice as compared to that when administered intramuscularly. In particular, compared with the saline + inactivated pseudorabies virus intravenous injection, the intravenous administration of inactivated *E. faecium* + inactivated PRV could provide higher protection to mice against PRV infection. This fully reflects the good vaccine adjuvant effect of inactivated *E. faecium*. Thus, this indicates that this study has certain potential research value.

According to a previous report, the BCG vaccine could maximize the protective effect of the vaccine on animals after intravenous administration to rhesus monkeys and mice [26]. In 2020, Darrah et al. obtained the same results experimentally and elucidated the mechanism of action as follows: the cellular immunity of animals plays an important role in immunization; intravenous immunization significantly increases the antibody level in animals; and “trained immunity”-induced epigenetically modified macrophages show enhanced resistance to *Mycobacterium tuberculosis* infection [27]. In the present study, we observed similar results, wherein the mortality rate of mice in the inactivated PRV intravenous injection group after the virus challenge was significantly lower than that in the inactivated PRV intramuscular injection group (Figure 1); furthermore, the level of antibodies produced by mice was significantly higher in the intravenous injection group than in the intramuscular injection group (Figure 2). An ideal vaccination route can reduce animal mortality or substantially reduce clinical signs. The survival curves of mice from the different groups at 21 days after the virus challenge (Figure 2) and the lung pathology of mice from each group (Figure 3) showed that the intravenous administration of inactivated *E. faecium* + inactivated PRV significantly reduced the mortality rate and alleviated the pathological damage caused by virus infection, thus exhibiting an excellent immunization effect. Previous studies have indicated that humoral immunity plays an important secondary role in the regeneration of a specific cellular immune response by the host and is an indispensable component of the organism’s ability to trigger an effective immune response against viral infection [28,29]. In the present experiment, the level of

antibodies in the serum of mice in the saline + inactivated PRV intravenous injection group and the inactivated *E. faecium* + inactivated PRV intravenous injection group was significantly higher than that in the remaining experimental groups. This finding indicates the vital effect of intravenous administration of a vaccine on the humoral immunity of animals and also lays the foundation for the rapid generation of specific cellular immunity in animals after the reinvasion of the virus.

Immunomodulation is one of the essential properties of probiotics, and the good immunomodulatory effect of inactivated *E. faecium* can significantly enhance the nonspecific primary and specific immune responses of animals [25]. Similar results were reported by Brisbin et al., thus suggesting that probiotics such as lactic acid bacteria can modulate the innate and adaptive immune responses of animals [30–35]. In previous studies, probiotics have been used as adjuvants for oral and intramuscular vaccines for experimental purposes, with some success [7,36–38]. The immunomodulatory effect of inactivated *E. faecium* as a vaccine adjuvant was also demonstrated in the present experiment: inactivated *E. faecium*, when co-injected with inactivated PRV as a vaccine adjuvant, significantly increased the number of immune cells such as Th cells, Tc cells, and NK cells in the spleen (Table 4). This in turn had a significant effect on the induction of cellular and humoral immunity and the initial and recovery periods of resistance to the viral infection after the mice were immunized with the vaccine. Thus, inactivated *E. faecium* as a vaccine adjuvant plays a vital role in the production of cellular and humoral immunity and the initial and recovery phases of resistance to viral infection.

In the present study, with regard to serum cytokine levels, mice in the saline + inactivated PRV intravenous injection group showed significantly higher levels of IL-1 β than the remaining groups; IL-1 β promotes the antigen-presenting ability of antigen-presenting cells (APCs) such as monocytes and macrophages and enhances B cell growth and differentiation and antibody formation. We speculate that the higher antibody levels (OD) in the mice of the saline + inactivated PRV intravenous injection group than in the remaining experimental groups is related to IL-1 β concentration. The inactivated *E. faecium* + inactivated PRV intravenous injection group showed significantly higher levels of IFN- γ than the saline + inactivated PRV intravenous injection group. IFN- γ exerts an excellent immunomodulatory effect, regulates the immune functions of T and B lymphocytes, promotes the differentiation of quiescent CD4 $^+$ T cells into Th1 cells, promotes the expression of Th1-type cytokines, and enhances cellular immune functions. *E. faecium* as a vaccine adjuvant demonstrated good immunomodulatory effects, as reported earlier by Mohammadi et al. [7,36,37]. IL-10 can promote the survival, expansion, and lethality (cytotoxicity) of CD8 $^+$ T immune cells in the animal immune system, better promoting long-term protective immunity. The serum IL-10 level was significantly higher in the inactivated *E. faecium* + inactivated PRV intravenous injection group than in the saline + inactivated PRV intravenous injection group, thus demonstrating that *E. faecium* as a vaccine adjuvant exhibited a good immunomodulatory effect; this result was similar to the findings of Mohammadi [7].

Probiotics can influence the immune system of animals through the production of their metabolites, cell wall components, and DNA; furthermore, dead probiotic cells or probiotic-derived ingredients, such as peptidoglycan fragments or DNA, can induce the immunomodulatory effects on animals [39,40]. Even after inactivation, the cytoskeleton of *E. faecium* remains intact; this feature enables to better utilize its probiotic properties. Although probiotics have a high potential and exert good immunomodulatory effects on animals, treatment with probiotics alone does not protect the animal from virus infection. In our study, we found that the administration of inactivated *E. faecium* alone did not enable mice to resist PRV infection; moreover, the inactivated *E. faecium* intravenous injection group and the PRV model group showed no difference in time to onset of death and number of deaths; this result was consistent with the findings of Bavananthasivam et al. [31]. The high survival rate of mice in the inactivated *E. faecium* + inactivated PRV intravenous injection group might contribute to the combination of high humoral immunity

produced by intravenous vaccine administration and the fact that inactivated *E. faecium* could adequately stimulate the cellular immunity of the animal.

In the present study, inactivated PRV was used as the antigen, and inactivated *E. faecium* was used as the adjuvant. Inactivated *E. faecium* was co-administered intravenously with the inactivated pathogen. The differences in the protective properties and antibody production in mice following various immunization protocols were compared, and it was concluded that co-administration of inactivated *E. faecium* and the inactivated PRV antigen can provide better protection to animals against PRV infection; this is the innovation aspect of the present study. This study also demonstrates the good immunomodulatory effect of inactivated *E. faecium* and provides new ideas for developing vaccines for infectious diseases and for designing innovative immunization methods.

This study was initiated with the discovery that *E. faecium* is present in the blood of animals [41]. Intravenous administration of *E. faecium* after hyperbaric inactivation led to a significant increase in nonspecific immune function in mice and restored the normal immune function of immunosuppressed mice [25]. Previous studies have shown that an intravenous injection of bacteria or viruses alone can treat tumors with good therapeutic effects [42–45]. The intravenous administration of the BCG vaccine yielded excellent experimental results as compared to those obtained following other immunization routes, including increased antibody levels in animals, reduced mortality in animals after challenge, and a significant reduction in pathological lesions as observed in autopsy; this confirmed that the BCG vaccine provides the most effective immunization effect on animals when administered intravenously [26,27]. These studies reported that the intravenous administration of bacterial or viral components could exert good immunomodulatory and therapeutic effects on the disease. However, there are no reports on intravenous co-administration of bacterial and viral components in a specific ratio. In the present study, we found that the intravenous injection of inactivated *E. faecium* alone could not enable mice to resist PRV infection. Therefore, we combined inactivated *E. faecium* with inactivated PRV and co-administered them intravenously in mice to test the experimental results. We expect that this approach could serve as a reference to treat some diseases that cannot be prevented and cured by conventional treatment strategies; moreover, this approach could also provide a model for vaccine development and clinical application.

Author Contributions: Conceptualization, Y.S.; methodology, Y.S.; software, L.H.; validation, Y.C., G.W. and Y.S.; formal analysis, J.L.; investigation, J.L.; resources, Y.S.; data curation, Y.C., G.W. and Y.S.; writing—original draft preparation, Y.C. and G.W.; writing—review and editing, Y.C., G.W. and Y.S.; visualization, Y.C., G.W., L.H. and Y.S.; supervision, G.W. and Y.S.; project administration, Y.S.; funding acquisition, Y.S. All authors have read and agreed to the published version of the manuscript.

Funding: This work was supported by the Fund of “Tai’an Special Project for Prevention and Control of Pneumonia Epidemic in 2020” (2020FYZX05), and the Fund of “Natural Science Foundation of Shandong Province” (ZR2021MC161).

Institutional Review Board Statement: Institutional Review Board Statement: The study protocol and the poultry studies were approved by the Animal Care and Use Committee of Shandong Agricultural University, Tai’an, China (Ethical Approval Number SDAUA-2018-027).

Informed Consent Statement: Not applicable.

Data Availability Statement: Not applicable.

Conflicts of Interest: The authors declare no conflict of interest.

References

1. Pomeranz, L.E.; Reynolds, A.E.; Hengartner, C.J. Molecular biology of pseudorabies virus: Impact on neurovirology and veterinary medicine. *Microbiol. Mol. Biol. Rev.* **2005**, *69*, 462–500. [CrossRef] [PubMed]
2. Li, X.D.; Fu, S.H.; Chen, L.Y.; Li, F.; Deng, J.H.; Lu, X.C.; Wang, H.Y.; Tian, K.G. Detection of Pseudorabies Virus Antibodies in Human Encephalitis Cases. *Biomed. Environ. Sci.* **2020**, *33*, 444–447. [CrossRef] [PubMed]

3. Liu, Q.; Wang, X.; Xie, C.; Ding, S.; Yang, H.; Guo, S.; Li, J.; Qin, L.; Ban, F.; Wang, D.; et al. A Novel Human Acute Encephalitis Caused by Pseudorabies Virus Variant Strain. *Clin. Infect. Dis.* **2021**, *73*, e3690–e3700. [CrossRef]
4. Wang, D.; Tao, X.; Fei, M.; Chen, J.; Guo, W.; Li, P.; Wang, J. Human encephalitis caused by pseudorabies virus infection: A case report. *J. Neurovirol.* **2020**, *26*, 442–448. [CrossRef] [PubMed]
5. Yang, X.; Guan, H.; Li, C.; Li, Y.; Wang, S.; Zhao, X.; Zhao, Y.; Liu, Y. Characteristics of human encephalitis caused by pseudorabies virus: A case series study. *Int. J. Infect. Dis.* **2019**, *87*, 92–99. [CrossRef]
6. Berdeu, I.; Spataru, D.; Paraschiv, A. Vaccines: Past, present and future. *One Health Risk Manag.* **2021**, *2*, 27–35. [CrossRef]
7. Mohammadi, E.; Golchin, M. High protection of mice against *Brucella abortus* by oral immunization with recombinant probiotic *Lactobacillus casei* vector vaccine, expressing the outer membrane protein OMP19 of *Brucella* species. *Comp. Immunol. Microbiol. Infect. Dis.* **2020**, *70*, 101470. [CrossRef]
8. Plotkin, S.A. Vaccines: Past, present and future. *Nat. Med.* **2005**, *11*, S5–S11. [CrossRef]
9. Boyle, J.; Eastman, D.; Millar, C.; Camuglia, S.; Cox, J.; Pearse, M.; Good, J.; Drane, D. The utility of ISCOMATRIX adjuvant for dose reduction of antigen for vaccines requiring antibody responses. *Vaccine* **2007**, *25*, 2541–2544. [CrossRef]
10. Reed, S.G.; Orr, M.T.; Fox, C.B. Key roles of adjuvants in modern vaccines. *Nat. Med.* **2013**, *19*, 1597–1608. [CrossRef]
11. Ahiwe, E.U.; Abdallah, M.E.; Chang'a, E.P.; Omede, A.A.; Al-Qahtani, M.; Gausi, H.; Graham, H.; Iji, P.A. Influence of dietary supplementation of autolyzed whole yeast and yeast cell wall products on broiler chickens. *Asian-Australas. J. Anim. Sci.* **2020**, *33*, 579–587. [CrossRef] [PubMed]
12. Lee, B.B.; Yang, T.S.; Goo, D.; Choi, H.S.; Pitargue, F.M.; Jung, H.; Kil, D.Y. Effects of dietary beta-mannanase supplementation on the additivity of true metabolizable energy values for broiler diets. *Asian-Australas. J. Anim. Sci.* **2018**, *31*, 564–568. [CrossRef] [PubMed]
13. Galdeano, C.M.; Perdigon, G. The probiotic bacterium *Lactobacillus casei* induces activation of the gut mucosal immune system through innate immunity. *Clin. Vaccine Immunol.* **2006**, *13*, 219–226. [CrossRef] [PubMed]
14. Lymbery, A.; Song, S.; Hosseini Shekarabi, S.P. Adjuvant effects of medicinal herbs and probiotics for fish vaccines. *Rev. Aquac.* **2018**, *11*, 1325–1341. [CrossRef]
15. Ma, S.; Wang, L.; Huang, X.; Wang, X.; Chen, S.; Shi, W.; Qiao, X.; Jiang, Y.; Tang, L.; Xu, Y.; et al. Oral recombinant *Lactobacillus* vaccine targeting the intestinal microfold cells and dendritic cells for delivering the core neutralizing epitope of porcine epidemic diarrhea virus. *Microb. Cell Factories* **2018**, *17*, 20. [CrossRef]
16. Dadar, M.; Shahali, Y.; Mojjani, N. Role of immunobiotic lactic acid bacteria as vaccine adjuvants. In *Probiotics in the Prevention and Management of Human Diseases*; Academic Press: Cambridge, MA, USA, 2022; pp. 417–430. [CrossRef]
17. Shi, S.H.; Yang, W.T.; Yang, G.L.; Cong, Y.L.; Huang, H.B.; Wang, Q.; Cai, R.P.; Ye, L.P.; Hu, J.T.; Zhou, J.Y.; et al. Immunoprotection against influenza virus H9N2 by the oral administration of recombinant *Lactobacillus plantarum* NC8 expressing hemagglutinin in BALB/c mice. *Virology* **2014**, *464–465*, 166–176. [CrossRef] [PubMed]
18. Nouri Gharajalar, S.; Mirzai, P.; Nofouzi, K.; Madadi, M.S. Immune enhancing effects of *Lactobacillus acidophilus* on Newcastle disease vaccination in chickens. *Comp. Immunol. Microbiol. Infect. Dis.* **2020**, *72*, 101520. [CrossRef]
19. Li, E.; Chi, H.; Huang, P.; Yan, F.; Zhang, Y.; Liu, C.; Wang, Z.; Li, G.; Zhang, S.; Mo, R.; et al. A Novel Bacterium-Like Particle Vaccine Displaying the MERS-CoV Receptor-Binding Domain Induces Specific Mucosal and Systemic Immune Responses in Mice. *Viruses* **2019**, *11*, 799. [CrossRef]
20. Maldonado Galdeano, C.; Cazorla, S.I.; Lemme Dumit, J.M.; Velez, E.; Perdigon, G. Beneficial Effects of Probiotic Consumption on the Immune System. *Ann. Nutr. Metab.* **2019**, *74*, 115–124. [CrossRef]
21. Song, M.; Hong, H.A.; Huang, J.M.; Colenutt, C.; Khang, D.D.; Nguyen, T.V.; Park, S.M.; Shim, B.S.; Song, H.H.; Cheon, I.S.; et al. Killed *Bacillus subtilis* spores as a mucosal adjuvant for an H5N1 vaccine. *Vaccine* **2012**, *30*, 3266–3277. [CrossRef]
22. Hayashi, R.M.; Lourenco, M.C.; Kraieski, A.L.; Araujo, R.B.; Gonzalez-Esquerria, R.; Leonardecz, E.; da Cunha, A.F.; Carazzolle, M.F.; Monzani, P.S.; Santin, E. Effect of Feeding *Bacillus subtilis* Spores to Broilers Challenged with *Salmonella enterica* serovar Heidelberg Brazilian Strain UFPR1 on Performance, Immune Response, and Gut Health. *Front. Vet. Sci.* **2018**, *5*, 13. [CrossRef] [PubMed]
23. Hong, J.E.; Kye, Y.C.; Park, S.M.; Cheon, I.S.; Chu, H.; Park, B.C.; Park, Y.M.; Chang, J.; Cho, J.H.; Song, M.K.; et al. Alveolar Macrophages Treated With *Bacillus subtilis* Spore Protect Mice Infected With Respiratory Syncytial Virus A2. *Front. Microbiol.* **2019**, *10*, 447. [CrossRef] [PubMed]
24. Lee, J.E.; Kye, Y.C.; Park, S.M.; Shim, B.S.; Yoo, S.; Hwang, E.; Kim, H.; Kim, S.J.; Han, S.H.; Park, T.S.; et al. *Bacillus subtilis* spores as adjuvants against avian influenza H9N2 induce antigen-specific antibody and T cell responses in White Leghorn chickens. *Vet. Res.* **2020**, *51*, 68. [CrossRef] [PubMed]
25. Yu, L.; Zhang, W.; Wang, X.; Zhang, K.; Yin, Y.; Li, J.; Shi, Y. Selection of an Inactivated *Enterococcus faecium* and Evaluation of its Potential as an Immunomodulator via Intravenous Injection. *J. Biotechnol. Biomed.* **2022**, *5*, 42–62. [CrossRef]
26. Barclay, W.R.; Anacker, R.L.; Brehmer, W.; Leif, W.; Ribic, E. Aerosol-Induced Tuberculosis in Subhuman Primates and the Course of the Disease After Intravenous BCG Vaccination. *Infect. Immun.* **1970**, *2*, 574. [CrossRef]
27. Darrach, P.A.; Zeppa, J.J.; Maiello, P.; Hackney, J.A.; Wadsworth, M.H., 2nd; Hughes, T.K.; Pokkali, S.; Swanson, P.A., 2nd; Grant, N.L.; Rodgers, M.A.; et al. Prevention of tuberculosis in macaques after intravenous BCG immunization. *Nature* **2020**, *577*, 95–102. [CrossRef]

28. De Bruin, M.G.; De Visser, Y.E.; Kimman, T.G.; Bianchi, A.T. Time course of the porcine cellular and humoral immune responses in vivo against pseudorabies virus after inoculation and challenge: Significance of in vitro antigenic restimulation. *Vet. Immunol. Immunopathol.* **1998**, *65*, 75–87. [CrossRef] [PubMed]
29. Kimman, T.G.; Bruin, T.M.G.D.; Voermans, J.J.M.; Peeters, B.P.H.; Bianchi, A.T.J. Development and antigen specificity of the lymphoproliferation response of pigs to pseudorabies virus: Dichotomy between secondary Band T-cell responses. *Immunology* **1995**, *86*, 372–378.
30. Alizadeh, M.; Shojadoost, B.; Astill, J.; Taha-Abdelaziz, K.; Karimi, S.H.; Bavananthasivam, J.; Kulkarni, R.R.; Sharif, S. Effects of in ovo Inoculation of Multi-Strain Lactobacilli on Cytokine Gene Expression and Antibody-Mediated Immune Responses in Chickens. *Front. Vet. Sci.* **2020**, *7*, 105. [CrossRef]
31. Bavananthasivam, J.; Alizadeh, M.; Astill, J.; Alqazlan, N.; Matsuyama-Kato, A.; Shojadoost, B.; Taha-Abdelaziz, K.; Sharif, S. Effects of administration of probiotic lactobacilli on immunity conferred by the herpesvirus of turkeys vaccine against challenge with a very virulent Marek's disease virus in chickens. *Vaccine* **2021**, *39*, 2424–2433. [CrossRef]
32. Bermudez-Brito, M.; Plaza-Diaz, J.; Munoz-Quezada, S.; Gomez-Llorente, C.; Gil, A. Probiotic mechanisms of action. *Ann. Nutr. Metab.* **2012**, *61*, 160–174. [CrossRef] [PubMed]
33. Brisbin, J.T.; Gong, J.; Parvizi, P.; Sharif, S. Effects of lactobacilli on cytokine expression by chicken spleen and cecal tonsil cells. *Clin. Vaccine Immunol.* **2010**, *17*, 1337–1343. [CrossRef] [PubMed]
34. Pender, C.M.; Kim, S.; Potter, T.D.; Ritzi, M.M.; Young, M.; Dalloul, R.A. In ovo supplementation of probiotics and its effects on performance and immune-related gene expression in broiler chicks. *Poult. Sci.* **2017**, *96*, 1052–1062. [CrossRef] [PubMed]
35. Plaza-Diaz, J.; Ruiz-Ojeda, F.J.; Gil-Campos, M.; Gil, A. Mechanisms of Action of Probiotics. *Adv. Nutr.* **2019**, *10*, S49–S66. [CrossRef] [PubMed]
36. Hori, T.; Kiyoshima, J.; Shida, K.; Yasui, H. Augmentation of cellular immunity and reduction of influenza virus titer in aged mice fed Lactobacillus casei strain Shirota. *Clin. Diagn. Lab. Immunol.* **2002**, *9*, 105–108. [CrossRef]
37. Olivares, M.; Diaz-Roperero, M.P.; Sierra, S.; Lara-Villoslada, F.; Fonolla, J.; Navas, M.; Rodriguez, J.M.; Xaus, J. Oral intake of Lactobacillus fermentum CECT5716 enhances the effects of influenza vaccination. *Nutrition* **2007**, *23*, 254–260. [CrossRef]
38. Xu, J.; Ren, Z.; Cao, K.; Li, X.; Yang, J.; Luo, X.; Zhu, L.; Wang, X.; Ding, L.; Liang, J.; et al. Boosting Vaccine-Elicited Respiratory Mucosal and Systemic COVID-19 Immunity in Mice With the Oral Lactobacillus plantarum. *Front. Nutr.* **2021**, *8*, 789242. [CrossRef]
39. Oelschlaeger, T.A. Mechanisms of probiotic action—A review. *Int. J. Med. Microbiol.* **2010**, *300*, 57–62. [CrossRef]
40. Rodriguez-Nogales, A.; Algieri, F.; Vezza, T.; Garrido-Mesa, N.; Olivares, M.; Comalada, M.; Riccardi, C.; Utrilla, M.P.; Rodriguez-Cabezas, M.E.; Galvez, J. The viability of Lactobacillus fermentum CECT5716 is not essential to exert intestinal anti-inflammatory properties. *Food Funct.* **2015**, *6*, 1176–1184. [CrossRef]
41. Jimenez, E.; Fernandez, L.; Marin, M.L.; Martin, R.; Odriozola, J.M.; Nueno-Palop, C.; Narbad, A.; Olivares, M.; Xaus, J.; Rodriguez, J.M. Isolation of commensal bacteria from umbilical cord blood of healthy neonates born by cesarean section. *Curr. Microbiol.* **2005**, *51*, 270–274. [CrossRef]
42. Franco, L.; Torres-Dominguez, L.; Mamola, J.; Lemos de Matos, A.; Abrantes, M.; Walker, B.; Tacner, Z.; Kien, C.; Elliott, N.; McFadden, G.; et al. Abstract PO091: Armed Myxoma virus demonstrates efficacy in syngeneic tumor models alone and in combination with immune checkpoint inhibitors. *Cancer Immunol. Res.* **2021**, *9*, PO091. [CrossRef]
43. Park, S.; Moshiri, A.; Hadi, R.; Green, A.; Gardner, J.; Doolittle-Amieva, C. 593 Tumoral melanosis mimicking residual melanoma After T-VEC treatment. *J. ImmunolTherapy Cancer* **2020**, *8* (Suppl. S3), A355–A356. [CrossRef]
44. Rahman, M.M.; McFadden, G. Oncolytic Virotherapy with Myxoma Virus. *J. Clin. Med.* **2020**, *9*, 171. [CrossRef] [PubMed]
45. Yi, X.; Zhou, H.; Chao, Y.; Xiong, S.; Zhong, J.; Chai, Z.; Yang, K.; Liu, Z. Bacteria-triggered tumor-specific thrombosis to enable potent photothermal immunotherapy of cancer. *Sci. Adv.* **2020**, *6*, eaba3546. [CrossRef]

Disclaimer/Publisher's Note: The statements, opinions and data contained in all publications are solely those of the individual author(s) and contributor(s) and not of MDPI and/or the editor(s). MDPI and/or the editor(s) disclaim responsibility for any injury to people or property resulting from any ideas, methods, instructions or products referred to in the content.

Article

Isolation and Characterization of a Novel Recombinant Classical Pseudorabies Virus in the Context of the Variant Strains Pandemic in China

Zhengmin Lian¹, Panrao Liu¹, Zhenbang Zhu¹, Zhe Sun², Xiuling Yu², Junhua Deng², Ruichao Li¹, Xiangdong Li^{1,2,*} and Kegong Tian^{2,*}

¹ Jiangsu Co-Innovation Center for Prevention and Control of Important Animal Infectious Diseases and Zoonoses, College of Veterinary Medicine, Yangzhou University, Yangzhou 225009, China; lian_zm@126.com (Z.L.); 007617@yzu.edu.cn (P.L.)

² Luoyang Putai Biotech Co., Ltd., Luoyang 471003, China

* Correspondence: 007352@yzu.edu.cn (X.L.); tiankg@263.net (K.T.)

Abstract: Pseudorabies virus (PRV) variants were discovered in immunized pigs in Northern China and have become the dominant strains since 2011, which caused huge economic losses. In this study, a classical PRV strain was successfully isolated in a PRV gE positive swine farm. The complete genome sequence was obtained using a high-throughput sequencing method and the virus was named JS-2020. The nucleotide homology analysis and phylogenetic tree based on complete genome sequences or gC gene showed that the JS-2020 strain was relatively close to the classical Ea strain in genotype II clade. However, a large number of amino acid variations occurred in the JS-2020 strain compared with the Ea strain, including multiple immunogenic and virulence-related genes. In particular, the gE protein of JS-2020 was similar to earlier Chinese PRV strains without Aspartate insertion. However, the amino acid variations analysis based on major immunogenic and virulence-related genes showed that the JS-2020 strain was not only homologous with earlier PRV strains, but also with strains isolated in recent years. Moreover, the JS-2020 strain was identified as a recombinant between the GXGG-2016 and HLJ-2013 strains. The pathogenicity analysis proved that the PRV JS-2020 strain has typical neurogenic infections and a strong pathogenicity in mice. Together, a novel recombinant classical strain was isolated and characterized in the context of the PRV variant pandemic in China. This study provided some valuable information for the study of the evolution of PRV in China.

Keywords: pseudorabies virus; classical strain; phylogenetic analysis; recombination; pathogenicity



Citation: Lian, Z.; Liu, P.; Zhu, Z.; Sun, Z.; Yu, X.; Deng, J.; Li, R.; Li, X.; Tian, K. Isolation and Characterization of a Novel Recombinant Classical Pseudorabies Virus in the Context of the Variant Strains Pandemic in China. *Viruses* **2023**, *15*, 1966. <https://doi.org/10.3390/v15091966>

Academic Editor: Ronald N. Harty

Received: 22 August 2023

Revised: 18 September 2023

Accepted: 20 September 2023

Published: 20 September 2023



Copyright: © 2023 by the authors. Licensee MDPI, Basel, Switzerland. This article is an open access article distributed under the terms and conditions of the Creative Commons Attribution (CC BY) license (<https://creativecommons.org/licenses/by/4.0/>).

1. Introduction

Pseudorabies virus (PRV) is a highly pathogenic and infectious pathogen in pigs, which causes pseudorabies (PR) or Aujeszky's disease (AD) and is characterized by neurological symptoms, fever and itchiness. AD leads to abortion and stillbirth in swine, growth retardation in growing pigs, and high mortality in piglets, resulting in huge economic losses in pig production. PRV is a double-stranded linear DNA virus belonging to the Herpesviridae family, Alphaherpesvirinae subfamily and Varicellovirus genus. The genomes of herpesvirus were divided into six classes (A to F). The PRV genome belongs to the D class, which is similar to the varicella-zoster virus (VZV) genome [1]. The first complete DNA sequence of the PRV genome was obtained from several published incomplete sequences and multiple newly sequenced fragments derived from different strains [2]. The first full genome characterization of a single PRV strain (Bartha strain) was revealed using Illumina high-throughput sequencing [3]. These studies showed that PRV was organized into a unique long (UL) region, a unique short (US) region and two large inverted and terminal repeats (IR, TR) flanking the US region.

The earliest sporadic outbreaks of PRV were reported in the United States in 1813 and then PRV was spread around the world [1]. With the widespread use of the PRV Bartha-K61 strain, an attenuated live vaccine, PRV was effectively controlled in pigs [4]. Furthermore, it has been eradicated in the United States, Netherlands and various European countries [5]. In China, PRV was discovered in 1950s. With the use of the commercial Bartha-K61 vaccine since the 1970s, PRV was effectively controlled in Chinese swine farms. However, since 2011, the PRV variant strain was discovered in pigs immunized with the Bartha-K61 vaccine in Northern China, and then spread rapidly almost nationwide [6,7]. The epidemiological investigation revealed that the positive rate of wild-type PRV was 8.27% between 2012 and 2017, and it even reached 12% between 2012 and 2013 [8]. Although the Bartha-K61 vaccine was widely used in swine farms, more and more outbreaks of PRV were reported in vaccinated swine farms since the variant strain was discovered [9–11]. Several research studies have shown that the Bartha-K61 vaccine could not provide full protection against the PRV variant strains [7,12,13]. Compared with classical PRV strains, the PRV variant showed stronger pathogenicity in pigs [10,14]. In recent years, several novel vaccines based on PRV variant strains have been developed and evaluated, including the gE/gI-deleted inactivated vaccine based on the PRV ZJ01 strain [15], the inactivated vaccine (gE-deleted) and the live attenuated vaccine (gE/gI/TK-deleted) based on the PRV HN1201 strain [16,17].

With the wide application of high-throughput sequencing technology, multiple complete genome sequences of PRV variant strains were reported and characterized. However, the novel classical strains were less reported on. In this study, a novel classical PRV strain was isolated in the context of the PRV variant pandemic in China. Its complete genome sequence was obtained using Illumina high-throughput sequencing. The genome characteristics, genetic evolution and amino acid variations were analyzed. Furthermore, the biological characteristics and pathogenicity were further revealed and tested.

2. Materials and Methods

2.1. Cells and Virus Infection

PK-15 cells were purchased from the American Type Culture Collection (ATCC) and cultured in Dulbecco's modified Eagle medium (DMEM) (Solarbio, Shanghai, China) supplemented with 10% fetal bovine serum (FBS, Thermo Fisher Scientific, Waltham, MA, USA) at 37 °C in 5% CO₂. Clinical brain tissue samples were collected from a case of PRV-suspected aborted swine in Jiangsu Province of China in 2020. The fever and loss of appetite were observed from aborted swine. It was a PRV negative farm, and the pigs were not vaccinated with any PRV vaccines in recent years. Samples were homogenized and the PK-15 cells were infected with filtered supernatant for 1 h. Next, the infected cells were washed with phosphate-buffered saline (PBS) and incubated in DMEM supplemented with 1% FBS.

2.2. PCR Identification and Growth Curves

The supernatant samples from infected PK-15 cells which showed PRV-like cytopathic effects (CPEs), were purified using three rounds of plaque purification to obtain purified PRV. Total DNA strands of purified PRV samples were extracted using viral genomic DNA extraction kit according to the manufacturer's instructions (TIANGEN, China). Next, purified DNA samples were identified with polymerase chain reaction (PCR) using PRV specific primers pairs for gD gene (F: 5' CAG GAG GAC GAG CTG GGG CT -3' and R: 5' GTC CAC GCC CCG CTT GAA GCT -3').

The purified PRV JS-2020 and Bartha strain were inoculated with PK-15 cells at 0.1 MOI in DMEM supplemented with 1% FBS, and the supernatants were harvested at 2, 6, 12, 24, 36 and 48 h post infection. The viral titers of supernatants were tested using PK-15 cells.

2.3. Immunofluorescence

PK-15 cells were infected with JS-2020 at 0.1 MOI in DMEM and supplemented with 1% FBS; cell samples were collected at 24 h post infection. For immunofluorescence, the infected PK-15 cells were fixed with 4% paraformaldehyde for 10 min and permeabilized with 0.5% Triton X-100 at room temperature. Cells were blocked with 3% bovine serum albumin (BSA) for 1 h at room temperature and incubated with PRV gB protein antibody (A general gift from Prof. Beibei Chu at Henan Agricultura University) overnight at 4 °C. Following three washes with PBS, cells were incubated with an Alexa fluor 555-conjugated anti-mouse IgG (Cell Signaling Technology, Danvers, MA, USA) for 1 h at the room temperature. The cells were visualized with an inverted fluorescence microscope (U-HGLGPS, OLYMPUS, Tokyo, Japan).

2.4. Complete Genome Sequencing and Analysis

Purified genomic DNA of PRV JS-2020 strain was sequenced through next-generation sequencing (NGS) technology using Illumina paired-end sequencing (Sangon Biotech, Shanghai, China). The complete genome sequence was annotated using SnapGene 6.0 software and submitted to the GenBank database (GenBank accession number: OR271601).

The complete sequences of JS-2020 strain were aligned with other 15 PRV strains (Table 1), the nucleotide homology analysis was performed using MegAlign module of DNASTAR Lasergene 7 software. Phylogenetic trees of genomic and gC sequences were constructed using maximum likelihood (ML) method of MEGA11 software (V11.0.13).

Table 1. Information of pseudorabies virus strains for gC gene and complete genome analysis.

Strain	Accession Number	Country	Isolation Date
HeNZM/2017	MW560175.1	China	2017
JX/CH/2016	MK806387.1	China	2016
LA	KU552118.1	China	1997
Ea	KU315430.1	China	1990
Fa	KM189913.1	China	2012
FB	ON005002.1	China	1986
hSD-1/2019	MT468550.1	China	2019
PRV XJ	MW893682.1	China	2015
PRV-GD	OK338076.1	China	2021
SX1911	OP376823.1	China	2019
Becker	JF797219.1	USA	1970
SC	KT809429.1	China	1986
Bartha	JF797217.1	Hungary	1961
GXGG-2016	OP605538.1	China	2016
HLJ-2013	MK080279.1	China	2013
JS-2020	OR271601	China	2020

2.5. Amino Acid Variations Analysis

Amino acid sequence alignment of JS-2020 ORFs were performed using BLAST on the NCBI website (https://blast.ncbi.nlm.nih.gov/Blast.cgi?PROGRAM=blastp&PAGE_TYPE=BlastSearch&LINK_LOC=blasthome, accessed on 20 June 2023). The amino acid sequence homology and phylogenetic trees of PRV major immunogenic and virulence-related genes (including gB, gC, gD, gE, gI and TK) were analyzed using maximum likelihood (ML) method with MEGA11 software (V11.0.13).

2.6. Recombination Analysis

RDP4 software (V4.101) was used to detect the potential recombination signals in JS-2020 strain with Bootscan, 3seq, PhylPro, Maxchi, SiScan and Chimaera algorithms. Then, the major recombination events were further validated with SimPlot 3.5.1 software with a sliding window of 2000 nucleotides which moved every 200 nucleotide steps.

2.7. Animal Experiments

The purified PRV JS-2020 strain was diluted to $10^{4.5}$ TCID₅₀/mL in DMEM. Six-week-old specific pathogen-free (SPF) BALB/c mice (Comparative Medicine Center of Yangzhou University) were randomly divided into two groups including DMEM group and PRV infected group. The 5 mice of PRV infected group were infected with $10^{3.5}$ TCID₅₀ PRV JS-2020 strain in 100 μ L DMEM by injecting intraperitoneally. Another 5 mice of DMEM group were intraperitoneally injected with 100 μ L DMEM. Mice were monitored daily, and the survival rates were recorded for 7 days.

2.8. Histopathology and Immunohistochemistry Staining

Brain tissues samples were collected from dead mice of PRV JS-2020 strain infected group and surviving mice of DMEM group. Samples were fixed with 10% formaldehyde, placed into paraffin blocks, and cut into sections. The hematoxylin and eosin staining were applied to sections for histopathological examination. PRV specific antibody (anti-gB protein) was used for immunohistochemistry staining as described previously [18].

3. Results

3.1. Isolation and Identification of PRV JS-2020 Strain

The PRV gE positive brain tissue samples from aborted piglets were identified with the real-time PCR method. Supernatants of the PRV gE-positive tissues were incubated in PK-15 cells and typical CPEs of PRV were observed within 24 h post infection (hpi) (Figure 1A). Moreover, the results of IFA showed that PRV gB protein was detected in infected PK-15 cells (Figure 1A). After three rounds of plaque purification and PCR identification (Figure 1B), the purified PRV was obtained and named JS-2020. Results of growth curves showed the highly efficient replication capability of JS-2020 in PK-15 cells (Figure 1C). The viral titers of JS-2020 in infected cells' supernatants increased rapidly from 6 hpi to 12 hpi, and peaked with a viral copy number of more than 10^9 TCID₅₀/mL after 36 hpi (Figure 1C). This result was similar to the Bartha-K61's outcome. These results indicated that a field strain of PRV was successfully isolated from the clinical samples and grew well in PK-15 cells.

3.2. Genomic Characterization of the JS-2020 Strain

To identify the genetic characteristics of the JS-2020 strain, the complete genome sequences were obtained using the high-throughput sequencing method. The complete genome length of the JS-2020 strain was 143,246 bp, which encodes 69 open reading frames (ORFs) (Figure 2A). The genome sequence was divided into the following four parts: UL (101,287 bp), US (9183 bp), IR (16,388 bp) and TR (16,388 bp) (Table 2). GC content was 74%, which was similar to other published PRV strains [4].

Table 2. Genome organization and location of PRV JS-2020 strain.

Region	Start (5')	End (3')	Length (bp)
UL	1	101,287	101,287
IR	101,288	117,675	16,388
US	117,676	126,858	9183
TR	126,858	143,246	16,388

Based on complete genome sequences, the nucleotide homology analysis revealed that JS-2020 shared 91.3–99% homology with other PRV strains. In addition, it had the highest homology with the Ea strain (99.8%), which is a Chinese classical PRV strain isolated in 1990

(Table 3). Moreover, the phylogenetic trees based on both genomic and gC sequences were constructed and analyzed (Figure 2B,C). The phylogenetic tree based on gC showed that the PRV strains were classified into genotype I and genotype II, and the JS-2020 strain was clustered within genotype II. The results based on the complete genome showed that the JS-2020 strain also clustered with Chinese PRV strains and had the closest genetic evolutionary relationship with the Ea strain, which was a Chinese classical PRV strain isolated in 1990. These results, which were based on the analysis of genome sequences, suggested that a classical PRV strain was isolated in the context of the PRV variant pandemic in China.

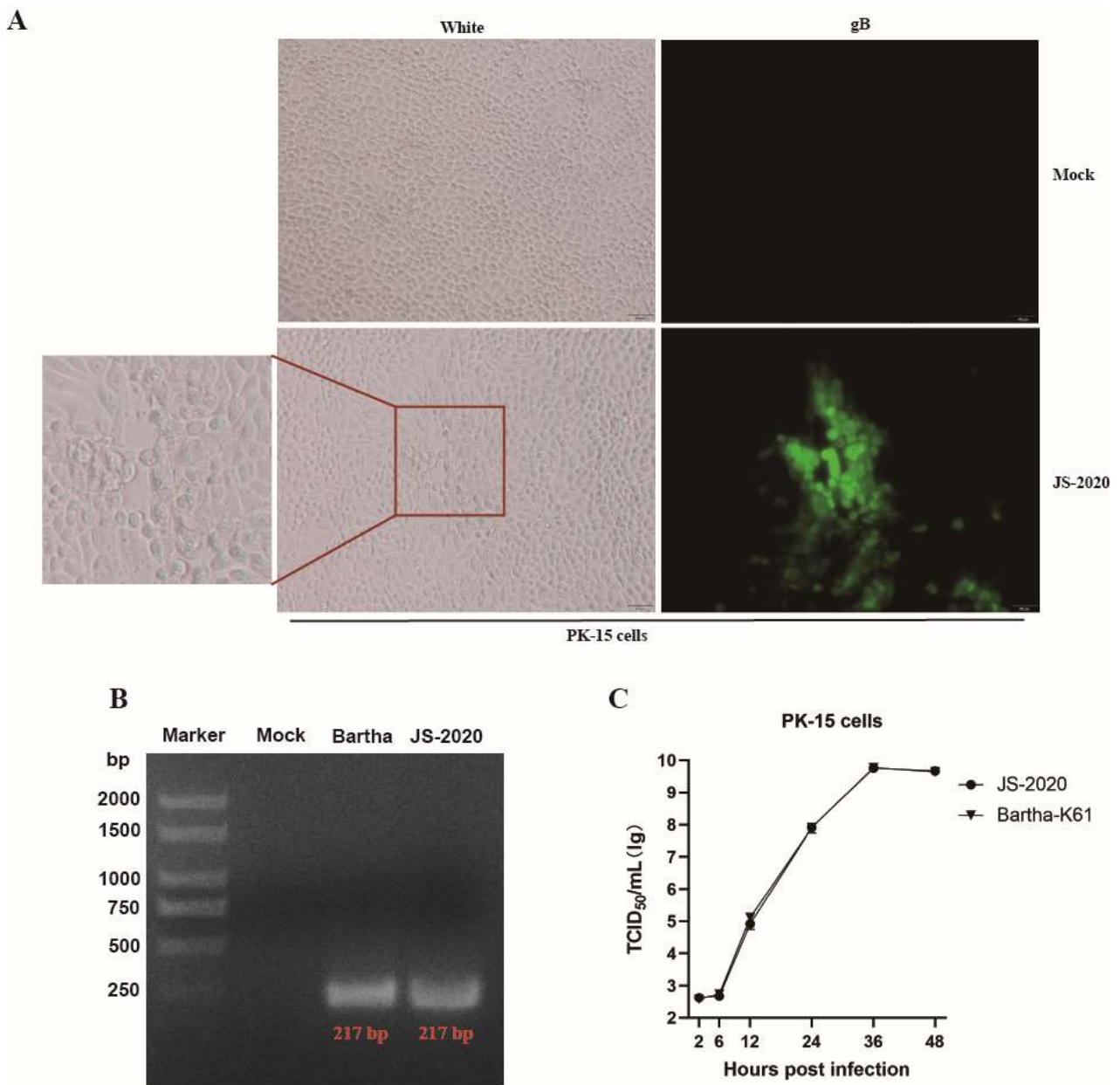


Figure 1. Isolation and identification of PRV JS-2020 strain. (A) PRV-like CPEs were observed within 24 h post infection, and the gB protein of PRV was positive (IFA). (B) PCR identification of purified JS-2020 strain (gD gene, where Bartha was used as a positive control). (C) Growth curves of JS-2020 strain.

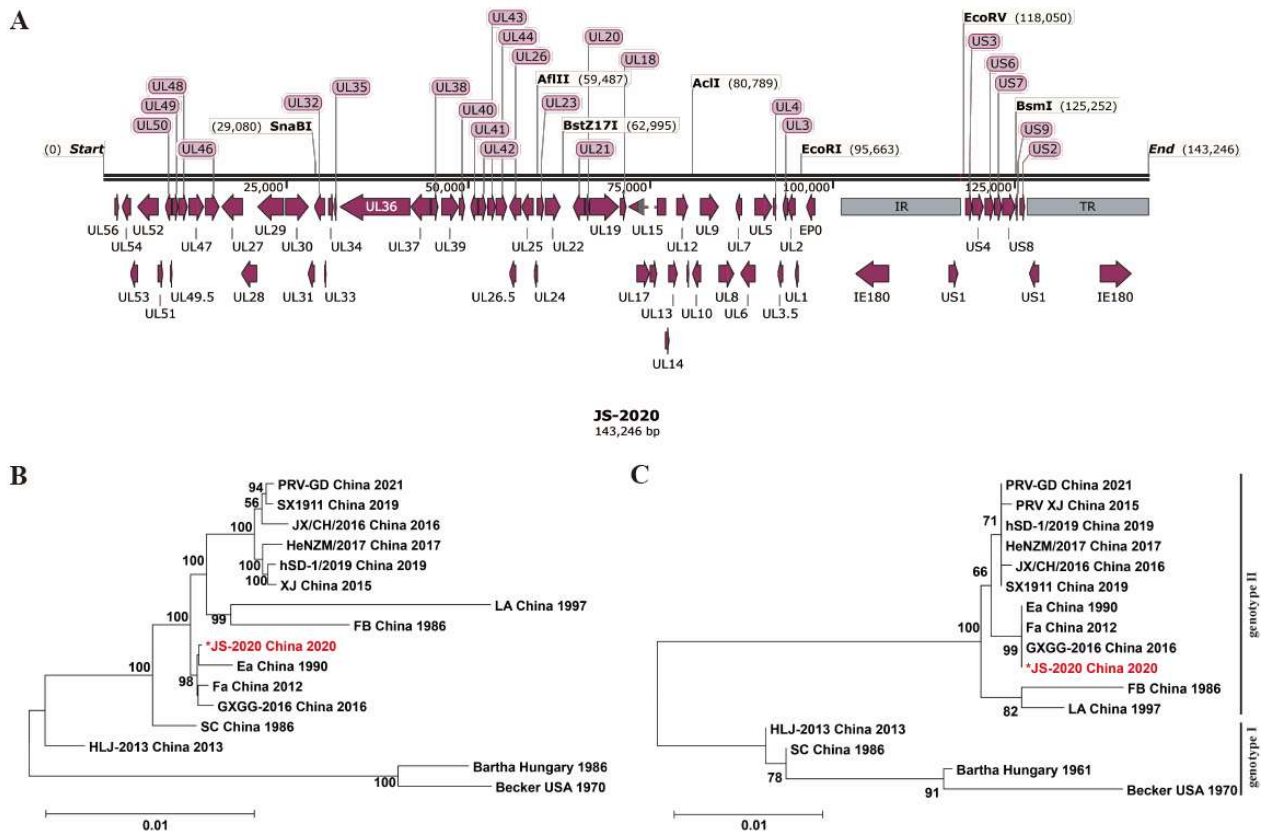


Figure 2. Genomic characterization of PRV JS-2020 strain. Complete genome distribution of JS-2020 strain (A) and the phylogenetic trees based on both complete sequences (B) and gC (C). “*” indicates the target PRV strain in this study.

Table 3. Nucleotide homology of 13 PRV strains compared with JS-2020 strain.

PRV Strain	Nucleotide Homology % (Complete Genome)														
	JX/CH/2016	LA	Ea	Fa	FB	hSD-1/2019	PRV XJ	PRV-GD	SX1911	Becke	SC	Bartha	HLJ-2013	GXGG-2016	JS-2020
HeNZM/2017	97.1	94.1	96.4	96.1	94.6	96.6	96.9	95.6	97.2	91.7	95.7	90.3	95.5	96.3	96.8
JX/CH/2016		94.7	97.1	97	95.4	97.6	98.4	95.6	97.8	91.9	96.7	90.9	96.5	97.1	97.8
LA			94.9	94.8	93.5	94.3	94.7	93.3	94.3	92.1	94.2	90.6	94.7	94.7	95.1
Ea				98.3	95.8	96.4	96.9	94.7	96.6	91.9	96.9	90.9	97.1	99.2	99
Fa					96.9	96.1	96.6	94.6	96.5	91.8	96.9	90.8	97.1	98.2	98.8
FB						95.5	95.1	94	95.6	91.1	95.7	90.1	95.7	95.8	96.4
hSD-1/2019							98.6	96.3	98.3	91.4	97.8	90.1	96.1	96.4	97
PRV XJ								95.7	98	91.8	97.4	90.4	96.4	96.8	97.5
PRV-GD									96.7	90.8	95.4	88.9	94.4	94.6	95.3
SX1911										92.1	97.2	90.5	96.3	96.6	97.3
Becker											92	93.8	93	91.7	92.3
SC												91.1	97.3	96.9	97.6
Bartha													92.3	90.8	91.3
HLJ-2013														97.1	97.9
GXGG-2016															98.9

3.3. Amino Acid Variations Analysis of the JS-2020 Strain

Compared with the Ea strain, a total of 27 proteins of the JS-2020 strain were different, containing 86 mutations, 7 deletions and 20 insertions (Table 4). The major amino acid variations occurred in UL47 (7 aa), UL27 (6 aa), UL36 (34 aa), IE180 (7 aa), US1 (21 aa) and US3 (5 aa).

Table 4. Protein coding variations of JS-2020 strain compared with Ea strain.

Protein Name	Number (aa)	Amino Acid Residues and Location
UL50	1	24 (+E)
UL49.5	1	4 (+S)
UL48	4	R161Q T216M T271A H397P
UL47	7	P399A V404L D406E T411A 414–415(TL > AV) P419A
UL46	2	C494Y A666T
UL27	6	P735L H560Q G393D V114G T112P
UL28	1	V428G
UL30	1	P150L
UL32	1	T402A
UL34	1	A78V
UL35	1	P102S
UL36	34	G3167D 2510–2512(Δ APP) K2267T 279–280(Δ QS) 942–968(GAAGRAVGGRRGGGRGDARAGCARSPTR> ALQAALSAAVAAVEMLGRLRAQPDE
UL39	1	L571F
UL41	2	S218T Y111H
UL15	2	F545S K169E
UL17	1	D209A
UL10	4	L200H V158A R116Q Q107R
UL9	1	C218R
UL3.5	1	S195P
UL2	2	42–43(Δ GA)
EP0	3	A270G C200S V161M
IE180	7	V999A Q943E N908K P865S V757A T724A Q524R
US1	21	P81A G136C K236E 342–343 (+EDEDEDEDEDEDEDEDEDE)
US3	5	S24G R115P P135R V177D G214A
US6	2	F169S S278R
US7	1	V148L
US2	1	Y265S

Note: Single amino acid variation is indicated by the amino acid in Ea strain, position and amino acid in JS-2020 strain, e.g., R161Q. Insertions in JS-2020 strain are indicated by position in Ea strain followed by a plus sign and the amino acids of JS-2020 strain, e.g., 24(+E). Deletions are indicated by position, symbol " Δ " and the amino acids in Ea strain, e.g., 279–280(Δ QS). Sequential variations are indicated by position, the amino acid in Ea strain, symbol ">" and the amino acid of JS-2020 strain, e.g., 414–415(TL > AV).

To assess the variations of major immunogenic and virulence-related genes (including gB, gC, gD, gE, gI and TK), the amino acid sequence of the JS-2020 strain was compared with 24 Chinese PRV strains and the Bartha strain. The homology analysis results showed that the gI and TK of JS-2020 was highly conserved (sharing 100% homology with most of the Chinese PRV strains) and gB, gC, gD and gE shared lower homology with other PRV strains (gB 96.5–99.7%, gC 92.4–100%, gD 97.3–100% and gE 83.9–100%). Moreover, the phylogenetic trees based on amino acid sequence of gB, gC, gD, gE, gI and TK were constructed and analyzed (Figure 3). The gB protein of the JS-2020 strain had the highest homology with the Fa, GXGG-2016 and SC strain (99.7%), but their evolutionary relationships belong to different branches (Figure 3A). The gC protein has 100% homology and the closest evolutionary relationship with the Ea, Fa and GXGG-2016 strain (Figure 3B). The gD protein has the highest homology (100%) and belongs to same branch of evolutionary relationship with the Fa, GXGG-2016, HLJ-2013 and SC strain. (Figure 3C). The gE protein has the highest homology (100%) and the closest evolutionary relationship with Ea, Fa, HLJ-2013 and SC strain (Figure 3D). The evolutionary relationships of highly conserved gI and TK proteins are similar to homology analysis results, which are also similar to most of the Chinese PRV strains (Figure 3E,F).

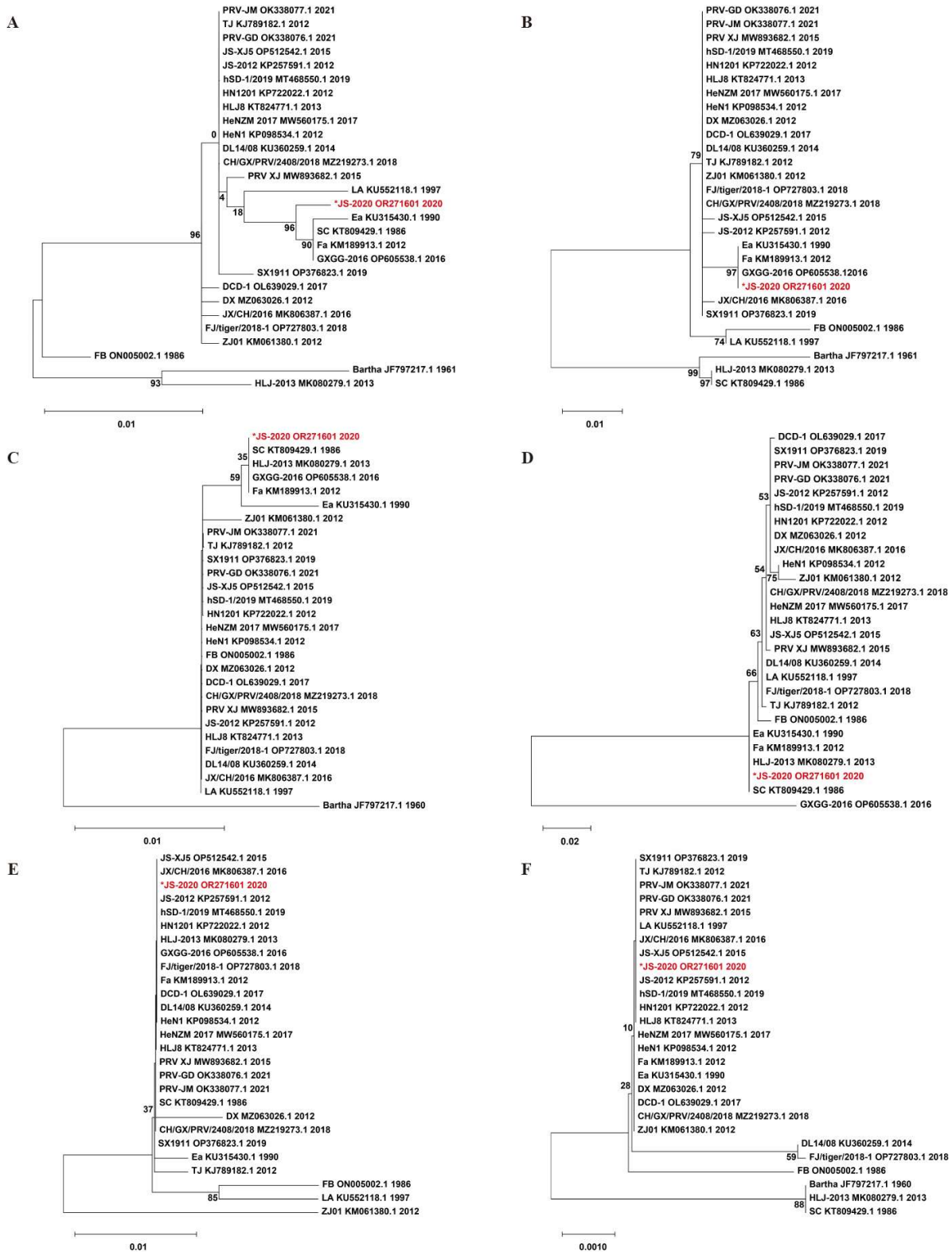


Figure 3. Phylogenetic trees that are based on amino acid sequences of gB (A), gC (B), gD (C), gE (D), gI (E) and TK (F). “*” indicates the PRV isolate in this study.

The results of previous studies showed that the gE protein of the PRV variant strain contained two Aspartate (Asp, D) insertions when compared with earlier PRV strains that were isolated from China. Although Asp insertions were also observed in a few early PRV strains, the insertions in the variant strains were highly conserved [7,9]. The results of the amino acid sequence analysis showed that the gE protein of the JS-2020 strain is similar to the earlier Chinese PRV strains without the Asp insertion at the amino acid position 497 (Figure 4). These results further proved that a classical PRV strain was isolated, which is similar to earlier Chinese PRV strains.

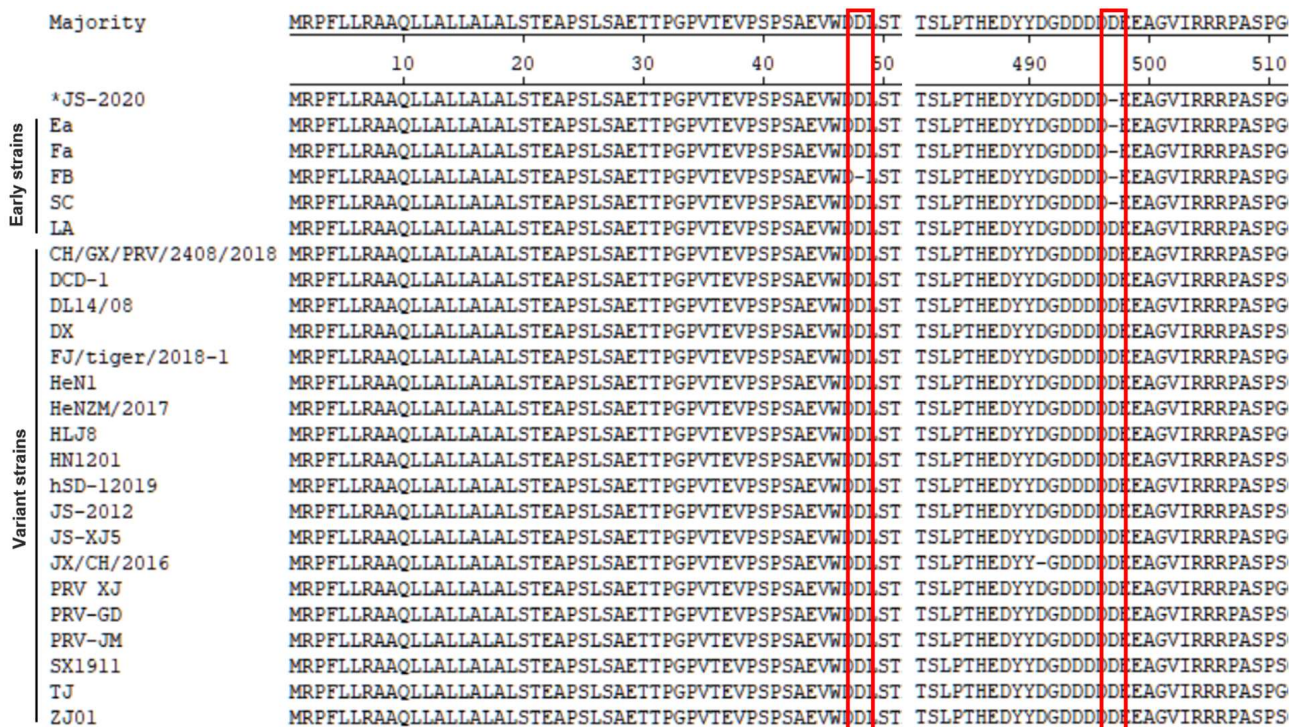


Figure 4. Alignment of amino acid sequences of PRV gE protein. JS-2020 strain is similar to earlier Chinese PRV strains without Asp insertion at amino acid position 497. Red lines indicate two Asp insertions in the variant strains.

3.4. Recombination Analysis

Multiple studies have shown that recombinant events were found in a few isolated Chinese PRV strains [9,19,20]. The homology analysis of the JS-2020 results showed that partial genes of the JS-2020 have high homology and close evolutionary relationship not only with earlier PRV strain (Ea), but also with recent strains (GXGG-2016). These results suggested that the JS-2020 might be a recombinant strain. To test whether there are any recombination signals in the JS-2020 with other Chinese PRV strains (as shown in Table 5) and the Bartha strain, recombinant analysis was performed using RDP4 software (V4.101). The results showed that several major recombination events were detected in the JS-2020 strain with Bootscan, 3seq, PhylPro, Maxchi, SiScan and Chimaera algorithms. In addition, the major backbone of the JS-2020 was the GXGG-2016 strain, and the major recombination regions were obtained from the HLJ-2013 strain (minor backbone). There were no Ea and Fa strains associated with the recombination signals in the JS-2020 strain, although they shared high homology. Moreover, the recombination events were further verified using Simplot 3.5.1 software. The result showed that four potential major recombination regions which form the HLJ-2013 strain were detected and that they were located at 15,201 to 17201; 31,401 to 33,201; 109,401 to 119,401 and 126,401 to 132,001 (Figure 5). The major recombination regions include partial UL46, UL27, UL34, UL36 and US3 ORFs and complete UL35, US1 and US2 ORFs (Figure 5). The other regions of the JS-2020 strain were highly similar to the

GXGG-2016 strain. These results indicated that the JS-2020 and the GXGG-2016 strain share a common parental strain and most of the fragments in the JS-2020 strain come from the GXGG-2016 strain. However, there is a continuous deletion of 69 amino acids in the TK gene of the GXGG-2016 strain [20], but the JS-2020 does not undergo deletion. Therefore, this indicates that the TK gene of the JS-2020 comes from other PRV strains.

Table 5. Amino acid homology of major immunogenic and virulence-related genes.

PRV Strain	Homology of Amino Acid Sequence (%)					
	gB	gC	gD	gE	gI	TK
Bartha	96.5	92.7	97.3	-	-	99.4
CH/GX/PRV/2408/2018	99.3	99.4	99.8	99.3	100.0	100.0
DCD-1	99.2	99.4	99.8	99	100.0	100.0
DL14/08	99.3	99.4	99.8	99.5	100.0	99.7
DX	99.2	99.4	99.8	99.1	99.5	100.0
Ea	99.5	100.0	99.5	100.0	99.7	100.0
Fa	99.7	100.0	100.0	100.0	100.0	100.0
FB	98.3	97.3	99.8	99.1	98.6	99.7
FJ/tiger/2018-1	99.5	99.4	99.8	99.5	100.0	99.7
GXGG-2016	99.7	100.0	100.0	83.9	100.0	-
HeN1	99.3	99.4	99.8	98.8	100.0	100.0
HeNZM/2017	99.3	99.4	99.8	99.3	100.0	100.0
HLJ-2013	97.8	94.4	100.0	99.8	100.0	99.4
HLJ8	99.3	99.4	99.8	99.3	100.0	100.0
HN1201	99.3	99.4	99.8	99.1	100.0	100.0
hSD-1/2019	99.3	99.4	99.8	99.1	100.0	100.0
JS-2012	99.3	99.2	99.8	99.1	100.0	100.0
JS-XJ5	99.3	99.2	99.8	99.3	100.0	100.0
JX/CH/2016	99.2	99.2	99.8	99.1	100.0	100.0
LA	98.8	98.3	99.7	99.5	98.6	100.0
PRV XJ	99.2	99.4	99.8	99.1	100.0	100.0
PRV-GD	99.3	99.4	99.8	99.1	100.0	100.0
PRV-JM	99.3	99.4	99.8	99.1	100.0	100.0
SC	99.7	94.4	100.0	100.0	100.0	99.4
SX1911	99.1	99.4	99.8	99.1	100.0	100.0
TJ	99.3	99.4	99.8	99.3	99.7	100.0
ZJ01	99.2	99.4	99.5	98.4	97.3	100.0

Note: “-” indicates the deletion of this gene.

3.5. Pathogenicity Analysis

Mice are commonly used as animal models since they show neurogenic infections of the central nervous systems (CNS) with high mortalities in a productive PRV infection [21,22]. To assess the pathogenicity of the JS-2020 strain, the six-week-old specific pathogen-free (SPF) BALB/c mice were infected with the PRV JS-2020 strain or the DMEM by injecting, intraperitoneally. The results showed that the mice infected with the PRV JS-2020 strain began to die on the third day post infection (Figure 6A). All PRV infected mice died on fifth day post infection and the symptoms associated with the PRV infection (nervous symptoms and dead mice) were not observed in the DMEM group. In our previous study results, the higher dose of PRV Bartha -K61 (50 μ L 1×10^5 TCID₅₀/mL) infected mice started to die as early as the fifth day post infection. Therefore, the JS-2020 showed higher pathogenicity than Bartha-K61 in mice [23].

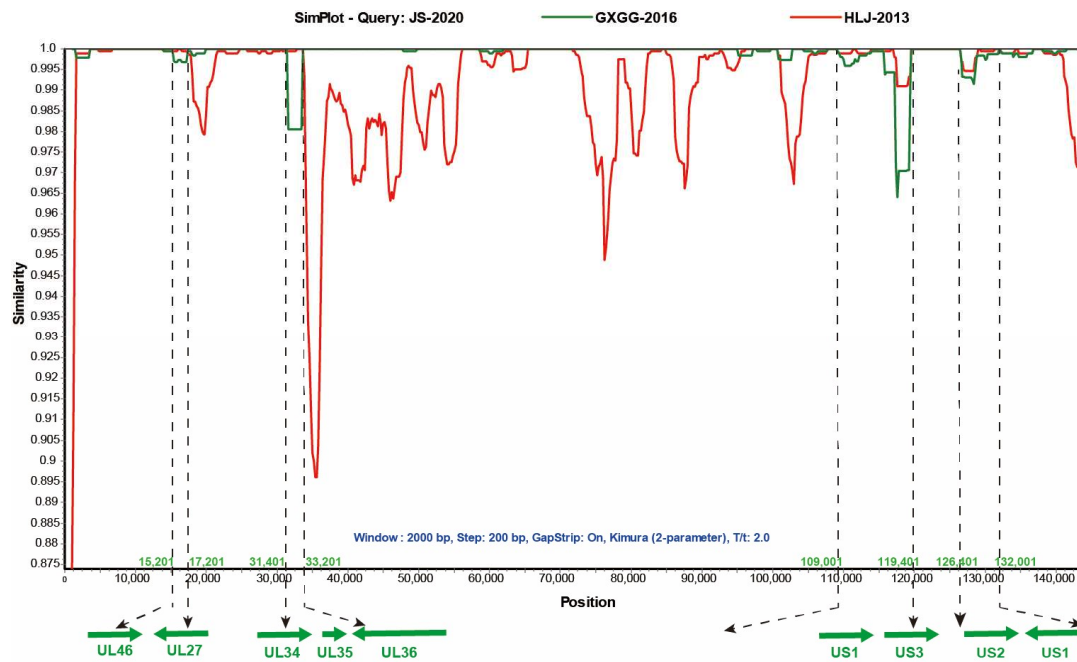


Figure 5. Recombination analysis of JS-2020 strain using Simplot 3.5.1 software. The four recombination regions are shown with dotted lines. Parameters: Window 2000 bp, Step 200 bp, GapStrip On, Kimura (2-parameter), T/t 2.0.

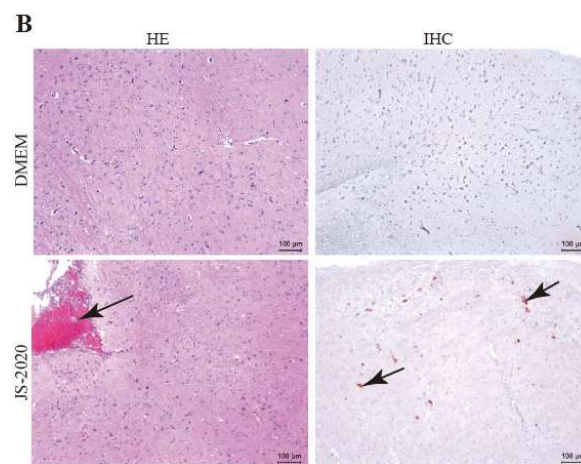
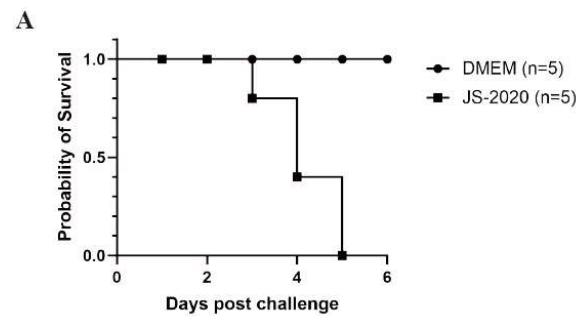


Figure 6. Pathogenicity of JS-2020 strain in mice. (A) Six-week-old SPF BALB/c mice were infected with $10^{3.5}$ TCID₅₀ PRV JS-2020, survival of each group was recorded and the survival curves were generated. (B) The histopathological examination (HE) and immunohistochemistry staining (IHC) of brain tissues.

Next, histopathological examination and immunohistochemistry staining of brain tissues were performed to evaluate the neurovirulence of the JS-2020 strain. The hematoxylin-eosin (HE) staining results showed that the meningeal congestion was observed in mice infected with the PRV JS-2020 strain (Figure 6B, HE). Immunohistochemistry staining results revealed that PRV antigens were positive in brain tissues of the mice infected with the PRV JS-2020 strain (Figure 6B, IHC). No lesions or PRV antigens were observed in the brain tissues of mice in the DMEM group. These results indicated that the PRV JS-2020 strain has typical neurogenic infections and a strong pathogenicity in mice.

4. Discussion

Since the PRV variant strains were discovered in 2011 in China, it has spread to most areas of China and caused huge economic losses. Next, more and more PRV variant strains were isolated and identified. To control the spread of newly emerged PRV variants, several effective vaccines based on PRV variants have been developed and applied in recent years in China. However, PRV exhibits a definite neurotropism and results in acute infection in piglets or in the establishment of latent infection in trigeminal ganglion neurons [1,21]. Based on its characteristic of latent infection, the earlier PRV strains were able to maintain long-term infection in swine farms. These PRV strains can be reactivated and spread to healthy pigs. In this study, a classical PRV strain (JS-2020) was isolated and identified from PRV-infected pigs in 2020. It proved that the earlier PRV strains still persist in Chinese swine farms in the context of the PRV variant pandemic.

The complete genomic sequences of the PRV JS-2020 strain were obtained using a high-throughput sequencing method. It had similar genome organization, including a unique long (UL) region, a unique short (US) region and two inverted repeats (IR and TR) along with other published PRV strains. Based on complete genome sequences, the JS-2020 strain has high homology and a close evolutionary relationship with the Ea strain (an earlier classical PRV strain isolated in 1990 in China). In addition, it was classified into genotype II with most of the other Chinese PRV strains based on the gC phylogenetic tree. Compared with the Ea strain, a large number of amino acid variations occurred in the JS-2020 strain, including multiple immunogenic and virulence-related genes.

It was reported that the gB, gC, gD, gE, gI and TK genes are major immunogenic and virulence-related genes of PRV. The gB protein is one of envelope glycoproteins and major viral antigen in PRV, participates in the processes of viral entry and cell-to-cell spread [24–26]. The gC protein was regarded as a viral adhesion and immune response related glycoprotein [27]. The cell receptor nectin-1, an immunoglobulin-like cell adhesion molecule, is engaged by the gD protein at an early step of PRV infection. It was reported that the special antibody of gD protein was able to block PRV attachment to cell [28,29]. Both gE and gI are neurovirulence associated proteins of PRV. Deletion of gE or gI severely reduces anterograde spread capacity of PRV in processes of axonal transport [30,31]. The TK gene codes thymidine kinase of PRV. The pathogenicity of TK mutant PRV was highly attenuated in mice, rabbits and pigs [1]. The amino acid variations analysis based on these immunogenic and virulence-related genes showed that the gB, gC, gD and gE genes of the JS-2020 strain were not only homologous with earlier PRV strains (the Ea, Fa or SC strains), but also with strains isolated in recent years (the GXGG-2016 or HLJ-2013 strains). In particular, the gE gene of the JS-2020 strain was most similar to the earlier strains without an Asp insertion when compared to those with variant strains isolated in recent years. Both the gI and TK gene of the JS-2020 strain were highly conserved compared with most of the Chinese PRV strains.

It was reported that the GXGG-2016 and HLJ-2013 strains were classical PRV strains, and they were also homologous with earlier Chinese strains from previous studies [20,32]. The analysis of homology and variations based on nucleotide or amino acid sequences suggested that the JS-2020 strain might have evolved from the GXGG-2016 or HLJ-2013 strain. In recent studies, multiple recombinant PRV strains were identified, such as the JSY13, SC and FJ strains. The recombination regions of the JSY13 and SC strains were

regarded as a Bartha strain [9,19]. The FJ strain was regarded as a recombination strain between the HLJ8 and Ea strains [33]. The evolutionary and recombination analysis based on a large number of PRV complete genome sequences indicated that novel PRV variants might evolve from classical PRV strains through recombination mechanisms [34]. In this study, the recombination events were further predicted using related software. The JS-2020 strain was identified as a recombinant, its major sequences was highly similar to GXGG-2016 strain and a fraction of recombination regions were from the HLJ-2013 strain. In summary, a recombinant classical PRV strain was isolated and characterized in this study. These results will provide some evidence for the PRV-evolution-related studies. Moreover, it indicated that the classical PRV strains were still spreading among Chinese swine farms in the context of the PRV variant pandemic and that the novel natural recombinant virus is constantly being produced.

Author Contributions: Conceptualization, K.T. and X.L.; methodology, Z.L. and Z.Z.; software, Z.L. and R.L.; validation, Z.L., Z.Z. and P.L.; formal analysis, Z.L.; investigation, Z.L., Z.S., X.Y. and J.D.; resources, X.L., Z.S., X.Y. and J.D.; data curation, Z.L.; writing—original draft preparation, Z.L.; writing—review and editing, Z.L. and X.L.; visualization, Z.L.; supervision, K.T. and X.L.; project administration, X.L.; funding acquisition, X.L. All authors have read and agreed to the published version of the manuscript.

Funding: This work was funded by the National Natural Science Foundation of China (No. 32172823 and No. 32102637), the Postgraduate Research and Practice Innovation Program of Jiangsu Province (Yangzhou University) (No. SJCX22_1805) and the Project of the Priority Academic Program Development of Jiangsu Higher Education Institutions (PAPD).

Institutional Review Board Statement: All the animal experiments were approved by the Jiangsu Administrative Committee for Laboratory Animals (Permission Number: 202304001) and complied with the Guidelines of Laboratory Animal Welfare and Ethics of Jiangsu Administrative Committee and Laboratory Animal Welfare and Ethics Committee of Yangzhou University for Laboratory Animals.

Data Availability Statement: All the data generated during this study are included in the manuscript. Additional data related to this article may be requested from the corresponding authors.

Conflicts of Interest: The authors declare no conflict of interest.

References

1. Pomeranz, L.E.; Reynolds, A.E.; Hengartner, C.J. Molecular biology of pseudorabies virus: Impact on neurovirology and veterinary medicine. *Microbiol. Mol. Biol. Rev.* **2005**, *69*, 462–500. [CrossRef]
2. Klupp, B.G.; Hengartner, C.J.; Mettenleiter, T.C.; Enquist, L.W. Complete, annotated sequence of the pseudorabies virus genome. *J. Virol.* **2004**, *78*, 424–440. [CrossRef]
3. Szpara, M.L.; Tafuri, Y.R.; Parsons, L.; Shamim, S.R.; Verstrepen, K.J.; Legendre, M.; Enquist, L.W. A wide extent of inter-strain diversity in virulent and vaccine strains of alphaherpesviruses. *PLoS Pathog.* **2011**, *7*, e1002282. [CrossRef]
4. Zheng, H.H.; Fu, P.F.; Chen, H.Y.; Wang, Z.Y. Pseudorabies Virus: From Pathogenesis to Prevention Strategies. *Viruses* **2022**, *14*, 1638. [CrossRef]
5. Zhou, J.; Li, S.; Wang, X.; Zou, M.; Gao, S. Bartha-k61 vaccine protects growing pigs against challenge with an emerging variant pseudorabies virus. *Vaccine* **2017**, *35*, 1161–1166. [CrossRef]
6. Yu, X.; Zhou, Z.; Hu, D.; Zhang, Q.; Han, T.; Li, X.; Gu, X.; Yuan, L.; Zhang, S.; Wang, B.; et al. Pathogenic pseudorabies virus, China, 2012. *Emerg. Infect. Dis.* **2014**, *20*, 102–104. [CrossRef]
7. An, T.Q.; Peng, J.M.; Tian, Z.J.; Zhao, H.Y.; Li, N.; Liu, Y.M.; Chen, J.Z.; Leng, C.L.; Sun, Y.; Chang, D.; et al. Pseudorabies virus variant in Bartha-K61-vaccinated pigs, China, 2012. *Emerg. Infect. Dis.* **2013**, *19*, 1749–1755. [CrossRef]
8. Sun, Y.; Liang, W.; Liu, Q.; Zhao, T.; Zhu, H.; Hua, L.; Peng, Z.; Tang, X.; Stratton, C.W.; Zhou, D.; et al. Epidemiological and genetic characteristics of swine pseudorabies virus in mainland China between 2012 and 2017. *PeerJ* **2018**, *6*, e5785. [CrossRef]
9. Bo, Z.; Miao, Y.; Xi, R.; Gao, X.; Miao, D.; Chen, H.; Jung, Y.S.; Qian, Y.; Dai, J. Emergence of a novel pathogenic recombinant virus from Bartha vaccine and variant pseudorabies virus in China. *Transbound. Emerg. Dis.* **2021**, *68*, 1454–1464. [CrossRef]
10. Luo, Y.; Li, N.; Cong, X.; Wang, C.H.; Du, M.; Li, L.; Zhao, B.; Yuan, J.; Liu, D.D.; Li, S.; et al. Pathogenicity and genomic characterization of a pseudorabies virus variant isolated from Bartha-K61-vaccinated swine population in China. *Vet. Microbiol.* **2014**, *174*, 107–115. [CrossRef]
11. Tan, L.; Yao, J.; Yang, Y.; Luo, W.; Yuan, X.; Yang, L.; Wang, A. Current Status and Challenge of Pseudorabies Virus Infection in China. *Virol. Sin.* **2021**, *36*, 588–607. [CrossRef] [PubMed]

12. Tong, W.; Liu, F.; Zheng, H.; Liang, C.; Zhou, Y.J.; Jiang, Y.F.; Shan, T.L.; Gao, F.; Li, G.X.; Tong, G.Z. Emergence of a Pseudorabies virus variant with increased virulence to piglets. *Vet. Microbiol.* **2015**, *181*, 236–240. [CrossRef] [PubMed]
13. Wang, C.H.; Yuan, J.; Qin, H.Y.; Luo, Y.; Cong, X.; Li, Y.; Chen, J.; Li, S.; Sun, Y.; Qiu, H.J. A novel gE-deleted pseudorabies virus (PRV) provides rapid and complete protection from lethal challenge with the PRV variant emerging in Bartha-K61-vaccinated swine population in China. *Vaccine* **2014**, *32*, 3379–3385. [CrossRef] [PubMed]
14. Yang, Q.Y.; Sun, Z.; Tan, F.F.; Guo, L.H.; Wang, Y.Z.; Wang, J.; Wang, Z.Y.; Wang, L.L.; Li, X.D.; Xiao, Y.; et al. Pathogenicity of a currently circulating Chinese variant pseudorabies virus in pigs. *World J. Virol.* **2016**, *5*, 23–30. [CrossRef] [PubMed]
15. Gu, Z.; Dong, J.; Wang, J.; Hou, C.; Sun, H.; Yang, W.; Bai, J.; Jiang, P. A novel inactivated gE/gI deleted pseudorabies virus (PRV) vaccine completely protects pigs from an emerged variant PRV challenge. *Virus Res.* **2015**, *195*, 57–63. [CrossRef]
16. Wang, T.; Xiao, Y.; Yang, Q.; Wang, Y.; Sun, Z.; Zhang, C.; Yan, S.; Wang, J.; Guo, L.; Yan, H.; et al. Construction of a gE-Deleted Pseudorabies Virus and Its Efficacy to the New-Emerging Variant PRV Challenge in the Form of Killed Vaccine. *Biomed. Res. Int.* **2015**, *2015*, 684945. [CrossRef]
17. Zhang, C.; Guo, L.; Jia, X.; Wang, T.; Wang, J.; Sun, Z.; Wang, L.; Li, X.; Tan, F.; Tian, K. Construction of a triple gene-deleted Chinese Pseudorabies virus variant and its efficacy study as a vaccine candidate on suckling piglets. *Vaccine* **2015**, *33*, 2432–2437. [CrossRef]
18. Yan, S.; Huang, B.; Bai, X.; Zhou, Y.; Guo, L.; Wang, T.; Shan, Y.; Wang, Y.; Tan, F.; Tian, K. Construction and Immunogenicity of a Recombinant Pseudorabies Virus Variant With TK/gI/gE/11k/28k Deletion. *Front. Vet. Sci.* **2021**, *8*, 797611. [CrossRef] [PubMed]
19. Ye, C.; Guo, J.C.; Gao, J.C.; Wang, T.Y.; Zhao, K.; Chang, X.B.; Wang, Q.; Peng, J.M.; Tian, Z.J.; Cai, X.H.; et al. Genomic analyses reveal that partial sequence of an earlier pseudorabies virus in China is originated from a Bartha-vaccine-like strain. *Virology* **2016**, *491*, 56–63. [CrossRef]
20. Qin, Y.; Qin, S.; Huang, X.; Xu, L.; Ouyang, K.; Chen, Y.; Wei, Z.; Huang, W. Isolation and identification of two novel pseudorabies viruses with natural recombination or TK gene deletion in China. *Vet. Microbiol.* **2023**, *280*, 109703. [CrossRef]
21. Klopffleisch, R.; Klupp, B.G.; Fuchs, W.; Kopp, M.; Teifke, J.P.; Mettenleiter, T.C. Influence of pseudorabies virus proteins on neuroinvasion and neurovirulence in mice. *J. Virol.* **2006**, *80*, 5571–5576. [CrossRef]
22. Klopffleisch, R.; Teifke, J.P.; Fuchs, W.; Kopp, M.; Klupp, B.G.; Mettenleiter, T.C. Influence of tegument proteins of pseudorabies virus on neuroinvasion and transneuronal spread in the nervous system of adult mice after intranasal inoculation. *J. Virol.* **2004**, *78*, 2956–2966. [CrossRef] [PubMed]
23. Li, Y.; Yan, S.; Li, X.; Yang, Q.; Guo, L.; Wang, Y.; Xiao, Y.; Tan, F.; Li, X.; Tian, K. From mouse to pig: Is PRV vaccine safe across two species? *Virus Res.* **2017**, *236*, 44–49. [CrossRef] [PubMed]
24. Peeters, B.; de Wind, N.; Hooisma, M.; Wagenaar, F.; Gielkens, A.; Moormann, R. Pseudorabies virus envelope glycoproteins gp50 and gII are essential for virus penetration, but only gII is involved in membrane fusion. *J. Virol.* **1992**, *66*, 894–905. [CrossRef]
25. Rauh, I.; Mettenleiter, T.C. Pseudorabies virus glycoproteins gII and gp50 are essential for virus penetration. *J. Virol.* **1991**, *65*, 5348–5356. [CrossRef] [PubMed]
26. Zaripov, M.M.; Morenkov, O.S.; Fodor, N.; Braun, A.; Schmatchenko, V.V.; Fodor, I.; Brown, A. Distribution of B-cell epitopes on the pseudorabies virus glycoprotein B. *J. Gen. Virol.* **1999**, *80 Pt 3*, 537–541. [CrossRef]
27. Rue, C.A.; Ryan, P. Pseudorabies virus glycoprotein C attachment-proficient revertants isolated through a simple, targeted mutagenesis scheme. *J. Virol. Methods* **2008**, *151*, 101–106. [CrossRef]
28. Li, A.; Lu, G.; Qi, J.; Wu, L.; Tian, K.; Luo, T.; Shi, Y.; Yan, J.; Gao, G.F. Structural basis of nectin-1 recognition by pseudorabies virus glycoprotein D. *PLoS Pathog.* **2017**, *13*, e1006314. [CrossRef]
29. Zhang, T.; Liu, Y.; Chen, Y.; Wang, J.; Feng, H.; Wei, Q.; Zhao, S.; Yang, S.; Liu, D.; Zhang, G. A monoclonal antibody neutralizes pseudorabies virus by blocking gD binding to the receptor nectin-1. *Int. J. Biol. Macromol.* **2021**, *188*, 359–368. [CrossRef]
30. Ch'ng, T.H.; Enquist, L.W. Neuron-to-cell spread of pseudorabies virus in a compartmented neuronal culture system. *J. Virol.* **2005**, *79*, 10875–10889. [CrossRef]
31. Kratchmarov, R.; Kramer, T.; Greco, T.M.; Taylor, M.P.; Ch'ng, T.H.; Cristea, I.M.; Enquist, L.W. Glycoproteins gE and gI are required for efficient KIF1A-dependent anterograde axonal transport of alphaherpesvirus particles in neurons. *J. Virol.* **2013**, *87*, 9431–9440. [CrossRef] [PubMed]
32. Liu, H.; Shi, Z.; Liu, C.; Wang, P.; Wang, M.; Wang, S.; Liu, Z.; Wei, L.; Sun, Z.; He, X.; et al. Implication of the Identification of an Earlier Pseudorabies Virus (PRV) Strain HLJ-2013 to the Evolution of Chinese PRVs. *Front. Microbiol.* **2020**, *11*, 612474. [CrossRef] [PubMed]
33. Huang, J.; Tang, W.; Wang, X.; Zhao, J.; Peng, K.; Sun, X.; Li, S.; Kuang, S.; Zhu, L.; Zhou, Y.; et al. The Genetic Characterization of a Novel Natural Recombinant Pseudorabies Virus in China. *Viruses* **2022**, *14*, 978. [CrossRef] [PubMed]
34. Hu, R.; Wang, L.; Liu, Q.; Hua, L.; Huang, X.; Zhang, Y.; Fan, J.; Chen, H.; Song, W.; Liang, W.; et al. Whole-Genome Sequence Analysis of Pseudorabies Virus Clinical Isolates from Pigs in China between 2012 and 2017 in China. *Viruses* **2021**, *13*, 1322. [CrossRef]

Disclaimer/Publisher's Note: The statements, opinions and data contained in all publications are solely those of the individual author(s) and contributor(s) and not of MDPI and/or the editor(s). MDPI and/or the editor(s) disclaim responsibility for any injury to people or property resulting from any ideas, methods, instructions or products referred to in the content.

Article

Brincidofovir Effectively Inhibits Proliferation of Pseudorabies Virus by Disrupting Viral Replication

Huihui Guo^{1,2,†}, Qingyun Liu^{1,2,†}, Dan Yang^{1,2}, Hao Zhang^{1,2}, Yan Kuang^{1,2}, Yafei Li^{1,2}, Huanchun Chen^{1,2,3,4} and Xiangru Wang^{1,2,3,4,*} 

¹ National Key Laboratory of Agricultural Microbiology, College of Veterinary Medicine, Huazhong Agricultural University, Wuhan 430070, China; guohuihui@webmail.hzau.edu.cn (H.G.); liuqy@mail.hzau.edu.cn (Q.L.); danyang6211@webmail.hazu.edu.cn (D.Y.); 2022302110193@webmail.hzau.edu.cn (H.Z.); ky19981459286@163.com (Y.K.); lyfovlyf@163.com (Y.L.); chenhch@mail.edu.cn (H.C.)

² Key Laboratory of Preventive Veterinary Medicine in Hubei Province, The Cooperative Innovation Center for Sustainable Pig Production, Huazhong Agricultural University, Wuhan 430070, China

³ Frontiers Science Center for Animal Breeding and Sustainable Production, Huazhong Agricultural University, Wuhan 430070, China

⁴ International Research Center for Animal Disease, Ministry of Science and Technology of China, Wuhan 430070, China

* Correspondence: wangxr228@mail.hzau.edu.cn

† These authors contributed equally to this work.

Abstract: Pseudorabies is an acute and febrile infectious disease caused by pseudorabies virus (PRV), a member of the family Herpesviridae. Currently, PRV is predominantly endemoepidemic and has caused significant economic losses among domestic pigs. Other animals have been proven to be susceptible to PRV, with a mortality rate of 100%. In addition, 30 human cases of PRV infection have been reported in China since 2017, and all patients have shown severe neurological symptoms and eventually died or developed various neurological sequelae. In these cases, broad-spectrum anti-herpesvirus drugs and integrated treatments were mostly applied. However, the inhibitory effect of the commonly used anti-herpesvirus drugs (e.g., acyclovir, etc.) against PRV were evaluated and found to be limited in this study. It is therefore urgent and important to develop drugs that are clinically effective against PRV infection. Here, we constructed a high-throughput method for screening antiviral drugs based on fluorescence-tagged PRV strains and multi-modal microplate readers that detect fluorescence intensity to account for virus proliferation. A total of 2104 small molecule drugs approved by the U.S. Food and Drug Administration (FDA) were studied and validated by applying this screening model, and 104 drugs providing more than 75% inhibition of fluorescence intensity were selected. Furthermore, 10 drugs that could significantly inhibit PRV proliferation in vitro were strictly identified based on their cytopathic effects, virus titer, and viral gene expression, etc. Based on the determined 50% cytotoxic concentration (CC₅₀) and 50% inhibitory concentration (IC₅₀), the selectivity index (SI) was calculated to be 26.3–3937.2 for these 10 drugs, indicating excellent drugability. The antiviral effects of the 10 drugs were then assessed in a mouse model. It was found that 10 mg/kg brincidofovir administered continuously for 5 days provided 100% protection in mice challenged with lethal doses of the human-origin PRV strain hSD-1/2019. Brincidofovir significantly attenuated symptoms and pathological changes in infected mice. Additionally, time-of-addition experiments confirmed that brincidofovir inhibited the proliferation of PRV mainly by interfering with the viral replication stage. Therefore, this study confirms that brincidofovir can significantly inhibit PRV both in vitro and in vivo and is expected to be an effective drug candidate for the clinical treatment of PRV infections.

Keywords: pseudorabies virus; human infection; antiviral drugs; brincidofovir



Citation: Guo, H.; Liu, Q.; Yang, D.; Zhang, H.; Kuang, Y.; Li, Y.; Chen, H.; Wang, X. Brincidofovir Effectively Inhibits Proliferation of Pseudorabies Virus by Disrupting Viral Replication. *Viruses* **2024**, *16*, 464. <https://doi.org/10.3390/v16030464>

Academic Editor: Raymond Rowland

Received: 5 February 2024

Revised: 11 March 2024

Accepted: 11 March 2024

Published: 18 March 2024



Copyright: © 2024 by the authors. Licensee MDPI, Basel, Switzerland. This article is an open access article distributed under the terms and conditions of the Creative Commons Attribution (CC BY) license (<https://creativecommons.org/licenses/by/4.0/>).

1. Introduction

Pseudorabies virus (PRV) belongs to the family Herpesviridae, the subfamily Alpha-herpesvirus, and the genus Varicella. It is enveloped and harbors a double-stranded DNA genome. PRV infection has been reported in a wide range of mammals, including pigs, cattle, sheep, cats, dogs, and other domestic animals, as well as wild animals. Among them, pigs are the exclusive natural reservoir of PRV [1]. After being infected, newborn piglets suffer from fatal encephalitis, resulting in 100% mortality, breeding pigs exhibit reproductive disorders, and fattening pigs experience stunted growth. PRV infection in other susceptible animals is characterized by severe pruritus and central nervous system (CNS) dysfunction, ultimately resulting in 100% mortality [2]. Apparently, PRV is neurotropic and lethal for a wide range of hosts.

The global pig industry has suffered significant economic losses due to the high prevalence of PRV. Despite vaccination and eradication measures, PRV remains endemic in wild boars and domestic pigs worldwide, posing a major threat to pig farming as one of the most important animal infectious diseases. China has experienced two outbreaks of porcine pseudorabies caused by classical and variant strains, respectively [3]. Several studies have demonstrated that the virulence of variant PRV strains is significantly enhanced compared to classical strains [4]. These variant PRV strains have been circulating in Chinese pig populations since 2011.

It has long been controversial as to whether humans can be infected with PRV. In 1914, two researchers who were studying PRV were suspected of being infected with PRV after coming to contact with contaminated materials and exhibited symptoms such as weakness, agitation, sore throat, and pruritus [5]. From then until 1992, there were 17 reported cases of suspected human infection with PRV [6].

From 2017 to the present, there have been a total of 30 clinical cases of PRV infection in humans reported in China, all of which were classified as pseudorabies encephalitis. All patients exhibited fever and neurological symptoms such as seizures and impaired consciousness. Over half of the patients experienced severe visual impairment, presenting as acute retinal detachment, vitreous clouding or blindness. Of the 30 reported cases, 28 individuals were involved in industries related to pig production and pork marketing, including veterinarians, butchers, and pork salesman. Next-generation sequencing (NGS) revealed variable reads and coverage of PRV sequences in the tissues of these patients, while some patients also exhibited detectable levels of PRV antibodies in their sera [2,7–15]. In addition, we previously isolated the PRV strain hSD-1/2019 from the cerebrospinal fluid of a patient, providing direct pathogenetic evidence to support PRV infection in humans [2]. After receiving aggressive treatment, unfortunately, the majority of these patients had a poor prognosis, with neurological sequelae or even death. Currently, vaccination against pseudorabies is the primary effective measure for preventing and controlling porcine pseudorabies. However, comprehensive treatment is typically employed for human pseudorabies encephalitis, as there are currently no specific antiviral drugs available for PRV infection. Due to the disabling and lethal effects of pseudorabies on both animals and humans, it is imperative to identify effective antiviral drugs for controlling PRV infection.

Some natural products have been reported to exhibit anti-PRV activity, such as isobavachalcone [16], (-)-epigallocatechin-3-gallate [17], resveratrol [18], kaempferol [19], and quercetin [20], etc. These drugs exhibited potential antiviral effects *in vivo* or *in vitro*; however, their inhibitory effects on PRV proliferation were mostly observed at high effective concentrations. The effective concentration of (-)-epigallocatechin-3-gallate and kaempferol in inhibiting PRV was as high as 50 μ M *in vitro* and 240 mg/kg *in vivo*, respectively. Hydroquinone and adefovir dipivoxil, approved by the U.S. Food and Drug Administration (FDA), have demonstrated certain antiviral efficacy against classical PRV strains; however, their effectiveness against prevalent variant PRV strains in China and human-origin PRV strains remains uncertain [21,22]. So far, all of the studies on the development of anti-PRV drugs have been in the phase of laboratory screening and validation.

In cases of human pseudorabies encephalitis caused by PRV infection, patients were administered commonly used anti-herpesvirus drugs (such as acyclovir, ganciclovir, and penciclovir) along with other medical interventions. Despite treatment, several patients succumbed to the disease, while all surviving patients experienced varying degrees of neurological sequelae. Most importantly, the inhibitory effect of acyclovir on the human-origin PRV strain hSD-1/2019 was evaluated at different drug concentrations. The results indicated that in vitro, acyclovir did not significantly inhibit the virus and failed to provide adequate protection for challenged mice. In this study, a high-throughput screening method for anti-PRV drugs was established and utilized to screen 2104 FDA-approved drugs. Brincidofovir was identified as having notable antiviral effects against hSD-1/2019 in vitro and in vivo, providing 100% protection for lethally challenged mice. This effective anti-PRV drug is of great significance for the clinical treatment of PRV infection.

2. Materials and Methods

2.1. Cells and Viruses

Porcine kidney cells (PK-15) were purchased from the China Center for Type Culture Collection (CCTCC) and preserved in our laboratory. PK-15 cells were grown in Dulbecco's modified Eagle's high-glucose medium (DMEM) supplemented with 10% fetal bovine serum (FBS) (GIBCO, Grand Island, NY, USA) at 37 °C with 5% CO₂. The classical PRV strain Ea was isolated from the infected pig and the variant PRV strain hSD-1/2019 was isolated from cerebrospinal fluid of the infected patient. These PRV strains were isolated and preserved in our laboratory [2].

2.2. Construction of Fluorescently Labeled Viruses

The fluorescence-labeled viruses were constructed and rescued by inserting mCherry in front of the terminator of the PRV UL35 gene through homologous recombination. Briefly, the genomic DNA of hSD-1/2019 and Ea strains was extracted using TIANamp Genomic DNA Kit (TIANGEN, Beijing, China). Polymerase chain reactions (PCRs) were then conducted to amplify the homologous sequences and the red fluorescent protein expressing gene mCherry with primers listed in Table 1. The homologous recombinant transfer plasmids were constructed by sequentially inserting these sequences into pcDNA3.1 (+) vector (Biofeng, Shanghai, China). The correct homologous recombinant plasmids were named as pcDNA3.1 (+)-mCherry-hSD and pcDNA3.1 (+)-mCherry-Ea, respectively.

Table 1. Primers used for PCR in this study.

Target Sequences	Primer	Sequences (5'-3')
Upstream homologous arm	PRV-HindIII-F	CCCAAGCTTAGGCCGCGTACCCTCCG
	PRV-KpnI-R	CGGGGTACCGGGCGAGGGGCGAGGG
mCherry	mCherry-KpnI-F	CGGGGTACCGGTGGAGGCGGTTTCAGGCGGAG
	mCherry-BamHI-R	GTGGCTCTATGGTGAGCAAGGGCGAGGA CGCGGATCCCTTGTACAGCTCGTCCATGC
Downstream homologous arm	PRV-BamHI-F	CGCGGATCCTAGCCCCGCGGATCAATAAAG
	PRV-EcoRI-R	CCGGAATTCCC GCGCGTGGTGGAGTCG

The combined linear fragments of the homologous arms and mCherry were amplified from the recombinant plasmid and purified. The purified fragments were transfected into PK-15 cells in a 6-well plate using Lipofectamine[®] 2000 Reagent (Life, Carlsbad, CA, USA) according to manufacturer's instructions. At 4 h post transfection, the cells were infected with hSD-1/2019 or Ea at a multiplicity of infection (MOI) of 0.001 and then incubated at 37 °C with 5% CO₂ for 1–2 days. During the incubation, red fluorescent cytopathic effects (CPEs) were observed. When the cells showed 80% CPEs, the culture was collected and a "freeze–thaw cycle" was conducted three times. After that, virus plaque purification was

performed 5 times to obtain the recombinant mutants hSD-mCherry and Ea-mCherry as previously described [2].

2.3. Cytotoxicity Test

The cytotoxicity of the drugs on PK-15 cells was assessed with the Cell Counting Kit-8 assay (CCK-8) according to the instructions provided by the manufacturers of the CCK-8 kit (Beyotime, Shanghai, China). Briefly, the drug was diluted to 320, 160, 80, 40, 20, and 10 μM , respectively, and added to PK-15 cells at 80% confluence in a 96-well plate. Six replicate wells were set for each dilution as well as the cell control without drug treatment. After 36 h of incubation at 37 °C with 5% CO_2 , 10 μL of CCK-8 reagent was added per well and the plate was then incubated for another 1 h. Absorbance values at 450 nm were measured. The viability of cells treated with drugs was calculated according to the following formula: Average absorbance value (cells treated with the drug)/Average absorbance value (cell control). Nonlinear regression (curve fitting) analysis was then conducted to obtain the 50% cytotoxicity concentration 50% (CC_{50}), which was defined as the drug concentration that reduced cell viability by 50% when compared to untreated controls.

2.4. Half Maximal Inhibitory Concentration (IC_{50}) Determination

The IC_{50} of the drugs against PRV was assessed in PK-15 cells using the CCK-8 assay. In a 96-well plate, PK-15 cells monolayers at 80% confluence were treated with drugs at different concentrations and infected with hSD-1/2019 at 0.01 MOI. After 36 h of incubation at 37 °C with 5% CO_2 , 10 μL of CCK-8 reagent was added per well. Absorbance values at 450 nm were measured after another 1 h of incubation. The inhibition ratio of each drug against PRV was calculated according to the following formula: (Average absorbance value (cells infected with PRV) – Average absorbance value (cells treated with drugs and infected with PRV))/Average absorbance value (cell infected with PRV). The IC_{50} was illustrated by means of nonlinear regression analysis using GraphPad Prism, indicating the concentration of the drug that inhibited virus replication by 50%.

2.5. The 50% Tissue Culture Infectious Dose (TCID_{50}) Assay

The virus titer was determined by means of TCID_{50} assay as previously described, with some modifications [23]. Then, 100 μL of a PK-15 cell suspension containing 2×10^4 cells was added to each well. Negative controls containing only PK-15 cells were set up in two columns. The virus solution was 10-fold diluted serially from approximately 10^{-1} to 10^{-8} in FBS-free DMEM medium, and 100 μL of each dilution was added into a 96-well plate with 8 replicates. The 96-well plates were incubated at 37 °C with 5% CO_2 for 7 days, and CPEs were checked daily and recorded. After the observation, TCID_{50} was calculated according to the Reed–Muench method.

2.6. Quantitative PCR (qPCR) Detecting *gE* Gene

PRV *gE* gene copies were detected by means of TaqMan qPCR as previously described [2]. The standard recombinant plasmid was prepared and the standard curve was constructed. Viral DNA was extracted from the samples using the TIANamp Genomic DNA Kit (TIANGEN, Beijing, China) and the *gE* gene of the extracted DNA was amplified by TaqMan qPCR. The *gE* copies were calculated according to the detected cycle threshold value of the sample and the standard curve.

2.7. One-Step Growth Curve

Confluent monolayer PK-15 cells were infected with PRV at a dose of 0.1 MOI followed by incubation at 37 °C with 5% CO_2 for 2 h. After incubation, the medium was discarded and cells were washed twice with PBS before adding fresh DMEM supplemented with 3% FBS (the maintenance medium). Both cells and supernatant were collected at 0, 4, 8, 12, 16, 20, 24, 28, 32, 36, 40 and 48 h post incubation in the maintenance medium. After three

freeze–thaw cycles, the supernatant of lysates was collected via centrifugation and titrated as TCID₅₀ in PK-15 cells.

2.8. In Vivo Assessment of Antiviral Effects of the Drugs

The antiviral effects of the drugs were assessed in mice, which was conducted in the Experimental Animal Center of Huazhong Agricultural University (animal welfare assurance number HZAUMO-2022-0143). Mice were randomly grouped, with 5 mice in each group. Except for 5 mice injected with DMEM as a blank control, other mice were challenged with hSD-1/2019 at a dose of 500 TCID₅₀ via hind footpad injection. Treatment was started at the same time as the challenge, and all drugs were injected intraperitoneally using a dose of 10 mg/kg/d for 5 days. Five challenged mice were set as the hSD-1/2019 control with intraperitoneal injection of DMEM. The clinical symptoms and mortality of the mice were observed daily and recorded for 14 days. The clinical symptoms of mice in each group were scored according to the scoring criteria in Table 2.

Table 2. Scoring criteria of clinical symptoms in mice.

Score	Clinical Symptoms
0	No symptoms
1	Excitement, restlessness, occasional itching and scratching
2	Ataxia, severe itching, persistent gnawing on hind limbs
3	Gnawing on the hind limbs resulting in bone disruption and tissue necrosis
4	Dead or dying

Upon the onset of mortality in the hSD-1/2019 control group, two mice were humanely euthanized and dissected. Additionally, two mice from both the Brincidofovir administration group and the blank control group were also euthanized and dissected. The brain, lung, and spleen tissues were collected, fixed in 4% paraformaldehyde (Biosharp, Beijing, China), and sent for the preparation of sections with hematoxylin-eosin (HE) staining at HYcell Biotechnology Co., Ltd. (Wuhan, China).

2.9. Time-of-Addition Assay

The time-of-addition assay was performed to determine the stage of viral replication cycle targeted by the drug by adjusting the order in which the drug and viruses were added into cells. During all the experiments, monolayer PK-15 cells in 96-well plates were infected with PRV-mCherry at an MOI of 0.01 and treated with the drug at 10 µM. (I) Virus inactivation: The mixture of viruses and drug was incubated at 37 °C for 1 h and then added to the cells for continued incubation. After 36 h, the cultures were collected. (II) Pre-treatment effect: A concentration of 10 µM of the drug was added to the cells for 1 h of incubation at 37 °C and then replaced by the viral suspension. The cells were covered with fresh medium 1 h post infection and incubated for 36 h before harvesting. (III) Virus internalization: The cells were infected with PRV-mCherry and incubated at 4 °C for 1 h. Then, the supernatant was replaced with the drug, followed by 1 h of incubation at 37 °C. The drug was removed and fresh medium was added. The cultures were collected after 36 h. (IV) Virus replication: The cells were infected with PRV-mCherry and incubated at 37 °C for 1 h. Then, the supernatant was replaced with the drug and the cells were incubated at 37 °C for 36 h before collection. These collected cultures were applied for fluorescence intensity detection and virus titer determination.

2.10. Statistical Analysis

Data are presented as the mean ± standard deviation (SD) from 3 independent experiments. GraphPad Prism version 6.0 software (GraphPad, La Jolla, CA, USA) was used for statistical analysis. The significant difference between groups was analyzed using Student's *t*-test or two-way ANOVA. A level of 0.01 < *p* < 0.05 (*) was considered significant,

$p < 0.01$ (**) or $p < 0.001$ (***) was considered statistically highly significant and extremely significant, respectively. $p > 0.05$ (ns) was considered not significant.

3. Results

3.1. Fluorescence Intensity of the Recombinant PRV-mCherry Could Indicate Virus Proliferation Titers

The recombinant PRV strains hSD-mCherry and Ea-mCherry, which were fluorescently labeled, were generated by inserting the mCherry gene upstream of the terminator sequence within the UL35 gene of PRV (Figure 1A). After plaque purification, virions with red fluorescence were obtained (Figure 1B). The recombinant hSD-mCherry and Ea-mCherry were passaged in PK-15 cells, and the fluorescence intensity of the culture in different passages was found to be comparable, indicating a consistent expression of mCherry during virus replication (Figure 1C). With an increasing infection dose, the fluorescence intensity and virus titer of cell culture exhibited a parallel increase (Figure 1D), indicating that PRV-mCherry's fluorescence intensity can serve as a direct indicator of the virus proliferation titer. Additionally, the one-step growth curves of WT PRV strains and mCherry-labeled strains were comparable, despite the lower virus titers observed in the recombinant strains compared to their parental WT counterparts (Figure 1E). These findings suggest that PRV-mCherry strains can be effectively utilized for subsequent drug screening.

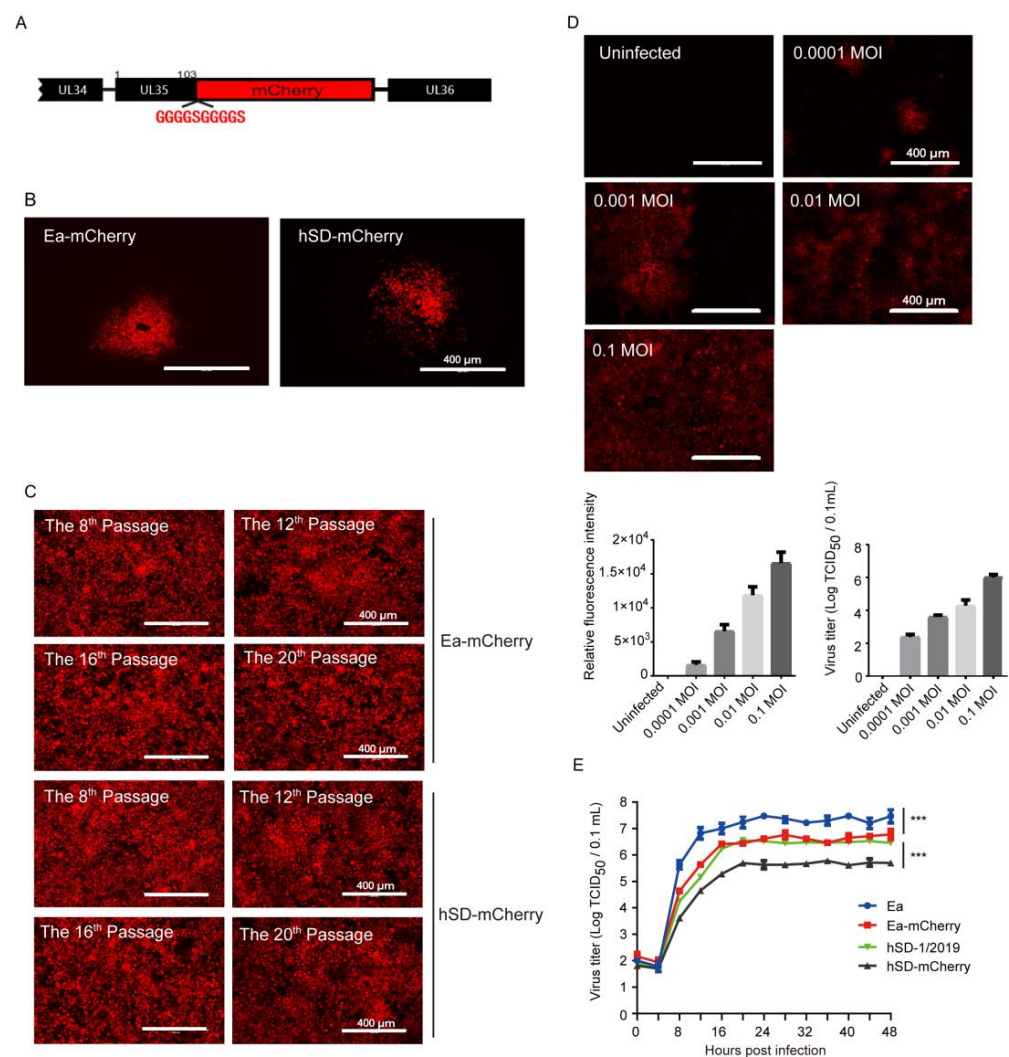


Figure 1. The PRV strains labeled with mCherry could express the protein stably and exhibited a proliferation trend similar to that of the wild-type strains. (A) The coding sequences of mCherry

were fused upstream of the terminator region of PRV UL35 gene to generate PRV-mCherry strains; (B) plaque purification of recombinant Ea-mCherry and hSD-mCherry; (C) Ea-mCherry and hSD-mCherry were passaged in PK-15 cells and their fluorescence intensity of the 8th, 12th, 16th, and 20th passages were observed and compared; (D) the PK-15 cells were infected with PRV-mCherry at different MOI. Fluorescence intensity and virus titers were measured at 24 hpi, revealing a similar increasing trend; (E) one-step growth curves of PRV-mCherry strains and wild-type strains in PK-15 cells with an MOI of 0.01. Virus titers between groups were analyzed by Student's *t*-test. A level of $p < 0.001$ (***) was considered statistically extremely significant.

3.2. The Anti-Herpesvirus Drugs Commonly Used in Clinical Practice Exhibited Limited Efficacy against the PRV Variant Strain hSD-1/2019

Of the 30 previously reported PRV-infected patients, 15 received antiviral medication containing acyclovir, 5 received antiviral medication containing ganciclovir, and 1 received antiviral medication containing penciclovir. However, the efficacy of these drugs against PRV remains to be studied given their poor final outcomes [24]. Subsequently, the efficacy of several clinical anti-herpesvirus medications against the human-origin PRV variant strain hSD-1/2019 were evaluated in this study. The IC_{50} of acyclovir against hSD-1/2019 was determined to be 110.4 μ M (Figure 2A). At a concentration of 160 μ M, acyclovir significantly attenuated the fluorescence intensity of PK-15 cells infected with hSD-mCherry compared to the lower concentrations (Figure 2B). However, noticeably, the IC_{50} values of acyclovir against herpes simplex virus type-1 and Varicella Zoster virus were both less than 10 μ M [25,26], indicating much higher susceptibility to acyclovir than the PRV variant strain hSD-1/2019. The anti-PRV effect of acyclovir was further investigated in mice challenged with a lethal dose of hSD-1/2019. Mice that received no medication showed severe neurological symptoms and 100% mortality, while those treated with acyclovir at doses of 10 mg/Kg and 90 mg/Kg had the same clinical symptom scores and mortality rates as the untreated group, indicating that acyclovir did not protect mice from lethal PRV infection (Figure 2C,D).

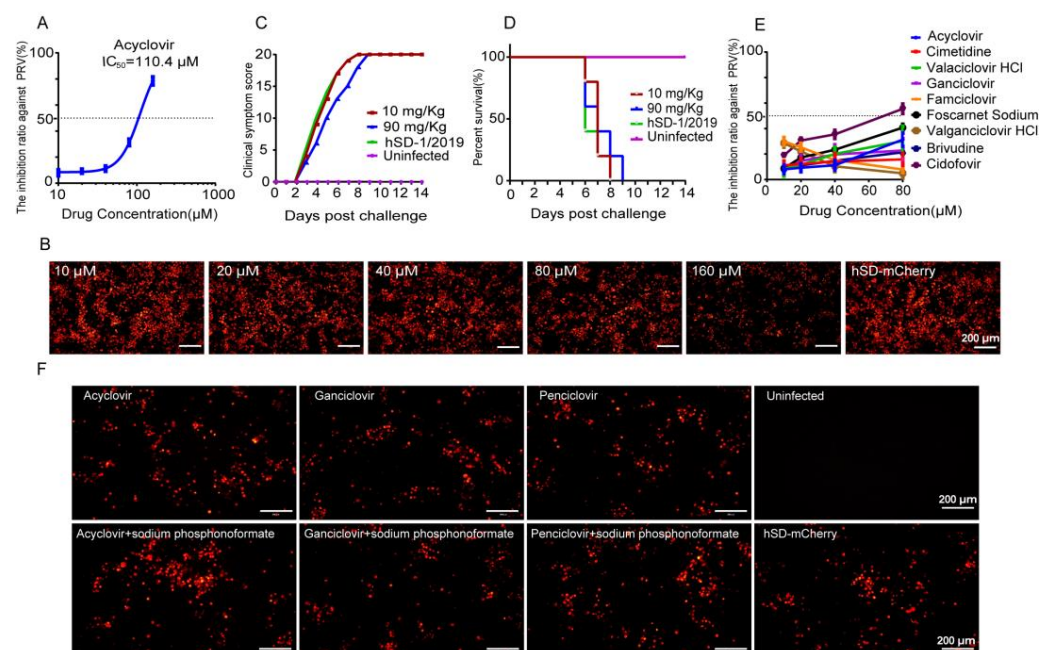


Figure 2. The commonly used clinical anti-herpesvirus drugs exhibited limited efficacy against the PRV variant strain hSD-1/2019. (A) IC_{50} of acyclovir against PRV. The dotted line represents 50% inhibition; (B) PK-15 cells were infected with hSD-mCherry at 0.01 MOI and treated with different

concentrations of acyclovir. Fluorescence intensity was observed at 48 hpi; (C) clinical symptom scores of the mice according to the scoring criteria in Table 2. The data are presented as the total daily score for each group of mice; (D) survival curves of the mice. Daily mortality rates for each group were recorded over a period of 14 days, and survival curves were plotted using GraphPad Prism; (E) inhibition ratio of nine anti-herpesvirus drugs at different concentrations against PRV. PK-15 cells were infected with hSD-mCherry at 0.01 MOI and treated with drugs at various concentrations. The fluorescence intensity was measured by a multimode microplate reader at 48 hpi, and drug inhibition ratios were calculated using the following formula: $(\text{Fluorescence intensity [cells infected with PRV]} - \text{Fluorescence intensity [cells treated with drug and infected with PRV]}) / (\text{Fluorescence intensity [cells infected with PRV]}) \times 100\%$; (F) PK-15 cells were infected with hSD-mCherry at 0.01 MOI and treated with drugs individually or in combination groups consisting of treatment with either 10 μM acyclovir, ganciclovir, or penciclovir alone, or combined treatment involving both antiviral drugs and sodium phosphonoformate at a concentration of 10 μM each, respectively. Fluorescence intensity was observed at 48 hpi, showing similar fluorescence intensities across all groups.

Furthermore, the anti-PRV effects of nine anti-herpesvirus drugs were additionally assessed *in vitro*. The results revealed that cidofovir at a concentration of 80 μM exhibited an inhibition rate of 56% against PRV, while the remaining eight drugs demonstrated less than 50% inhibition, even at their highest tested concentrations (80 μM) (Figure 2E). The clinical application of combining antiviral drugs with sodium phosphonoformate has been commonly employed to enhance the antiviral effect. Therefore, we added sodium phosphonoformate to test the antiviral effects of acyclovir, ganciclovir, and penciclovir. The fluorescence intensity of the combined medication groups did not show any significant differences compared to that of the individual medication groups or the non-medicated group (Figure 2F). The aforementioned data indicate that the clinically utilized anti-herpesvirus drugs, including acyclovir, exhibit ineffectiveness against the human-origin PRV strain hSD-1/2019 both *in vitro* and *in vivo*. Therefore, there is an imperative and urgent need to conduct a comprehensive screening for efficacious anti-PRV drugs to combat PRV infection.

3.3. Eighteen Drugs Effectively Inhibiting PRV-mCherry Proliferation Were Screened out from 2104 FDA-Approved Drugs through the High-Throughput Screening Method

A high-throughput method was developed based on the fluorescently labeled PRV strains described above. The optimization results for inoculation dose and infection time demonstrated that cells infected with Ea-mCherry at 0.01 MOI for 36 h exhibited peak fluorescence intensity and virus titers, which remained stable (Figure 3A,B). Accordingly, the established high-throughput method for drug screening involved infecting PK-15 cell monolayers in 96-well plates with Ea-mCherry at 0.01 MOI, followed by treatment with a 10 μM drug. Cells infected with PRV served as the infection control group. After incubation for 36 h, the fluorescence intensity of cells was measured using a multimode microplate reader instrument with excitation light at 587 nm and emission light at 610 nm. The inhibition ratio of the drug against Ea-mCherry was calculated as the percentage difference in fluorescence intensity between infected cells and drug-treated cells.

Through this high-throughput screening method, a total of 2104 drugs approved by the FDA for the market and clinical disease treatment were tested (Figure 3C). The dotted line at “75” in Figure 3C is the threshold for judgement of effective inhibition on PRV proliferation. A drug was considered to inhibit PRV proliferation effectively if its inhibition ratio against PRV was greater than or equal to 75%. Each symbol represents a kind of drug. As illustrated in Figure 3C, 104 drugs exhibited the inhibition ratio against PRV higher than 75%. Subsequently, the cell morphology of each group was individually observed, and 18 out of the 104 drugs were confirmed to effectively reduce the CPEs induced by virus infection without exhibiting obvious cytotoxic effects on the cells. The names of the 18 selected drugs are shown in Table 3. They are tanespimycin (17-AAG), ganetespib (STA-9090), triapine, topotecan HCl, floxuridine, amonafide, TAS-102, adefovir dipivoxil, trifluridine, tenofovir alafenamide hemifumarate, tenofovir alafenamide fumarate, barici-

tinib phosphate, pixantrone Maleate, cerdulatinib (PRT062070), camptothecin, cytarabine hydrochloride, methotrexate, and brincidofovir.

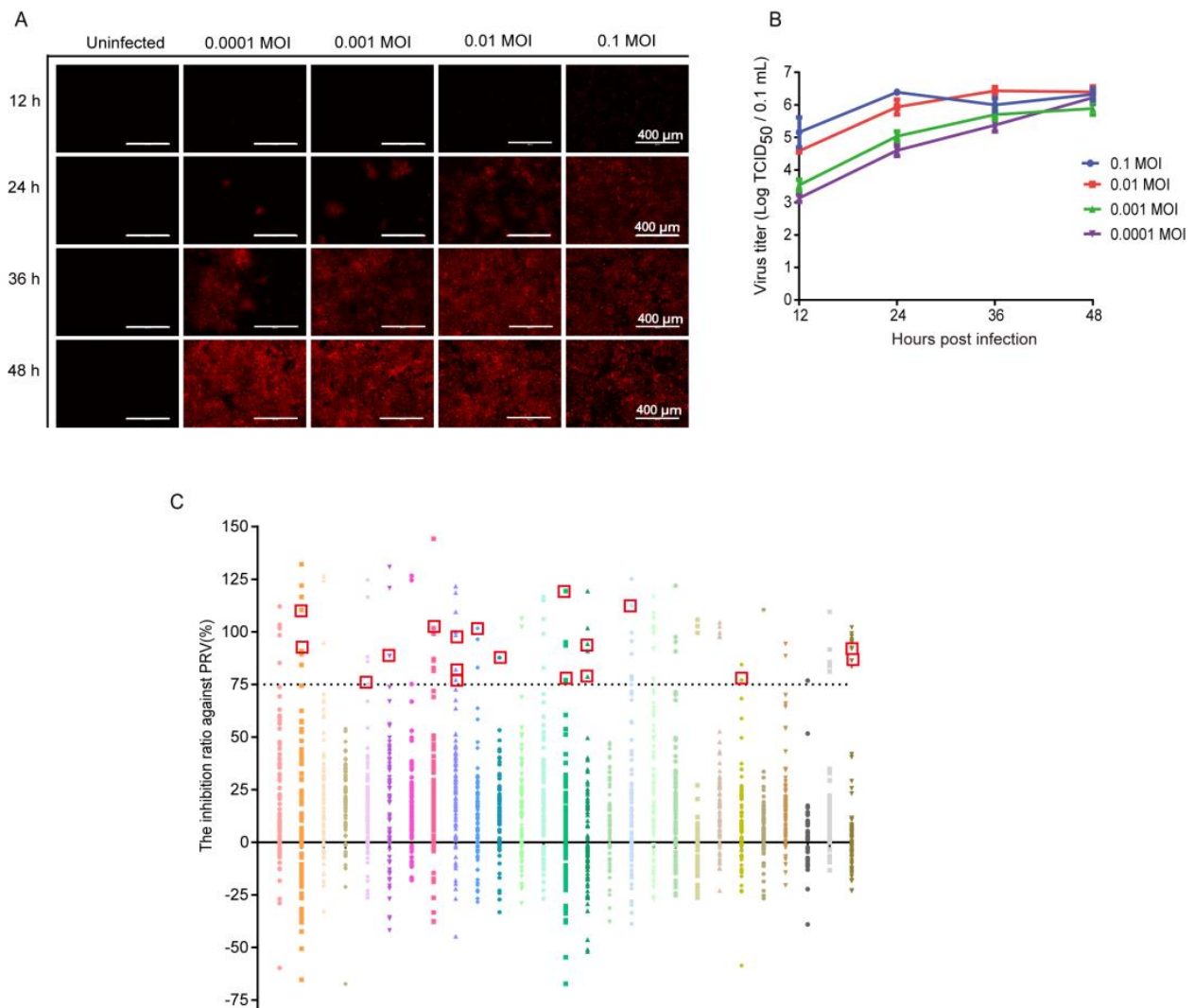


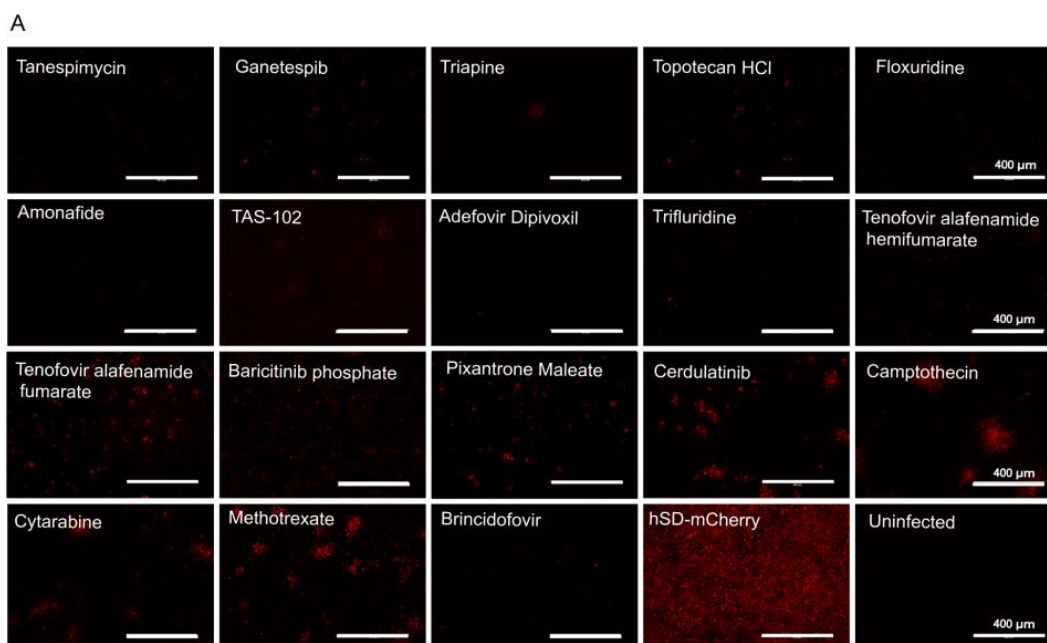
Figure 3. A high-throughput method for screening anti-PRV drugs was developed, resulting in the identification of 18 out of 2104 FDA-approved drugs based on this approach. (A,B) PK-15 cells were infected with Ea-mCherry at different dose. The fluorescence intensity and virus titer of each group was observed and determined at 12, 24, 36, and 48 hpi, respectively. The virus titer is expressed as the mean \pm standard deviation of 3 independent analyses. In cells infected with Ea-mCherry at 0.01 MOI for 36 h, the fluorescence intensity was the strongest, while the virus titer reached its highest level; (C) PK-15 cells were infected with Ea-mCherry at 0.01 MOI and were treated with the drug at a concentration of 10 μ M. After incubation for 36 h, the inhibition ratio of the drugs against PRV was calculated according to the following formula: $(\text{Fluorescence intensity}_{(\text{cells infected with PRV})} - \text{Fluorescence intensity}_{(\text{cells treated with drug and infected with PRV})}) / \text{Fluorescence intensity}_{(\text{cells infected with PRV})} \times 100\%$. A total of 2104 drugs were tested here. Each color represents a parallel screening of 96-well plate. The Y axis shows the inhibition rate of drugs on PRV calculated as described above. Each symbol represents a kind of drug. The symbols above the dotted line at “75” represent the drugs showing an inhibition ratio against PRV greater than or equal to 75%, 18 drugs (red squares) were confirmed to effectively reduce the CPEs induced by virus infection without exhibiting obvious cytotoxic effects on the cells. These drugs are considered as effective anti-PRV drugs in vitro. Data are expressed as the mean \pm standard deviation of 3 independent analyses.

Table 3. The 18 drugs effectively inhibiting PRV and screened out by the high-throughput method.

Number	Drug	Target
1	Tanespimycin (17-AAG)	Cytoskeletal Signaling
2	Ganetespib (STA-9090)	Cytoskeletal Signaling
3	Triapine	DNA/RNA Synthesis
4	Topotecan HCl	DNA Damage
5	Floxuridine	DNA Damage
6	Amonafide	DNA Damage
7	TAS-102	DNA/RNA Synthesis
8	Adefovir Dipivoxil	Microbiology
9	Trifluridine	DNA Damage
10	Tenofovir alafenamide hemifumarate	Reverse Transcriptase
11	Tenofovir alafenamide fumarate	Reverse Transcriptase
12	Baricitinib phosphate	JAK/STAT
13	Pixantrone Maleate	DNA Damage
14	Cerdulatinib (PRT062070)	JAK/STAT
15	Camptothecin	Topoisomerase
16	Cytarabine hydrochloride	DNA Damage
17	Methotrexate	Metabolism
18	Brincidofovir	DNA/RNA Synthesis

3.4. In Vitro Evaluation of the Anti-PRV Drug Candidates

The inhibitory effects of the 18 screened drug candidates on hSD-mCherry proliferation were evaluated in vitro. All 18 drugs demonstrated significant reductions in fluorescence intensity, viral gE gene copies, and virus titers in cells infected with hSD-mCherry (Figure 4A–C). The top 10 drugs exhibiting the highest inhibition of viral gE gene expression and virus titers were selected for further testing. The CC_{50} values of these 10 drugs ranged from 22.32 to 1124.00 μ M, while their IC_{50} values against PRV ranged from 0.075 to 4.076 μ M (Table 4, Figures S1 and S2). Consequently, all of these selected drugs exhibited a calculated select index (SI) greater than or equal to 25, indicating their potential as effective anti-PRV agents (Table 4).

**Figure 4.** Cont.

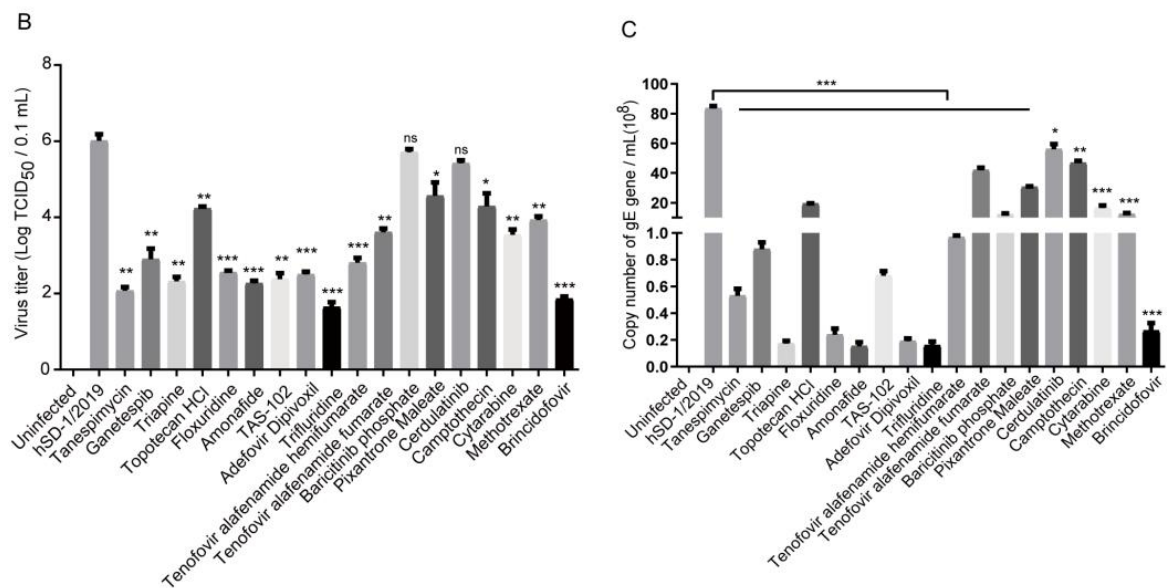


Figure 4. The inhibitory activity of 18 candidate drugs against PRV was evaluated in vitro. (A) PK-15 cells were infected with hSD-mCherry at an MOI of 0.01 and treated with the 18 drugs at a concentration of 10 μ M. After 36 h of infection, the fluorescence intensity of the cells was observed; (B,C) viral gE gene copies and virus titers were quantified using TaqMan qPCR and TCID₅₀ determination, respectively. All data were presented as the mean \pm standard deviation from three independent analyses. Statistical analysis using Student's *t*-test was performed to determine significant differences between the hSD-mCherry-infected group and the medication group. A level of 0.01 < *p* < 0.05 (*) was considered significant, and *p* < 0.01 (**) or *p* < 0.001 (***) was considered statistically highly significant and extremely significant, respectively. *p* > 0.05 (ns) was considered not significant.

Table 4. CC₅₀, IC₅₀ and SI of 10 drug candidates.

Number	Drug	CC ₅₀ (μ M)	IC ₅₀ (μ M)	SI (CC ₅₀ /IC ₅₀)
1	Tanespimycin (17-AAG)	48.89	0.46	106.08
2	Ganetespib (STA-9090)	294.51	0.07	3937.17
3	Triapine	78.66	2.99	26.29
4	Floxuridine	375.43	0.23	1653.74
5	Amonafide	241.71	1.24	194.76
6	TAS-102	1124.00	0.95	1186.66
7	Adefovir Dipivoxil	227.61	4.08	55.84
8	Trifluridine	352.40	1.43	246.09
9	Tenofovir hemifumarate	225.95	2.79	81.09
10	Brincidofovir	22.32	0.54	41.04

3.5. In Vivo Evaluation of the 10 Drug Candidates

The 10 drug candidates showing significant in vitro anti-PRV effects were further assessed in mice to validate their therapeutic efficacy against PRV infection in vivo. As shown in Figure 5A, mice were exposed to hSD-1/2019 at a lethal dose of 500 TCID₅₀ and intraperitoneally administered the candidate drug at a dose of 10 mg/kg for 5 consecutive days. Starting from the fourth day post infection, severe symptoms including abdominal scratching, persistent gnawing on the hind injected limbs leading to bone mutilation and tissue necrosis, and mortality (Figure 5B) were observed in both the hSD-1/2019 group and most drug groups. In contrast, mice treated with brincidofovir only exhibited mild clinical signs, such as bedding rubbing and abdominal scratching, on day 4 after infection, which completely disappeared by day 7 (Figure 5B). Consistently, survival curve analysis demonstrated that brincidofovir could provide complete protection against lethal hSD-1/2019 infection, while all mice in the other medication groups succumbed to the infection

(Figure 5C). These findings suggest that brincidofovir exhibits comprehensive protective effects in hSD-1/2019-infected mice.

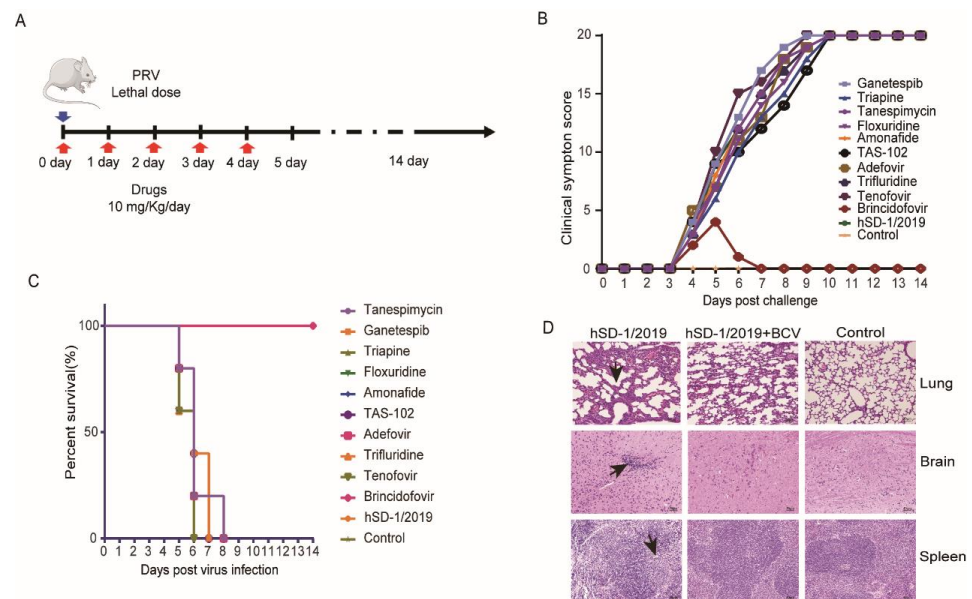


Figure 5. Therapeutic effect of the 10 drugs in mice infected with a lethal dose of hSD-1/2019 (A) Schematic diagram of the mouse model. The red arrows indicate drug medication and the blue arrow indicates the virus challenge. Mice were challenged with PRV hSD-1/2019 at 500 TCID₅₀ via hind foot pad injection. The medication groups were intraperitoneally treated with the drugs at a daily dose of 10 mg/Kg for five days. The observation period lasted for 14 days; (B) clinical symptoms in each group were scored daily and the total score of mice in a group is displayed, where higher scores indicate more severe clinical symptoms. A score of 20 represents death of all 5 mice in a group; (C) survival curve analysis was performed using Kaplan–Meier survival plots to evaluate the survival rates among different groups. The color lines represent different drug treatment groups; (D) histopathological examination was conducted on lung, brain and spleen tissues collected from three groups when mice died in the hSD-1/2019 group.

The brain, lung, and spleen tissues were collected from mice in the brincidofovir medication group, the hSD-1/2019 group, and the blank control group for section preparation and histopathological analysis. In the hSD-1/2019 group, the lung tissues of mice exhibited pulmonary congestion, thickened alveolar septa, enlarged alveolar cavities that fused to form large pulmonary alveoli, and significant intra-alveolar inflammatory cell infiltration. Massive monocyte infiltration was observed in the brain tissues. The spleen showed the disappearance of acini lienalis and blurred boundaries between red and white marrow (left column images of Figure 5D). Compared to the hSD-1/2019 group, mice treated with brincidofovir displayed reduced pulmonary congestion and alveolar septum thickening, more intact alveolar profiles, and a smaller amount of inflammatory cell infiltration in the alveolar lumen. No pathological changes were observed in the brain or spleen tissues (middle column images of Figure 5D). None of the tissues from mice in the blank control group showed any pathological changes (right column images of Figure 5D). Therefore, brincidofovir demonstrated a significant therapeutic effect on mice with lethal PRV infection.

3.6. Brincidofovir Inhibits Virus Proliferation Mainly by Interfering with the Viral Replication Phase

We subsequently evaluated and verified the antiviral efficacy of brincidofovir against PRV virus proliferation. The findings demonstrate a significant dose-dependent reduction in PRV virus titer upon treatment with brincidofovir (Figure 6A–C). To further elucidate

the specific stage of the PRV life cycle targeted by brincidofovir, time-of-addition assays were conducted (Figure 6D). Following the experimental protocol outlined in the Section 2, a concentration of 10 μM of brincidofovir was used along with a virus dose of 0.1 MOI. The results revealed that group IV treated with brincidofovir exhibited significantly lower fluorescence intensity compared to the control group (Figure 6E), indicating an enhanced inhibitory effect on viral replication (Figure 6F) and a substantial decrease in virus titer (Figure 6G). These observations suggest that brincidofovir primarily acts during the replication stage of PRV. However, no notable changes were observed in terms of the virus fluorescence intensity or titer in groups I, II, and III, implying that direct virucidal activity or interference with PRV adsorption or internalization is not among the mechanisms employed by brincidofovir.

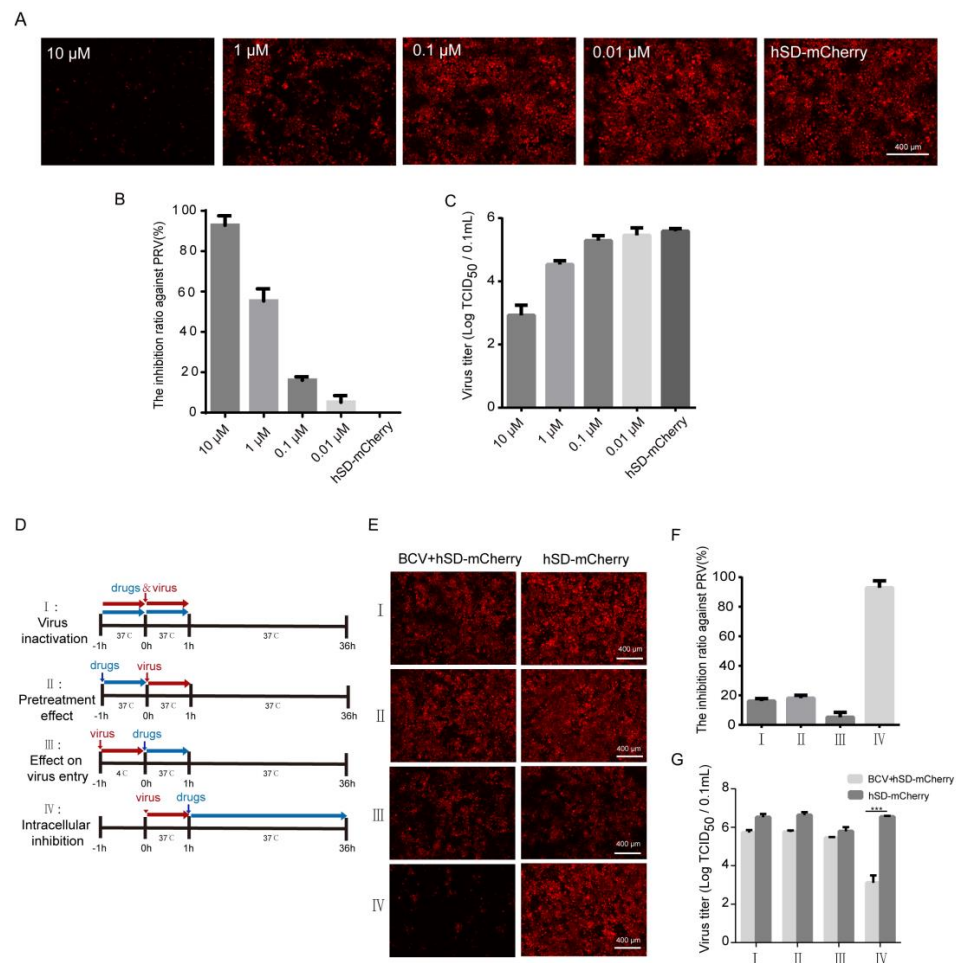


Figure 6. The stage of BCV inhibiting PRV virus infection. (A–C) PRV was inoculated into an 80% confluence of PK-15 cells at the dose of 0.01 MOI, and different concentrations of BCV were added. After incubation for 24 h, the fluorescence intensity was measured to calculate the inhibition rate of PRV based on the fluorescence intensity. Simultaneously, the virus titers were determined at different drug concentrations; (D) schematic illustration of the time-of-addition experiment; (E–G) resuscitated PK-15 cells were cultured in a cell incubator to form a monolayer for subsequent use. PRV virus infection and drug treatment followed a time-of-addition test diagram approach. The inhibition rate of drugs at different stages of PRV replication was assessed using fluorescence intensity measurements, and further confirmed by detecting the viral titer. A level of $p < 0.001$ (***) was considered statistically extremely significant.

4. Discussion

PRV infection is currently epidemic in various areas worldwide with dense pig populations, including Asia, South America, and Europe. Although pseudorabies has been successfully eliminated from domestic pigs in some countries, there is still a risk of virus transmission to domestic pig populations from wild animals, particularly wild boars [27,28]. Pseudorabies is one of the major infectious diseases in China, with a seropositivity rate of 35% in the last five years in 24 provinces. PRV infection has caused substantial economic losses to the Chinese pig farming industry. Vaccination has been the primary method of controlling and eliminating PRV infection in pigs [29]. As a typical alpha herpesvirus, PRV can build latent infection and be reactivated under certain stimulations. The reactivated virus can spill out and cause infection in pig herds. Moreover, latent PRV cannot be detected and therefore cannot be eliminated in time [1]. Vaccination cannot prevent PRV from establishing latent infection nor block the virus from spilling out after infection [30]. Effective anti-PRV drugs can potentially suppress latent infection and virus reactivation, preventing the virus from spilling out, which is of great importance for pseudorabies elimination in pigs and the treatment of human pseudorabies encephalitis.

Since 2017, 30 cases of PRV infection in humans have been reported in China. The human-origin PRV strain hSD-1/2019 was previously isolated from the cerebrospinal fluid of a patient in our laboratory. It was highly genomically and biologically similar to the PRV variant strains currently prevalent in pigs in China, suggesting the potential transmission risk of the PRV variant strains from pigs to humans [2]. The current worldwide spread of PRV in pigs has increased the contact degree between the virus and humans, promoting its potential to become a zoonotic disease and highlighting its threat to public health. In the 30 cases of human pseudorabies encephalitis, all patients developed neurological symptoms soon after the onset of febrile symptoms. After the treatment, five patients ultimately died and most survivors suffered from sequelae, including a coma (7/30), visual impairment (13/30), and delayed responses (4/26) [24]. The antiviral treatment of the patients did not prevent the rapid progression of neurological damage. PRV usually causes fatal infections in non-natural hosts, and the infected animals die within 24 h of developing neurological signs [31]. Therefore, early and effective antiviral treatment is particularly important for preventing neurological dysfunction and death caused by PRV infection.

The commonly used clinical anti-herpesvirus drugs include acyclovir, ganciclovir, famciclovir, valaciclovir, cidofovir, penciclovir, valganciclovir, trifluridine, vidarabine, cytarabine, and edoxudine [32]. These drugs are mostly nucleosides or nucleotide analogs, which could inhibit or interfere with the synthesis of viral DNA [33]. Antiviral drugs including acyclovir, ganciclovir, and penciclovir were administered to the 30 patients with a PRV infection after the initial diagnosis of viral encephalitis. Considering the poor progression of the patients, the antiviral effect of these drugs on PRV remained to be evaluated. Here, it was found that these clinically used anti-herpesvirus drugs showed few antiviral effects against the human-origin PRV strain hSD-1/2019 in vitro and in vivo (Figure 2), suggesting the urgency of developing more effective anti-PRV drugs.

It was reported that resveratrol showed effective anti-PRV effects with an IC_{50} of 17.17 μ M in vitro [34], and 30 mg/kg resveratrol could completely protect piglets intranasally infected with PRV at a dose of 2×10^6 TCID₅₀ [18]. However, the antiviral mechanism of these natural products is unclear and requires more research before clinical application. Hydroquinone and adefovir dipivoxil, which are listed in the FDA-approved drug library, were found to have a significant antiviral effect in vitro and in vivo against classical PRV strains, while the effects against the variant PRV strains and human-origin strains are unclear [21,22]. Although the valproic acid derivative valpromide (VPD) could inhibit PRV proliferation in PK-15 and Neuro-2a cells in the concentration range of 0.5 to 1.5 mM, no data support its medicative effect in vivo [35]. Ivermectin, an antiparasitic drug, also exhibited 100% inhibition of PRV replication at 2.0 μ M in vitro and reduced mortality by 50% in PRV-infected mice with attenuated brain damage [23].

According to the results in Figure 6, it can be suggested that brincidofovir primarily acts during the replication stage of PRV. However, it remains unclear as to which specific events in the PRV replication cycle are regulated by brincidofovir. Brincidofovir is a lipid conjugate of the acyclic nucleotide phosphonate cidofovir (CDV) [36]. The lipid side chain of brincidofovir hydrolyzes in cells to release CDV, which is then phosphorylated into CDV-diphosphate (CDV-DP). This compound inhibits the DNA polymerase enzyme that aids in viral DNA synthesis and suppresses viral DNA replication by disrupting the function of viral DNA polymerase and destabilizing viral DNA [37,38]. The addition of a lipid moiety increases the bioavailability and half-life while reducing nephrotoxic side effects associated with brincidofovir [39]. Therefore, brincidofovir is more effective in vivo than many other antiviral drugs. Based on these previous studies, the inhibition of brincidofovir on PRV DNA replication will be focused on in future investigations. At present, this drug is undergoing clinical trials for the treatment of patients severely infected with DNA viruses, including cytomegalovirus [40], adenovirus [38], herpes simplex virus [41], polyomavirus [42], smallpox virus [43], and monkeypox virus [44]. Moreover, it has been approved by the FDA for the treatment of smallpox virus [36], highlighting its high potential as a clinical medication in humans. In this study, brincidofovir was identified as a significant antiviral drug against both classical and variant PRV strains in vitro and in vivo. The IC_{50} of brincidofovir against PRV was remarkably low, at 0.5439 μ M (Table 4), while the administration of 10 mg/kg brincidofovir provided complete protection to mice from fatal infections caused by the human-origin variant PRV strain hSD-1/2019 (Figure 5). Since 2017, there has been an increasing number of reported cases involving human pseudorabies encephalitis. This emerging viral encephalitis poses serious risks such as severe neurological damage, death, and long-term complications, even with adequate clinical treatments, thus necessitating further attention towards elucidating its pathogenic mechanisms and developing effective antiviral drugs through future research.

5. Conclusions

In this study, we assessed the inhibitory efficacy of commonly utilized anti-herpesvirus medications (e.g., acyclovir, etc.) against PRV strains and observed their limited effectiveness. Herein, we developed a high-throughput screening method for identifying PRV antiviral drugs based on fluorescently labeled PRV strains and a multimode microplate reader that quantified fluorescence intensity to depict virus proliferation. A total of 2104 small-molecule drugs approved by the FDA were screened and validated using this model. Remarkably, the continuous administration of brincidofovir at a dosage of 10 mg/kg for 5 days provided complete protection in mice challenged with a lethal dose of a human-origin PRV strain. Experimental evidence confirmed that brincidofovir primarily impedes viral replication, thereby significantly inhibiting PRV both in vitro and in vivo. Consequently, these findings establish brincidofovir as a promising drug candidate for the clinical treatment of PRV infection.

Supplementary Materials: The following supporting information can be downloaded at: <https://www.mdpi.com/article/10.3390/v16030464/s1>, Figure S1: The 50% cytotoxic concentration (CC_{50}) measurement of 10 drugs. Figure S2: Half maximal inhibitory concentration (IC_{50}) of the 10 candidate drugs.

Author Contributions: Conceptualization, H.G., Q.L. and X.W.; Methodology, H.G., Q.L. and D.Y.; Formal analysis, D.Y.; Investigation, H.G. and H.Z.; Visualization, H.G., Q.L., H.Z. and Y.K.; Validation, Q.L.; Writing—original draft, H.G. and Q.L.; Resources, Y.K., Y.L. and H.C.; Software, Y.L.; Funding acquisition, H.C. and X.W.; Project administration, H.C. and X.W.; Supervision, X.W.; Writing—review and editing, X.W. All authors have read and agreed to the published version of the manuscript.

Funding: This work was supported by grants from the National Natural Science Foundation of China (32122086), the National Key Research and Development Program of China (2021YFD1800800), the Natural Science Foundation of Hubei Province (2021CFA016), the Fundamental Research Funds for

the Central Universities (2662023PY005), and the China Agriculture Research System of MOF and MARA (CARS-35). The funders had no role in the study design, data collection, data analysis, data interpretation, or manuscript writing.

Institutional Review Board Statement: Not applicable.

Informed Consent Statement: Not applicable.

Data Availability Statement: Data are contained within the article and Supplementary Materials.

Acknowledgments: We sincerely thank Song Li and Wu Zhong (National Engineering Research Center for the Emergency Drug, Beijing, China) for providing the compound.

Conflicts of Interest: The authors declare no conflicts of interest.

References

1. Pomeranz, L.E.; Reynolds, A.E.; Hengartner, C.J. Molecular biology of pseudorabies virus: Impact on neurovirology and veterinary medicine. *Microbiol. Mol. Biol. Rev. MMBR* **2005**, *69*, 462–500. [CrossRef]
2. Liu, Q.; Wang, X.; Xie, C.; Ding, S.; Yang, H.; Guo, S.; Li, J.; Qin, L.; Ban, F.; Wang, D.; et al. A novel human acute encephalitis caused by pseudorabies virus variant strain. *Clin. Infect. Dis.* **2020**, *73*, 3690–3700. [CrossRef]
3. Wu, T.; Fei, L.; Hao, Z.; Liang, C.; Tong, G.Z. Emergence of a Pseudorabies virus variant with increased virulence to piglets. *Vet. Microbiol.* **2015**, *181*, 236–240.
4. Wang, C.H.; Yuan, J.; Qin, H.Y.; Luo, Y.; Cong, X.; Li, Y.; Chen, J.; Li, S.; Sun, Y.; Qiu, H.J. A novel gE-deleted pseudorabies virus (PRV) provides rapid and complete protection from lethal challenge with the PRV variant emerging in Bartha-K61-vaccinated swine population in China. *Vaccine* **2014**, *32*, 3379–3385. [CrossRef]
5. Skinner, G.; Ahmad, A.; Davies, J.A. The infrequency of transmission of herpesviruses between humans and animals; postulation of an unrecognised protective host mechanism. *Comp. Immunol. Microbiol. Infect. Dis.* **2001**, *24*, 255–269. [CrossRef]
6. Tan, L.; Shu, X.; Xu, K.; Liao, F.; Song, C.; Duan, D.; Yang, S.; Yao, J.; Wang, A. Homologous recombination technology generated recombinant pseudorabies virus expressing EGFP facilitates to evaluate its susceptibility to different cells and screen antiviral compounds. *Res. Vet. Sci.* **2022**, *145*, 125–134. [CrossRef]
7. Fan, S.; Yuan, H.; Liu, L.; Li, H.; Wang, S.; Zhao, W.; Wu, Y.; Wang, P.; Hu, Y.; Han, J.; et al. Pseudorabies virus encephalitis in humans: A case series study. *J. Neurovirol.* **2020**, *26*, 556–564. [CrossRef]
8. Zhao, W.; Wu, Y.; Li, H.; Li, S.; Fan, S.; Wu, H.; Li, Y.; Lü, Y.; Han, J.; Zhang, W.; et al. Clinical experience and next-generation sequencing analysis of encephalitis caused by pseudorabies virus. *Zhonghua Yi Xue Za Zhi* **2018**, *98*, 1152–1157. [CrossRef]
9. Wang, D.; Tao, X.; Fei, M.; Chen, J.; Guo, W.; Li, P.; Wang, J. Human encephalitis caused by pseudorabies virus infection: A case report. *J. Neurovirol.* **2020**, *26*, 442–448. [CrossRef]
10. Wang, Y.; Nian, H.; Li, Z.; Wang, W.; Wang, X.; Cui, Y. Human encephalitis complicated with bilateral acute retinal necrosis associated with pseudorabies virus infection: A case report. *Int. J. Infect. Dis. IJID Off. Publ. Int. Soc. Infect. Dis.* **2019**, *89*, 51–54. [CrossRef]
11. Yang, X.; Guan, H.; Li, C.; Li, Y.; Wang, S.; Zhao, X.; Zhao, Y.; Liu, Y. Characteristics of human encephalitis caused by pseudorabies virus: A case series study. *Int. J. Infect. Dis. IJID Off. Publ. Int. Soc. Infect. Dis.* **2019**, *87*, 92–99. [CrossRef]
12. Zheng, L.; Liu, X.; Yuan, D.; Li, R.; Lu, J.; Li, X.; Tian, K.; Dai, E. Dynamic cerebrospinal fluid analyses of severe pseudorabies encephalitis. *Transbound. Emerg. Dis.* **2019**, *66*, 2562–2565. [CrossRef]
13. Yang, H.; Han, H.; Wang, H.; Cui, Y.; Liu, H.; Ding, S. A Case of Human Viral Encephalitis Caused by Pseudorabies Virus Infection in China. *Front. Neurol.* **2019**, *10*, 534–542. [CrossRef] [PubMed]
14. Hu, F.; Wang, J.; Peng, X. Bilateral Necrotizing Retinitis following Encephalitis Caused by the Pseudorabies Virus Confirmed by Next-Generation Sequencing. *Ocul. Immunol. Inflamm.* **2020**, *29*, 922–925. [CrossRef]
15. Ai, J.W.; Weng, S.S.; Cheng, Q.; Cui, P.; Li, Y.J.; Wu, H.L.; Zhu, Y.M.; Xu, B.; Zhang, W.H. Human Endophthalmitis Caused By Pseudorabies Virus Infection, China, 2017. *Emerg. Infect. Dis.* **2018**, *24*, 1087–1090. [CrossRef] [PubMed]
16. Wang, Y.; Liu, T.X.; Wang, T.Y.; Tang, Y.D.; Wei, P. Isobavachalcone inhibits Pseudorabies virus by impairing virus-induced cell-to-cell fusion. *Virol. J.* **2020**, *17*, 39–48. [CrossRef] [PubMed]
17. Huan, C.; Xu, W.; Guo, T.; Pan, H.; Gao, S. (-)-Epigallocatechin-3-Gallate Inhibits the Life Cycle of Pseudorabies Virus In Vitro and Protects Mice Against Fatal Infection. *Front. Cell. Infect. Microbiol.* **2021**, *10*, 895–908. [CrossRef]
18. Zhao, X.; Tong, W.; Song, X.; Jia, R.; Li, L.; Zou, Y.; He, C.; Liang, X.; Cheng, L.; Bo, J. Antiviral Effect of Resveratrol in Piglets Infected with Virulent Pseudorabies Virus. *Viruses* **2018**, *10*, 457. [CrossRef]
19. Li, L.; Wang, R.; Hu, H.; Chen, X.; Yin, Z.; Liang, X.; He, C.; Yin, L.; Ye, G.; Zou, Y.; et al. The antiviral activity of kaempferol against pseudorabies virus in mice. *BMC Vet. Res.* **2021**, *17*, 247–258. [CrossRef]
20. Sun, Y.; Li, C.; Li, Z.; Shanguan, A.; Jiang, J.; Zeng, W.; Zhang, S.; He, Q. Quercetin as an antiviral agent inhibits the Pseudorabies virus in vitro and in vivo. *Virus Res.* **2021**, *305*, 556–564. [CrossRef]
21. Fang, L.; Gao, Y.; Lan, M.; Jiang, P.; Bai, J.; Li, Y.; Wang, X. Hydroquinone inhibits PRV infection in neurons in vitro and in vivo. *Vet. Microbiol.* **2020**, *250*, 864–871. [CrossRef] [PubMed]

22. Wang, G.; Chen, R.; Huang, P.; Hong, J.; Cao, J.; Wu, Q.; Zheng, W.; Lin, L.; Han, Q.; Chen, Y.; et al. Adefovir dipivoxil efficiently inhibits the proliferation of pseudorabies virus in vitro and in vivo. *Antivir. Res.* **2021**, *186*, 14–25. [CrossRef]
23. Lv, C.; Liu, W.; Wang, B.; Dang, R.; Qiu, L.; Ren, J.; Yan, C.; Yang, Z.; Wang, X. Ivermectin inhibits DNA polymerase UL42 of pseudorabies virus entrance into the nucleus and proliferation of the virus in vitro and vivo. *Antivir. Res.* **2018**, *159*, 55–62. [CrossRef] [PubMed]
24. Zhou, Y.; Nie, C.; Wen, H.; Long, Y.; Zhou, M.; Xie, Z.; Hong, D. Human viral encephalitis associated with suid herpesvirus 1. *Neurol. Sci. Off. J. Ital. Neurol. Soc. Ital. Soc. Clin. Neurophysiol.* **2022**, *43*, 2681–2692. [CrossRef] [PubMed]
25. Russ, P.; Schelling, P.; Scapozza, L.; Folkers, G.; Clercq, E.; Marquez, V. Synthesis and biological evaluation of 5-substituted derivatives of the potent antiherpes agent (north)-methanocarbathymine. *J. Med. Chem.* **2003**, *46*, 5045–5054. [CrossRef] [PubMed]
26. Brancale, A.; McGuigan, C.; Algain, B.; Savy, P.; Benhida, R.; Fourrey, J.; Andrei, G.; Snoeck, R.; De Clercq, E.; Balzarini, J. Bicyclic anti-VZV nucleosides: Thieno analogues retain full antiviral activity. *Bioorganic Med. Chem. Lett.* **2001**, *11*, 2507–2510. [CrossRef] [PubMed]
27. Pedersen, K.; Turnage, C.T.; Gaston, W.D.; Arruda, P.; Alls, S.A.; Gidlewski, T. Pseudorabies detected in hunting dogs in Alabama and Arkansas after close contact with feral swine (*Sus scrofa*). *BMC Vet. Res.* **2018**, *14*, 388–395. [CrossRef]
28. Chiari, M.; Ferrari, N.; Bertolotti, M.; Avisani, D.; Cerioli, M.; Zanoni, M.; Alborali, L.G.; Lanfranchi, P.; Lelli, D.; Martin, A.M. Long-Term Surveillance of Aujeszky's Disease in the Alpine Wild Boar (*Sus scrofa*). *EcoHealth* **2015**, *12*, 563–570. [CrossRef]
29. Sun, Y.; Luo, Y.; Wang, C.H.; Yuan, J.; Li, N.; Song, K.; Qiu, H.J. Control of swine pseudorabies in China: Opportunities and limitations. *Vet. Microbiol.* **2016**, *183*, 119–124. [CrossRef]
30. Lu, J.J.; Yuan, W.Z.; Zhu, Y.P.; Hou, S.H.; Wang, X.J. Latent pseudorabies virus infection in medulla oblongata from quarantined pigs. *Transbound. Emerg. Dis.* **2021**, *68*, 543–551. [CrossRef]
31. Tan, L.; Yao, J.; Yang, Y.; Luo, W.; Yuan, X.; Yang, L.; Wang, A. Current Status and Challenge of Pseudorabies Virus Infection in China. *Virol. Sin.* **2021**, *36*, 588–607. [CrossRef] [PubMed]
32. Bialas, K.M.; Swamy, G.K.; Permar, S.R. Perinatal cytomegalovirus and varicella zoster virus infections: Epidemiology, prevention, and treatment. *Clin. Perinatol.* **2015**, *42*, 61–75. [CrossRef] [PubMed]
33. Evans, C.M.; Kudesia, G.; Mckendrick, M. Management of herpesvirus infections. *Int. J. Antimicrob. Agents* **2013**, *42*, 119–128. [CrossRef] [PubMed]
34. Zhao, X.; Cui, Q.; Fu, Q.; Song, X.; Jia, R.; Yang, Y.; Zou, Y.; Li, L.; He, C.; Liang, X. Antiviral properties of resveratrol against pseudorabies virus are associated with the inhibition of κ B kinase activation. *Sci. Rep.* **2017**, *7*, 782–790. [CrossRef] [PubMed]
35. Andreu, S.; Ripa, I.; Praena, B.; López-Guerrero, J.A.; Bello-Morales, R. The Valproic Acid Derivative Valpromide Inhibits Pseudorabies Virus Infection in Swine Epithelial and Mouse Neuroblastoma Cell Lines. *Viruses* **2021**, *13*, 2522. [CrossRef] [PubMed]
36. Florescu, D.F.; Keck, M.A. Development of CMX001 (Brincidofovir) for the treatment of serious diseases or conditions caused by dsDNA viruses. *Expert Rev. Anti-Infect. Ther.* **2014**, *12*, 1171–1178. [CrossRef]
37. Feghoul, L.; Mercier-Delarue, S.; Salmona, M.; Ntsiba, N.; Dalle, J.-H.; Baruchel, A.; Klonjkowski, B.; Richardson, J.; Simon, F.; LeGoff, J. Genetic diversity of the human adenovirus species C DNA polymerase. *Antivir. Res.* **2018**, *159*, 1–9. [CrossRef]
38. Alvarez-Cardona, J.J.; Whited, L.K.; Chemaly, R.F. Brincidofovir: Understanding its unique profile and potential role against adenovirus and other viral infections. *Future Microbiol.* **2020**, *15*, 389–400. [CrossRef]
39. Hutson, C.L.; Kondas, A.V.; Mauldin, M.R.; Doty, J.B.; Olson, V.A. Pharmacokinetics and Efficacy of a Potential Smallpox Therapeutic, Brincidofovir, in a Lethal Monkeypox Virus Animal Model. *mSphere* **2021**, *6*, 927–932. [CrossRef]
40. Randall, L.E.; Scott, F.; Tom, B.; Sunwen, C.; Prichard, M.N.; Steven, K.; Chad, W.; Donella, C.; Herve, M.M. Analysis of Mutations in the Gene Encoding Cytomegalovirus DNA Polymerase in a Phase 2 Clinical Trial of Brincidofovir Prophylaxis. *J. Infect. Dis.* **2016**, *214*, 32–35.
41. Quenelle, D.C.; Lampert, B.; Collins, D.J.; Rice, T.L.; Painter, G.R.; Kern, E.R. Efficacy of CMX001 against Herpes Simplex Virus Infections in Mice and Correlations with Drug Distribution Studies. *J. Infect. Dis.* **2010**, *202*, 1492–1499. [CrossRef] [PubMed]
42. Gosert, R.; Rinaldo, C.H.; Wernli, M.; Major, E.O.; Hirsch, H.H. CMX001 (1-O-Hexadecyloxypropyl-Cidofovir) Inhibits Polyomavirus JC Replication in Human Brain Progenitor-Derived Astrocytes. *Antimicrob. Agents Chemother.* **2011**, *55*, 2129–2136. [CrossRef] [PubMed]
43. Olson, V.A.; Smith, S.K.; Foster, S.; Li, Y.; Lanier, E.R.; Gates, I.; Trost, L.C.; Damon, I.K. In Vitro Efficacy of Brincidofovir against Variola Virus. *Antimicrob. Agents Chemother.* **2014**, *58*, 5570–5571. [CrossRef]
44. Lanier, R.; Trost, L.; Tippin, T.; Lampert, B.; Robertson, A.; Foster, S.; Rose, M.; Painter, W.; O'Mahony, R.; Almond, M.; et al. Development of CMX001 for the Treatment of Poxvirus Infections. *Viruses* **2010**, *2*, 2740–2762. [CrossRef] [PubMed]

Disclaimer/Publisher's Note: The statements, opinions and data contained in all publications are solely those of the individual author(s) and contributor(s) and not of MDPI and/or the editor(s). MDPI and/or the editor(s) disclaim responsibility for any injury to people or property resulting from any ideas, methods, instructions or products referred to in the content.

MDPI
St. Alban-Anlage 66
4052 Basel
Switzerland
www.mdpi.com

Viruses Editorial Office
E-mail: viruses@mdpi.com
www.mdpi.com/journal/viruses



Disclaimer/Publisher's Note: The statements, opinions and data contained in all publications are solely those of the individual author(s) and contributor(s) and not of MDPI and/or the editor(s). MDPI and/or the editor(s) disclaim responsibility for any injury to people or property resulting from any ideas, methods, instructions or products referred to in the content.



Academic Open
Access Publishing

mdpi.com

ISBN 978-3-7258-1297-4